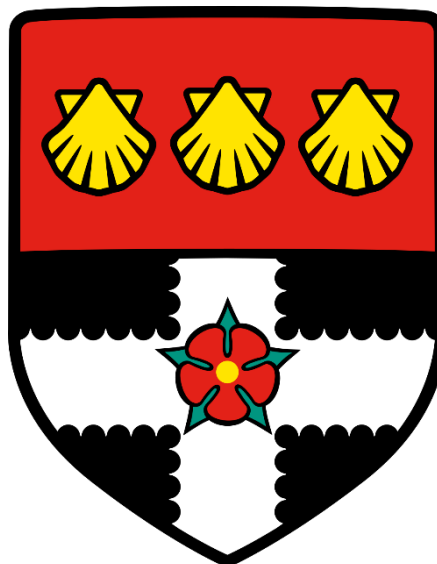


**University of Reading**



**Echocardiography for  
Assessment of Cardiac  
Hypertrophy in Mice**

PhD Biomedicine

School of Biological Sciences

**Joshua James Cull**

**March 2024**

## **Declaration of Authorship**

I, Joshua Cull, confirm that this is my own work and that the use of all material from other sources has been properly and fully acknowledged.

**Name:**

Joshua Cull

**Signed:**

## **Abstract**

**Background:** Multiple diseases, including hypertension, induce stress on the heart, causing cardiac hypertrophy and eventually heart failure. Associated with these disease states are altered protein interactions, which modify cardiac function. Hypertension is estimated to affect 1.28 billion adults worldwide, with heart failure affecting 64 million people. While preclinical models exist and are used in research, they often focus on late-stage hypertension. This thesis presents a series of studies for which a standardised echocardiography protocol was developed to assess the roles of different proteins in the early stages of hypertension-induced cardiac pathology. **Aims:** To develop a robust, standardised and reproducible *in vivo* assessment of the effect of early-stage hypertension on the hearts of mouse models. This protocol must adhere to the principles of replacement, reduction, and refinement in animal research. These studies aim to show that it is possible to study the effects of early-stage hypertension on cardiac function and protein signalling. This would provide insights into how alterations in protein signalling contribute to the pathology before significant illness occurs. **Methods:** An *in vivo* echocardiography protocol was developed and performed on genetically altered mouse models (e.g., STRN, STRN3, PKN2) and their wild-type (WT) littermates, or through pharmacological inhibition in C57BL/6J mice (e.g. the effect of dabrafenib targeting BRAF). The protocol was used to assess the effect of AngII treatment on cardiac function, cardiac dimensions and arterial blood flow. AngII-induced hypertension causes haemodynamic overload of the heart which induces cardiac hypertrophy. Echocardiography was performed twice before treatment (for baseline normalisation) and sequentially post-AngII administration until the end of the experiment-specific timeline. After the final echocardiography session, tissues were harvested for biochemical and histological analysis. **Results:** Three papers are presented in this thesis, summarised by the following results. Echocardiography provided insights into the differential roles of STRN, STRN3, and PKN2 genetically altered mice in the cardiac adaptation to AngII-induced hypertension. For the STRN/STRN3 and PKN2 studies, the global heterozygote offspring were successfully produced and appear phenotypically normal. However, homozygote gene deletion was embryonic lethal, suggesting a compensatory mechanism in the heterozygous mice. Consistent with this, the effects of gene deletion or inhibition appeared to have a minimal effect at baseline. However, under stress, each study demonstrated that the genes are required for the heart to adapt. Since the global model affected all cardiac cells other than just cardiomyocytes, it was not clear if these genes were significant in cardiomyocytes themselves. Conditional cardiomyocyte-specific knockouts were successfully generated and applied to demonstrate that these genes play

a significant role in cardiomyocyte adaptation to AngII-induced hypertension. Echocardiography also helped identify the cardioprotective effects of RAF inhibition by dabrafenib against AngII-induced hypertrophy. **Conclusion:** Overall, this thesis contributes to the understanding of protein kinase signalling pathways in cardiac remodelling. It demonstrated that early-stage hypertension-associated cardiac hypertrophy can be assessed, providing insights into potential novel therapeutic interventions. Each chapter demonstrates the importance of echocardiography for the non-invasive assessment of these models. Exploring echocardiography, histology and biochemical analysis further will uncover the full implications of these pathways in the heart.

## **Dedication**

This thesis is dedicated to my dad. I love you and miss you more than words can express. Your belief in me has inspired me to pursue my dreams and finish this PhD.

## **Acknowledgements**

First and foremost, I would like to express my profound gratitude to Professor Angela Clerk, whose exceptional teaching and mentorship have been invaluable to my academic journey. Your guidance and support have enabled me to navigate and understand the complexities of this PhD. The foundations of this body of work are products of her efforts. I also want to express my admiration for Dr Hajed Alharbi, my friend and colleague. Your extensive assistance, resolute spirit and comradery throughout the PhD were greatly appreciated.

I want to especially thank my amazing fiancé, Alice Filipe, whose constant love and unwavering support made this achievement possible. Alice my angel, I love you more than words can express. I will forever be grateful for your encouragement and belief in me. We have been through the worst the world can offer and now are thriving. This thesis is proof that together we can achieve anything! I cannot wait for our future adventures as doctors. The world awaits us.

I would also like to thank my loving family: Tracey, Richard, Sam, Nick, Miranda, Anne, Geoffrey, Jane, Jose, and Lily. You all have always believed in me, even when I may not have believed in myself. Your love, support and motivation throughout my PhD and illness will never be forgotten. I am forever indebted to you all.

This thesis would have been impossible without the invaluable assistance of numerous individuals, whose names may not all be listed here. I wholeheartedly appreciate and acknowledge all their efforts and contributions in every possible way. Finally, I am grateful to the British Heart Foundation for its funding, which has enabled me to pursue this research. I am honoured to have had the opportunity to contribute to their mission of advancing cardiovascular research. I hope this work will positively impact the lives of those affected by cardiovascular disease.

## **Contents Page**

<b>Echocardiography for Assessment of Cardiac Hypertrophy in Mice.....</b>	<b>1</b>
<b>Declaration of Authorship.....</b>	<b>2</b>
<b>Abstract .....</b>	<b>3</b>
<b>Dedication .....</b>	<b>5</b>
<b>Acknowledgements .....</b>	<b>6</b>
<b>Contents Page.....</b>	<b>7</b>
<b>List of Figures .....</b>	<b>10</b>
<b>List of Tables .....</b>	<b>11</b>
<b>Abbreviations .....</b>	<b>12</b>
<b>Chapter 1 - Introduction .....</b>	<b>17</b>
<b>1.1 Aims of the Research .....</b>	<b>18</b>
<b>1.2 Themes Between the Presented Studies .....</b>	<b>18</b>
<b>1.3 Experimental Design .....</b>	<b>20</b>
<b>1.3.1 Experimental Controls for Genetic Modification .....</b>	<b>20</b>
<b>1.3.2 The 3 Rs .....</b>	<b>21</b>
<b>1.4 Summary of Results Chapters .....</b>	<b>26</b>
<b>1.4.1 Chapter 3: Striatin, but not striatin 3, plays a major role in angiotensin II-induced cardiomyocyte and cardiac hypertrophy in mice <i>in vivo</i>.....</b>	<b>26</b>
<b>1.4.2 Chapter 4: PKN2 deficiency leads both to prenatal 'congenital' cardiomyopathy and defective angiotensin II stress responses.....</b>	<b>28</b>
<b>1.4.3 Chapter 5: The anti-cancer drug dabrafenib is not cardiotoxic and inhibits cardiac remodelling and fibrosis in a murine model of hypertension. ....</b>	<b>28</b>
<b>Chapter 2 - Background .....</b>	<b>31</b>
<b>2.1 Hypertension and Heart Failure.....</b>	<b>32</b>
<b>2.1.1 Types of Heart Failure .....</b>	<b>32</b>
<b>2.1.2 Risk Factors for Hypertension and Heart Failure .....</b>	<b>33</b>
<b>2.2 Cardiac Anatomy and Physiology.....</b>	<b>34</b>
<b>2.2.1 Gross Anatomy .....</b>	<b>34</b>
<b>2.2.2 The Cardiac Cycle and Electrical Conduction System .....</b>	<b>39</b>
<b>2.2.3 Cellular Content of the Heart.....</b>	<b>42</b>
<b>2.2.4 Cardiac Contractile Apparatus .....</b>	<b>44</b>
<b>2.2.5 Cardiac Hypertrophy .....</b>	<b>48</b>

2.2.6 Effect of Hypertension on the Heart .....	49
<b>2.3 RAAS and Blood Pressure Regulation .....</b>	<b>51</b>
<b>2.4 Therapeutic Options for Hypertension Management.....</b>	<b>54</b>
2.4.1 Lifestyle Modifications.....	54
2.4.2 Antihypertensive Medications.....	54
<b>2.5 Rodent Models of Hypertension.....</b>	<b>57</b>
2.5.1 Inbred Genetic Models.....	58
2.5.2 Drug-Induced vs Surgical Models of Hypertension.....	59
2.5.3 Genetically-Altered Mice .....	60
<b>2.6 Echocardiography.....</b>	<b>68</b>
2.6.1 Overview .....	68
2.6.2 Imaging Methods .....	71
2.6.3 Echocardiography vs Magnetic Resonance Imaging.....	81
<b>2.7 Regulation of Cellular Responses .....</b>	<b>83</b>
2.7.1 Intra- and Inter-Cellular Signalling: General Concepts.....	83
2.7.2 Striatins, PP2A and STRIPAK Complexes .....	86
2.7.3 PKN2 in the Heart.....	94
2.7.4 The ERK1/2 Pathway and its Inhibitors .....	95
<b>Chapter 3 - Striatin plays a major role in angiotensin II-induced cardiomyocyte and cardiac hypertrophy in mice <i>in vivo</i>.....</b>	<b>98</b>
<b>Chapter 4 - PKN2 deficiency leads both to prenatal ‘congenital’ cardiomyopathy and defective angiotensin II stress responses.....</b>	<b>99</b>
<b>Chapter 5 - The anti-cancer drug dabrafenib is not cardiotoxic and inhibits cardiac remodelling and fibrosis in a murine model of hypertension .....</b>	<b>100</b>
<b>Chapter 6 - Discussion and Conclusion .....</b>	<b>101</b>
<b>6.1 Key Conclusions from the Research .....</b>	<b>102</b>
6.1.1 The Role of Striatins in the Heart (Chapter 3).....	102
6.1.2 The Role of PKN2 in the Heart (Chapter 4).....	103
6.1.3 The Effects of Dabrafenib on the Heart (Chapter 5) .....	104
<b>6.2 Theoretical and Practical Implications of <i>In Vivo</i> Studies.....</b>	<b>105</b>
6.2.1 Choice of Preclinical Model and Use of Genetically-Altered Mice.....	106
6.2.2 Selection of Genetically Altered Model for Gene Deletion.....	107
6.3.2 Limitations of <i>In Vivo</i> Studies with Preclinical Models of Disease .....	111
<b>6.3 Concluding Remarks .....</b>	<b>113</b>

<b>References .....</b>	114
<b>Appendix .....</b>	140
<b>Appendix I: Publications .....</b>	140

## List of Figures

<b>Figure 1: The Basic Structure of the Heart.....</b>	36
<b>Figure 2: The Structure of the Walls of the Heart.....</b>	38
<b>Figure 3: A Representation of an Electrocardiogram (ECG) Trace.....</b>	41
<b>Figure 4: The Sliding-Filament Model of Muscle Contraction.....</b>	47
<b>Figure 5: The Renin-Angiotensin-Aldosterone System (RAAS).....</b>	53
<b>Figure 6: Generation of the Strn and Strn Knockout Mouse Models.....</b>	63
<b>Figure 7: STRN<sup>tm1a(KOMP)WTsi</sup> Knockout First (Promoter Driven) System for the Generation of Cardiac Specific, Inducible Strn+/- Mice.....</b>	66
<b>Figure 8: Summary of the Strn<sup>f1/f1</sup>/Cre<sup>WT/MCM</sup> Mouse Breeding Program.....</b>	67
<b>Figure 9: Schematic, Positioning and B-mode Image Demonstrating the PSAX Cardiovascular Orientations.....</b>	72
<b>Figure 10: Schematic, Positioning and B-mode Image Demonstrating the PLAX Cardiovascular Orientation.....</b>	73
<b>Figure 11: Representative Mouse Cardiac B-mode Images.....</b>	75
<b>Figure 12: Representative Mouse Cardiac M-mode Images.....</b>	77
<b>Figure 13: Representative Analysis of Aorta and Pulmonary Artery Function.....</b>	80
<b>Figure 14: A Representation of a Signalling Pathway.....</b>	85
<b>Figure 15: The Gene Structure of the Striatin Family Proteins.....</b>	88
<b>Figure 16: STRIPAK Complexes and the Germinal Centre Kinase (GCK) Subfamilies.....</b>	89
<b>Figure 17: Activation of the ERK1/2 Signalling Pathway by EGF.....</b>	97

## **List of Tables**

<b>Table 1: Animal Monitoring Scoring System .....</b>	<b>24</b>
<b>Table 2: Key Anti-Hypertensive Medications.....</b>	<b>56</b>
<b>Table 3: Components of the STRIPAK Complex.....</b>	<b>90</b>

## **Abbreviations**

<b>Abbreviation</b>	<b>Expansion</b>
2D	Two-Dimensional
2K1C	Two-Kidney, One Clip
3D	Three-Dimensional
ACE	Angiotensin-Converting Enzyme
ADP	Adenosine Diphosphate
AngI	Angiotensin I
AngII	Angiotensin II
ANP	Atrial Natriuretic Peptide
ARVC	Arrhythmogenic Right Ventricular Cardiomyopathy
ASK	Apoptosis Signal-Regulating Kinase
AT1R	Angiotensin II Receptor Type 1
ATP	Adenosine Triphosphate
AWERB	Animal Welfare and Ethical Review Body
BALB/c	Bagg Albino/c Mice (a strain of inbred mice)
BMI	Body Mass Index
B-Mode	Brightness Mode
BNP	B-Type Natriuretic Peptide
BRU	BioResource Unit
CaM	Calmodulin Binding Domain
Cas9	CRISPR-Associated Protein 9
CaV	Caveolin Binding Domain
C-C	Coiled-Coil
CCM3	Cerebral Cavernous Malformation 3

Col1a1	Fibrillar Collagen Type I
Col3a1	Fibrillar Collagen Type III
CRE	Cyclic Recombinase
CRISPR	Clustered Regularly Interspaced Short Palindromic Repeats
CTTNBP2	Cortactin-Binding Protein 2
CTTNBP2NL	Cortactin-Binding Protein 2 N-Terminal-Like
DMSO	Dimethyl Sulfoxide
DNA	Deoxyribonucleic Acid
ECG	Electrocardiogram
ECM	Extracellular Matrix
EGF	Epidermal Growth Factor
EGFR	Epidermal Growth Factor Receptor
ERK	Extracellular Signal-Regulated Kinase
FGFR1OP2	Fibroblast Growth Factor Receptor 1 Overexpressed in Prostate Cancer 2
FLP	Flippase
FRT	Flippase Recognition Target
GAPDH	Glyceraldehyde 3-phosphate Dehydrogenase
GCK	Germinal Centre Kinase
GDP	Guanosine Diphosphate
GEF	Guanine Nucleotide Exchange Factor
GPCR	G Protein-Coupled Receptor
GRB2	Growth Factor Receptor-Bound Protein 2
GTP	Guanosine Triphosphate
HFmrEF	Heart Failure with Mid-Range Ejection Fraction
HFpEF	Heart Failure with Preserved Ejection Fraction

HFrEF	Heart Failure with Reduced Ejection Fraction
HOLC	Home Office Liaison Contact
IMPC	International Mouse Phenotyping Consortium
IVS	Interventricular Septum
JNK	c-Jun N-Terminal Kinase
KOMP	Knockout Mouse Project
LoxP	Locus of Crossing-Over P
LV	Left Ventricle
LVAW	Left Ventricular Anterior Wall
LVID	Left Ventricular Internal Diameter
LVPW	Left Ventricular Posterior Wall
MAPK	Mitogen-Activated Protein Kinase
MAPs	Microtubule-Associated Proteins
MCM	Myh6-MERCeMER
MEK	Mitogen-Activated Protein Kinase Kinase
MLCK	Myosin Light Chain Kinase
MLK	Mixed Lineage Kinase
M-Mode	Motion Mode
MRI	Magnetic Resonance Imaging
mRNA	Messenger RNA
MST	Mammalian STE20-Like Protein Kinase
Myh6	Myosin Heavy Chain 6
Myh7	Myosin Heavy Chain 7
NACWO	Named Animal Care and Welfare Officer
NO	Nitric Oxide

NTCO	Named Training and Competency Officer
NVS	Named Veterinary Surgeon
PAT/AAT	Pulmonary/Aortic Acceleration Time
PEG	Polyethylene Glycol
PET/AET	Pulmonary/Aortic Ejection Time
P <sub>i</sub>	Inorganic phosphate
PKA/B/C/N	Protein Kinase A/B/C/N
PLAX	Parasternal Long Axis View
PP2A	Protein Phosphatase 2A
PP2A <sub>A</sub>	Protein Phosphatase 2A Structural Subunit
PP2A <sub>B</sub>	Protein Phosphatase 2A Regulatory Subunit
PP2A <sub>Cat</sub>	Protein Phosphatase 2A Catalytic Subunit
PSAX	Parasternal Short Axis View
PSR	Picrosirius Red
RAAS	Renin-Angiotensin-Aldosterone System
RAF	Rapidly Accelerated Fibrosarcoma
RNA	Ribonucleic Acid
ROSA26	Reverse Orientation Splice Acceptor 26
Ser/Thr	Serine/Threonine
SH2	Src Homology 2 Domain
SHR	Spontaneously Hypertensive Rat
SIKE	Suppressor of IKKepsilon
SLMAP	Sarcolemmal Membrane-Associated Protein
SM22 $\alpha$	Smooth Muscle Protein 22 $\alpha$
SOP	Standard Operating Procedure

SOS	Sons of Sevenless
STRIP2	Striatin-Interacting protein 2
STRIPAK	Striatin Interacting Phosphatase And Kinase
SG2NA	S/G2 Nuclear Autoantigen
TAC	Transverse Aortic Constriction
TGF	Transforming Growth Factor
TRAF3	Tumour Necrosis Factor Receptor-Associated Factor 3
TRAF3IP3	TRAF3 Interacting Protein 3
T-tubules	Transverse Tubules
Tyr	Tyrosine
VEGF	Vascular Endothelial Growth Factor
VEGFR	Vascular Endothelial Growth Factor Receptor
VTI	Velocity Time Interval
WD	Tryptophan-Aspartate-Repeat
XMLC2	Xenopus Laevis Myosin Light-Chain 2
YSK1	Yeast Stress-Activated Protein Kinase 1

## **Chapter 1 - Introduction**

## 1.1 Aims of the Research

The primary aim of the research presented in this thesis was the development of a robust, standardised and reproducible *in vivo* echocardiography protocol for non-invasive visualisation and assessment of the lateral (PSAX) and longitudinal (PLAX) axes of the heart in early-stage mouse models. The technique was to be applied across genetically altered models with global gene deletion (e.g. STRN, STRN3 or PKN2 deletion; see **Chapters 3** (Cull *et al.*, 2023) and **4** (Marshall *et al.*, 2022), respectively) or gene deletion or mutation in cardiomyocytes such as STRN (**Chapter 3**) (Cull *et al.*, 2023) or BRAF deletion (Alharbi *et al.*, 2022) or BRAF(V600E) mutation (Clerk *et al.*, 2022) using a tamoxifen-inducible system for genetic modulation. The technique was also to be applied in models of cardiac hypertrophy including hypertension induced by angiotensin II (AngII) and in the context of small molecule inhibitors of protein kinases that have been developed for cancer as with dabrafenib (**Chapter 5**) (Meijles, Cull, *et al.*, 2021) and other drugs targeting BRAF (Clerk *et al.*, 2022).

The methodology was initially developed to image the left ventricle in these mice, measuring key cardiac parameters, including ejection fraction, fractional shortening, and chamber dimensions, all of which are essential in gauging cardiac function. It was extended to using Döppler flow methodologies to assess blood flow in the pulmonary artery and aorta, and to capture images of the ascending aorta and aortic arch. This research was conducted with the intention that a well-constructed, standardised approach to mouse echocardiography could make a significant contribution to the scientific community. A particular feature of the studies is the focus on early time points of intervention (usually 3-7 days of treatment) when cardiac changes can be detected before symptoms of heart failure develop. This contrasts with most other studies in which the emphasis is on end-stage disease (Failer *et al.*, 2022; Gubra, 2021; Haggerty *et al.*, 2015; Li *et al.*, 2022).

## 1.2 Themes Between the Presented Studies

The primary focus of the research was initially to investigate the role(s) of STRN and STRN3 in the heart generally and in cardiomyocytes specifically. However, this rapidly expanded to incorporate other studies of BRAF and various BRAF inhibitors, ASK1 inhibitors and PKN2, leading to several publications as shown in **Appendix I** (Alharbi *et al.*, 2022; Clerk *et al.*, 2022; Cull *et al.*, 2023; Fuller *et al.*, 2021; Marshall *et al.*, 2022; Meijles, Cull, *et al.*, 2021; Meijles *et al.*, 2020; Meijles, Fuller, *et al.*, 2021). The papers selected as the focus for this thesis are those for which the echocardiography played a

substantial role and which demonstrate the robust nature of the methodology developed. The particular themes between them are highlighted below.

**(i) Effects of pathophysiological stress on the heart.** All three papers in **Chapters 3, 4 and 5**, investigate the role of specific genes or pathways in cardiac hypertrophy under basal conditions and in a context in which the heart was subjected to stress (infusion with AngII). In all cases, effects of heterozygote gene deletion or inhibition appeared to have a minimal effect at baseline, but they are required for the heart to adapt to stress. Therefore, it can be determined that the heart has limited use of these pathways until there is physiological stress.

**(ii) Consideration of embryonic lethality.** For STRN/STRN3 and PKN2 (**Chapters 3 and 4**, respectively), global homozygote gene deletion is embryonic lethal, while heterozygote offspring are successfully produced and appear phenotypically normal. The resilience suggests a compensatory mechanism such that haploinsufficiency does not affect development. Consistent with this, when assessed using echocardiography, all models demonstrated no significant difference in cardiac function or dimensions compared with wild-type littermates. When stressed with AngII, however, there were significant effects of gene haploinsufficiency.

**(iii) Development of models for conditional gene deletion.** Although information could be obtained for heterozygote global gene deletion of STRN, STRN3 and PKN2, since the heart contains cells other than just cardiomyocytes, it was not clear if these genes were significant in cardiomyocytes themselves. For PKN2, conditional models had been developed for constitutive cardiomyocyte-specific gene deletion to show that cardiomyocyte PKN2 was important in the heart. A model of STRN gene deletion in cardiomyocytes was also developed. This used an inducible system for conditional deletion on the administration of tamoxifen to overcome the problems with embryonic development.

**(iv) Combinations of drug treatments.** The study of dabrafenib (**Chapter 5**) (Meijles, Cull, *et al.*, 2021) demonstrates the use of small molecule inhibitors in combination with AngII. This provides a useful contrast to the studies using genetic alteration.

## **1.3 Experimental Design**

The specific experimental design for each study will be discussed in the relevant chapters. All of the studies presented in this thesis only used young (8-12 week) male mice. Female littermates or a combination of both genders were not appropriate for these experiments mainly because young female mice are resistant to AngII-induced hypertension due to their oestrogen levels (Milner *et al.*, 2008). Related studies of the role of BRAF in female mice in phenylephrine-induced cardiac hypertrophy indicate that females also have a reduced response in this model (Alharbi *et al.*, 2022). It is also a consideration that we used tamoxifen to induce genetic modification. Although this was a single injection, because we were studying early-stage disease development, there could be some additional effects due to interference with the hormonal status in female mice. While tamoxifen typically leaves the body within 2-3 days (Sohal *et al.*, 2001), how it behaves in females and with strain-specific responses may be different. This means there is a chance lingering effects from the drug could be present. Overall, although it is desirable and important to also study females, such studies need to be undertaken independently to account for the effect of fluctuating oestrogen levels, age and tamoxifen administration.

### **1.3.1 Experimental Controls for Genetic Modification**

**(i) Genetic modification.** Genetically-altered mice, may exhibit variations in their background genetics even with extensive in-breeding. These variations can introduce additional confounding variables and make it challenging to distinguish the specific effects of the genetic modification being studied. To avoid this (as in **Chapters 2 and 3**), when genetically-altered animal models were used with germline gene modification, wild-type littermates are needed as one of the controls. These share the same genetic background as the experimental group, therefore by comparing experimental data obtained from wild-type and genetically-altered animals, researchers can better isolate and attribute any observed effects specifically to the genetic modification. For mice with tamoxifen-inducible CRE (for cardiomyocyte-specific gene deletion), the genetic background is controlled for by treating mice with tamoxifen or vehicle. However, it was important to ensure that the CRE enzyme itself did not have toxic effects on the heart. To control for this, studies were conducted using heterozygous CRE mice generated from the same lines of mice being used to generate the model (**Figure 9**). Heterozygous CRE mice (rather than homozygous CRE mice) were used to minimise the effects of CRE on the heart (McLellan *et al.*, 2017).

**(ii) Delivery of AngII and small molecule inhibitors.** Osmotic minipumps were used to deliver AngII or small molecule inhibitors with the drugs dissolved in an appropriate

vehicle (Almoshari, 2022). Osmotic minipumps, while commonly used for controlled drug delivery, may introduce confounding factors such as mechanical stress, local tissue response, or direct effects on the mouse's physiology. To control for the vehicle and surgical procedure, along with any discomfort from the minipumps themselves, control animals were implanted with minipumps containing the vehicle only. By comparing the outcomes in the drug-treated group to those in the vehicle-treated group, any observed effects can be attributed to the drug itself rather than other factors associated with the delivery system or vehicle components. In the same sense, if any experimental outcomes are observed in each treatment group, the effect may be attributed to the vehicle alone, rather than an effect of the drug.

For **Chapter 5**, AngII was dissolved in an aqueous buffer system (acidified phosphate buffered saline (PBS)) whilst the small molecule inhibitors were only soluble in a DMSO/PEG mix (**Meijles, Cull, et al., 2021**). Consequently, it was necessary to deliver them with separate minipumps. In these cases, two mini-pumps were also given to the mice in the control group. By using multiple mini-pumps in both the control and treated groups, this maintains consistency across the groups and takes into account these confounding factors, minimising the potential impact of procedural variations on the study outcomes. This ensures that any observed effects are specifically attributed to the treatment being studied, rather than any unintended consequences of the mini-pump delivery system.

### 1.3.2 The 3 Rs

The three R's (Replacement, Reduction and Refinement) are essential principles to be followed when planning and conducting animal research (Flecknell, 2002; Hubrecht & Carter, 2019; MacArthur Clark, 2018; Prescott, 2017; Richmond, 2002). Each principle is aimed at minimising the use of animals, reducing their suffering if avoidable, and refining experimental procedures to ensure quality of life.

**(i) Replacement.** Replacement focuses on finding alternative methods that can completely replace the use of animals in scientific experiments (MacArthur Clark, 2018). This can include the use of *in vitro* models, *in silico* models, or other non-animal testing methods. In the studies presented in this thesis, complete replacement of animal models is not possible due to the biological complexity of hypertension and heart failure and the lack of suitable models to fully assess these complexities (Richmond, 2002).

**(ii) Reduction.** If animal models are required, reduction should be considered to minimise the number of animals used in the experiments, while still obtaining reliable results (MacArthur Clark, 2018; Richmond, 2002). For each study, power calculations were performed based on previous experiments to determine the expected number of animals necessary to obtain a representative cohort and obtain sufficient statistical significance. A pilot study was then conducted as a smaller-scale version of each study and as proof-of-concept. The pilot study aimed to evaluate the feasibility of the experimental design, identify potential issues or challenges, and confirm the sample size estimated by the power calculations (Muasya & Mulwa, 2023). The methodology and experimental conditions were optimised, and any adjustments to the experimental procedure were thought out and implemented before proceeding to larger-scale studies. The use of small groups of animals for the experimental stage of the study allowed for analysis of the datasets before the next experimental group was investigated. As each experimental group were completed and analysed, the data were combined together to produce the cohort for the entire study. If a greater response was obtained than originally predicted and statistically significant changes detected with fewer animals, the study was halted. This allowed us to obtain statistically significant results while using fewer animals. This was the case for one particular group of animals treated with SB590885 (a BRAF “inhibitor”) compared with SB590885 plus trametinib (a MEK inhibitor) (Clerk *et al.*, 2022).

**(iii) Refinement.** In the context of animal research, refinement involves reducing any pain, suffering, or distress experienced by the animals during the experiments while enhancing animal welfare during and outside of the experiments (MacArthur Clark, 2018; Richmond, 2002). Increasing animal welfare can be as simple as adapting the housing conditions to improve interactivity or adopting tube-handling procedures to reduce the amount of stress the animal experiences when interacting with humans (Wells *et al.*, 2006). To refine our procedures, I developed an SOP for sterile surgery for minipump implantation and for echocardiography. In addition, I developed a comprehensive scoring system to assess and monitor various aspects of the animal's welfare. The scoring system encompasses the following factors.

- **Appearance:** Assess the general appearance of the animals, including coat condition, grooming, and body posture. Note any signs of abnormal appearance, such as piloerection, hunched posture, or abnormal skin coloration, which may indicate potential health issues or distress.

- **Food and water intake:** Monitor the animals' consumption of food and water. Decreased or increased intake can be indicative of health problems or changes in the animals' well-being.
- **Temperature:** Observe any significant temperature change, both increase or decrease, during experimental procedures.
- **Provoked behaviour:** Assess the animals' response to external stimuli or handling. Observe if they display usual motility with and without stimulation.
- **Natural behaviour:** Monitor the animals' engagement in their natural behaviours, such as exploration, social interaction, or grooming. A decrease or absence of these behaviours may indicate a decrease in overall well-being or the presence of external environmental stressors.
- **Wounds:** Inspect any surgical wounds, suture integrity, or other wounds that may have occurred during the experimental timeframe. Monitor for signs of infection, inflammation, or poor healing. Proper wound management is crucial to prevent pain, infection, or other complications.
- **Ejection fraction:** Assess the animals' cardiac function. Abnormalities in ejection fraction may indicate cardiac dysfunction or compromised cardiovascular health.
- **Respiration:** Monitor the animals' respiratory rate and pattern. Rapid or laboured breathing can be indicative of respiratory distress or cardiovascular issues (side effects of procedures or potential infection).

Each parameter is assigned a numerical score and graded using a standardised scoring system. This system is summarised in **Table 1**. Assessments were conducted during each procedure, as well as the days before and after surgery. Any abnormal scores or significant changes triggered appropriate interventions, such as veterinary consultation, analgesics, adjustments to the experimental procedures or full termination of the experiment, to ensure the welfare of the animals.

**Table 1: Animal Monitoring Scoring System**

Factor	Score	Criteria
Appearance	0	Normal
	1	General lack of grooming
	2	Coat staring, ocular and nasal discharge
	3	Piloerection, grimace and hunched
Food and water intake	0	No weight lost
	1	Weight loss: <5% decrease in body weight
	2	Decreased intake: 5-15% decrease in body weight
	3	No food or water intake: >15% decrease in body weight
Natural behaviour	0	Normal
	1	Minor changes
	2	Less mobile and alert, isolated from group
	3	Vocalisation, self-mutilation, restless or still
Provoked behaviour	0	Normal
	1	Subdued, but normal when stimulated
	2	Subdued even when stimulated
	3	Limited response to stimulation
Wounds (Surgical, Sutures etc)	0	Normal, healing well
	1	Inflamed, slow healing
	2	Open wound
	3	Infected wound
Temperature	0	No change
	1	Minor changes
	2	T +/- 5°C
	3	T +/- 10°C
Ejection fraction	0	≥ 40-50%
	2	< 40%
	3	< 30%
Respiration	0	Normal
	1	Intermittent/abnormal
	2	Intermittent/laboured
	3	Persistently laboured
Score adjustment	1	Extra point awarded for each score of 3
	Total Score	Judgement (Adjusted according to protocol)
	0 - ≤4	Normal
	5 - ≤9	Monitor carefully, consider analgesics or other treatment
	10 - ≤14	Suffering, provide relief, observe regularly, seek NACWO/NVS advice. Consider termination.

Table legend: Each factor has a score of 0 to 3, with 0 being “normal” and 3 being the most severe. The total score is the sum of the scores for all factors. The judgement is based on the total score and is adjusted according to the protocol.

Another way to refine the experiments is by conducting and assessing sequential echocardiograms. This is particularly important for the first pilot studies for any gene-modification or drug treatment. For this, baseline echocardiograms were collected (prior to treatment) followed by echocardiograms at 3 and 7 days post-treatment (or at intervals thereafter if experiments were for longer duration; see Chapters **4** and **5**). Assessment at multiple time points post-treatment enables a comprehensive assessment of changes in the animals' cardiac function and structure over time. The baseline measurements provided the starting point for comparison, while subsequent echocardiograms allowed changes in the development and progression of any cardiac responses to the experimental interventions to be tracked, whether that be genotype or drug treatments. Sequential echocardiograms also enable early detection of any adverse effects of the experiment on normal physiological functioning. This allows for timely interventions and adjustments to minimise any potential harm or distress experienced by the animals.

## 1.4 Summary of Results Chapters

### 1.4.1 Chapter 3: Striatin, but not striatin 3, plays a major role in angiotensin II-induced cardiomyocyte and cardiac hypertrophy in mice *in vivo*.

**Authors:** Cull JJ, Cooper STE, Alharbi HO, Chothani SP, Rackham OJL, Dash PR, Risto Kerkelä, Ruparelia N, Sugden PH, Clerk A.

My primary focus for developing the mouse echocardiography in-house at University of Reading was striatin (STRN) and striatin 3 (STRN3) and their impact on cardiac adaptation to increased AngII. Additional details of striatin biology are provided in **Chapter 2**. The hypothesis was that decreased expression of STRN or STRN3 would disrupt adaptation to hypertension by interfering with signalling cascades involved in cardiac remodelling and cell death (**Cull et al., 2023**).

**Contribution:** I had full responsibility for and execution of the breeding strategies for the experiments with the mice with global heterozygous STRN and STRN3 gene deletion. I also developed the lines for cardiomyocyte-specific STRN homozygous gene deletion. This included animal husbandry and ear-notching at the University of Reading (global gene deletion studies) and genotyping for line development at St. George's University of London (cardiomyocyte-specific STRN gene deletion). I developed the SOPs for echocardiography and for surgery for minipump implantation. I was also responsible for training of assistants for surgery and echocardiography in both institutions, in addition to taking the lead tissue harvesting, tissue processing (histology, DNA, RNA and protein extraction), and data analysis for the aforementioned. Because of the large amount of data, not all of it could be presented within the paper and additional imaging and analysis were performed that were not included (e.g. pulmonary flow data). All images and samples obtained during the project remain available for further analysis.

**Project aims:** The three aims were

- **Aim 1:** To investigate the effect of global heterozygous STRN deletion on AngII-induced cardiac remodelling in mice.
- **Aim 2:** To investigate the effect of global heterozygous STRN3 deletion on AngII-induced cardiac remodelling in mice.
- **Aim 3:** To investigate the effect of cardiomyocyte-specific STRN deletion on AngII-induced cardiac remodelling in mice.

These aims were addressed through the generation of mouse models with either a global knockdown or cardiomyocyte-specific knockout of STRN or STRN3. Tamoxifen was used for inducible gene deletion of the cardiomyocyte knockouts using the CRE/LoxP system to prevent embryonic lethality seen in global homozygote STRN/STRN3 mouse models (Cull *et al.*, 2023; Sohal *et al.*, 2001). Analysis of the echocardiograms, histology, RNA, DNA and protein expression were used to assess the effect of the genes on AngII induced cardiac remodelling.

## Outcomes of the Study

**(i) Methodology.** I developed and implemented a comprehensive SOP for *in vivo* mouse echocardiography and osmotic minipump implantation surgeries. The success of the study can be measured by the SOPs developed being transferred to and adopted by collaborators at the University of Reading (ASK1 and BRAF associated projects), Francis Crick Institute (PKN2 studies) and St. George's University London (BRAF gene deletion and PKN2 studies). For each institution, I had to gain approval on the procedures from home office liaison contact (HOLC). I was responsible for the training and sign-off of post-doctoral researchers and other PhD students at each of these institutions. Criteria included competency to independently perform the procedures to the standards of the named animal care and welfare officer (NACWO) and named training and competency officer (NTCO).

During my PhD, I successfully trained and signed off the following for both procedures:

- Dr Hajed Alharbi
- Dr Susanna Cooper
- Dr Daniel Meijles
- Dr Feroz Ahmad
- Dr Tayab Afzal
- Dr Viridiana Alonso

**(ii) Understanding of the role(s) of STRN and STRN3 in AngII-induced cardiac hypertrophy.** The study determined that the heterozygous knockout of STRN, but not STRN3, reduces cardiac hypertrophy induced by AngII in mice. This suggests that STRN plays a more important global role than STRN3 in the development of cardiac hypertrophy in this context. Cardiomyocyte-specific deletion of striatin was also shown to inhibit AngII-induced cardiac hypertrophy and fibrosis, suggesting that striatin significantly influences

the development of hypertension-induced cardiac hypertrophy acting within the contractile cardiomyocytes.

#### **1.4.2 Chapter 4: PKN2 deficiency leads both to prenatal ‘congenital’ cardiomyopathy and defective angiotensin II stress responses.**

**Authors:** Marshall JJT, Cull JJ, Alharbi HO, Zaw Thin M, Cooper STE, Barrington C, Vanyai H, Snoeks T, Siow B, Suárez-Bonnet A, Herbert E, Stuckey DJ, Cameron AJM, Prin F, Cook AC, Priestnall SL, Chotani S, Rackham OJL, Meijles DN, Mohun T, Clerk A, Parker PJ).

The main objective for this study overall was to investigate the role of PKN2 in cardiomyocytes during embryogenesis and in the development adult heart diseases, with my focus being on the adult. Additional information on PKN2 is in **Chapter 2**. The hypothesis for this aspect of the work was that decreased expression of PKN2 interferes with signalling cascades involved in cardiac remodelling and cell death, disrupting the stress response of the heart to hypertension (Marshall *et al.*, 2022).

#### **Outcomes of the Study**

*(i) Transfer of protocols to other institutions.* As discussed in relation to **Chapter 3**, I developed and implemented a comprehensive SOP for *in vivo* mouse echocardiography and minipump surgery. The success of the study can be measured by the SOPs developed being transferred to and adopted by collaborators at St. George’s University London and the Francis Crick Institute.

*(ii) Understanding of the role(s) of PKN2 in AngII-induced cardiac hypertrophy.* The study discovered that heterozygote PKN2 gene deletion compromises cardiac adaptation to hypertension in adult mouse hearts. It also affects cardiac function in aged mice.

#### **1.4.3 Chapter 5: The anti-cancer drug dabrafenib is not cardiotoxic and inhibits cardiac remodelling and fibrosis in a murine model of hypertension.**

**Authors:** Meijles DN, Cull JJ, Cooper STE, Markou T, Hardyman MA, Fuller SJ, Alharbi HO, Haines ZHR, Alcantara-Alonso V, Glennon PE, Sheppard MN, Sugden PH, Clerk A.

This study investigated the effect of dabrafenib, a Type 1.5 BRAF inhibitor, and its potential effects on cardiac hypertrophy in AngII-induced hypertension. BRAF is the protein kinase that initiates activation of the extracellular signal-regulated kinase 1/2 (ERK1/2) cascade. This pathway plays a crucial role in cell cycle regulation and is involved in cardiomyocyte hypertrophy and cell death in the heart. Dabrafenib is used clinically to inhibit the ERK1/2 signalling in forms of cancer that result from BRAF(V600E) mutations (primarily melanoma). Additional information on BRAF and ERK1/2 signalling is in **Chapter 2**. The hypothesis was that dabrafenib inhibition of the ERK1/2 cascade would inhibit cardiac hypertrophy and changes in cardiac function from AngII treatment, but that this could be detrimental (Meijles, Cull, *et al.*, 2021).

**Contribution:** I played a major role in conducting the *in vivo* studies for this project. This involved the purchase of the mice (C57Bl/6J) and subsequent monitoring, surgical implants of minipumps, echocardiography and tissue harvest. My contributions extended to training of Dr. Daniel Meijles to assist with these studies. I was also involved with data analysis, review and editing of the publication. As for the study of STRN/STRN3 and PKN2, because of the large amount of data, not all of it could be presented within the paper and additional imaging and analysis were performed that were not included (e.g. pulmonary flow data). All images and samples obtained during the project remain available for further analysis.

**Project aims:** The project had two aims.

- Aim 1. To determine the effects of dabrafenib on heart failure resulting from AngII-induced hypertension.
- Aim 2: To determine if dabrafenib has cardiotoxic effects.

These aims were addressed using wild-type C57Bl/6J mice treated with vehicle, dabrafenib or AngII only, or AngII with dabrafenib. Cardiac function/dimensions were measured using echocardiography. Analysis of the echocardiograms, histology, RNA, DNA and protein expression were used to assess the effect of dabrafenib inhibition on AngII-induced cardiac remodelling.

## **Outcomes of the Study**

**(i) Treatment and analysis.** The study was conducted over a duration of either 7 or 28 days with the administration of AngII to assess the effects in both acute and chronic settings. This was the first study in our research group to extend the duration of AngII

treatment for 28 days which required more careful monitoring since (as expected) the initial cardiac hypertrophy progressed towards a heart failure phenotype. It was also the first study in which speckle-tracking and strain analysis was used to gain a more refined and detailed characterisation of cardiac function and dynamics (see **Chapter 2**). This methodology requires high quality brightness-mode (B-mode) images of the left ventricle that had not been possible before the detailed SOP developed for the STRN/STRN study.

**(ii) Effects of dabrafenib on AngII-induced cardiac hypertrophy.** The study demonstrated that dabrafenib itself is not cardiotoxic over the duration of the experiment. Surprisingly, dabrafenib mitigated both the acute and chronic effects of AngII on the heart having a particularly notable effect in reducing cardiac fibrosis.

## **Chapter 2 - Background**

## 2.1 Hypertension and Heart Failure

The cardiovascular system is of vital importance to every cell in the body, delivering oxygen and nutrients while removing waste. At the centre of this system lies the heart. The heart is a resilient structure, physically adapting to physiological demands (e.g. exercise) to maintain optimal blood flow and tissue perfusion. However, its resiliency is tested when faced with pathophysiological stressors such as hypertension. The protective mechanisms of the heart can gradually falter over time, resulting in heart failure. Heart failure is characterised by the impaired ability of the heart to effectively pump blood throughout the body, often resulting from damage to the heart muscle (e.g. following myocardial infarction (Savarese *et al.*, 2023). Hypertension and heart failure are closely linked (Georgiopoulou *et al.*, 2012). Sustained hypertension can damage the heart muscle, making efficient blood flow and perfusion increasingly difficult, putting more strain on the heart, eventually causing the heart to fail.

In the United Kingdom, it is estimated that heart failure cases exceed 900,000 individuals, with 200,000 new cases reported each year (Conrad *et al.*, 2018). It is of significant concern that despite 40% of patients exhibiting symptoms that should trigger early assessment, almost 80% of heart failure diagnoses in England occur during hospital admissions (Bottle *et al.*, 2018). These figures shed light on the significant impact of heart failure within the UK. However, it is important to recognise that hypertension and heart failure are global health challenges: hypertension affects approximately 1.28 billion adults worldwide (Nadar & Lip, 2021; World Health Organization, 2023) and heart failure affects around 64 million people (Savarese *et al.*, 2023). Hypertension is the most common and preventable risk factor for cardiovascular disease, contributing to one in five deaths globally and affecting around 30% of adults. Approximately two-thirds of people with hypertension are either unaware of the condition, have not received treatment, or their treatment is not effective at controlling blood pressure (Parati *et al.*, 2022). Managing both hypertension and heart failure poses a substantial challenge due to the diverse array of causes and underlying factors (Mills *et al.*, 2020; Savarese *et al.*, 2023). There is an urgent need for further expansion of scientific discovery, therapeutic options and a personalised medicinal approach. Achieving these goals will require further research into the underlying mechanisms and improvements in preclinical models of heart failure.

### 2.1.1 Types of Heart Failure

Heart failure has been most commonly characterised as a reduction in contractile ability (systolic function) associated with a reduction in ejection fraction (HFrEF) (Murphy *et al.*,

2020; Simmonds *et al.*, 2020). However, it is also recognised that heart failure also occurs with preserved ejection fraction (HFpEF) (Miranda-Silva *et al.*, 2021; Shimizu & Minamino, 2016). Despite both resulting in the reduced ability to pump blood to the body, they have different causes and presentations. HFpEF generally occurs when the left ventricular (LV) muscle loses the ability to relax fully, becoming stiff. As a result, the heart cannot fill properly between each contraction. HFpEF is characterised clinically by an ejection fraction  $\geq 50\%$  (Redfield & Borlaug, 2023). HFrEF, on the other hand, occurs when the left ventricle demonstrates decreased efficiency of myocardial contraction. As a result, the heart cannot pump with sufficient force to push enough blood into circulation. This is displayed clinically by an ejection fraction  $\leq 40\%$  (Murphy *et al.*, 2020; Simmonds *et al.*, 2020). HFrEF may also have impaired relaxation, although reduced contractility is the primary concern. HFpEF is more commonly caused by conditions such as hypertension, which can progress to ventricular stiffening and impaired relaxation (Miranda-Silva *et al.*, 2021; Redfield & Borlaug, 2023). HFrEF, on the other hand, is often a consequence of damage to the heart muscle as occurs with myocardial infarctions or cardiomyopathies (Banerjee, 2017). This leads to reduced contractile function of the heart.

The type of heart failure with which an individual presents is potentially influenced by factors such as age and gender. HFpEF is more common in older adults and women, while HFrEF is more common in middle-aged adults and men. It is also worth considering that heart failure with mid-range ejection fraction (HFmrEF) also occurs (Redfield & Borlaug, 2023). Characterised by ejection fraction between 40-50%, HFmrEF is intermediate between HFrEF and HFpEF. It shares characteristics of HFrEF, such as association with coronary artery disease (Simmonds *et al.*, 2020).

### **2.1.2 Risk Factors for Hypertension and Heart Failure**

Hypertension is the leading cause of heart failure (Maeda *et al.*, 2023). Hypertension and heart failure are both complex multifactorial conditions but share common risk factors that contribute to their development. Age is one of the most significant risk factors. As individuals get older, the likelihood of developing high blood pressure increases, which, in turn, predisposes them to heart failure (Masenga & Kirabo, 2023). Over a lifetime, men have a higher risk compared to women for cardiovascular diseases, although the risk for women increases after menopause

(Lawson *et al.*, 2020; Maas *et al.*, 2021). Ethnicity plays a role in the occurrence of cardiovascular diseases. For example, black ethnicities have elevated rates of heart failure compared to white ethnicities (Georgiopoulou *et al.*, 2012; Lawson *et al.*, 2020). This is likely due to the higher prevalence of conditions like hypertension and diabetes in these groups (Lawson *et al.*, 2020).

Family history is another important risk factor, and having a first-degree relative with hypertension or heart failure can elevate the patient's risk by up to 70% when compared to individuals without a familial history (Watson, 2023). Various medical conditions also lead to both hypertension and, eventually, heart failure by damaging the heart muscle. Examples include coronary artery disease, diabetes and chronic kidney disease (Anthamatten, 2023; Damman *et al.*, 2013; Lawson *et al.*, 2020; Parker & Wigger, 2023; Vidal-Petiot *et al.*, 2018). Related to all of these conditions, are lifestyle factors such as smoking, excessive alcohol use, obesity, poor diet, and immobility (Masenga & Kirabo, 2023). These factors all contribute to disease progression by promoting various cardiovascular diseases, such as atherosclerosis and blood clots (Lawson *et al.*, 2020).

## 2.2 Cardiac Anatomy and Physiology

### 2.2.1 Gross Anatomy

Anatomically, a healthy adult heart consists of four chambers: the left atrium (LA), right atrium (RA), left ventricle (LV), and right ventricle (RV) (**Figure 1**). The atria are separated by the interatrial septum whilst the ventricles are separated by the interventricular septum (IVS) (Boron & Boulpaep, 2012; Whitaker, 2018). Blood flow between the atria, ventricles and connecting vessels is regulated by valves. The tricuspid valve lies between the right atrium and right ventricle, the pulmonary valve is between the right ventricle and pulmonary artery, the mitral or bicuspid valve is between the left atrium and left ventricle, and the aortic valve is between the left ventricle and aorta (Mori *et al.*, 2019). The septa and valves ensure that blood flows through the heart in coordination with the cardiac cycle as follows. The superior and inferior vena cava brings deoxygenated blood from the body into the right atrium during diastole. From there, the blood enters the right ventricle and is expelled through the pulmonary artery to the lungs (pulmonary circulatory system) during systole. Oxygenated blood returns to the heart via the pulmonary veins, entering the left atrium during diastole. The left ventricular wall propels the oxygenated blood into the aorta during systole, distributing it to the rest of the body (Boron & Boulpaep, 2012; Pollock &

Makaryus, 2024). It is worth noting that, the left ventricular wall is larger than the right ventricular wall due to its requirement to circulate blood at increased pressure around the systemic circulatory system (Whitaker, 2018).

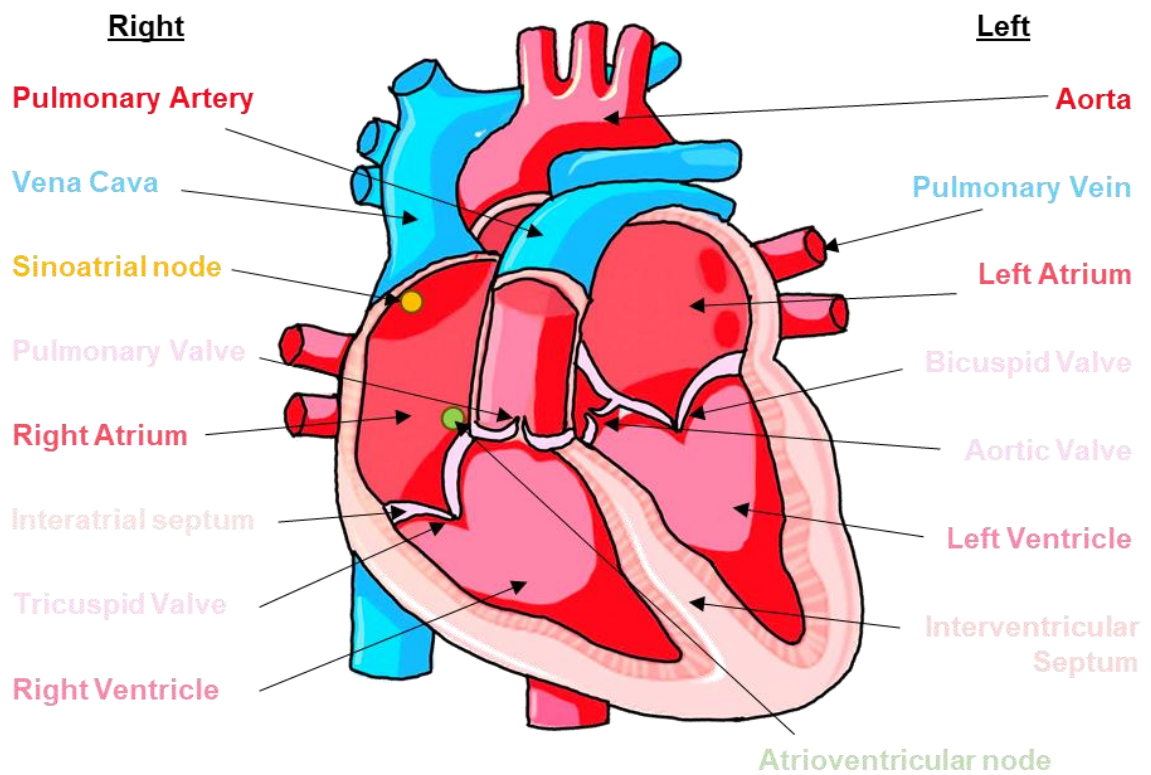


**Figure 1: The Basic Structure of the Heart.**

The diagram shows the relative positions of the major heart structures. Adapted from (Boron & Boulpaep, 2012).

The muscular wall of the heart is composed of three distinct layers: the epicardium (outer layer), myocardium (middle muscular layer), and endocardium (inner lining) (**Figure 2**) (Lin *et al.*, 2012; Ovalle & Nahirney, 2013). The endocardium and epicardium are composed of endothelial cells lining the inside and outside of the heart, respectively. The endocardium protects the valves and heart chambers from damage by providing a barrier to protect subsequent layers. The epicardium has the same protective function on the heart's surface. Sandwiched between these layers lies the myocardium, a thick layer primarily composed of cardiomyocytes (cardiac muscle cells). Cardiomyocytes are specialised muscle cells that produce coordinated contractions necessary to generate the pressure required for systemic blood circulation (Boron & Boulpaep, 2012).

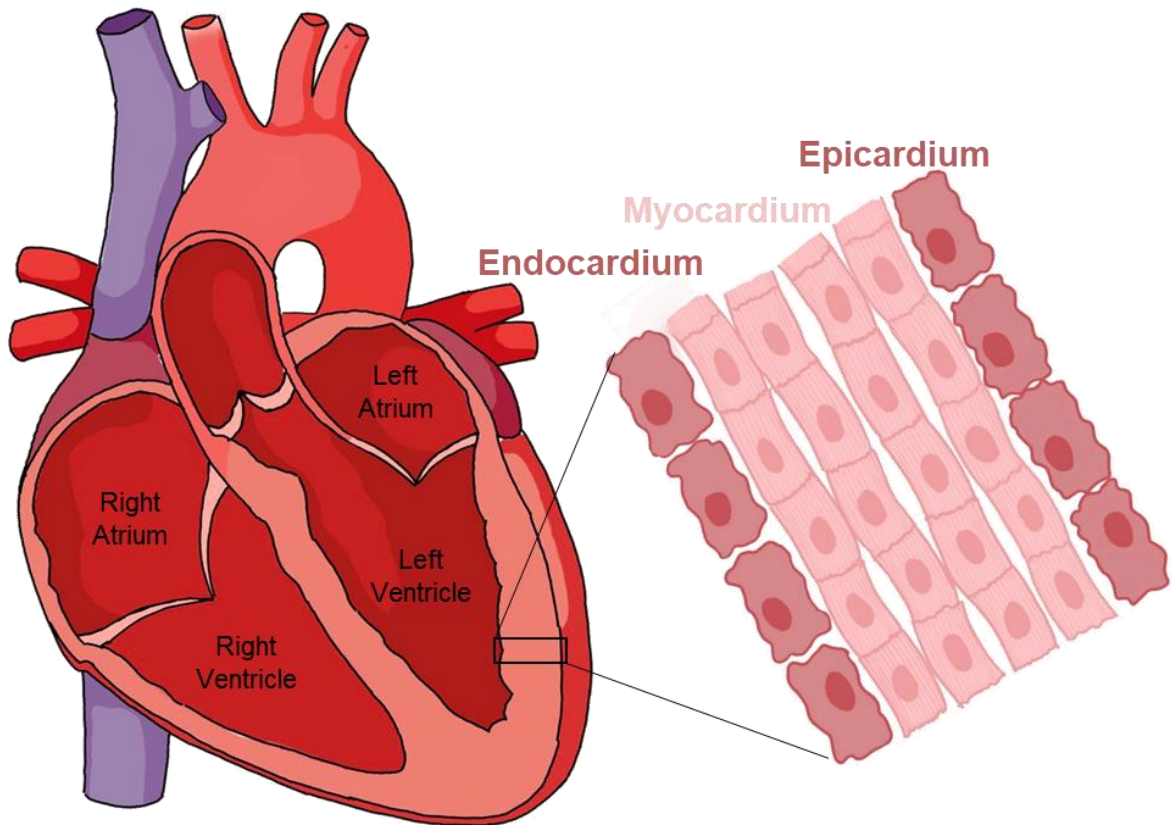


**Figure 2: The Structure of the Walls of the Heart.**

The endocardium is situated within the heart's internal structure with the epicardium on its external surface. The myocardium is situated between these two structures. Adapted from (Lin *et al.*, 2012; Tanti *et al.*, 2023).

## 2.2.2 The Cardiac Cycle and Electrical Conduction System

The cardiac cycle is a series of sequential events that occurs during one complete heartbeat. The electrical conduction system of the heart is essential for coordination of these events, ensuring the synchronised contraction of the chambers of the heart, allowing efficient circulation of blood. The system consists of specialised cells that can generate and transmit electrical impulses, orchestrating the rhythmic beating of the heart. The origins of the cardiac cycle begin with the generation of an electrical impulse by the sinoatrial node. The sinoatrial node is a small cluster of cells located in the right atrium near the superior vena cava (**Figure 1**) (Boron & Boulpaep, 2012; Chambers & Matthews, 2019). The sinoatrial node serves as the natural pacemaker of the heart, initiating the cardiac cycle and consequently, each heartbeat. The sinoatrial node produces the electrical signal, which spreads across the atria, depolarising the tissue, and stimulating the contraction of the atrial cardiomyocytes. This is known as atrial systole.

Cardiomyocyte contraction propels the blood from the atria into the ventricles. This depolarisation of the atria is represented by the P wave on the ECG (**Figure 3**) (Barros, 2019). Signal transduction continues until the electrical impulse reaches the interatrial septum (the junction between the atria and ventricles). The interatrial septum prevents the electrical impulse from continuing into the ventricle (Boron & Boulpaep, 2012).

The electrical signal is transferred into the atrioventricular node, residing within the Koch triangle near the base of the IVS (**Figure 1**). The atrioventricular node briefly delays the electrical signal. This pause allows the atria to contract fully, ensuring optimal blood flow into the ventricles before ventricular contraction begins. This delay is represented by the PR interval on the ECG (Barros, 2019). From the atrioventricular node, the electrical impulse travels down a pathway of cells called the bundle of His, which then branches into the right and left bundle branches (Boron & Boulpaep, 2012). These branches extend along the interventricular septum, delivering the electrical signal to the Purkinje fibres. The depolarisation of the interventricular septum is represented on an ECG by the Q wave (**Figure 3**) (Barros, 2019). The Purkinje fibres are specialised conducting fibres that distribute the electrical impulses rapidly and uniformly throughout the ventricles (Boyden *et al.*, 2010). This coordinated transmission causes simultaneous depolarisation of ventricular myocytes. Consequently, depolarisation causes contraction of the ventricles, expelling blood from the heart into circulation. This is known as ventricular systole. The synchronised contraction maximises the force generated by cardiomyocyte contraction, generating the high pressures required to circulate the blood systemically. The

depolarisation of the left ventricle is represented on an ECG by the RS wave (Barros, 2019; Boron & Boulpaep, 2012).

After ventricular contraction, the ventricles enter a phase of relaxation known as ventricular diastole. This relaxation period is represented by the ST segment on the ECG, which occurs between the end of the QRS complex and the beginning of the T wave (**Figure 3**). During this time, the ventricles repolarise, preparing for the next cycle. Repolarisation of the ventricles is represented by the T wave on the ECG (Barros, 2019). It represents the recovery phase of the ventricular muscle as the electrical activity returns to the baseline (Boron & Boulpaep, 2012). The ventricles relax further during this phase, allowing for the filling of blood from the atria in preparation for the next cardiac cycle.

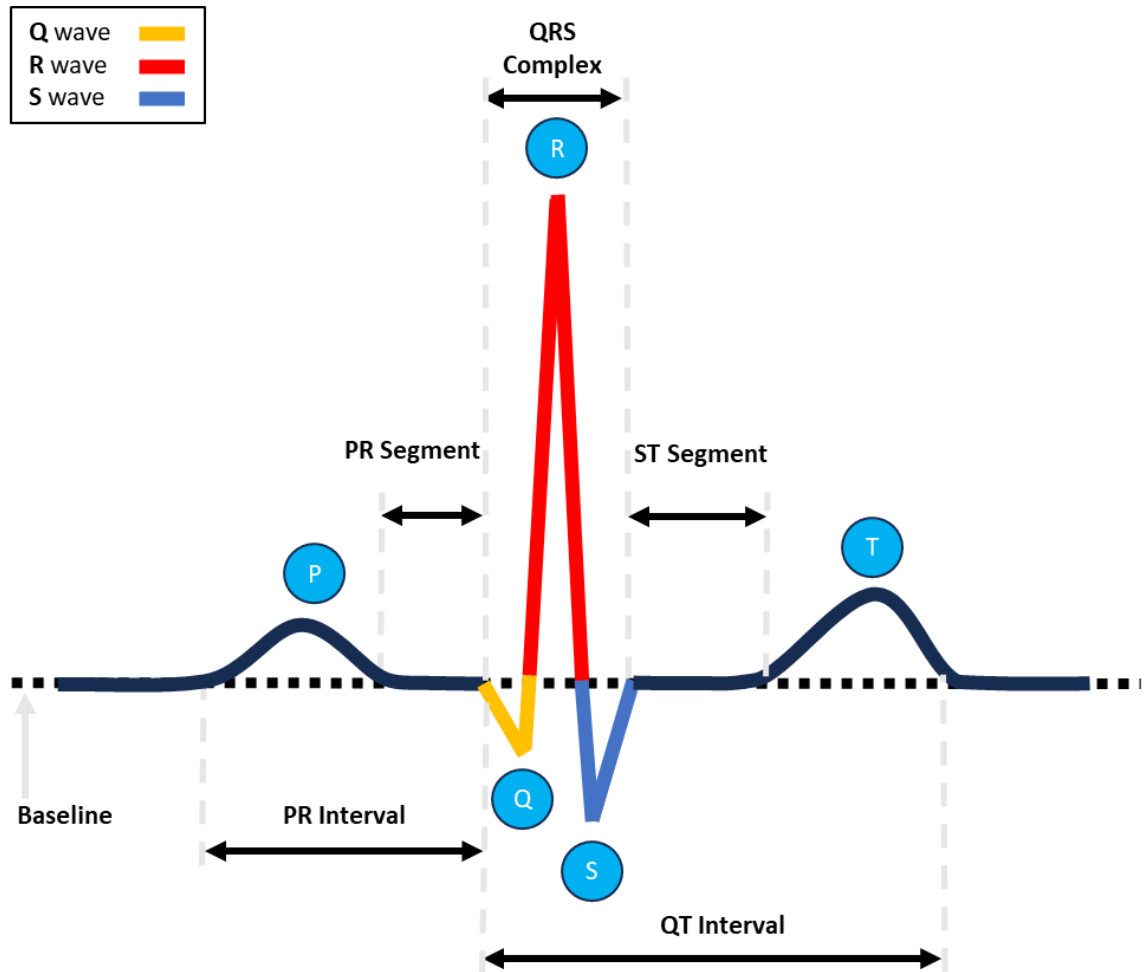


**Figure 3: A Representation of an Electrocardiogram (ECG) Trace.**

The ECG is a recording of the electrical activity of the heart. Each wave on the ECG corresponds to a different part of the cardiac cycle. PR interval: the time taken for the electrical impulse to travel from the sinoatrial node (the heart's pacemaker) to the ventricles. QRS complex: the time for the ventricles to depolarise and contract. QT interval: the time for the ventricles to repolarise and relax. PR segment: the time between the end of the P wave and the beginning of the QRS complex. ST segment: the time between the end of the QRS complex and the beginning of the T wave. T wave: the time at which the ventricles to repolarise. Adapted from (Barros, 2019).

### 2.2.3 Cellular Content of the Heart

The normal structure of heart wall (myocardium) contains three main cell types: cardiomyocytes, fibroblasts and endothelial cells (Pinto *et al.*, 2016).

#### Cardiomyocytes

Cardiomyocytes are the contractile cells of the heart, comprising of approximately 70% of the heart's cardiac cellular volume while (because they are large cells) only accounting for approximately 30% of cardiac cells (Zhou & Pu, 2016). Cardiomyocytes are striated cells that, in mammals, are usually mononucleated or binucleated and they have an optimised ultrastructure for continuous contraction. The cytoplasm of cardiomyocytes (the sarcoplasm) houses densely packed myofibrils, the contractile units of the cell. These myofibrils are comprised of thick myosin filaments and thin actin filaments, arranged in a highly organised sarcomeric pattern with Z-discs anchoring the thin filaments. Surrounding the cell is the sarcolemma, the plasma membrane, which dips inwards at regular intervals forming T-tubules. These T-tubules stretch deep into the cell, ensuring a rapid and even distribution of electrical signals throughout the cardiomyocyte (Kartha, 2021).

Cardiomyocytes interconnect at intercalated discs to form myocardial fibres. The intercalated discs are specialised junctions that facilitate the transmission of ions, enabling simultaneous initiation or termination of muscle contractions (Kartha, 2021). Myocardial fibres are arranged in a spiral pattern, allowing for a twisting motion during contraction. This motion allows cardiomyocytes to generate the strong, involuntary and coordinated contractions necessary for efficient blood circulation. Compared with skeletal muscle fibres, cardiomyocytes are shorter in length and contain an increased number of calcium ion channels, enabling enhanced calcium ion exchange, contributing to their exceptional contractile capabilities. They are also highly resistant to fatigue. This endurance stems from large numbers of mitochondria and a high myoglobin content. Together, these adaptations ensure a constant supply of energy for cellular respiration and, in turn, continuous muscle contraction (Saxton *et al.*, 2023).

Cardiomyocytes are terminally-differentiated cells, lacking the ability to regenerate (Ahuja *et al.*, 2007). Therefore, once damaged, they cannot be replaced. In response to damage, the surviving cardiomyocytes undergo a compensatory process known as hypertrophy, where individual cells increase in size to compensate for the loss of contractile cells. This hypertrophic response aims to sustain cardiac function. However, over time, this compensatory mechanism may fail, leading to decompensation. Decompensation is

characterised by an enlargement of the heart's internal diameter and the development of fibrosis within the ventricular walls. These structural changes result in decreased pumping power, ultimately leading to heart failure (Mangini *et al.*, 2013).

### **Endothelial cells**

The heart is a highly vascularised organ. The coronary arteries provide blood to the heart via arterioles and the heart is perfused with a dense network of capillaries that allows for efficient gaseous and waste exchange. Capillaries are composed of a thin layer of endothelial cells and a basal lamina, which together form a diffusion barrier that separates the blood from the surrounding tissue. Endothelial cells are not terminally-differentiated, unlike cardiomyocytes. This means that they can grow and proliferate when required to produce new capillary networks (angiogenesis) or to repair any damage to blood vessel (Muñoz-Chápuli *et al.*, 2004; Oka *et al.*, 2014). For example, endothelial cells produce vascular endothelial growth factor (VEGF), which is a potent stimulator of angiogenesis. VEGF is produced in response to a number of stimuli, including tissue hypoxia, inflammation, and injury (Shibuya, 2011). The number and arrangement of endothelial cells can also change depending on the environmental conditions. This plasticity is essential for tissue repair, angiogenesis, growth, and development (Tombor & Dimmeler, 2022). When endothelial cells are permanently damaged, they lose the ability to proliferate. This can lead to areas of the heart without capillary networks, which become hypoxic (low in oxygen). As the tissue cannot exchange the materials it needs to function, cells may die through stress-induced programmed cell death (apoptosis) (Alberts *et al.*, 2002).

### **Fibroblasts**

Fibroblasts are non-excitable, mesenchymal cells that surround structures of the heart and are responsible for forming and maintaining the connective tissue (Plikus *et al.*, 2021). This tissue acts as a scaffold for the cardiomyocytes and provides structure to the heart. Fibroblasts achieve this by producing type 1 collagen and other extracellular matrix (ECM) components, such as fibronectin (Kendall & Feghali-Bostwick, 2014). This creates an intricate network of protein fibres that provide strength and structure to the heart, stabilising the myocardial wall and aiding force transmission (Gourdie *et al.*, 2016).

When the heart experiences injury, fibroblasts become activated and ramp up production of collagen and other ECM components. Fibrosis occurs when fibroblasts produce excessive ECM in response to damage (Kendall & Feghali-Bostwick, 2014). Although the

aim of the fibroblasts is to heal the damaged tissue, fibrosis results in the thickening of the affected area, forming scar tissue. Overtime, scaring stiffens the heart, hindering its ability to contract and relax effectively, contributing to heart failure.

In hypertensive hearts, excess collagen and ECM is produced, causing an increased stiffness of the myocardial wall and structural remodelling of the myocardium (Alberts *et al.*, 2002; Jiang *et al.*, 2021). This can increase ventricular wall thickness, but not overall heart size, causing decreased ventricular volume. As the scar tissue is unable to contract effectively, normal diastolic and systolic function is prevented. This is because the heart is unable to stretch to maximum capacity in response to changing blood volumes. As a result, the heart must work harder to circulate the same blood volume as a healthy heart, as a significant pumping force cannot be generated (Nakamura & Sadoshima, 2018; Ruwhof & van der Laarse, 2000). Dysregulation of cardiac fibroblasts in disease can cause excessive collagen deposition, resulting in fibrosis. Fibrosis is one contributor to the development of heart failure (Moore-Morris *et al.*, 2015) (Rog-Zielinska *et al.*, 2016).

### **Other cardiac cells**

Although cardiomyocytes, endothelial cells and fibroblasts are the key cells of the heart, there are minor cell types including smooth muscle cells (e.g. in arterioles) and some resident immune cells (Zhou & Pu, 2016). The proportion of immune cells in particular changes in pathophysiology. There has also been debate about the presence of resident stem cells known as cardiac stem cells (Zhang *et al.*, 2015).

## **2.2.4 Cardiac Contractile Apparatus**

### **Specialised Components**

Cardiomyocytes are composed of muscle fibres (myofibers) constructed from cylindrical bundles of proteins called myofibrils, the sarcolemma (plasma membrane) and the sarcoplasm (cytoplasm). Intercalated discs are specialised junctions connecting adjacent cardiomyocytes. Intercalated discs provide mechanical stability and ensure coordinated contraction of the collective heart muscle. Myofibrils are further divided into repeating units called sarcomeres, creating the striated appearance of heart muscle. Sarcomeres are the fundamental units of muscle contraction containing two major protein types; actin and myosin (**Figure 4**) (Kartha, 2021; Powers *et al.*, 2021). Actin forms thin double-stranded filaments containing binding sites for myosin (Henderson & Gregorio, 2015; Skwarek-Maruszewska *et al.*, 2009)). Myosin forms thick, rod-shaped filaments featuring globular

heads. These heads contain ATP-binding sites which form cross-bridges to interact with actin. This interaction allows myosin to bind to and "pull" on actin filaments, generating the contractile force (Altman, 2020; Knight, 2023; Powers *et al.*, 2021). The actin filament also contains the proteins tropomyosin and troponin. Tropomyosin is a long, fibrous protein located along the actin filament groove. In the relaxed state, it blocks the myosin binding sites on actin (David, 2018). Troponin, a regulatory protein associated with tropomyosin, binds  $\text{Ca}^{2+}$  to initiate a conformational change in tropomyosin, exposing the myosin binding sites on the actin filament (Gusev, 2013; Kartha, 2021).

### **Sliding Filament Theory**

The sliding filament theory describes the cellular process that occurs to generate muscular contraction. With cardiomyocytes in their relaxed state, contraction starts with an electrical signal generated by the sinoatrial node. The electrical signal stimulates the opening of voltage-gated  $\text{Ca}^{2+}$  channels, causing an influx of  $\text{Ca}^{2+}$  into the sarcoplasm (da Silva & Reinach, 1991). This influx stimulates a  $\text{Ca}^{2+}$ -induced  $\text{Ca}^{2+}$  release system, where the sarcoplasmic/endoplasmic reticulum calcium ATPase (SERCA) pumps  $\text{Ca}^{2+}$  stored within the endoplasmic reticulum into the sarcoplasm. This drastically increases  $\text{Ca}^{2+}$  concentration within the cardiomyocyte (Zhihao *et al.*, 2020).

Once in the sarcoplasm,  $\text{Ca}^{2+}$  binds to troponin, inducing a conformational change in tropomyosin, which exposes the myosin binding sites on the actin filaments (**Figure 4.1**) (Gordon *et al.*, 2000). The exposed myosin binding sites attract the high energy myosin heads, forming a cross-bridge between the two filaments and subsequently causing the release of inorganic phosphate (Pi) in the process (**Figure 4.2**) (Powers *et al.*, 2021; Spudich, 2001). ADP (adenosine diphosphate) is then released, the energy of which fuels the power stroke (**Figure 4.3**). A power stroke is a rapid change in the shape of the myosin head that pulls the actin filament towards the centre of the sarcomere, shortening the sarcomere and ultimately the entire cardiomyocyte. An ATP molecule binds the myosin head, stimulating its dissociation from the actin binding site (**Figure 4.4**). An ATPase within the myosin head then hydrolyses the ATP into ADP and Pi. With continued electrical stimulation,  $\text{Ca}^{2+}$  will remain in the sarcoplasm and the cycle repeats. The myosin head attaches to a new actin binding site further along the filament, pulling it again, producing further contraction.

Relaxation occurs with the cessation of signalling from the sinoatrial node.  $\text{Ca}^{2+}$  is pumped back into the sarcoplasmic reticulum, decreasing sarcoplasmic  $\text{Ca}^{2+}$  concentrations and

causing  $\text{Ca}^{2+}$  to dissociate from troponin, which undergoes a conformational change (Gordon *et al.*, 2000; Powers *et al.*, 2021). This causes a reversal in the conformational change of tropomyosin, blocking the myosin binding sites on actin and preventing further cross bridge formation. Unlike skeletal muscle, which relies on the large protein titin for recoil, cardiac muscle utilises the inherent elasticity of its sarcomere. As cross-bridges break and binding sites are covered, the elastic recoil of the protein filaments within the sarcomere pulls the actin and myosin filaments back towards their original lengthened positions. The myocyte is now in its relaxed state, ready for initiation at the start of the next cardiac cycle (Spudich, 2001).

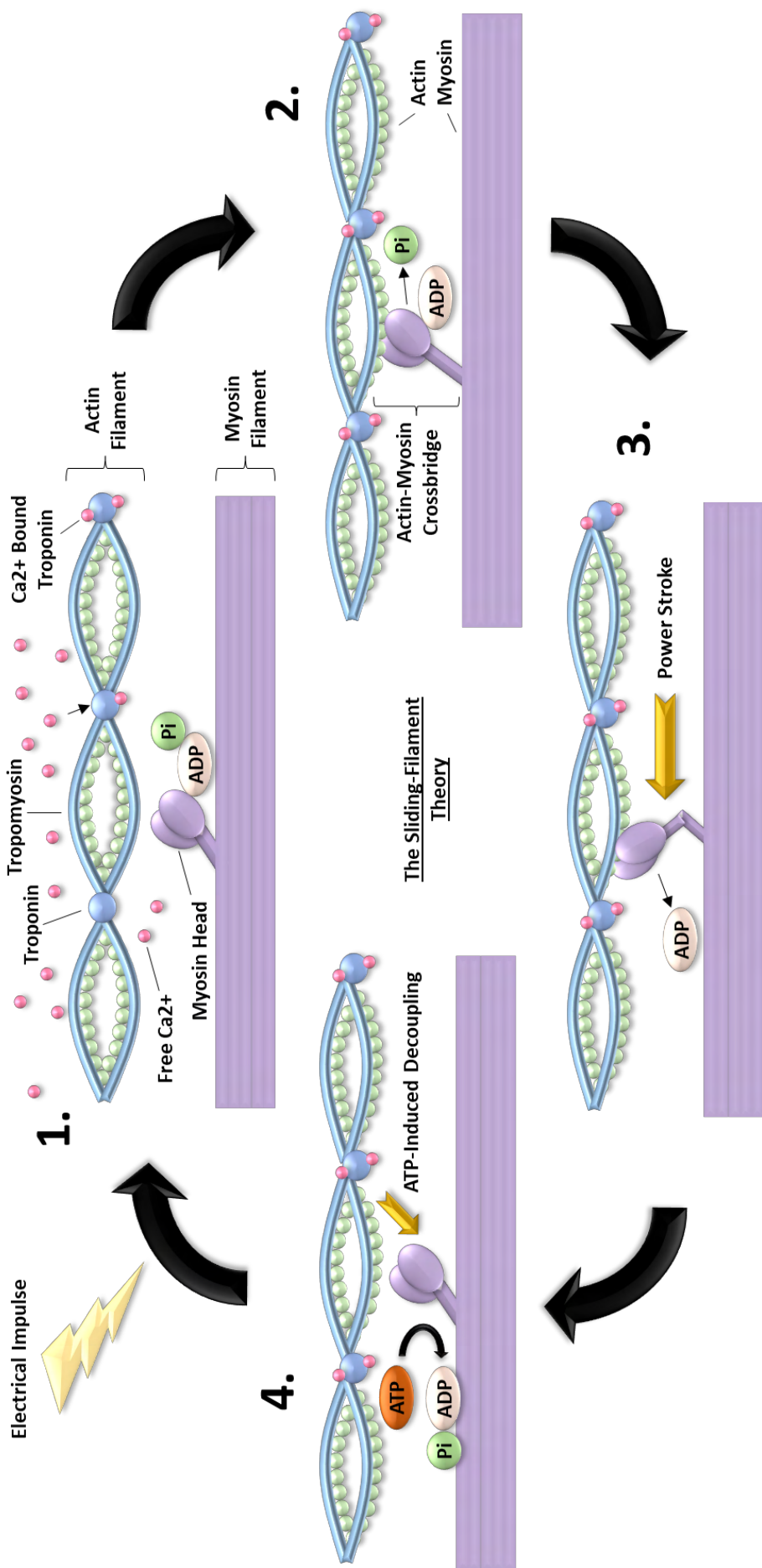


**Figure 4: The Sliding-Filament Model of Muscle Contraction.**

(1). A tropomyosin protein complex blocks myosin from binding to actin. (2). Calcium ions trigger a conformational change in tropomyosin, exposing the binding site for myosin. (3). Myosin then attaches to actin, forming a cross-bridge. (4). The myosin head pivots using energy from ATP hydrolysis, pulling the actin filament and generating force for contraction. Adapted from (Powers *et al.*, 2021).

## 2.3 Pathophysiological Stresses and Cardiac Hypertrophy

### 2.2.5 Cardiac Hypertrophy

The heart responds to physiological stresses to maintain optimal perfusion of blood to the tissues of the body (e.g. to increase cardiac output during exercise). However, pathophysiological stressors such as hypertension can, over time, cause the protective responses to fail (Nakamura & Sadoshima, 2018). Such stresses induces remodelling of the myocardium, increasing fibrosis, causing loss of capillaries and inducing cardiomyocyte hypertrophy, consequently reducing the efficacy of heart function until it fails entirely (Grossman & Paulus, 2013). Heart failure occurs when the heart cannot supply the required blood volume for normal tissue and organ activity. Heart failure is the terminal phase of many diseases, including hypertension, ischaemic heart disease and diabetes (Kemp & Conte, 2012), which are multifactorial in their aetiology. Analogous to these diseased states are altered protein-protein interactions, which affect cardiac function.

Cardiac hypertrophy is an increase in heart size and may result from either physiological or pathological hypertrophy (Dorn *et al.*, 2003; Nakamura & Sadoshima, 2018; Tardiff, 2006). Physiological hypertrophy is a normal response of the heart to increased demand for contractile ability. This occurs, for example, in athletes and during pregnancy in women to accommodate the increased demand for oxygen (Shimizu & Minamino, 2016).

Physiological hypertrophy is generally reversible on removal of the stress. Pathological hypertrophy is caused by an underlying disease or condition and can lead to serious complications such as heart failure and an increased risk of heart attack (Dorn *et al.*, 2003; Nakamura & Sadoshima, 2018). In most cases, pathological hypertrophy occurs in the left ventricle of the heart. However, right ventricular hypertrophy occurs in congenital disorders and as a result of lung diseases (e.g. pulmonary hypertension) (Bartelds *et al.*, 2021; Iacobazzi *et al.*, 2016; Vonk Noordegraaf & Galiè, 2011).

Cardiac hypertrophy is often described according to gross morphological changes as concentric and eccentric hypertrophy (Müller & Dhalla, 2013). Concentric hypertrophy occurs when the heart is subjected to an increased workload (as with hypertension), requiring the heart to pump blood harder. This places stress on the heart, which compensates by increasing the thickness of the myocardial walls, particularly in the left ventricle (Müller & Dhalla, 2013; Tardiff, 2006). This form of hypertrophy is a compensatory mechanism that enables the heart to pump more blood with each contraction. Eccentric hypertrophy arises from the enlargement and dilation of the heart's

chambers. This results in an increase in the size of the heart's chambers rather than the increase in the thickness of the heart's muscle walls. This form of hypertrophy leads to weaker heart function as more blood accumulates in the chamber and less is pumped out (Shimizu & Minamino, 2016).

### **2.2.6 Effect of Hypertension on the Heart**

High blood pressure requires increased pumping power of the heart, inducing stress on the tissue (Ruwhof & van der Laarse, 2000). This stress can induce apoptosis of cardiomyocytes and the endothelium. Elevated systemic arterial blood pressures impacting the left ventricular wall cause further apoptosis by stressing and damaging these cells (Georgiopoulou *et al.*, 2012; Susic & Frohlich, 2000). As cardiomyocytes are terminally-differentiated and therefore cannot proliferate, they undergo hypertrophy to compensate for the reduced cardiomyocyte population and manage the workload. This increases the left ventricular wall thickness, subsequently reducing the ventricular volume and efficiency of muscle relaxation (Alberts *et al.*, 2002; Nadar & Lip, 2021). Damaged endothelial cells lose the ability to proliferate (termed senescence) or undergo apoptosis. Consequently, the remaining capillary network cannot enable efficient exchange of materials required for tissue function (Carmeliet, 2005). This, in combination with the disproportionate increase in left ventricular wall thickness causes inadequate microvasculature perfusion of the myocardium (Georgiopoulou *et al.*, 2012), leading to localised hypoxia and cell death. After removal of cell debris by surrounding cells, fibroblasts then infiltrate the damaged tissue and induce fibrosis. Fibrosis occurs when excessive ECM, particularly collagen, is produced in response to damage and the resulting area forms stiff, poorly-contracting scar tissue (Rog-Zielinska *et al.*, 2016). This increases ventricular wall thickness, but not overall heart size, and contributes to the decreased ventricular volume. If the increase in pressure is in the pulmonary artery (feeding the lungs), the impact is initially on the right ventricle which hypertrophies (Vonk Noordegraaf & Galiè, 2011). However, this eventually has a secondary effect on the left ventricle.

Collectively, the cellular response to hypertension prevents optimal blood circulation due to a decreased diastolic and systolic volume, clinically defined as diastolic dysfunction (Rog-Zielinska *et al.*, 2016). Consequentially, the heart must "work" harder to circulate the same blood volume as an unstressed heart due to the significant loss in pumping force. Increased fibrotic stiffness further exacerbates the decrease in functional cardiomyocytes by impeding the electrical impulses required for cardiac contraction, which independently

increases the risk of developing heart failure (Segura *et al.*, 2014). The heart will stretch in response to the reduced ventricular volume (decompensates), but the cardiomyocytes are consequently weakened. This alongside the increased stiffness and remodelling of the myocardium causes a decrease in myocardial contractility which progresses to heart failure (**Figure 5**) (Georgiopoulou *et al.*, 2012; Mangini *et al.*, 2013).

## 2.3 RAAS and Blood Pressure Regulation

The renin-angiotensin aldosterone system (RAAS) is a hormonal system responsible for regulating blood pressure homeostasis in humans through electrolyte balance and fluid retention (**Figure 6**) (Boron & Boulpaep, 2012; Nehme *et al.*, 2019). Pressure sensitive baroreceptors within the carotid sinus detect a drop in blood pressure and stimulate RAAS via the sympathetic nervous system. RAAS is also stimulated by renal hypoperfusion (decrease filtrate flow rate through the macula densa of the kidneys) or a decrease in filtrate NaCl concentration (Nehme *et al.*, 2019). In response to these signals, juxtaglomerular cells release the enzyme renin into the bloodstream (Ames *et al.*, 2019). Angiotensinogen is also released from the liver in response to low blood pressure or NaCl concentrations. Renin binds and cleaves angiotensinogen within the blood stream to form angiotensin I (AngI). AngI is then converted into angiotensin II (AngII) by angiotensin converting enzyme (ACE) (Patel *et al.*, 2017; Pugliese *et al.*, 2020). ACE is produced in the vascular endothelium of most tissues. However, it is highly expressed in tissues of the cardiovascular and pulmonary circulatory systems.

AngII binds to and activates the type 1 AngII receptor (AT1R) present on the surface of the endothelium within blood vessels (Ames *et al.*, 2019). AT1R activation causes an increase in intracellular calcium within the endothelial cells, inducing vasoconstriction (Nehme *et al.*, 2019). Vasoconstriction is the narrowing of the blood vessels, increasing vascular resistance which in turn, increases blood pressure. In addition, ACE degrades bradykinin, a peptide hormone that promotes synthesis of nitric oxide (NO) that causes vasodilation (Ancion *et al.*, 2019). Therefore, decreases in NO resulting from reduced bradykinin promotes vasoconstriction. AngII binding to AT1R also impairs NO synthesis (Ding *et al.*, 2020). These mechanisms help to restore blood pressure and maintain perfusion to vital organs in response to low blood pressure or blood volume. Once blood pressure has been increased to an appropriate level, renin production is reduced in order to maintain homeostasis.

Apart from its effects on vasoconstriction, AngII also stimulates aldosterone and vasopressin production which further increases blood pressure (Mehta & Griendling, 2007; Nehme *et al.*, 2019; Steckelings *et al.*, 2017). Aldosterone is secreted from the adrenal glands and acts on the renal tubules in the kidneys, promoting sodium reabsorption and potassium excretion. With increasing blood aldosterone levels, the kidneys become more efficient at reabsorbing sodium from the urine and excreting potassium (Boron & Boulpaep, 2012; Nehme *et al.*, 2019). Vasopressin acts on the

kidneys to promote water reabsorption. Vasopressin interacts with renal vasopressin V2 receptors, increasing the permeability of the collecting ducts within the nephrons. Consequently, this stimulates the reabsorption of water from the urine back into the bloodstream, increasing blood volume and in turn blood pressure (Boone & Deen, 2008). Both hormones work in conjunction with one another to enhance sodium ion exchange which is accompanied by increased water retention. Sodium ion retention consequently increases blood volume and blood pressure.

The RAAS is precisely controlled through negative feedback mechanisms to prevent overactivity (**Figure 6**). Once blood pressure and volume are restored to normal physiological levels, negative feedback loops suppress further RAAS activation. On detecting blood pressure and volume increases, the kidneys respond by inhibiting the release of renin (Thomas & Tikellis, 2009). This normalisation promotes vasodilation, preventing the further increase of blood pressure and volume. The RAAS is also balanced by counter-regulatory hormone systems. Hormones like atrial natriuretic peptide (ANP) and brain natriuretic peptide (BNP) act paradoxically to the RAAS (Pandey, 2021). ANP and BNP promote vasodilation of blood vessels, increasing sodium and water excretion by the kidneys as well as directly inhibiting renin release.

As described above, the RAAS is essential in maintaining homeostasis for the body's fluid balance and blood pressure. Dysregulation of this system can lead to pathophysiological conditions such as hypertension and the development of heart failure (Ames *et al.*, 2019; Sayer & Bhat, 2014). Due to this, the AngII hypertension model is one of the most widely used preclinical *in vivo* mammalian models of hypertension. The AngII model involves external administration of AngII to artificially increase systemic blood pressure. This model is characterised by vasoconstriction, increased water and salt retention and subsequent increase in blood volume and pressure (Humphrey, 2021). As AngII plays a significant role in blood pressure homeostasis in humans, the effect of AngII on mammalian models can be translated reasonably accurately to a clinical setting (reproducible across species). In both humans and *in vivo* models, prolonged AngII-induced hypertension causes haemodynamic overload of the heart, which induces hypertrophy of the ventricle walls (**section 2.2**), as well as AngII causing myocardial dysfunction and fibrosis directly (Rosenkranz, 2004).

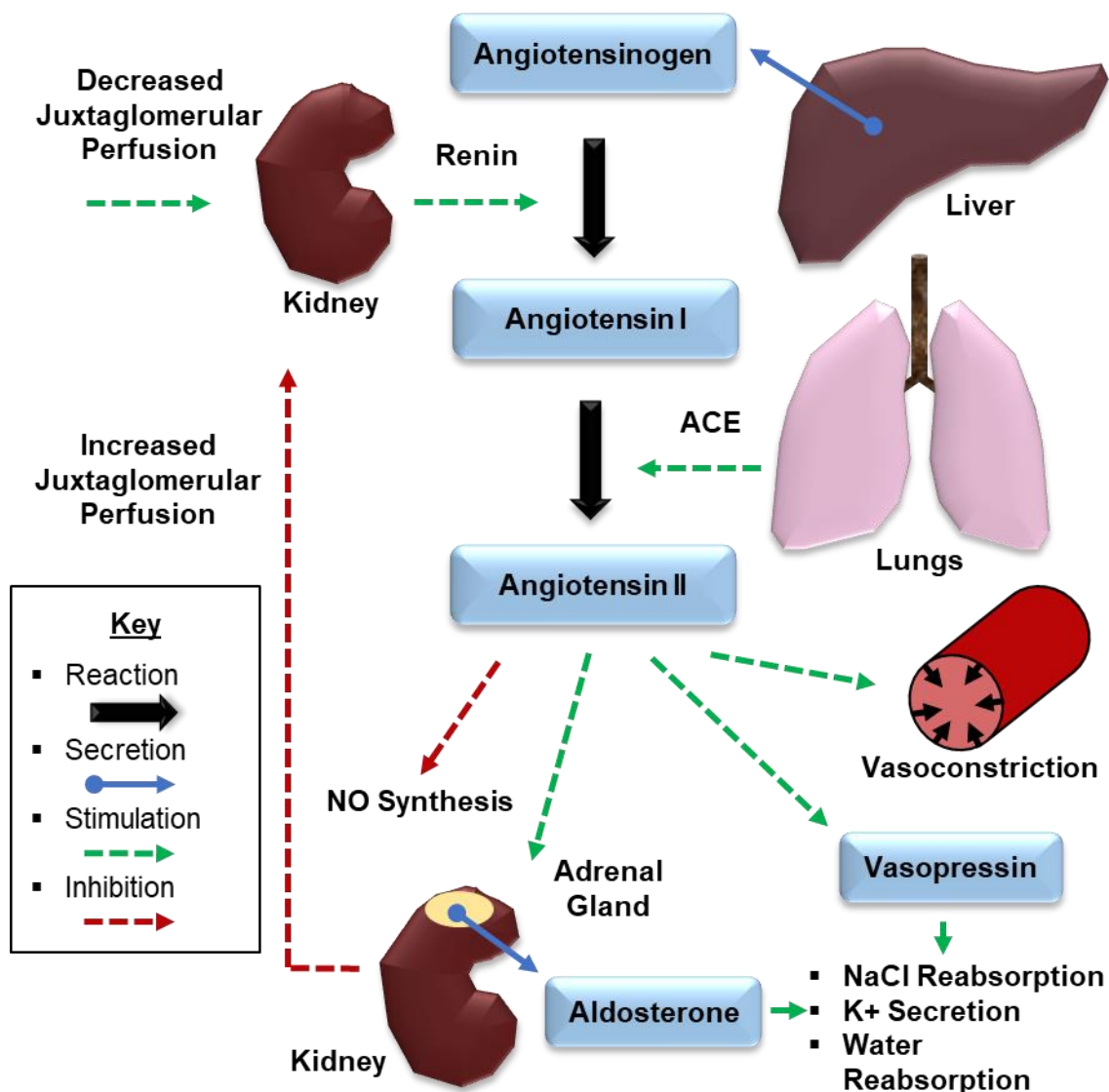


**Figure 5: The Renin-Angiotensin-Aldosterone System (RAAS).**

The RAAS is a complex hormonal system that helps regulate blood pressure, blood volume, and electrolyte balance in the body. When blood pressure drops, the RAAS is activated, leading to the release of renin. Renin cleaves angiotensinogen (produced by the liver) to produce angiotensin I, which is converted to angiotensin II, which stimulates vasopressin. Aldosterone is released by the kidney, and the hormones work together to increase blood pressure by constricting blood vessels, increasing blood volume, and reabsorbing sodium and water. Conversely, when blood pressure rises, the RAAS is inhibited.

## 2.4 Therapeutic Options for Hypertension Management

### 2.4.1 Lifestyle Modifications

Patients with a risk of or presenting with hypertension can adjust their lifestyle to actively control their blood pressure levels (Appel *et al.*, 1997; Georgiopoulou *et al.*, 2012; Goetsch *et al.*, 2021; Parati *et al.*, 2022).

- **Diet:** Maintain a healthy diet. This includes, limiting intake of sodium (Appel *et al.*, 1997), saturated fats and cholesterol while increasing consumption of fruits, vegetables, whole grains, and lean proteins (Parati *et al.*, 2022)
- **Weight:** Achieving and maintaining a healthy body weight. A BMI of 18-25 is considered to be a healthy range for most adults or a body fat percentage of 20 to 30% (Goetsch *et al.*, 2021; Narkiewicz, 2006). A healthy body weight is case specific with healthy ranges dependant on height, age, sex, and overall body composition.
- **Physical activity:** Engaging in regular aerobic exercise, such as brisk walking, swimming, or cycling, can contribute to lowering blood pressure levels. Patients have an increased risk (30-50%) of developing hypertension with low physical activity and fitness (Georgiopoulou *et al.*, 2012). The recommended amount of physical activity typically includes at least 150 minutes of moderate-intensity exercise per week (Goetsch *et al.*, 2021).
- **Stress:** Chronic stress can exacerbate hypertension. If the patient is unable to remove themselves from the stress, techniques for stress reduction, such as mindfulness meditation, deep breathing exercises, and yoga, can help patients manage their stress and, in turn, their blood pressure (Dickinson *et al.*, 2008; Goetsch *et al.*, 2021).
- **Alcohol consumption:** Excessive alcohol intake can lead to elevated blood pressure. Moderating alcohol consumption is advised, with guidelines suggesting no more than one drink per day for women and two drinks per day for men (Goetsch *et al.*, 2021; Stranges *et al.*, 2004).
- **Smoking:** Smoking increases risk of developing hypertension.

### 2.4.2 Antihypertensive Medications

Antihypertensive medications are commonly prescribed to control blood pressure. By specifically targeting pathways and regulatory systems involved in regulating blood pressure, antihypertensive medications exert a precise and modulated influence on blood

pressure, thereby mitigating the risks associated with uncontrolled hypertension (Kannan & Janardhanan, 2014). After failure to manage the condition through lifestyle modifications, antihypertensive treatment generally starts as monotherapy (Khalil & Zeltser, 2023). **Table 2** displays the common medications used and how they function. Combination therapy can be employed when one antihypertensive medication is not sufficient to significantly reduce the effects of hypertension. Combination therapy involves using multiple medications with complementary actions (Whelton *et al.*, 2018). Combination therapy not only enhances treatment effectiveness but also minimises any adverse side effects. However, in ~10% of hypertension cases, hypertensive medications are not successful in reducing blood pressure (Myat *et al.*, 2012; Noubiap *et al.*, 2019) and new therapeutic approaches are needed. Thus, further research into mechanisms associated with hypertension is needed.

**Table 2: Key Anti-Hypertensive Medications**

Medication	Effects	Examples
<b>Diuretics</b>	Increase urine output, reducing fluid volume and blood pressure by helping the body remove excess salt and water	Hydrochlorothiazide (HCTZ), furosemide (Lasix)
<b>ACE inhibitors</b>	Inhibits the production of angiotensin II	Lisinopril (Zestril), enalapril (Vasotec)
<b>Angiotensin II receptor blockers (ARBs)</b>	Antagonises the action of angiotensin II on blood vessels	Losartan (Cozaar), valsartan (Diovan)
<b>Calcium channel blockers (CCBs)</b>	Inhibit calcium entry into smooth muscle cells, leading to vasodilation	Amlodipine (Norvasc), diltiazem (Cardizem)

Table legend: This table summarises key anti-hypertensive medications, listing their medication class, mechanism of action, and some common examples. Adapted from (Khalil & Zeltser, 2023).

## 2.5 Rodent Models of Hypertension

Rodent models play an essential role in advancing our understanding of the pathophysiology of hypertension in humans. Rodent models can simulate the aetiology of human hypertension, the induction of cardiac hypertrophy and the progression to heart failure (Jama *et al.*, 2022). This enables researchers to investigate the underlying mechanisms of the diseases and evaluate the safety of new treatments. As discussed previously, cardiac hypertrophy is characterised by an increase in the size of heart cells and an increase in the thickness of the heart wall. There are several ways to assess hypertrophy in animal models. This includes the following:

- **Histological Analysis:** Measure changes in the size and number of myocytes as well as the extent of fibrosis in the heart at the end of the experiment after the heart has been removed from the animal, fixed, cut into sections and stained. An increase in myocyte size and fibrosis is indicative of cardiac hypertrophy.
- **In Vivo Echocardiography:** Measure changes in the thickness of the heart wall, the size of the heart chambers and the functional capacity of the heart *in vivo* using non-invasive imaging. Echocardiography can be used to monitor changes in cardiac hypertrophy over an extended time period. Other methods (e.g. small animal magnetic resonance imaging (MRI) require more expensive equipment and more prolonged periods of imaging (Phuah *et al.*, 2023).
- **Molecular Markers:** Gene expression and protein levels can also indicate changes in the heart associated with cardiac hypertrophy at the end of the study. While both provide specific insights, gene expression is especially useful in early-stage assessment of cardiac hypertrophy. Changes in mRNA levels often precede changes in protein levels, providing an early indication of the cellular response to hypertrophy. For example, changes in the mRNA expression of cell-specific genes (Myh7 is upregulated whilst Myh6 is downregulated in rodent cardiomyocytes with hypertrophy) (Forough *et al.*, 2011), stress (Nppb) (Man *et al.*, 2018) or fibrosis (Col1a, Col3a1 - collagen genes) (Hinderer & Schenke-Layland, 2019) can be indicative of the development of cardiac hypertrophy.

There is a range of different types of rodent models that are commonly used in hypertension research, as discussed below. The advantages of using animal models in scientific research are numerous. However, serious consideration of ethical and moral necessity should be raised before their involvement. The researcher should first explore alternative methods, such as cell culture and computational models, in which the

technology is improving year after year. Researchers should also consider that the results obtained through these model organisms may not directly translate to humans, and thus, additional validation may be required. Therefore, selecting the optimal model is essential for a successful study. It is important to consider the specific research question, the study's goals and the differing advantages and disadvantages of each model before determining which model to select.

For the reasons explained below, the studies in **Chapters 3, 4 and 5** were conducted using the AngII model in mice with a C57BL6/J background coupled with genetic alteration of specific genes (**Chapters 3 and 4**) or to assess the effects of an anti-cancer drug (**Chapter 5**).

### 2.5.1 Inbred Genetic Models

Inbred models are created by breeding animals with desirable genetic characteristics, in this case hypertension, over many generations to obtain offspring that reliably and reproducibly present with these characteristics. Two common examples of inbred genetic models for hypertension are the Dahl salt-sensitive rat and the spontaneously hypertensive rat (SHR) (Jama *et al.*, 2022).

The Dahl salt-sensitive rat strain is a well-established model. The model is hypersensitive to the effects of dietary salt intake due to a genetic predisposition. An increased salt intake results in an increase in systemic blood pressure (Kurtz & Morris, 1985). The Dahl salt-sensitive strain is also prone to developing other hypertension-related complications. Such complications include left ventricular hypertrophy and renal damage (Abais-Battad *et al.*, 2019; Dutta & Mukherjee, 2019).

The SHR strain is another established genetic model of hypertension. Originally derived from Wistar rats, SHRs display a progressive rise in arterial blood pressure beginning at around 6 weeks of age (Doggrell & Brown, 1998). By 4-6 months of age, SHRs have severe hypertension with systolic blood pressures over 200 mmHg (Doggrell & Brown, 1998). This hypertension progresses with age and is accompanied by end-organ damages similar to human hypertensive disease, such as left ventricular hypertrophy, renal impairment, and vascular damage (Susic & Frohlich, 2011). Unlike most other rodent models, the hypertension of SHRs does not require manipulation such as high-salt diet or administration of exogenous chemicals. The spontaneous hypertension of SHRs

consistently develops as the rats age, mimicking the development of primary hypertension in humans. The SHR model has been extensively used to investigate the genetic and molecular mechanisms underlying hypertension, as well as to evaluate the efficacy of antihypertensive interventions (Jama *et al.*, 2022).

### 2.5.2 Drug-Induced vs Surgical Models of Hypertension

Drug-induced models of hypertension utilise pharmacological agents to artificially elevate blood pressure in laboratory animals. Common infusion models include the AngII and phenylephrine models (Jama *et al.*, 2022). As described previously (**Section 2.4**), AngII promotes vasoconstriction, increasing vascular resistance and in turn, elevating blood pressure. Therefore, the administration of exogenous AngII, either through regular injections or using osmotic mini-pumps implanted under the skin for constant delivery, artificially induces hypertension. Phenylephrine demonstrates similar vasoconstriction properties. Phenylephrine is an  $\alpha_1$ -adrenergic receptor agonist which induces a cascade of events that can result in vasoconstriction and in turn, raises blood pressure (Richards *et al.*, 2023). Drug-induced models allow researchers a rapid, yet controlled and specific method of studying mechanisms involved in blood pressure regulation. This allows for the assessment of these drug-related pathways in the development of hypertension.

There are several surgical models of hypertension which have been developed. These models involve surgical interventions to replicate various aspects of hypertension, allowing researchers to investigate the physiological and pathophysiological changes they induce. The two-kidney, one-clip (2K1C) model of renal artery stenosis is another one of the most commonly used surgical models of hypertension. In the 2K1C model, a surgical clip is placed on one renal artery, inducing hypertension by reducing blood flow to one kidney. This simulates the pathology of human renal artery stenosis. This surgical technique has been applied in previous research to investigate the effects of hypertension on various organ systems (Wiesel *et al.*, 1997). A model of direct pressure overload on the heart involves transverse aortic constriction (TAC). The TAC model involves constricting the transverse aorta using a surgical clip or suture. This increases the pressure required by the left ventricle to circulate the blood volume, leading to cardiac hypertrophy and remodelling (Liu *et al.*, 2020). It is also worth mentioning the abdominal aortic banding (AAB) model, which partially constricts the aorta in the abdomen. Compared to TAC, AAB creates a milder pressure overload on the heart. This typically leads to compensated hypertrophy, where the heart muscle thickens (hypertrophy) but

remains functional, unlike TAC, which can rapidly progress to heart failure (HF) (Seymour *et al.*, 2015).

AngII infusion and TAC surgical models are both widely used experimental methods in cardiovascular research, both causing pressure overload on the left ventricle of the heart as occurs in hypertension (Humphrey, 2021). Each model has its advantages and disadvantages. The osmotic mini-pump implantation surgery required for the AngII model is a simple procedure which is easy to implement, only entering into sub-cutaneous structures (Lu *et al.*, 2015). It is also reliable since a predefined dose can be administered to vary the degree of hypertension. Finally, it is truly representative of the effects of systemic hypertension. The TAC surgical model, however, requires more invasive and technically challenging surgery, entering into the internal cavity of the animal (Liu *et al.*, 2020). TAC is more variable in terms of degree of pressure overload since this depends on the tightness of the clip or suture. It is also not truly representative of systemic effects of hypertension on the heart.

### **2.5.3 Genetically-Altered Mice**

Genetically altered mice are often used as models in hypertension research to study the underlying mechanisms, test potential treatments, and gain insights into the genetics of the disease (Jama *et al.*, 2022). These mice are usually used in combination with drug or surgery-induced hypertension models. Alterations to the genome can be in the form of additions or deletions which cause overexpression, knockdown (reduction in expression) or knockout (complete removal) of the targeted gene. Overexpression approaches generally use a system in which a gene of interest is inserted into the genome. Early studies were non-targeted and effects could result from disruption of an alternative gene. Moreover, the degree of overexpression was rarely controlled. More recent studies take advantage of a “safe-harbour” locus where the gene is introduced into a part of the genome known to not interfere with any other gene (e.g. ROSA26 locus in mice) (Ma *et al.*, 2022).

Gene deletion approaches have been developed to eliminate a crucial exon(s) causing a frameshift mutation that results in introduction of a nonsense mutation and lack of functional protein. This gene editing now often employs CRISPR/Cas9 for specific targeting (El Marjou *et al.*, 2021; Ma *et al.*, 2014; Muñoz-Santos *et al.*, 2020; Yang *et al.*, 2014). While gene deletion and overexpression can both be used to study the role of a gene, gene deletion is generally considered to be more accurate. This is because gene

deletion creates a loss-of-function mutation, usually producing a more severe phenotype which is more likely to reflect the gene's true function. Overexpression may stimulate compensatory mechanisms that counteract the effects of overexpression. As a result, these mechanisms may conceal the true effects of the gene's expression. Deleting the gene may still produce compensatory mechanisms. However, the response produced due to the deletion, will more precisely reflect the gene's function.

Advanced models may use a knock-in approach to introduce a specific mutation. Here, a coding sequence is usually introduced to replace the existing gene, leaving the new sequence under control of the endogenous promoter (e.g. BRAFV600E model) (Landa & Knauf, 2019). These targeted mutations offer advantages over non-specific mutations when developing new genetically-altered models. Targeted mutations typically target the coding region of the gene, disrupting the production of a functional protein product by modifying the protein's amino acid sequence. The aim is to produce a protein of the similar spatial arrangement, where the active or catalytic site is non-functioning, but allows for the protein's usual interactions with other molecules. Non-specific mutations while still inactivating the enzyme, may cause more extensive alterations to the enzyme's structure. These structural changes may disrupt the enzyme's usual interactions with other molecules, complicating research aimed at understanding protein function and its role in disease mechanisms.

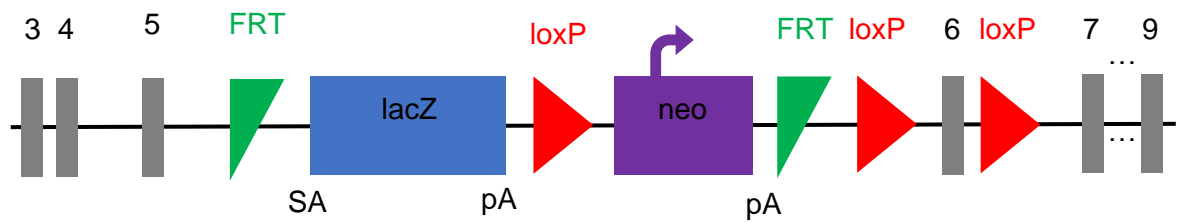
### **Global Genetic Alterations**

Global alteration of specific genes in mice is widely used and, in these mice, the genetic alteration occurs in all cells at all stages of development. These models are useful for studying the overall function of a gene, allowing researchers to observe the overall effects of gene or protein manipulation before focusing on specific cell types or tissues. However, if a gene product is essential for development, studies with global mutation become problematical either because of serious malformations of the embryo that result in early or premature death or because gene manipulation (e.g. gene deletion) results in the embryo not developing at all (embryonic lethality). This thesis contains three examples of this. *Strn* or *Strn3* gene deletion (Chapter 3) and *PKN2* gene deletion (Chapter 4) are all embryonic lethal in the homozygous state (Cull *et al.*, 2023; Danno *et al.*, 2017; Marshall *et al.*, 2022; Quétier *et al.*, 2016) and it is not possible to use homozygous global gene knockout systems to study their role in the heart. In each case, the heterozygotes (with reduced gene expression) are viable and fertile with no overt abnormalities. Thus,

heterozygote mice were used to study the roles of these proteins in hypertension-associated hypertrophy. However, it was not possible to confirm the exact roles of the proteins in cardiomyocytes specifically from the consequences of loss of the gene in cardiac non-myocytes. It was also not possible to be certain that there were no additional influences from the knockout in other organs (e.g. kidney).

The use of mice with global genetic alterations is reasonably straightforward in terms of strategy. My studies focused particularly on the Striatin project, where we generated heterozygote *Strn*<sup>+/−</sup> and *Strn3*<sup>+/−</sup> mice. *Strn*<sup>+/−</sup> and *Strn3*<sup>+/−</sup> founder mice were obtained from a cryopreserved repository (KOMP; STRN/STRN3<sup>tm1a(KOMP)WTSi</sup>) and backcrossed with C57Bl/6J mice (Charles River Ltd) for eight generations prior to experimentation. C57Bl/6J mice were used as C57Bl/6N are not suitable for cardiac research. This is because of inherent differences in the background genetics of C57Bl/6N mice which makes their hearts more sensitive to stressors (Garcia-Menendez *et al.*, 2013; Moreth *et al.*, 2014; Williams *et al.*, 2020; Zhou *et al.*, 2021). The colony was maintained as heterozygotes and outbred with C57Bl/6J mice to generate heterozygote knockout mice with wild-type littermates for the study. The model used a knockout first (promoter-driven) system involving the insertion of LacZ/neo cassette between critical exons of the target protein (exons 5 and 6) (**Figure 7**) ((IMPC), 2023). This insertion prevents the production of *Strn*/*Strn3* mRNA, which (in the heterozygote) decreases global protein expression by approximately 50% (Cull *et al.*, 2023; Skarnes *et al.*, 2011).

**(A)**



**(B)**

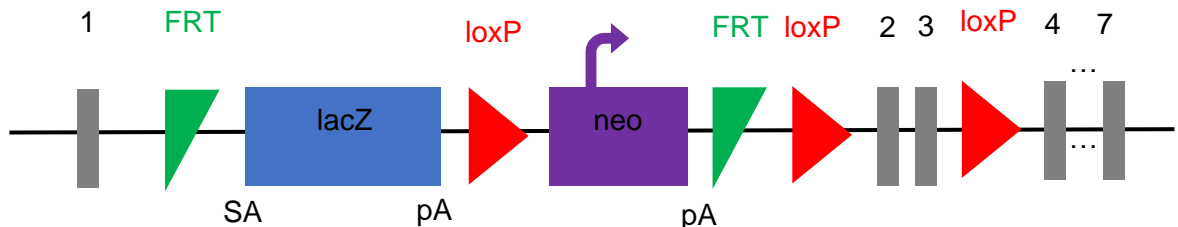


**Figure 6: Generation of the Strn and Strn Knockout Mouse Models.**

A knockout first (promoter driven) system using a lacZ/neo cassette was applied to generate the (A) Strn ( $STRN^{tm1a(KOMP)WTs1}$ ) or (B) Strn3 ( $STRN3^{tm1a(KOMP)WTs1}$ ) knockout mouse models. The insertion of the lacZ/neo cassette between critical exons prevents production of the relevant mRNA. The  $STRN^{tm1a(KOMP)WTs1}$  and  $STRN3^{tm1a(KOMP)WTs1}$  mouse models were obtained from the KOMP repository. The Figure was adapted from (Skarnes *et al.*, 2011) and based on the Allele map for  $STRN^{tm1a(KOMP)WTs1}$  and  $STRN3^{tm1a(KOMP)WTs1}$  from ((IMPC), 2023).

## Conditional Genetic Alterations

To avoid the developmental problems associated with gene modification, systems have been developed for conditional gene alteration. These usually employ a recombinase enzyme (usually Cre, sometimes FLP), which targets specific sequences (LoxP or FRT, respectively) for recombination. For cell-specificity, the enzyme is expressed under the control of a cell-specific promoter (e.g. Myh6 is usually used for cardiomyocytes (Huang *et al.*, 2021; Yan *et al.*, 2015)). In some cases, for inducible expression, the enzyme may be modified so that it is only active in the presence of a drug or hormone (e.g. tamoxifen) (Sohal *et al.*, 2001). Thus, in mice with cell-specific genetic alterations, the other (non-targeted) cell types in the organism will retain the original, unmutated gene. This targeted approach allows for investigations into the impact of the mutations in a specific tissue or cell type on biological mechanisms and the development of diseases.

Examples of cell-specific genetic alterations are presented in **Chapters 3 and 4** for Strn and PKN2 (Cull *et al.*, 2023; Marshall *et al.*, 2022). The breeding strategy for Strn is explained here as an example. The model involves inducible cardiomyocyte-specific knockout of Strn, on administration of tamoxifen. To achieve this, heterozygote Strn<sup>+/−</sup> mice from KOMP were used. These mice were generated as “knockout first” lines that can be converted for conditional gene deletion using FLP recombinase (**Figure 8**).

Cryopreserved mice were resuscitated from sperm simultaneously with the introduction of the FLP enzyme. This removed the lacZ STOP cassette, revealing the loxP sites surrounding the targeted exon 5. Viable heterozygous floxed (fl) Strn (Strn<sup>WT/fl</sup>) mice were generated and backcrossed onto a C57Bl/6J background, removing the FLP gene. The Strn<sup>WT/fl</sup> mice were then crossed with mice that were homozygous for tamoxifen-inducible Cre (MerCreMer, MCM) under the control of an MYH6 promoter (Sohal *et al.*, 2001). This generated mice that were heterozygous for floxed Strn and Cre (Strn<sup>WT/fl</sup>/Cre<sup>WT/MCM</sup> mice) (**Figure 9.A**).

One potential problem with the Cre enzyme is that it can cause cardiotoxicity itself if it is expressed at high levels or for prolonged duration (Bersell *et al.*, 2013). So, although it is important to have homozygous gene deletion for Strn (i.e. Strn<sup>fl/fl</sup> mice are needed) it is necessary to have mice heterozygous for CRE (McLellan *et al.*, 2017). Thus, upon generation of the Strn<sup>WT/fl</sup>/Cre<sup>WT/MCM</sup> double heterozygous mice, further breeding was required to obtain the Strn<sup>fl/fl</sup>/Cre<sup>WT/MCM</sup> genotype required for *in vivo* experimentation. First, the Strn<sup>WT/fl</sup>/Cre<sup>WT/MCM</sup> mice were crossed again with Cre<sup>MCM/MCM</sup> mice to generate mice with the heterozygous Strn<sup>WT/fl</sup> and homozygous Cre<sup>MCM/MCM</sup> genotypes (Strn<sup>fl/fl</sup>/Cre<sup>MCM/MCM</sup>)

(**Figure 9.B**). The  $\text{Strn}^{\text{WT/ffl}}/\text{Cre}^{\text{MCM/MCM}}$  mice were then bred with other  $\text{Strn}^{\text{WT/ffl}}/\text{Cre}^{\text{MCM/MCM}}$  mice to generate double homozygous  $\text{Strn}^{\text{ffl/ffl}}/\text{Cre}^{\text{MCM/MCM}}$  mice (**Figure 9.C**).

Simultaneously, the  $\text{Strn}^{\text{WT/ffl}}$  mice were bred together to generate homozygous floxed  $\text{Strn}$  ( $\text{Strn}^{\text{ffl/ffl}}$ ) mice (**Figure 9.D**). The  $\text{Strn}^{\text{ffl/ffl}}/\text{Cre}^{\text{MCM/MCM}}$  mice were then crossed with  $\text{Strn}^{\text{ffl/ffl}}$  mice to generate the experimental model,  $\text{Strn}^{\text{ffl/ffl}}/\text{Cre}^{\text{WT/MCM}}$  mice (**Figure 9.E**).

Heterozygous Cre mice were generated from the same colonies as a control.

### A. Heterozygous global Strn expression (tm1a)

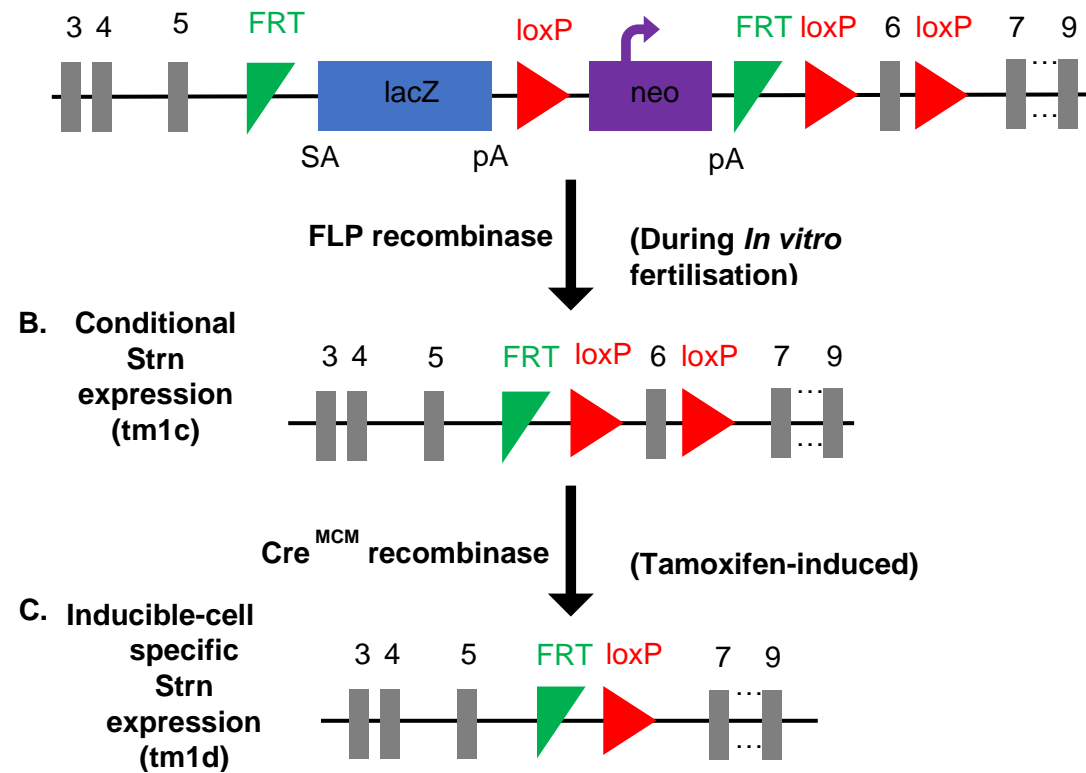


**Figure 7: STRN<sup>tm1a(KOMP)WT<sup>si</sup></sup>** Knockout First (Promoter Driven) System for the Generation of Cardiac Specific, Inducible Strn+/- Mice.

(A). Global heterozygous knockout of Strn by the STRN<sup>tm1a(KOMP)WT<sup>si</sup> knockout first (promoter driven) system using the lacZ/neo STOP cassette between exons 5 and 6 to prevent the production of Strn mRNA. (B). Generation of conditional Strn expression mice. During *in vitro* fertilisation, allele conversion was performed to generate floxed homozygote Strn mice (Strn<sup>f/f</sup>). The Strn<sup>f/f</sup> mice possess FLP recombinase which excised the lacZ/neo cassette at the FRT sites, inducing recombination. (C). Tamoxifen-induced recombination using Cre recombinases excises exon 6, inducing a frameshift and loss of cardiac gene expression. Cardiac specificity is generated from breeding a Cre mouse with a myosin heavy chain ( $\alpha$ MHC) promoter (Cre<sup>MHC/MHC</sup>). Adapted from (Skarnes *et al.*, 2011) and based on the Allele map for Strn<sup>tm1a(KOMP)WT<sup>si</sup> from ((IMPC), 2023).</sup></sup>

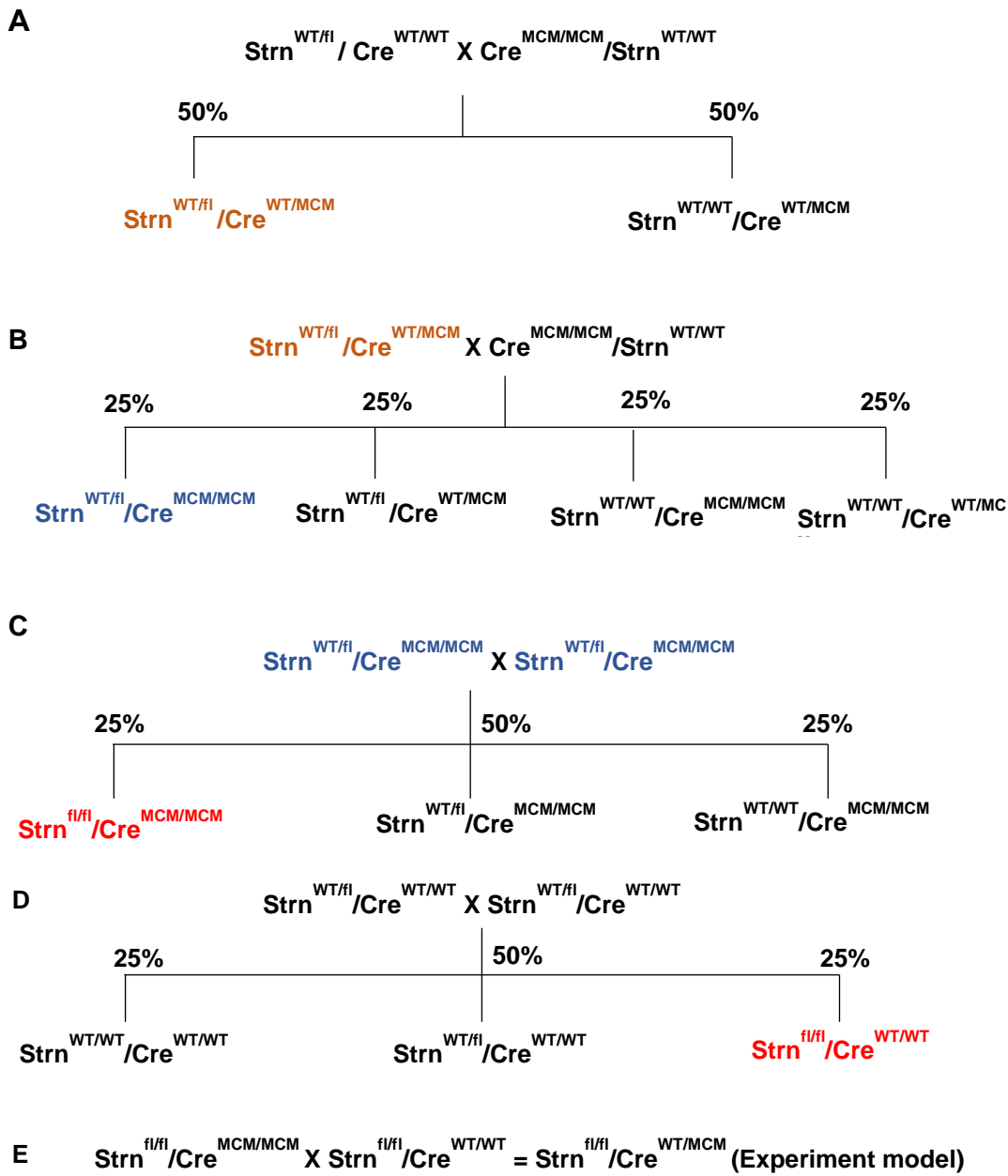


**Figure 8: Summary of the  $\text{Strn}^{\text{fl/}\text{fl}}/\text{Cre}^{\text{WT/MCM}}$  Mouse Breeding Program.**

(A). Floxed Strn mice were crossed with Cre mice. (B). Generation of the heterozygous Strn and homozygous Cre genotype. (C). Generation of the double homozygous Strn/Cre genotype. (D). Generation of the homozygous floxed Strn mice. (E). Generation of the test experimental mouse model.

## 2.6 Echocardiography

### 2.6.1 Overview

Ultrasound imaging utilises pulses of high frequency sound waves. The ultrasonic pulses reflect off the tissues of the body, allowing the production of ultrasound images (Wong, 2014). Each tissue type has differing tissue densities and therefore reflection properties. The varying reflection properties allow for the differentiation of tissues and structures within the ultrasound image. Echocardiography applies ultrasound imaging to allow for non-invasive real-time imaging of the heart's structure and movement (Garbi *et al.*, 2016). In a clinical setting, echocardiography assists in the diagnosis and monitoring of cardiovascular diseases. Diagnosis includes estimating heart function including cardiac output (the amount of blood expelled from the heart per minute), ejection fraction (the percentage of blood expelled with each contraction) and diastolic function (how efficiently the heart can relax). It can also be used to locate any tissue damage or structural changes in the heart. To understand how ultrasound can be used to accurately generate non-invasive real-time images of internal structures, the following principles must be known.

### Piezoelectric Effect

The Piezoelectric effect is how ultrasound pulses are generated. Within the ultrasound probe resides a piezoelectric (electric accumulating) crystal (Wong, 2014). When an electric current is applied to the crystal, the crystal structure is deformed, causing the crystal to vibrate. The vibrations result in the production of high-frequency ultrasound waves. The frequency of a sound wave is the number of wave cycles completed every second. The frequency of the ultrasound wave is predetermined by the size and shape of the crystal within the ultrasound probe. The higher the frequency of the ultrasound wave, the higher the resolution of the image produced (Garbi *et al.*, 2016). However, with a higher frequency, the ultrasound wave has a shorter wavelength (they are inversely proportional). The wavelength of a sound wave is the distance needed to complete one wave cycle. Shorter ultrasound wavelengths cannot penetrate to deeper tissues before being reflected. Therefore, the optimal frequency of the ultrasound wave must be predetermined to ensure the highest resolution and penetrating power to image the area of interest.

### Pulse-Echo Principle

Because the same crystals are used to produce and interpret the reflected ultrasound waves, the ultrasound waves are not continuously produced. The initial ultrasound wave produced must first interact, reflect and return to the ultrasound probe's crystal before the

next ultrasound impulse is generated (Wong, 2014). The reflected ultrasound waves need to interact and deform the crystals within the ultrasound probe to produce a new electrical current which is relayed to and interpreted by a computer. The computer calculates the distance from the probe to the tissue (based on the speed of sound through tissue) and the time for the ultrasound to be produced and return to the probe (millionths of a second). The machine then displays the distances and intensities of the echoes on a screen, forming a two-dimensional image. Once the first ultrasound wave signal is interpreted, a new ultrasound wave can be generated. Therefore, the ultrasound waves must be generated in pulses.

### **The Döppler Effect**

The Döppler effect is how moving objects interact and change the characteristics of sound waves (Garbi *et al.*, 2016). When an ultrasound wave reflects off an object moving towards a detector (ultrasound probe), the crest of the reflected ultrasound wave is produced at a position closer to the ultrasound probe compared to that of the previous ultrasound wave. Therefore, as an object moves towards the ultrasound probe, each ultrasound wave reflecting off that object takes less time to return to the ultrasound probe. Resultantly, the arrival time of each successive wave crest gets subsequently smaller. This causes the wavefronts to shorten and cluster together, increasing the frequency of the ultrasound waves (Wong, 2014). On the other hand, if the object is moving away from the ultrasound probe, the crest of the reflected ultrasound wave is produced at a position further away from the ultrasound probe compared to that of the previous ultrasound wave. Therefore, as an object moves away from the ultrasound probe, each ultrasound wave reflecting off that object takes more time to return to the ultrasound probe. Resultantly, the arrival time of each successive wave crest increases. This causes the wavefronts to increase and spread out, decreasing the frequency of the ultrasound waves. Therefore, it is possible to differentiate between objects moving towards or away from a detector (Garbi *et al.*, 2016).

In the context of echocardiography, the ultrasound probe emits a predetermined frequency which reflects off red blood cells. The reflected ultrasound waves from red blood cells return to the probe with a Döppler shift that is translated by a computer into a positive (towards) or negative (away) velocity (Wong, 2014). There are two different types of Döppler modes which were employed to assist in this study. Colour Döppler: blood velocity is depicted as colour overlayed onto a B-mode image. The intensity of the colour correlates to velocity. The more intense the colour, the higher the velocity. The red colour

represents blood flowing towards the probe whilst the blue colour represents blood flowing away from the ultrasound probe (Garbi *et al.*, 2016). Pulsed-wave Döppler: short impulses of ultrasound waves enable measurement of blood flow within a defined area of a two-dimensional B-mode image. The pulsed-wave Döppler allows measurements such as blood acceleration and ejection time through the vessel.

## 2.6.2 Imaging Methods

Echocardiography is an imaging technique that utilises ultrasound waves to create visual representations of the heart structure and function. Different modes and orientations of the echocardiography probe provide unique views and details about cardiac structure and motion.

### PSAX vs PLAX Orientations

The parasternal short axis (PSAX) orientation offers a bird's-eye view of the heart, showcasing the left ventricle in a clear circular format (**Figure 10**). To obtain the PSAX view, a transducer is applied perpendicular at 90° to the mouse's longitudinal axis, capturing a cross-sectional image (VisualSonics, 2008b). PSAX allows for the visual assessment of cardiac function and structures through various imaging modes and techniques discussed below (B-mode and M-mode, 3D and speckle-tracking). To obtain the parasternal long axis (PLAX) view, a transducer is applied parallel at 160° to the mouse's longitudinal axis (**Figure 11**), creating an image of the heart from a lateral angle (VisualSonics, 2008b). The PLAX view displays the heart in a longitudinal orientation, as the ultrasound beam is orientated parallel to the long axis of the heart. As with PSAX, the resulting image obtained with PLAX reveals the left ventricle chamber (though as an elongated view), but PLAX also allows views of the cardiac valves, pulmonary artery and aorta. The PLAX view therefore allows for the Döppler imaging of these vessels (VisualSonics, 2008a).

The PLAX view provides a wider perspective of the heart, giving a broader view of the left ventricle and its motion. On the other hand, the PSAX view is generally considered to provide a more specific assessment of chamber dimensions and structures as it assesses a perpendicular cross-section of the heart at a single point (Garbi *et al.*, 2016). In combination, assessing both viewpoints provides the most representative perspective of the heart and of any changes that may have occurred. By obtaining baseline measurements of the heart prior to treatment, researchers can determine any change that may occur over the course of an experiment (Garbi *et al.*, 2016).

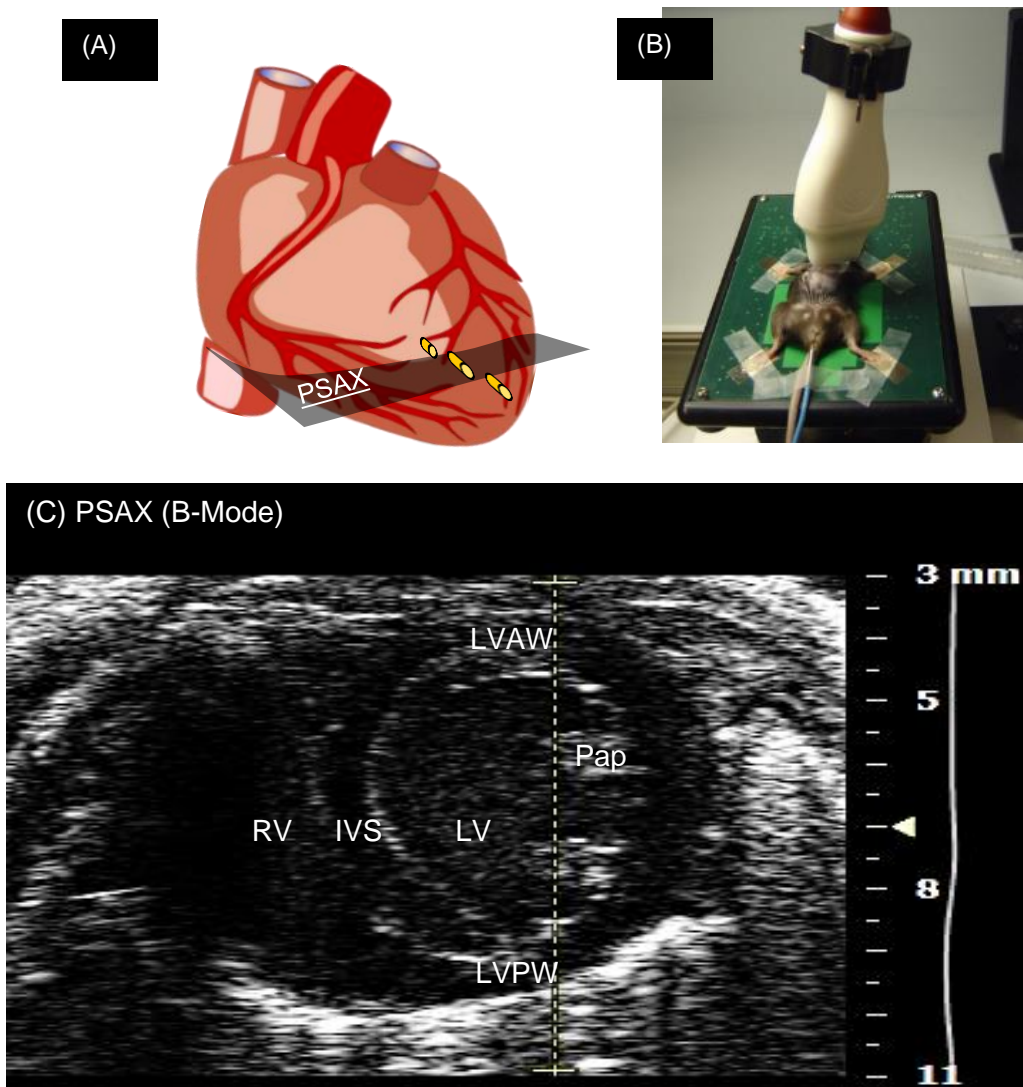


**Figure 9: Schematic, Positioning and B-mode Image Demonstrating the PSAX Cardiovascular Orientations.**

(A). Schematic demonstrating the PSAX cross-sectional area. (B). Transducer positioning for visualisation of a mouse PSAX. (C). PSAX B-mode image. Echocardiograms of eight-week-old C57BL/6J mice were produced using a Vevo 2100 system with a 38 MHz MS400 transducer. The yellow line represents the axis which the M-Mode trace is generated. Abbreviations: LV = Left ventricle, AW = anterior wall, PW = posterior wall, IVS = Interventricular septum, Pap = papillary muscle. Image (B) was taken from (VisualSonics, 2008b).

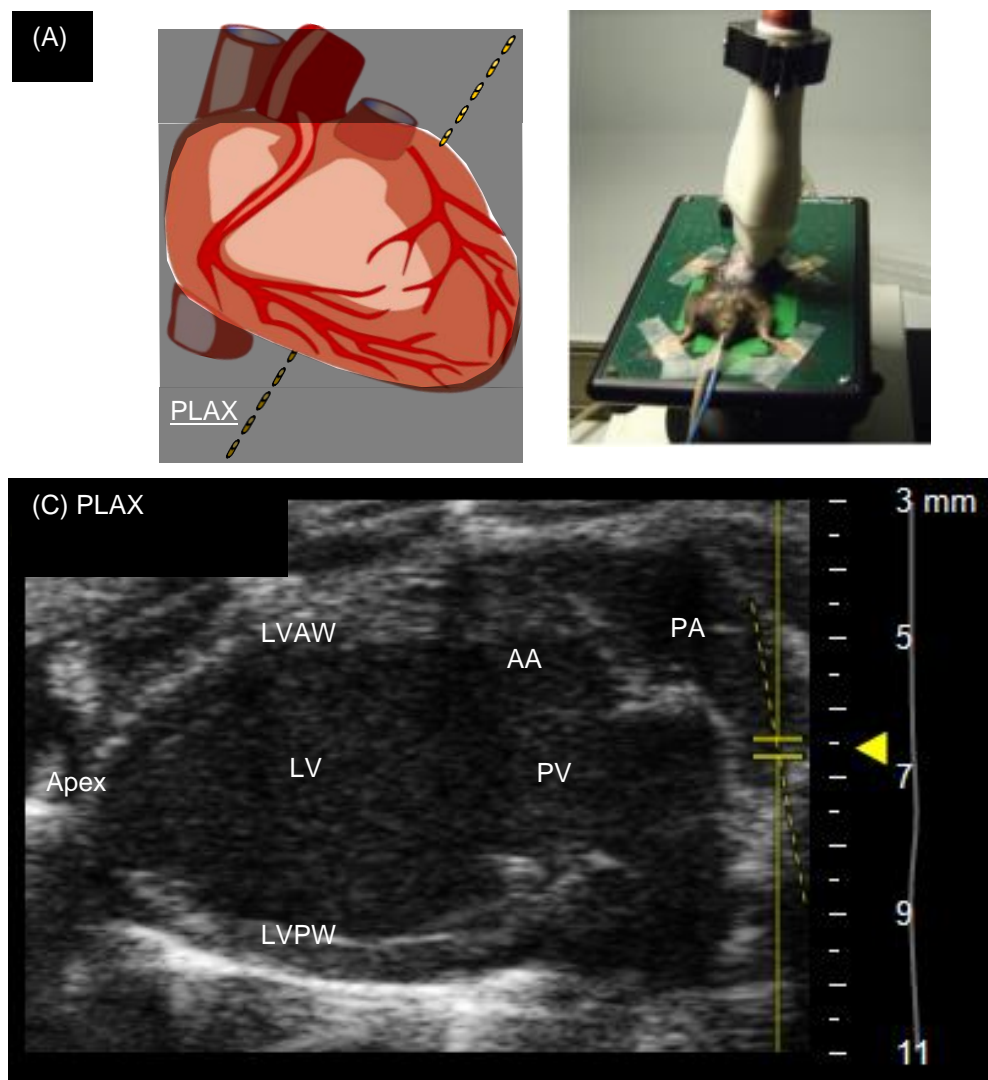


**Figure 10: Schematic, Positioning and B-mode Image Demonstrating the PLAX Cardiovascular Orientation.**

(A). Schematic demonstrating the PLAX cross-sectional area on a 3D-heart. The yellow line represents the axis which the M-mode trace is generated. (B). Transducer positioning for visualisation of a mouse PSAX. (C). PLAX B-mode image. The yellow line represents the axis which the pulmonary artery doppler flow is generated. Echocardiograms of eight-week-old C57Bl/6J mice were produced using a Vevo 2100 system with a 38 MHz MS400 transducer. Abbreviations: LV = Left ventricle, AW = anterior wall, PW = posterior wall, ID= Internal diameter. AA = ascending aorta, PA = pulmonary artery, PV = Pulmonary vein. Image (B) was taken from (VisualSonics, 2008b).

### **B-mode (Brightness mode) Imaging**

B-mode imaging produces two-dimensional cross-sectional images, entirely constructed of white dots (*Garbi et al., 2016*). Each dot represents a reflected ultrasound wave. Therefore, B-mode images are constructed of multiple ultrasound waves (**Figure 12**). The brightness of the dot represents the density of the structure from which the ultrasound wave is reflected. The brighter the dot, the higher the density of the structure. B-mode images offer excellent spatial resolution, allowing for detailed visualisation of anatomical features and abnormalities. For example, it can be used to quantify IVS wall thickness and aortic diameter (VisualSonics, 2008a).

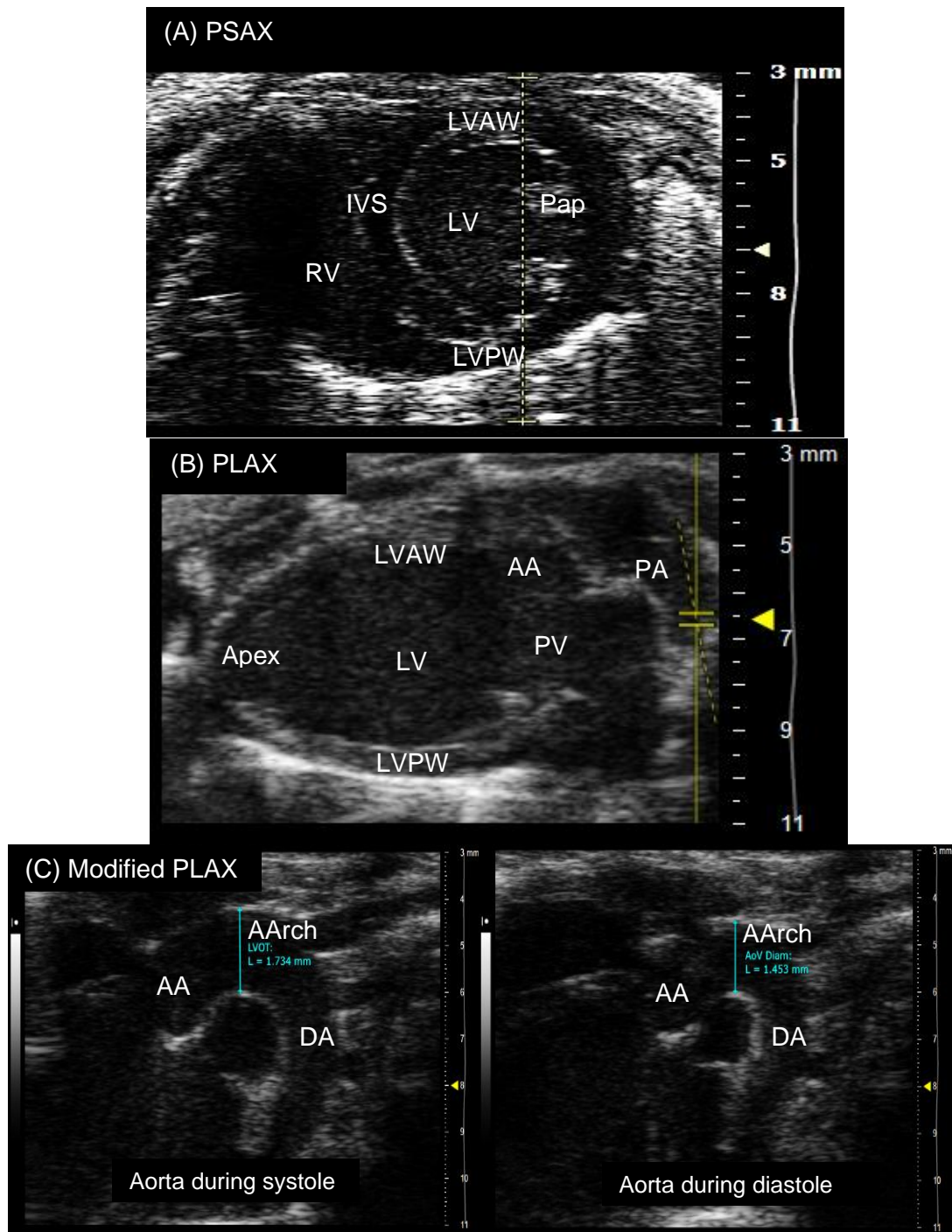


**Figure 11: Representative Mouse Cardiac B-mode Images.**

(A). Parasternal short axis (PSAX) B-mode image of the heart. (B). Parasternal long axis (PLAX) B-mode image of the heart. (C). Modified PLAX B-mode image of the aorta during systole (left) and diastole (right). Echocardiograms of eight-week-old C57Bl/6J mice were captured using a Vevo 2100 system with a 38 MHz MS400 transducer. The yellow line represents the axis which the M-Mode trace is generated. Abbreviations: LV = left ventricle, AW = anterior wall, PW = posterior wall, IVS= intraventricular septum, Pap = papillary muscle, RV = right ventricle. PA = pulmonary artery, PV = pulmonary vein, AA = ascending aorta, DA = descending aorta, AArch = aortic arch.

## M-Mode Imaging

For Motion Mode (M-mode) imaging, pulses of ultrasound waves are produced along a single axis. The pulses produce multiple B-mode images, which are linked together to create a live video, providing a one-dimensional representation of motion over time (**Figure 13**) (Garbi *et al.*, 2016). As the axis of the ultrasound beam remains the same, any movement within the area of focus would correlate with structural displacement. This displacement is detected as the structure moves in and out of focus of the single ultrasound beam. In the context of this thesis, M-Mode imaging in echocardiography was used to assess changes in left ventricle wall structure and function. As the left ventricle contracts and relaxes, displacements in left ventricular size and shape can be observed. These displacements enable calculations of systolic and diastolic function and dimensions, including ejection fraction, and changes in left ventricular wall thickness (anterior wall (LVAW) and posterior (LVPW)) (Lindsey *et al.*, 2018; VisualSonics, 2008a). M-mode imaging can, therefore, be used to evaluate any wall motion abnormalities of a diseased heart.

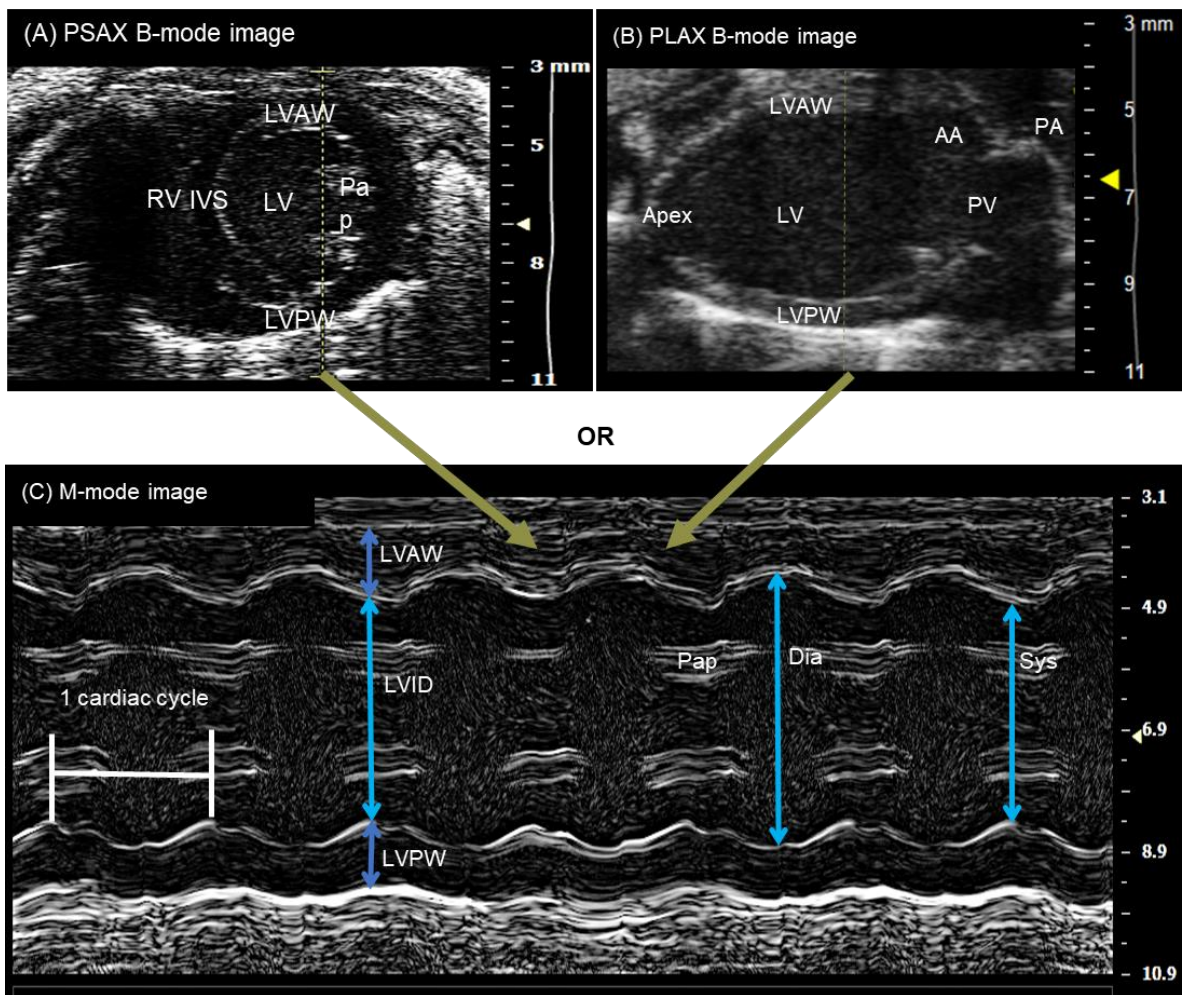


**Figure 12: Representative Mouse Cardiac M-mode Images.**

(A). Parasternal short axis (PSAX) B-mode image of the heart. (B). Parasternal long axis (PLAX) B-mode image of the heart. (C). M-mode image of the heart can be done from either PSAX or LSAX imaging. Echocardiograms of eight-week-old C57Bl/6J mice were produced using a Vevo 2100 system with a 38 MHz MS400 transducer. The yellow lines on (A) and (B) represent the axes from which the M-Mode trace (C) is generated. Abbreviations: LV = left ventricle, AW = anterior wall, PW = posterior wall, IVS= intraventricular septum, Pap = papillary muscle, RV = right ventricle, PA = pulmonary artery, PV = pulmonary vein, AA = ascending aorta, Dia = diastolic, Sys = systolic, ID = internal diameter. Adapted from (VisualSonics, 2008a).

## 3D Imaging

In recent years, technological advancements in medical imaging have led to improvements in cardiac echocardiography. Although not used in this thesis, one such innovation is three-dimensional (3D) echocardiography. Traditional two-dimensional (2D) echocardiography has long been a cornerstone of cardiac imaging. However, it has certain limitations, particularly for accurate visualisation and assessment of changes across the whole heart. As previously described, 2D echocardiography involves capturing 2D cross-sectional images of the heart in real time using ultrasound waves. 3D echocardiography combines multiple planes of 2D images to generate a live 3D model of the heart (Garbi *et al.*, 2016). So how does 3D echocardiography provide a more comprehensive assessment of cardiac anatomy? In 2D echocardiography, measurements of 2D cross-sectional images provide a perspective of the heart on a single plane. As the heart is a dynamic organ that constantly moves and changes shape throughout the cardiac cycle, this can lead to inaccuracies in measurements in a 2D plane. These inaccuracies are especially prevalent when the heart has irregular shapes or complex structures as a consequence of disease. 3D echocardiography, on the other hand, allows for gating of the heartbeat and creates a 3D image of the entire heart. This allows for a more precise quantification of parameters like cardiac volumes and ejection fraction, as well as dimensions such as volume and wall thickness (Garbi *et al.*, 2016). It accounts for the entire cardiac structure rather than a single cross-section, reducing errors associated with assumptions about shape and geometry. Capturing the entire heart with 3D echocardiography may enable the detection of any subtle abnormalities that 2D echocardiography may miss or even be able to identify these abnormalities earlier in their development. However, the time for echocardiography is greater for 3D echocardiography.

## Pulsed-Wave Döppler

Pulsed wave Döppler is widely used in sonography to assess blood flow in major vessels, such as the aorta, pulmonary artery, carotid arteries, renal arteries, and peripheral vessels (Garbi *et al.*, 2016). In this thesis, the focus was the pulmonary artery (**Figure 14A**) and the aorta (**Figure 14B**). Pulsed wave Döppler provides valuable information for diagnosing and monitoring cardiovascular conditions. Pulsed wave Döppler enables measurement of blood flow velocities at specific points along the vessel, enabling calculation of important hemodynamic parameters, such as peak velocity and the velocity time interval (VisualSonics, 2008a), so that researchers can identify any deviations from the norm.

Pulsed wave Döppler is highly effective in evaluating the presence and severity of stenosis or other obstructions within vessels (*Garbi et al., 2016*). Detecting these issues early is critical for diagnosis and ongoing monitoring of conditions that hinder blood flow.

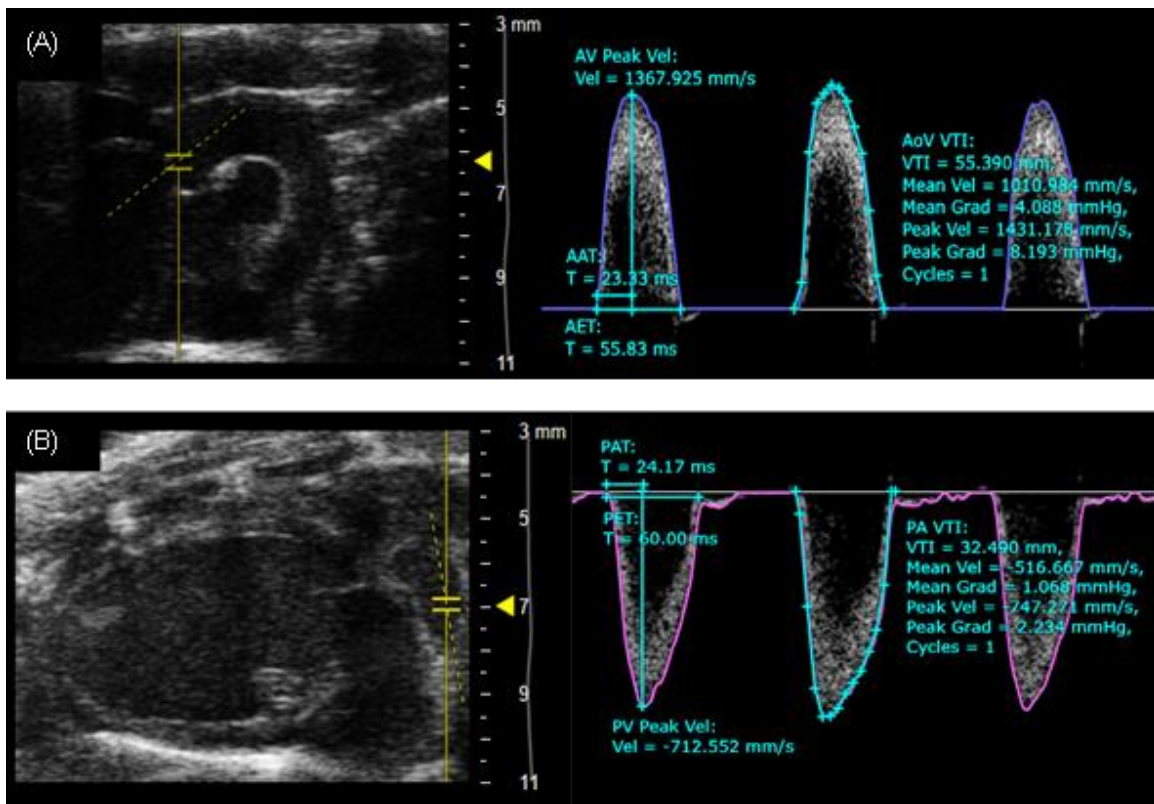


**Figure 13: Representative Analysis of Aorta and Pulmonary Artery Function.**

(A). Pulsed-wave Doppler trace assessing aortic blood flow. (B). A pulse wave Doppler trace assessing pulmonary artery blood flow. Echocardiograms of eight-week-old mice were obtained using a Vevo 2100 system. VevoLab analysis was used to assess the blood flow in the aorta and pulmonary artery and the effects of each treatment. The yellow dotted line represents the single ultrasound beam which generates the trace. Abbreviations: PA = pulmonary artery, AoV = aortic valve, VTI = velocity time interval of blood flow, PAT/AAT = pulmonary/aortic acceleration time, PET/AET = pulmonary/aortic ejection time. Adapted from (VisualSonics, 2008a).

## **Mitral Flow**

Although not used in this thesis, pulsed wave Döppler can be used to assess blood flow across the mitral valve (separating the left atrium and left ventricle of the heart) (Madalina Garbi *et al.*, 2016). Mitral flow provides an insight into the performance of the left ventricle's diastolic function, e.g. E-wave/A-wave ratio and mitral deceleration time (Kitzman & Little, 2012; Schirmer *et al.*, 2000). Efficient blood flow is essential for proper cardiac function, ensuring an adequate supply of oxygen-rich blood to be pumped out to the body. Therefore, an assessment of mitral flow can help evaluate the efficiency of ventricular filling and therefore identify any deviations in cardiovascular diseases, e.g., ischemia or heart failure (Madalina Garbi *et al.*, 2016).

## **Speckle-Tracking and Strain Analysis**

Speckle-tracking is an advanced echocardiographic method used to assess the deformation of cardiac structures (such as the myocardium) during each cardiac cycle (Garbi *et al.*, 2016). It relies on the identification and tracking of "speckles", unique patterns created within the cardiac tissue on interaction with ultrasound waves. As the heart contracts and relaxes during the cardiac cycle, these speckles move. The speckle-tracking technology precisely follows the displacement of these speckles over time (Kinno *et al.*, 2017). The quantitative measurement of this tissue deformation is known as strain, expressed as a percentage change in length. Strain assesses the extent to which the heart muscle stretches or contracts during each phase of the cardiac cycle, offering detailed information about both regional and global myocyte contractility during both diastole or systole (Garbi *et al.*, 2016). Speckle-tracking allows for the assessment of strain in multiple directions, including longitudinal, circumferential, and radial strain (Garbi *et al.*, 2016). Together, these techniques can detect subtle changes in myocardial mechanics, enabling early detection of myocardial dysfunction even before traditional measures of cardiac function are affected. This is because they provide a more comprehensive evaluation of myocardial function compared to conventional echocardiography. Speckle-tracking and strain analysis can be performed with 2D or 3D echocardiograms.

### **2.6.3 Echocardiography vs Magnetic Resonance Imaging**

Medical imaging plays a significant role in diagnosing and managing cardiovascular diseases. Two of the most commonly used imaging methods are echocardiography and

MRI, each offering distinct advantages. Both echocardiography and MRI play crucial roles in cardiovascular disease diagnosis and patient monitoring in a clinical setting (Phuah *et al.*, 2023) (Aimo *et al.*, 2021) (Kinno *et al.*, 2017). Both can also be used for preclinical assessment of cardiac function and dimensions.

Echocardiography has numerous advantages in comparison to cardiac MRI. Ultrasound equipment is much cheaper in comparison to MRI equipment. Echocardiography also has substantially lower maintenance and operational costs, which further reduces financial investment in running the equipment. This affordability makes echocardiography more accessible for medical facilities with lower financial support, particularly because it has more portability and can be deployed rapidly. This portability enables usage at the patient's bedside or in external hospital settings. For preclinical studies, echocardiography can be performed much quicker in the context of *in vivo* experiments. This reduces the time animals are under anaesthetic and therefore any complications which may arise from prolonged anaesthetic exposure (e.g. deteriorating thermoregulation, lung and cardiovascular function) (Tremoleda *et al.*, 2012). The speed of echocardiography does not compromise accuracy of the recorded data therefore can be used to reduce the duration of time for which animals are under anaesthesia.

MRI equipment is much larger, stationary and requires lengthy technical setup procedure. However, MRI has unhindered imaging capabilities compared with echocardiography which is limited due to photoacoustic interference with dense structures such as bone. Dense structures obscure acoustic access of the ultrasound waves to underlying tissue (the ultrasound waves are reflected off the dense structure, rather than passing through), preventing imaging of the underlying tissues (Grant *et al.*, 2021). However, for preclinical models, animals need to be anaesthetised for more prolonged periods of time for MRI and small animal MRI is vastly more expensive, requiring specialised facilities that are not available in all units.

## 2.7 Regulation of Cellular Responses

The studies presented in this thesis use mouse echocardiography to assess the roles of specific genes (Striatins in Chapter 3 and PKN2 in Chapter 4, respectively) or the effects of a small molecule inhibitor of protein kinases (the RAF inhibitor dabrafenib in Chapter 5) in cardiac hypertrophy resulting from AngII-induced hypertension. The context of the signalling is described in the publications in each of the chapters. The main scientific focus of my work was the Striatins (see **Chapter 1**), and these are explained in detail **below**, with brief summaries for the chapters on PKN2 (**Section 2.9.3**) and the dabrafenib (**Section 2.9.4**) projects.

### 2.7.1 Intra- and Inter-Cellular Signalling: General Concepts

Signalling pathways are dynamic networks of interconnected proteins and small molecules that enable cells to communicate, interpret, and respond to stimuli from their internal and external environments (Alberts *et al.*, 2002; Kotob, 2021). Signalling pathways play a fundamental role in regulating cellular processes. Without signalling pathways, essential processes such as cell growth, differentiation, metabolism, and apoptosis, would not be possible (Pan & Zhang, 2021). Conversely, deviations in signalling pathways are responsible for the pathogenesis of various diseases (Alberts *et al.*, 2002). Signalling pathways consist of four fundamental components: receptors, signalling molecules, transducers, and effectors (**Figure 15**) (Kotob, 2021). Receptors detect and bind to specific signalling molecules, known as ligands, which convey information from the intracellular or extracellular environment. Ligand-receptor interactions trigger a cascade of intracellular biochemical events, initiated by transducers that amplify the initial signal and regulate downstream signalling components. Finally, effectors execute the ultimate responses, translating the amplified signal into changes in gene expression, protein activity, cellular morphology, or metabolic processes (Alberts *et al.*, 2002; Kotob, 2021).

Protein kinases and phosphatases are essential for intracellular signalling, contributing to a diverse number of cellular processes essential for human physiology. The human kinome and phosphatome (all of the protein kinases/phosphatases encoded within the genome) consists of ~530 protein kinases (Bhullar *et al.*, 2018; Sergienko *et al.*, 2022) and ~200 phosphatases (Chen *et al.*, 2017; Sergienko *et al.*, 2022). Protein kinases phosphorylate proteins by transferring the gamma phosphate from adenosine triphosphate to the target protein. Protein phosphatases antagonise the effects of kinases, dephosphorylating their substrates producing inorganic phosphate. These post-

translational modifications alter protein conformation and, therefore, function. The effect depends on the residue's function within the target protein (Shchemelinin *et al.*, 2006) and can mediate/disrupt signal transduction and the generation of signalling cascades (Alberts *et al.*, 2002; Kotob, 2021). This affects fundamental processes including mRNA transcription and subsequent protein expression. The antagonistic role of kinases and phosphatases enables cellular signalling to be regulated to ensure the correct responses are generated from the initiating signalling molecules or stressors. Their importance in modulating signalling cascades means they must be tightly regulated. This includes phosphorylation/dephosphorylation by other kinases/phosphatases or themselves (i.e. autophosphorylation). There are three main types of eukaryotic kinases, serine/threonine (Ser/Thr) protein kinases, tyrosine (Tyr) protein kinases and dual-specificity kinases that can phosphorylate Ser/Thr and Tyr residues (Bhullar *et al.*, 2018).

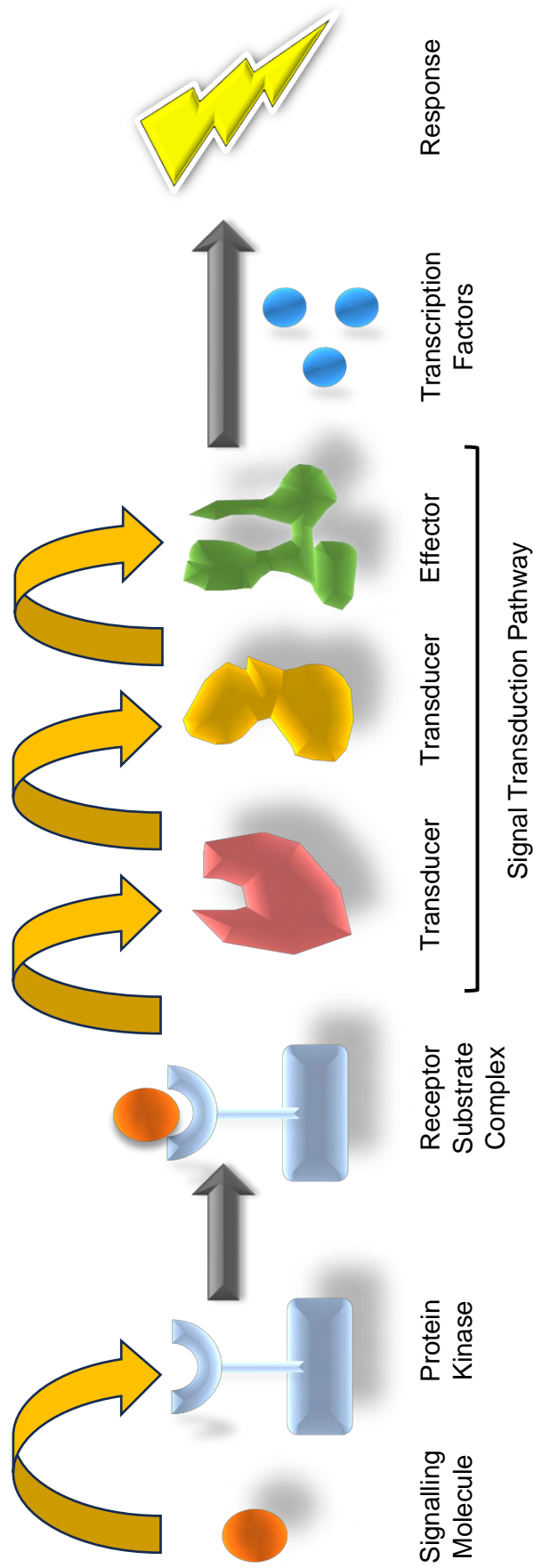


**Figure 14: A Representation of a Signalling Pathway.**

Each shape represents a protein involved in the signalling pathway. The final protein in this cascade (green), upon activation, interacts with transcription factors, which alter gene expression within the cell, ultimately producing the desired cellular response. The signalling pathway can consist of a wide variety and number of proteins, each capable of activating multiple downstream targets. This extensive chain reaction allows for a significant response to be produced from a single signalling molecule. Adapted from (Kotob, 2021).

## 2.7.2 Striatins, PP2A and STRIPAK Complexes

PP2A is a heterotrimeric Ser/Thr protein phosphatase, ubiquitously expressed in human cell types, which is responsible for a large proportion of eukaryotic phosphatase activity (Hwang & Pallas, 2014). The common residue targeting of PP2A is essential for intracellular signalling as it gives PP2A a broad substrate specificity, allowing influence over a diverse number of cellular functions. The structure of PP2A is comprised of structural (A), regulatory (B) and catalytic (C) subunits (Baskaran & Velmurugan, 2018; Moreno *et al.*, 2000). PP2A has a dimeric core consisting of PP2A<sub>A</sub> and PP2A<sub>C</sub>, which further complexes with PP2A<sub>B</sub> to form a heterotrimeric PP2A holoenzyme. PP2A<sub>B</sub> directs the dimeric core to specific substrates and/or required intracellular locations as well as regulates the activity of PP2A<sub>C</sub> (Gordon *et al.*, 2011). The holoenzyme provides variability upon association of the A and C subunits with B, producing unique characteristics and functions.

PP2A<sub>A</sub> is essential to establish the heterotrimeric complex in order to alter the catalytic activity of PP2A<sub>cat</sub>. This process occurs even in the absence of PP2A<sub>B</sub>. PP2A<sub>A</sub> and PP2A<sub>C</sub> each comprise of only two isoforms ( $\alpha$ ,  $\beta$ ) with sequence conservation within eukaryotes (Gordon *et al.*, 2011; Goudreault *et al.*, 2009). PP2A<sub>B</sub> is more heterogenic in comparison and is classified into four classes: B, B', B'' and B''', with at least 16 genes contributing to these subfamilies (Baskaran & Velmurugan, 2018; Hwang & Pallas, 2014). The striatin family of proteins comprise the fourth (B''') family, as they can bind to and alter the activity of the dimeric core in the absence of other B-type subunits (Gordon *et al.*, 2011; Moreno *et al.*, 2000). Therefore, the striatin family in complex with PP2A<sub>A</sub> and PP2A<sub>C</sub> are essential for targeting proteins to PP2A for dephosphorylation. Further modifications either post-translational or via accessory proteins, manipulate PP2A subunit association and activity.

The striatin family consists of striatin (Strn), Strn3 (originally referred to as S/G2 nuclear autoantigens or SG2NA) and Strn4 (also known as Zinedin) (Tanti *et al.*, 2023) (Hwang & Pallas, 2014). The striatin family are homologous, characterised by four protein-protein interacting domains: (1) the caveolin (CaV) binding domain, (2) a  $\text{Ca}^{2+}$ - calmodulin (CaM) binding domain, (3) a coiled-coil (C-C) domain and (4) a Tryptophan-Aspartate-repeat (WD) domain (Sanghamitra *et al.*, 2008) (**Figure 16**). In addition to forming the B''' subunit of PP2A, striatins form a hub for protein kinase signalling by interacting with a range of different proteins, thus forming **STR**iatin-**I**nteracting **P**hosphatase **A**nd **K**inase (**STRIPAK**)

complexes each complex having striatins at the core (**Figure 17**). STRIPAK complexes incorporates combinations of over 20 types of proteins from 10 protein families (**Table 3**), producing over 100 different variants (Goudreault *et al.*, 2009). The function of the STRIPAK complex is determined by the proteins comprising the complex (Tanti *et al.*, 2023). The functional diversity of the STRIPAK proteins indicates that the STRIPAK complex influences a variety of processes which contribute to maintain cardiac function. Therefore, it can be assumed that abnormalities in PP2A/STRIPAK core would disrupt usual cardiac function (Baskaran & Velmurugan, 2018; Hwang & Pallas, 2014; Nader, 2019; Sergienko *et al.*, 2022).

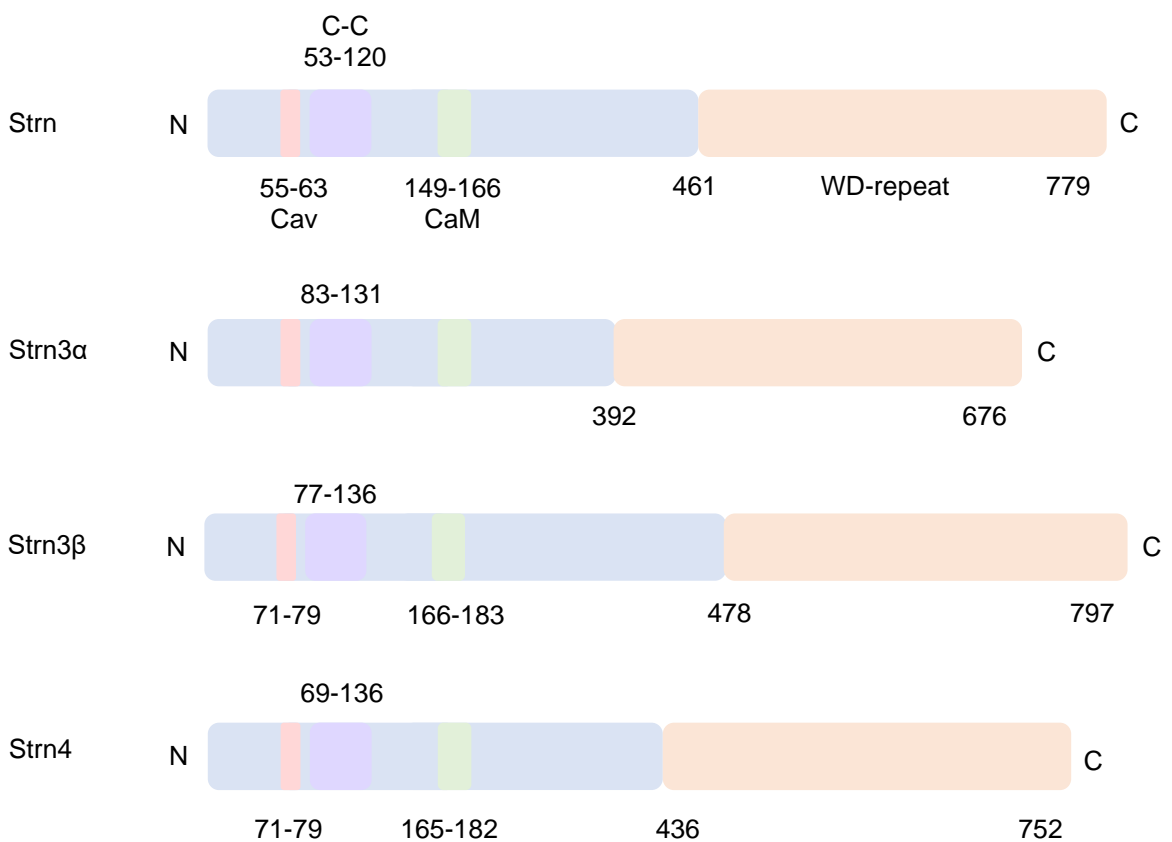
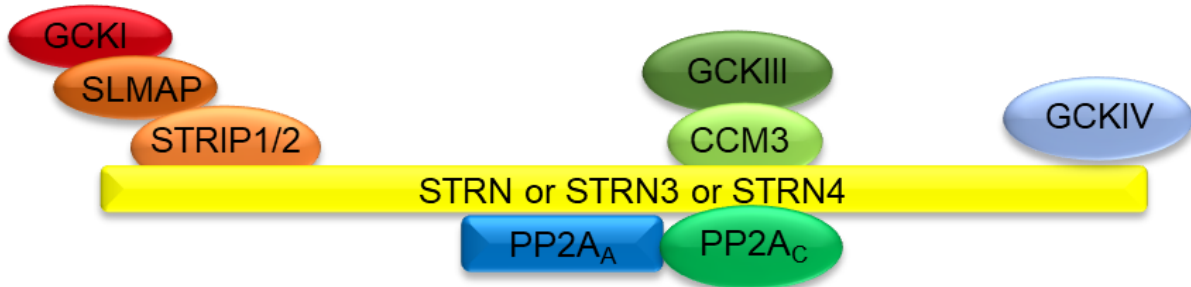


**Figure 15: The Gene Structure of the Striatin Family Proteins.**

The four highly conserved domains are annotated as follows: CaV = caveolin-binding domain, C-C = coiled-coil domain, CaM = calmodulin binding domain and the WD-repeat = Tryptophan-Aspartate-repeat domain. The data were obtained from Uniprot codes: O43815 = Strn, K7DCS6 = Strn3 alpha isoform, Q13033 = Strn3 Beta isoform, Q9NRL3 = Strn4 (UniProt Consortium., 2018). Adapted from (Hwang & Pallas, 2014).

### A. Activation



### B. Inhibition

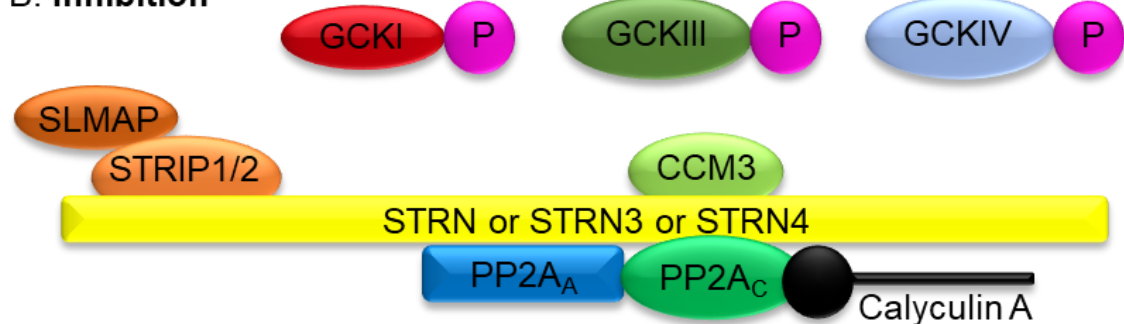


**Figure 16: STRIPAK Complexes and the Germinal Centre Kinase (GCK) Subfamilies.**

(A) Activated PP2A: Striatin family proteins associate with PP2A<sub>A</sub> and PP2A<sub>C</sub>, enabling dephosphorylation of the GCKs in complex with the striatins. GCKs are either bound with the striatins directly (e.g. GCKIV) or indirectly through adaptor proteins (e.g. GCKIII). (B). Inhibited PP2A: Inhibition of PP2A (e.g. by Calyculin A) or dissociation of GCK from the complex enables kinase autophosphorylation and activation of GCK. Adapted from (Goudreault *et al.*, 2009).

**Table 3: Components of the STRIPAK Complex**

Protein group	Protein name	Structural motif	Biological role
1	PP2A <sub>cα</sub>	Phosphatase catalytic	Multiple substrate protein dephosphorylation
	PP2A <sub>cβ</sub>	Phosphatase catalytic	Multiple substrate protein dephosphorylation
2	PP2A <sub>Aα</sub>	PP2A scaffold, HEAT repeats	Phosphatase scaffold
	PP2A <sub>Aβ</sub>	PP2A scaffold, HEAT repeats	Phosphatase scaffold
3	Striatin	Caveolin-binding, Ca2+-CaM-binding, C-C, WD-repeat	Scaffold protein which modulates numerous signalling pathways.
	Striatin 3	Caveolin-binding, Ca2+-CaM-binding, C-C, WD-repeat	Scaffold protein which modulates numerous signalling pathways.
	Striatin 4	Caveolin-binding, Ca2+-CaM-binding, C-C, WD-repeat	Scaffold protein which modulates numerous signalling pathways.
4	Mob3	Mob domain	Vesicular trafficking
5	STRIP1	Proline-rich	Cellular morphology and migration through mediating cytoskeletal organisation
	STRIP2	Poly-Leucine	
6	CTTNBP2NL	C-C, Proline rich	Regulating cytoskeletal organisation and transporter activity
	CTTNBP2	C-C, Proline rich	Regulates dendritic spine distribution
7	SLMAP	C-C, FHA, Leucine zipper, hydrophobic membrane anchor	Component of the cardiac sarcolemma associated

			with myoblast fusion and contraction
	TRAF3IP3	C-C	Modulates TRAF3-mediated JNK activation associated with stress response and apoptosis induction
8	SIKE	C-C	Negative regulator of the interferon pathway
	FGFR1OP2	C-C	Contributes to wound healing
9	CCM3	Lyase 2-enoyl-coa Hydratase, nucleotidyltransferases	Intermediate to stabilise GCKIII and therefore modulates GCKIII activity
10	MST3	Ste20 Kinase, Nuclear localisation signal, nuclear export signal	Serine/threonine kinase which promotes apoptosis in response to stress stimuli and caspase activation.
	YSK1	Ste20 Kinase	Oxidant stress-activated serine/threonine kinase that may play a role in the response to environmental stress
	MST4	Ste20 Kinase	Modulates apoptosis and cell growth

Table legend: The STRIPAK complex can be comprised of 20 different proteins from 10 different protein families, producing over 100 variants of the STRIPAK complex. This table lists the structural motifs and biological functions for each protein within the complex. This table was adapted from (Goudreault *et al.*, 2009).

The purpose of the STRIPAK complexes appears to bring PP2A into proximity of protein kinases to keep them in a dephosphorylated and inactivated form of the enzyme (Hwang & Pallas, 2014; Tanti *et al.*, 2023). Inhibition of PP2A (e.g. with an inhibitor such as Calyculin A) (Wakimoto *et al.*, 2002) or removal of either the kinase or phosphatase from the complex results in autophosphorylation and activation of the kinase that can then phosphorylate downstream substrates (Hwang & Pallas, 2014).

The best characterised of the striatin-regulated kinases belong to the Germinal Center Kinase superfamily (GCKs) (Hwang & Pallas, 2014). These are a family of 22 Ser/Thr kinases composed of two domains: a conserved catalytic domain and a variable regulatory domain. The regulatory domain is divided into eight subcategories, and the STRIPAK complex predominantly interacts with GCKIII and GCKIV. GCKs are involved in cellular survival/apoptosis and proliferation (Deloire, 2009). This suggests that they may play a role in the hypertrophic response and heart failure. However, the mechanisms of regulation and function of GCKs in cardiac myocytes are poorly understood, especially in the context of heart failure aetiology.

The best characterised interaction between the Striatins and GCKs is the interaction of GCKIII with Strn and Strn3. GCKIII interacts with Strn and Strn3 using cerebral cavernous malformation 3 (CCM3) as an intermediate to stabilise GCKIII (Gordon *et al.*, 2011; Goudreault *et al.*, 2009; Kean *et al.*, 2011). PP2A then dephosphorylates residues such as Thr<sup>178</sup> within the activation loop of MST3, inactivating MST3 (Gordon *et al.*, 2011). PP2A inhibition (e.g. by Calyculin A), or the modulation of STRIPAK components, causes MST3 to dissociate and become activated (**Figure 17**). This occurs through autophosphorylation of Thr<sup>178</sup> within the catalytic domain followed simultaneously by cis-autophosphorylation of Thr<sup>328</sup> within the regulatory domain of MST3 (Fuller *et al.*, 2012).

Other interactions of STRIPAK members with the striatin family are less well-characterised. GCK activity is regulated within the STRIPAK complex by PP2A dephosphorylation through various protein interactions (Hwang & Pallas, 2014). For example, Strn4 has been shown to directly associate with GCKIVs. GCKIs, through sarcolemmal membrane-associated protein (SLMAP) intermediates, can target any of the Striatins. GCKIIIs and GCKIVs have been demonstrated to interact with the Striatins through associations with CTTNBP2NL (cortactin-binding protein 2 (CTTNBP2) N-terminal-like). STRIPAKs have also been demonstrated to be involved in the Hippo (Kuck *et al.*, 2019; Ma *et al.*, 2019), MAPK/ERK (Shi *et al.*, 2016), cytoskeletal (Fletcher &

Mullins, 2010) (Charrin & Alcover, 2006) and the oestrogen receptor pathways (Fuentes & Silveyra, 2019; Shi *et al.*, 2016).

As within many organ systems, there is a limited understanding on the role of the striatin family and the STRIPAK complex in the heart. Evidence for STRIPAK and cardiac disease was demonstrated first when the striatin gene was identified within one of 22 loci correlating with recurrent variants of cardiac ventricular conduction and QRS interval length (Sotoodehnia *et al.*, 2010). This association correlated with findings from Meurs *et al.*, 2010 who identified an 8 base-pair deletion that decreased Strn mRNA in Boxer dogs. This mutation increased the risk of developing arrhythmogenic right ventricular cardiomyopathy (ARVC) (Meurs *et al.*, 2010) and dilated cardiomyopathy (Meurs *et al.*, 2013). ARVC and sudden cardiac death commonly presents with a prolonged QRS interval, the condition which the mutated Strn isoform is associated.

Nader *et al.*, 2012 demonstrated that Strn interacts with caveolin-3 and calmodulin in the presence of  $\text{Ca}^{2+}$  to mediate spontaneous contraction rate of cultured cardiac myocytes (Nader *et al.*, 2012). Strn is localised to the intercalated discs (Meurs *et al.*, 2010) where it may influence cardiac contractility and intercellular communication. Nader *et al.*, 2017 found that Strn overexpression increased the spontaneous contraction rate of cultured cardiac myocytes 2-fold, whilst knockout Strn decreased contraction rate by 40% from the control (Nader *et al.*, 2017). This demonstrates that Strn plays a significant role in moderating cardiomyocyte contraction rate and could be considered as a therapeutic treatment for cardiac arrhythmias.

Heterozygote knockdown of Strn (Strn $^{+/-}$ ) in mice causes a significant increase in salt-dependent hypertension in comparison to wild-type mice (Garza *et al.*, 2015). A single nucleotide polymorphism (rs2540923) human Strn is also linked to salt-sensitive hypertension, correlating with the relationship identified in mice (Garza *et al.*, 2015; Gholami *et al.*, 2024; Gupta *et al.*, 2017). Strn $^{+/-}$  mice are more sensitive to aldosterone-induced injury, but the Strn $^{+/-}$  mice showed no significant modification of aldosterone mediated cardiac and kidney damage when compared to their wild-type littermates (Garza *et al.*, 2020). A clinical trial (Stone *et al.*, 2021) has recruited for a study investigating the effect of a mineralocorticoid receptor antagonist on blood pressure in participants with the Striatin rs2540923 SNP (i.e. the SNP identified previously (Garza *et al.*, 2015)).

There appear to be no current studies published so far that have assessed the effect of Strn3 on the heart. However, Strn3 is an important regulator in endoplasmic reticulum

homeostasis, preventing cellular damage from oxidative stress and promoting cellular survival. Depletion of Strn3 promotes cell death in BALB/c mice in response to endoplasmic reticulum stress (Jain *et al.*, 2017). Previous investigations have correlated increased endoplasmic reticulum stress with cardiac hypertrophy and heart failure (Wang *et al.*, 2018). Therefore, it can be predicted that Strn3 may play a role in this process.

Many of the other components of the STRIPAK complex are associated with cardiac dysfunction (Hwang & Pallas, 2014). This includes SLMAP, STRIP2, CCM3 and MAP4K4. SLMAP has many functions within the heart and heart disease, including organisation of the excitation-contraction coupling complex, recruitment of STRIPAK components and in the pathology of Brugada syndrome (Antzelevitch & Patocskai, 2016; Guzzo *et al.*, 2005; Ishikawa *et al.*, 2012). STRIP2 knockdown in zebrafish causes structural heart defects including ventricular stagnancy, an enlarged atrium and vascular defects (Wagh *et al.*, 2014). The studies also found associations with a reduction in STRIP2 expression with a reduction of cardiac myosin light chain 2 and ventricular heavy chain expression. Mutations within CCM3 have been associated with cerebral cavernous malformation, a disorder associated with cardiac dysfunction (Kean *et al.*, 2011; Retta & Glading, 2016). MAP4K4 is regulated by STRIPAK complexes within cardiomyocytes. This regulation was shown to influence the cytoskeletal dynamics, adhesion, differentiation and migration of the cell. MAP4K4 may contribute to cardiac dysfunction when these systems go awry (Fuller *et al.*, 2021; Kim *et al.*, 2020; Nicholls, 2019; Seo *et al.*, 2020).

### 2.7.3 PKN2 in the Heart

The PKN (Protein Kinase N) family of Ser/Thr kinases is a subset of the protein kinase C (PKC) superfamily. These kinases have an N-terminal regulatory domain and a C-terminal catalytic domain and interactions between the N- and C-terminal regions maintains the enzyme in an inactive form (Sophocleous *et al.*, 2021). Unlike some other PKCs, the three PKN isoforms (PKN1, PKN2, and PKN3) are not regulated by diacylglycerol or  $\text{Ca}^{2+}$ . PKN activation is tightly regulated by the Rho GTPase family of proteins, RhoA, RhoB, and RhoC. PKNs are activated by binding GTP-bound Rho proteins to its Rho-binding domain. This binding causes a conformational change, activating it by exposing its catalytic domain. Activated PKNs phosphorylate various downstream targets, such as myosin light chain kinase (MLCK), microtubule-associated proteins (MAPs), and transcription factors. These phosphorylation events modulate cellular processes such as cell motility, cytoskeleton dynamics, and gene expression. However, despite many years of investigation, the details of PKN regulation and roles remain to be determined.

Of the PKNs, only PKN2 is embryonic lethal (Danno *et al.*, 2017). Homozygous PKN1 or PKN3 knockout mice are viable and fertile with no overt abnormalities. Heterozygous PKN2 knockout mice also appear normal, but homozygous PKN2 knockout mice die at embryonic day E10.5 with cardiac defects indicating that PKN2 plays a significant role in the development of the heart (as shown in Chapter 4). The publication shown in **Chapter 4** demonstrated that, although PKN2 may not be required for functioning of the adult heart, it is required for the heart to respond to a pathophysiological stress such as hypertension.

#### 2.7.4 The ERK1/2 Pathway and its Inhibitors

The ERK1/2 pathway (**Figure 18**) plays a pivotal role in regulating cell proliferation, differentiation, and survival (Lavoie *et al.*, 2020). As a consequence, the ERK1/2 pathway is a key target for cancer (Ali *et al.*, 2022; Lavoie *et al.*, 2020; Marampon *et al.*, 2019). Anti-cancer drugs have been or are being developed to target each component of the pathway with small molecule inhibitors of the small G protein Ras and the key protein kinases of the pathway (RAF, MEK1/2 and ERK1/2).

Classically, the pathway is initiated by the binding of a peptide growth factor such as epidermal growth factor (EGF) to its receptor, the EGF receptor (EGFR), leading to the autophosphorylation of the tyrosine kinase domain of the receptor (**Figure 18A**). This phosphorylation event creates docking sites for proteins like growth factor receptor-bound protein 2 (GRB2), which contain Src homology 2 (SH2) domains capable of binding to the phosphotyrosine residues on the activated receptor (Zarich *et al.*, 2006). Once bound, GRB2 brings SOS (son of sevenless), a guanine nucleotide exchange factor (GEF) to the membrane. SOS catalyses the removal of guanosine diphosphate (GDP) from a member of the rat sarcoma protein (Ras) subfamily (e.g., H-Ras or K-Ras) (**Figure 18B**). This enables the binding of guanosine triphosphate (GTP) to Ras, activating the protein (**Figure 18C**).

Activated Ras then initiates a downstream signalling cascade by recruiting RAF (rapidly accelerated fibrosarcoma) kinase to the membrane for phosphorylation and activation (**Figure 18D**) (Avruch *et al.*, 2001). RAF kinase subsequently phosphorylates and activates the mitogen-activated protein kinase kinase 1/2 (MEK1 and MEK2) (**Figure 18E**). MEK, in turn, phosphorylates and activates extracellular signal-regulated kinase 1/2 (ERK1/2) (**Figure 18F**). Activated ERK1/2 translocates to the nucleus, where it

phosphorylates and regulates the activity of various transcription factors such as Myc, Fos, Elk, and Ets (**Figure 18G**) (Ali *et al.*, 2022; Kong *et al.*, 2019; Lavoie *et al.*, 2020; Plotnik *et al.*, 2014; Sears *et al.*, 2000; Tanos *et al.*, 2005). This phosphorylation modulates the transcriptional activity of these factors, ultimately influencing the expression of genes involved in cell proliferation, differentiation, and survival.

Vemurafenib, dabrafenib, and encorafenib are all approved anti-cancer therapies that target RAF kinases (Bahar *et al.*, 2023; Maik-Rachline *et al.*, 2018). These therapies are generally used in combination with a MEK1/2 inhibitor (e.g. dabrafenib is used with trametinib) (Ullah *et al.*, 2022). However, the ERK1/2 cascade is also important in cardiac development and in cardiac pathology (Gallo *et al.*, 2019), raising the question of the effects of the anti-cancer drugs that target the pathway on cardiac function, and whether they may be cardiotoxic.

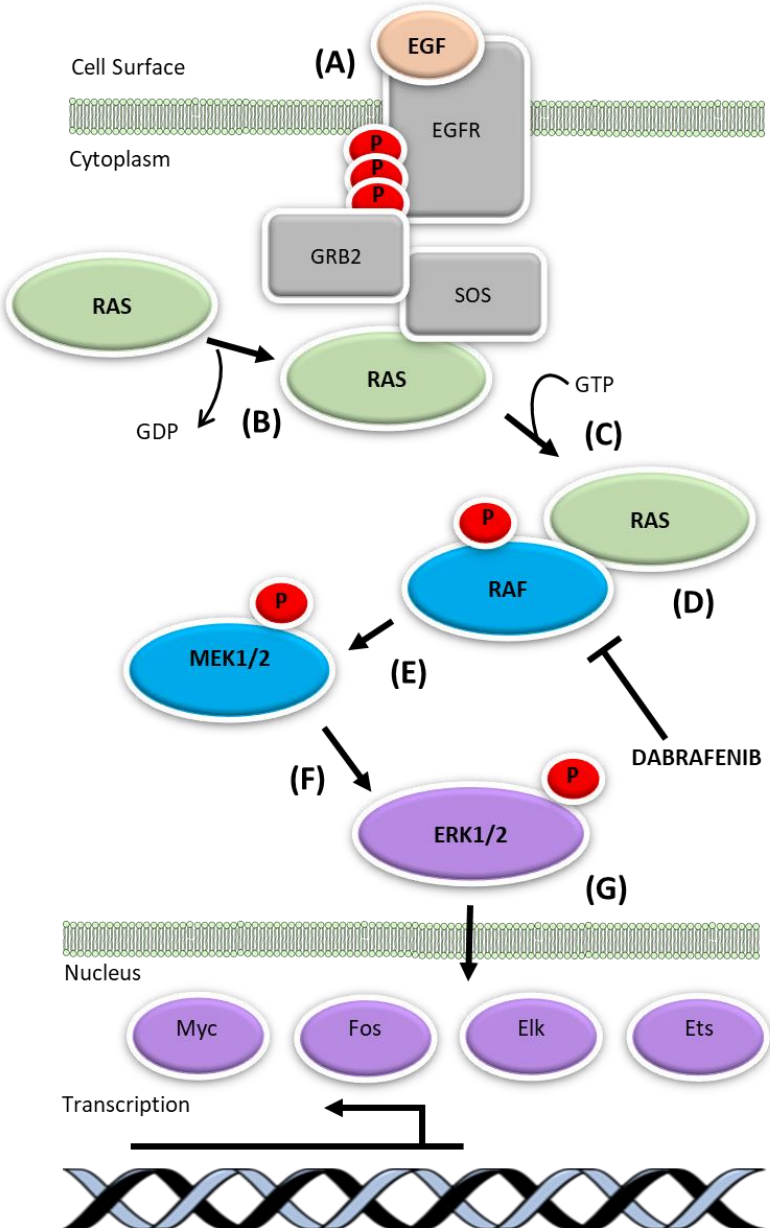


**Figure 17: Activation of the ERK1/2 Signalling Pathway by EGF.**

(A). EGF binds EGFR causing autophosphorylation of the associated tyrosine kinase. (B). Activated SOS then promotes the removal of GDP from Ras. (C). Ras binds GTP and becomes activated. (D). Activated Ras recruits RAF for phosphorylation. (E). RAF phosphorylates and activates MEK1/2. (F) MEK1/2 phosphorylates and activates ERK1/2. (G). ERK translocates into the nucleus where it regulates the activities of several transcription factors. Dabrafenib targets BRAF but inhibits all RAF isoforms (ARAF, BRAF and RAF1). Abbreviations: EGFR, epidermal growth factor receptor; GRB2, growth factor receptor-bound protein 2; SOS, son of sevenless; MEK, mitogen-activated protein kinase kinase; ERK, extracellular signal-regulated kinase. Adapted from (Lavoie *et al.*, 2020).

## **Chapter 3 - Striatin plays a major role in angiotensin II-induced cardiomyocyte and cardiac hypertrophy in mice *in vivo*.**

**Title:** Striatin plays a major role in angiotensin II-induced cardiomyocyte and cardiac hypertrophy in mice *in vivo*.

**Authors:** Cull JJ, Cooper STE2, Alharbi HO, Chothani SP, Rackham OJL, Meijles DN, Dash PR, Risto Kerkelä, Ruparelia N, Sugden PH, Clerk A.

**Contributions:** J.J.C. was responsible for and conducted the breeding for the experiments with the STRN<sup>+/−</sup> and STRN3<sup>+/−</sup> mice, and the echocardiography and analysis. H.O.A. assisted with these experiments. Studies with mice for cardiomyocyte knockout of STRN were conducted by J.J.C and S.T.E.C. S.P.C and O.J.L.R were responsible for the analysis of RNASeq data from dilated cardiomyopathy patients compared with normal controls. P.H.S., N.R, R.K and P.R.D. assisted with writing and reviewing the manuscript. P.H.S. and A.C. initiated the studies. A.C. obtained funding, designed the experiments and wrote the manuscript.

**DOI:** <https://doi.org/10.1042/CS20240496>

Research Article

# Striatin plays a major role in angiotensin II-induced cardiomyocyte and cardiac hypertrophy in mice *in vivo*

Joshua J. Cull<sup>1</sup>, Susanna T.E. Cooper<sup>2,\*</sup>, Hajed O. Alharbi<sup>1,†</sup>, Sonia P. Chothani<sup>3</sup>, Owen J.L. Rackham<sup>3,4</sup>,  
Daniel N. Meijles<sup>2</sup>, Philip R. Dash<sup>1</sup>, Risto Kerkelä<sup>5</sup>, Neil Ruparelia<sup>1,6</sup>, Peter H. Sugden<sup>1</sup> and Angela Clerk<sup>1</sup>

<sup>1</sup>School of Biological Sciences, University of Reading, Reading, U.K.; <sup>2</sup>Molecular and Clinical Sciences Institute, St. George's University of London, London, U.K.; <sup>3</sup>Program in Cardiovascular and Metabolic Disorders, Duke-National University of Singapore Medical School, Singapore; <sup>4</sup>School of Biological Sciences, University of Southampton, Southampton, U.K.; <sup>5</sup>Research Unit of Biomedicine and Internal Medicine, Medical Research Centre Oulu (Oulu University Hospital) and Biocenter Oulu, University of Oulu, Oulu, Finland; <sup>6</sup>Department of Cardiology, Royal Berkshire Hospital, Reading, U.K.

Correspondence: Angela Clerk (a.clerk@reading.ac.uk)



The three striatins (STRN, STRN3, STRN4) form the core of **STR**iatin-**I**nteracting **P**hosphatase and **K**inase (STRIPAK) complexes. These place protein phosphatase 2A (PP2A) in proximity to protein kinases thereby restraining kinase activity and regulating key cellular processes. Our aim was to establish if striatins play a significant role in cardiac remodelling associated with cardiac hypertrophy and heart failure. All striatins were expressed in control human hearts, with up-regulation of STRN and STRN3 in failing hearts. We used mice with global heterozygote gene deletion to assess the roles of STRN and STRN3 in cardiac remodelling induced by angiotensin II (AngII; 7 days). Using echocardiography, we detected no differences in baseline cardiac function or dimensions in STRN<sup>+/−</sup> or STRN3<sup>+/−</sup> male mice (8 weeks) compared with wild-type littermates. Heterozygous gene deletion did not affect cardiac function in mice treated with AngII, but the increase in left ventricle mass induced by AngII was inhibited in STRN<sup>+/−</sup> (but not STRN3<sup>+/−</sup>) mice. Histological staining indicated that cardiomyocyte hypertrophy was inhibited. To assess the role of STRN in cardiomyocytes, we converted the STRN knockout line for inducible cardiomyocyte-specific gene deletion. There was no effect of cardiomyocyte STRN knockout on cardiac function or dimensions, but the increase in left ventricle mass induced by AngII was inhibited. This resulted from inhibition of cardiomyocyte hypertrophy and cardiac fibrosis. The data indicate that cardiomyocyte striatin is required for early remodelling of the heart by AngII and identify the striatin-based STRIPAK system as a signalling paradigm in the development of pathological cardiac hypertrophy.

\*Present address: Institute of Developmental and Regenerative Medicine, Department of Physiology, Anatomy and Genetics, University of Oxford, Oxford, U.K.

†Present address: Department of Medical Laboratory, College of Applied Medical Sciences, Quassim University, Buraydah, Saudi Arabia.

Received: 18 March 2024

Revised: 07 May 2024

Accepted: 08 May 2024

Version of Record published:  
00 xx 00

## Introduction

The development of heart failure is associated with significant morbidity and a poor prognosis despite optimal medical therapy. It affects millions of people worldwide [1]. A leading cause of heart failure is hypertension that affects ~30% of all adults [1,2]. Whilst the identification of patients suffering from hypertension and their management has significantly improved in recent years, a number of patients present acutely with end-organ damage or progress to complications of hypertension in spite of maximal therapy. Broader therapeutic options for individual patients to manage hypertensive heart disease are clearly needed, but this requires greater understanding of the underlying mechanisms. Striatin (STRN) is associated with salt-dependent hypertension in mice. Thus, mice that are heterozygotic for STRN gene deletion have a similar blood pressure profile to wild-type littermates when provided with a low salt diet, but have a greater increase in blood pressure with higher dietary salt [3]. This probably results from effects

in endothelial cells and enhanced vasoconstriction [4]. These mice also have increased renal damage in response to aldosterone [5]. Further evidence for a role for STRN in heart failure comes from boxer dogs with arrhythmogenic right ventricular cardiomyopathy (ARVC) and heart failure, resulting from an 8 bp deletion in the 3'UTR of STRN and reduced STRN expression [6,7]. In humans, SNPs in the STRN gene are linked to blood pressure regulation [3,8,9], PR/QRS interval [10,11], hypertrophic cardiomyopathy [12] and heart failure [13]. SNPs in a second isoform, striatin 3 (STRN3, also known as SG2NA) are also linked to hypertension [14]. STRN, STRN3 and the third isoform, STRN4, are all expressed in the heart. Understanding the roles of these proteins may increase therapeutic options in patients with hypertension to both reduce the risk and to manage the development of heart failure complications.

The heart mainly contains contractile cardiomyocytes, endothelial cells in the capillary network and fibroblasts producing extracellular matrix [15]. Since adult mammalian cardiomyocytes are terminally-differentiated, they respond to increased cardiac workload (e.g., resulting from hypertension) with hypertrophic growth to increase contractile function [16]. The increase in cell size is associated with increased contractile apparatus and changes in gene expression (e.g., up-regulation of *Myh7*, *Nppa* and *Nppb* mRNAs). Cardiomyocytes may undergo necrosis or programmed cell death in situations of extreme or prolonged stress, compromising cardiac function and leading to heart failure [17]. Loss of endothelial cells and capillary rarefaction is another feature of developing heart failure [18], along with increased fibrosis in the myocardium (interstitial fibrosis) that compromises cardiac function by increasing ventricular wall stiffness, and around the arterioles (perivascular fibrosis) [19,20]. Fibrosis is associated with increased numbers of myofibroblasts which may derive from activation of resident fibroblasts or other cardiac cells (e.g., endothelial cells may undergo endothelial to mesenchymal transition and increase numbers of myofibroblasts) [21,22].

Cellular changes associated with cardiac remodelling are regulated by protein phosphorylation/dephosphorylation. Whilst much is known about protein kinase signalling cascades, specific roles of phosphatases and dephosphorylation are less well understood. The Ser-/Thr- phosphatase PP2A is highly abundant and ubiquitously expressed [23]. It is formed of one of two catalytic subunits (PP2A<sub>C</sub>), one of two regulatory subunits (PP2A<sub>A</sub>) and one of many targeting 'B' subunits that direct PP2A to its substrates. Striatins form a class of B subunits (B<sup>'''</sup>) for PP2A, but also interact with protein kinases, particularly those of the Germinal Centre Kinase (GCK) family [24]. Because of this, striatin-based complexes have been termed *STRiatin-Interacting Phosphatase and Kinase* (STRIPAK) complexes [25,26]. This system places GCKs in close proximity to PP2A which maintains the kinase in a dephosphorylated (inactive) state. Inhibition of PP2A or removal of the phosphatase or kinase results in kinase activation, most probably through autophosphorylation. Striatins have an N-terminal domain that binds caveolins, potentially directing them to the plasma membrane and a Ca<sup>2+</sup>/calmodulin-binding domain. A coiled-coil domain and C-terminal WD repeats facilitate binding of other proteins. Interactome studies have identified many proteins in STRIPAK complexes, some of which probably direct different complexes to different subcellular targets and/or subdomains [27–29]. Striatins, GCKs and STRIPAKs regulate a diverse array of cellular processes including cell survival/proliferation/migration, key features of cardiac remodelling. As described above, STRN is linked to various forms of heart failure and conductance irregularities. Consistent with the latter, STRN is of significant importance in composite junctions between cells, and immunostaining experiments place STRN at intercalated discs between cardiomyocytes, potentially regulating ion fluxes between cells [6,30].

Our hypothesis is that STRIPAKs play a significant role in cardiac remodelling associated with developing heart failure. Here, we show that STRN, STRN3 and STRN4 are all dysregulated in human failing hearts compared with normal controls, with up-regulation of STRN and STRN3. Our data in mouse models with heterozygote knockout of STRN and STRN3 identified STRN, but not STRN3, as a potential mediator of the early phase of cardiac remodelling (i.e., prior to heart failure development and cardiac dysfunction) induced by developing hypertension in mice resulting from angiotensin II (AngII) infusion. Further studies using mice with inducible cardiomyocyte-specific STRN deletion confirmed that cardiomyocyte striatin plays a key role in this early remodelling phase.

## Methods

### Ethics statement

#### Human heart samples

Human heart samples were from the University of Pittsburgh, U.S.A. Failing human heart samples were from patients who consented to a protocol reviewed and approved by the University of Pittsburgh Institutional Review Board. Non-failing heart samples were collected under University of Pittsburgh CORID #451 (Committee for Oversight of Research and Clinical Training Involving Decedents) and with consent being obtained by the local Organ Procurement Organization (OPO), CORE (Center for Organ Recovery and Education).

## Mouse studies

Mice were housed at the BioResource Unit at University of Reading (colonies for STRN and STRN3 global knockout) or St. George's University of London (colonies for cardiomyocyte-specific deletion of STRN), both UK registered with a Home Office certificate of designation. Procedures were performed in accordance with UK regulations and the European Parliament Directive 2010/63/EU for animal experiments. All work was undertaken in accordance with local institutional animal care committee procedures at the University of Reading and the U.K. Animals (Scientific Procedures) Act 1986. Studies were conducted under Project Licences 70/8248, 70/8249 and P8BAB0744.

## Studies of striatin isoforms in human hearts

mRNA expression of *STRN* (ENSG00000115808), *STRN3* (ENSG00000196792) and *STRN4* (ENSG00000090372) was determined using a previously published RNASeq dataset derived from left ventricular samples of patients with end-stage dilated cardiomyopathy ( $n=97$ ) taken at the time of transplantation or left ventricular assist device implantation, compared with non-diseased controls ( $n=108$ ) [31]. Differential expression analysis was performed with DESeq2 (V1.18.1, Wald test) [32].

Human heart samples used in this study were previously used to study RAF kinases [33]. Transmural tissue at the level of the anterior papillary muscle was collected at the time of cardiac transplantation from the left ventricle of end-stage heart failure patients. Samples were collected in the operating room and transported in ice-cold St. Thomas' cardioplegia solution, flash frozen within 20 min of excision, and stored at  $-80^{\circ}\text{C}$  prior to utilisation. Control left ventricular tissues were collected from hearts that were rejected for transplant for varying reasons. Tissues were collected and stored in a similar manner as the failing hearts, with between 20 and 45 min of time elapsing between cross-clamp and freezing of the tissue. Hearts were ground to powder under liquid  $\text{N}_2$ , and samples taken for RNA and protein preparation as described below.

## Animal husbandry and randomisation

Housing conditions were as described in [33,34]. Animals were checked daily and breeding was conducted with mice between 6 weeks and 8 months with a maximum of 6 litters per female. Mice undergoing procedures were monitored using a score sheet and routinely culled if they reached a predefined endpoint agreed with the Named Veterinary Surgeon. Weights were taken before, during and at the end of the procedures. Mouse weights from the start and end of procedures are provided in Supplementary Table S1. These studies used only male mice because of the intention to convert the line for conditional gene deletion using tamoxifen (see below), an approach which has not been fully characterised for female mice. Furthermore, our recent studies of inducible deletion of BRAF indicated that males and females responded very differently to this regime [35]. Mice were allocated to specific groups on a random basis with randomisation performed independently of the individual leading the experiment. Four mice receiving AngII that died and all data for these were excluded from analysis (one wild-type from the STRN colony that died on day 2, two *STRN*<sup>fl/fl</sup>/Cre<sup>MCM/−</sup> mice treated with corn-oil that died on day 7 and one *STRN*<sup>fl/fl</sup>/Cre<sup>MCM/−</sup> mouse treated with tamoxifen that died on day 7). Post-mortem analysis showed rupture of a major blood vessel in all cases. Otherwise, no mice were excluded after randomisation. Individuals conducting the studies were not blinded to experimental conditions for welfare monitoring purposes. Data and sample analysis (e.g., echocardiography and histology) was performed by individuals who were blinded to intervention.

## Mouse lines and gene deletion strategy

Mice for STRN or STRN3 knockout were from the Knockout Mouse Project (KOMP). Both lines ("Knockout first" *STRN*<sup>tm1a(KOMP)WTsi</sup> and *STRN3*<sup>tm1a(KOMP)WTsi</sup>) were on a C57Bl/6N background and, following resuscitation, were backcrossed with C57Bl/6J mice (Charles River Laboratories) for at least eight generations prior to experimentation and sperm preservation (at the Mary Lyon Centre, MRC Harwell, UK). Colonies were maintained as heterozygotes with ongoing breeding with C57Bl/6J mice to generate heterozygote and wild-type (WT) littermates for experiments (N.B. Global homozygous knockout of any striatin isoform is embryonic lethal).

*Myh6*-MERCeMER mice expressing tamoxifen-inducible Cre recombinase under control of a mouse *Myh6* promoter [Tg(*Myh6-cre*)1Jmk/J, strain no. 009074] [36] were from Jackson Laboratories, imported into the UK and transported to St. George's University of London for breeding in-house. These mice are on a C57Bl/6J background. Mice for cardiomyocyte-specific knockout of STRN were derived from the sperm banked at the Mary Lyon Centre from the STRN mice. The line was resuscitated and allele conversion using FLP recombinase to generate the conditional ready floxed line was performed by the Mary Lyon Centre (MRC Harwell). Heterozygous floxed STRN (*STRN*<sup>WT/fl</sup>) mice were transported to St. George's University of London and backcrossed onto a C57Bl/6J background

for four generations maintaining the line as heterozygotes before generating the homozygote line (STRN<sup>fl/fl</sup>). They were then crossed with homozygous Cre (Cre<sup>+/+</sup>) mice to generate mice that were heterozygous STRN and hemizygous for Cre (STRN<sup>WT/fl</sup>/Cre<sup>+/−</sup>); these were used to generate double homozygotes (STRN<sup>fl/fl</sup>/Cre<sup>+/+</sup>). STRN<sup>fl/fl</sup> mice were bred with STRN<sup>fl/fl</sup>/Cre<sup>+/+</sup> mice to generate mice hemizygous for Cre and homozygous for floxed STRN (STRN<sup>fl/fl</sup>/Cre<sup>+/−</sup>).

Tamoxifen was dissolved in 0.25 ml ethanol which was then mixed with 4.75 ml corn oil. Male mice (8–9 weeks) were treated with a single dose of tamoxifen (40 mg/kg i.p.; Sigma-Aldrich) to induce recombination or corn-oil vehicle as a control at 4 days relative to mini-pump implantation (see below). Our previous studies of mice hemizygous for Cre<sup>MCM/−</sup> treated in this way demonstrated that this is sufficient to induce recombination but has no overt effect on cardiac function or dimensions at baseline or on AngII-induced cardiac hypertrophy [33,35].

### Genotyping and confirmation of recombination

Ear notches were taken for identification using a 0.5 mm ear punch and used for genotyping. For confirmation of recombination in the heart, hearts and kidneys were collected from mice treated with tamoxifen or corn-oil vehicle, the tissues were ground to powder under liquid N<sub>2</sub> and samples were taken. DNA was extracted using Purelink genomic DNA (gDNA) mini-kits (Invitrogen) according to the manufacturer's instructions. gDNA was purified through Purelink spin columns and eluted in 30 µl of elution buffer. PCR amplification used GoTaq Hot Start Polymerase (Promega). PCR conditions were 95°C for 3 min, followed by up to 35 cycles of 95°C denaturations for 30 s, 30 s annealing, elongation at 72°C for 30 s, followed by a 7-minute 72°C final extension. Details of primers and conditions are in Supplementary Table S2. PCR products were separated using gel electrophoresis (25 min, 80 V) on 2% (w/v) agarose gels and visualised under UV light.

### AngII-induced cardiac hypertrophy

Alzet osmotic minipumps (supplied by Charles River Laboratories) were used for continuous delivery of 0.8 mg/kg/d AngII or vehicle for 7 d. Mice were anaesthetised in an induction chamber using vaporised 5% isoflurane in a constant oxygen supply of 2 l/min. Anaesthesia was maintained at 2.5% isoflurane using a nose cone. Mice were positioned on a heated mat in the prone position. Buprenorphine (Vetgesic, Ceva Animal Health Ltd.) (0.05 mg/kg, diluted in sterile PBS) was administered subcutaneously for analgesia. The fur covering the mid-scapular region was removed using an electric razor and the area was sterilised with HIBISCRUB® (VioVet). Under aseptic conditions, a 2 cm incision was made at the mid-scapular region and blunt dissection generated a pocket towards the lower-left flank of the mouse for the minipump to be inserted. The wound was closed with two simple interrupted sutures using polypropylene 4-0 thread (Prolene, Ethicon) and then sterilised with HIBISCRUB®. Mice were recovered singly and returned to a clean cage once fully recovered.

### Mouse echocardiography

Echocardiography was performed using a high-frequency ultrasound system (Vevo 2100™, Visualsonics) equipped with a 38 MHz MS400 transducer. Baseline echocardiograms were collected at 8 weeks (prior to tamoxifen treatment and/or minipump implantation) with additional scans taken at the end of the study. Mice were anaesthetised in an induction chamber using vaporised 5% isoflurane in a constant oxygen supply of 1 l/min. Anaesthesia was maintained with 1.5% isoflurane using a nose cone. Mice were positioned on a heating physiological monitoring stage in a supine position. Heart rate, respiration rate and body temperature were monitored. Chest fur was removed with an electric razor and hair removal cream. Pre-warmed ultrasound gel was applied to the chest as a coupling medium for the transducer. The transducer was orientated and lowered into the ultrasound gel until a clear image was centralised on the monitor. Imaging was completed within a maximum time of 30 min, and usually within 15 min. Mice were recovered singly and transferred to the home cage once fully recovered. Cardiac function and left ventricular wall dimensions were measured from M-mode short axis images using VevoLab software with assistance from the autoLV tool. Cardiac function and global longitudinal strain were measured from B-mode long axis images using VevoStrain software for speckle tracking. B-mode images of the ascending aorta were also captured and the diameter of the aorta measured using VevoLab software, before the beginning of the arch and perpendicular to the walls. Measurements were collected at the end of ventricular contraction when the diameter was at its largest and following contraction of the aorta when at its narrowest. At the end of the experiment, whilst still under anaesthesia, mice were culled by cervical dislocation with severance of the femoral artery to ensure cessation of life. Hearts were excised quickly, washed in PBS, dried and snap-frozen in liquid N<sub>2</sub> or fixed for histology.

## Histology and analysis

Histological sections for the global STRN and STRN3 knockout mouse studies were prepared and stained by HistologiX Limited. Sections for the cardiomyocyte-specific STRN knockout study were prepared and stained at St. George's University of London (as described in [37]). Haematoxylin and eosin staining was used for analysis of myocyte cross-sectional area. Cells around the periphery of the left ventricle (excluding epicardial layer) were chosen at random (ensuring that the cells were in cross-section and with a clear, rounded nucleus) and outline traced using NDP.view2 software (Hamamatsu). This approach was taken to ensure cells were captured in the same region of the myocardium, to avoid issues relating to different levels of stress and orientation of cells across the myocardial wall, along with interdigitation of individual cardiomyocytes. Because of the rigorous approach, limited numbers of cells were available for selection and all, or up to 30 cells were measured per section by a single independent assessor and the mean value taken for each mouse. To assess interstitial fibrosis, sections were stained with Masson's trichrome or picrosirius red and analysis used Image-J as in [37]. The collagen fraction was calculated as the ratio between the sum of the total area of fibrosis (blue colour for Masson's trichrome, red colour for picrosirius red) to the sum of the total tissue area (including the myocyte area) for the entire image and expressed as a percentage. For perivascular fibrosis (because there was not a constant number of vessels apparent in each section), picrosirius red staining was used and the whole section was scored for perivascular fibrosis around arterioles (identified by a clear elastic layer). Values were 1 (negligible increase in fibrosis around any vessel), 2 (mild-to-moderate fibrosis around 1 or more vessels), 3 (significant fibrosis permeating tissue around 1 or more vessels) and 4 (extensive fibrosis around multiple vessels, penetrating into the myocardium).

## RNA preparation and qPCR

Heart powders (10–15 mg) were weighed into safelock Eppendorf tubes and kept on dry ice. RNA Bee (AMS Biotechnology Ltd.) was added (1 ml) and the samples homogenised on ice using a pestle. RNA was prepared according to the manufacturer's instructions and dissolved in nuclease-free water. The purity was assessed from the  $A_{260}/A_{280}$  measured using an Implen NanoPhotometer (values were 1.8–2.0) and concentrations determined from the  $A_{260}$ . Quantitative PCR (qPCR) analysis was performed as described in [38]. Total RNA was reverse transcribed to cDNA using High Capacity cDNA Reverse Transcription Kits with random primers (Applied Biosystems). qPCR was performed using a StepOnePlus Real-Time PCR system (ThermoFisher Scientific) using 1/40 of the cDNA produced. Optical 96-well reaction plates were used with iTaq Universal SYBR Green Supermix (Bio-Rad Laboratories Inc.) according to the manufacturer's instructions. See Supplementary Table S3 for primer sequences. Results were normalised to *GAPDH*, and relative quantification was obtained using the  $\Delta Ct$  (threshold cycle) method; relative expression was calculated as  $2^{-\Delta\Delta Ct}$ , and normalised as indicated in the Figure Legends.

## Immunoblotting

Heart powders (15–20 mg) were homogenised in 6 vol extraction buffer [20 mM Tris pH 7.5, 1 mM EDTA, 10% (v/v) glycerol, 1% (v/v) Triton X-100, 100 mM KCl, 5 mM NaF, 0.2 mM Na<sub>3</sub>VO<sub>4</sub>, 5 mM MgCl<sub>2</sub>, 0.05% (v/v) 2-mercaptoethanol, 10 mM benzamidine, 0.2 mM leupeptin, 0.01 mM trans-epoxy succinyl-L-leucylamido-(4-guanidino)butane, 0.3 mM phenylmethylsulphonyl fluoride, 4 µM microcystin]. Samples were extracted on ice with intermittent vortex mixing (10 min), then centrifuged (10,000  $\times g$ , 10 min, 4°C) to pellet insoluble material. The supernatants were removed, a sample was taken for protein assay and the rest boiled with 0.33 vol sample buffer (300 mM Tris-HCl pH 6.8, 10% (w/v) SDS, 13% (v/v) glycerol, 130 mM dithiothreitol, 0.2% (w/v) bromophenol blue). Protein concentrations were determined by BioRad Bradford assay using a 1/5 dilution (v/v) in H<sub>2</sub>O of the dye reagent concentrate and BSA standards.

Proteins (100 µg for human heart samples, 40 µg for rat and mouse heart samples) were separated by SDS-PAGE (200 V) using 8% (for striatin isoforms), or 12% (GAPDH) polyacrylamide resolving gels with 6% stacking gels until the dye front reached the bottom of the gel (~50 min). Proteins were transferred electrophoretically to nitrocellulose using a BioRad semi-dry transfer cell (10 V, 60 min). Non-specific binding sites were blocked (15 min) with 5% (w/v) non-fat milk powder in Tris-buffered saline (20 mM Tris-HCl pH 7.5, 137 mM NaCl) containing 0.1% (v/v) Tween 20 (TBST). Blots were incubated with primary antibodies in TBST containing 5% (w/v) BSA (overnight, 4°C), then washed with TBST (3  $\times$  5 min, 21°C), incubated with horseradish peroxidase-conjugated secondary antibodies in TBST containing 1% (w/v) non-fat milk powder (60 min, 21°C) and then washed again in TBST (3  $\times$  5 min, 21°C). Rabbit polyclonal antibodies to STRN and STRN4 were from Novus Biologicals Ltd (STRN: catalogue number NB110-74571; STRN4: catalogue no. NBP2-36537) and were used at 1/1000 dilution. Goat polyclonal antibodies to STRN3 (SG2NA) were from Santa Cruz Biotechnology Inc (catalogue no. E1704). Rabbit polyclonal antibodies to

GAPDH were from Cell Signaling Technologies (catalogue no. 14C10). All primary antibodies were used at 1/1000 dilutions. Horseradish-peroxidase-conjugated goat anti-rabbit immunoglobulins (catalogue no. P0448) and rabbit anti-goat immunoglobulins (catalogue no. P0449) were from Dako (supplied by Agilent) and were used at 1/5000 dilution. Bands were detected by enhanced chemiluminescence using ECL Prime with visualisation using an Image-Quant LAS4000 system (Cytiva). ImageQuant TL 8.1 software (GE Healthcare) was used for densitometric analysis. Raw values for phosphorylated kinases were normalised to the total kinase. Values for all samples were normalised to the mean of the controls.

## Image processing and statistical analysis

Images were exported from the original software as .tif or .jpg files and cropped for presentation with Adobe Photoshop CC maintaining the original relative proportions. Data analysis used Microsoft Excel and GraphPad Prism 9. Statistical analysis was performed using GraphPad Prism 9. A Grubb's outlier test was applied to the data, and outliers excluded from the analysis. Statistical significance was determined using two-tailed unpaired Mann–Whitney tests, or two-tailed one-way or two-way ANOVA as indicated in the Figure Legends. A Holm–Sidak's multiple comparison test was used in combination with ANOVA. Graphs were plotted with GraphPad Prism 9 or 10. Specific *P* values are provided with significance levels of *P*<0.05 in bold type.

## Results

### Striatin and striatin 3 are up-regulated in human failing hearts

To assess which of the striatin isoforms is most likely to promote human heart failure, we mined an RNASeq database of heart samples from patients with dilated cardiomyopathy (DCM; *n*=97) compared with normal controls (*n*=108) [31]. *STRN*, *STRN3* and *STRN4* transcripts were readily detected, with a rank order of expression of *STRN4*>*STRN*>*STRN3* in control samples (Figure 1A). Expression of *STRN4* declined in DCM hearts whilst expression of *STRN* and *STRN3* increased. To establish if this reflects a broader spectrum of heart failure and determine how mRNA expression correlates with protein expression, we also assessed expression of striatins in samples from 12 patients with heart failure of mixed non-ischaemic aetiology compared with normal controls (previously reported in [33]). These showed a significant increase in only *STRN3* mRNA expression in heart failure samples (Figure 1B), although protein expression of all striatins was significantly increased in failing hearts (Figure 1C,D). Thus, although *STRN* and *STRN3* have a similar profile overall with up-regulation in disease, *STRN4* may have more specific and selective roles in different forms of heart failure.

### Global heterozygous knockout of *STRN* in mice, but not *STRN3*, reduces cardiac hypertrophy induced by AngII

Since *STRN* and *STRN3* were up-regulated in DCM and human failing hearts of other aetiology, we focused on these isoforms for further investigation. We used commercially-available knockout-first mice, engineered with a removable STOP cassette to permit conversion for conditional gene deletion (Figure 1E; Supplementary Figure S1A). Homozygous global deletion of any striatin isoform is embryonic lethal, so we assessed the effects of heterozygous gene deletion (*STRN*<sup>+/−</sup> and *STRN3*<sup>+/−</sup>), comparing responses with wild-type littermates. We studied male mice taking baseline echocardiograms at 8 weeks and, using M-mode assessment of short axis images, or B-mode images with speckle-tracking/strain analysis, we detected no differences in cardiac function or dimensions in *STRN*<sup>+/−</sup> or *STRN3*<sup>+/−</sup> mice compared with the wild-types (Supplementary Table S4). Mice were then treated for 7 days with acidified PBS (AcPBS) vehicle or with 0.8 mg/kg/d AngII using osmotic minipumps (Figure 1F). This 'slow-pressor' dose gradually induces hypertension over 7–14 days [39–41]. We did not assess the effects in female mice because premenopausal mice are resistant to AngII-induced hypertension [42,43] (see Discussion).

We assessed protein expression of the three striatins in mouse hearts by immunoblotting. The only antibody for *STRN* that we could identify detected *STRN* protein in mouse hearts as a band of ~110 kDa (the upper band on the immunoblots), and this was reduced in hearts from *STRN*<sup>+/−</sup> mice (Figure 1G,H). Other bands were detected below this but, since there is no evidence for alternatively spliced isoforms of *STRN* and we detected no difference in expression of these bands in the *STRN*<sup>+/−</sup> mice, we assume these are non-specific. *STRN* knockdown did not significantly affect expression of *STRN3* or *STRN4*. AngII increased expression of *STRN* in wild-type littermates from the *STRN* colony, and this was accompanied by a significant increase in *STRN3*. *STRN3* was reduced in hearts from *STRN3*<sup>+/−</sup> mice with no significant change in expression of *STRN* or *STRN4* (Supplementary Figure 1C,D). In contrast to the *STRN* colony, we did not detect an increase in any striatin isoform with AngII in hearts from

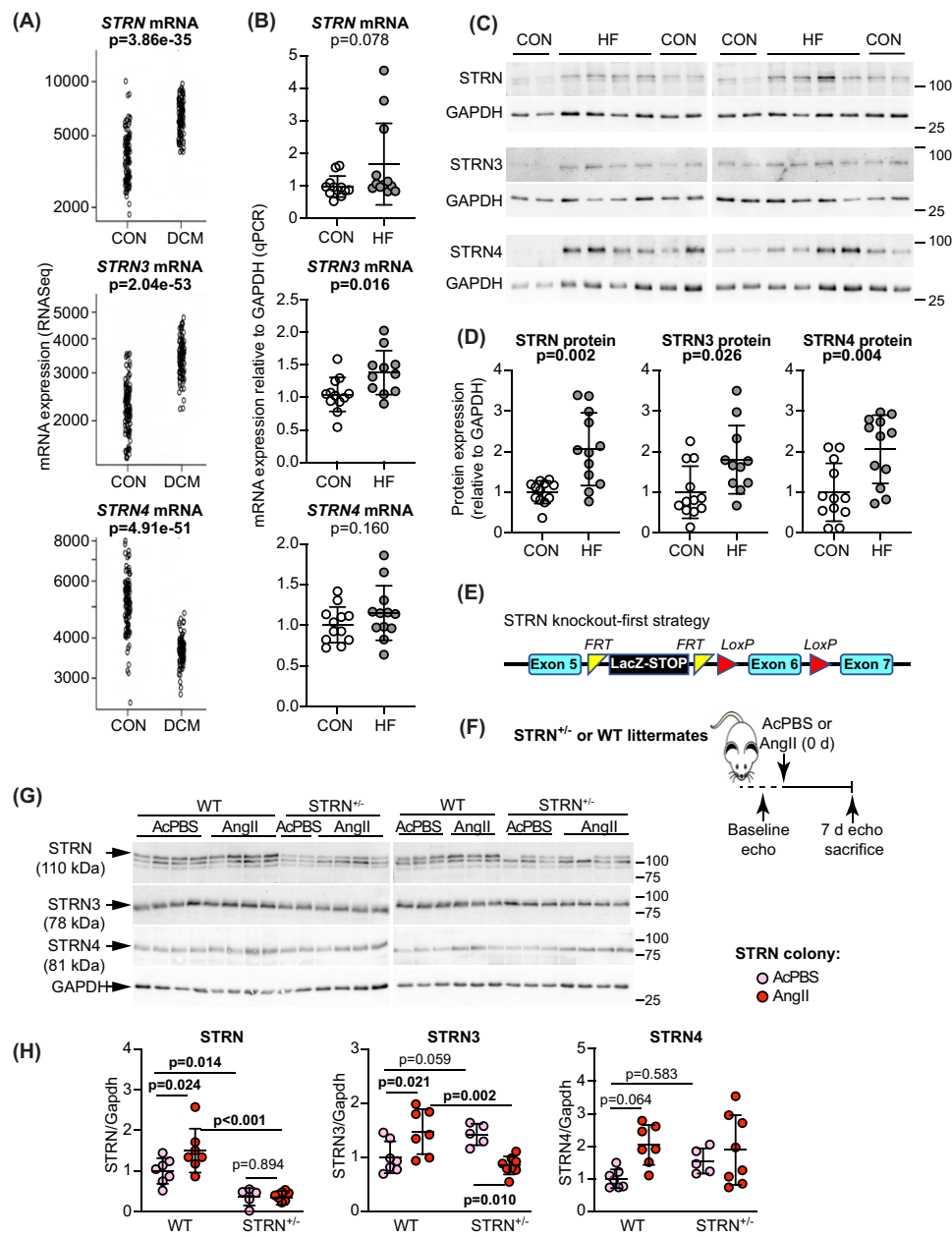


**Figure 1. Expression of striatin isoforms in human failing hearts and global heterozygous STRN knockout in mice**

(A) Data for mRNA expression of striatin isoforms in human hearts were from an RNASeq database of patients with dilated cardiomyopathy (DCM,  $n=97$ ) and normal controls (CON,  $n=108$ ). Data for individual samples are shown with adjusted  $P$  values. (B–D) Samples from control hearts (CON) or explanted hearts from patients with heart failure (HF) were used to prepare RNA for qPCR analysis (B) or protein for immunoblots (C,D). Representative immunoblots (100  $\mu$ g protein per lane) are in (C) with densitometric analysis in (D). Individual values are shown with means  $\pm$  SD. Results are relative to GAPDH and normalised to the mean of the CON hearts. Mann–Whitney tests were used for statistical analysis. (E) ‘Knockout-first’ strategy for global deletion of STRN in mice involved positioning of a STOP cassette flanked by FRT sites upstream of a critical exon that was also flanked with LoxP sites. (F) Experimental approach for assessment of effects of STRN deletion on cardiac function. Homozygous global knockout of STRN is embryonic lethal, so heterozygote STRN<sup>+/−</sup> male mice (8 weeks) were used in comparison with wild-type (WT) littermates from each colony. Following baseline echocardiography (echo), minipumps were implanted for delivery of acidified PBS vehicle (AcPBS) or 0.8 mg/kg/d angiotensin II (AngII). Following echocardiography at 7 d, mice were killed. (G,H) Heart powders were used for immunoblotting (40  $\mu$ g protein per lane). Representative immunoblots of the striatin isoforms and GAPDH (G) are shown with densitometric analysis (H). Results are relative to GAPDH and normalised to the means for WT mice treated with AcPBS. N.B. The upper band of the STRN blot used for densitometry correlates with the predicted molecular weight of STRN protein (110 kDa).

wild-type mice from the STRN3 colony, presumably reflecting differences in the background strain despite extensive backcrossing onto the same C57Bl/6J background.

We determined the effects of AngII on STRN<sup>+/−</sup> and STRN3<sup>+/−</sup> mouse hearts using echocardiography, assessing the changes induced at 3 and 7 d after minipump implantation. We analysed short axis M-mode images to obtain information on cardiac function and left ventricle dimensions (wall thickness and internal diameter) as is usual, but also employed the newer modality of speckle-tracking/strain analysis of long axis B-mode images. The latter offers a significant advantage in monitoring changes around the entire ventricle wall rather than across a single point in the myocardium. For cardiac function (heart rate, ejection fraction, fractional shortening and cardiac output), we obtained similar measurements with either M-mode analysis or B-mode speckle-tracking software (Figure 2; Supplementary Figure S2 and Supplementary Tables S5–7). We detected no significant changes in cardiac function with AngII treatment in STRN<sup>+/−</sup> and STRN3<sup>+/−</sup> mouse hearts or their wild-type littermates.

M-mode analysis was used to assess wall thickness and internal diameter at the level of the papillary muscle across the left ventricle. AngII induced a significant increase in left ventricle wall thickness in wild-type mice from both STRN<sup>+/−</sup> and STRN3<sup>+/−</sup> colonies at 3 d, together with a decrease in internal diameter, consistent with concentric hypertrophy (Figure 2; Supplementary Figure S2 and Supplementary Tables S5–7). Wall thickness was also increased in STRN<sup>+/−</sup> mice treated with AngII, but this was significantly less than in the wild-type littermates (Figure 2A). By 7 d, the increase in wall thickness induced by AngII in STRN<sup>+/−</sup> mice was no longer significantly different from the wild-type littermates (Figure 2B), presumably a consequence of further remodelling of the heart. B-mode imaging confirmed this was likely to be the case since AngII induced a significant increase in estimated left ventricle mass in wild-type mice with a significantly reduced overall response in STRN<sup>+/−</sup> mice (Figure 2C). This was not associated with any differences in global longitudinal strain between wild-type and STRN<sup>+/−</sup> mice which, along with the absence of change in cardiac functional measurements, indicated that the hypertrophic response was still in a compensatory phase. In contrast to STRN<sup>+/−</sup> mice, the responses to AngII of STRN3<sup>+/−</sup> mouse hearts were similar to those of wild-type littermates with increases in left ventricle wall thickness (using M-mode analysis) and estimated left ventricle mass (with B-mode speckle-tracking) (Supplementary Figure S2). This was accompanied by a small increase in global longitudinal strain suggesting there could be some gain of contractile function but, together with the standard measures of cardiac function, the data indicate that these hearts were also in a compensatory phase.

Heart sections were stained with haematoxylin and eosin and the cross-sectional area of myocytes at the periphery of the left ventricle measured. AngII increased cardiomyocyte cross-sectional area (indicative of cardiomyocyte hypertrophy) in wild-type mice from both STRN and STRN3 colonies (Figure 3A,B and Supplementary Figure S3A,B), and increased expression of hypertrophic gene markers (Figure 3C and Supplementary Figure S3C). The AngII-induced increase in cross-sectional area and expression of *Myh7* mRNA (though not *Nppa* or *Nppb*) was reduced in hearts from STRN<sup>+/−</sup> mice (but not STRN3<sup>+/−</sup> mice) compared with their wild-type littermates. Other genes associated with cardiac non-myocytes (*Ng2* for pericytes, *Tagln* for smooth muscle cells, *Ddr2* for fibroblasts, *Cdh1* and *Cdh5* for endothelial cells) were not significantly changed with AngII treatment or between wild-type and STRN<sup>+/−</sup> mice, suggesting the responses were not associated with significant changes in the proportions of cardiac cell types at this stage (Figure 3C).

Heart sections were stained with picrosirius red to assess cardiac fibrosis (Figure 4A–E and Supplementary Figure S3D–E). At this 7-day time point, AngII induced only a small, non-significant increase in interstitial fibrosis and this was most commonly detected in the area at the junction between the interventricular septum and the ventricular wall. However, there was a greater, significant increase in perivascular fibrosis. The degree of fibrosis induced by AngII was similar in STRN<sup>+/−</sup>, STRN3<sup>+/−</sup> and their wild-type littermates. AngII also upregulated mRNAs encoding fibrotic genes (Figure 4F,G). This was not significantly different in STRN<sup>+/−</sup> or STRN3<sup>+/−</sup> mouse hearts compared with their wild-type littermates, but there was an indication of reduced expression of some genes in the STRN<sup>+/−</sup> mouse hearts.

Overall, the data indicate that reduction of STRN3 does not substantially affect cardiac hypertrophy induced by AngII, at least over the short term. In contrast, reduction of STRN compromises the cardiac response to AngII, having a clear effect on cardiomyocyte hypertrophy, though not cardiac fibrosis.

## Cardiomyocyte-specific deletion of STRN inhibits AngII-induced cardiac hypertrophy

To determine if the reduced hypertrophic response to AngII in STRN<sup>+/−</sup> mice was due to reduced expression of STRN in cardiomyocytes rather than other cardiac cells, we converted the STRN knockout-first line for conditional gene deletion using FLP recombinase (Figure 5A). These mice were used to generate homozygous floxed STRN mice with

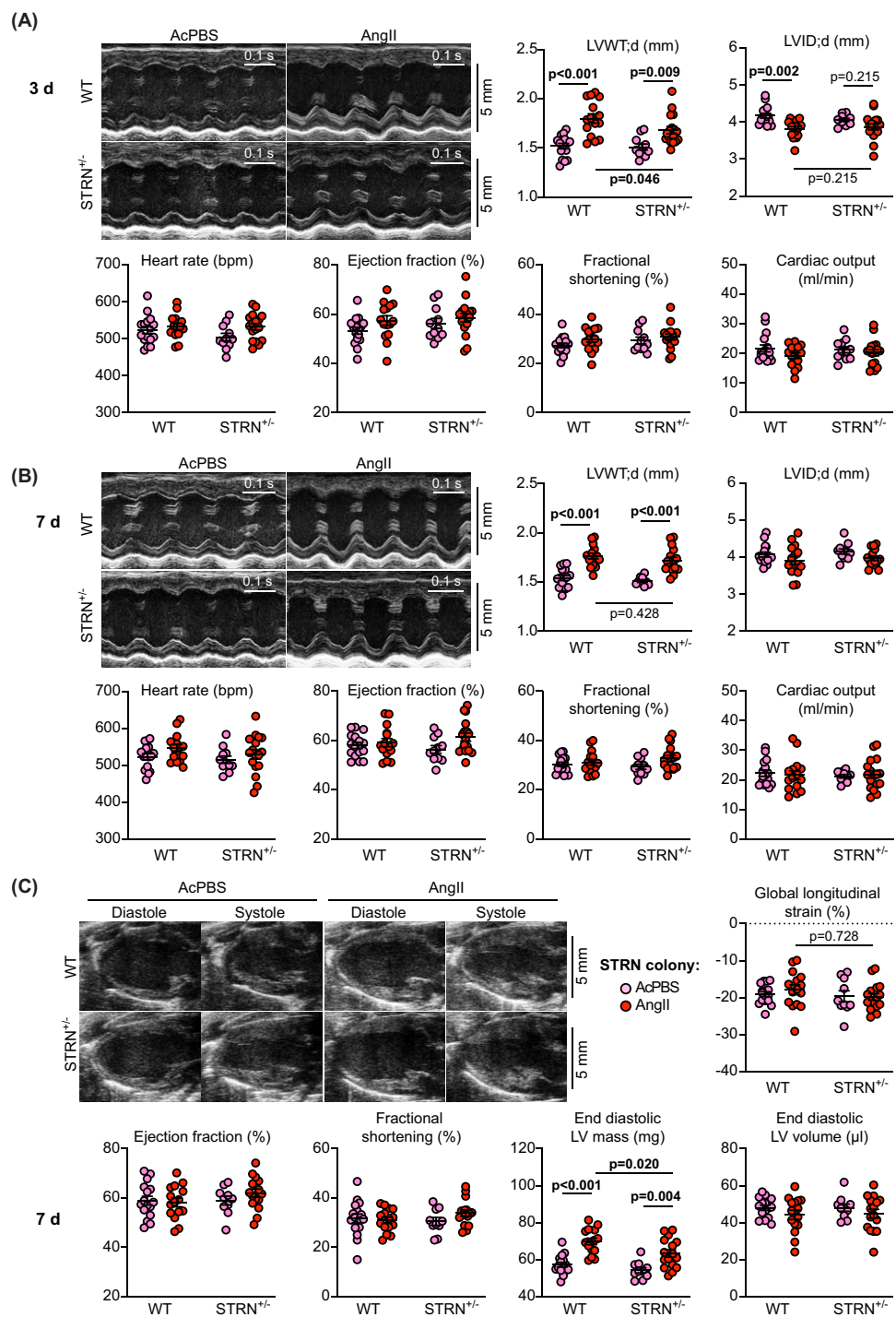


**Figure 2. Heterozygous global deletion of STRN compromises the hypertrophic response to AngII**

Male mice (8 wks) heterozygote for STRN knockout (STRN<sup>+/−</sup>) and wild-type (WT) littermates from the same colony were treated with acidified PBS (AcPBS) vehicle or AngII (0.8 mg/kg/d). Cardiac function and dimensions were assessed by echocardiography using M-mode imaging of the short axis at 3 d (A) or 7 d (B), or B-mode imaging of the long axis at 7 d with speckle-tracking and strain analysis (C). For M-mode imaging, diastolic values for left ventricle (LV) wall thickness (WT) or internal diameter (ID) are shown and end diastolic LV mass and volume are provided for B-mode imaging. Cardiac function measurements are shown for M-mode and B-mode analysis for comparison. Representative images are in the upper left of each panel. Individual datapoints are plotted with means  $\pm$  SEM. Statistical analysis used two-way ANOVA with Holm-Sidak's post-test (N.B.: All echocardiography data are provided in Supplementary Tables S4, S5 and S7).

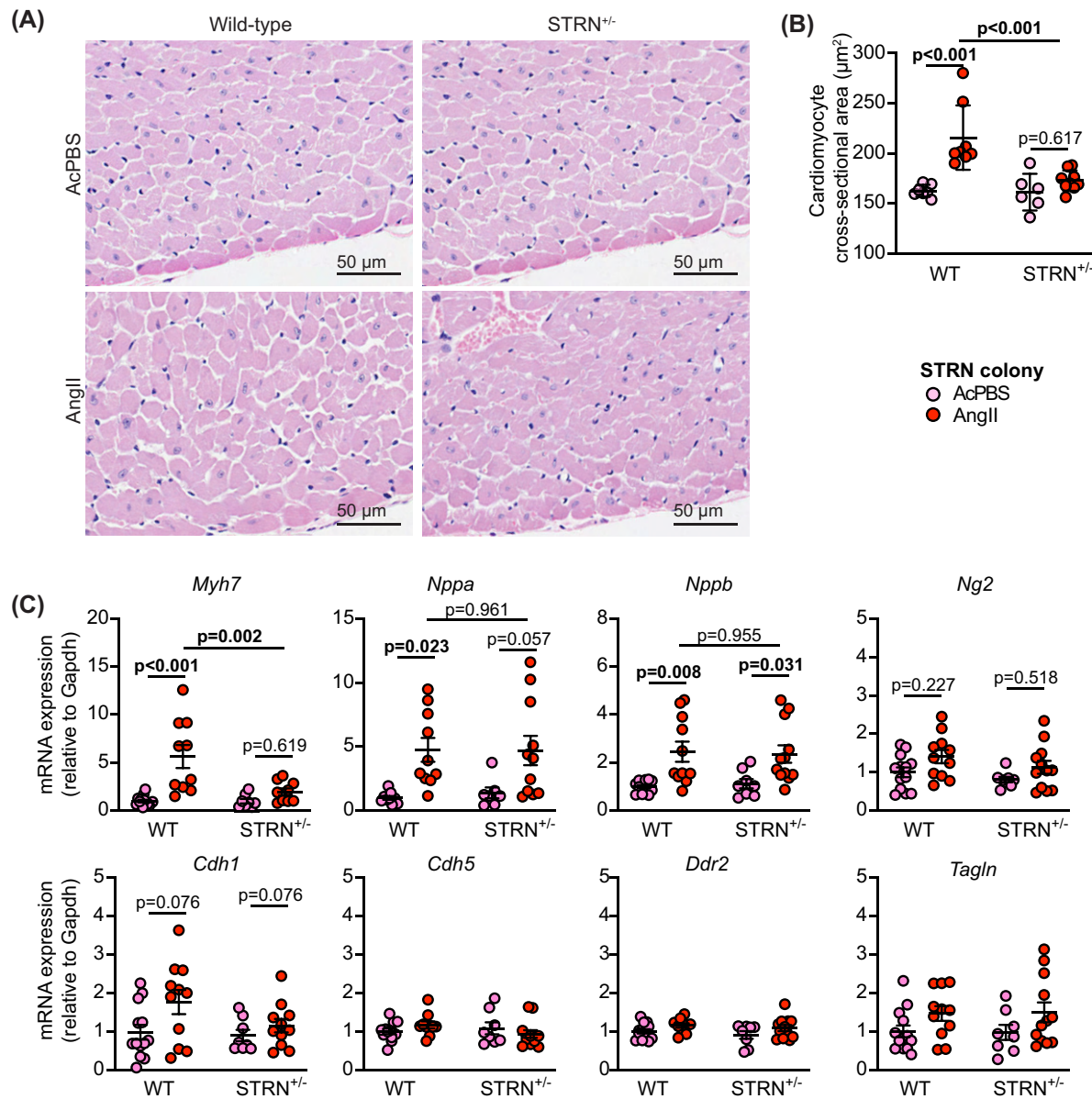


**Figure 3. Heterozygous global deletion of STRN, reduces cardiomyocyte hypertrophy and the increase in expression of *Myh7* induced by AngII**

8 wk male  $\text{STRN}^{+/-}$  mice, plus their wild-type (WT) littermates were treated with acidified PBS (AcPBS) vehicle or 0.8 mg/kg/d AngII (7 d). Hearts were fixed and sections stained with haematoxylin and eosin. Representative images (A) show areas from the outer perimeter of the left ventricular wall opposite the interventricular septum. (B) Cardiomyocyte cross-sectional areas are shown. (C) RNA was extracted from mouse heart powders and analysed by qPCR for the mRNAs shown. Individual datapoints are plotted with means  $\pm$  SEM. Results are relative to GAPDH and normalised to the means for WT mice treated with AcPBS. Statistical analysis used two-way ANOVA with Holm-Sidak's post-test.

a single allele for tamoxifen-inducible Cre under the control of a *Myh6* promoter [36]. Male  $\text{STRN}^{\text{fl/fl}}/\text{Cre}^{+/-}$  mice (8 weeks) were treated with a single dose of tamoxifen (40 mg/kg) to induce recombination, an approach which is not associated with significant cardiotoxicity from the Cre enzyme [33,35]. Recombination was detected in hearts but not kidneys from  $\text{STRN}^{\text{fl/fl}}/\text{Cre}^{+/-}$  mice treated with tamoxifen (Figure 5B), confirming cardiac-specific gene deletion. Osmotic minipumps were implanted 4 days after tamoxifen treatment (by which time the tamoxifen has been cleared

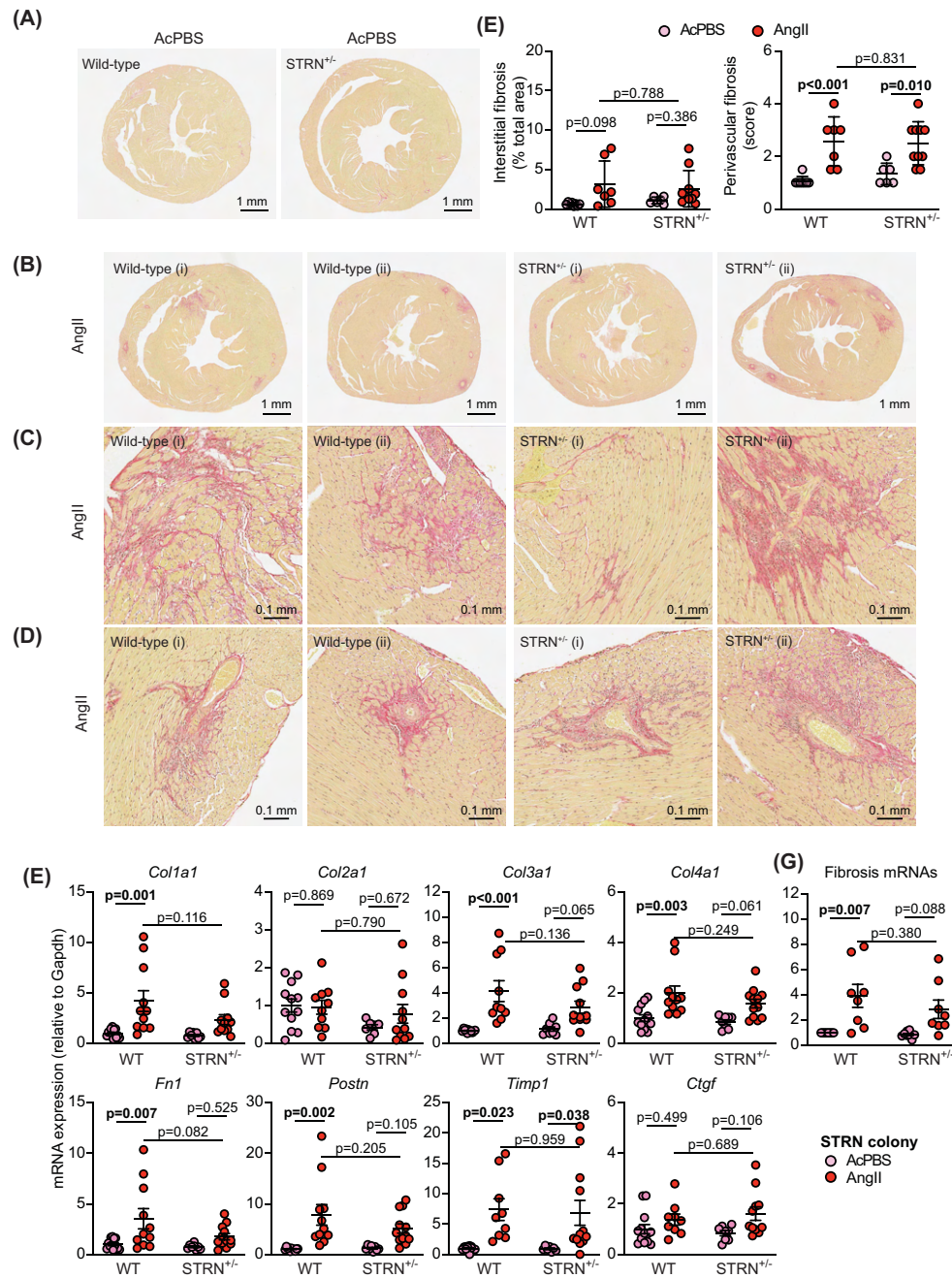


**Figure 4. Heterozygous knockout of STRN does not reduce cardiac fibrosis induced by AngII**

Eight-week male STRN<sup>+/-</sup> mice, plus their wild-type (WT) littermates were treated with acidified PBS (AcPBS) vehicle or 0.8 mg/kg/d AngII (7 d). Hearts were fixed and sections stained with picrosirius red. Representative short axis views of the whole heart are shown for wild-type and STRN<sup>+/-</sup> mice treated with AcPBS (A) or AngII (B). For AngII-treated hearts, an average (i) or maximum (ii) response is shown. Enlarged regions of the AngII-treated hearts in (B) are shown below for interstitial fibrosis (C) or perivascular fibrosis (D). (E) Interstitial fibrosis was measured using ImageJ and is presented as the % of the total area (excluding regions around the blood vessels). Perivascular fibrosis was scored (1: negligible increase in fibrosis around any vessel; 2: mild-to-moderate fibrosis around 1 or more vessels; 3: significant fibrosis permeating tissue around 1 or more vessels; 4: extensive fibrosis around multiple vessels, penetrating into the myocardium). A scoring system was used for the latter because of the variation in numbers of vessels seen in different heart sections. (F) RNA was extracted from mouse heart powders and analysed by qPCR for fibrosis mRNAs as indicated. (G) The average value for each condition for each of the genes shown in (F) was taken. qPCR results are relative to GAPDH and normalised to the means for WT mice treated with AcPBS. Individual datapoints are plotted with means  $\pm$  SEM. Statistical analysis used two-way ANOVA with Holm-Sidak's post-test.

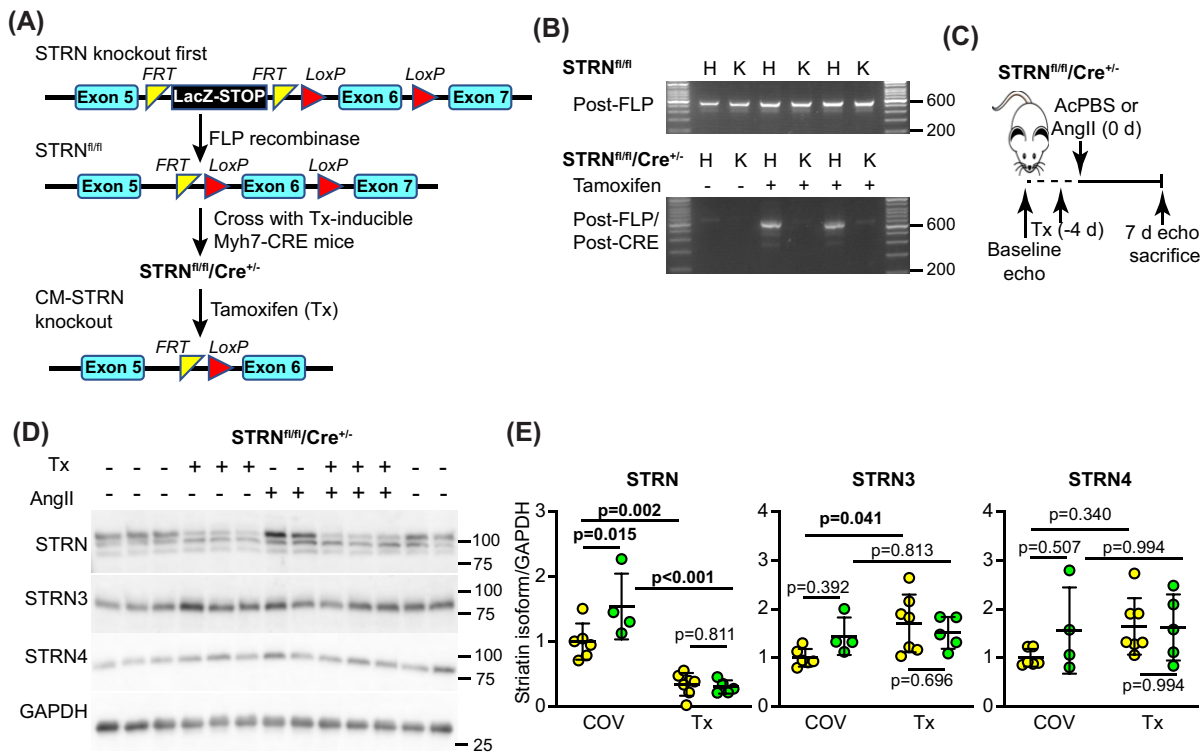


**Figure 5. Cardiomyocyte-specific knockout of STRN inhibits cardiac hypertrophy induced by AngII**

**(A)** Strategy for cardiomyocyte (CM) specific knockout of STRN in mice. STRN knockout first mice were converted to 'conditional-ready' using FLP recombinase, removing the STOP cassette between exons 5 and 6, whilst leaving the LoxP sites surrounding exon 6 in place (STRN<sup>fl/fl</sup> mice). These were bred with mice expressing tamoxifen- (Tx-) activated Cre to generate mice homozygous for floxed striatin and hemizygous for Cre (STRN<sup>fl/fl/Cre+/-</sup>) for experiments. Treatment with tamoxifen induced recombination and deletion of exon 6. **(B)** Hearts (H) and kidneys (K) from male mice were genotyped to confirm that the mice were conditional-ready (upper panel) and that tamoxifen treatment (40 mg/kg) induced recombination in the heart but not kidney (lower panel). **(C)** Strategy for experiments. Male STRN<sup>fl/fl/Cre+/-</sup> mice (8 weeks) were used. Following baseline echocardiography (echo), mice were treated with corn-oil vehicle (COV) or Tx in COV (40 mg/kg; day -4) and minipumps were implanted (day 0) to deliver acidified PBS (AcPBS) vehicle or 0.8 mg/kg/d AngII for 7 days, after which a final echocardiogram was taken before the mice were sacrificed. **(D,E)** Heart powders were used for immunoblotting (40 µg protein per lane). Representative immunoblots of the striatin isoforms and GAPDH are in **(D)** with densitometric analysis in **(E)**. Results are relative to GAPDH and normalised to the means for mice treated with vehicle only. The upper band of the STRN blot used for densitometry correlates with the predicted molecular weight of STRN protein.

from the body [44]) to deliver acidified PBS vehicle or 0.8 mg/kg/d AngII for 7 days. Immunoblotting confirmed that tamoxifen induced a significant and substantial decrease in STRN expression in the hearts of STRN<sup>fl/fl/Cre+/-</sup> mice, and this was associated with a significant increase in expression of STRN3 (Figure 5D,E). As with global heterozygous STRN<sup>+/−</sup> mice (Figure 1F,G), AngII increased expression of STRN, but there was no increase in the hearts of cardiomyocyte STRN knockout mice (Figure 5D,E).

We used echocardiography to assess the changes in cardiac function and dimensions induced by AngII 3 and 7 d after minipump implantation in mice with and without cardiomyocyte STRN knockout (Figure 6 and Supplementary Tables S8,9). As with global heterozygous STRN gene deletion, we detected no significant differences in cardiac function between any of the conditions at either of the times studied using either M-mode or B-mode analysis. AngII induced a significant increase in left ventricle wall thickness and decrease in internal diameter after 3 d in mice without cardiomyocyte STRN knockout as assessed by M-mode imaging, but there was no increase in wall thickness in mice with cardiomyocyte STRN knockout. As with the STRN<sup>+/−</sup> colony, this hypertrophy was no longer detectable at 7 d using M-mode imaging. However, using B-mode imaging and speckle-tracking for the entire wall of the left ventricle, at 7 d, AngII induced a significant overall increase in estimated left ventricle mass in mice with cardiomyocyte STRN that was lost with cardiomyocyte STRN knockout (Figure 6C).

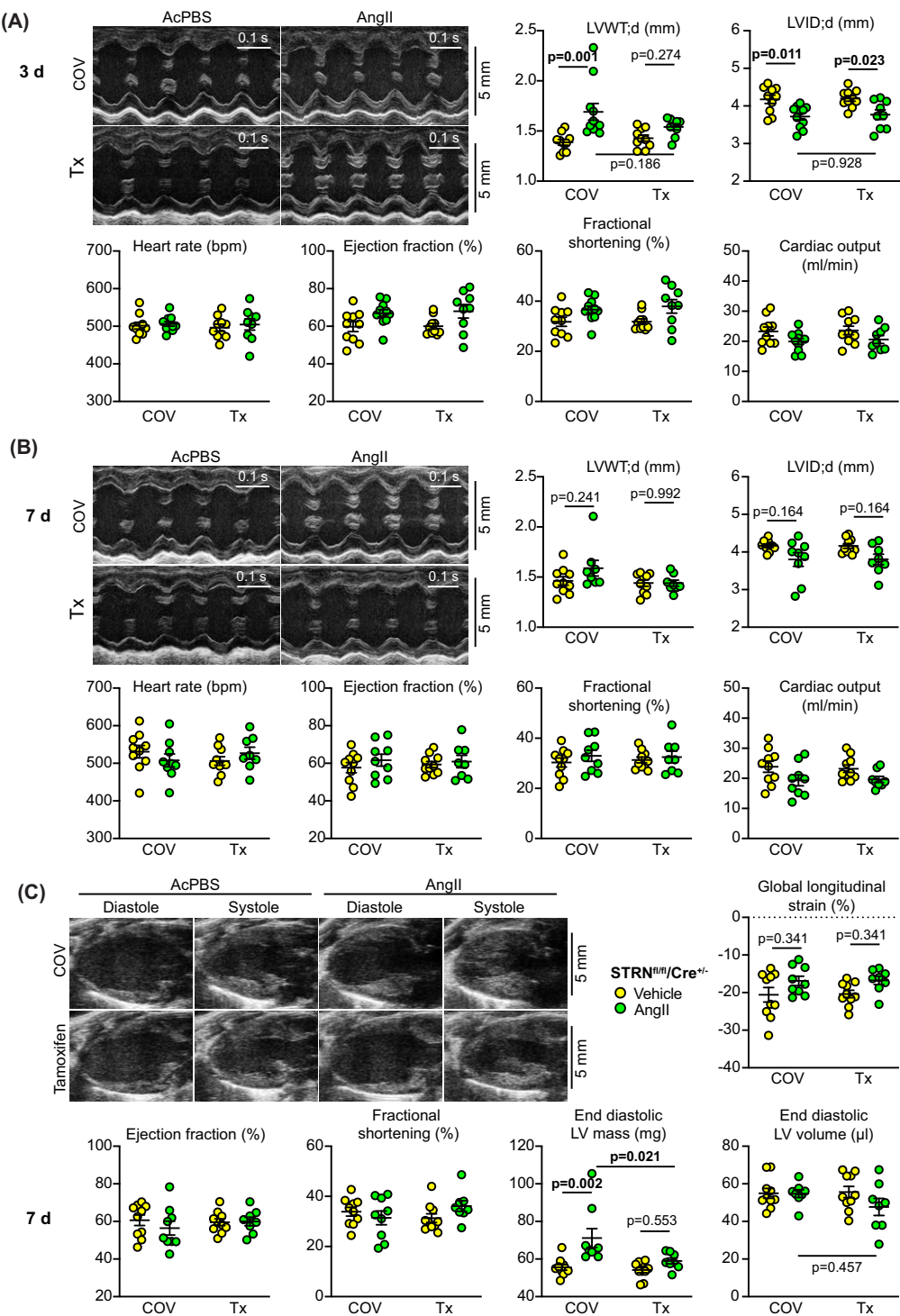


**Figure 6. Cardiomyocyte-specific knockout of STRN compromises the hypertrophic response to AngII**

Male STRN<sup>fl/fl</sup>/Cre<sup>+/−</sup> mice (8 weeks) were treated with corn-oil vehicle (COV) or tamoxifen (Tx; 40 mg/kg) and minipumps implanted to deliver acidified PBS (AcPBS) or 0.8 mg/kg/d AngII for 7 days. Cardiac function and dimensions were assessed by echocardiography using M-mode imaging of the short axis at 3 d (A) or 7 d (B), or B-mode imaging of the long axis at 7 d with speckle-tracking and strain analysis (C). For M-mode imaging, diastolic values for left ventricle (LV) wall thickness (WT) or internal diameter (ID) are shown and end diastolic LV mass and volume are provided for B-mode imaging. Cardiac function measurements are shown for both M-mode and B-mode for comparison. Individual datapoints are plotted with means  $\pm$  SEM. Statistical analysis used two-way ANOVA with Holm-Sidak's post-test. (N.B. All echocardiography data are provided in Supplementary Tables S9 and S10).

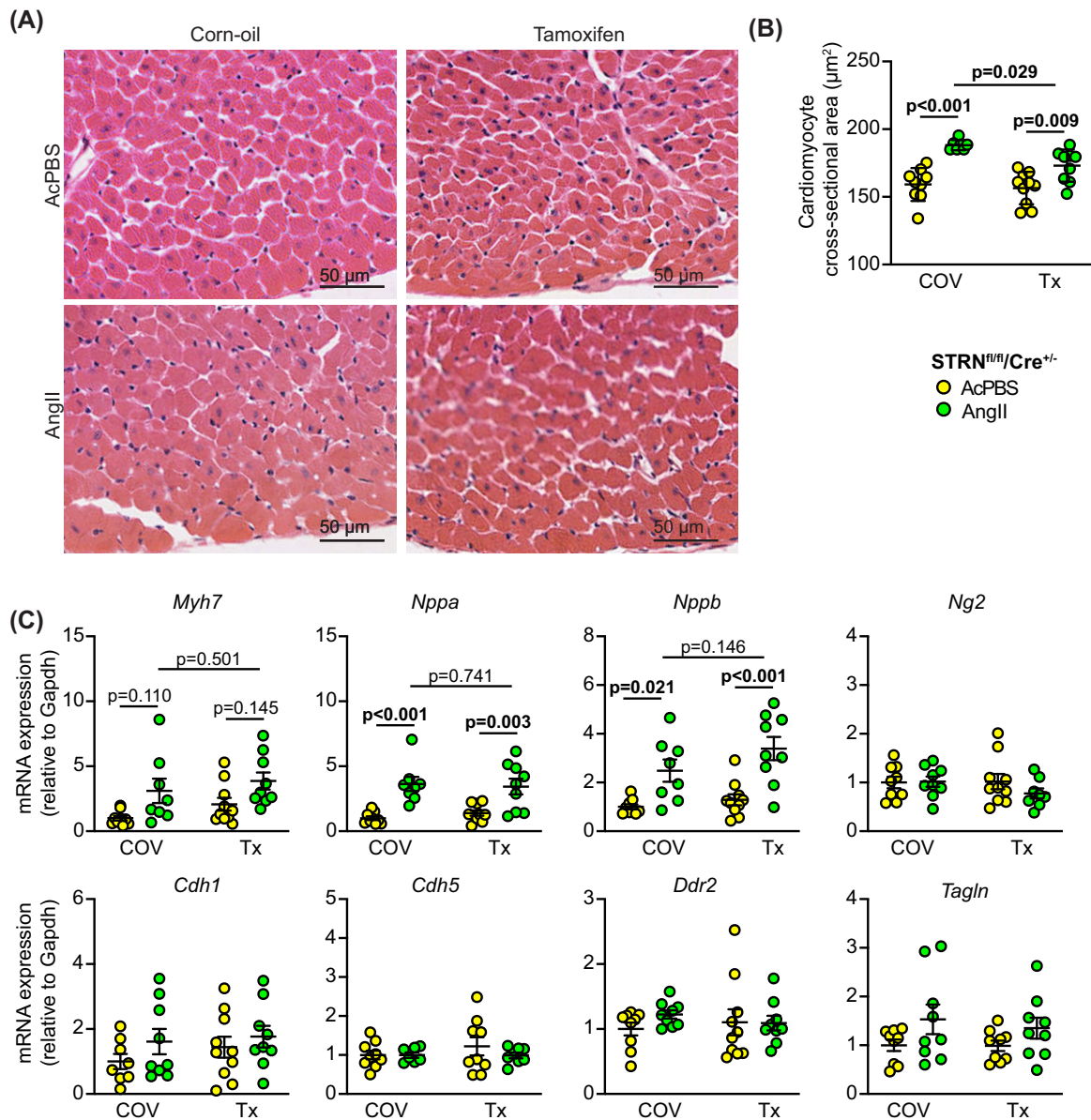


**Figure 7. Cardiomyocyte-specific knockout of STRN inhibits the increase in cardiomyocyte cross-sectional area induced by AngII**

Male STRN<sup>fl/fl</sup>/Cre<sup>+/−</sup> mice (8 wks) were treated with corn-oil vehicle (COV) or tamoxifen (Tx; 40 mg/kg) and minipumps implanted to deliver acidified PBS (AcPBS) or 0.8 mg/kg/d AngII for 7 days. Hearts were fixed or snap-frozen in liquid N<sub>2</sub> before grinding to powder. Representative images of sections stained with haematoxylin and eosin (A) show areas from the outer perimeter of the left ventricular wall opposite the interventricular septum. (B) Cardiomyocyte cross-sectional areas. (C) RNA extracted from mouse heart powders was analysed by qPCR for the mRNAs shown. Results are relative to GAPDH and normalised to the means for mice treated with vehicle only.

AngII increased cardiomyocyte cross-sectional area and this was significantly reduced with cardiomyocyte STRN knockout (Figure 7A,B). However, hypertrophic gene marker expression (*Myh7*, *Nppa* and *Nppb*) was similar with or without tamoxifen treatment (Figure 6C) suggesting the cells continued to undergo pathological stress. As with the STRN<sup>+/−</sup> colony, gene markers for cardiac non-myocytes showed no significant change in expression. In contrast with the effect of global heterozygous STRN knockout (Figure 4A–C), the increase in interstitial and perivascular fibrosis induced by AngII was significantly inhibited with cardiomyocyte STRN knockout and this was associated with

reduced expression of fibrotic gene markers (Figure 8). We conclude that cardiomyocyte STRN plays an important role in early adaptive remodelling of the heart induced by AngII, with effects at the level of the cardiomyocytes themselves to promote hypertrophic growth and to increase cardiac fibrosis.

Finally, to determine if there were likely to be secondary consequences of the compromised cardiac response to AngII in mice with cardiomyocyte STRN knockout, we assessed the responsiveness of the aorta, focusing on the Windkessel effect [45]. This is seen in the large elastic arteries that distend when blood pressure increases with cardiac contraction in systole and recoil as blood pressure falls during diastole. The Windkessel effect is a system that dampens the large variation in blood pressure during the cardiac cycle and is lost with arterial stiffening resulting from aging or atherosclerosis [46]. We measured the width of the ascending aorta (immediately after the aortic valve and before the aortic arch) after systolic contraction when the aortic diameter is at its largest, and the narrowest diameter following cardiac relaxation. At 7 d, AngII had no significant effect on either measurement in mice treated with corn-oil vehicle alone. However, with cardiomyocyte deletion of STRN, the width of the aorta following relaxation (i.e., the smallest diameter) was significantly greater in mice treated with AngII than the aortas from the vehicle treated mice (Figure 9). This resulted in a significant decrease in the width ratio, suggesting that the loss of striatin in the heart had a secondary effect on the aorta with loss of compliance and reduction in the Windkessel effect.

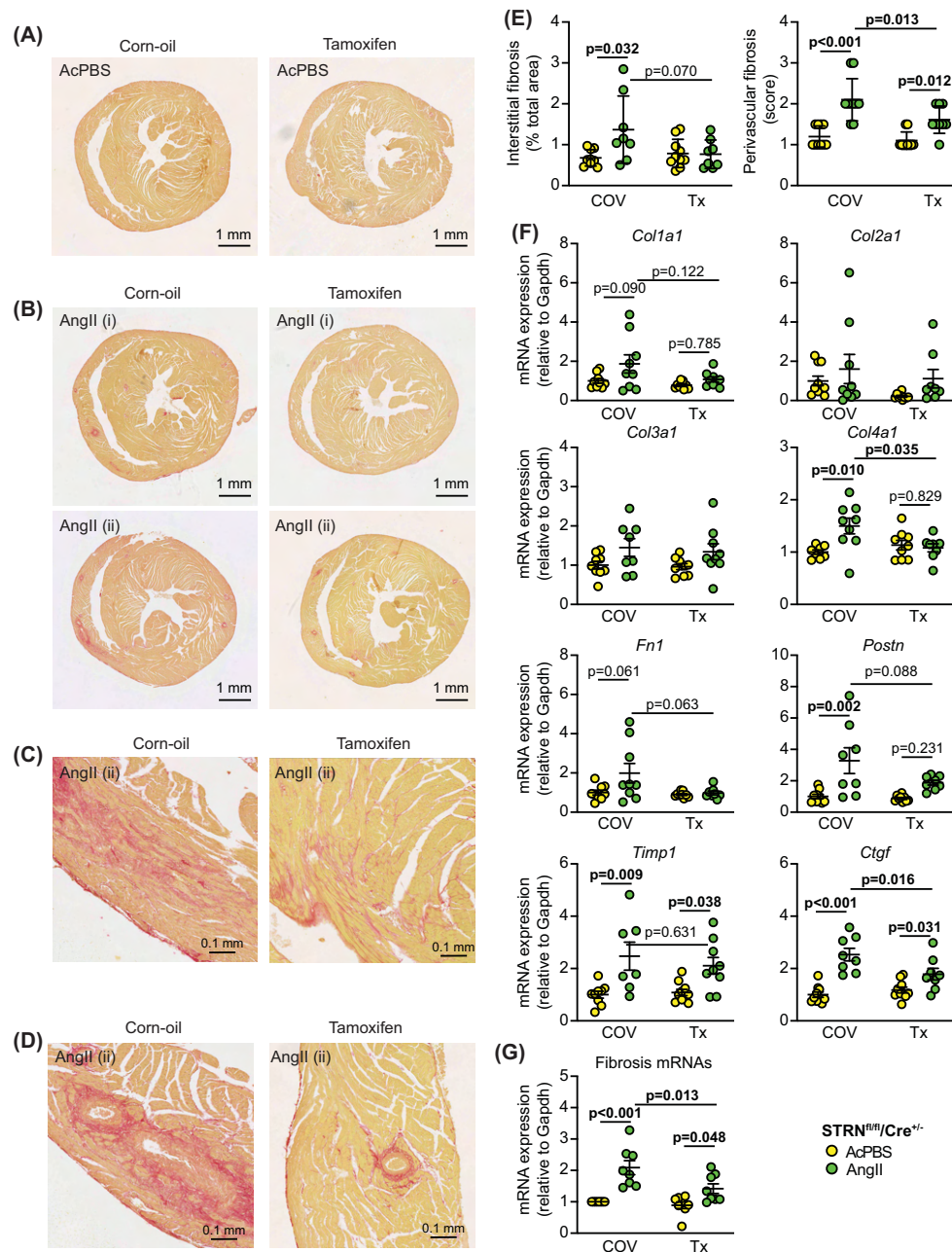
## Discussion

Eukaryotic cellular responses are regulated by vast numbers of protein phosphorylation reactions, catalysed by over 500 different protein kinases in the mammalian kinome [47,48] and countered by a range of protein phosphatases [49]. We have detailed knowledge of how some key signalling pathways operate, but the regulation and roles of many protein kinases remain to be unravelled. Here, we focused on a relatively uninvestigated system, the STRIPAK complexes with a striatin isoform at the core, bringing together the most abundant protein phosphatase in the cell (PP2A) with key protein kinases (e.g., GCKs) to regulate their activation [25,26]. Our data indicate that the three striatin isoforms are all dysregulated in human failing hearts, but our studies with genetically altered mice place a particular emphasis on STRN itself in the development of cardiac hypertrophy induced by AngII treatment and, therefore, in the broader context of hypertensive heart disease.

Our study was conducted in a context of the working model shown in Figure 10 in which STRN-based STRIPAKs operate in all cardiac cells. In addition to global effects of AngII to increase blood pressure, there are local effects of AngII on cardiac cells. The primary effect of both is likely to be on the vascular cells within the heart that are in direct contact with or close proximity to the blood, and which are highly responsive to this hormone (i.e., endothelial cells, smooth muscle cells and/or pericytes). Amongst other effects, AngII stimulates release of pro-hypertrophic factors (e.g., endothelin-1, *Edn1* [50]) that act on cardiomyocytes, inducing cardiomyocyte hypertrophy. In turn, cardiomyocytes release factors that promote fibrosis (e.g., fibroblast growth factor 2, FGF2) and proliferation (e.g., EGF family ligands) in other cardiac cells. Our previous studies with BRAF knockout mice support this concept since *Edn1* and *FGF2* mRNAs are up-regulated in mouse hearts by AngII, but manipulation of cardiomyocyte signalling (with cardiomyocyte knockout of BRAF) selectively inhibit the increase in *FGF2* [34]. We propose that the response involves striatin-based STRIPAKs with activation of GCKs in one or more of the cardiac cell types.

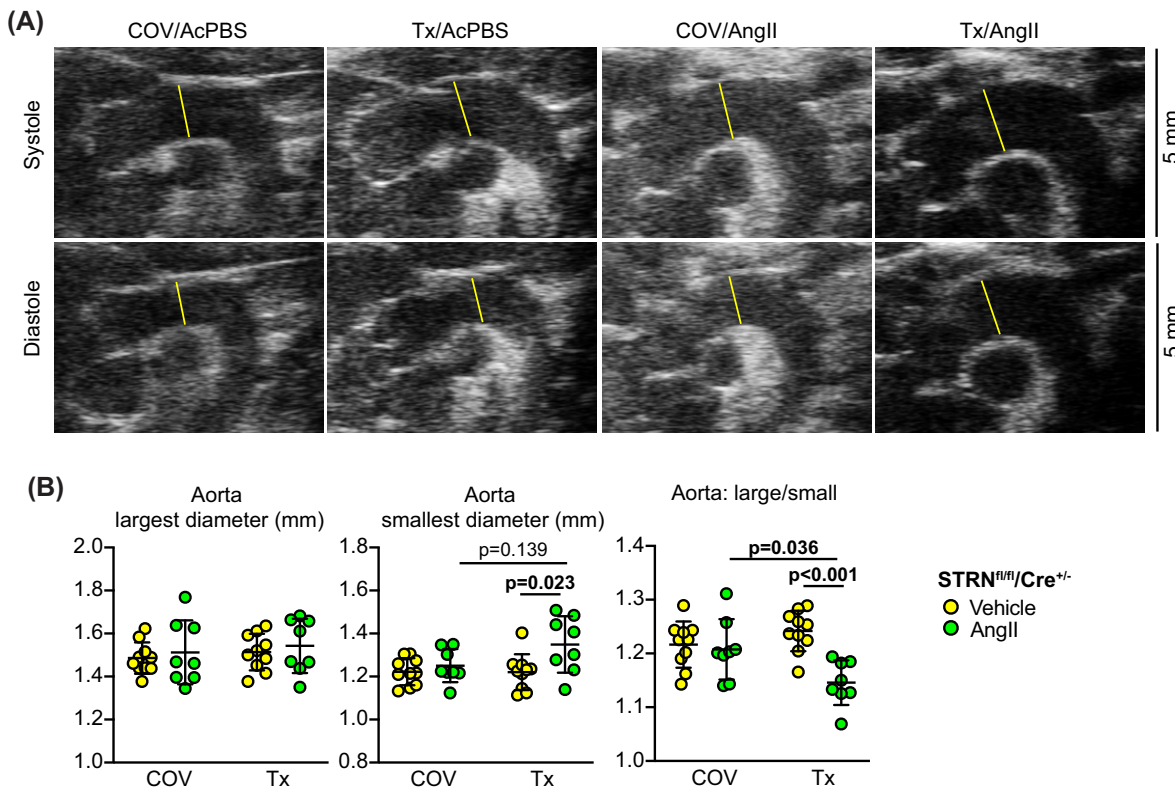
Cardiomyocyte-specific knockout of STRN (with potential dysregulation and mislocalisation of one or more GCK) was sufficient to reduce cardiomyocyte hypertrophy (Figures 6–8). Pro-fibrotic cardiomyocyte-derived factors were also reduced, resulting in inhibition of fibrotic genes and overall reduction in cardiac fibrosis. Thus, striatin-based STRIPAKs are required for cardiomyocyte and cardiac hypertrophy in AngII-induced hypertension. With heterozygous global STRN knockout, there was no significant effect on interstitial or perivascular fibrosis induced by AngII compared with wild-type littermates, but there was greater suppression of cardiomyocyte hypertrophy (Figures 2–4). This model is more complicated, with reduction of STRN-based STRIPAKs in all cardiac cells, potentially disrupting the entire local cardiac response to AngII. Furthermore, loss of STRN in vascular smooth muscle and endothelial cells in peripheral resistance blood vessels carries a potential to affect blood pressure as discussed below. The loss of cardiomyocyte hypertrophy could be a combination of reduced hypertrophic signals from other cells and reduced cardiomyocyte hypertrophy signalling. The apparent lack of effect on fibrosis could be due to changes in pro- vs anti-fibrotic factors that were counterbalanced. However, we can only speculate and further research is needed on the role(s) of STRN in cardiac non-myocytes.

Previous studies in mice with global heterozygous STRN knockout used the same knockout-first system as we used here. The earlier studies developed from prior work demonstrating up-regulation of STRN in mouse heart and aorta by aldosterone, modulation of dietary salt or a combination of L-NAME (to inhibit NO production) and AngII [51]. STRN<sup>+/−</sup> mice and their wild-type littermates have similar blood pressure when fed a restricted salt or normal



**Figure 8. Cardiomyocyte-specific knockout of STRN inhibits the increase in cardiac fibrosis induced by AngII**

Male STRN<sup>fl/fl</sup>/Cre<sup>+/−</sup> mice (8 wks) were treated with corn-oil vehicle (COV) or tamoxifen (Tx; 40 mg/kg) and minipumps implanted to deliver acidified PBS (AcPBS) or 0.8 mg/kg/d AngII for 7 days. Hearts were fixed and sections stained with picrosirius red. Representative short axis views of the whole heart are shown for mice treated with AcPBS (A) or AngII (B). For AngII-treated hearts, the average (i) or maximum (ii) response is shown. Enlarged regions of the AngII-treated hearts in (B) are shown below for interstitial fibrosis (C) or perivascular fibrosis (D). (E) Interstitial fibrosis was measured using ImageJ and is presented as the % of the total area (excluding regions around the blood vessels). Perivascular fibrosis was scored (1: negligible increase in fibrosis around any vessel; 2: mild to moderate fibrosis around 1 or more vessels; 3: Significant fibrosis permeating tissue around 1 or more vessels; 4: extensive fibrosis around multiple vessels, penetrating into the myocardium). A scoring system was used for the latter because of the variation in numbers of vessels seen in different heart sections. (F) RNA was extracted from mouse heart powders and analysed by qPCR for fibrosis mRNAs as indicated. (G) The average value for each condition for each of the genes shown in (F) was taken. aPCR results are relative to GAPDH and normalised to the means for WT mice treated with AcPBS. Individual datapoints are plotted with means  $\pm$  SEM. Statistical analysis used two-way ANOVA with Holm-Sidak's post-test.

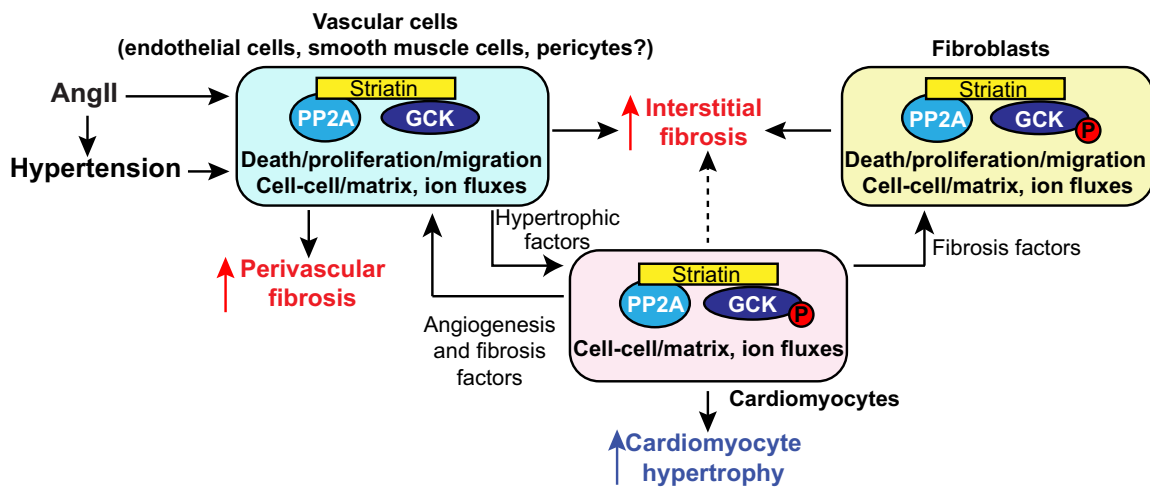


**Figure 9. Loss of aortic elasticity in mice with cardiomyocyte-specific knockout of STRN**

Male STRN<sup>fl/fl</sup>/Cre<sup>+/−</sup> mice (8 wks) were treated with corn-oil vehicle (COV) or tamoxifen (Tx; 40 mg/kg) and minipumps implanted to deliver acidified PBS (AcPBS) or 0.8 mg/kg/d AngII for 7 days. **(A)** B-mode images of the aorta at cardiac systole or diastole (upper and lower panels, respectively; images from each condition are from the same mouse). Aortic width measured after the aortic valve at its largest (i.e., immediately following cardiac contraction) and smallest diameter (with cardiac relaxation) as shown by the yellow lines. **(B)** Analysis of aortic diameter at cardiac systole and diastole plus the ratio between the two values. Individual datapoints are plotted with means ± SEM. Statistical analysis used two-way ANOVA with Holm-Sidak's post-test.

diet (0.03% or 0.3–0.5% NaCl, respectively), but have an exaggerated increase in blood pressure on a higher salt diet (1.6% NaCl) along with enhanced contraction of aortic rings and reduced relaxation [3–5]. STRN<sup>+/−</sup> mice also have an enhanced response to aldosterone with increased renal (though not cardiac) damage [5].

Interestingly, there is no significant difference in the renal or cardiac responses of STRN<sup>+/−</sup> and wild-type mice in a hypertension model using L-NAME and AngII, despite an increase in blood pressure. This apparently contradicts our data, but L-NAME inhibits NO production and compromises endothelial cell function and vessel relaxation [52]. In Garza et al. [4], mice were treated with L-NAME for 7 d, before implantation of minipumps for delivery of 0.7 mg/kg/d AngII for 3 d in a regime that increased blood pressure. We used a similar dose of AngII over 7 d without L-NAME, a regime with a minimal effect on blood pressure over this time [39–41] and, arguably, a milder model. It remains possible that the blood pressure response to AngII alone (not measured in this study) could be affected in STRN<sup>+/−</sup> mice if STRN-based STRIPAKs are involved in AngII receptor signalling in vascular smooth muscle and/or endothelial cells in peripheral resistance blood vessels. Deletion of type 1 AngII receptors (AT<sub>1</sub>Rs) in vascular smooth muscle cells in resistance vessels in mice reduces baseline blood pressure and inhibits the increase in blood pressure induced by AngII by 30% [53,54]. Thus, although there is no baseline difference between STRN<sup>+/−</sup> mice and their wild-type littermates [3–5], the effect of AngII on blood pressure in heterozygote STRN<sup>+/−</sup> mice could be compromised to some degree, possibly contributing to some of the effects on the heart that we detected (Figures 2–4). However, AngII increases NO production in endothelial cells [55], and expression of constitutively-active AT<sub>1</sub>Rs in endothelial cells decreases basal blood pressure with increased production of NO [56], potentially countering the effects in vascular smooth muscle cells. Further research is clearly important to assess the specific roles of STRN-based

**Working model:****Effects of STRN knockout:**

**Global heterozygote STRN knockout**

- Interstitial fibrosis
- Perivascular fibrosis
- Reduced cardiomyocyte hypertrophy

**Cardiomyocyte STRN knockout**

- Reduced interstitial fibrosis
- Reduced perivascular fibrosis
- Reduced cardiomyocyte hypertrophy

**Figure 10. Working model of striatin signalling in cardiac hypertrophy induced by angiotensin II and conclusions from this study**

Previous studies place striatin at the core of STRIPAK complexes in which PP2A is brought into the vicinity of protein kinases (particularly those of GCK family). Here, PP2A dephosphorylates and inactivates GCKs. STRIPAKs are targeted to subcellular domains where they modulate cell–cell and cell–matrix interactions, regulate cell death or influence cell growth, proliferation and migration. In our working model, in addition to global effects of AngII to increase blood pressure, there are also local effects of AngII on cardiac cells. The increase in blood pressure, along with AngII itself have a primary effect on endothelial cells that are in direct contact with the blood and highly responsive to this hormone. In arterioles, there is additional interaction of AngII with smooth muscle cells that are also directly affected by blood pressure. These cells release pro-hypertrophic factors to promote cardiomyocyte hypertrophy. Cardiomyocytes release additional pro-fibrotic and pro-proliferative factors that affect other cardiac cells. The response involves STRN-based STRIPAKs in one or more of the cardiac cell types with, potentially, protein kinases such as GCKs being activated by reduced PP2A activity in the STRIPAK complex. The data from this study show that cardiomyocyte-specific knockout of STRN in mice reduced cardiomyocyte hypertrophy and cardiac fibrosis resulting from AngII treatment. AngII-induced cardiomyocyte hypertrophy was also inhibited in heterozygous global STRN knockout mice compared with wild-type littermates, but there was no effect on interstitial or perivascular fibrosis.

STRIPAKs in vascular smooth muscle cells and endothelial cells not only in the heart but also in peripheral blood vessels and the effects on blood pressure, alongside tissue pathologies.

Our studies assessed the effects of STRN deletion only in young male mice and in a context of AngII-induced hypertension using a dose of 0.8 mg/kg/d. The dosage was selected carefully because our pilot studies with a higher dose (0.9 mg/kg/d) resulted in increased mortality (20–30% over 3–7 d) due to rupture of a major blood vessel (unpublished data). The concentration of AngII we used is recognised as a slow pressor dose [39–41] and induced features of hypertensive heart disease in all three genetic models with cardiomyocyte hypertrophy and cardiac fibrosis even over 7 days. We have used the same dose in previous experiments including an assessment of the effects of dabrafenib (a BRAF inhibitor) on AngII-induced hypertension, in which we also demonstrated how the disease progresses towards heart failure over 28 d [57]. Further studies of STRN over this longer period may be useful to determine whether it plays a significant role in later stages of the disease. We have yet to assess the role of STRN or STRN3 in female mice. Here, it is necessary to consider that hypertension develops in males at an earlier age than females, and females have some protection against hypertension until after the menopause [58]. Thus, young female mice are resistant to

AngII-induced hypertension and induction of menopause results in loss of this resistance [42,43]. Notably, protection is restored if mice continue to receive oestrogen. Overall, although there is emphasis on assessing and comparing males and females in all studies, particularly for hypertension, it seems more appropriate and necessary to consider the sexes separately allowing for menopausal status in females.

STRN3 was first identified as a nuclear antigen (S/G2 nuclear antigen, SG2NA) subject to cell cycle regulation [59] and, consequently, there is greater emphasis on its role in proliferating cells and cancer (e.g., [60]). However, it is expressed at significant levels in the heart and, of the multiple splice-variants, the dominant isoform is reported to be 78 kD, lacking two exons from the full-length 87 kDa variant [61,62]. Although other variants are reported in the heart, we detected a single dominant band above the 75 kDa marker, presumably corresponding to the 78 kDa STRN3 isoform (Supplementary Figures S4–S7). We are not aware of other published studies of STRN3 in the heart or of *in vivo* studies in STRN3 knockout mice. STRN3 was expressed in mouse and human hearts and was significantly upregulated in human failing hearts (Figure 1A–C). However, we did not detect any significant differences in cardiac function or dimensions between STRN3<sup>+/−</sup> mice and their wild-type littermates, either at baseline or in response to AngII (Supplementary Figures S2,3, and Supplementary Tables S4, S6 and S7). The studies of STRN3<sup>+/−</sup> and STRN<sup>+/−</sup> mice were done in parallel and the negative results with STRN3<sup>+/−</sup> mice emphasize the potential importance of STRN in the early adaptive response to AngII. However, STRN3 may play an important role in later phases of hypertension-induced cardiac dysfunction and/or in other cardiac pathologies (e.g., myocardial infarction that results in acute injury). It also has to be considered that we studied mice with heterozygote rather than homozygote gene deletion and study of homozygotes (not possible because of embryonic lethality) may have been more revealing. Because of this, it was important to adopt a conditional deletion approach to avoid problems during development.

Immunostaining studies place STRN at the intercalated disc in the heart suggesting it may regulate ion fluxes [6,30]. Consistent with this concept, reduced expression of STRN in boxer dogs is associated with ARVC and heart failure [6,7], both of which are associated with a higher risk of life-threatening ventricular arrhythmia and poor prognosis [63]. In addition, studies in cultured cardiomyocytes indicate that overexpression of striatin enhances contraction and STRN knockdown reduces contractility [64]. Human genome-wide association studies (GWAS) link the STRN gene with QRS/PR interval [10,11], further suggesting a role in regulating ion fluxes and contractility in cardiomyocytes. We did not detect any differences in cardiac function between STRN<sup>+/−</sup> mice and their wild-type littermates, but it is unlikely that we would have detected arrhythmias with echocardiography in the relatively young mice we studied with a relatively low level of stress resulting from the dose and duration of AngII treatment. Greater differences would perhaps have been detected in older mice or with a more severe or prolonged stress (e.g., in a myocardial infarction model, prolonged treatment with AngII or with transverse aortic constriction).

Even though we saw no effect of heterozygous STRN knockout on cardiac function using echocardiography, the overall hypertrophic response induced by AngII was inhibited (Figure 2). This was due to a reduction in cardiomyocyte hypertrophy rather than fibrosis (Figures 3 and 4), suggesting that the phenotype resulted from decreased STRN expression in cardiomyocytes. To address this, we developed a model for homozygous cardiomyocyte-specific STRN knockout adopting a system for inducible and conditional gene deletion. This used a well-established approach using a tamoxifen-inducible Cre enzyme under the regulation of the MYH6 promoter [36], a system which avoids problems associated with development but raises additional concerns of potential cardiotoxicity from the Cre enzyme. This was minimised by only using mice hemizygous for Cre and by restraining temporal activation of the enzyme with just a single dose of tamoxifen to induce recombination. In hemizygous Cre<sup>+/−</sup> mice, we detect no cardiotoxicity with or without AngII for at least the duration of the experiments reported here [33,35]. Others have used a similar approach and also report little cardiotoxicity [65]. Given the results with STRN<sup>+/−</sup> mice, we anticipated that the hypertrophic response induced by AngII would be compromised by cardiomyocyte STRN knockout, and the increase in predicted LV mass estimated on echocardiograms was, indeed, reduced (Figure 6C). However, the degree of inhibition of cardiomyocyte hypertrophy appeared less than with the STRN<sup>+/−</sup> mice and, in contrast to the STRN<sup>+/−</sup> mice, there was substantial reduction in fibrosis (Figures 7 and 8). The mice were derived from sperm from our STRN<sup>+/−</sup> colony so the difference is unlikely to be due to the genetic background. Thus, the effect on fibrosis is most probably a true reflection of the knockout system.

SNPs in the STRN gene have been linked to regulation of blood pressure and the development of heart failure using GWAS, but there are some difficulties with interpretation. The first SNP to be linked to QRS interval (rs17020136 [66]) was originally placed in the STRN gene, but is now linked to the adjacent HEATR5B gene in the EMBL-EBI GWAS Catalog (<https://www.ebi.ac.uk/gwas>), along with others associated with increased systolic blood pressure (rs146074994, 13408514 [9,67]). HEATR5B (HEAT repeat containing 5B) is a ubiquitously expressed protein-coding gene of unknown function and further studies of its role in blood pressure regulation may be useful. Nevertheless, SNPs in the STRN gene are also linked to increased blood pressure (rs2540923 [3], rs3770770 [9]) in addition to

QRS/PR interval (rs3770770 [10], rs17496249 [11]), hypertrophic cardiomyopathy and heart failure (rs2003585 [12]). Many of the identified STRN SNPs associated with cardiac dysfunction are intronic, so the functional consequences are not clear. Nevertheless, linkage of the STRN gene with blood pressure along with studies in STRN<sup>+/−</sup> mice have led to a clinical trial for use of mineralocorticoid receptor antagonists in hypertensive patients carrying STRN risk alleles [68].

Our data implicate cardiomyocyte STRN in cardiac hypertrophy, but provide limited insight into the mechanism of action. Striatin itself becomes hyperphosphorylated on inhibition of PP2A in cardiomyocytes [69], a modification which may modify subcellular localisation and/or binding partners. It may also be subject to ADP-ribosylation [70], although this has not been studied in the heart. The protein kinases identified in STRIPAK complex signalling belong to the GCK family with the GCKII (MST1 and MST2 [71]), GCKIII (MST3, MST4, YSK [60,72–74]), GCKV (SLIK in *Drosophila*; SLK and LOK are mammalian homologues [73,75]) and GCKVI (MAP4K4, TNIK, MINK1 [76–78]) subfamilies being specifically implicated to date. MST1/2, MST3, SLK and MAP4K4 are relatively highly expressed in adult rat cardiomyocytes [79], so these are the candidate kinases for cardiac adaptation to AngII. MST1/MST2 are involved in HIPPO signalling and regulation of cell survival/cell death in the heart [80]. Since cardiomyocyte MST1 knockout increases autophagic flux to alleviate AngII-induced cardiac damage [81], dysregulation of MST1 as a result of cardiomyocyte STRN knockout could have a similar effect and reduce cardiomyocyte hypertrophy. MAP4K4 associates with striatins in cardiomyocytes and is linked to human heart failure [69,82,83], so could also be involved. MST3 plays an important role in cell migration and is regulated acutely by phosphatase activity in cardiomyocytes [84,85], but there is little/no information on the role of SLK in heart. Whilst all of the kinases may interact with each of the striatins in experiments conducted *in vitro* or using overexpression approaches, specificity in terms of STRIPAK binding partners or subcellular targeting remains to be determined.

We tried to gain insight into which kinases may be involved in our study and whether global knockdown of STRN or STRN3, or cardiomyocyte STRN knockout had any effect on GCKs by immunoblotting mouse heart extracts (data not shown). Although the antibodies were adequate for studies of MST3 and MAP4K4 in rat cardiomyocytes [69,84], we failed to obtain reliable signals for these kinases in mouse hearts. Of a range of other antibodies, only MST1 produced a band of an appropriate molecular weight, but the results were variable and the reliability of the data is questionable. Even if we could detect these proteins, it would have been difficult to interpret the data because of the interconnecting networks of STRIPAK complexes. Clearly further studies are required to determine the nature of specific STRIPAK complexes in cardiomyocytes and the heart, along with their subcellular localisation, but *in vivo* gene deletion studies are probably not the best approach. For this stage of the research, it may be more appropriate to increase knowledge and understanding of the biochemical basis of the signalling pathway before trying to understand the implications for heart disease. These studies may benefit from the use of genetically modified systems for direct labelling of near-neighbour proteins that can then be identified and tracked. This technology is becoming available (e.g., Bio-ID [86]) and will be invaluable for understanding multiprotein systems such as those involved in STRIPAK signalling.

This study only considers the role of STRN and STRN3 in the early stages of cardiac remodelling induced by AngII, not the later stages associated with heart failure and decreased ejection fraction. Extending the study over a more prolonged period would enable further assessment of whether STRN knockdown or cardiomyocyte deletion could prevent this deterioration of cardiac function. Longer term studies would also help to determine if STRN3 plays an important role in developing heart failure, as suggested by the minor abnormalities in longitudinal strain we detected in STRN3<sup>+/−</sup> mice treated with AngII over 7 d. We also did not consider the possible effects of STRN on arrhythmias and sudden death. We noted that the STRN mice under investigation in this study appeared more prone to sudden death than other genetically altered mice (e.g., those associated with BRAF [33,35]) we studied in parallel. However, there was no correlation with STRN expression (Supplementary Table S1), suggesting it was either coincidental or related to the background strain. Given the link between STRN and ARVC in boxer dogs [6,7] and SNPs in the STRN gene to hypertrophic cardiomyopathy, it will be important to conduct additional studies to assess possible arrhythmias in mice with STRN knockdown. Probably the greatest limitation of this study is the lack of knowledge of the STRIPAK complexes themselves. Thus, although the data suggest that inhibiting STRN will reduce cardiac hypertrophy induced by AngII, STRN potentially acts at the core of multiple complexes that regulate different GCKs, and one or more of these GCKs may be involved. Knowing which GCKs are involved and how they are regulated will be a crucial element for identifying specific targets for therapeutic manipulation of STRIPAK signalling.

In conclusion, our data indicate that STRN, but probably not STRN3, plays an important role in the early remodelling processes induced in the heart to AngII. There is clearly much research on STRN still to be done to understand its role in hypertensive heart disease, not only for cardiac pathologies (e.g., to understand the role of STRN in cardiac

non-myocytes) but also for the rest of the cardiovascular system (e.g., STRIPAK complex involvement in blood pressure regulation and the peripheral vasculature). In addition, STRN3 and STRN4 remain to be investigated, along with the involvement of individual GCKs in specific STRIPAK complexes in each of the aforementioned cells. Nevertheless, the data in this study clearly identify striatin-based STRIPAKs as a novel signalling paradigm in the development of pathological cardiac hypertrophy. Understanding this system may provide therapeutic options for modulating the responses and managing progression of hypertensive heart disease.

## Clinical perspectives

- **Background:** Striatins form the core of ***STR*iatin-*I*nteracting ***P*hosphatase ***A*nd *K*inase**** (STRIPAK) complexes that regulate crucial cellular processes such as those associated with heart failure.**
- **Summary:** The three striatins are expressed in human hearts, with up-regulation of STRN and STRN3 in failing hearts, whilst studies in mice indicate that STRN is required in cardiomyocytes for early remodelling of the hypertensive heart.
- **Potential significance of results to human health and disease:** STRN-based STRIPAKs represent a novel signalling paradigm in the development of pathological cardiac hypertrophy, and modulating this system may provide therapeutic options for managing the cardiac effects of hypertensive heart disease.

## Data Availability

All primary data are available from the corresponding author upon reasonable request.

## Competing Interests

The authors declare that there are no competing interests associated with the manuscript.

## Funding

This work was supported by the British Heart Foundation [grant numbers PG/15/41/31560, FS/18/33/33621, PG/15/24/31367, and FS/19/24/34262] and Qassim University, Saudi Arabia (to H.O.A).

## Open Access

Open access for this article was enabled by the participation of University of Reading in an all-inclusive *Read & Publish* agreement with Portland Press and the Biochemical Society under a transformative agreement with JISC.

## CRedit Author Contribution

**Joshua J. Cull:** Investigation, Writing—review & editing. **Susanna T.E. Cooper:** Investigation, Writing—review & editing. **Hajed O. Alharbi:** Investigation, Writing—review & editing. **Sonia P. Chothani:** Investigation, Writing—review & editing. **Owen J.L. Rackham:** Supervision, Writing—review & editing. **Daniel N. Meijles:** Supervision, Investigation, Writing—review & editing. **Philip R. Dash:** Writing—review & editing. **Risto Kerkelä:** Writing—review & editing. **Neil Ruparelia:** Writing—review & editing. **Peter H. Sugden:** Conceptualization, Writing—original draft, Writing—review & editing. **Angela Clerk:** Conceptualization, Resources, Data curation, Formal analysis, Supervision, Funding acquisition, Validation, Methodology, Writing—original draft, Project administration.

## Acknowledgements

We thank Andrew Cripps, Mhairi Baxter and Wayne Knight (University of Reading), and Robert Bond, Emma Mustafa and Rene Ocho (St. George's University of London) for support for the *in vivo* mouse studies.

## Abbreviations

AT<sub>1</sub>R, type 1 AngII receptor; COV, corn-oil vehicle; DCM, dilated cardiomyopathy; FGF2, fibroblast growth factor 2; GCK, Germline Centre Kinase; GWAS, genome-wide association studies; STRIPAK, ***STR*iatin-*I*nteracting ***P*hosphatase ***A*nd *K*inase****; WT, wild-type.**

## References

- 1 Savarese, G., Becher, P.M., Lund, L.H., Seferovic, P., Rosano, G.M.C. and Coats, A. (2023) Global burden of heart failure: a comprehensive and updated review of epidemiology. *Cardiovasc. Res.* **118**, 3272–3287, <https://doi.org/10.1093/cvr/cvac013>
- 2 Mills, K.T., Stefanescu, A. and He, J. (2020) The global epidemiology of hypertension. *Nat. Rev. Nephrol.* **16**, 223–237, <https://doi.org/10.1038/s41581-019-0244-2>
- 3 Garza, A.E., Rariy, C.M., Sun, B., Williams, J.S., Lasky-Su, J., Baudrand, R. et al. (2015) Variants in striatin gene are associated with salt-sensitive blood pressure in mice and humans. *Hypertension* **65**, 211–217, <https://doi.org/10.1161/HYPERTENSIONAHA.114.04233>
- 4 Garza, A.E., Pojoga, L.H., Moize, B., Hafiz, W.M., Opsasnick, L.A., Siddiqui, W.T. et al. (2015) Critical role of striatin in blood pressure and vascular responses to dietary sodium intake. *Hypertension* **66**, 674–680, <https://doi.org/10.1161/HYPERTENSIONAHA.115.05600>
- 5 Garza, A.E., Trefts, E., Katayama Rangel, I.A., Brooks, D., Baudrand, R., Moize, B. et al. (2020) Striatin heterozygous mice are more sensitive to aldosterone-induced injury. *J. Endocrinol.* **245**, 439–450, <https://doi.org/10.1530/JOE-19-0562>
- 6 Meurs, K.M., Mauceli, E., Lahmers, S., Acland, G.M., White, S.N. and Lindblad-Toh, K. (2010) Genome-wide association identifies a deletion in the 3' untranslated region of striatin in a canine model of arrhythmogenic right ventricular cardiomyopathy. *Hum. Genet.* **128**, 315–324, <https://doi.org/10.1007/s00439-010-0855-y>
- 7 Meurs, K.M., Stern, J.A., Sisson, D.D., Kittleson, M.D., Cunningham, S.M., Ames, M.K. et al. (2013) Association of dilated cardiomyopathy with the striatin mutation genotype in boxer dogs. *J. Vet. Intern. Med.* **27**, 1437–1440, <https://doi.org/10.1111/jvim.12163>
- 8 Gupta, T., Connors, M., Tan, J.W., Manosroi, W., Ahmed, N., Ting, P.Y. et al. (2017) Striatin gene polymorphic variants are associated with salt sensitive blood pressure in normotensives and hypertensives. *Am. J. Hypertens.* **31**, 124–131, <https://doi.org/10.1093/ajh/hpx146>
- 9 Plotnikov, D., Huang, Y., Khawaja, A.P., Foster, P.J., Zhu, Z., Guggenheim, J.A. et al. (2022) High blood pressure and intraocular pressure: a Mendelian randomization study. *Invest. Ophthalmol. Vis. Sci.* **63**, 29, <https://doi.org/10.1167/iovs.63.6.29>
- 10 van der Harst, P., van Setten, J., Verweij, N., Vogler, G., Franke, L., Maurano, M.T. et al. (2016) Genetic loci influencing myocardial mass. *J. Am. Coll. Cardiol.* **68**, 1435–1448, 52, <https://doi.org/10.1016/j.jacc.2016.07.729>
- 11 Ntalla, I., Weng, L.C., Cartwright, J.H., Hall, A.W., Sveinbjornsson, G., Tucker, N.R. et al. (2020) Multi-ancestry GWAS of the electrocardiographic PR interval identifies 202 loci underlying cardiac conduction. *Nat. Commun.* **11**, 2542, <https://doi.org/10.1038/s41467-020-15706-x>
- 12 Harper, A.R., Goel, A., Grace, C., Thomson, K.L., Petersen, S.E., Xu, X. et al. (2021) Common genetic variants and modifiable risk factors underpin hypertrophic cardiomyopathy susceptibility and expressivity. *Nat. Genet.* **53**, 135–142, <https://doi.org/10.1038/s41588-020-00764-0>
- 13 Levin, M.G., Tsao, N.L., Singhal, P., Liu, C., Vy, H.M.T., Paranjpe, I. et al. (2022) Genome-wide association and multi-trait analyses characterize the common genetic architecture of heart failure. *Nat. Commun.* **13**, 6914, <https://doi.org/10.1038/s41467-022-34216-6>
- 14 Surendran, P., Feofanova, E.V., Lahrouchi, N., Ntalla, I., Karthikeyan, S., Cook, J. et al. (2020) Discovery of rare variants associated with blood pressure regulation through meta-analysis of 1.3 million individuals. *Nat. Genet.* **52**, 1314–1332, <https://doi.org/10.1038/s41588-020-00713-x>
- 15 Zhou, P. and Pu, W.T. (2016) Recounting cardiac cellular composition. *Circ. Res.* **118**, 368–370, <https://doi.org/10.1161/CIRCRESAHA.116.308139>
- 16 Dorn, II, G.W., Robbins, J. and Sugden, P.H. (2003) Phenotyping hypertrophy: eschew obfuscation. *Circ. Res.* **92**, 1171–1175, <https://doi.org/10.1161/01.RES.0000077012.11088.BC>
- 17 Sheng, S.Y., Li, J.M., Hu, X.Y. and Wang, Y. (2023) Regulated cell death pathways in cardiomyopathy. *Acta Pharmacol. Sin.* **44**, 1521–1535, <https://doi.org/10.1038/s41401-023-01068-9>
- 18 Gogiraju, R., Bochenek, M.L. and Schafer, K. (2019) Angiogenic endothelial cell signaling in cardiac hypertrophy and heart failure. *Front Cardiovasc. Med.* **6**, 20, <https://doi.org/10.3389/fcvm.2019.00020>
- 19 Suthahar, N., Meijers, W.C., Sillje, H.H.W. and de Boer, R.A. (2017) From inflammation to fibrosis—molecular and cellular mechanisms of myocardial tissue remodelling and perspectives on differential treatment opportunities. *Curr. Heart Fail Rep.* **14**, 235–250, <https://doi.org/10.1007/s11897-017-0343-y>
- 20 Mishra, S. and Kass, D.A. (2021) Cellular and molecular pathobiology of heart failure with preserved ejection fraction. *Nat. Rev. Cardiol.* **18**, 400–423, <https://doi.org/10.1038/s41569-020-00480-6>
- 21 Kurose, H. (2021) Cardiac fibrosis and fibroblasts. *Cells* **10**, 1716, <https://doi.org/10.3390/cells10071716>
- 22 Kovacic, J.C., Dimmeler, S., Harvey, R.P., Finkel, T., Aikawa, E., Krenning, G. et al. (2019) Endothelial to mesenchymal transition in cardiovascular disease: JACC State-of-the-Art Review. *J. Am. Coll. Cardiol.* **73**, 190–209, <https://doi.org/10.1016/j.jacc.2018.09.089>
- 23 Reynhout, S. and Janssens, V. (2019) Physiologic functions of PP2A: lessons from genetically modified mice. *Biochim. Biophys. Acta Mol. Cell. Res.* **1866**, 31–50, <https://doi.org/10.1016/j.bbamcr.2018.07.010>
- 24 Delpire, E. (2009) The mammalian family of sterile 20p-like protein kinases. *Pflugers Archiv* **458**, 953–967, <https://doi.org/10.1007/s00424-009-0674-y>
- 25 Hwang, J. and Pallas, D.C. (2014) STRIPAK complexes: structure, biological function, and involvement in human diseases. *Int. J. Biochem. Cell Biol.* **47**, 118–148, <https://doi.org/10.1016/j.biocel.2013.11.021>
- 26 Kuck, U., Radchenko, D. and Teichert, I. (2019) STRIPAK, a highly conserved signaling complex, controls multiple eukaryotic cellular and developmental processes and is linked with human diseases. *Biol. Chem.* **400**, 1005–1022, <https://doi.org/10.1515/hsz-2019-0173>
- 27 Goudreault, M., D'Ambrosio, L.M., Kean, M.J., Mullin, M.J., Larsen, B.G., Sanchez, A. et al. (2009) A PP2A phosphatase high density interaction network identifies a novel striatin-interacting phosphatase and kinase complex linked to the cerebral cavernous malformation 3 (CCM3) protein. *Mol. Cell. Proteomics* **8**, 157–171, <https://doi.org/10.1074/mcp.M800266-MCP200>
- 28 Herzog, F., Kahraman, A., Boehringer, D., Mak, R., Bracher, A., Walzthoeni, T. et al. (2012) Structural probing of a protein phosphatase 2A network by chemical cross-linking and mass spectrometry. *Science* **337**, 1348–1352, <https://doi.org/10.1126/science.1221483>

29 Couzens, A.L., Knight, J.D., Kean, M.J., Teo, G., Weiss, A., Dunham, W.H. et al. (2013) Protein interaction network of the mammalian Hippo pathway reveals mechanisms of kinase-phosphatase interactions. *Sci. Signal.* **6**, rs15, <https://doi.org/10.1126/scisignal.2004712>

30 Franke, W.W., Rickett, S., Zimbelmann, R., Dorflinger, Y., Kuhn, C., Frey, N. et al. (2014) Striatins as plaque molecules of zonulae adherentes in simple epithelia, of tessellate junctions in stratified epithelia, of cardiac composite junctions and of various size classes of lateral adherens junctions in cultures of epithelia- and carcinoma-derived cells. *Cell Tissue Res.* **357**, 645–665

31 Heinig, M., Adriaens, M.E., Schafer, S., van Deutekom, H.W.M., Lodder, E.M., Ware, J.S. et al. (2017) Natural genetic variation of the cardiac transcriptome in non-diseased donors and patients with dilated cardiomyopathy. *Genome Biol.* **18**, 170, <https://doi.org/10.1186/s13059-017-1286-z>

32 Love, M.I., Huber, W. and Anders, S. (2014) Moderated estimation of fold change and dispersion for RNA-seq data with DESeq2. *Genome Biol.* **15**, 550, <https://doi.org/10.1186/s13059-014-0550-8>

33 Clerk, A., Meijles, D.N., Hardyman, M.A., Fuller, S.J., Chothani, S.P., Cull, J.J. et al. (2022) Cardiomyocyte BRAF and type 1 RAF inhibitors promote cardiomyocyte and cardiac hypertrophy in mice in vivo. *Biochem. J.* **479**, 401–424, <https://doi.org/10.1042/BCJ20210615>

34 Marshall, J.J., Cull, J.J., Alharbi, H.O., Zaw Thin, M., Cooper, S.T., Barrington, C. et al. (2022) PKN2 deficiency leads both to prenatal congenital cardiomyopathy and defective angiotensin II stress responses. *Biochem. J.* **479**, 1467–1486, <https://doi.org/10.1042/BCJ20220281>

35 Alharbi, H.O., Hardyman, M.A., Cull, J.J., Markou, T., Cooper, S.T.E., Glennon, P.E. et al. (2022) Cardiomyocyte BRAF is a key signalling intermediate in cardiac hypertrophy in mice. *Clin. Sci. (Lond.)* **136**, 1661–1681, <https://doi.org/10.1042/CS20220607>

36 Sohal, D.S., Nghiem, M., Crackower, M.A., Witt, S.A., Kimball, T.R., Tymitz, K.M. et al. (2001) Temporally regulated and tissue-specific gene manipulations in the adult and embryonic heart using a tamoxifen-inducible Cre protein. *Circ. Res.* **89**, 20–25, <https://doi.org/10.1161/hh1301.092687>

37 Meijles, D.N., Cull, J.J., Markou, T., Cooper, S.T.E., Haines, Z.H.R., Fuller, S.J. et al. (2020) Redox regulation of cardiac ASK1 (Apoptosis Signal-Regulating Kinase 1) controls p38-MAPK (mitogen-activated protein kinase) and orchestrates cardiac remodeling to hypertension. *Hypertension* **76**, 1208–1218, <https://doi.org/10.1161/HYPERTENSIONAHA.119.14556>

38 Marshall, A.K., Barrett, O.P.T., Cullingford, T.E., Shannmugasundram, A., Sugden, P.H. and Clerk, A. (2010) ERK1/2 signaling dominates over RhoA signaling in regulating early changes in RNA expression induced by endothelin-1 in neonatal rat cardiomyocytes. *PLoS ONE* **5**, e10027, <https://doi.org/10.1371/journal.pone.0010027>

39 Zimmerman, M.C., Lazartigues, E., Sharma, R.V. and Davison, R.L. (2004) Hypertension caused by angiotensin II infusion involves increased superoxide production in the central nervous system. *Circ. Res.* **95**, 210–216, <https://doi.org/10.1161/01.RES.0000135483.12297.e4>

40 Patel, J., Douglas, G., Kerr, A.G., Hale, A.B. and Channon, K.M. (2018) Effect of irradiation and bone marrow transplantation on angiotensin II-induced aortic inflammation in ApoE knockout mice. *Atherosclerosis* **276**, 74–82, <https://doi.org/10.1016/j.atherosclerosis.2018.07.019>

41 Capone, C., Faraco, G., Peterson, J.R., Coleman, C., Anrather, J., Milner, T.A. et al. (2012) Central cardiovascular circuits contribute to the neurovascular dysfunction in angiotensin II hypertension. *J. Neurosci.* **32**, 4878–4886, <https://doi.org/10.1523/JNEUROSCI.6262-11.2012>

42 Pollow, Jr, D.P., Romero-Aleshire, M.J., Sanchez, J.N., Konhilas, J.P. and Brooks, H.L. (2015) ANG II-induced hypertension in the VCD mouse model of menopause is prevented by estrogen replacement during perimenopause. *Am. J. Physiol. Regul. Integr. Comp. Physiol.* **309**, R1546–R1552, <https://doi.org/10.1152/ajpregu.00170.2015>

43 Brooks, H.L., Pollow, D.P. and Hoyer, P.B. (2016) The VCD mouse model of menopause and perimenopause for the study of sex differences in cardiovascular disease and the metabolic syndrome. *Physiology (Bethesda)* **31**, 250–257, <https://doi.org/10.1152/physiol.00057.2014>

44 Jahn, H.M., Kasakow, C.V., Helfer, A., Michely, J., Verkhratsky, A., Maurer, H.H. et al. (2018) Refined protocols of tamoxifen injection for inducible DNA recombination in mouse astroglia. *Sci. Rep.* **8**, 5913, <https://doi.org/10.1038/s41598-018-24085-9>

45 Belz, G.G. (1995) Elastic properties and Windkessel function of the human aorta. *Cardiovasc. Drugs Ther.* **9**, 73–83, <https://doi.org/10.1007/BF00877747>

46 Pierce, G.L., Coutinho, T.A., DuBose, L.E. and Donato, A.J. (2022) Is it good to have a stiff aorta with aging? Causes and consequences. *Physiology (Bethesda)* **37**, 154–173, <https://doi.org/10.1152/physiol.00035.2021>

47 Manning, G., Whyte, D.B., Martinez, R., Hunter, T. and Sudarsanam, S. (2002) The protein kinase complement of the human genome. *Science* **298**, 1912–1934, <https://doi.org/10.1126/science.1075762>

48 Caenepeel, S., Charydczak, G., Sudarsanam, S., Hunter, T. and Manning, G. (2004) The mouse kinome: discovery and comparative genomics of all mouse protein kinases. *Proc. Natl. Acad. Sci. U.S.A.* **101**, 11707–11712, <https://doi.org/10.1073/pnas.0306880101>

49 Nguyen, H. and Kettenbach, A.N. (2023) Substrate and phosphorylation site selection by phosphoprotein phosphatases. *Trends Biochem. Sci.* **48**, 713–725, <https://doi.org/10.1016/j.tibs.2023.04.004>

50 Marasciulo, F.L., Montagnani, M. and Potenza, M.A. (2006) Endothelin-1: the yin and yang on vascular function. *Curr. Med. Chem.* **13**, 1655–1665, <https://doi.org/10.2174/092986706777441968>

51 Pojoga, L.H., Coutinho, P., Rivera, A., Yao, T.M., Maldonado, E.R., Youte, R. et al. (2012) Activation of the mineralocorticoid receptor increases striatin levels. *Am. J. Hypertens.* **25**, 243–249, <https://doi.org/10.1038/ajh.2011.197>

52 Evora, P.R., Evora, P.M., Celotto, A.C., Rodrigues, A.J. and Joviliano, E.E. (2012) Cardiovascular therapeutics targets on the NO-sGC-cGMP signaling pathway: a critical overview. *Curr. Drug Targets* **13**, 1207–1214, <https://doi.org/10.2174/138945012802002348>

53 Sparks, M.A., Stegbauer, J., Chen, D., Gomez, J.A., Griffiths, R.C., Azad, H.A. et al. (2015) Vascular type 1A angiotensin II receptors control BP by regulating renal blood flow and urinary sodium excretion. *J. Am. Soc. Nephrol.* **26**, 2953–2962, <https://doi.org/10.1681/ASN.2014080816>

54 Rianto, F., Hoang, T., Revoori, R. and Sparks, M.A. (2021) Angiotensin receptors in the kidney and vasculature in hypertension and kidney disease. *Mol. Cell. Endocrinol.* **529**, 111259, <https://doi.org/10.1016/j.mce.2021.111259>

55 Yan, C., Kim, D., Aizawa, T. and Berk, B.C. (2003) Functional interplay between angiotensin II and nitric oxide: cyclic GMP as a key mediator. *Arterioscler. Thromb. Vasc. Biol.* **23**, 26–36, <https://doi.org/10.1161/01.ATV.0000046231.17365.9D>

56 Ramchandran, R., Takezako, T., Saad, Y., Stull, L., Fink, B., Yamada, H. et al. (2006) Angiotensinergic stimulation of vascular endothelium in mice causes hypotension, bradycardia, and attenuated angiotensin response. *Proc. Natl. Acad. Sci. U.S.A.* **103**, 19087–19092, <https://doi.org/10.1073/pnas.0602715103>

57 Meijles, D.N., Cull, J.J., Cooper, S.T.E., Markou, T., Hardyman, M.A., Fuller, S.J. et al. (2021) The anti-cancer drug dabrafenib is not cardiotoxic and inhibits cardiac remodelling and fibrosis in a murine model of hypertension. *Clin. Sci. (Lond.)* **135**, 1631–1647, <https://doi.org/10.1042/CS20210192>

58 Pitha, J., Vaneckova, I. and Zicha, J. (2023) Hypertension after the menopause: what can we learn from experimental studies? *Physiol. Res.* **72**, S91–S112, <https://doi.org/10.33549/physiolres.935151>

59 Muro, Y., Chan, E.K., Landberg, G. and Tan, E.M. (1995) A cell-cycle nuclear autoantigen containing WD-40 motifs expressed mainly in S and G2 phase cells. *Biochem. Biophys. Res. Commun.* **207**, 1029–1037, <https://doi.org/10.1006/bbrc.1995.1288>

60 Madsen, C.D., Hooper, S., Tozluoglu, M., Bruckbauer, A., Fletcher, G., Erler, J.T. et al. (2015) STRIPAK components determine mode of cancer cell migration and metastasis. *Nat. Cell Biol.* **17**, 68–80, <https://doi.org/10.1038/ncb3083>

61 Jain, B.P., Chauhan, P., Tanti, G.K., Singarapu, N., Ghaskadbi, S. and Goswami, S.K. (2015) Tissue specific expression of SG2NA is regulated by differential splicing, RNA editing and differential polyadenylation. *Gene* **556**, 119–126, <https://doi.org/10.1016/j.gene.2014.11.045>

62 Sanghamitra, M., Talukder, I., Singarapu, N., Sindhu, K.V., Kateriya, S. and Goswami, S.K. (2008) WD-40 repeat protein SG2NA has multiple splice variants with tissue restricted and growth responsive properties. *Gene* **420**, 48–56, <https://doi.org/10.1016/j.gene.2008.04.016>

63 Krahn, A.D., Wilde, A.A.M., Calkins, H., La Gerche, A., Cadri-Tourigny, J., Roberts, J.D. et al. (2022) Arrhythmogenic right ventricular cardiomyopathy. *JACC Clin. Electrophysiol.* **8**, 533–553, <https://doi.org/10.1016/j.jacep.2021.12.002>

64 Nader, M., Alotaibi, S., Alsolme, E., Khalil, B., Abu-Zaid, A., Alsomali, R. et al. (2017) Cardiac striatin interacts with caveolin-3 and calmodulin in a calcium sensitive manner and regulates cardiomyocyte spontaneous contraction rate. *Can. J. Physiol. Pharmacol.* **95**, 1306–1312, <https://doi.org/10.1139/cjpp-2017-0155>

65 Hougen, K., Aronsen, J.M., Stokke, M.K., Enger, U., Nygard, S., Andersson, K.B. et al. (2010) Cre-loxP DNA recombination is possible with only minimal unspecific transcriptional changes and without cardiomyopathy in Tg(alphaMHC-MerCreMer) mice. *Am. J. Physiol. Heart Circ. Physiol.* **299**, H1671–H1678, <https://doi.org/10.1152/ajpheart.01155.2009>

66 Sotoodehnia, N., Isaacs, A., de Bakker, P.I., Dorr, M., Newton-Cheh, C., Nolte, I.M. et al. (2010) Common variants in 22 loci are associated with QRS duration and cardiac ventricular conduction. *Nat. Genet.* **42**, 1068–1076, <https://doi.org/10.1038/ng.716>

67 Giri, A., Hellwege, J.N., Keaton, J.M., Park, J., Qiu, C., Warren, H.R. et al. (2019) Trans-ethnic association study of blood pressure determinants in over 750,000 individuals. *Nat. Genet.* **51**, 51–62, <https://doi.org/10.1038/s41588-018-0303-9>

68 Stone, I.B., Green, J., Koefoed, A.W., Hornik, E.S., Williams, J.S., Adler, G.K. et al. (2021) Striatin genotype-based, mineralocorticoid receptor antagonist-driven clinical trial: study rationale and design. *Pharmacogenet Genomics* **31**, 83–88, <https://doi.org/10.1097/FPC.0000000000000425>

69 Fuller, S.J., Edmunds, N.S., McGuffin, L.J., Hardyman, M.A., Cull, J.J., Alharbi, H.O. et al. (2021) MAP4K4 expression in cardiomyocytes: multiple isoforms, multiple phosphorylations and interactions with striatins. *Biochem. J.* **478**, 2121–2143, <https://doi.org/10.1042/BCJ20210003>

70 Guettler, S., LaRose, J., Petsalaki, E., Gish, G., Scotter, A., Pawson, T. et al. (2011) Structural basis and sequence rules for substrate recognition by Tankyrase explain the basis for cherubism disease. *Cell* **147**, 1340–1354, <https://doi.org/10.1016/j.cell.2011.10.046>

71 Tang, Y., Chen, M., Zhou, L., Ma, J., Li, Y., Zhang, H. et al. (2019) Architecture, substructures, and dynamic assembly of STRIPAK complexes in Hippo signaling. *Cell Discov.* **5**, 3, <https://doi.org/10.1038/s41421-018-0077-3>

72 Gordon, J., Hwang, J., Carrier, K.J., Jones, C.A., Kern, Q.L., Moreno, C.S. et al. (2011) Protein phosphatase 2a (PP2A) binds within the oligomerization domain of striatin and regulates the phosphorylation and activation of the mammalian Ste20-Like kinase Mst3. *BMC Biochem.* **12**, 54, <https://doi.org/10.1186/1471-2091-12-54>

73 Kean, M.J., Ceccarelli, D.F., Goudreault, M., Sanches, M., Tate, S., Larsen, B. et al. (2011) Structure-function analysis of core STRIPAK proteins: a signaling complex implicated in Golgi polarization. *J. Biol. Chem.* **286**, 25065–25075, <https://doi.org/10.1074/jbc.M110.214486>

74 Ceccarelli, D.F., Laister, R.C., Mulligan, V.K., Kean, M.J., Goudreault, M., Scott, I.C. et al. (2011) CCM3/PDCD10 heterodimerizes with germinal center kinase III (GCKIII) proteins using a mechanism analogous to CCM3 homodimerization. *J. Biol. Chem.* **286**, 25056–25064, <https://doi.org/10.1074/jbc.M110.213777>

75 De Jamblinne, C.V., Decelle, B., Dehghani, M., Joseph, M., Sriskandarajah, N., Leguay, K. et al. (2020) STRIPAK regulates Slik localization to control mitotic morphogenesis and epithelial integrity. *J. Cell Biol.* **219**, e201911035, <https://doi.org/10.1083/jcb.201911035>

76 Hyodo, T., Ito, S., Hasegawa, H., Asano, E., Maeda, M., Urano, T. et al. (2012) Misshapen-like kinase 1 (MINK1) is a novel component of striatin-interacting phosphatase and kinase (STRIPAK) and is required for the completion of cytokinesis. *J. Biol. Chem.* **287**, 25019–25029, <https://doi.org/10.1074/jbc.M112.372342>

77 Kim, J.W., Berrios, C., Kim, M., Schade, A.E., Adelman, G., Yeerna, H. et al. (2020) STRIPAK directs PP2A activity toward MAP4K4 to promote oncogenic transformation of human cells. *Elife* **9**, e53003, <https://doi.org/10.7554/elife.53003>

78 Migliavacca, J., Zullig, B., Capdeville, C., Grotzer, M.A. and Baumgartner, M. (2022) Cooperation of striatin 3 and MAP4K4 promotes growth and tissue invasion. *Commun. Biol.* **5**, 795, <https://doi.org/10.1038/s42003-022-03708-y>

79 Fuller, S.J., Osborne, S.A., Leonard, S.J., Hardyman, M.A., Vaniotis, G., Allen, B.G. et al. (2015) Cardiac protein kinases: the cardiomyocyte kinome and differential kinase expression in human failing hearts. *Cardiovasc. Res.* **108**, 87–98, <https://doi.org/10.1093/cvr/cvv210>

80 Wang, J., Liu, S., Heallen, T. and Martin, J.F. (2018) The Hippo pathway in the heart: pivotal roles in development, disease, and regeneration. *Nat. Rev. Cardiol.* **15**, 672–684, <https://doi.org/10.1038/s41569-018-0063-3>

81 Cheng, Z., Zhang, M., Hu, J., Lin, J., Feng, X., Wang, S. et al. (2018) Mst1 knockout enhances cardiomyocyte autophagic flux to alleviate angiotensin II-induced cardiac injury independent of angiotensin II receptors. *J. Mol. Cell Cardiol.* **125**, 117–128, <https://doi.org/10.1016/j.yjmcc.2018.08.028>

82 Golforoush, P.A., Narasimhan, P., Chaves-Guerrero, P.P., Lawrence, E., Newton, G., Yan, R. et al. (2020) Selective protection of human cardiomyocytes from anthracycline cardiotoxicity by small molecule inhibitors of MAP4K4. *Sci. Rep.* **10**, 12060, <https://doi.org/10.1038/s41598-020-68907-1>

83 Fiedler, L.R., Chapman, K., Xie, M., Maifoshie, E., Jenkins, M., Golforoush, P.A. et al. (2019) MAP4K4 inhibition promotes survival of human stem cell-derived cardiomyocytes and reduces infarct size in vivo. *Cell Stem Cell.* **24**, 579e512–591e512, <https://doi.org/10.1016/j.stem.2019.01.013>

84 Fuller, S.J., McGuffin, L.J., Marshall, A.K., Giraldo, A., Pikkarainen, S., Clerk, A. et al. (2012) A novel non-canonical mechanism of regulation of MST3 (mammalian Sterile20-related kinase 3). *Biochem. J.* **442**, 595–610, <https://doi.org/10.1042/BJ20112000>

85 Sugden, P.H., McGuffin, L.J. and Clerk, A. (2013) S0ck, MiSTs, MASK and STicKs: the germinal centre kinase III (GCKIII) kinases and their heterologous protein-protein interactions. *Biochem. J.* **454**, 13–30, <https://doi.org/10.1042/BJ20130219>

86 Roux, K.J., Kim, D.I., Burke, B. and May, D.G. (2018) BioID: a screen for protein-protein interactions. *Curr. Protoc. Protein Sci.* **91**, 19.23.11–19.23.15, <https://doi.org/10.1002/cpp.51>

## **Supplementary information:**

### **STRN, but not STRN3, plays a major role in angiotensin II-induced cardiomyocyte and cardiac hypertrophy**

Joshua J Cull<sup>1</sup>, Susanna TE Cooper<sup>2\*</sup>, Hajed O Alharbi<sup>1#</sup>, Sonia P Chothani<sup>3</sup>, Owen JL Rackham<sup>3,4</sup>, Daniel N Meijles<sup>2</sup>, Philip R Dash<sup>1</sup>, Risto Kerkelä<sup>5</sup>, Neil Ruparelia<sup>1,6</sup>, Peter H Sugden<sup>1</sup>, Angela Clerk<sup>1</sup>

<sup>1</sup>School of Biological Sciences, University of Reading, Reading, UK.

<sup>2</sup>Molecular and Clinical Sciences Institute, St. George's University of London, London, UK.

<sup>3</sup>Program in Cardiovascular and Metabolic Disorders, Duke-National University of Singapore Medical School, Singapore.

<sup>4</sup>School of Biological Sciences, University of Southampton, Southampton, UK.

<sup>5</sup>Research Unit of Biomedicine and Internal Medicine, Medical Research Centre Oulu (Oulu University Hospital) and Biocenter Oulu, University of Oulu, Oulu, Finland.

<sup>6</sup>Department of Cardiology, Royal Berkshire Hospital, Reading, UK.

#### **Supplementary Table S1. Mouse weights.**

#### **Supplementary Table S2. Primers for genotyping and confirmation of recombination.**

#### **Supplementary S3. qPCR primers.**

#### **Supplementary Table S4. Baseline echocardiography data for STRN<sup>+/−</sup> and STRN3<sup>+/−</sup> male mice and their wild-type (STRN<sup>+/+</sup> and STRN3<sup>+/+</sup>) male littermates.**

#### **Supplementary Table S5. Echocardiography data for STRN<sup>+/−</sup> male mice and wild-type (STRN<sup>+/+</sup>) male littermates treated with acidified PBS (AcPBS) or 0.8 mg/kg/d AngII for 3 or 7 d: M-mode data.**

#### **Supplementary Table S6. Echocardiography data for STRN3<sup>+/−</sup> male mice and wild-type (STRN3<sup>+/+</sup>) male littermates treated with acidified PBS (AcPBS) or 0.8 mg/kg/d AngII for 3 or 7 d: M-mode data**

#### **Supplementary Table S7. Echocardiography data for STRN<sup>+/−</sup> and STRN3<sup>+/−</sup> male mice and wild-type (STRN<sup>+/+</sup> and STRN3<sup>+/+</sup>) male littermates treated with acidified PBS (AcPBS) or 0.8 mg/kg/d AngII for 7 d: B-mode data and speckle tracking.**

#### **Supplementary Table S8. Echocardiography data for STRN3<sup>floxed/floxed</sup>/Cre<sup>+/−</sup> mice: M-mode data.**

#### **Supplementary Table S9. Echocardiography data for STRN3<sup>floxed/floxed</sup>/Cre<sup>+/−</sup> mice: B-mode data and speckle tracking.**

#### **Supplementary Figure S1. Global heterozygous STRN3 knockout in mice.**

#### **Supplementary Figure S2. Heterozygous global deletion of STRN does not affect the hypertrophic response to AngII.**

#### **Supplementary Figure S3. Heterozygous global deletion of STRN3 does not affect cardiomyocyte hypertrophy or cardiac fibrosis induced by AngII.**

#### **Supplementary Figure S4. Full images for immunoblots in Figure 1C.**

#### **Supplementary Figure S5. Full images for immunoblots in Figure 1F.**

#### **Supplementary Figure S6. Full images for immunoblots in Supplementary Figure S2C.**

#### **Supplementary Figure S7. Full images for immunoblots in Figure 5D.**

**Supplementary Table S1. Mouse weights.** Male mice (8 weeks) were allocated to groups on a random basis. STRN<sup>+/+</sup> and STRN3<sup>+/−</sup> heterozygous knockout mice and their wild-type (WT) STRN<sup>+/+</sup> and STRN3<sup>+/−</sup> littermates were treated with acidified PBS (AcPBS) or 0.8 mg/kg/d angiotensin II (AngII). STRN<sup>fl/fl</sup>/Cre<sup>+/−</sup> mice were treated with 40 mg/kg tamoxifen in corn-oil or with corn-oil vehicle (COV) with or without AcPBS or AngII. Weights (g) were taken at the start of the study with the first baseline echocardiogram (Start), immediately after minipump surgery, and when mice were culled (End). Weights post-surgery and at the end included the minipumps. N values are provided with exclusions due to mortality indicated in parentheses.

Study	Condition	Start		Post-minipump		End		n
		Mean	SD	Mean	SD	Mean	SD	
<b>STRN study group</b>								
STRN <sup>+/+</sup> (WT)	AcPBS	25.16	1.38	26.94	1.46	27.59	1.49	16
	AngII	24.77	1.57	26.46	1.42	26.65	1.38	15 (1)
STRN <sup>+/−</sup>	AcPBS	25.00	0.92	26.76	0.95	27.52	0.78	10
	AngII	24.78	1.38	26.49	1.26	26.85	1.57	17
<b>STRN3 study group</b>								
STRN3 <sup>+/+</sup> (WT)	AcPBS	23.62	2.11	25.44	1.71	26.07	1.66	16
	AngII	24.31	1.46	25.79	1.44	26.41	1.69	14
STRN3 <sup>+/−</sup>	AcPBS	23.26	2.20	24.85	2.01	25.76	2.15	11
	AngII	23.32	1.68	25.64	1.43	25.78	1.21	11
<b>STRN<sup>fl/fl</sup>/Cre<sup>+/−</sup></b>								
	COV/AcPBS	22.21	1.53	24.58	2.06	25.27	1.76	10
	Tx/AcPBS	22.82	1.70	25.79	1.73	26.40	1.31	10
	COV/AngII	21.98	2.04	24.12	1.61	24.04	1.66	9 (2)
	Tx/AngII	25.38	1.70	25.38	1.70	25.48	1.86	8 (1)

**Supplementary Table S2. Primers for genotyping and confirmation of recombination.**

Mouse strain	Forward primer	Reverse primer	Size (bp)	Annealing temp.
<b>Genotyping</b>				
STRN knockout	GAGATGGCGCAACGCAATTAATG	GAAGTGCATGGGAAGTCAGTACACG	296	51°C
STRN3 knockout	GAGATGGCGCAACGCAATTAATG	ACCTGAGCAAATTCACCCAAAACC	334	51°C
Cre <sup>−</sup>	TCTATTGCACACAGCAATCCA	CCAACTCTTGTGAGAGGAGCA	305	52°C
Cre <sup>+</sup>	TCTATTGCACACAGCAATCCA	CCAGCATTGTGAGAACAGG	285	52°C
<b>Recombination</b>				
Post-FLP	TGAATTATTGGAGTTTGTTCAGACC	GCACAGACAGACCTTCATGCTAACCC	630	53°C
Post-FLP Post-Cre	TGAATTATTGGAGTTTGTTCAGACC	GAAGTGCATGGGAAGTCAGTACACG	666	53°C

**Supplementary S3. qPCR primers.**

Gene Symbol	Accession No.	Sense Primer (5'→3')	Antisense Primer (5'→3')
Cdh1	NM_009864.3	GTCTCCTCATGGCTTGC	CTTAGATGCCGCTTCAC
Cdh5	NM_009868.4	TCTGCCAGCAAACCTCTCCT	TTGGAATCAAATGCACATCG
Col1a1	NM_007742	TCGTGGCTTCTGGTCTC	CCGTTGAGTCCGTCTTGC
Col2a1	NM_00111351	GACGAGGCAGACAGTACCTG	GATGCTCTCAATCTGGTTGTCAG
Col3a1	NM_009930.2	GGAACCTGGTTCTTCTCACC	TAGGACTGACCAAGGTGGCT
Col4a1	NM_009931.2	TGTGGGCCAGCCAGGCATTG	CAGGGGGTCCGATCGCTCCA
Ctgf	NM_010217	GCACACCGCACAGAACCA	ATGGCAGGCCACAGGTCTTG
Ddr2	NM_022563.2	GCACTTGGTGAATTATTAGAACCTG	GGACAACATAATGGTCCCTCCC
Fn1	NM_010233	AAGAGGACGTTGCAGAGCTA	AGACACTGGAGACACTGACTAA
Gapdh	NM_008084.2	TCACCACCATGGAGAACGGC	GCTAACGAGTTGGTGGTGC
Myh7	NM_080728	CATGCCAACCGTATGGCTG	GTTCACGATGGCGATGTT
Ng2 (Cspg4)	NM_139001.2	TTGGCTACGTAAAGATAGGG	AGCACGATGACTCTGAGACC
Nppa	NM_008725	GATGGATTCAAGAACCTGCTAGA	CTTCCTCAGTCTGCTCACTCA
Nppb	NM_008726	TCCAGCAGAGACCTAAAATTC	CAGTGCAGTTACAGCCCCAAA
Postn	NM_015784	TTCCCTCCTGCCCTATATGC	CCTGATCCCAGCCCCCTGAT
Tagln	NM_011526.5	GAATGCACCTCTCGGCTCAT	CCGAAGCTACTCTCCTCCA
Timp1	NM_011593	TACGCCTACACCCCAGTCAT	GCCCGTGATGAGAAACTCTTC

**Supplementary Table S4. Baseline echocardiography data for STRN<sup>+/−</sup> and STRN3<sup>+/−</sup> male mice and their wild-type (STRN<sup>+/+</sup> and STRN3<sup>+/+</sup>) male littermates.** Short axis M-mode images were analysed using VevoLab software. LV, left ventricle; ID, internal diameter; AW, anterior wall; PW, posterior wall; d, diastole; s, systole; wall thickness (WT) = AW+ PW; SV, stroke volume; CO, cardiac output; EF, ejection fraction; FS, fractional shortening. Long axis B-mode images were analysed using speckle-tracking software. EDV, End diastolic volume; ESV, End systolic volume; EDLVM, End diastolic left ventricle mass; ESLVM, End systolic left ventricle mass; GLS, global longitudinal strain; GCS, Global circumferential strain.

	STRN <sup>+/+</sup> (n=31)		STRN <sup>+/−</sup> (n=26)		STRN3 <sup>+/+</sup> (n=27)		STRN3 <sup>+/−</sup> (n=19)	
	Mean	SD	Mean	SD	Mean	SD	Mean	SD
<b>M-Mode</b>								
Heart Rate (bpm)	483	28	471	44	502	38	498	19
SV (μl)	42.16	8.83	42.31	6.27	40.68	4.94	41.36	7.78
CO (ml/min)	20.33	7.85	19.97	7.01	20.71	6.32	20.56	6.00
EF (%)	57.41	5.31	55.65	4.58	53.41	4.17	56.14	4.02
FS (%)	30.10	4.33	28.90	3.87	27.48	3.13	29.25	3.83
LVID; d (mm)	2.853	0.319	2.954	0.300	3.018	0.274	2.894	0.272
LVID; s (mm)	4.076	0.295	4.147	0.239	4.153	0.209	4.084	0.274
LVAW; d (mm)	1.043	0.099	1.039	0.094	1.072	0.079	1.078	0.077
LVAW; s (mm)	0.789	0.062	0.790	0.079	0.780	0.058	0.757	0.051
LVPW; d (mm)	0.999	0.116	0.991	0.093	0.986	0.081	1.007	0.083
LVPW; s (mm)	0.703	0.068	0.702	0.050	0.698	0.039	0.697	0.048
WT; d (mm)	2.042	0.201	2.030	0.150	2.059	0.148	2.085	0.141
WT; s (mm)	1.492	0.114	1.492	0.096	1.477	0.086	1.454	0.083
<b>B-mode</b>								
Heart Rate (bpm)	484	31	473	54	480	40	472	40
SV (μl)	29.96	5.84	31.49	6.06	28.89	4.64	28.16	7.25
CO (ml/min)	14.46	2.85	14.99	3.82	13.87	2.47	13.13	2.71
EF (%)	57.54	6.86	58.14	6.45	56.26	8.10	57.38	7.83
FS (%)	30.73	5.68	30.71	4.96	28.34	6.38	30.24	5.82
EDV (μl)	52.07	9.17	54.17	9.96	51.57	8.40	48.86	9.88
ESV (μl)	22.12	5.61	22.68	5.88	22.68	6.52	20.70	5.43
EDLVM (mg)	53.90	5.43	54.21	5.83	53.24	5.20	50.75	5.79
ESLVM (mg)	56.03	5.76	56.11	6.20	55.99	5.94	52.99	6.01
GLS (%)	-20.27	2.91	-19.80	3.44	-20.76	4.97	-20.06	3.16
GCS (%)	-20.84	3.48	-20.83	3.40	-20.30	4.01	-19.98	3.34

**Supplementary Table S5. Echocardiography data for  $\text{STRN}^{+/-}$  male mice and wild-type ( $\text{STRN}^{+/+}$ ) male littermates treated with acidified PBS (AcPBS) or 0.8 mg/kg/d AngII for 3 or 7 d: M-mode data.** Short axis M-mode images were analysed using VevoLab software. LV, left ventricle; ID, internal diameter; AW, anterior wall; PW, posterior wall; d, diastole; s, systole; wall thickness (WT) = AW+ PW; SV, stroke volume; CO, cardiac output; EF, ejection fraction; FS, fractional shortening.

	$\text{STRN}^{+/+}/\text{AcPBS}$ (n=16)		$\text{STRN}^{+/-}/\text{AcPBS}$ (n=10)		$\text{STRN}^{+/+}/\text{AngII}$ (n=15)		$\text{STRN}^{+/-}/\text{AngII}$ (n=16)	
3 d	Mean	SD	Mean	SD	Mean	SD	Mean	SD
Heart Rate (bpm)	524	39	505	34	534	33	533	36
SV (µl)	41.62	9.01	42.19	6.64	36.18	6.95	38.00	7.92
CO (ml/min)	21.75	5.60	21.27	6.74	19.29	7.44	20.25	7.19
EF (%)	53.28	3.65	56.27	4.58	57.39	4.93	58.53	4.89
FS (%)	27.30	4.67	29.28	3.48	29.88	3.72	30.70	4.43
LVID; d (mm)	3.032	0.192	2.913	0.270	2.675	0.254	2.691	0.339
LVID; s (mm)	4.174	0.246	4.116	0.225	3.816	0.245	3.872	0.339
LVAW; d (mm)	1.052	0.081	1.051	0.112	1.171	0.099	1.103	0.090
LVAW; s (mm)	0.820	0.071	0.805	0.083	0.919	0.070	0.856	0.073
LVPW; d (mm)	0.988	0.085	0.999	0.074	1.193	0.139	1.164	0.123
LVPW; s (mm)	0.698	0.058	0.704	0.041	0.879	0.126	0.825	0.098
WT; d (mm)	2.040	0.146	2.050	0.157	2.364	0.221	2.267	0.202
WT; s (mm)	1.518	0.112	1.509	0.102	1.799	0.181	1.681	0.151
7 d	Mean	SD	Mean	SD	Mean	SD	Mean	SD
Heart Rate (bpm)	523	34	515	33	546	38	529	53
SV (µl)	42.54	7.43	43.27	6.78	39.74	10.93	41.09	7.74
CO (ml/min)	22.24	4.86	22.27	5.17	21.61	6.47	21.84	6.75
EF (%)	57.95	3.29	56.38	3.46	59.12	4.55	61.36	4.87
FS (%)	30.28	4.23	29.33	3.89	31.10	5.70	32.71	5.19
LVID; d (mm)	2.839	0.226	2.941	0.228	2.698	0.343	2.641	0.314
LVID; s (mm)	4.072	0.261	4.157	0.228	3.912	0.413	3.919	0.311
LVAW; d (mm)	1.092	0.068	1.043	0.064	1.210	0.088	1.206	0.100
LVAW; s (mm)	0.826	0.059	0.813	0.133	0.927	0.078	0.898	0.074
LVPW; d (mm)	1.047	0.083	1.052	0.068	1.184	0.095	1.234	0.169
LVPW; s (mm)	0.713	0.075	0.738	0.042	0.837	0.085	0.862	0.158
WT; d (mm)	2.139	0.123	2.095	0.082	2.394	0.171	2.440	0.259
WT; s (mm)	1.539	0.100	1.551	0.143	1.764	0.110	1.761	0.209

**Supplementary Table S6. Echocardiography data for STRN3<sup>+/−</sup> male mice and wild-type (STRN3<sup>+/+</sup>) male littermates treated with acidified PBS (AcPBS) or 0.8 mg/kg/d AngII for 3 or 7 d: M-mode data.** Short axis M-mode images were analysed using VevoLab software. LV, left ventricle; ID, internal diameter; AW, anterior wall; PW, posterior wall; d, diastole; s, systole; wall thickness (WT) = AW+ PW; SV, stroke volume; CO, cardiac output; EF, ejection fraction; FS, fractional shortening.

	STRN3 <sup>+/+</sup> /AcPB S (n=16)		STRN3 <sup>+/−</sup> /AcPBS (n=10)		STRN3 <sup>+/+</sup> /AngII (n=15)		STRN3 <sup>+/−</sup> /AngII (n=16)	
3 d	Mean	SD	Mean	SD	Mean	SD	Mean	SD
Heart Rate (bpm)	520	31	508	37	528	39	525	52
SV (µl)	41.52	6.73	41.17	7.08	37.98	7.18	34.55	6.63
CO (ml/min)	54.83	6.73	60.16	5.28	61.65	9.40	56.03	8.25
EF (%)	28.36	4.29	31.77	3.69	33.02	6.70	28.98	5.30
FS (%)	21.48	3.05	20.97	4.38	20.02	3.72	18.10	3.45
LVID; d (mm)	2.973	0.355	2.699	0.210	2.551	0.391	2.703	0.371
LVID; s (mm)	4.140	0.317	3.955	0.231	3.795	0.316	3.795	0.331
LVAW; d (mm)	1.079	0.075	1.098	0.138	1.249	0.163	1.221	0.180
LVAW; s (mm)	0.772	0.065	0.773	0.086	0.890	0.106	0.897	0.138
LVPW; d (mm)	1.034	0.052	1.070	0.109	1.259	0.185	1.220	0.230
LVPW; s (mm)	0.713	0.035	0.733	0.083	0.898	0.127	0.923	0.178
WT; d (mm)	2.113	0.119	2.168	0.232	2.508	0.316	2.441	0.394
WT; s (mm)	1.485	0.086	1.506	0.125	1.788	0.199	1.821	0.294
7 d	Mean	SD	Mean	SD	Mean	SD	Mean	SD
Heart Rate (bpm)	533	42	521	35	539	48	534	34
SV (µl)	42.79	5.38	42.98	7.60	41.75	7.13	39.76	5.10
CO (ml/min)	59.23	6.87	61.24	7.05	61.63	6.35	65.24	3.46
EF (%)	31.25	4.76	32.70	5.28	32.92	4.56	35.25	2.50
FS (%)	22.74	2.84	22.43	4.63	22.50	4.15	21.23	3.24
LVID; d (mm)	2.802	0.373	2.697	0.307	2.650	0.273	2.445	0.209
LVID; s (mm)	4.063	0.311	4.002	0.276	3.944	0.256	3.770	0.236
LVAW; d (mm)	1.130	0.085	1.126	0.119	1.210	0.110	1.294	0.095
LVAW; s (mm)	0.789	0.068	0.781	0.071	0.876	0.089	0.913	0.090
LVPW; d (mm)	1.113	0.084	1.071	0.139	1.258	0.151	1.290	0.164
LVPW; s (mm)	0.741	0.050	0.728	0.058	0.868	0.108	0.929	0.165
WT; d (mm)	2.243	0.160	2.197	0.243	2.468	0.243	2.583	0.243
WT; s (mm)	1.530	0.091	1.509	0.111	1.744	0.163	1.842	0.208

**Supplementary Table S7. Echocardiography data for STRN<sup>+/−</sup> and STRN3<sup>+/−</sup> male mice and wild-type (STRN<sup>+/+</sup> and STRN3<sup>+/+</sup>) male littermates treated with acidified PBS (AcPBS) or 0.8 mg/kg/d AngII for 7 d: B-mode data and speckle-tracking.** Long axis B-mode images were analysed using speckle-tracking software. EDV, End diastolic volume; ESV, End systolic volume; EDLVM, End diastolic left ventricle mass; ESLVM, End systolic left ventricle mass; GLS, global longitudinal strain; GCS, Global circumferential strain; SV, stroke volume; CO, cardiac output; EF, ejection fraction; FS, fractional shortening.

	STRN <sup>+/+</sup> /AcPBS (n=16)		STRN <sup>+/−</sup> /AcPBS (n=10)		STRN <sup>+/+</sup> /AngII (n=15)		STRN <sup>+/−</sup> /AngII (n=16)	
	Mean	SD	Mean	SD	Mean	SD	Mean	SD
Heart Rate (bpm)	507	35	502	38	541	45	526	49
SV (μl)	29.23	5.17	28.53	5.11	25.68	5.62	27.55	5.01
CO (ml/min)	14.81	2.75	14.34	2.93	13.82	2.95	14.44	2.77
EF (%)	58.93	7.05	58.94	5.63	58.19	6.84	61.99	6.51
FS (%)	31.68	7.28	30.46	5.10	30.96	4.65	33.88	5.27
EDV (μl)	49.58	8.16	48.05	6.21	44.21	9.66	44.80	9.51
ESV (μl)	20.35	5.27	19.52	3.24	18.53	5.82	17.25	5.49
EDLVM (mg)	57.23	5.12	54.27	4.70	69.82	6.81	63.32	7.95
ESLVM (mg)	59.03	5.17	55.47	4.94	72.29	7.61	65.45	9.16
GLS (%)	-19.07	2.66	-19.65	4.71	-17.86	5.06	-19.78	3.70
GCS (%)	-21.45	3.73	-21.47	2.15	-19.61	3.25	-22.01	5.01
	STRN3 <sup>+/+</sup> /AcPBS (n=13)		STRN3 <sup>+/−</sup> /AcPBS (n=9)		STRN3 <sup>+/+</sup> /AngII (n=14)		STRN3 <sup>+/−</sup> /AngII (n=10)	
	Mean	SD	Mean	SD	Mean	SD	Mean	SD
Heart Rate (bpm)	517	40	520	46	529	51	517	31
SV (μl)	28.78	5.20	28.15	5.31	27.87	4.67	25.41	5.72
CO (ml/min)	14.85	2.72	14.80	4.11	14.69	2.59	13.08	2.75
EF (%)	58.04	6.77	61.92	3.13	58.94	7.01	62.44	6.16
FS (%)	31.61	7.49	34.72	4.31	31.84	7.56	33.24	7.33
EDV (μl)	50.60	13.75	45.20	7.87	47.45	8.97	40.79	9.88
ESV (μl)	21.82	9.25	17.05	3.08	19.57	6.22	15.38	5.34
EDLVM (mg)	53.99	6.23	53.83	5.42	68.06	7.48	69.43	7.30
ESLVM (mg)	57.12	7.14	56.01	5.81	71.12	7.46	73.15	7.28
GLS (%)	-19.46	1.96	-20.56	2.92	-18.79	4.11	-22.72	4.00
GCS (%)	-20.39	3.51	-23.53	3.81	-22.95	2.46	-22.80	3.68

**Supplementary Table S8. Echocardiography data for STRN3<sup>f1/f1</sup>/Cre<sup>+/−</sup> mice: M-mode data.**

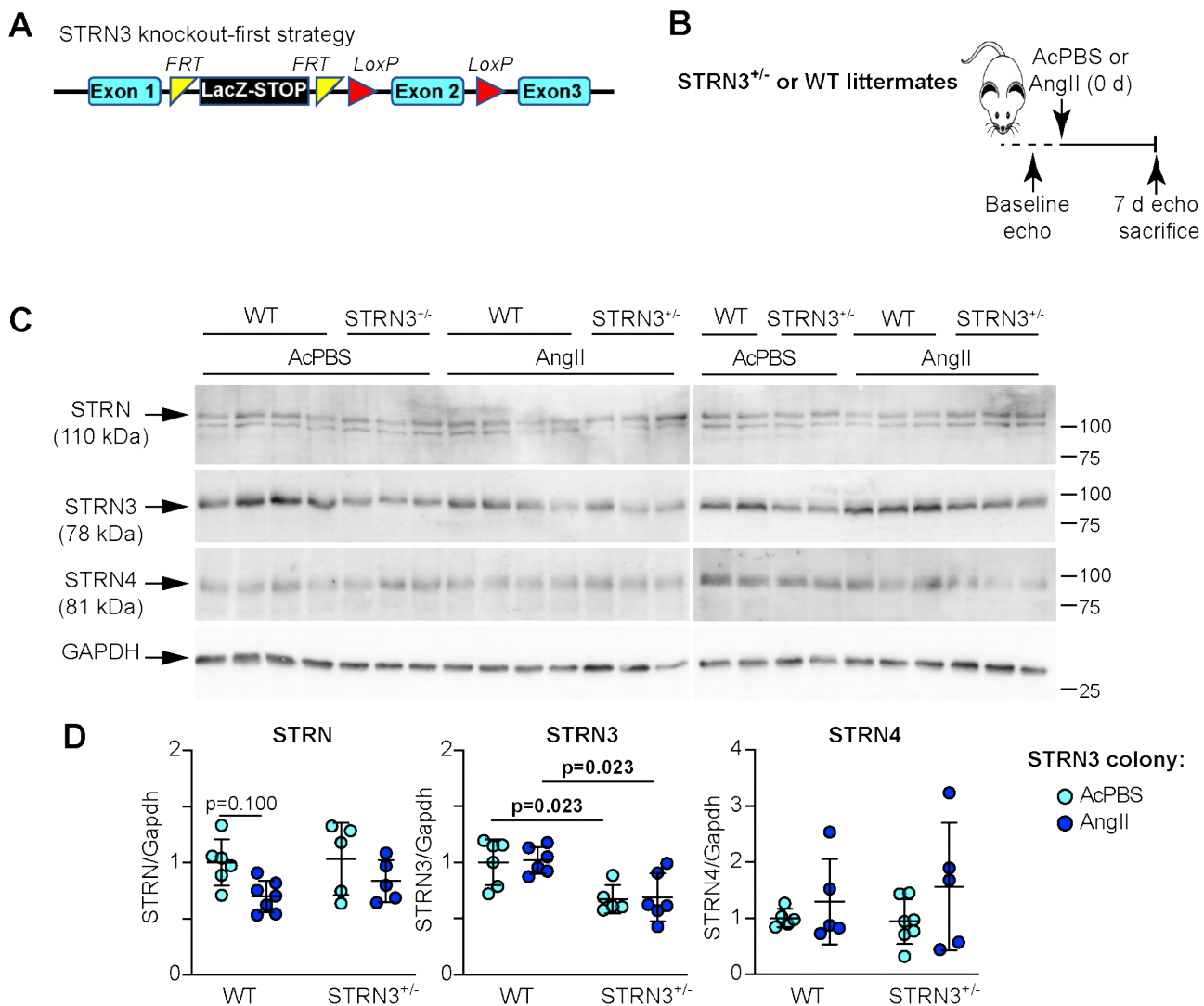
Male mice (8 wks) were treated with corn-oil vehicle (COV) or 40 mg/kg tamoxifen (Tx) 4 days and then with acidified PBS (AcPBS) or 0.8 mg/kg/d AngII in AcPBS. Short axis M-mode images were analysed using VevoLab software. LV, left ventricle; ID, internal diameter; AW, anterior wall; PW, posterior wall; d, diastole; s, systole; wall thickness (WT) = AW+ PW; SV, stroke volume; CO, cardiac output; EF, ejection fraction; FS, fractional shortening.

	COV/AcPBS		Tx/AcPBS		COV/AngII		Tx/AngII	
Baseline	Mean	SD	Mean	SD	Mean	SD	Mean	SD
Heart Rate (bpm)	481	27	479	30	485	22	492	26
SV (µl)	44.48	6.53	44.44	6.18	45.37	6.23	41.20	6.24
CO (ml/min)	57.28	6.55	57.40	4.50	60.48	5.30	59.01	5.51
EF (%)	30.04	4.54	29.99	2.94	32.16	3.72	31.11	3.64
FS (%)	21.44	3.72	21.31	3.68	21.94	3.02	20.15	2.38
LVID; d (mm)	2.929	0.279	2.932	0.328	2.793	0.164	2.767	0.325
LVID; s (mm)	4.180	0.241	4.177	0.330	4.115	0.154	4.003	0.313
LVAW; d (mm)	0.949	0.055	0.974	0.038	0.990	0.056	0.978	0.047
LVAW; s (mm)	0.693	0.028	0.696	0.043	0.720	0.031	0.722	0.028
LVPW; d (mm)	0.954	0.072	0.930	0.060	0.959	0.049	0.961	0.049
LVPW; s (mm)	0.637	0.063	0.642	0.041	0.644	0.025	0.653	0.039
WT; d (mm)	1.904	0.107	1.904	0.087	1.949	0.097	1.939	0.091
WT; s (mm)	1.329	0.083	1.338	0.072	1.364	0.048	1.374	0.058
<hr/>								
3 d	Mean	SD	Mean	SD	Mean	SD	Mean	SD
Heart Rate (bpm)	502	28	496	29	506	21	505	45
SV (µl)	46.38	8.99	47.36	7.12	39.34	5.58	40.99	8.15
CO (ml/min)	59.78	8.29	60.04	4.78	66.91	6.04	67.97	10.76
EF (%)	31.79	5.74	31.82	3.50	36.63	4.38	37.92	8.11
FS (%)	23.25	4.67	23.61	4.52	19.92	2.93	20.59	3.89
LVID; d (mm)	2.855	0.397	2.862	0.215	2.365	0.283	2.357	0.491
LVID; s (mm)	4.176	0.354	4.197	0.232	3.719	0.253	3.768	0.378
LVAW; d (mm)	1.033	0.080	1.043	0.058	1.180	0.112	1.138	0.119
LVAW; s (mm)	0.720	0.050	0.744	0.043	0.873	0.065	0.803	0.053
LVPW; d (mm)	0.993	0.067	1.005	0.076	1.210	0.115	1.139	0.123
LVPW; s (mm)	0.667	0.059	0.684	0.059	0.818	0.122	0.738	0.058
WT; d (mm)	2.026	0.132	2.048	0.112	2.390	0.214	2.277	0.233
WT; s (mm)	1.387	0.092	1.429	0.096	1.691	0.185	1.541	0.091
<hr/>								
7 d	Mean	SD	Mean	SD	Mean	SD	Mean	SD
Heart Rate (bpm)	531	52	506	36	508	54	527	45
SV (µl)	44.56	7.98	45.64	5.26	38.49	10.59	37.49	6.47
CO (ml/min)	57.67	8.51	59.35	5.18	61.65	8.59	60.91	9.30
EF (%)	30.33	5.69	31.34	3.65	33.00	6.04	32.47	6.72
FS (%)	23.87	5.79	23.21	3.91	19.33	5.00	19.63	2.90
LVID; d (mm)	2.900	0.249	2.860	0.235	2.562	0.408	2.586	0.469
LVID; s (mm)	4.164	0.148	4.161	0.199	3.801	0.428	3.804	0.390
LVAW; d (mm)	1.062	0.090	1.049	0.069	1.159	0.093	1.035	0.074
LVAW; s (mm)	0.764	0.058	0.747	0.043	0.851	0.078	0.755	0.049
LVPW; d (mm)	1.018	0.117	1.013	0.089	1.177	0.159	1.034	0.122
LVPW; s (mm)	0.697	0.083	0.693	0.061	0.873	0.151	0.684	0.040
WT; d (mm)	2.079	0.185	2.062	0.131	2.337	0.240	2.070	0.168
WT; s (mm)	1.461	0.131	1.440	0.099	1.723	0.222	1.439	0.085

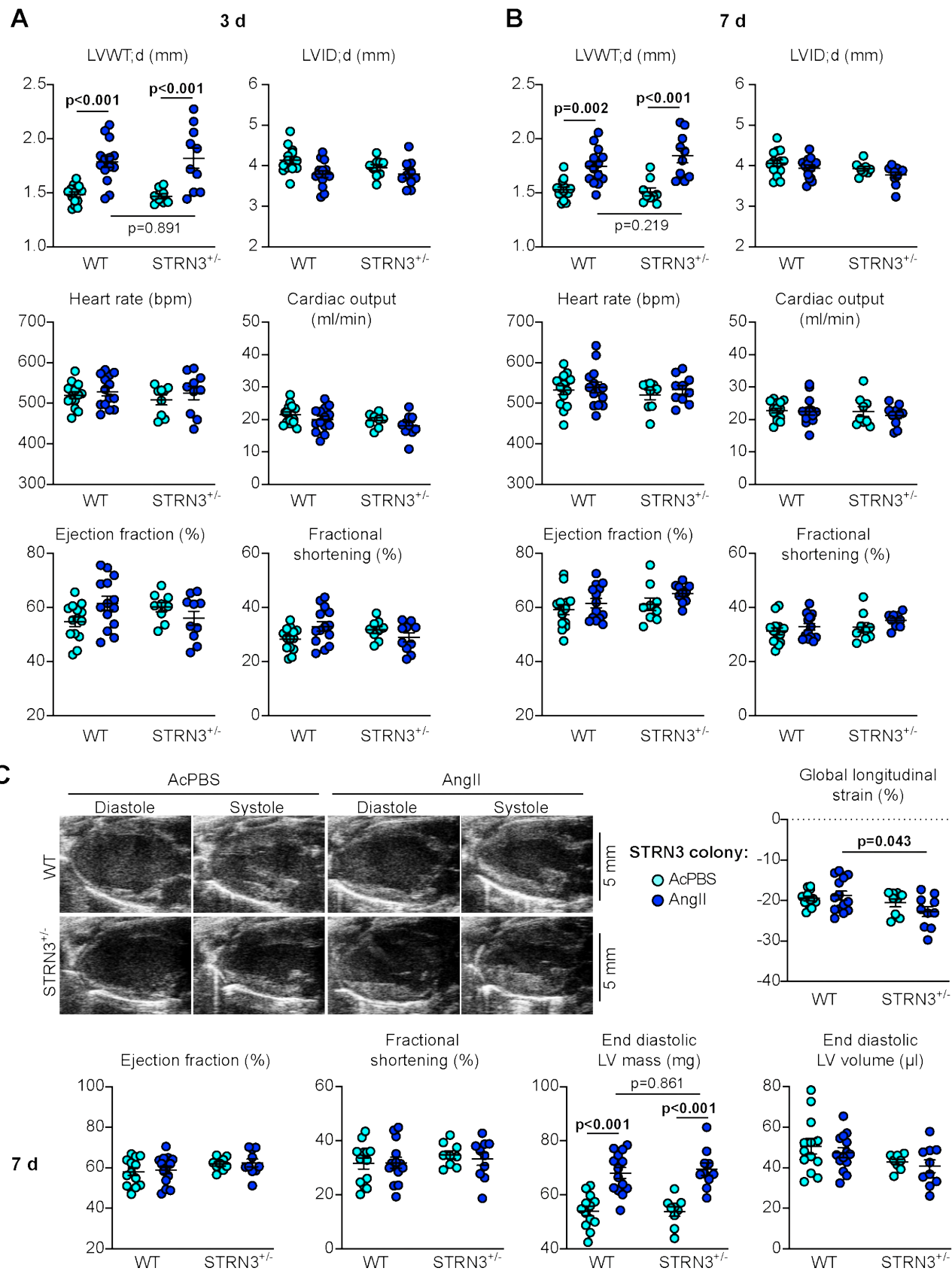
**Supplementary Table S9. Echocardiography data for STRN3<sup>f1/f1</sup>/Cre<sup>+/+</sup> mice: B-mode data and speckle-tracking.** Male mice (8 wks) were treated with corn-oil vehicle (COV) or 40 mg/kg tamoxifen (Tx) 4 days before minipumps were implanted for delivery of acidified PBS (AcPBS) or 0.8 mg/kg/d AngII in AcPBS for 7 d. Long axis B-mode images were analysed using speckle-tracking software. Tx, tamoxifen; EDV, End diastolic volume; ESV, End systolic volume; EDLVM, End diastolic left ventricle mass; ESLVM, End systolic left ventricle mass; GLS, global longitudinal strain; GCS, Global circumferential strain; SV, stroke volume; CO, cardiac output; EF, ejection fraction; FS, fractional shortening.

	COV/AcPBS		Tx/AcPBS		COV/AngII		Tx/AngII	
	Mean	SD	Mean	SD	Mean	SD	Mean	SD
<b>Baseline</b>								
Heart Rate (bpm)	460	27	465	25	468	32	476	26
SV (µl)	33.26	5.25	34.35	4.56	32.10	2.68	32.60	4.42
CO (ml/min)	15.36	2.82	15.96	2.23	15.04	1.89	15.43	1.67
EF (%)	56.56	6.96	56.64	3.44	57.21	4.71	58.42	5.15
FS (%)	30.20	6.91	30.39	3.74	31.37	4.54	31.26	4.14
EDV (µl)	58.76	6.92	60.69	8.28	56.20	4.25	56.26	9.59
ESV (µl)	25.50	5.09	26.34	4.57	24.11	3.79	23.65	6.47
EDLVM (mg)	54.62	3.78	53.42	3.39	52.82	2.94	52.05	3.08
ESLVM (mg)	57.36	3.85	56.82	4.77	54.63	3.53	54.95	3.08
GLS (%)	-19.96	2.84	-20.84	2.71	-19.27	2.64	-20.92	3.20
GCS (%)	-21.19	3.27	-21.68	2.51	-21.65	2.71	-21.15	2.96
<b>7 d</b>								
Heart Rate (bpm)	514	56	496	38	490	59	515	62
SV (µl)	33.40	6.21	33.09	4.79	27.74	7.67	28.14	5.35
CO (ml/min)	17.26	3.90	16.34	2.16	13.45	3.74	14.30	2.12
EF (%)	60. 64	8.7 7	59. 54	5.6 9	56. 44	11. 08	59. 95	6.4 1
FS (%)	33.88	5.48	31.30	5.47	31.45	8.26	36.14	6.01
EDV (µl)	54.94	8.31	55.63	9.49	50.47	13.99	47.69	12.79
ESV (µl)	21.54	6.55	22.54	6.21	22.73	8.55	19.55	7.94
EDLVM (mg)	55.58	4.65	54.17	4.56	71.19	15.02	58.98	4.37
ESLVM (mg)	58.04	5.17	57.22	4.79	72.26	15.07	60.15	4.38
GLS (%)	-20.57	6.10	-20.37	3.09	-16.90	3.76	-16.74	3.10
GCS (%)	-23.04	4.23	-22.75	3.28	-22.03	3.48	-21.28	5.52

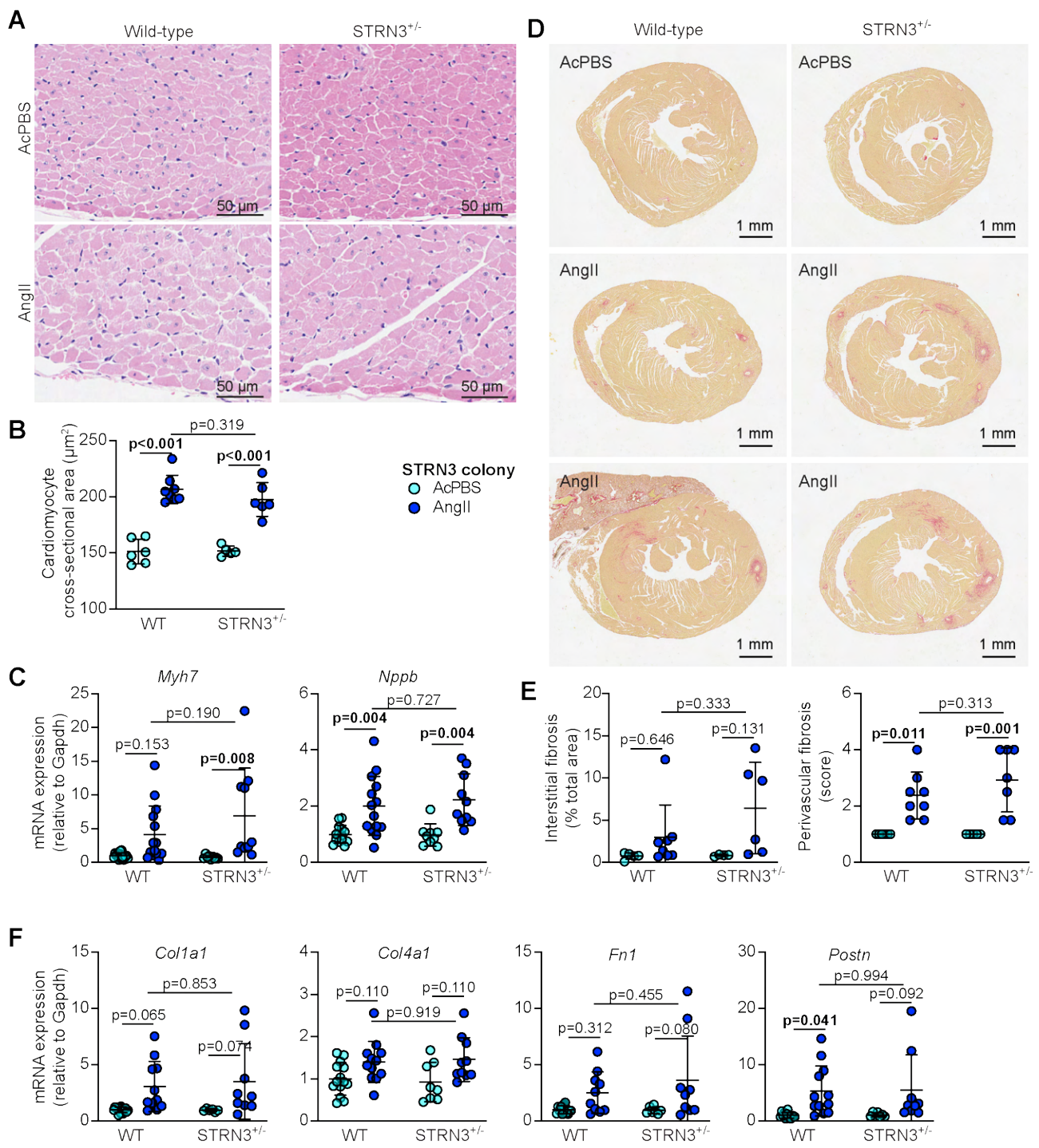
**Supplementary Figure S1. Global heterozygous STRN3 knockout in mice.** **A**, “Knockout-first” strategy for global deletion of STRN3 in mice involved positioning of a STOP cassette flanked by FRT sites upstream of a critical exon that was also flanked with LoxP sites. **B**, Experimental approach for assessment of effects of STRN3 deletion on cardiac function. Homozygous global knockout of STRN3 is embryonic lethal, so heterozygote STRN3<sup>+/−</sup> male mice (8 wks) were used in comparison with wild-type (WT) littermates from each colony. Following baseline echocardiography (echo), minipumps were implanted for delivery of acidified PBS vehicle (AcPBS) or 0.8 mg/kg/d angiotensin II (AngII). Following echocardiography at 7 d, mice were sacrificed. **C**, **D**, Heart powders were used for immunoblotting (40 µg protein per lane). Representative immunoblots of the striatin isoforms and GAPDH (**C**) are shown with densitometric analysis (**D**). Results are relative to GAPDH and normalised to the means for WT mice treated with AcPBS. Individual datapoints are plotted with means ± SEM. N.B. The upper band of the STRN blot used for densitometry correlates with the predicted molecular weight of STRN protein (110k Da).



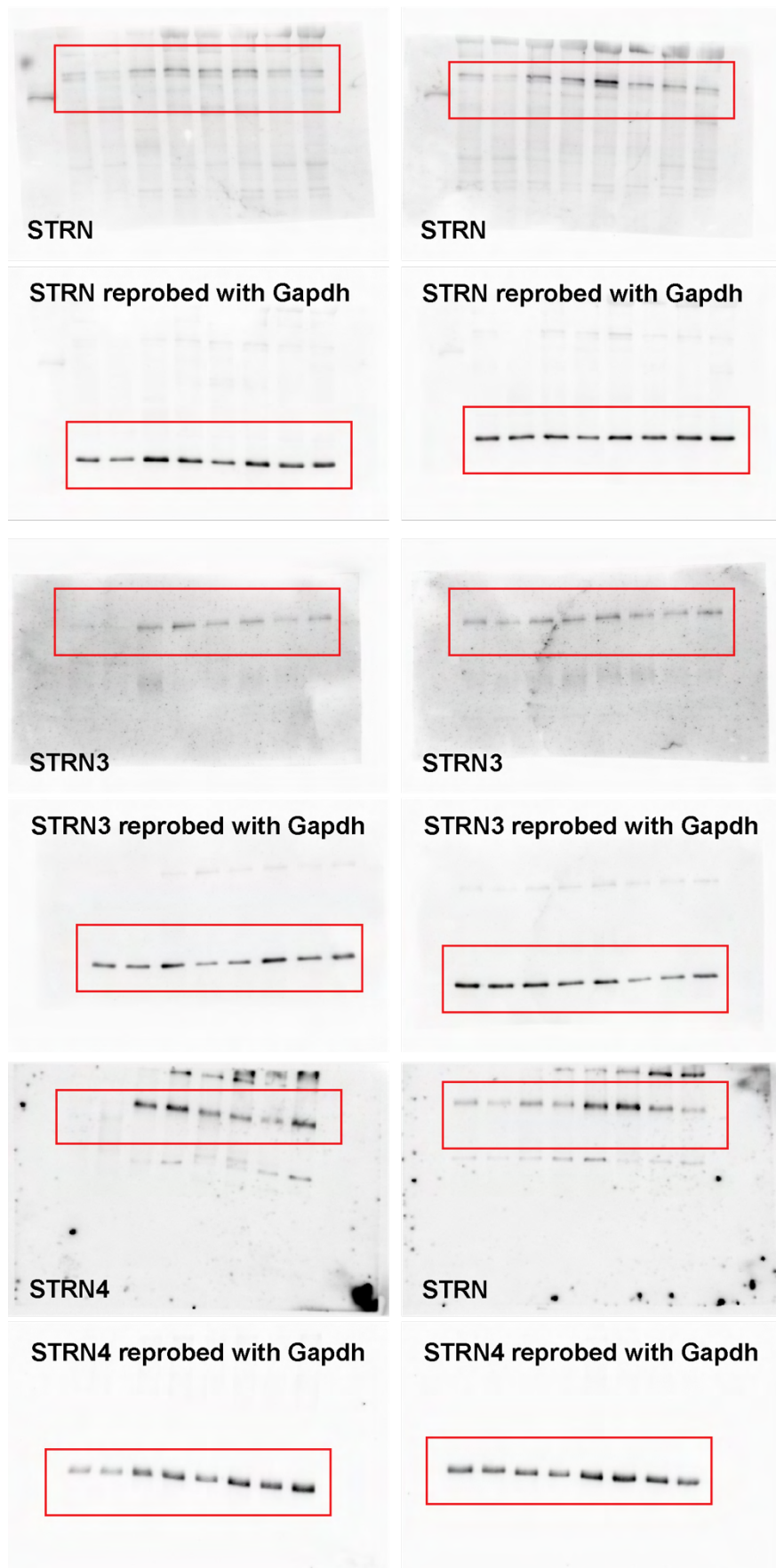
**Supplementary Figure S2. Heterozygous global deletion of STRN does not affect the hypertrophic response to AngII.** Male mice (8 wks) heterozygote for STRN3 knockout (STRN3<sup>+/</sup>) and wild-type (WT) littermates from each colony were treated with acidified PBS (AcPBS) vehicle or AngII (0.8 mg/kg/d). Cardiac function and dimensions were assessed by echocardiography using M-mode imaging of the short axis at 3 d (**A**) or 7 d (**B**), or B-mode imaging of the long axis at 7 d with speckle-tracking and strain analysis (**C**). For M-mode imaging, diastolic values for left ventricle (LV) wall thickness (WT) or internal diameter (ID) are shown and end diastolic LV mass and volume are provided for B-mode imaging. Cardiac function measurements are shown for both M-mode and B-mode for comparison. Individual datapoints are plotted with means  $\pm$  SEM. Statistical analysis used 2-way ANOVA with Holm-Sidak's post-test. (N.B. All echocardiography data are provided in **Supplementary Tables S4, S6 and S7**).



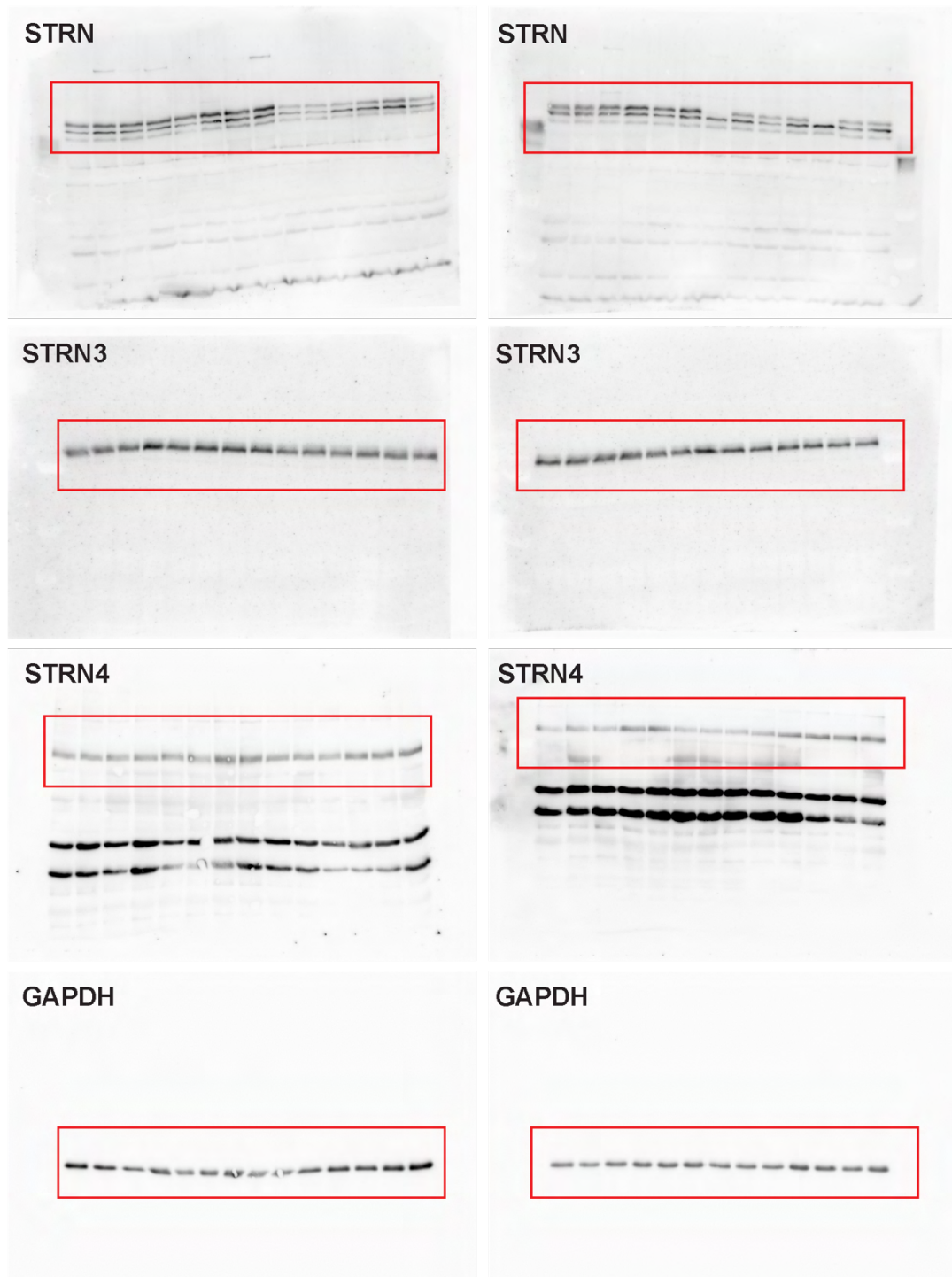
**Supplementary Figure S3. Heterozygous global deletion of STRN3 does not affect cardiomyocyte hypertrophy or cardiac fibrosis induced by AngII.** 8 wk male STRN<sup>+/−</sup> mice, plus their respective wild-type (WT) littermates were treated with acidified PBS (AcPBS) vehicle or 0.8 mg/kg/d AngII (7 d). **A-B**, Hearts were fixed and sections stained with haematoxylin and eosin. Representative images (**A**) show areas from the outer perimeter of the left ventricular wall opposite the interventricular septum and cardiomyocyte cross-sectional areas are shown (**B**). **C**, RNA was extracted from mouse heart powders and analysed by qPCR for *Myh7* and *Nppb* mRNAs. **D-E**, Hearts were fixed and sections stained with picrosirius red. Representative short axis views of the whole heart are shown for wild-type and STRN<sup>+/−</sup> mice treated with AcPBS or AngII (**D**). For AngII-treated hearts, the minimum or maximum response is shown in the middle and lower panels, respectively. **E**, Interstitial fibrosis was measured using Image J and is presented as the % of the total area (excluding regions around the blood vessels). Perivascular fibrosis was scored (1: negligible increase in fibrosis around any vessel; 2: mild to moderate fibrosis around 1 or more vessels; 3: Significant fibrosis permeating tissue around 1 or more vessels; 4: extensive fibrosis around multiple vessels, penetrating into the myocardium). A scoring system was used for the latter because of the variation in numbers of vessels seen in different heart sections. **F**, RNA was extracted from mouse heart powders and analysed by qPCR for fibrosis mRNAs as indicated. Results for qPCR are relative to GAPDH and normalised to the means for WT mice treated with AcPBS. Individual datapoints are plotted with means ± SD. Statistical analysis used 2-way ANOVA with Holm-Sidak's post-test.



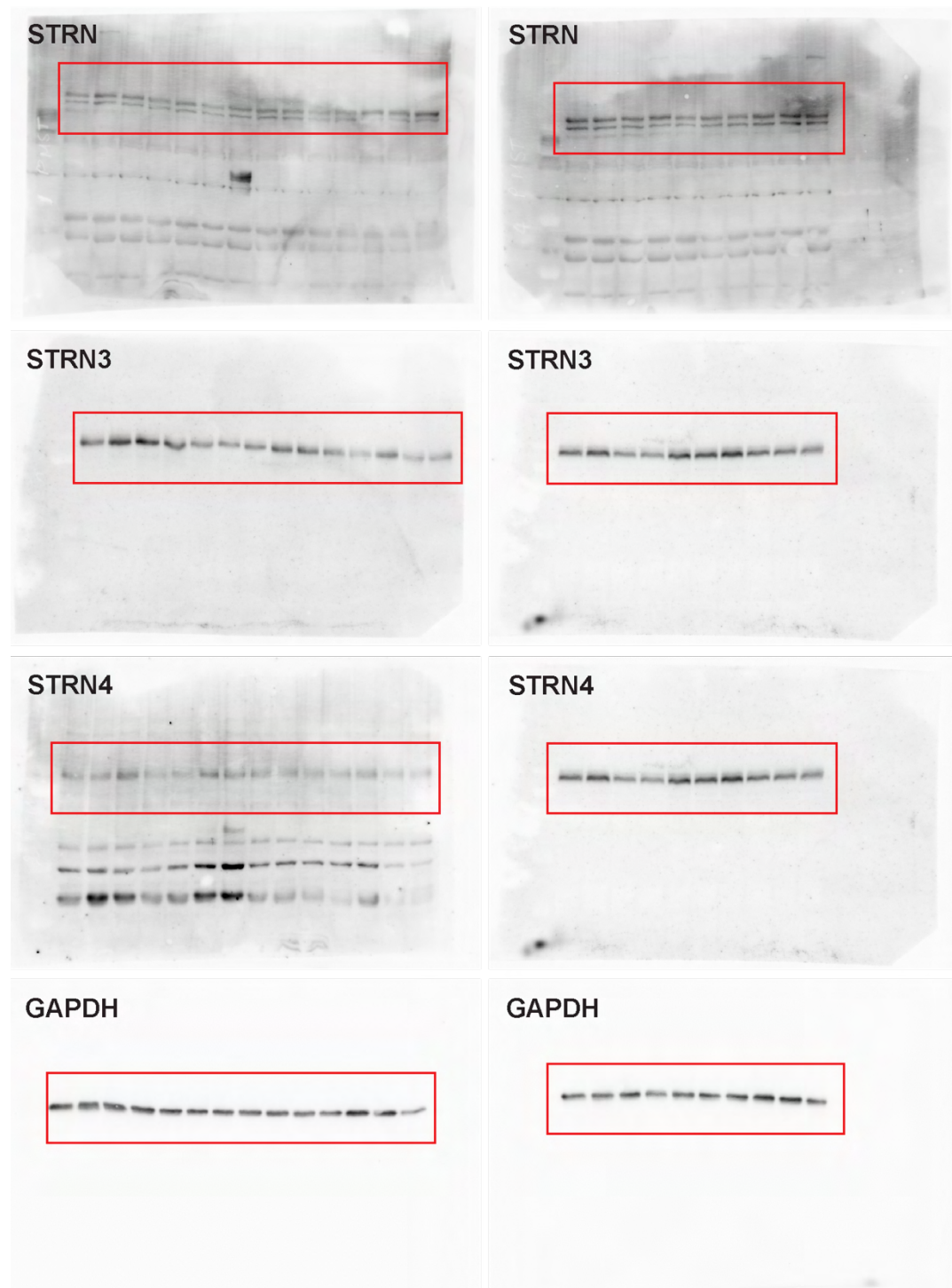
**Supplementary Figure S4. Full images for immunoblots in Figure 1C.** Proteins were separated on 10% polyacrylamide gels. Red boxes highlight the bands of interest.



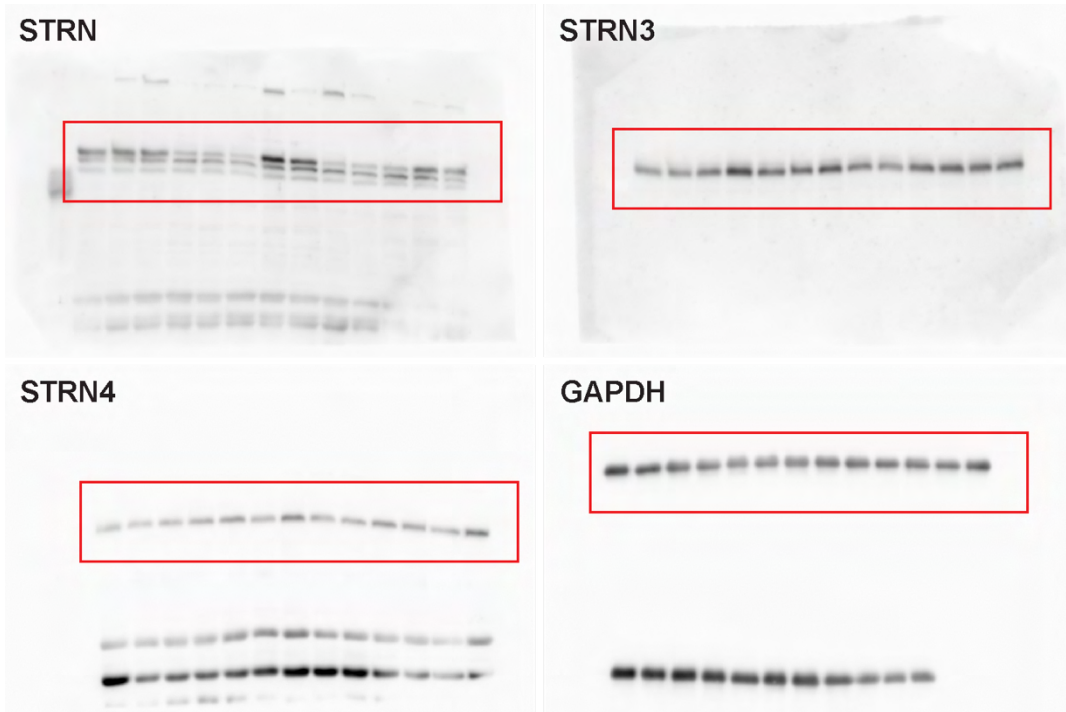
**Supplementary Figure S5. Full images for immunoblots in Figure 1G.** Proteins were separated on 8% and 12% polyacrylamide gels for striatins and GAPDH, respectively. Red boxes highlight the bands of interest.



**Supplementary Figure S6. Full images for immunoblots in Supplementary Figure S1C.**  
Proteins were separated on 8% and 12% polyacrylamide gels for striatins and GAPDH, respectively.  
Red boxes highlight the bands of interest.



**Supplementary Figure S7. Full images for immunoblots in Figure 5D.** Proteins were separated on 8% and 10% polyacrylamide gels for striatins and GAPDH, respectively. (N.B. Two half blots for GAPDH from different experiments were imaged together giving upper and lower bands). Red boxes highlight the bands of interest.



## **Chapter 4 - PKN2 deficiency leads both to prenatal 'congenital' cardiomyopathy and defective angiotensin II stress responses**

**Title:** PKN2 deficiency leads both to prenatal 'congenital' cardiomyopathy and defective angiotensin II stress responses.

**Authors:** Jacqueline J.T. Marshall, Joshua J. Cull, Hajed O. Alharbi, May Zaw Thin, Susanna T.E. Cooper, Christopher Barrington, Hannah Vanyai, Thomas Snoeks, Bernard Siow, Alejandro Suárez-Bonnet, Eleanor Herbert, Daniel J. Stuckey, Angus J.M. Cameron, Fabrice Prin, Andrew C. Cook, Simon L. Priestnall, Sonia Chotani, Owen J. L. Rackham, Daniel N. Meijles, Tim Mohun, Angela Clerk and Peter J. Parker.

**Contributions:** Peter J. Parker: Conceptualization, Resources, Formal analysis, Supervision, Funding acquisition, Writing — original draft, Project administration, Writing — review and editing. Jacqueline JT Marshall: Conceptualization, Formal analysis, Investigation, Writing — original draft, Project administration, Writing — review and editing. Joshua J. Cull: Investigation, Writing — review and editing. Hajed O. Alharbi: Investigation, Writing — review and editing. May Zaw Thin: Investigation, Writing — review and editing. Susanna TE Cooper: Investigation, Writing — review and editing. Christopher Barrington: Formal analysis, Writing — review and editing. Hannah Vanyai: Investigation, Writing — review and editing. Thomas Snoeks: Investigation, Writing — review and editing. Bernard Siow: Investigation, Writing — review and editing. Alejandro Suárez-Bonnet: Investigation, Writing — review and editing. Eleanor Herbert: Investigation, Writing — review and editing. Daniel J. Stuckey: Investigation, Writing — review and editing. Angus Cameron: Conceptualization, Supervision, Investigation, Writing — review and editing. Fabrice Prin: Investigation, Writing — review and editing. Andrew C. Cook: Conceptualization, Writing — review and editing. Simon L. Priestnall: Investigation, Writing — review and editing. Sonia Chotani: Investigation, Writing — review and editing. Owen JL Rackham: Investigation, Writing — review and editing. Daniel Meijles: Conceptualization, Supervision, Investigation, Writing — review and editing. Timothy Mohun: Supervision, Investigation, Writing — review and editing. Angela Clerk: Conceptualization, Resources, Supervision, Investigation, Writing — original draft, Writing — review and editing.

**DOI:** <https://doi.org/10.1042/BCJ20220281>

Research Article

# PKN2 deficiency leads both to prenatal ‘congenital’ cardiomyopathy and defective angiotensin II stress responses

Jacqueline J.T. Marshall<sup>1,\*</sup>, Joshua J. Cull<sup>2</sup>, Hajed O. Alharbi<sup>2</sup>, May Zaw Thin<sup>3</sup>, Susanna T.E. Cooper<sup>4</sup>, Christopher Barrington<sup>5</sup>, Hannah Vanyai<sup>6,†</sup>, Thomas Snoeks<sup>7</sup>, Bernard Siow<sup>7</sup>, Alejandro Suárez-Bonnet<sup>8,9</sup>, Eleanor Herbert<sup>8,9</sup>, Daniel J. Stuckey<sup>3</sup>, Angus J.M. Cameron<sup>10</sup>, Fabrice Prin<sup>11</sup>, Andrew C. Cook<sup>12</sup>, Simon L. Priestnall<sup>8,9</sup>, Sonia Chotani<sup>13</sup>, Owen J. L. Rackham<sup>13</sup>,  Daniel N. Meijles<sup>4</sup>, Tim Mohun<sup>11</sup>,  Angela Clerk<sup>2</sup> and  Peter J. Parker<sup>1,14</sup>

<sup>1</sup>Protein Phosphorylation Laboratory, Francis Crick Institute, 1 Midland Road, London NW1 1AT, U.K.; <sup>2</sup>School of Biological Sciences, University of Reading, Reading RG6 2AS, U.K.; <sup>3</sup>UCL Centre for Advanced Biomedical Imaging, Division of Medicine, University College London, London WC1E 6DD, U.K.; <sup>4</sup>Molecular and Clinical Sciences Institute, St George's University of London, London SW17 0RE, U.K.; <sup>5</sup>Bioinformatics and Biostatistics, Francis Crick Institute, 1 Midland Road, London NW1 1AT, U.K.; <sup>6</sup>Epithelial Biology Laboratory, Francis Crick Institute, 1 Midland Road, London NW1 1AT, U.K.; <sup>7</sup>In Vivo Imaging, Francis Crick Institute, 1 Midland Road, London NW1 1AT, U.K.; <sup>8</sup>Experimental Histopathology, Francis Crick Institute, 1 Midland Road, London NW1 1AT, U.K.; <sup>9</sup>Department of Pathobiology & Population Sciences, The Royal Veterinary College, North Mymms, Hatfield, Hertfordshire AL9 7TA, U.K.; <sup>10</sup>Kinase Biology Laboratory, John Vane Science Centre, Barts Cancer Institute, Queen Mary University of London, Charterhouse Square, London EC1M 6BQ, U.K.; <sup>11</sup>Heart Formation in Vertebrates Laboratory, Francis Crick Institute, 1 Midland Road, London NW1 1AT, U.K.; <sup>12</sup>Centre for Morphology and Structural Heart Disease, Institute of Institute of Cardiovascular Science, Zayed Centre for Research, 20 Guilford Street, London WC1N 1DZ, U.K.; <sup>13</sup>Program in Cardiovascular and Metabolic Disorders, Duke-NUS Medical School, Singapore, Singapore; <sup>14</sup>School of Cancer and Pharmaceutical Sciences, New Hunt's House, Guy's Campus, London SE1 1UL, U.K.

Correspondence: Peter J. Parker (peter.parker@crick.ac.uk) or Angela Clerk (a.clerk@reading.ac.uk)



The protein kinase PKN2 is required for embryonic development and PKN2 knockout mice die as a result of failure in the expansion of mesoderm, cardiac development and neural tube closure. In the adult, cardiomyocyte PKN2 and PKN1 (in combination) are required for cardiac adaptation to pressure-overload. The specific role of PKN2 in contractile cardiomyocytes during development and its role in the adult heart remain to be fully established. We used mice with cardiomyocyte-directed knockout of PKN2 or global PKN2 haploinsufficiency to assess cardiac development and function using high resolution episcopic microscopy, MRI, micro-CT and echocardiography. Biochemical and histological changes were also assessed. Cardiomyocyte-directed PKN2 knockout embryos displayed striking abnormalities in the compact myocardium, with frequent myocardial clefts and diverticula, ventricular septal defects and abnormal heart shape. The sub-Mendelian homozygous knockout survivors developed cardiac failure. RNASeq data showed up-regulation of PKN2 in patients with dilated cardiomyopathy, suggesting an involvement in adult heart disease. Given the rarity of homozygous survivors with cardiomyocyte-specific deletion of PKN2, the requirement for PKN2 in adult mice was explored using the constitutive heterozygous PKN2 knockout. Cardiac hypertrophy resulting from hypertension induced by angiotensin II was reduced in these haploinsufficient PKN2 mice relative to wild-type littermates, with suppression of cardiomyocyte hypertrophy and cardiac fibrosis. It is concluded that cardiomyocyte PKN2 is essential for heart development and the formation of compact myocardium and is also required for cardiac hypertrophy in hypertension. Thus, PKN signalling may offer therapeutic options for managing congenital and adult heart diseases.

\*Current address: Cancer Research UK, 2 Redman Place, London E20 1JQ, U.K.

†Current address: The Walter and Eliza Hall Institute, 1G Royal Parade, Parkville, 3052, Australia

Received: 30 May 2022

Revised: 21 June 2022

Accepted: 21 June 2022

Accepted Manuscript online:

22 June 2022

Version of Record published:

12 July 2022

## Introduction

Heart disease, a major cause of death and disability worldwide, develops from numerous underlying causes. These include genetic/environmental interactions causing congenital cardiac defects [1, 2], in addition to diseases in later life resulting from various pathophysiological stressors (e.g. coronary artery disease, hypertension, diabetes, obesity) [3–8]. The increasing prevalence of heart disease worldwide accounts for an expanding patient cohort who go on to develop and die of heart failure. The heart contains three main cell types (cardiomyocytes, endothelial cells, fibroblasts) with cardiomyocytes providing the contractile force. In the embryo/foetus, cardiomyocytes proliferate whilst the heart develops, but then withdraw from the cell cycle in the perinatal/postnatal period, becoming binucleated and fully terminally differentiated [9, 10]. Further growth of the heart to the adult size requires an increase in size and sarcomeric/myofibrillar apparatus of individual cardiomyocytes (maturational growth). The adult heart experiences pathophysiological stresses (e.g. hypertension) requiring an increase in contractile function. This is accommodated by cardiomyocyte hypertrophy (sarcomeric replication in parallel or series) with associated cardiac hypertrophy (enlargement of the heart) [11]. This adaptation is initially beneficial, but pathological hypertrophy develops over prolonged periods with cardiomyocyte dysfunction and death, loss of capillaries and deposition of inelastic fibrotic scar tissue [11]. These processes are all regulated by a complex interplay of intracellular signalling pathways, driven by numerous protein kinases that play central roles both in mammalian development and in adult tissue homeostasis [12]. These regulatory proteins offer themselves as potential targets for intervention both in management of congenital cardiomyopathies and in pathological states. Insight into the key regulatory players at each and every stage is central for prevention, in addition to the development and delivery of improved treatments and outcomes.

The Protein Kinase N (PKN) family of kinases are emerging as potential therapeutic targets for heart disease [13]. Whilst PKN1 and PKN2 are ubiquitously expressed in tissues throughout the body, PKN3 is expressed in a smaller subset of tissues, especially endothelial cell types [14, 15]. Of the three PKNs, only *Pkn2* knockout is embryonic lethal. This is due to failure in the expansion of mesoderm tissues, failure of cardiac development and compromised neural tube closure [16, 17]. Further studies with conditional knockouts of *Pkn2* employed cell-targeted Cre under the control of a smooth muscle protein 22 $\alpha$  (SM22 $\alpha$ ) promoter [17]. SM22 $\alpha$  (and therefore SM22 $\alpha$ -Cre) is expressed in the heart tube from embryonic day E7.5/8 [18], with expression declining from E10.5 and becoming restricted to the right ventricle by E12.5. By E13.5, SM22 $\alpha$  is undetectable in the heart [19] and expression is subsequently confined to smooth muscle cells and myofibroblasts [18, 20–22]. Conditional gene deletion of *Pkn2* results in sub-Mendelian survival of SM22 $\alpha$ -Cre $^{+/-}$  *Pkn2* $^{fl/fl}$  offspring, with ~1/3 of mice surviving to 4 weeks postnatally [17]. These data indicate that PKN2 is not only important in the heart during embryonic development, but (whilst the phenotype is not fully penetrant in the SM22 $\alpha$ -Cre model) is also required for maturational growth of the heart. This raises the question of what is compromised and how loss of PKN2 manifests in the adult.

There are few studies of PKNs in the adult heart. PKN1 is activated in neonatal cardiomyocytes by hyperosmotic shock [23] and reduces ischaemia/reperfusion injury in *ex vivo* perfused hearts [24]. *In vivo* studies suggest there may be redundancy between PKN1 and PKN2 in cardiomyocytes, and double knockout of both kinases simultaneously in cardiomyocytes inhibits cardiac hypertrophy in pressure-overload conditions induced by transverse aortic constriction (TAC) or angiotensin II (AngII) [25]. Fundamental questions remain concerning the functional redundancy of PKN1 and 2 in cardiomyocytes. Here, we demonstrate that the loss of PKN2 in cardiomyocytes has a catastrophic effect on ventricular myocardial development, suggesting that alterations in PKN2 signalling may contribute to congenital cardiac problems cardiomyopathy. We also demonstrate that PKN2 haploinsufficiency compromises cardiac adaptation to hypertension in adult mouse hearts. We conclude that PKN2 plays a significant and non-redundant role in cardiac development and adaptation.

## Results

### Cardiac-specific knockout of *Pkn2*

Evidence from the SM22 $\alpha$ -Cre conditional *Pkn2* knockout indicates reduced survival (Table 1 and [17]), which might reflect in part an impact on heart function but may also be determined by loss of *Pkn2* expression in smooth muscle. To dissect the functional contributions more selectively, we sought to refine the pattern of knockout by using the *XMLC-Cre* line, where *Cre* expression is cardiac restricted [26]. Genotyping pups from the *Pkn2* $^{fl/fl}$  mice crossed with *XMLC2-Cre* $^{+/-}$  *Pkn2* $^{fl/+}$  animals at 2–4 weeks of age identified only one *XMLC2-Cre* $^{+/-}$  *Pkn2* $^{fl/fl}$  mouse (of 126), consistent with a severe phenotype with this *Cre* line (Table 1). This potentially results from higher efficiency of *XMLC2-Cre* activity in cardiomyocytes (95% [26]) compared with

**Table 1** *SM22αCre* and *XMLC2Cre* mouse strain crosses are indicated in column 1, with numbers of experimentally determined genotypes shown in rows for the age ranges defined

Parent genotypes	Age	Cre negative		Cre positive		Fisher's test	Representation
		PKN2 <sup>fl/+</sup>	PKN2 <sup>fl/fl</sup>	PKN2 <sup>fl/+</sup>	PKN2 <sup>fl/fl</sup>		
SM22α-Cre <sup>+/−</sup> × PKN2 <sup>fl/+</sup> × PKN2 <sup>fl/fl</sup>	E14.5–E18.5	54	43	33	46	>0.5	Mendelian under-represented
	3 weeks	166	215	176	44	0.0001	
XMLC2-Cre <sup>+/−</sup> × PKN2 <sup>fl/+</sup> × PKN2 <sup>fl/fl</sup>	E14.5–E18.5	5	3	10	6	>0.5	Mendelian under-represented
	3 weeks	37	41	47	1	0.0001	

The representation of the PKN2 knockout (i.e. PKN2<sup>fl/fl</sup> in the context of Cre expression) was analysed as a function of the all genotypes using Fisher's test.

*SM22α-Cre* (75–80% [20]) and more specifically indicates that there are cardiac-associated phenotypes of PKN2 loss. The single surviving male was small (11.2 g relative to 22.4 g for a *XMLC2-Cre<sup>+/−</sup> Pkn2<sup>fl/+</sup>* littermate) and was culled at 5 weeks due to poor condition. Histological analysis of the heart from this animal showed that it was highly abnormal. Both ventricles were dilated, with a hypertrophic right ventricle and thin-walled (hypotrophic) and disorganised left ventricular myocardium and interventricular septum. There were partial discontinuities in the cardiac muscle of the compact layer, and sections with highly disorganised cardiomyocytes and fibrosis (Figure 1a). It was noted also that the lungs from the *XMLC2-Cre<sup>+/−</sup> Pkn2<sup>fl/fl</sup>* mouse displayed grossly enlarged alveolar spaces (Figure 1b).

To explore this impact of PKN2 further, we genotyped gestational day 14.5 embryos from *Pkn2<sup>fl/fl</sup>* mice crossed with *XMLC2-Cre<sup>+/−</sup> Pkn2<sup>fl/+</sup>* and found that 6 of 24 were *XMLC2-Cre<sup>+/−</sup> Pkn2<sup>fl/fl</sup>* consistent with a Mendelian distribution at this developmental stage. However, analysis of the hearts using high resolution episcopic microscopy (HREM) showed various abnormalities (Figure 1c; Video 1 see also Supplementary Figure S1). Notably, hearts from these mouse embryos displayed multiple surface nodules (diverticula; see below) distributed across both ventricles, unusually large perimembranous ventricular septal defects and thin compact myocardium indicative of significant cardiac developmental complications.

## Characterising the cardiac requirement of PKN2

Whilst the *XMLC*-driven knockout of *Pkn2* clearly demonstrated a cardiac phenotype associated with PKN2 loss, the fatal consequences of the *XMLC*-driven knockout of *Pkn2* led us instead to investigate in more detail the more frequent survivors derived in the *SM22α-Cre* model. On re-derivation of the *SM22α* model into a new facility and crossing the *Pkn2<sup>fl/fl</sup>* with *SM22α-Cre<sup>+/−</sup> Pkn2<sup>fl/+</sup>* animals, we found there remained a sub-Mendelian distribution of the *SM22α-Cre<sup>+/−</sup> Pkn2<sup>fl/fl</sup>* genotype (28% of expected numbers with no male/female bias; Table 1). Crossing 10 of these mice with *Pkn2<sup>fl/fl</sup>* animals produced 62 weaned pups but again a sub-Mendelian representation of the *SM22α-Cre<sup>+/−</sup> Pkn2<sup>fl/fl</sup>* genotype (32% of expected).

Typically, surviving *SM22α-Cre<sup>+/−</sup> Pkn2<sup>fl/fl</sup>* mice became overtly unwell as they aged, displaying a range of adverse phenotypes including body weight differences compared with littermates, loss of condition, hunched appearance or reduced activity. Amongst a cohort of 23 animals, there were 50% asymptomatic *SM22α-Cre<sup>+/−</sup> Pkn2<sup>fl/fl</sup>* mice at 24 weeks of age, with the oldest two mice reaching 72 weeks and only then started to display phenotypes (echocardiography showed aortic valve stenosis and echo-dropout across the long-axis view of the left ventricle in one, suggestive of mitral annular calcification; see below). A typical example of an aging *SM22α-Cre<sup>+/−</sup> Pkn2<sup>fl/fl</sup>* animal was a 38-week-old fertile female which upon culling due to loss of condition displayed a heart weight: body weight ratio = 0.99% (compared with 0.37–0.48% for female littermates).

Similar to the single weaned *XMLC2-Cre<sup>+/−</sup> Pkn2<sup>fl/fl</sup>* mouse, histology of the *SM22α-Cre<sup>+/−</sup> Pkn2<sup>fl/fl</sup>* mice showed hypertrophic ventricular walls with disorganised cardiomyocytes and extensive fibrosis, consistent with a form of cardiomyopathy and heart failure (Figure 2a,b; Supplementary Figure S2). Histological assessment of the lungs showed *SM22α-Cre<sup>+/−</sup> Pkn2<sup>fl/fl</sup>* mice culled with breathlessness had grossly enlarged alveolar spaces (Figure 2c), corresponding to the anecdotal finding in the one *XMLC-Cre<sup>+/−</sup> Pkn2<sup>fl/fl</sup>* survivor. The timing of symptom onset is illustrated in Figure 2d. Functional cardiac MRI analysis of a further set of five surviving *SM22α-Cre<sup>+/−</sup> Pkn2<sup>fl/fl</sup>* mice with initial symptoms of heart failure, indicated that they had reduced left ventricular ejection fraction (Figure 2e,f). Imaging did not identify a single unifying cause, with examples of

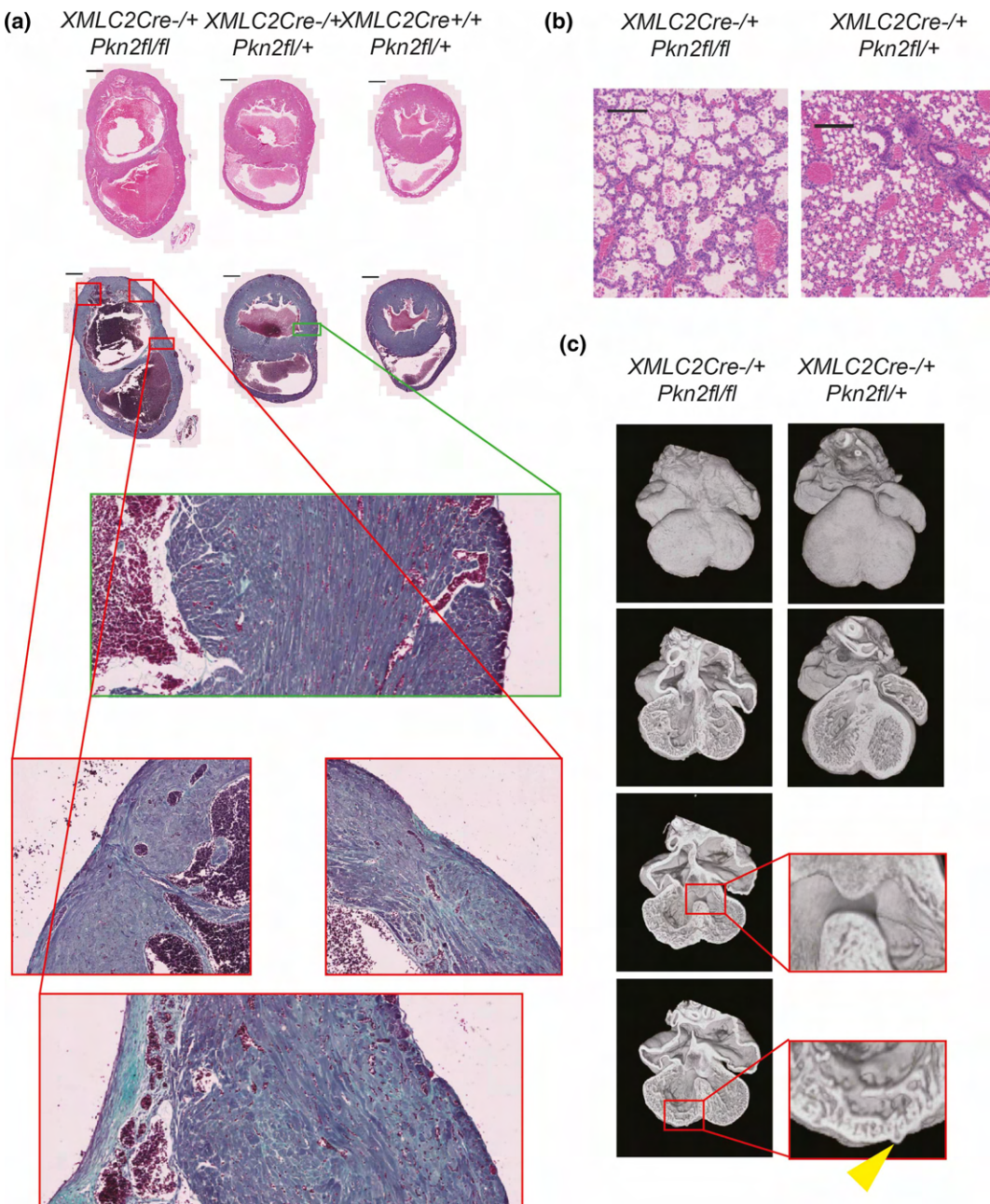


**Figure 1. PKN2 knockout in cardiomyocytes causes defective embryonic heart development leading to failure prior to adulthood.**

(a) H&E and Gomori's Trichrome stained histological cardiac short-axis sections of the longest surviving *XMLC2Cre<sup>+-</sup> Pkn2<sup>fl/fl</sup>* genotype mouse (left; male), and two littermates (middle & right; male *XMLC2Cre<sup>+-</sup> Pkn2<sup>fl/+</sup>* & female *XMLC2Cre<sup>++</sup> Pkn2<sup>fl/+</sup>*, respectively) all culled aged 5 weeks. Scale bars are 1 mm. In lower boxed regions, various sections are also shown at 20 $\times$  zoom relative to whole-heart cross-sections. (b) H&E sections of lungs of the same *XMLC2Cre<sup>+-</sup> Pkn2<sup>fl/fl</sup>* genotype mouse (left), and its *XMLC2Cre<sup>+-</sup> Pkn2<sup>fl/+</sup>* littermate (right; both male). Scale bars are 200  $\mu$ m. (c) Images of High-Resolution Episcopic Microscopy (HREM) reconstructions of E14.5 embryo hearts for the genotypes indicated, showing surface and four chamber views. Boxed regions of sections are shown at 4 $\times$  zoom; a diverticulum is indicated by the yellow arrowhead.

reduced right ventricular mass, potentially associated with pulmonary hypertension ( $n = 2$  of 5), or completely abnormal architecture with hearts exhibiting a bulbous shape ( $n = 3$  of 5) (see histology and HREM in Supplementary Figures S2 and S3).

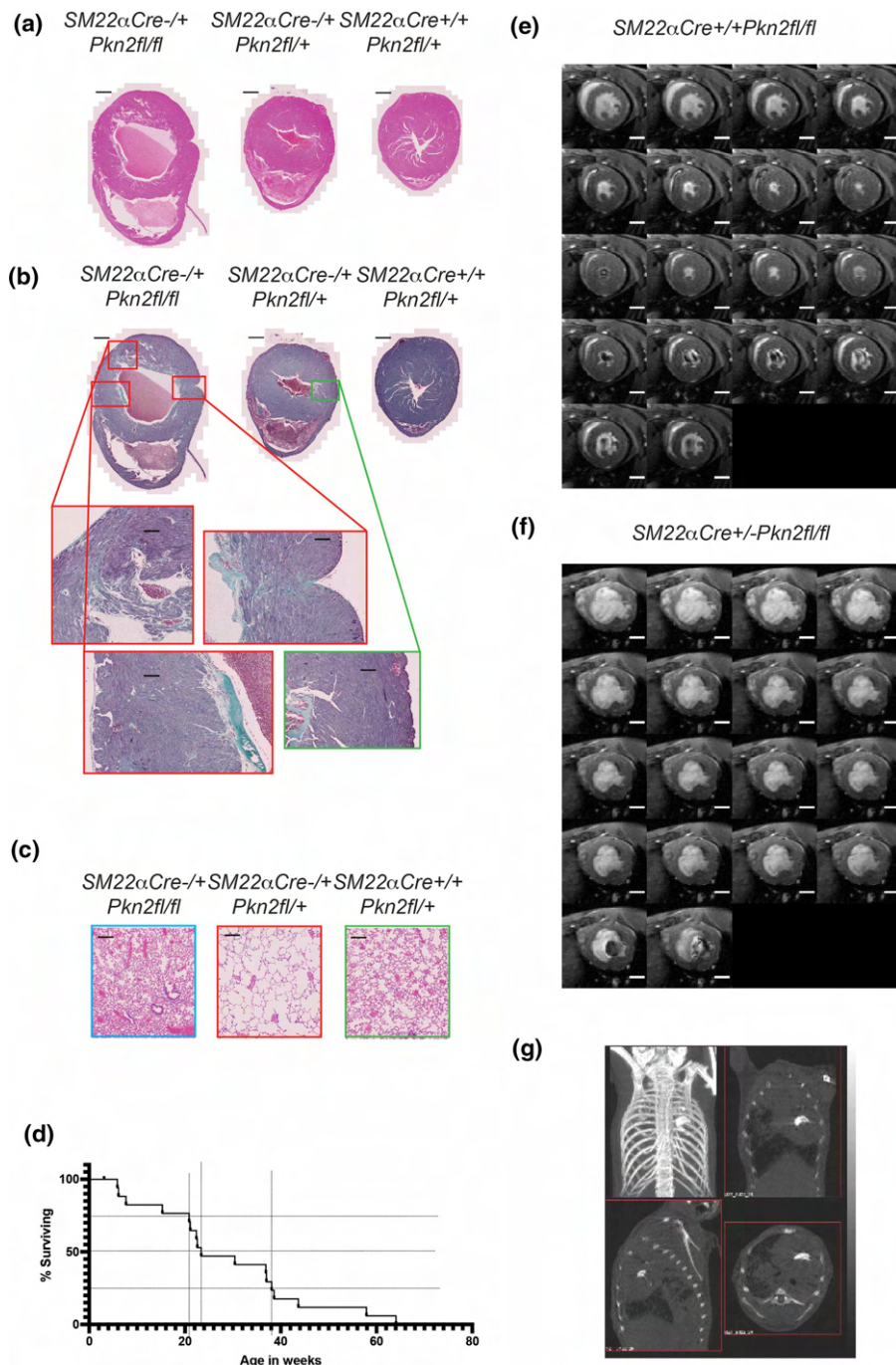


**Figure 2. *SM22aCre*<sup>+/−</sup> *Pkn2*<sup>fl/fl</sup> mice suffer cardiac failure on aging.**

(a and b) Short-axis mid-ventricle sections of hearts of 39 week male littermates of the genotypes indicated, stained with H&E (a), or Gomori's Trichrome (b). (c) H&E stained sections of lungs, littermates as in (a and b). (d) Time course of symptom onset for mice of genotype *SM22aCre*<sup>+/−</sup> *Pkn2*<sup>fl/fl</sup> ( $n = 23$ ). (e and f) Montage of time-series through the cardiac cycle recorded by cine-cardiac-MRI through the short-axis plane at mid-ventricle from *SM22aCre*<sup>+/+</sup> *Pkn2*<sup>fl/fl</sup> (e) and *SM22aCre*<sup>+/−</sup> *Pkn2*<sup>fl/fl</sup> (f) 32 week old female littermates. (g) micro-CT of the thorax of a 24 week *SM22aCre*<sup>+/−</sup> *Pkn2*<sup>fl/fl</sup> female shown as a projected image and slice images in three planes. Scale-bars in histopathology images are 1 mm in whole heart sections (panels a and b) and 200  $\mu$ m in zoomed sections (panels b and c). Scale-bars in MRI montages are 2 mm (panels e and f).

Micro-CT imaging was used to assess disease in a further subset of survivors. This revealed variously: pulmonary oedema and pleural effusion, and marked, unusual calcification in the centre of the rib cage (Figure 2g). Subsequent micro-CT of fixed hearts showed that calcification appeared to be associated with both the aortic and mitral valves (Supplementary Video S2). The evidence suggests that surviving  $SM22\alpha$ -*Cre*<sup>+/−</sup>  $Pkn2^{fl/fl}$  mice had congenital defects in the heart and/or lungs resulting in heart failure and as with human congenital heart disease, there was heterogeneity with respect to age of disease onset, severity of disease and specific cardiac phenotype.

### Cardiomyocyte PKN2 is essential for normal cardiac development

Although previous studies reported that PKN2 is essential for embryonic development, E13.5 embryos were produced at a normal Mendelian ratio [17]. Data from surviving  $SM22\alpha$ -*Cre*<sup>+/−</sup>  $Pkn2^{fl/fl}$  mice (above) suggest the cardiac defect is most likely the result of developmental cardiac abnormalities, however defects in lung development resulting from loss of  $Pkn2$  in smooth muscle cells would impact cardiac function and also lead to heart failure. We therefore collected embryos at E14.5–E18.5 generated by crossing  $Pkn2^{fl/fl}$  and  $SM22\alpha$ -*Cre*<sup>+/−</sup>  $Pkn2^{fl/+}$  mice for further analysis to examine the Mendelian ratios at these later embryonic stages, and to enable pathological examination of the developing hearts and lungs. Genotype distribution was Mendelian at both E14.5 and E18.5 (Table 1). Notably, histological analysis failed to identify any difference between lungs from  $SM22\alpha$ -*Cre*<sup>+/−</sup>  $Pkn2^{fl/fl}$  embryos and those from littermates that were either *Cre* negative or heterozygous for the floxed  $Pkn2$  allele or both (Figure 3a), suggesting normal lung development to E18.5 and implying that the enlarged alveolar spaces in some of the rare surviving adults may be a secondary consequence of cardiac abnormalities.

Given that the E18.5 genotype distribution was Mendelian but only ~30% of  $SM22\alpha$ -*Cre*<sup>+/−</sup>  $Pkn2^{fl/fl}$  mice survived to weaning, this suggested that lethality occurred in the perinatal period. Analysis of deceased pups including part-cannibalised carcasses demonstrated that this genotype was selectively lost in this very early neonatal stage (Table 1). Veterinary pathologist characterisation of P1.5–P5.5 carcasses showed that all had normal palates, lungs that floated and milk spots. There were no observations of pericardial bleeding, which might have been observed if one of the cardiac diverticula had ruptured causing tamponade (see below).

Analysis of embryo hearts using HREM showed that of 16  $SM22\alpha$ -*Cre*<sup>+/−</sup>  $Pkn2^{fl/fl}$  E14.5 embryos, 15 had overt defects in cardiac development compared with littermates (exemplified in Figure 3b; see also Supplementary Figure S3). Defects included perimembranous ventricular septal defects (pVSDs), small muscular VSDs (mVSDs), thin compact myocardium (right and left ventricle) and overt nodules on the external surface of either or both ventricles. The degree of phenotype varied, with the most abnormal hearts showing pVSD with overriding of the aorta (OA), and many showing an overall abnormally squat shape with an indistinct apex. The nodules on the surface of the ventricles were examined histologically and identified as diverticula with internal lumens connected to the ventricular cavities (Figure 3c).

Cardiac septation would expect to be completed by E15, however of 60 embryos analysed in crosses of  $Pkn2^{fl/fl}$  and  $SM22\alpha$ -*Cre*<sup>+/−</sup>  $Pkn2^{fl/+}$  mice, we obtained 18  $SM22\alpha$ -*Cre*<sup>+/−</sup>  $Pkn2^{fl/fl}$  embryos of which seven had persistent VSDs along with thin compact myocardium/ventricular walls. The nodules on the ventricle surfaces apparent at E14.5 also persisted. There was additional abnormal development of the trabecular layer in the ventricular walls — analogous to hypertrabeculation (Figure 3d).

The congruence of developmental defects in the  $SM22\alpha$ -*Cre* and the  $XMLC$ -*Cre* strains indicates that the dominant effect of tissue-specific  $Pkn2$  loss relates to the shared aspect between these models, namely an impact on cardiomyocytes rather than, for example any later embryonic stage stromal loss of  $Pkn2$ . Although there is the potential for additional influences of the  $SM22\alpha$ -*Cre*  $Pkn2$  knockout model via vascular smooth muscle, this is unlikely to have any profound impact given the phenotype of the  $XMLC$ -*Cre* strain is more penetrant not less so. It is surmised that this reflects the higher efficiency of this latter promoter in cardiomyocytes [26]. These observations of developmental abnormalities in the heart are consistent with the conclusion that the failure of these  $Cre$ <sup>+/−</sup>  $Pkn2^{fl/fl}$  mice to thrive, and in particular the cardiac abnormalities in the rare survivors, reflect congenital problems. The rarity of these survivors and the legacy of the developmental defects compromise the assessment of the role of PKN2 in adults in these models and alternative strategies are required.

### Expression of PKN2 in the adult heart

$Pkn2$  is expressed in adult cardiomyocytes [12]. Although expression levels relative to total protein decline during postnatal development, this is because cardiomyocyte size increases substantially, and the relative

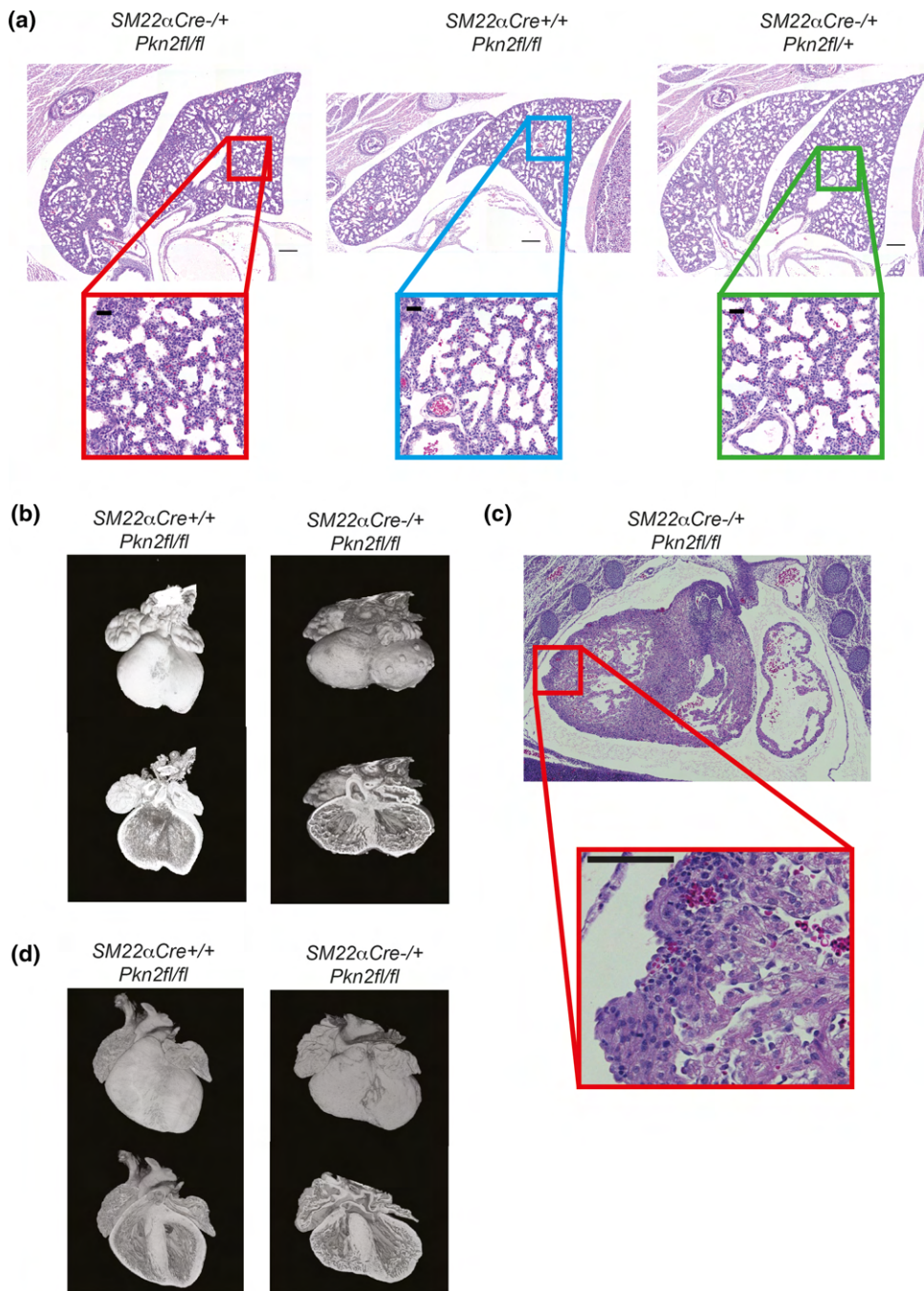


**Figure 3. The heart-specific defects in *SM22αCre+/-Pkn2fl/fl* mice.**

(a) H&E stained sections of (E18.5) lungs of littermates with the indicated genotypes. Lower boxed panels are 5 $\times$  zoomed; scale bars indicate 200  $\mu$ m in upper panels and 40  $\mu$ m in lower zoomed panels. (b) Reconstructions of E14.5 hearts imaged by HREM are shown in surface (top images) and slice (lower images) views. The genotypes are as indicated. (c) H&E stained E14.5 heart sections featuring an outer ventricular surface nodule, identified as a diverticulum. Scale bars are 100  $\mu$ m. (d) Reconstructions of E18.5 hearts imaged by HREM shown as per panel (b). Genotypes are indicated.

amount of PKN2 per cell increases in the adult (Supplementary Figure S4). To determine if variations in *PKN2* expression may be associated with human heart failure, we mined an RNASeq database of patients with dilated cardiomyopathy ( $n = 97$ ) vs normal controls ( $n = 108$ ) [27]. All PKN isoforms were detected in human hearts,

but *PKN2* expression increased in dilated cardiomyopathy (DCM) hearts relative to controls, whilst *PKN1* and *PKN3* declined (Figure 4a). To determine if *PKN2* may be involved in disease aetiology, we assessed expression in a mouse model of hypertension induced by angiotensin II (AngII; 0.8 mg/kg/d, 7 days). Expression of *PKN2*, but not *PKN1*, increased with AngII treatment relative to vehicle-treated controls (Figure 4b). This suggests that altered expression may contribute to the adaptive response to hypertension and/or may be associated with progression towards a pathological state. To assess whether altered expression might impact this response and in view of the impact of *Pkn2* knockout as described above, we focused on the effects of haploinsufficiency (global loss of a single allele, i.e. *Pkn2*Het mice). *PKN2* protein expression was reduced in hearts from male *Pkn2*Het mice relative to WT littermates (Figure 4c). There was no compensatory increase in *PKN1* expression although the relative level of phosphorylation of *PKN2* was increased. *Pkn2*Het mice thus provide a model for assessment of altered expression in the adult heart.

### The role of *PKN2* in the adult heart

We assessed the baseline dimensions and function of the hearts from *Pkn2*Het mice and WT littermates using echocardiography (Figure 4d,e; Supplementary Table S1). M-mode imaging of the short-axis view revealed that *Pkn2*Het mice had a small but significant reduction in left ventricle (LV) wall thickness compared with WT littermates. Assessment of cardiac function using speckle-tracking strain analysis confirmed that overall LV mass was significantly decreased in *Pkn2*Het mice and there was a small, albeit non-significant, increase in ejection fraction (Figure 4e; Supplementary Table S1). We conclude that there are abnormalities in surviving *Pkn2*Het mice and, although these changes appear relatively minor, they may compromise cardiac adaptation to pathophysiological stresses such as hypertension.

To determine if the hearts from *Pkn2*Het mice can adapt to hypertension, adult male *Pkn2*Het mice or WT littermates (aged 11–14 weeks) were treated with AngII or vehicle for 7 d and cardiac dimensions/function were assessed by echocardiography (Figure 4f–h; Supplementary Table S2). As in previous studies[28, 29], AngII promoted cardiac hypertrophy in WT mice, with decreased LV internal diameter and significantly increased LV wall thickness (Figure 4f,h). AngII promoted similar changes in *Pkn2*Het mice, although ventricular wall thickening appeared reduced with no significant difference relative to vehicle-treated mice (Figure 4h). Strain analysis of B-mode images confirmed that the increase in LV mass induced by AngII was attenuated in *Pkn2*Het mice (Figure 4g,h). In addition, AngII significantly increased ejection fraction and fractional shortening in WT mice, but not *Pkn2*Het mice, indicating that cardiac adaptation to hypertension in response to AngII was attenuated. Histological staining showed that AngII increased cardiomyocyte cross-sectional area in WT mice, but not in *Pkn2*Het mice (Figure 5a). AngII increased cardiac fibrosis in interstitial areas of the myocardium, particularly at the junctions between the outer LV wall and the interventricular septum, but this was similar in both WT and *Pkn2*Het mice (Figure 5b). AngII also increased fibrosis in the perivascular regions of arteries/arterioles, and this was reduced in *Pkn2*Het hearts compared with hearts from WT mice (Figure 5c). Overall, cardiac adaptation to hypertension was reduced in *Pkn2*Het mice compared with WT littermates, with both reduced cardiomyocyte hypertrophy and perivascular fibrosis.

To gain mechanistic insight into the effects of *PKN2* in the cardiac response to hypertension, we used RNASeq to assess the transcriptional differences in the AngII response of hearts from *Pkn2*Het mice compared with WT littermates (Figure 5d). No differentially expressed genes (DEGs) were identified when comparing *Pkn2*Het and WT hearts from mice treated with either vehicle or AngII. AngII-treatment resulted in 2272 DEGs in hearts from WT or *Pkn2*Het mice ( $P < 0.01$ ): 699 were identified in both genotypes, 1371 were only detected in WT hearts and 202 were only detected in *Pkn2*Het hearts (Figure 5d(i), Supplementary Tables S3–S8). Clustering the DEGs according to function highlighted significant changes in a subset of genes for the myofibrillar apparatus and cytoskeletal structures, particularly the actin cytoskeleton, but there were no overall differences between the genotypes/treatment in these gene classes as a whole (Figure 5d(ii)). In contrast, genes associated with fibrosis were significantly up-regulated by AngII (Figure 5d(iii)), particularly those associated with collagen production (Figure 5d(iv)). The response in hearts from *Pkn2*Het mice was reduced relative to WT littermates, consistent with a reduction in perivascular fibrosis seen by histology (Figure 5c). Another notable feature of the AngII response was the reduction in the expression of genes for mitochondrial proteins (Figure 5d(v)). The overall response was reduced in *Pkn2*Het mice, but the effect was more pronounced for some genes, particularly those of the tricarboxylic acid (TCA) cycle (Figure 5d(vi)). AngII cardiac hypertrophy is associated with inflammation and we detected a clear interferon response (Figure 5d(vii)) with up-regulation of the complement pathway (Figure 5d(viii)). Both of these responses were reduced in hearts from *Pkn2*Het

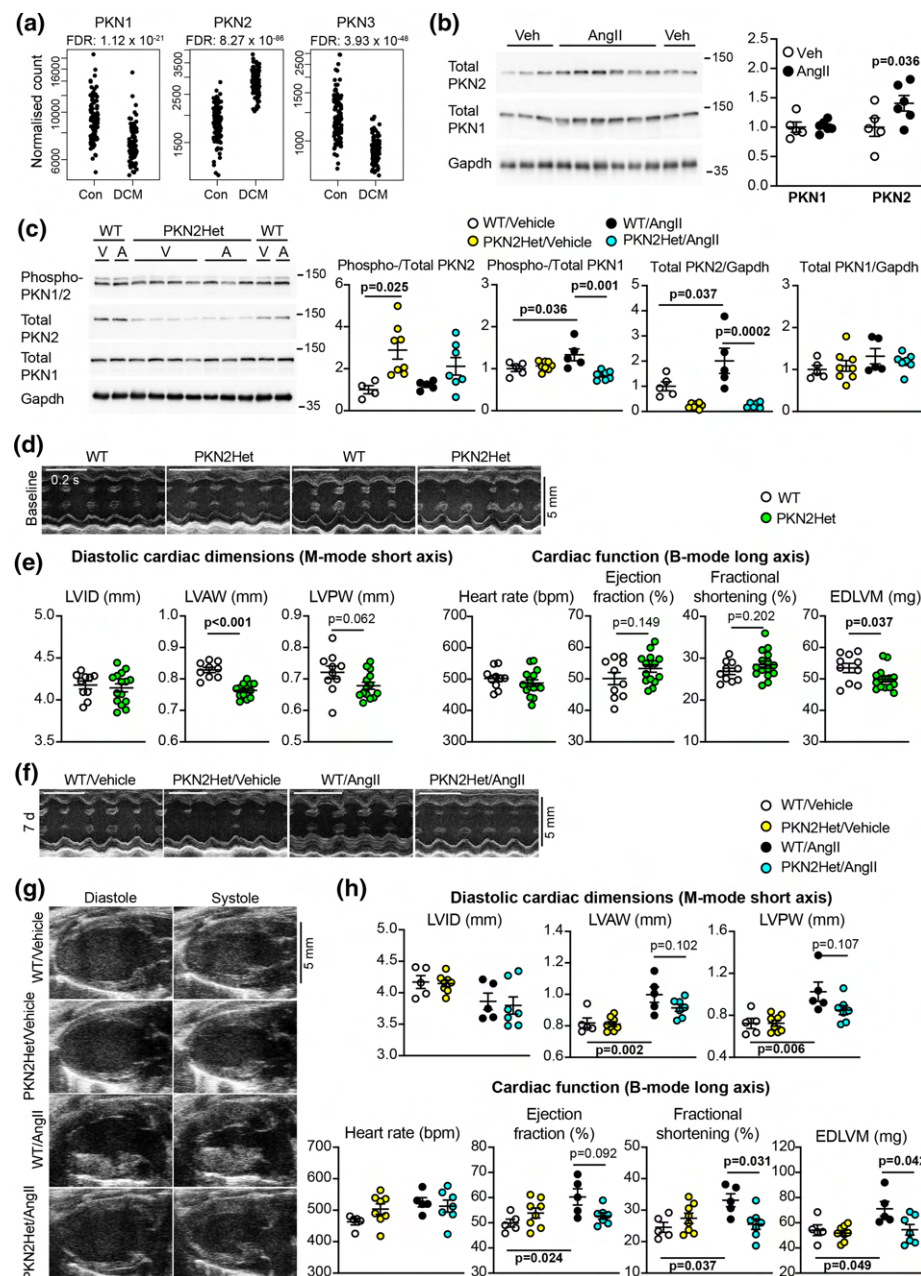


**Figure 4. PKN2 is associated with human heart failure and required for cardiac adaptation to hypertension in mice.**

(a), Expression of *PKN1*, *PKN2* and *PKN3* in human hearts. Data were mined from an RNASeq database of patients with dilated cardiomyopathy (DCM;  $n = 97$ ) and normal controls (Con;  $n = 108$ ). Data for individual samples are shown with false discovery rates (FDR). (b and c) Immunoblotting of phospho-PKN1/2, total PKN1, total PKN2 and GAPDH in hearts from wild-type (WT) or *Pkn2Het* mice treated for 7 days with vehicle (Veh, V) or 0.8 mg/kg/d angiotensin II (AngII, A). Immunoblots are shown on the left with densitometric analysis on the right (normalised to the mean of vehicle-treated controls). Individual data points are provided with means  $\pm$  SEM. Analysis used two-way ANOVA with Holm–Sidak's post-test. (d–h), Echocardiography of hearts from WT and *Pkn2Het* mice at baseline (d and e) or treated with vehicle or AngII for 7 days (f–h). Representative short-axis M-mode images used for assessment of cardiac dimensions are shown at baseline (d) and after treatment (f) (the same animals are shown). (g), Representative long-axis B-mode images used for speckle-tracking and strain analysis to assess cardiac function are shown after 7 days treatment. (e and h), Echocardiograms were analysed. Individual data points are provided with means  $\pm$  SEM. Additional data are provided in Supplementary Table S1 and histology in S2. Analysis used unpaired, two-tailed *t*-tests (e) or two-way ANOVA with Holm–Sidak's post-test (g). LV, Left ventricle; ID, internal diameter; AW, anterior wall; PW, posterior wall; EDLVM, end diastolic LV mass.

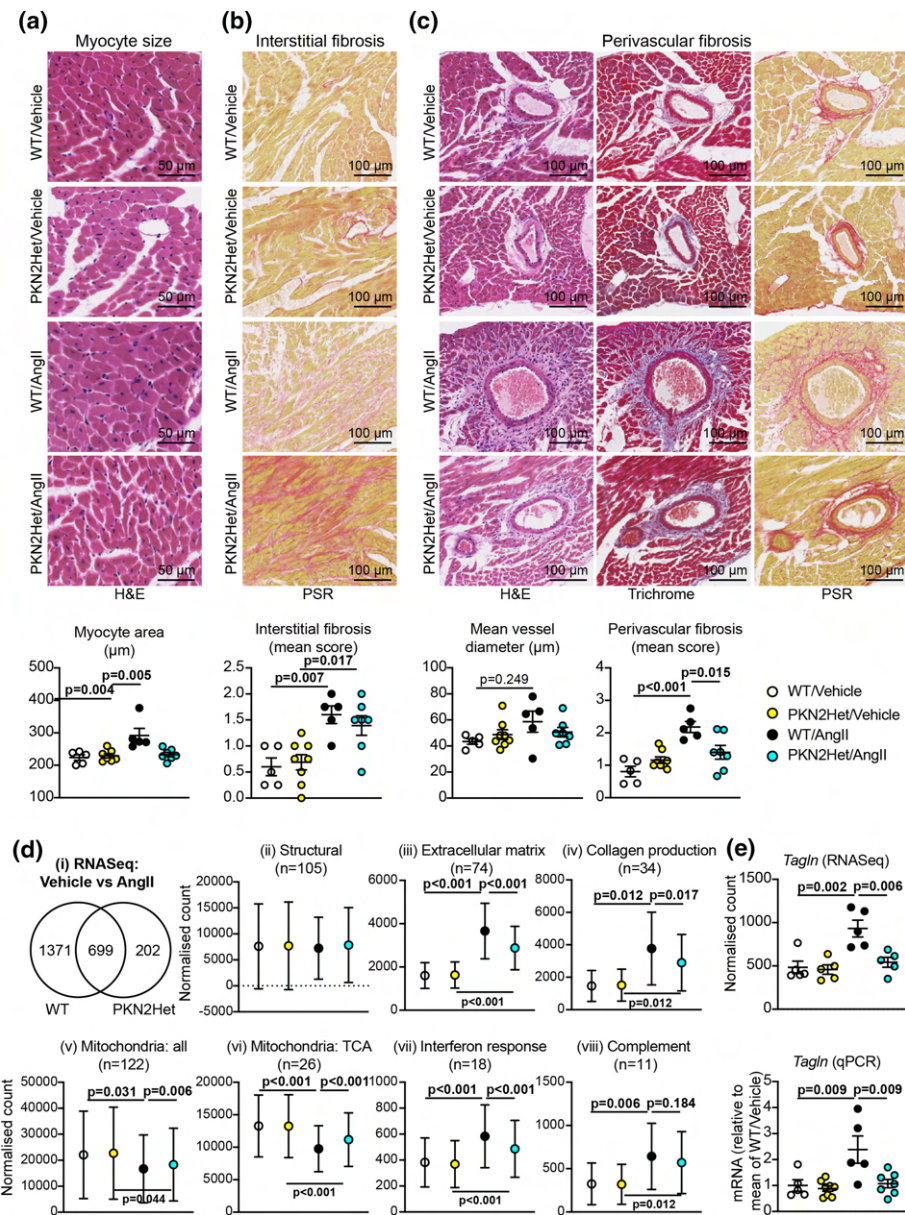


**Figure 5. *Pkn2* haploinsufficiency reduces cardiac adaptation to hypertension, affecting cardiomyocyte size, perivascular fibrosis and gene expression.**

WT or *Pkn2*Het mice were treated with vehicle or AngII (0.8 mg/kg/d) for 7 days. (a–c), Sections of WT and *Pkn2*Het mouse hearts were stained with haematoxylin and eosin (H&E), picrosirius red (PSR), or Masson's Trichrome. Representative images are shown with quantification provided below. Individual data points are provided with means ± SEM. Analysis used two-way ANOVA with Holm–Sidak's post-test. (d), RNASeq analysis of hearts from WT and *Pkn2*Het mice. (i) Summary of differentially-expressed genes ( $P < 0.01$  resulting from AngII treatment). (ii)–(viii) Clusters of DEGs according to function. Results are the mean normalised count values with 95% CI for the  $n$  values indicated. Analysis used one-way ANOVA with Holm–Sidak's post-test. (e) Comparison of *Tagln* ( $SM22\alpha$ ) mRNA expression assessed by RNASeq and qPCR. Individual data points are shown with means ± SEM. Analysis used two-way ANOVA with Holm–Sidak's post-test.

mice relative to WT littermates. Data for individual genes in each of the clusters are in Supplementary Table S9. We mined the data for classical markers of cardiac hypertrophy and detected increased expression of *Myh7*, *Nppa* and *Nppb* with AngII as expected [11], but expression was similar in *Pkn2*Het and WT mice (Supplementary Figure S5). We also detected up-regulation of *Tagln* ( $SM22\alpha$ ) by AngII in WT, but not

*Pkn2*Het mouse hearts (Figure 5e). SM22 $\alpha$  is a marker of smooth muscle cells in the adult, and this is potentially a reflection of the perivascular fibrosis induced by AngII around arteries/arterioles.

The importance of PKN2 in cardiac development and disease led us to investigate what the consequences might be with aging, comparing echocardiography data for male mice with an average age of 12 weeks with those obtained from mice with an average age of 42 weeks. As expected, hearts from the older mice had a significantly greater LV mass than the 12 week animals, but there was no difference between WT and *Pkn2*Het mice (Figure 6a). The largest diameter of the aortae (measured during cardiac systole) increased with age to some extent in both genotypes, but the distensibility of the aorta was compromised in the older mice as shown by a reduction in the ratio between the diameter measured at cardiac systole and after the aortic valve has closed when the diameter is at its narrowest (Figure 6b). This appeared to be mitigated to some degree in the *Pkn2*Het mice. Pulsed-wave Doppler was used to assess blood flow from the heart into the aorta and the pulmonary artery. We detected no differences in blood flow in either vessel in the young mice (Figure 6c–f; Supplementary Table S1). Older WT and *Pkn2*Het mice had reduced pulmonary velocity time interval (VTI), with a reduction in velocity and gradient, and the degree of change was similar (Figure 6c,d; Supplementary Table S1). In WT mice, the aortic velocity time interval (VTI), along with the mean/peak velocity and gradient were all significantly reduced in older mice compared with the young mice, but aortic VTI, velocity and gradients were relatively preserved in the older *Pkn2*Het mice (Figure 6e,f; Supplementary Table S1). This may be a consequence of greater flexibility/elasticity of the aorta in these mice compared with the WT animals (Figure 6b). This raises the possibility that some of the long survival of a minor subset of *SM22aCre*<sup>+/−</sup> *Pkn2*<sup>f/f</sup> mice may have been supported by loss of PKN2 in the aorta.

Overall, our studies of PKN2 in the adult heart indicate that it plays a significant role in cardiovascular adaptation to pathophysiological stresses, both in disease and as animals age, affecting both the contractile cardiomyocytes themselves and the major vessels.

## Discussion

This study addresses the role of PKN2 throughout development, from its importance in cardiomyocytes in the embryo, through influence on cardiac remodelling in pathological cardiac hypertrophy in the adult heart and to a potential role in aging. It shows that there can be a continuous spectrum between heart disease defined as being ‘congenital’ and what might be considered as ‘acquired’ heart disease in adults. As previously reported [16, 17], PKN2 is critical for embryonic cardiac development but our data demonstrate that PKN2 plays a crucial role in cardiomyocytes, having a particular effect on development of the compact myocardium. PKN2 also supports cardiac remodelling in response to hypertension, but has apparently little impact on the aging heart, potentially having a greater effect on the vasculature.

Previous studies using the SM22 $\alpha$  promoter in mice suggested that PKN2 is required in cardiomyocytes for embryonic cardiac development [17]. Our data, using the XMLC promoter for specific cardiomyocyte deletion of *Pkn2* reinforce this conclusion and XMLC-driven knockout of *Pkn2* was of even greater severity, with only one homozygote survivor from the XMLC-driven knockout. In both models, embryos were produced at a normal Mendelian ratio, but the ventricular walls of the hearts in E14.5–E18.5 embryos were very thin, and the integrity and contiguity of these walls was compromised, impacting on the overall architecture of the heart as it developed *in utero*. The heart is the earliest functioning organ to form in the embryo and, in mice, cardiac looping is generally completed by E9.0 with chamber development apparent by E9.5 [30–32]. Although looping may be delayed, cardiac development appears relatively normal through to E11.5 with SM22 $\alpha$ -driven *Pkn2* knockout, with no evidence of any significant effect on cardiomyocyte proliferation or global cardiac structure [17]. Here, we showed that by E14.5, there were significant effects of *Pkn2* deletion in cardiomyocytes (Figures 1 and 3): cardiac trabeculae had developed between E9.5 and E14.5, projecting into the ventricular chambers as expected, but there was a failure in formation of the compact myocardium, resulting in thin walls. Consistent with this, amongst other changes, there is a decrease in expression of the compact layer marker, *Hey2* [33] in these mutant embryos (unpublished observations). This phase of cardiac development is still poorly understood, but cardiomyocytes required for compaction develop largely from a different pool of cells from the base of the trabeculae that are less differentiated and have higher proliferative potential [30, 31]. The compaction process requires proliferation of these cells and, although the trabecular cells contribute to the compact myocardium, they also form part of the vasculature within the myocardium and the Purkinje fibre network. PKN2 can control migration and influence intercellular adhesion in other cells (e.g. fibroblasts, epithelial cells, skeletal muscle myoblasts [14, 17, 34, 35]), factors that potentially influence cardiac compaction in embryonic development.

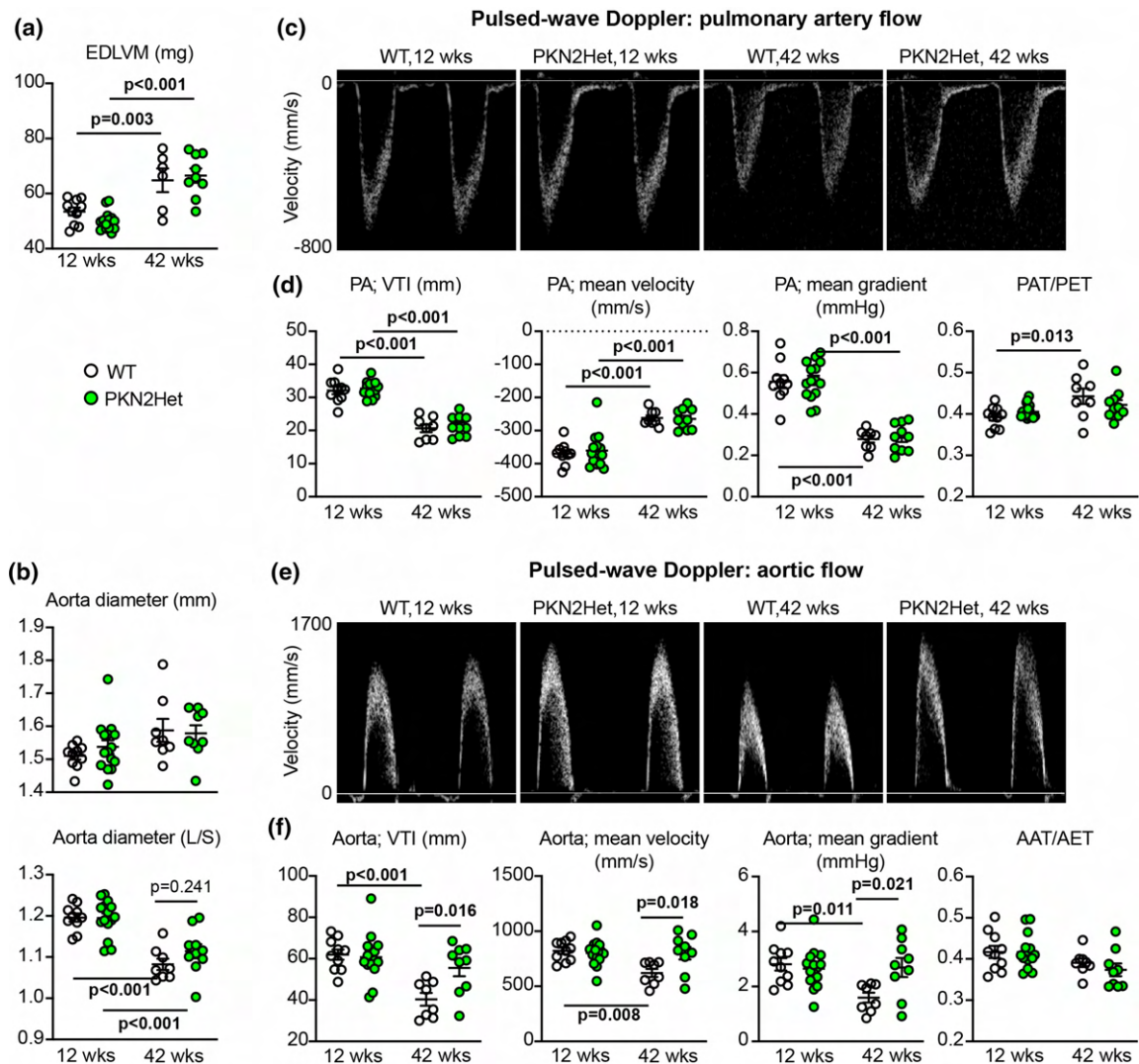


**Figure 6. Effects of aging on aortic and pulmonary blood flow in WT and *Pkn2*Het mice.**

Echocardiograms were taken for *Pkn2*Het and WT littermates with an average age of 12 or 42 weeks. (a), End diastolic left ventricular mass (EDLVM) was measured from long-axis B-mode images using speckle-tracking strain analysis. (b), The width of the aorta was measured from B-mode images from the widest diameter taken at cardiac systole (upper panel) and assessing the ratio of this to the narrowest diameter taken after the aortic valve closed (L/S). (c–f), Pulsed wave Doppler was used to assess blood flow as it leaves the heart into the pulmonary artery (c and d) and the aorta (e and f). Additional data are provided in Supplementary Table S1. Representative images are shown (c and e) and with the analysis (d and f). Individual data points are shown with means  $\pm$  SEM. Analysis used two-way ANOVA with Holm–Sidak's post-test.

Although mice with cardiomyocyte *Pkn2* knockout had normal Mendelian ratios throughout embryonic development, even with the milder *SM22 $\alpha$* -driven knockout model, only  $\sim$ 30% survived the perinatal phase. This is probably because of myocardial developmental malformations, in particular the lack of an adequate compact myocardium, compromising neonatal cardiac adaptation to an increased workload and oxidative metabolism, along with cell cycle withdrawal of cardiomyocyte and a switch from hyperplasia to maturational (hypertrophic) growth [32]. The data have clear implications for congenital heart disease both with respect to *PKN2* itself and its downstream signalling, particularly in relation to a potential role in the formation of the compact myocardium and left ventricular non-compaction. Although left ventricular hypertrabeculation or non-compaction is a recognised genetic disease, it varies in presentation and severity. Cardiomyocyte *Pkn2*

knockout appears to have the greatest similarity with the most severe form associated with fetal/neonatal disease that is often lethal by or within the first year of life and which (as for the *Pkn2* knockout mice) is often associated with structural cardiac abnormalities [36, 37].

Mice with heterozygous PKN2 deletion have no obvious abnormalities and cardiac development appears normal [17]. Moreover, we did not detect any profound differences in cardiac function/dimensions between WT and *Pkn2*Het mice into middle/old age (42 weeks). This means that PKN2 is largely dispensable once the heart has formed and is only required for cardiac remodelling in response to a severe stress such as that induced by sudden imposition of pressure-overload in the AngII experiments. We did detect a difference in aortic flow and the reduction in flow in the WT mice was largely prevented in the *Pkn2*Het mice. The meaning of this is not currently clear, but there may be some adaptation of the aorta that preserved LV function. The difference was not apparent in pulmonary flow suggesting that the effect was specific for the highly muscularised aortic wall.

Even though it may have little role in a non-stressed heart, PKN2 is important in the adult cardiac response to pathophysiological stressors since expression is increased in patients with DCM and in mouse hearts subjected to pressure-overload resulting from AngII treatment. In our hands, PKN2 haploinsufficiency compromised cardiac adaptation to AngII, with reduced LV hypertrophy and an overall reduction in the increase in the LV mass, resulting from inhibition of cardiomyocyte enlargement and fibrotic ECM. This contrasts with a recent study reporting that tamoxifen-inducible, cardiomyocyte-specific knockout of both PKN1 or PKN2 (not either gene alone) in adult mice, reduced cardiac hypertrophy in models of pressure-overload, namely thoracic aortic constriction (TAC) or AngII [25]. The most obvious difference is our use of global heterozygotes rather than cardiomyocyte-specific knockout, and inhibition of fibrosis induced by AngII in our studies may result from PKN2 haploinsufficiency in cardiac non-myocytes, causing a reduction in fibrosis that reduces cardiomyocyte workload. Alternatively, the effect may be due to PKN2 haploinsufficiency in cardiomyocytes, and the differences reflect the higher degree of stress imposed on the heart in our studies (0.8 mg/kg/d AngII) compared with Sakaguchi et al., who used 0.1 mg/kg/d, a sub- or slow pressor dose [38]. Another difference is the duration of the experiment, here the study was conducted over 7 d, whilst the study by Sakaguchi et al. was over 28 d. It is possible that the heart may adapt such that differences in function/dimensions are no longer apparent by 28 d, however, our experience is that the phenotype becomes more pronounced with prolonged duration of treatment as heart failure develops [29]. With global knockout, there are also potential systemic effects on the heart that influence cardiac adaptation to AngII. Although PKN2 does not appear to play a significant role in endothelial cells during development [17], endothelial cell specific knockout in adult mice increases blood pressure *in vivo*, potentially due to loss of phosphorylation of eNOS with consequent reduction in NO production in the peripheral vasculature. There was no evidence for this in our studies of mice with global PKN2 haploinsufficiency, with no increase in fibrosis or cardiomyocyte hypertrophy at baseline. Furthermore, we detected no difference in phosphorylation of eNOS (data not shown). A final consideration relating to all of these studies is the background strain of the mice. Our studies used mice with a C57Bl/6J background, rather than C57Bl/6N and the cardiac responses of these two strains can differ substantially (see, for example, [39]).

The PKN family of enzymes remain poorly understood. PKN1 is the most well-investigated and is implicated in protection against ischaemia/reperfusion injury in *ex vivo* models but, even for this family member, there is little information on mechanism of action. For PKN2, there is less. It may influence gene expression directly via interaction and phosphorylation of HDAC5 [40], preventing HDAC5 import into the nucleus and thus increasing chromatin remodelling or it may act via MRTF to regulate hypertrophy-associated gene expression [25]. Our RNASeq data are not consistent with this because, although AngII induced changes in gene expression as expected with increases in classic hypertrophy-associated gene expression (e.g. *Nppa*, *Myh7*, *Nppb*), there was no apparent effect of *Pkn2* haploinsufficiency. Instead, *Pkn2* haploinsufficiency had a more general effect to moderate the changes induced by AngII on collagen production, mitochondrial TCA genes, interferon response genes and genes in the complement system (it is noted that mitochondrial TCA gene expression is also down-regulated in embryonic hearts from *SM22α-Cre*<sup>+/−</sup> *Pkn2*<sup>fl/fl</sup> mice; data not shown). The net effect would be to maintain cardiac energetics, reduce inflammation and reduce fibrosis. The marked inhibition of the induction of Transgelin (*Tagln*, or *SM22α*) upon AngII treatment of *Pkn2*Het mice compared with WT littermates, suggests a potential mechanism. *SM22α* is an actin binding protein although its function is still obscure. In vascular smooth muscle cells, *SM22α* facilitates stress fibre formation and contractility [41] so, with reduced *SM22α*, the response to AngII would be damped in *Pkn2*Het mice, as observed. The mechanism for *SM22α* up-regulation may be due to hypoxia and activation of HIF2α [42].

Irrespective of the mechanism of action, this study adds to an increasing body of work indicating that the PKNs play an important role in cardiac remodelling in the adult; for PKN2, haploinsufficiency impacting the response to AngII and on early knockout (driven by *XMLC2* or *SM22 $\alpha$* ) formation of the heart during development. With further understanding of regulation, specific targets and functions, PKN signalling may offer therapeutic options for managing congenital and adult heart diseases. This undoubtedly requires further research but, since the PKNs are not redundant and have specific roles in different cells/tissues, it will be essential to develop specific tools for inhibition and manipulation of the different family members.

The ROCK inhibitor Fasudil is a known broad specificity PKN inhibitor [43], already in clinical use in Japan and China as a vasodilator [44]. More discriminating inhibitors are necessary and, although it may prove challenging to target individual PKNs by small molecule approaches [43], other approaches may be useful. For example, an siRNA against *PKN3* (Atu027) has been in clinical trials as a novel chemotherapeutic agent for solid cancers and pancreatic cancer (in combination with Gemcitabine) [45–47], and exogenous application of the auto-inhibitory PLK peptide from PKN1 has been explored also [48]. Similar approaches might work for PKN2 [49] and, as with other protein kinases, developing these inhibitory systems will not only form the basis for novel therapeutics for the future, but their use as biochemical tools to elucidate mechanisms of action can facilitate the identification of other targets in the pathway.

## Materials and methods

### Mouse strains, *in vivo* mouse imaging and experiments, and *ex vivo* imaging

*Pkn2*Het, floxed *Pkn2* and *SM22 $\alpha$ -Cre* mouse strains were maintained on a C57Black6J background, and each sourced as described in Quetier et al. [17]. The *XMLC2-Cre* mouse strain [26] was provided from within the Francis Crick Institute and was on a mixed background, subsequently in this study back-crossed onto the C57Black6J background. Most Cre mice in this study also carried the mTmG reporter allele at the Rosa26 locus, sourced as described previously [17]. Genotyping was carried out by Transnetyx using real-time PCR, with methods based upon the PCR genotyping described in Quetier et al. [17].

*In vivo* imaging of mice from *SM22 $\alpha$ -Cre* and *XMLC2-Cre* crosses was carried out at UCL-CABI (up to 2017; *SM22 $\alpha$ -Cre* only) or the Francis Crick Institute (post 2017). MRI, micro-CT and ultrasound imaging technologies were utilised. All *in vivo* mouse imaging was carried out under continuous inhalation anaesthesia using isoflurane (1.5–5%) supplied with oxygen at 1–2 L/min, and with appropriate restraint. We note 5% isoflurane was used to induce anaesthesia initially, and maintenance was typically at 1.5–2%, but some strongly phenotypic *SM22 $\alpha$ -Cre*<sup>+/−</sup> *Pkn2*<sup>f/f</sup> mice required higher levels of isoflurane for successful maintenance. Procedures typically lasted only 20 min, with exception for cine-MRI, which necessitated longer non-recovery procedures. At UCL-CABI, the micro-CT was performed on mice in the supine position in a nanoScanPET/CT scanner (Mediso, Hungray) with a 50 kVp X-ray source, with 300 ms exposure time in 720 projections with an acquisition time of 8 min. Ultrasound of young *PKN2*Het mice (at St. George's University of London) and of a subset of *SM22 $\alpha$ -Cre*<sup>+/−</sup> *Pkn2*<sup>f/f</sup> mice (at UCL-CABI) was performed using VERO2100 ultrasound machines (VisualSonics Inc., Toronto, ON, Canada) with MS400 18–38 MHz transducer mouse probes, whilst middle-aged mice were imaged using a VERO3100 with a MS-550D 25–55 MHz transducer. Mice were restrained on a heated VERO Imaging Station, and cardiac scans of the parasternal long-axis and short-axis were recorded in B mode and M mode, and flow velocity waveforms of the aorta near the aortic valve were obtained with colour Doppler and then placing the pulsed wave Doppler sample gate over the colour Doppler signals. The ultrasound used at the Francis Crick Institute was a VERO3100, but otherwise scans were performed as described above. At the Francis Crick Institute, cardiac cine-MRI was performed using a 9.4T MRI (Bruker GmbH) equipped with a four-channel receive only mouse cardiac coil and 86 mm volume transmit coil, and Paravision 6.0.1 software. Mice were set up lying prone head-first with a heat pad and breathing movement sensor pad. A series of fast low-angle shot (FLASH) scans used for localisation of the heart and to determine the short-axis. Short-axis retrospectively-gated cine-MRI (intra-gate-FLASH sequence) was performed using the following parameters: 0.8 mm slices covering the entire left and right ventricles; 128 × 128 pixels matrix and field of view of 25 × 25 mm, giving a resolution of ~195  $\mu$ m; TR = 5.5 ms, TE = 2.233 ms, 10° flip angle; 300× oversampling with 24 cine frames reconstruction.

MRI data was converted using in-house MATLAB scripts to obtain tiffs, followed by ImageJ for image analysis, following published procedures [50]. This entailed determining the area of lumen in each the LV and RV in each slice at each systole and diastole, and calculating an approximate volume for the lumens of LV and RV at each systole and diastole based on the slice thickness of 0.8 mm. Stroke volumes and the ejection fractions

were determined by comparing diastolic and systolic chamber volumes. The relative volumes of the LV and RV, and number of slices containing LV and RV enabled assessment of abnormalities of shape of the hearts, as reported in Results.

*Ex vivo* imaging of 10% buffered formalin-fixed, and subsequently PBS-soaked (24 h) whole carcasses or extracted plucks (heart and lungs) from a cohort of mice from the SM22 $\alpha$ -Cre crosses was carried out at the Francis Crick Institute by micro-CT using a SkyScan1176 CT scanner (Bruker MicroCT, Kontich, Belgium). Three-hundred and ninety-four projections were acquired over a 180° trajectory with an exposure time of 65 ms, frame averaging of 3, X-ray source voltage and current of 50 kV and 500  $\mu$ A, and a 0.5 mm Al filter. Scans were reconstructed at a 34.2  $\mu$ m isotropic resolution using nRecon software (version 1.6.10.1, Bruker MicroCT). Video 2 was generated by segmentation of heart, lungs and cardiac calcification using Analyze (version 12.0, AnalyzeDirect, Overland Park, KS, U.S.A.) using threshold based segmentation.

For *in vivo* basal and AngII-challenge studies with young mice, male *Pkn2Het* and wild-type (WT) littermates (average age 11 weeks) on a C57Bl/6J background were imported into the BioResource Facility at St. George's University of London and allowed to acclimatise for 7 d. Mice were randomly allocated to each treatment group; body weights are provided in Supplementary Table S10. Drug delivery used 1007D Alzet osmotic pumps, filled according to the manufacturer's instructions. Mice received minipumps for delivery of 0.8 mg/kg/d AngII (Merck) or vehicle (acidified PBS). Minipumps were incubated overnight in sterile PBS (37°C), then implanted subcutaneously under continuous inhalation anaesthesia using isoflurane (induction at 5%, maintenance at 2–2.5%) mixed with 2 l/min O<sub>2</sub>. A 1 cm incision was made in the mid-scapular region and mice were given 0.05 mg/kg (s.c.) buprenorphine (Ceva Animal Health Ltd.) to repress post-surgical discomfort. Minipumps were implanted portal first in a pocket created in the left flank region of the mouse. Wound closure used a simple interrupted suture with polypropylene 4-0 thread (Prolene, Ethicon). Mice were allowed to recover singly and returned to their home cage once fully recovered. Echocardiography was performed on anaesthetised mice using the VEO2100 imaging system equipped with a MS400 18–38 MHz transducer (Visualsonics). Mice were anaesthetised in an induction chamber with isoflurane (5% flow rate) with 1 l/min O<sub>2</sub> then transferred to the heated Vevo Imaging Station. Anaesthesia was maintained with 1.5% isoflurane delivered via a nose cone. Baseline scans were taken prior to experimentation (–7 to –3 days). Further scans were taken at intervals following tamoxifen treatment or minipump implantation. Imaging was completed within 20 min. Mice were recovered singly and transferred to the home cage once fully recovered.

For *in vivo* studies with middle-aged mice, male *Pkn2Het* and wild-type (WT) littermates (average age 42 weeks) were housed in the Francis Crick Institute and echocardiograms were taken with the VEO3100 imaging system (Visualsonics).

Data analysis was performed using VevoLAB software (Visualsonics) by an independent assessor blinded to any AngII intervention. Left ventricular cardiac dimensions were assessed from short axis M-mode images with the axis placed at the mid-level of the left ventricle at the level of the papillary muscles. Data were gathered from two M-mode scans at each time point, taking mean values across four cardiac cycles for each echocardiogram. The diameter of the aorta was measured with the calliper function from B-mode images at the end of cardiac systole (with the aorta at its widest) and following aortic contraction, taking an average of measurements across two cardiac cycles. Cardiac function and left ventricular mass were measured B-mode long axis images using Vevo Strain software for speckle tracking. Blood flow was assessed using pulsed-wave Doppler.

Mice were killed either by cervical dislocation followed by exsanguination, or by CO<sub>2</sub> inhalation followed by cervical dislocation. Hearts were excised quickly, washed in PBS and blotted to remove excess PBS. The apex of the heart was snap-frozen in liquid N<sub>2</sub> and the remainder fixed in 10% buffered formalin for histology.

## Ethics statement for adult mouse experiments

Animals were housed in the Biological Resource Unit (BRU) at Cancer Research UK's London Research Institute (LRI to 2016), University College London (UCL)'s Centre for Advanced Biomedical Imaging (for pilot imaging experiments) and the Biological Research Facility (BRF) at the Francis Crick Institute (from 2016 onward), or the BioResource Facility at St. George's University of London. Each site is UK registered with a Home Office certificate of designation. Studies were performed in accordance with European Parliament Directive 2010/63/EU on the protection of animals used for scientific purposes, institutional animal care committee procedures (CRUK's London Research Institute, University College London, The Francis Crick Institute, University of Reading and St. George's University of London) and the UK Animals (Scientific Procedures) Act

1986 (under Procedure Project Licences 77/8066, P166DEA98, 70/7474, 70/8248, 70/8249, 70/8709 and P8BAB0744).

### HREM, histology and assessment of myocyte size and fibrosis

Samples for high resolution episcopic microscopy (HREM) were fixed in Bouin's for a minimum of 12 h followed by extensive washing in PBS, dehydration in a graded methanol series, incubation in JB-4 (Sigma) /Eosine (Sigma)/Acridine orange (Sigma) mix overnight to ensure proper sample infiltration and then embedded in fresh mix by adding the accelerator (see [51]). Once polymerised the blocks were imaged as previously described [52, 53]; details of the process can be found at: <https://dmdd.org.uk/hrem/>. Samples were sectioned on a Leica sledge microtome at 1 or 2  $\mu$ m or on a commercial HREM (Indigo Scientific) at 0.85 or 1.7  $\mu$ m. An image of the surface of the block was then acquired under GFP excitation wavelength light using Olympus MVX10 microscope and a high resolution camera (Jenoptik). After acquisition the stacks were adjusted for gray levels using Photoshop CS6 and then processed for isotropic scaling, orthogonal resectioning, 25% downscaling, using a mixture of commercial and homemade software (see Wilson R et al. NAR 2016, Vol. 44 D855–D861). 3D volume renderings of the datasets were typically produced from the 25% downscaled stack using OsirixMD or Horos.

Histological staining and analysis were performed as previously described [28], by board certified veterinary pathologists, assessing general morphology by haematoxylin and eosin (H&E), general fibrosis by Masson's or Gomori's trichrome (as indicated in figure legends and below) and collagen deposition using picrosirius red (PSR). Images of heart sections were captured and stored digitally using a Hamamatsu slide scanner. For analysis of myocyte cross-sectional area, cells stained by H&E within the LV (excluding epicardial and endocardial regions) were outline traced using NDP.view2 software (Hamamatsu). Only cells with a single nucleus that were clearly in cross-section were included in the analysis, and all cells in a given area meeting these criteria were measured. For assessment of interstitial fibrosis, PSR-stained sections were used and the areas of the myocardium in the middle of the left ventricular free wall, plus the points of intersection between the left ventricle and the interventricular septum were scored (0, no fibrosis; 1, limited fibrosis; 2, significant fibrosis; 3, extensive fibrosis permeating the tissue) and the mean value taken for each mouse. To assess perivascular fibrosis, Masson's Trichrome images were used. All arteries/arterioles with a clearly defined elastic lamina in cross section were measured across the diameter. Vessels >20  $\mu$ m diameter were scored as for interstitial fibrosis. The mean values for each mouse were taken. Data analysis was performed by an independent assessor blinded to treatment groups.

### RNASeq, qPCR and immunoblotting of adult mouse heart samples

The apex of each of the mouse hearts was ground to powder under liquid N<sub>2</sub>. Samples (10–15 mg) were homogenised with 1 ml RNA Bee (AMS Biotechnology Ltd). RNA was prepared according to the manufacturer's instructions and dissolved in nuclease-free water. The concentration and purity were assessed from the A<sub>260</sub> and A<sub>260</sub>/A<sub>280</sub> values measured using an Implen NanoPhotometer.

The nf-core/rnaseq pipeline version 3.1 [54] was used to prepare quantified expression matrices. The pipeline takes FastQ files as input and runs quality control checks on the data, trims reads for low quality nucleotides, aligns reads and quantifies aligned data to gene models. The GRCm38 reference and Ensembl release-95 gene models were provided. The ‘-aligner star\_rsem’ option was specified to align the reads with STAR [55] and quantify expression with RSEM [56] via RSEM version 1.3.1. Raw gene-level counts were imported into R using tximport [57] and DESeq2 version 1.32.0 [58] used to test for differential expression with a FDR threshold of 1%.

Quantitative PCR (qPCR) was performed as previously described [59]. Total RNA (0.5  $\mu$ g) was reverse transcribed to cDNA using High Capacity cDNA Reverse Transcription Kits with random primers (Applied Biosystems) according to the manufacturer's instructions. qPCR was performed using an ABI Real-Time PCR 7500 system (Applied Biosystems) using optical 96-well reaction plates and iTaq Universal SYBR Green Supermix (Bio-Rad Laboratories Inc.). GAPDH was used as the reference gene for the study. Results were normalised to GAPDH, and relative quantification was obtained using the  $\Delta\Delta Ct$  (threshold cycle) method; relative expression was calculated as  $2^{-\Delta\Delta Ct}$ , and normalised to vehicle or time 0. Primers were from Eurofins Genomics; sequences are provided in Supplementary Table S11.

Samples of heart powders (10–15 mg) were extracted in 8 vol (relative to powder weight) Buffer A [20 mM Tris pH 7.5, 1 mM EDTA, 10% (v/v) glycerol, 1% (v/v) Triton X-100, 100 mM KCl, 5 mM NaF, 0.2 mM

$\text{Na}_3\text{VO}_4$ , 5 mM  $\text{MgCl}_2$ , 0.05% (v/v) 2-mercaptoethanol, 10 mM benzamidine, 0.2 mM leupeptin, 0.01 mM trans-epoxy succinyl-l-leucylamido-(4-guanidino)butane, 0.3 mM phenylmethylsulphonyl fluoride, 4  $\mu\text{M}$  microcystin]. Samples were vortexed and extracted on ice (10 min). Extracts were centrifuged (10 000 $\times g$ , 10 min, 4°C). The supernatants were removed, a sample was taken for protein assay and the remainder boiled with 0.33 vol sample buffer [0.33 M Tris-HCl pH 6.8, 10% (w/v) SDS, 13% (v/v) glycerol, 133 M dithiothreitol, 0.2 mg/ml bromophenol blue]. Protein concentrations were determined by Bio-Rad Bradford assay using bovine serum albumin (BSA) standards.

Proteins were separated by SDS-PAGE using a Bio-Rad mini-gel system with 8% (w/v) polyacrylamide resolving gels and 6% stacking gels (200 V, 90 min) for PKN1/2 (40  $\mu\text{g}$  total protein), or 12% polyacrylamide resolving gels and 6% stacking gels (200 V, 50 min) for GAPDH (5  $\mu\text{g}$  total protein). Proteins were transferred electrophoretically to nitrocellulose using a Bio-Rad semi-dry transfer cell (10 V, 60 min) and detected as previously described [59]. Bands were visualised by enhanced chemiluminescence using ECL Prime Western Blotting detection reagents and using an ImageQuant LAS4000 system (GE Healthcare). ImageQuant TL 8.1 software (GE Healthcare) was used for densitometric analysis. Raw values for phosphorylated PKN1/2 were normalised to the total kinase. Values for all samples were normalised to the mean of the controls. Primary antibodies for total PKN2 (Cat. No. 2612), phospho-PKN1/2 (Cat. No. 2611) and GAPDH (Cat. No. 2118) were from Cell Signalling Technology. Antibodies for PKN1 were from BD Transduction Laboratories (Cat. No. 610686). Phospho- and total PKN antibodies were used at 1/750 dilution; GAPDH antibodies were used at 1/1000 dilution.

## Bioinformatics analysis for transcript expression in dilated cardiomyopathy

mRNA expression of *PKN1* (ENSG00000123143), *PKN2* (ENSG00000065243) and *PKN3* (ENSG00000160447) in control and diseased human hearts was determined using a published RNASeq dataset for left ventricular samples of 97 patients with end-stage dilated cardiomyopathy taken at the time of transplantation or left ventricular assist device implantation, and 108 non-diseased controls [27]. Differential expression analysis was carried out using DESeq2 (V1.18.1, Wald test) [58].

## Data Availability

The RNA sequence data generated in this study is available through GEO at GSE206779.

## Competing Interests

The authors declare that there are no competing interests associated with the manuscript.

## Funding

J.J.T.M., T.S., B.S., A.S.-B., E.H., S.L.P., T.M. and P.J.P. were supported by the Francis Crick Institute which receives its core funding from Cancer Research UK (CRUK) (FC001130), the UK Medical Research Council (MRC) (FC001130), and the Wellcome Trust (FC001130). A.C. acknowledges support from the British Heart Foundation FS/18/33/33621 (J.J.C.) and Qassim University, Saudi Arabia (H.O.A.). D.J.S. was supported by British Heart Foundation Intermediate and Senior Basic Science Research Fellowships (FS/15/33/31608, FS/SBSRF/21/31020), the BHF Centre for Regenerative Medicine RM/17/1/33377, the MRC MR/R026416/1, and the Wellcome Trust 212937/Z/18/Z. S.T.E.C. and D.M. were supported by BHF studentship FS/19/24/34262 and the Wellcome Trust 204809/16/z.

## CRediT Author Contribution

**Peter J. Parker:** Conceptualization, Resources, Formal analysis, Supervision, Funding acquisition, Writing — original draft, Project administration, Writing — review and editing. **Jacqueline JT Marshall:** Conceptualization, Formal analysis, Investigation, Writing — original draft, Project administration, Writing — review and editing. **Joshua J. Cull:** Investigation, Writing — review and editing. **Hajed O. Alharbi:** Investigation, Writing — review and editing. **May Zaw Thin:** Investigation, Writing — review and editing. **Susanna TE Cooper:** Investigation, Writing — review and editing. **Christopher Barrington:** Formal analysis, Writing — review and editing. **Hannah Vanyai:** Investigation, Writing — review and editing. **Thomas Snoeks:** Investigation, Writing — review and editing. **Bernard Siew:** Investigation, Writing — review and editing. **Alejandro Suaarez-Bonnet:** Investigation, Writing — review and editing. **Eleanor Herbert:** Investigation, Writing — review and editing. **Daniel J. Stuckey:** Investigation, Writing — review and editing. **Angus Cameron:** Conceptualization, Supervision,

Investigation, Writing — review and editing. **Fabrice Prin:** Investigation, Writing — review and editing. **Andrew C. Cook:** Conceptualization, Writing — review and editing. **Simon L. Priestnall:** Investigation, Writing — review and editing. **Sonia Chotani:** Investigation, Writing — review and editing. **Owen JL Rackham:** Investigation, Writing — review and editing. **Daniel Meijles:** Conceptualization, Supervision, Investigation, Writing — review and editing. **Timothy Mohun:** Supervision, Investigation, Writing — review and editing. **Angela Clerk:** Conceptualization, Resources, Supervision, Investigation, Writing — original draft, Writing — review and editing.

## Abbreviations

AngII, angiotensin II; DCM, dilated cardiomyopathy; DEGs, differentially expressed genes; FDR, false discovery rates; HREM, high resolution epicardial microscopy; LV, left ventricle; PKN, protein kinase N; PSR, picrosirius red; TAC, transverse aortic constriction; TCA, tricarboxylic acid; VTI, velocity time interval.

## References

- 1 Bouma, B.J. and Mulder, B.J. (2017) Changing landscape of congenital heart disease. *Circ. Res.* **120**, 908–922 <https://doi.org/10.1161/CIRCRESAHA.116.309302>
- 2 Hoffman, J.I. and Kaplan, S. (2002) The incidence of congenital heart disease. *J. Am. Coll. Cardiol.* **39**, 1890–1900 [https://doi.org/10.1016/S0735-1097\(02\)01886-7](https://doi.org/10.1016/S0735-1097(02)01886-7)
- 3 Jankauskas, S.S., Kansakar, U., Varzideh, F., Wilson, S., Mone, P., Lombardi, A. et al. (2021) Heart failure in diabetes. *Metabolism* **125**, 154910 <https://doi.org/10.1016/j.metabol.2021.154910>
- 4 Messerli, F.H., Rimoldi, S.F. and Bangalore, S. (2017) The transition from hypertension to heart failure: contemporary update. *JACC Heart Fail.* **5**, 543–551 <https://doi.org/10.1016/j.jchf.2017.04.012>
- 5 Ponikowski, P., Anker, S.D., AlHabib, K.F., Cowie, M.R., Force, T.L., Hu, S. et al. (2014) Heart failure: preventing disease and death worldwide. *ESC Heart Fail.* **1**, 4–25 <https://doi.org/10.1002/ehf2.12005>
- 6 Savarese, G. and Lund, L.H. (2017) Global public health burden of heart failure. *Card. Fail. Rev.* **3**, 7–11 <https://doi.org/10.15420/cfr.2016;25:2>
- 7 Walli-Attaei, M., Joseph, P., Rosengren, A., Chow, C.K., Rangarajan, S., Lear, S.A. et al. (2020) Variations between women and men in risk factors, treatments, cardiovascular disease incidence, and death in 27 high-income, middle-income, and low-income countries (PURE): a prospective cohort study. *Lancet* **396**, 97–109 [https://doi.org/10.1016/S0140-6736\(20\)30543-2](https://doi.org/10.1016/S0140-6736(20)30543-2)
- 8 Wenzl, F.A., Ambrosini, S., Mohammed, S.A., Kraier, S., Luscher, T.F., Costantino, S. et al. (2021) Inflammation in metabolic cardiomyopathy. *Front. Cardiovasc. Med.* **8**, 742178 <https://doi.org/10.3389/fcvm.2021.742178>
- 9 Ahuja, P., Sdeh, P. and MacLellan, W.R. (2007) Cardiac myocyte cell cycle control in development, disease, and regeneration. *Physiol. Rev.* **87**, 521–544 <https://doi.org/10.1152/physrev.00032.2006>
- 10 Broughton, K.M. and Sussman, M.A. (2019) Adult cardiomyocyte cell cycle detour: Off-ramp to quiescent destinations. *Trends Endocrinol. Metab.* **30**, 557–567 <https://doi.org/10.1016/j.tem.2019.05.006>
- 11 Dorn, II, G.W., Robbins, J. and Sugden, P.H. (2003) Phenotyping hypertrophy: eschew obfuscation. *Circ. Res.* **92**, 1171–1175 <https://doi.org/10.1161/01.RES.0000077012.11088.BC>
- 12 Fuller, S.J., Osborne, S.A., Leonard, S.J., Hardyman, M.A., Vaniotis, G., Allen, B.G. et al. (2015) Cardiac protein kinases: the cardiomyocyte kinome and differential kinase expression in human failing hearts. *Cardiovasc. Res.* **108**, 87–98 <https://doi.org/10.1093/cvr/cvw210>
- 13 Marrocco, V., Bogomolovas, J., Ehler, E., Dos Remedios, C.G., Yu, J., Gao, C. et al. (2019) PKC and PKN in heart disease. *J. Mol. Cell. Cardiol.* **128**, 212–226 <https://doi.org/10.1016/j.yjmcc.2019.01.029>
- 14 Lachmann, S., Jevons, A., De Rycker, M., Casamassima, A., Radtke, S., Collazos, A. et al. (2011) Regulatory domain selectivity in the cell-type specific PKN-dependence of cell migration. *PLoS ONE* **6**, e21732 <https://doi.org/10.1371/journal.pone.0021732>
- 15 Palmer, R.H., Ridden, J. and Parker, P.J. (1995) Cloning and expression patterns of two members of a novel protein-kinase-C-related kinase family. *Eur. J. Biochem.* **227**, 344–351 <https://doi.org/10.1111/j.1432-1033.1995.tb20395.x>
- 16 Danno, S., Kubouchi, K., Mehruba, M., Abe, M., Natsume, R., Sakimura, K. et al. (2017) PKN2 is essential for mouse embryonic development and proliferation of mouse fibroblasts. *Genes Cells* **22**, 220–236 <https://doi.org/10.1111/gtc.12470>
- 17 Quetier, I., Marshall, J.J.T., Spencer-Dene, B., Lachmann, S., Casamassima, A., Franco, C. et al. (2016) Knockout of the PKN family of Rho effector kinases reveals a Non-redundant role for PKN2 in developmental mesoderm expansion. *Cell Rep.* **14**, 440–448 <https://doi.org/10.1016/j.celrep.2015.12.049>
- 18 Lepore, J.J., Cheng, L., Min Lu, M., Mericko, P.A., Morrisey, E.E. and Parmacek, M.S. (2005) High-efficiency somatic mutagenesis in smooth muscle cells and cardiac myocytes in SM22alpha-Cre transgenic mice. *Genesis* **41**, 179–184 <https://doi.org/10.1002/gen.20112>
- 19 Li, L., Miano, J.M., Cserjesi, P. and Olson, E.N. (1996) SM22 alpha, a marker of adult smooth muscle, is expressed in multiple myogenic lineages during embryogenesis. *Circ. Res.* **78**, 188–195 <https://doi.org/10.1161/01.RES.78.2.188>
- 20 Malhowski, A.J., Hira, H., Bashiruddin, S., Warburton, R., Goto, J., Robert, B. et al. (2011) Smooth muscle protein-22-mediated deletion of Tsc1 results in cardiac hypertrophy that is mTORC1-mediated and reversed by rapamycin. *Hum. Mol. Genet.* **20**, 1290–1305 <https://doi.org/10.1093/hmg/ddq570>
- 21 Miano, J.M., Ramanan, N., Georger, M.A., de Mesy Bentley, K.L., Emerson, R.L., Balza, Jr, R.O. et al. (2004) Restricted inactivation of serum response factor to the cardiovascular system. *Proc. Natl. Acad. Sci. U.S.A.* **101**, 17132–17137 <https://doi.org/10.1073/pnas.0406041101>
- 22 Zhang, J.C., Kim, S., Helmke, B.P., Yu, W.W., Du, K.L., Lu, M.M. et al. (2001) Analysis of SM22alpha-deficient mice reveals unanticipated insights into smooth muscle cell differentiation and function. *Mol. Cell. Biol.* **21**, 1336–1344 <https://doi.org/10.1128/MCB.2001.21.4.1336-1344.2001>
- 23 Takagi, H., Hsu, C.P., Kajimoto, K., Shao, D., Yang, Y., Maejima, Y. et al. (2010) Activation of PKN mediates survival of cardiac myocytes in the heart during ischemia/reperfusion. *Circ. Res.* **107**, 642–649 <https://doi.org/10.1161/CIRCRESAHA.110.217554>

24 Francois, A.A., Obasanjo-Blackshire, K., Clark, J.E., Boguslavskyi, A., Holt, M.R., Parker, P.J. et al. (2018) Loss of Protein Kinase Novel 1 (PKN1) is associated with mild systolic and diastolic contractile dysfunction, increased phospholamban Thr17 phosphorylation, and exacerbated ischaemia-reperfusion injury. *Cardiovasc. Res.* **114**, 138–157 <https://doi.org/10.1093/cvr/cvx206>

25 Sakaguchi, T., Takefuji, M., Wettschureck, N., Hamaguchi, T., Amano, M., Kato, K. et al. (2019) Protein kinase N promotes stress-induced cardiac dysfunction through phosphorylation of myocardin-Related transcription factor A and disruption of its interaction With actin. *Circulation* **140**, 1737–1752 <https://doi.org/10.1161/CIRCULATIONAHA.119.041019>

26 Breckenridge, R., Kotecha, S., Towers, N., Bennett, M. and Mohun, T. (2007) Pan-myocardial expression of Cre recombinase throughout mouse development. *Genesis* **45**, 135–144 <https://doi.org/10.1002/dvg.20275>

27 Heinig, M., Adriaens, M.E., Schafer, S., van Deutekom, H.W.M., Lodder, E.M., Ware, J.S. et al. (2017) Natural genetic variation of the cardiac transcriptome in non-diseased donors and patients with dilated cardiomyopathy. *Genome Biol.* **18**, 170 <https://doi.org/10.1186/s13059-017-1286-z>

28 Meijles, D.N., Cull, J.J., Markou, T., Cooper, S.T.E., Haines, Z.H.R., Fuller, S.J. et al. (2020) Redox regulation of cardiac ASK1 (Apoptosis signal-Regulating kinase 1) controls p38-MAPK (mitogen-activated protein kinase) and orchestrates cardiac remodeling to hypertension. *Hypertension* **76**, 1208–1218 <https://doi.org/10.1161/HYPERTENSIONAHA.119.14556>

29 Meijles, D.N., Cull, J.J., Cooper, S.T.E., Markou, T., Hardiman, M.A., Fuller, S.J. et al. (2021) The anti-cancer drug dabrafenib is not cardiotoxic and inhibits cardiac remodelling and fibrosis in a murine model of hypertension. *Clin. Sci. (Lond)* **135**, 1631–1647 <https://doi.org/10.1042/CS20210192>

30 Choquet, C., Kelly, R.G. and Miquerol, L. (2019) Defects in trabecular development contribute to left ventricular noncompaction. *Pediatr. Cardiol.* **40**, 1331–1338 <https://doi.org/10.1007/s00246-019-02161-9>

31 D'Amato, G., Luxan, G. and de la Pompa, J.L. (2016) Notch signalling in ventricular chamber development and cardiomyopathy. *FEBS J.* **283**, 4223–4237 <https://doi.org/10.1111/febs.13773>

32 Tan, C.M.J. and Lewandowski, A.J. (2020) The transitional heart: from early embryonic and fetal development to neonatal life. *Fetal Diagn. Ther.* **47**, 373–386 <https://doi.org/10.1159/000501906>

33 Koibuchi, N. and Chin, M.T. (2007) CHF1/Hey2 plays a pivotal role in left ventricular maturation through suppression of ectopic atrial gene expression. *Circ. Res.* **100**, 850–855 <https://doi.org/10.1161/01.RES.0000261693.13269.bf>

34 Lim, M.A., Yang, L., Zheng, Y., Wu, H., Dong, L.Q. and Liu, F. (2004) Roles of PDK-1 and PKN in regulating cell migration and cortical actin formation of PTEN-knockout cells. *Oncogene* **23**, 9348–9358 <https://doi.org/10.1038/sj.onc.1208147>

35 Zeng, R., Wang, Z., Li, X., Chen, Y., Yang, S. and Dong, J. (2020) Cyclin-dependent kinase 1-mediated phosphorylation of protein kinase N1 promotes anchorage-independent growth and migration. *Cell Signal.* **69**, 109546 <https://doi.org/10.1016/j.cellsig.2020.109546>

36 Udeoji, D.U., Philip, K.J., Morrissey, R.P., Phan, A. and Schwarz, E.R. (2013) Left ventricular noncompaction cardiomyopathy: updated review. *Ther. Adv. Cardiovasc. Dis.* **7**, 260–273 <https://doi.org/10.1177/1753944713504639>

37 Ursell, P.C. (2013) Noncompaction in the fetus and neonate: an autopsy study. *Am. J. Med. Genet. C Semin. Med. Genet.* **163C**, 169–177 <https://doi.org/10.1002/ajmg.c.31367>

38 Kawada, N., Imai, E., Karber, A., Welch, W.J. and Wilcox, C.S. (2002) A mouse model of angiotensin II slow pressor response: role of oxidative stress. *J. Am. Soc. Nephrol.* **13**, 2860–2868 <https://doi.org/10.1097/01.ASN.0000035087.11758.ED>

39 Zi, M., Stafford, N., Prehar, S., Baudoin, F., Oceandy, D., Wang, X. et al. (2019) Cardiac hypertrophy or failure?: a systematic evaluation of the transverse aortic constriction model in C57BL/6NTac and C57BL/6J substrains. *Curr. Res. Physiol.* **1**, 1–10 <https://doi.org/10.1016/j.cophys.2019.10.001>

40 Harrison, B.C., Huynh, K., Lundgaard, G.L., Helmke, S.M., Perryman, M.B. and McKinsey, T.A. (2010) Protein kinase C-related kinase targets nuclear localization signals in a subset of class I histone deacetylases. *FEBS Lett.* **584**, 1103–1110 <https://doi.org/10.1016/j.febslet.2010.02.057>

41 Xie, X.L., Nie, X., Wu, J., Zhang, F., Zhao, L.L., Lin, Y.L. et al. (2015) Smooth muscle 22 $\alpha$  facilitates angiotensin II-induced signaling and vascular contraction. *J. Mol. Med. (Berl)* **93**, 547–558 <https://doi.org/10.1007/s00109-014-1240-4>

42 Zhang, R., Shi, L., Zhou, L., Zhang, G., Wu, X., Shao, F. et al. (2014) Transgelin as a therapeutic target to prevent hypoxic pulmonary hypertension. *Am. J. Physiol. Lung Cell. Mol. Physiol.* **306**, L574–L583 <https://doi.org/10.1152/ajplung.00327.2013>

43 Falk, M.D., Liu, W., Bolanos, B., Unsal-Kacmaz, K., Klippe, A., Grant, S. et al. (2014) Enzyme kinetics and distinct modulation of the protein kinase N family of kinases by lipid activators and small molecule inhibitors. *Biosci Rep.* **34**, e00097 <https://doi.org/10.1042/BSR20140010>

44 Zhao, J., Zhou, D., Guo, J., Ren, Z., Zhou, L., Wang, S. et al. (2006) Effect of fasudil hydrochloride, a protein kinase inhibitor, on cerebral vasospasm and delayed cerebral ischemic symptoms after aneurysmal subarachnoid hemorrhage. *Neurul. Med. Chir. (Tokyo)* **46**, 421–428 <https://doi.org/10.2176/hmc.46.421>

45 Aleku, M., Schulz, P., Keil, O., Santel, A., Schaeper, U., Dieckhoff, B. et al. (2008) Atu027, a liposomal small interfering RNA formulation targeting protein kinase N3, inhibits cancer progression. *Cancer Res.* **68**, 9788–9798 <https://doi.org/10.1158/0008-5472.CAN-08-2428>

46 Santel, A., Aleku, M., Röder, N., Möpert, K., Durieux, B., Janke, O. et al. (2010) Atu027 prevents pulmonary metastasis in experimental and spontaneous mouse metastasis models. *Clin. Cancer Res.* **16**, 5469–5480 <https://doi.org/10.1158/1078-0432.CCR-10-1994>

47 Schultheis, B., Strumberg, D., Santel, A., Vank, C., Gebhardt, F., Keil, O. et al. (2014) First-in-human phase I study of the liposomal RNA interference therapeutic Atu027 in patients with advanced solid tumors. *J. Clin. Oncol.* **32**, 4141–4148 <https://doi.org/10.1200/JCO.2013.55.0376>

48 Shiga, K., Takayama, K., Futaki, S., Hutt, J.E., Cantley, L.C., Ueki, K. et al. (2009) Development of an intracellularly acting inhibitory peptide selective for PKN. *Biochem. J.* **425**, 445–453 <https://doi.org/10.1042/BJ20090380>

49 Bauer, A.F., Sonzogni, S., Meyer, L., Zeuzem, S., Piiper, A., Biondi, R.M. et al. (2012) Regulation of protein kinase C-related protein kinase 2 (PRK2) by an intermolecular PRK2-PRK2 interaction mediated by its N-terminal domain. *J. Biol. Chem.* **287**, 20590–20602 <https://doi.org/10.1074/jbc.M111.327437>

50 Stuckey, D.J., Carr, C.A., Tyler, D.J., Aasum, E. and Clarke, K. (2008) Novel MRI method to detect altered left ventricular ejection and filling patterns in rodent models of disease. *Magn. Reson. Med.* **60**, 582–587 <https://doi.org/10.1002/mrm.21677>

51 Geyer, S.H., Maurer-Gesek, B., Reissig, L.F. and Weninger, W.J. (2017) High-resolution episcopic microscopy (HREM): simple and robust protocols for processing and visualizing organic materials. *J. Vis. Exp.* **125**, 56071 <https://doi.org/10.3791/56071>

52 Mohun, T.J. and Weninger, W.J. (2012) Embedding embryos for high-resolution episcopic microscopy (HREM). *Cold Spring Harb. Protoc.* **2012**, 678–680 <https://doi.org/10.1101/pdb.prot069583>

53 Weninger, W.J., Maurer-Gesek, B., Reissig, L.F., Prin, F., Wilson, R., Galli, A. et al. (2018) Visualising the cardiovascular system of embryos of biomedical model organisms with high resolution episcopic microscopy (HREM). *J. Cardiovasc. Dev. Dis.* **5**, 58 <https://doi.org/10.3390/jcdd5040058>

54 Ewels, P.A., Peltzer, A., Fillinger, S., Patel, H., Alneberg, J., Wilm, A. et al. (2020) The nf-core framework for community-curated bioinformatics pipelines. *Nat. Biotechnol.* **38**, 276–278 <https://doi.org/10.1038/s41587-020-0439-x>

55 Dobin, A., Davis, C.A., Schlesinger, F., Drenkow, J., Zaleski, C., Jha, S. et al. (2013) STAR: ultrafast universal RNA-seq aligner. *Bioinformatics* **29**, 15–21 <https://doi.org/10.1093/bioinformatics/bts635>

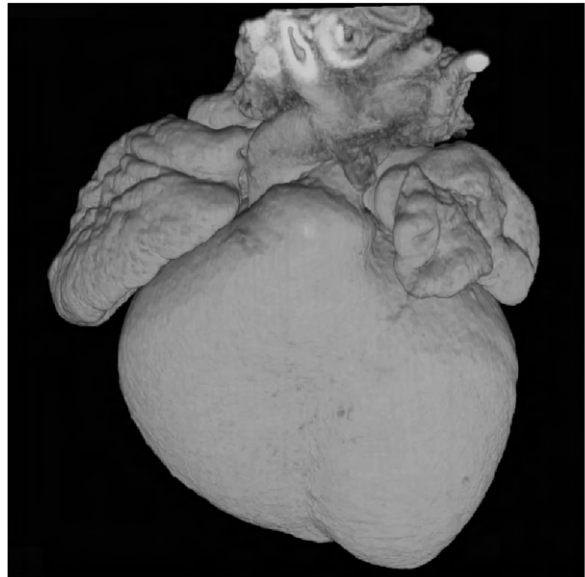
56 Li, B. and Dewey, C.N. (2011) RSEM: accurate transcript quantification from RNA-Seq data with or without a reference genome. *BMC Bioinformatics* **12**, 323 <https://doi.org/10.1186/1471-2105-12-323>

57 Soneson, C., Love, M.I. and Robinson, M.D. (2015) Differential analyses for RNA-seq: transcript-level estimates improve gene-level inferences. *F1000Res.* **4**, 1521 <https://doi.org/10.12688/f1000research.7563.1>

58 Love, M.I., Huber, W. and Anders, S. (2014) Moderated estimation of fold change and dispersion for RNA-seq data with DESeq2. *Genome Biol.* **15**, 550 <https://doi.org/10.1186/s13059-014-0550-8>

59 Marshall, A.K., Barrett, O.P.T., Cullingford, T.E., Shanmugasundram, A., Sugden, P.H. and Clerk, A. (2010) ERK1/2 signaling dominates over RhoA signaling in regulating early changes in RNA expression induced by endothelin-1 in neonatal rat cardiomyocytes. *PLoS One* **5**, e10027 <https://doi.org/10.1371/journal.pone.0010027>

XMLC2Cre<sup>+/+</sup>  
PKN2fl/+



XMLC2Cre<sup>-/-</sup>  
PKN2fl/fl

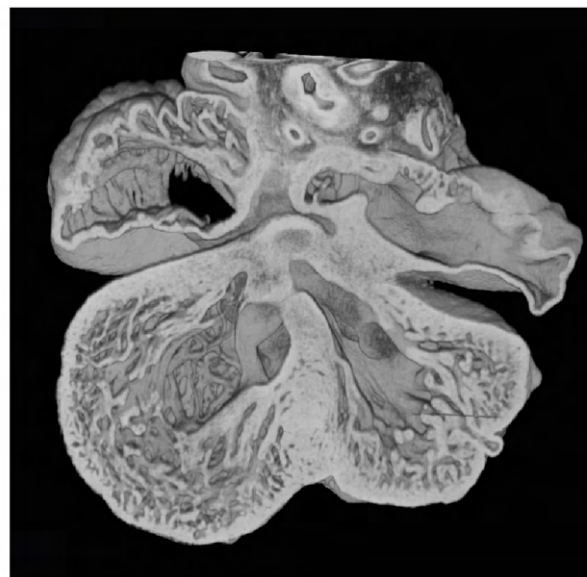
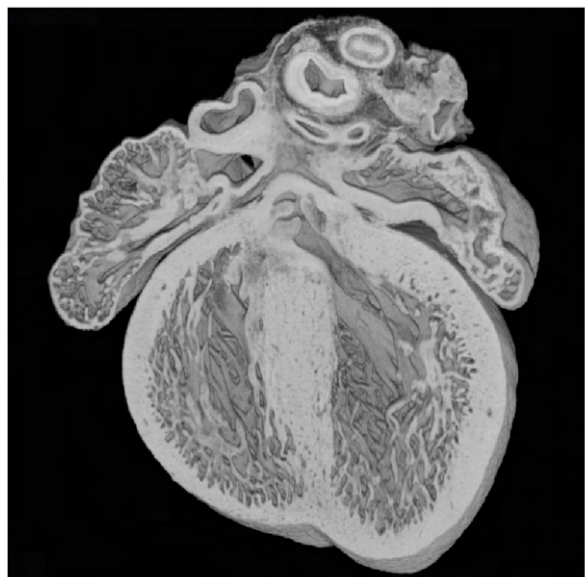
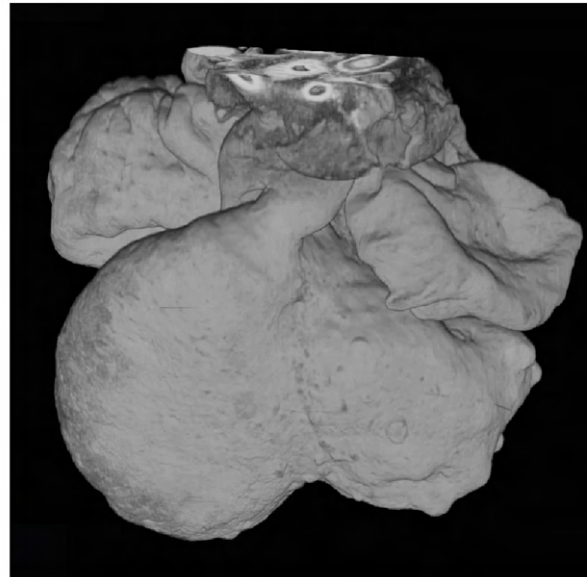


**Figure S1. HREM images of XMLC2 knockout of Pkn2**

HREM images are from a reconstruction of a 14.5d XMLC2Cre<sup>+/-</sup> *Pkn2*<sup>fl/+</sup> embryo (left) and of a XMLC2Cre<sup>+/-</sup> *Pkn2*<sup>fl/fl</sup> (right) from the same dam. The upper panels are surface images and the lower panels illustrate sections.

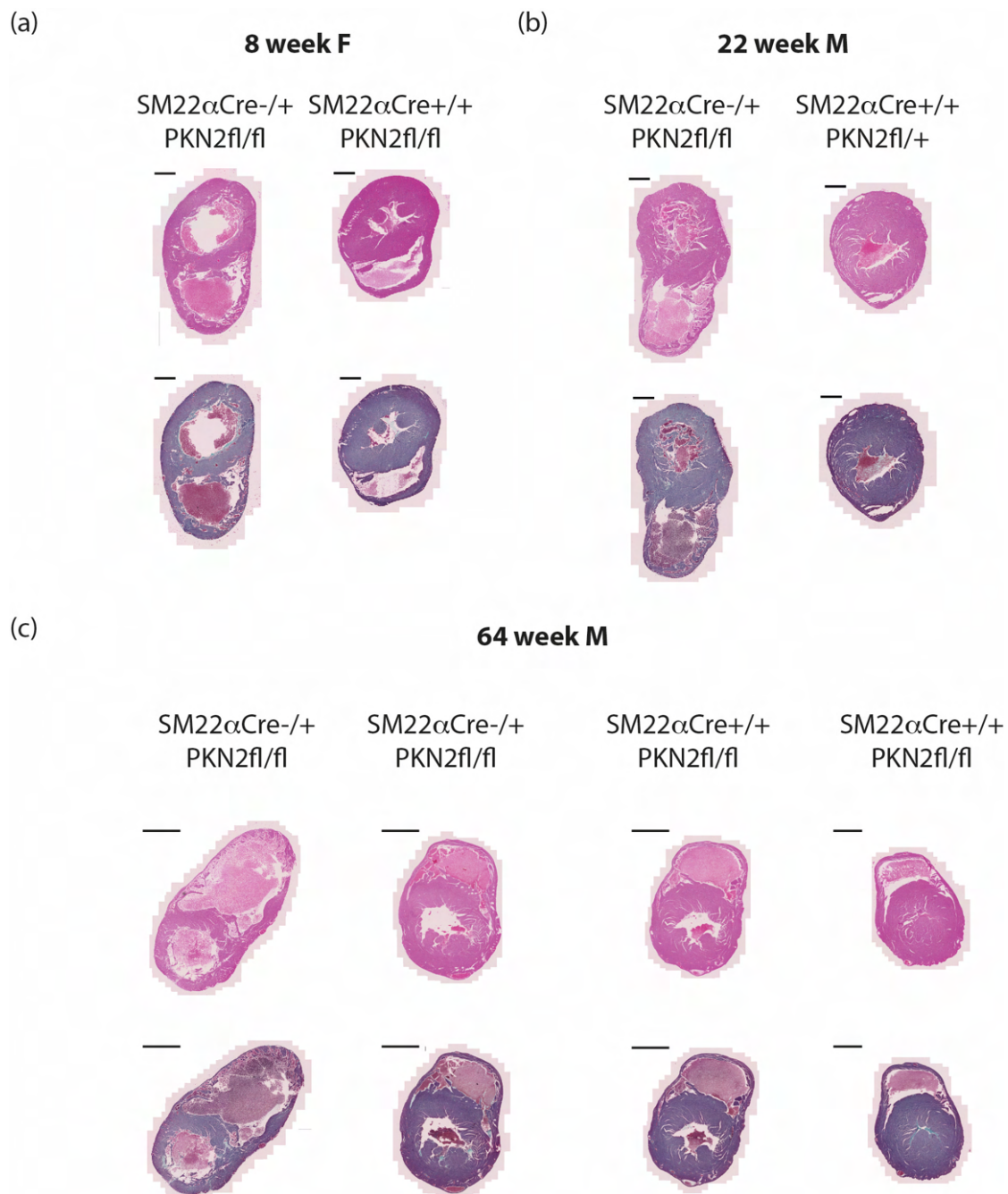


**Figure S2. Histology of sections from the SM22 $\alpha$  knockout of Pkn2 in adult hearts**

H&E (top rows) and Gomori's Trichrome (lower rows) stained sections through the short-axis of the heart, at 2-3 mm from the apex from littermates of (a) females culled at 8 weeks of age, (b) males at 22 weeks, and (c) males at 64 weeks, with genotypes as labelled. For each group, cull was triggered due to loss of condition of one littermate (left in each group). Scale bars are (a,b) 1 mm or (c) 2 mm.

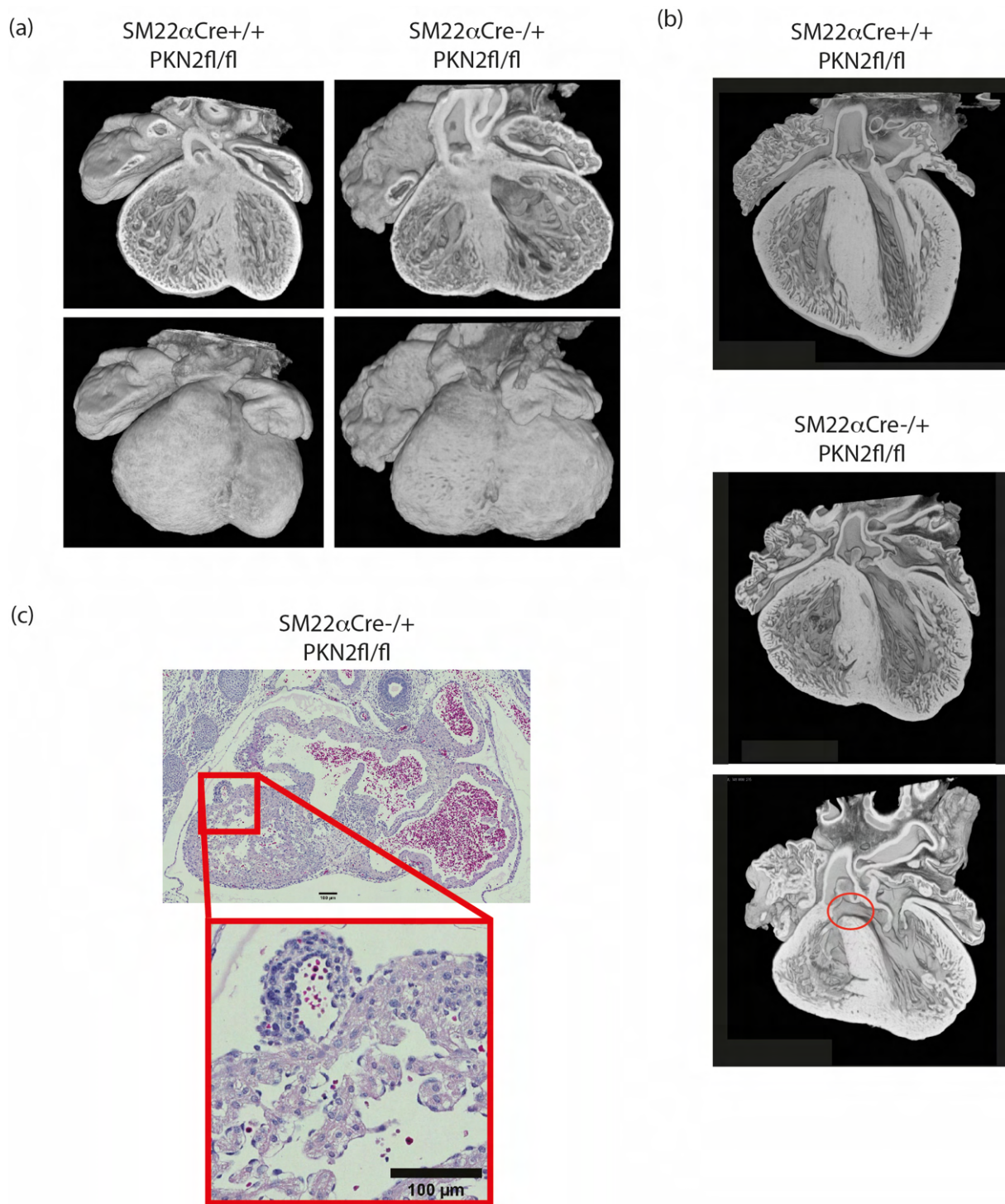


**Figure S3 Embryonic defects SM22 $\alpha$  Pkn2 mice**

HREM images are from reconstructions of embryos collected at (a) E14.5 and (b) E18.5 days gestation. Genotypes are as indicated. (c) H&E stained section of a SM22 $\alpha$ Cre $^{+/+}$  Pkn2fl/fl E14.5 heart with 100  $\mu$ m scale, as labelled.

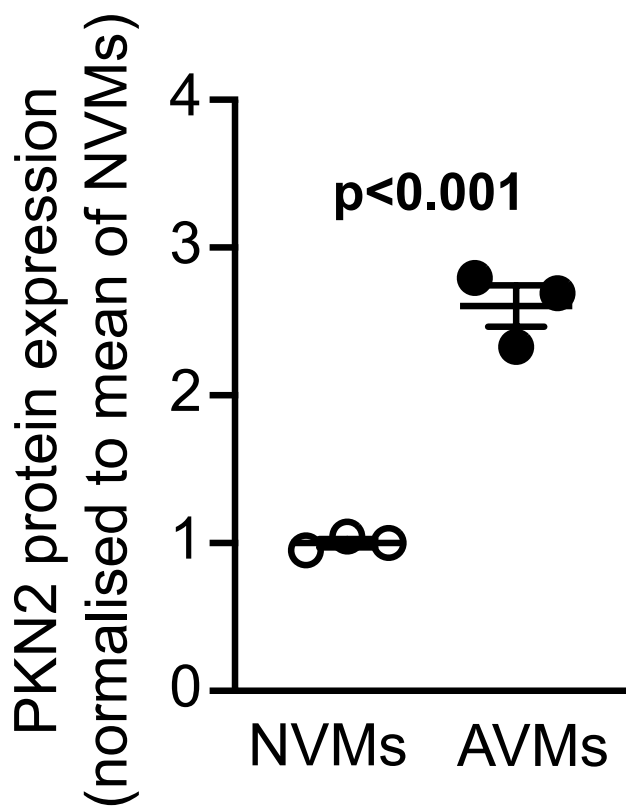


**Figure S4. Expression of PKN2 in neonatal rat ventricular myocytes (NVMs) compared with adult rat ventricular myocytes (AVMs) relative to cell size.** Expression data were from Fuller SJ et al. (Cardiovasc Res. 2015; 108: 87-98) adjusted for cell size according to membrane capacitance which increases from 13 pF in 1- to 2-day NVMs to 156 pF in AVMs [60, 61].

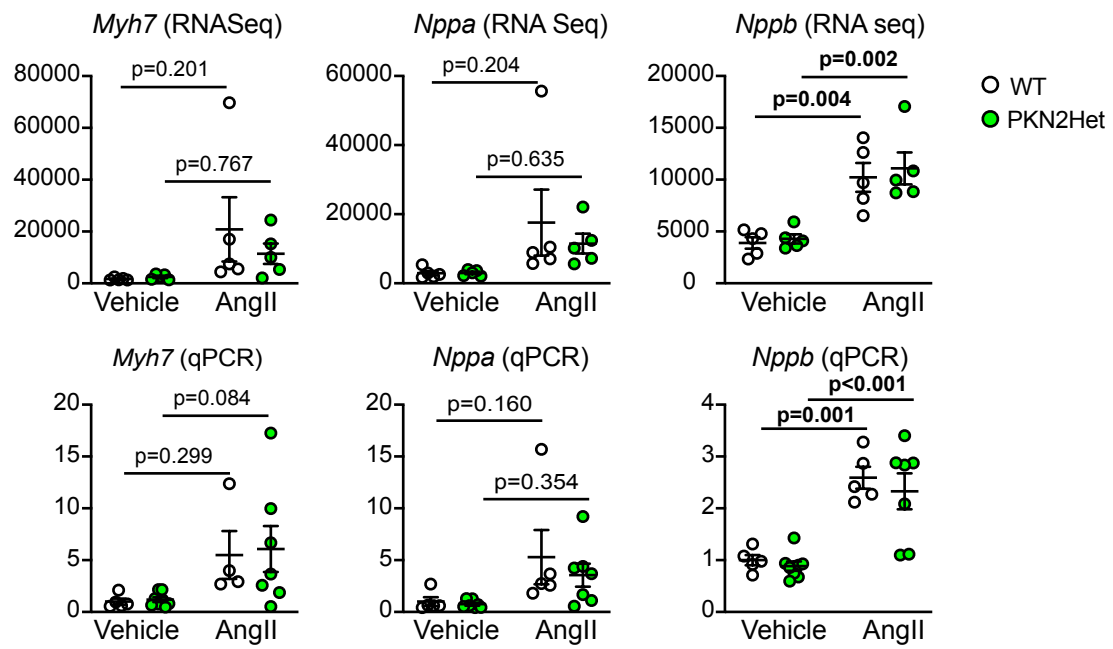


**Figure S5. Expression of hypertrophy associated genes in hearts from WT or Pkn2Het mice.** WT (white) or Pkn2Het (green) mice were treated with vehicle (left side of each graph) or AngII (0.8 mg/kg/d; right side of each graph) for 7 d. RNA was prepared and used for RNASeq (upper panels) or qPCR (lower panels). Individual data points are shown with means  $\pm$  SEM. Analysis used 2-way ANOVA with Holm-Sidak's post-test.

**Supplementary Table S1. Echocardiography data for 12 and 42 week male mice with heterozygous PKN2 gene deletion (PKN2Het) and wild-type (WT) mice: baseline data.** AAT, aortic acceleration time; AET, Aortic expulsion time; VTI, velocity time interval; PAT, pulmonary acceleration time; PET, pulmonary expulsion time; PA, pulmonary artery; LV, left ventricle; ID, internal diameter; AW, anterior wall; PW, posterior wall.

	WT: 12 wk (n=10)		PKN2Het: 12 wk (n=15)		WT: 42 wk (n=8)		PKN2Het: 42 wk (n=10)	
	Mean	SEM	Mean	SEM	Mean	SEM	Mean	SEM
<b>Aortic flow (Pulsed Wave Doppler)</b>								
AAT (ms)	23.80	0.82	23.59	0.72	18.98	0.72	20.03	1.08
AET (ms)	57.21	0.68	56.55	0.68	48.54	1.13	53.56	1.77
AAT/AET	0.42	0.01	0.42	0.01	0.39	0.01	0.37	0.01
Aorta VTI (mm)	61.95	2.47	60.71	2.86	40.31	3.09	55.47	3.77
Aorta Mean Velocity (mm/s)	821.32	29.33	800.96	29.24	620.71	36.58	800.88	54.81
Aorta Mean Gradient (mmHg)	2.81	0.23	2.65	0.19	1.59	0.18	2.69	0.33
Aorta Peak Velocity (mm/s)	1632.92	58.53	1592.77	53.01	1271.29	82.00	1620.63	104.77
Aorta Peak Grad (mmHg)	11.08	0.93	10.46	0.65	6.69	0.83	10.94	1.32
Aorta Peak Pressure (mmHg)	10.85	0.86	10.31	0.65	6.64	0.82	10.81	1.31
<b>Pulmonary flow (Pulsed Wave Doppler)</b>								
PAT (ms)	23.71	0.53	24.90	0.37	24.97	0.98	24.71	0.72
PET (ms)	60.47	0.92	61.43	0.65	56.74	2.15	58.94	2.42
PAT/PET	0.39	0.01	0.41	0.00	0.44	0.02	0.42	0.01
PA VTI	32.11	1.12	32.70	0.58	20.66	1.20	21.44	0.97
PA Mean Velocity (mm/s)	-369.58	10.38	-360.73	12.93	-262.10	8.32	-264.84	9.79
PA Mean Gradient (mmHg)	0.56	0.03	0.56	0.02	0.28	0.02	0.29	0.02
PA Peak Velocity (mm/s)	-764.05	17.63	-740.28	23.98	-551.01	13.94	-558.99	25.85
PA Peak Grad (mmHg)	2.37	0.11	2.36	0.08	1.22	0.06	1.28	0.12
<b>Aorta diameter (B-Mode)</b>								
Widest (mm)	1.51	0.01	1.54	0.02	1.59	0.03	1.60	0.03
Narrowest (mm)	1.28	0.02	1.29	0.02	1.47	0.04	1.44	0.04
Wide/narrow	1.20	0.01	1.19	0.01	1.08	0.01	1.11	0.02
<b>Left ventricle dimensions (short axis M-mode)</b>								
Heart Rate (bpm)	522.13	11.06	508.26	11.26	473.62	17.63	448.95	18.55
LVID;s (mm)	2.97	0.05	2.92	0.05	2.59	0.07	2.71	0.05
LVID;d (mm)	4.18	0.05	4.14	0.05	3.80	0.06	3.95	0.04
LVAW;s (mm)	1.11	0.02	1.05	0.01	1.10	0.04	1.07	0.03
LVAW;d (mm)	0.84	0.02	0.77	0.01	0.84	0.02	0.81	0.02
LVPW;s (mm)	1.03	0.03	1.01	0.02	1.16	0.03	1.11	0.05
LVPW;d (mm)	0.72	0.02	0.69	0.01	0.78	0.04	0.77	0.02
<b>Cardiac function (speckle-tracking strain analysis; long axis B-mode)</b>								
Heart rate (bpm)	502.23	10.29	487.39	10.63	459.97	22.21	460.58	22.49
Stroke volume (µl)	25.51	1.35	26.23	0.76	24.18	2.71	24.17	2.51
Fractional shortening (%)	26.85	0.76	28.45	0.85	28.04	1.43	29.33	2.73
Ejection fraction (%)	50.11	1.93	53.31	1.20	53.38	2.76	54.07	2.95
Cardiac output (ml/min)	12.76	0.59	12.79	0.49	10.94	1.10	11.01	1.04
End diastolic LV mass	53.48	1.45	49.95	0.88	64.83	4.30	66.52	2.59
End systolic LV mass	56.46	1.57	52.34	0.75	66.08	4.28	67.84	2.70

**Supplementary Table S2. Echocardiography data for 12 week male mice with heterozygous PKN2 gene deletion (PKN2Het) and wild-type (WT) mice treated for 7 d with 0.8 mg/kg/d angiotensin 2 or vehicle.** AAT, aortic acceleration time; AET, Aortic expulsion time; VTI, velocity time interval; PAT, pulmonary acceleration time; PET, pulmonary expulsion time; PA, pulmonary artery; LV, left ventricle; ID, internal diameter; AW, anterior wall; PW, posterior wall.

	WT: vehicle (n=5)		PKN2Het: vehicle (n=8)		WT: AngII (n=5)		PKN2Het: AngII (n=7)	
	Mean	SEM	Mean	SEM	Mean	SEM	Mean	SEM
<b>Aortic flow (Pulsed Wave Doppler)</b>								
AAT (ms)	23.50	1.19	22.76	0.86	24.42	1.23	22.53	1.44
AET (ms)	57.71	1.57	55.21	1.39	56.29	1.65	54.49	1.23
AAT/AET	0.41	0.03	0.41	0.01	0.43	0.02	0.41	0.02
Aorta VTI (mm)	61.67	5.44	58.84	4.05	58.82	3.16	61.60	5.13
Aorta Mean Velocity (mm/s)	780.00	63.10	819.21	59.70	811.40	45.61	864.12	57.41
Aorta Mean Gradient (mmHg)	2.53	0.41	2.80	0.37	2.68	0.30	3.08	0.42
Aorta Peak Velocity (mm/s)	1583.20	128.93	1607.53	109.14	1498.86	29.58	1689.25	81.15
Aorta Peak Grad (mmHg)	10.32	1.68	10.71	1.32	9.01	0.35	11.60	1.08
Aorta Peak Pressure (mmHg)	10.20	1.68	10.61	1.30	8.91	0.35	11.50	1.09
<b>Pulmonary flow (Pulsed Wave Doppler)</b>								
PAT (ms)	26.13	1.02	25.44	1.09	24.54	0.58	22.71	1.25
PET (ms)	62.38	1.29	63.13	1.47	58.68	2.93	56.67	1.72
PAT/PET	0.42	0.01	0.40	0.01	0.42	0.02	0.40	0.02
PA VTI	31.66	1.74	31.73	1.05	28.44	2.24	25.39	1.39
PA Mean Velocity (mm/s)	-362.61	16.48	-363.12	13.26	-333.86	18.50	-310.38	10.82
PA Mean Gradient (mmHg)	0.53	0.05	0.53	0.04	0.45	0.05	0.39	0.03
PA Peak Velocity (mm/s)	-755.55	28.94	-744.09	26.15	-704.73	33.94	-682.22	25.60
PA Peak Grad (mmHg)	2.30	0.18	2.24	0.16	2.01	0.20	1.88	0.14
<b>Aorta diameter (B-Mode)</b>								
Widest (mm)	1.51	0.02	1.51	0.01	1.63	0.06	1.69	0.08
Narrowest (mm)	1.21	0.02	1.27	0.03	1.44	0.09	1.56	0.09
Wide/narrow	1.24	0.02	1.19	0.03	1.14	0.04	1.09	0.01
<b>Left ventricle dimensions (short axis M-mode)</b>								
Heart Rate (bpm)	501.28	13.71	506.12	12.71	528.57	15.67	521.25	17.10
LVID;s (mm)	2.96	0.11	3.01	0.07	2.59	0.08	2.68	0.11
LVID;d (mm)	4.17	0.10	4.15	0.05	3.86	0.13	3.80	0.14
LVAW;s (mm)	1.08	0.04	1.07	0.01	1.29	0.06	1.15	0.02
LVAW;d (mm)	0.82	0.03	0.81	0.02	1.00	0.05	0.91	0.02
LVPW;s (mm)	1.03	0.06	1.02	0.03	1.31	0.07	1.18	0.02
LVPW;d (mm)	0.72	0.05	0.72	0.03	1.02	0.09	0.85	0.04
<b>Cardiac function (speckle-tracking strain analysis; long axis B-mode)</b>								
Heart rate (bpm)	462.84	9.65	503.48	16.63	525.26	14.72	512.86	19.44
Stroke volume (µl)	28.52	2.63	28.07	1.03	27.49	3.19	21.12	2.08
Fractional shortening (%)	24.54	1.58	27.42	1.62	33.15	2.06	25.56	1.69
Ejection fraction (%)	49.85	1.59	53.86	1.99	60.29	3.22	52.70	1.28
Cardiac output (ml/min)	13.21	1.31	14.22	0.90	14.41	1.70	10.68	0.90
End diastolic LV mass	54.15	4.23	51.75	2.14	71.11	5.80	54.44	4.21
End systolic LV mass	57.33	5.02	56.87	2.64	76.33	5.51	57.72	4.56

**Supplementary Table S3.** RNASeq analysis of effects of angiotensin II (AngII) on mRNA expression in hearts from PKN2Het vs WT littermates: mRNAs significantly upregulated by AngII in PKN2Het or WT hearts.

Gene Symbol	Ensembl gene id	WT Vehicle		WT AngII		PKN2Het Vehicle		PKN2Het AngII	
		Mean	SD	Mean	SD	Mean	SD	Mean	SD
Sept5	ENSMUSG00000072214	83	20	175	64	94	15	166	50
Sept9	ENSMUSG00000059248	865	99	1148	72	882	89	1148	182
Sept11	ENSMUSG00000058013	781	129	1170	161	705	99	998	196
1500009L16Rik	ENSMUSG00000087651	50	8	89	32	43	11	85	10
1700120C14Rik	ENSMUSG00000100599	84	4	153	41	76	23	122	23
2010111I01Rik	ENSMUSG00000021458	946	73	1185	106	902	74	1185	115
Abcg1	ENSMUSG00000024030	121	26	192	24	107	25	163	40
Acan	ENSMUSG00000030607	4	3	66	49	3	1	32	34
Ace	ENSMUSG00000020681	1467	152	2473	345	1594	190	2408	305
Acta1	ENSMUSG00000031972	6773	1395	24772	10833	8570	3863	28601	14894
Actn1	ENSMUSG00000015143	522	79	925	273	524	61	761	132
Actr3	ENSMUSG00000026341	2536	120	3001	264	2399	43	2908	199
Adam12	ENSMUSG00000054555	55	9	167	53	41	13	115	49
Adam15	ENSMUSG00000028041	1010	154	1434	80	997	96	1364	151
Adams12	ENSMUSG00000047497	91	12	261	100	100	8	204	80
Adams2	ENSMUSG00000036545	499	49	1369	604	526	39	1080	305
Adams8	ENSMUSG00000031994	16	4	76	21	15	2	57	28
Adamsl2	ENSMUSG00000036040	230	49	554	141	251	43	511	150
Adcy7	ENSMUSG00000031659	355	49	714	204	342	76	589	111
Adgre1	ENSMUSG00000004730	375	73	763	304	349	35	608	121
AI506816	ENSMUSG00000105987	463	36	655	41	454	52	676	86
Aif1	ENSMUSG00000024397	63	12	133	73	51	11	95	13
Aldh1a2	ENSMUSG00000013584	143	34	307	88	145	27	322	123
Ankrd1	ENSMUSG00000024803	20150	6483	57246	17002	19310	6244	49450	10874
Ankrd23	ENSMUSG00000067653	8223	1670	13521	3447	9104	579	14731	4085
Anln	ENSMUSG00000036777	56	22	225	55	56	7	174	50
Anxa1	ENSMUSG00000024659	596	70	1111	254	555	84	919	152
Anxa2	ENSMUSG00000032231	1328	74	2290	204	1236	149	1957	280
Anxa5	ENSMUSG00000027712	1991	157	2628	137	1995	184	2495	432
Apbb1ip	ENSMUSG00000026786	129	14	240	62	146	18	205	16
Apod	ENSMUSG00000022548	115	26	229	22	122	16	198	30
Apoe	ENSMUSG00000002985	3788	666	6913	2610	4103	455	5864	858
Arhgap1	ENSMUSG00000027247	496	38	622	41	520	32	610	36
Arhgap11a	ENSMUSG00000041219	76	15	183	32	69	9	158	44
Arhgap30	ENSMUSG00000048865	154	24	265	55	147	24	206	37
Arhgdib	ENSMUSG00000030220	506	27	664	56	483	58	627	60
Arhgef40	ENSMUSG0000004562	530	50	747	111	504	59	674	68
Arid5a	ENSMUSG00000037447	177	60	315	53	146	28	315	68
Arl4c	ENSMUSG00000049866	257	44	447	45	299	36	401	52
Arl6ip1	ENSMUSG00000030654	555	29	783	95	531	41	675	58
Arpc1b	ENSMUSG00000029622	814	81	1186	179	737	113	1071	150
Arpc3	ENSMUSG00000029465	1134	39	1490	168	1115	115	1392	88
Arpc5	ENSMUSG00000008475	864	45	1233	156	871	66	1121	40
Asap2	ENSMUSG00000052632	656	118	829	131	621	58	818	121
Aspm	ENSMUSG00000033952	46	20	147	29	43	10	129	39
Atad2	ENSMUSG00000022360	124	14	243	23	132	24	212	55
Atf4	ENSMUSG00000042406	1171	85	1374	69	1169	114	1319	150
Atp10a	ENSMUSG00000025324	58	4	114	20	63	11	98	18
Atp8a2	ENSMUSG00000021983	247	26	365	72	234	36	355	74
Atp8b1	ENSMUSG00000039529	239	30	380	49	213	28	351	75
Aurka	ENSMUSG00000027496	18	5	51	16	19	6	46	15
Aurkb	ENSMUSG00000020897	18	6	47	18	16	5	39	13
Axl	ENSMUSG0000002602	1982	499	2556	293	1813	317	2326	298
B3galnt1	ENSMUSG00000043300	50	8	82	21	50	8	80	7
Basp1	ENSMUSG00000045763	41	7	103	33	42	3	76	15
BC028528	ENSMUSG00000038543	144	14	227	38	130	24	206	24
Bgn	ENSMUSG00000031375	5175	520	12514	5386	5152	464	9491	2127
Birc5	ENSMUSG00000017716	20	10	66	13	18	6	66	24
Bmp1	ENSMUSG00000022098	505	77	897	297	496	46	796	219

Bub1	ENSMUSG00000027379	12	2	48	14	16	9	44	19
Bub1b	ENSMUSG00000040084	41	19	125	41	51	17	103	38
C1qa	ENSMUSG00000036887	895	96	1523	250	883	97	1362	183
C1qb	ENSMUSG00000036905	826	111	1513	429	782	128	1330	245
C1qc	ENSMUSG00000036896	886	106	1454	199	845	131	1290	171
C1qtnf6	ENSMUSG00000022440	122	21	426	250	120	11	348	107
C4b	ENSMUSG00000073418	231	28	604	141	295	41	861	703
Cald1	ENSMUSG00000029761	1649	323	2616	191	1624	256	2205	422
Cap1	ENSMUSG00000028656	1199	155	1633	55	1115	167	1503	127
Capg	ENSMUSG00000056737	183	29	364	36	182	36	328	70
Capzal1	ENSMUSG00000070372	1251	78	1608	138	1166	148	1428	124
Carhsp1	ENSMUSG00000008393	592	69	889	70	517	68	796	96
Casp4	ENSMUSG00000033538	79	11	119	19	74	18	113	27
Casp8	ENSMUSG00000026029	191	12	303	44	192	23	274	37
Cavin3	ENSMUSG00000037060	300	26	506	43	295	23	430	88
Ccdc80	ENSMUSG00000022665	1816	295	3479	1261	1843	168	2847	551
Ccl8	ENSMUSG00000009185	11	7	75	31	17	9	73	59
Ccna2	ENSMUSG00000027715	65	39	245	89	48	9	184	81
Ccnb1	ENSMUSG00000041431	24	11	73	20	14	4	71	30
Ccnb2	ENSMUSG00000032218	27	10	82	39	18	5	72	21
Cd109	ENSMUSG00000046186	101	22	257	86	92	18	181	52
Cd14	ENSMUSG00000051439	89	13	165	34	94	6	143	26
Cd248	ENSMUSG00000056481	285	55	497	49	278	22	431	86
Cd300c2	ENSMUSG00000044811	33	5	109	72	32	8	66	20
Cd300ld	ENSMUSG00000034641	151	30	245	51	133	23	238	49
Cd34	ENSMUSG00000016494	3352	231	5107	337	3106	396	4820	637
Cd44	ENSMUSG00000005087	292	53	505	44	273	42	409	82
Cd48	ENSMUSG00000015355	78	10	145	48	67	12	120	19
Cd68	ENSMUSG00000018774	205	25	321	48	181	27	308	61
Cd72	ENSMUSG00000028459	30	9	159	128	27	7	92	56
Cd84	ENSMUSG00000038147	88	19	178	51	80	9	164	32
Cd9	ENSMUSG00000030342	590	47	756	24	581	71	670	65
Cd93	ENSMUSG00000027435	3708	657	5435	821	3856	571	5157	633
Cdc20	ENSMUSG00000006398	28	11	91	19	23	7	80	21
Cdca3	ENSMUSG00000023505	16	5	56	20	12	5	59	28
Cdca5	ENSMUSG00000024791	5	2	21	8	5	3	21	10
Cdca8	ENSMUSG00000028873	14	3	49	5	13	6	38	18
Cdk1	ENSMUSG00000019942	33	11	194	49	35	17	130	47
Cdkn1a	ENSMUSG00000023067	351	153	609	89	367	175	544	152
Cenpe	ENSMUSG00000045328	62	41	172	56	38	21	116	38
Cep55	ENSMUSG00000024989	17	5	63	15	12	2	58	27
Cfb	ENSMUSG00000090231	36	7	140	61	33	15	114	78
Cfl1	ENSMUSG00000056201	2052	87	2670	304	1872	236	2490	204
Ch25h	ENSMUSG00000050370	11	6	32	14	13	5	34	17
Chd9	ENSMUSG00000056608	1089	68	1541	297	1030	53	1413	164
Cilp	ENSMUSG00000042254	294	76	3092	3273	401	134	2249	1515
Ckap2	ENSMUSG00000037725	33	16	131	46	25	5	95	45
Ckap2l	ENSMUSG00000048327	30	10	123	39	25	8	110	29
Ckap4	ENSMUSG00000046841	756	159	1094	75	815	103	1104	165
Cks2	ENSMUSG00000062248	13	1	50	13	9	2	35	11
Clec4d	ENSMUSG00000030144	9	3	26	14	4	2	18	9
Clec4n	ENSMUSG00000023349	32	6	110	48	34	9	86	29
Clec5a	ENSMUSG00000029915	57	11	99	10	54	23	89	10
Clic1	ENSMUSG00000007041	641	18	1053	159	606	66	943	94
Cmtm3	ENSMUSG00000031875	323	45	510	56	301	38	439	77
Cnn3	ENSMUSG00000053931	1009	125	1438	123	955	121	1319	119
Cnot6	ENSMUSG00000020362	832	68	999	41	747	64	909	122
Col12a1	ENSMUSG00000032332	47	12	495	623	42	10	315	288
Col14a1	ENSMUSG00000022371	466	75	1493	1179	377	75	1075	556
Col15a1	ENSMUSG00000028339	2833	383	5668	1135	3175	509	5335	1392
Col18a1	ENSMUSG00000001435	248	28	790	244	293	35	541	181
Col3a1	ENSMUSG00000026043	5494	744	25906	20347	5871	824	16747	9657
Col4a1	ENSMUSG00000031502	12856	2211	23909	1751	13123	855	20837	3837
Col4a2	ENSMUSG00000031503	9490	1105	15270	591	9814	526	14603	2361
Col4a4	ENSMUSG00000067158	345	73	497	114	364	54	494	37
Col5a1	ENSMUSG00000026837	1205	173	3410	1633	1238	85	2682	1054
Col5a2	ENSMUSG00000026042	878	65	4055	3237	927	105	2738	1563

Col6a1	ENSMUSG0000001119	2071	252	3943	1376	2047	155	3242	704
Col6a2	ENSMUSG0000020241	2038	291	3824	981	2062	139	3256	743
Col6a3	ENSMUSG0000048126	1170	165	2685	1137	1119	203	1895	452
Col8a1	ENSMUSG0000068196	704	96	3461	2170	747	153	2473	1081
Cotl1	ENSMUSG0000031827	234	40	369	66	208	50	335	22
Creb5	ENSMUSG0000053007	235	36	347	57	199	28	323	65
Crip1	ENSMUSG0000006360	686	77	907	72	645	76	846	125
Crlf1	ENSMUSG0000007888	11	7	82	61	12	6	50	29
Csf1r	ENSMUSG0000024621	1029	156	1681	243	1120	141	1491	195
Csrp2	ENSMUSG0000020186	180	37	542	354	165	20	315	127
Ctgf	ENSMUSG0000019997	1416	407	4434	1114	1381	216	3773	916
Ctla2a	ENSMUSG0000044258	445	55	611	63	463	136	614	55
Ctsc	ENSMUSG0000030560	1077	100	1506	162	1055	115	1329	214
Ctsz	ENSMUSG0000016256	454	61	730	152	421	29	666	78
Cxcl16	ENSMUSG0000018920	209	30	426	208	210	55	332	47
Dab2	ENSMUSG0000022150	1262	200	1666	115	1122	167	1571	239
Dbn1	ENSMUSG0000034675	170	35	385	71	169	25	330	74
Dchs1	ENSMUSG0000036862	677	75	906	45	647	56	875	104
Depdc1a	ENSMUSG0000028175	7	6	46	33	10	5	34	14
Diaph3	ENSMUSG0000022021	16	5	59	16	23	10	55	26
Dio2	ENSMUSG0000007682	59	18	224	44	57	23	165	64
Dlgap5	ENSMUSG0000037544	17	6	48	15	12	6	41	13
Dpysl3	ENSMUSG0000024501	1022	66	1824	480	1008	79	1535	363
Dtl	ENSMUSG0000037474	13	10	42	13	12	3	42	11
Dynll1	ENSMUSG0000009013	571	82	870	205	474	104	727	130
E2f1	ENSMUSG0000027490	21	5	59	13	23	8	56	20
E2f7	ENSMUSG0000020185	42	13	85	32	34	13	79	29
Ecm1	ENSMUSG0000028108	452	86	696	127	464	82	720	136
Ecsr	ENSMUSG0000073599	254	10	366	51	246	20	337	40
Ect2	ENSMUSG0000027699	21	8	80	27	24	9	75	24
Edem1	ENSMUSG0000030104	377	69	588	97	278	84	510	147
Eef1a1	ENSMUSG0000037742	19836	2225	28730	7994	17884	2426	23968	2075
Efhd2	ENSMUSG0000040659	427	47	656	180	426	31	620	78
Elf4	ENSMUSG0000031103	320	62	496	40	293	54	437	22
Emilin1	ENSMUSG0000029163	473	106	835	204	519	28	812	91
Emp1	ENSMUSG0000030208	1538	159	4210	1587	1504	221	3295	791
Emp3	ENSMUSG0000040212	145	17	216	17	152	17	192	12
Enah	ENSMUSG0000022995	2820	352	4077	860	3138	213	4243	467
Endod1	ENSMUSG0000037419	225	35	387	85	188	20	328	98
Entpd1	ENSMUSG0000048120	473	39	717	165	458	60	637	114
Ereg	ENSMUSG0000029377	2	1	20	9	2	1	13	5
Esco2	ENSMUSG0000022034	12	5	43	10	11	6	36	16
Esy1	ENSMUSG0000025366	578	37	738	64	571	38	697	35
F2r	ENSMUSG0000048376	819	41	1217	181	861	54	1112	37
F2rl1	ENSMUSG0000021678	27	6	56	22	20	7	44	13
Fads1	ENSMUSG0000010663	476	36	619	11	473	39	586	42
Fam111a	ENSMUSG0000024691	311	25	543	98	278	57	446	66
Fam114a1	ENSMUSG0000029185	316	44	511	131	316	48	398	46
Fam129b	ENSMUSG0000026796	610	83	785	85	572	21	715	78
Fam198b	ENSMUSG0000027955	1065	183	1845	423	1058	202	1912	390
Fbln2	ENSMUSG0000064080	1827	201	3200	493	1966	214	3008	422
Fbn1	ENSMUSG0000027204	2671	543	7690	2514	3011	303	6532	2277
Fcgr2b	ENSMUSG0000026656	275	47	507	137	255	41	437	94
Fcgr3	ENSMUSG0000059498	355	58	659	143	324	56	543	112
Fcgr4	ENSMUSG0000059089	20	9	70	53	17	3	41	16
Fcrls	ENSMUSG0000015852	197	22	463	184	186	29	357	109
Fign1l	ENSMUSG0000035455	26	6	57	22	21	4	51	17
Filip1l	ENSMUSG0000043336	880	82	1259	105	842	147	1084	69
Fkbp10	ENSMUSG0000001555	345	47	461	58	288	35	402	56
Flna	ENSMUSG0000031328	4014	455	5769	673	3783	774	4951	309
Fmnl3	ENSMUSG0000023008	757	91	963	63	730	56	931	86
Fndc1	ENSMUSG0000071984	473	60	1081	567	452	50	911	402
Foxm1	ENSMUSG0000001517	42	12	122	30	47	13	101	53
Frzb	ENSMUSG0000027004	70	18	272	183	82	24	208	55
Fscn1	ENSMUSG0000029581	817	47	1186	92	831	115	1140	241
Fstl1	ENSMUSG0000022816	2281	246	7581	4030	2354	314	5589	1854
Fstl3	ENSMUSG0000020325	58	10	114	21	45	10	101	24

Fuca2	ENSMUSG00000019810	4743	786	5774	464	4738	302	6270	543
Fxyd5	ENSMUSG00000009687	283	49	603	81	271	56	473	80
Gab2	ENSMUSG00000004508	804	49	1077	134	805	51	1017	130
Gas2l3	ENSMUSG00000074802	49	17	117	44	58	17	123	41
Gdf6	ENSMUSG00000051279	21	6	60	18	20	4	52	18
Glipr2	ENSMUSG00000028480	116	26	213	33	120	25	192	33
Gm42417	ENSMUSG00000109510	601	184	1052	250	572	93	1085	285
Gm47302	ENSMUSG00000105211	24	9	110	97	27	2	68	30
Gm4739	ENSMUSG00000112808	128	31	209	69	125	23	223	29
Gng2	ENSMUSG00000043004	106	30	205	31	90	14	161	60
Gpr153	ENSMUSG00000042804	289	39	472	87	284	32	390	64
Gprc5b	ENSMUSG00000008734	417	88	644	60	371	45	622	68
Gpx1	ENSMUSG00000063856	1007	59	1482	189	1015	47	1424	176
Grb10	ENSMUSG00000020176	1827	116	2380	316	1880	141	2271	196
Grn	ENSMUSG00000034708	1349	120	1891	216	1368	123	1853	161
Gtse1	ENSMUSG00000022385	12	4	37	7	11	3	35	14
Gusb	ENSMUSG00000025534	484	36	644	46	462	48	631	40
Haspin	ENSMUSG00000050107	7	3	26	4	7	2	20	10
Hcls1	ENSMUSG00000022831	234	38	352	48	191	20	308	52
Hectd2os	ENSMUSG00000087579	181	28	259	45	192	32	288	75
Hells	ENSMUSG00000025001	29	11	78	18	36	7	79	13
Hhip11	ENSMUSG00000021260	67	22	127	40	63	22	109	33
Hist1h2ap	ENSMUSG00000094777	37	19	118	39	33	8	97	65
Hmmr	ENSMUSG00000020330	21	9	98	40	21	6	82	33
Hspa11	ENSMUSG00000007033	134	25	210	54	130	20	216	41
Ifi204	ENSMUSG00000073489	206	34	433	95	196	40	334	43
Ifi27l2a	ENSMUSG00000079017	237	35	439	84	218	39	420	49
Ifitm2	ENSMUSG00000060591	875	131	1176	80	841	117	1097	135
Ifitm3	ENSMUSG00000025492	1226	258	1689	136	1126	147	1515	182
Ifngr1	ENSMUSG00000020009	1109	126	1400	78	1101	128	1324	109
Ift122	ENSMUSG00000030323	278	32	496	94	309	39	488	78
Igfbp7	ENSMUSG00000036256	2248	254	4619	1238	2198	173	3722	608
Igsf6	ENSMUSG00000035004	49	7	92	27	46	7	79	10
Il10ra	ENSMUSG00000032089	138	27	237	86	108	21	194	46
Il1rl2	ENSMUSG00000070942	95	8	139	17	75	7	130	22
Il2rg	ENSMUSG00000031304	249	26	354	25	214	37	325	48
Il4ra	ENSMUSG00000030748	359	66	598	83	333	48	463	59
Incenp	ENSMUSG00000024660	92	17	144	29	81	14	144	40
Inhba	ENSMUSG00000041324	65	15	199	57	61	18	178	55
Iqgap1	ENSMUSG00000030536	1656	342	2416	368	1438	279	2181	405
Iqgap3	ENSMUSG00000028068	31	20	115	32	27	10	119	46
Irf7	ENSMUSG00000025498	220	65	413	114	189	26	332	52
Itga5	ENSMUSG000000000555	986	110	1409	68	945	123	1366	142
Itga9	ENSMUSG00000039115	1864	139	2467	423	1953	131	2644	386
Itgam	ENSMUSG00000030786	190	26	365	31	200	68	269	58
Itih5	ENSMUSG00000025780	368	63	749	273	377	54	597	122
Itprpl2	ENSMUSG00000095115	1256	118	1751	114	1222	89	1508	115
Kcne4	ENSMUSG00000047330	64	17	119	36	59	9	95	7
Kctd11	ENSMUSG00000046731	99	17	174	7	96	16	157	31
Kctd17	ENSMUSG00000033287	312	32	468	35	317	29	437	78
Kif11	ENSMUSG00000012443	54	18	219	84	56	14	169	71
Kif15	ENSMUSG00000036768	14	6	40	11	16	8	57	20
Kif18b	ENSMUSG00000051378	13	3	50	17	14	3	49	16
Kif20a	ENSMUSG00000003779	45	12	135	43	44	5	120	29
Kif22	ENSMUSG00000030677	26	8	61	17	19	10	51	20
Kif23	ENSMUSG00000032254	53	21	153	63	39	12	144	59
Kif2c	ENSMUSG00000028678	15	5	39	8	8	2	33	12
Kif4	ENSMUSG00000034311	35	11	86	21	32	13	86	26
Kif5b	ENSMUSG00000006740	4524	195	5272	357	4610	339	5543	496
Kifc1	ENSMUSG00000079553	21	17	44	7	18	7	48	18
Kn11	ENSMUSG00000027326	29	18	66	14	21	8	59	16
Knstrn	ENSMUSG00000027331	28	8	90	28	24	3	76	21
Kntc1	ENSMUSG00000029414	13	8	61	43	19	11	63	21
Lama4	ENSMUSG00000019846	2464	138	3226	192	2291	264	3050	270
Lamb1	ENSMUSG00000002900	2656	308	3500	191	2690	265	3282	467
Lamc1	ENSMUSG00000026478	4969	490	7157	380	5155	283	6688	486
Laptm5	ENSMUSG00000028581	500	82	885	205	478	56	708	122

Lcp1	ENSMUSG00000021998	803	118	1421	200	781	112	1229	174
Lgals3	ENSMUSG00000050335	56	18	203	128	57	20	148	73
Lgals3bp	ENSMUSG00000033880	711	128	1195	145	721	83	1079	113
Lgals9	ENSMUSG0000001123	575	96	870	73	533	82	766	58
Lhfpl2	ENSMUSG00000045312	121	17	351	198	128	21	269	96
Lilr4b	ENSMUSG00000112023	154	32	309	106	138	41	252	97
Litaf	ENSMUSG00000022500	341	97	525	67	315	74	445	72
Lman11	ENSMUSG00000056271	6	2	21	5	6	5	23	11
Lockd	ENSMUSG00000098318	4	4	22	11	5	3	21	12
Lox11	ENSMUSG00000032334	618	97	1447	604	687	57	1181	257
Lox12	ENSMUSG00000034205	724	133	1635	127	683	84	1403	383
Lrp1	ENSMUSG00000040249	4010	495	5574	985	4250	358	5472	456
Lrp8	ENSMUSG00000028613	9	5	40	13	13	7	51	44
Ly6e	ENSMUSG00000022587	2929	530	3882	293	2782	305	3608	375
Ly86	ENSMUSG00000021423	93	6	221	112	92	20	181	43
Lyz2	ENSMUSG00000069516	4037	355	6768	1318	3852	675	5981	848
Mall	ENSMUSG00000027377	160	25	233	27	157	20	226	33
Map1b	ENSMUSG00000052727	582	102	873	51	444	82	777	113
Map4k4	ENSMUSG00000026074	3034	462	3619	383	2841	174	3784	234
Marcks1	ENSMUSG00000047945	104	18	211	70	107	9	183	4
Masp1	ENSMUSG00000022887	205	16	307	114	219	36	315	61
Mcam	ENSMUSG00000032135	1064	99	1678	301	970	129	1515	234
Medag	ENSMUSG00000029659	437	58	771	121	486	78	684	41
Melk	ENSMUSG00000035683	19	16	45	19	13	4	40	14
Meox1	ENSMUSG0000001493	296	46	905	284	323	49	767	246
Mest	ENSMUSG00000051855	193	22	598	325	156	26	417	154
Mfap4	ENSMUSG00000042436	202	18	1249	1153	245	36	712	324
Mfap5	ENSMUSG00000030116	411	43	1634	1033	404	45	1132	430
Mis18bp1	ENSMUSG00000047534	15	3	59	20	16	6	44	14
Mki67	ENSMUSG00000031004	305	108	1186	340	284	62	1009	362
Mmp2	ENSMUSG00000031740	991	124	2606	1435	1013	93	2013	656
Mmp23	ENSMUSG00000029061	80	8	179	97	80	19	146	38
Mpp1	ENSMUSG00000031402	302	30	434	51	294	38	387	21
Mrc1	ENSMUSG00000026712	1125	59	1641	55	1195	105	1622	319
Ms4a6b	ENSMUSG00000024677	163	35	265	79	109	27	237	58
Ms4a6c	ENSMUSG00000079419	117	24	273	106	108	30	198	50
Msn	ENSMUSG00000031207	4381	327	6174	266	4286	400	5734	498
Msr1	ENSMUSG00000025044	91	16	165	30	95	12	158	35
Mxd3	ENSMUSG00000021485	3	2	21	8	5	2	23	10
Mxra7	ENSMUSG00000020814	353	43	549	114	334	33	485	81
Mybl2	ENSMUSG00000017861	12	4	32	11	10	3	29	7
Mybpc2	ENSMUSG00000038670	292	36	901	354	321	110	773	309
Myh10	ENSMUSG00000020900	964	132	1462	186	988	96	1366	213
Myl1	ENSMUSG00000061816	777	84	1354	639	674	113	1186	282
Myl6	ENSMUSG00000090841	3039	174	4606	743	2959	365	4098	492
Myo1d	ENSMUSG00000035441	367	44	489	47	360	56	474	39
Myo1f	ENSMUSG00000024300	97	11	170	34	88	10	163	43
Myof	ENSMUSG00000048612	346	89	640	167	312	56	541	78
Nbl1	ENSMUSG00000041120	214	26	349	63	215	19	307	61
Ncapg	ENSMUSG00000015880	17	11	88	26	18	10	55	17
Ncapg2	ENSMUSG00000042029	78	9	184	50	101	31	166	54
Ncaph	ENSMUSG00000034906	32	7	80	27	35	11	78	26
Ncf1	ENSMUSG00000015950	112	33	201	54	124	31	190	42
Nckap11	ENSMUSG00000022488	260	42	511	159	240	40	412	73
Ndc80	ENSMUSG00000024056	18	8	69	23	19	4	56	15
Necap2	ENSMUSG00000028923	266	29	348	33	232	24	305	28
Nek2	ENSMUSG00000026622	16	10	60	22	15	3	46	11
Nes	ENSMUSG0000004891	1779	216	2677	688	1621	280	2378	347
Nid1	ENSMUSG0000005397	3926	530	6347	1387	3634	332	5323	725
Nid2	ENSMUSG00000021806	561	130	914	118	537	62	895	114
Nkd2	ENSMUSG00000021567	39	11	118	51	36	6	77	24
Nlrc3	ENSMUSG00000049871	58	17	139	45	66	12	140	43
Nppa	ENSMUSG00000041616	2919	1471	17568	21348	2998	848	11493	6461
Nppb	ENSMUSG00000029019	3896	1226	10218	3100	4287	995	11088	3450
Nuf2	ENSMUSG00000026683	21	9	86	40	16	4	77	34
Oaf	ENSMUSG00000032014	264	77	399	146	208	41	331	55
Olfml3	ENSMUSG00000027848	303	52	492	108	323	21	470	29

Otulin	ENSMUSG00000046034	372	28	492	30	374	38	498	73
P2ry6	ENSMUSG00000048779	103	15	191	33	95	15	152	28
P3h3	ENSMUSG00000023191	185	14	319	100	179	28	278	54
Pabpc1	ENSMUSG00000022283	2750	396	4424	589	2940	313	3983	663
Pam	ENSMUSG00000026335	13364	1232	16353	2118	13089	520	17039	1382
Pamr1	ENSMUSG00000027188	50	16	271	244	44	23	183	117
Pbk	ENSMUSG00000022033	18	15	71	30	16	9	69	28
Pcdhgc3	ENSMUSG00000102918	783	97	981	69	752	51	988	95
Pclaf	ENSMUSG00000040204	20	11	70	26	13	4	61	24
Pcolce	ENSMUSG00000029718	778	81	1236	178	675	91	1133	173
Peal5a	ENSMUSG00000013698	2146	275	2690	102	2035	242	2530	274
Pfkp	ENSMUSG00000021196	1083	101	1607	246	1116	108	1508	216
Pfn1	ENSMUSG00000018293	2349	50	2712	75	2362	104	2642	191
Phf11d	ENSMUSG00000068245	263	46	403	78	242	30	341	41
Phlda3	ENSMUSG00000041801	128	18	222	62	128	4	216	43
Pi16	ENSMUSG00000024011	1042	154	1987	337	1030	148	1793	499
Picalm	ENSMUSG00000039361	3682	311	4950	606	3495	243	4537	508
Pimreg	ENSMUSG00000020808	18	10	79	24	18	4	67	18
Pirb	ENSMUSG00000058818	142	22	283	84	134	30	266	92
Pla2g4a	ENSMUSG00000056220	118	46	201	50	118	39	188	22
Pla2g7	ENSMUSG00000023913	171	21	280	45	172	34	252	45
Plat	ENSMUSG00000031538	475	62	725	65	464	41	699	128
Plcg2	ENSMUSG00000034330	248	18	352	61	256	18	349	46
Plek	ENSMUSG00000020120	194	26	382	104	207	35	336	73
Plekhg2	ENSMUSG00000037552	415	79	602	42	355	76	498	81
Plekhh2	ENSMUSG00000040852	172	20	250	25	168	11	228	26
Plekho1	ENSMUSG00000015745	873	48	1229	109	927	54	1262	202
Plekho2	ENSMUSG00000050721	497	98	707	90	525	90	666	108
Pls3	ENSMUSG00000016382	1718	79	2436	255	1640	157	2091	235
Pmepa1	ENSMUSG00000038400	495	93	798	197	520	37	753	189
Pmp22	ENSMUSG00000018217	799	98	1125	49	732	79	1029	87
Postn	ENSMUSG00000027750	1288	354	16369	19036	1325	317	10262	8108
Ppic	ENSMUSG00000024538	424	29	954	416	413	41	706	107
Ppp1r9b	ENSMUSG00000038976	1114	96	1479	122	1143	53	1390	134
Praf2	ENSMUSG00000031149	91	14	155	27	90	17	137	19
Prc1	ENSMUSG00000038943	59	10	277	77	74	20	211	83
Prcp	ENSMUSG00000061119	378	31	583	113	369	43	525	62
Prelid1	ENSMUSG00000021486	540	47	753	58	476	49	647	93
Prnd	ENSMUSG00000027338	170	30	416	121	167	33	335	59
Prr11	ENSMUSG00000020493	26	9	79	21	18	6	65	19
Prrg3	ENSMUSG00000033361	304	49	476	60	309	45	455	53
Psat1	ENSMUSG00000024640	65	15	115	35	66	18	116	28
Psrc1	ENSMUSG00000068744	10	4	29	15	9	4	29	18
Ptgfrn	ENSMUSG00000027864	1116	158	1460	136	1089	77	1442	156
Ptgis	ENSMUSG00000017969	202	28	364	114	200	27	323	64
Ptma	ENSMUSG00000026238	4087	376	5328	376	3885	518	4897	607
Ptpj	ENSMUSG00000025314	404	60	631	75	427	56	571	83
Pxdn	ENSMUSG00000020674	2049	186	2790	214	2026	252	2556	286
Qsox1	ENSMUSG00000033684	551	17	792	82	588	46	765	102
Rab13	ENSMUSG00000027935	64	9	113	32	60	13	95	9
Rab31	ENSMUSG00000056515	515	47	841	272	486	52	743	141
Rab7b	ENSMUSG00000052688	114	17	216	47	113	25	187	28
Racgap1	ENSMUSG00000023015	51	13	168	39	47	22	147	53
Rbl1	ENSMUSG00000027641	92	18	142	31	88	10	137	16
Rcan1	ENSMUSG00000022951	2025	588	3577	1067	2237	187	3873	1294
Rcc2	ENSMUSG00000040945	364	24	453	17	354	21	462	57
Rcn3	ENSMUSG00000019539	304	49	526	177	289	35	431	74
Rgs16	ENSMUSG00000026475	42	13	97	25	41	22	76	17
Rhoc	ENSMUSG0000002233	1016	82	1471	147	963	60	1399	180
Ripk1	ENSMUSG00000021408	280	44	414	37	283	47	366	18
Rnase4	ENSMUSG00000021876	967	55	1292	169	990	104	1212	120
Rnd3	ENSMUSG00000017144	446	50	573	42	410	17	542	43
Rnf213	ENSMUSG00000070327	1921	265	2664	212	1732	232	2287	172
Rnf4	ENSMUSG00000029110	719	66	881	34	682	79	832	58
Rrm2	ENSMUSG00000020649	47	3	106	36	46	11	90	24
Rsd2	ENSMUSG00000020641	558	59	808	127	569	74	833	251
Rsu1	ENSMUSG00000026727	628	30	848	58	638	25	765	30

Runx3	ENSMUSG00000070691	15	6	40	18	11	6	33	8
S100a10	ENSMUSG00000041959	648	48	917	65	558	90	873	124
S100a11	ENSMUSG00000027907	541	79	1009	138	513	59	798	136
S100a4	ENSMUSG00000001020	101	23	185	48	95	20	157	48
S100a6	ENSMUSG00000001025	463	35	675	47	446	74	610	100
Samd9l	ENSMUSG00000047735	766	77	1115	179	714	95	898	111
Scml4	ENSMUSG00000044770	68	22	133	24	73	13	155	38
Sdc3	ENSMUSG00000025743	1679	201	2152	200	1603	123	1955	125
Sec61a1	ENSMUSG00000030082	772	59	1001	99	760	61	922	32
Sema3f	ENSMUSG00000034684	281	62	437	37	248	21	450	63
Serpib1c	ENSMUSG00000079049	2	1	40	44	2	1	21	10
Serpinf1	ENSMUSG00000000753	424	109	1021	469	419	39	783	209
Sgo1	ENSMUSG00000023940	10	3	30	10	11	4	27	6
Sh3bgrl3	ENSMUSG00000028843	283	45	439	75	294	39	393	63
Sh3bp2	ENSMUSG00000054520	69	26	114	31	61	7	106	12
Sh3pxd2b	ENSMUSG00000040711	249	93	530	157	247	52	411	85
Siglec1	ENSMUSG00000027322	120	21	202	53	128	32	195	28
Slamf9	ENSMUSG00000026548	102	15	214	66	105	27	174	36
Slc7a5	ENSMUSG00000040010	92	11	140	11	101	4	149	21
Slfn2	ENSMUSG00000072620	233	30	361	80	223	50	310	16
Slfn9	ENSMUSG00000069793	117	11	264	62	100	26	248	59
Slmap	ENSMUSG00000021870	4454	592	5686	709	4379	533	6028	274
Smc2	ENSMUSG00000028312	165	38	318	105	129	27	242	61
Snca	ENSMUSG00000025889	79	27	187	57	121	41	270	139
Sntb2	ENSMUSG00000041308	632	76	913	145	638	68	853	99
Socs3	ENSMUSG00000053113	83	19	176	67	83	9	171	89
Sox9	ENSMUSG00000000567	49	4	128	64	53	5	103	17
Spag5	ENSMUSG00000002055	26	31	54	13	19	10	55	17
Sparc	ENSMUSG00000018593	7512	635	18831	6579	7355	933	14409	2942
Spc25	ENSMUSG00000005233	14	8	61	17	18	8	51	25
Spdl1	ENSMUSG00000069910	14	4	33	8	11	3	28	11
Specc1	ENSMUSG00000042331	92	10	188	35	117	18	192	33
Spr1a	ENSMUSG00000050359	2	1	59	85	1	1	31	38
Sptlc2	ENSMUSG00000021036	532	46	684	85	500	56	646	54
Sri	ENSMUSG0000003161	820	36	947	43	794	58	937	33
Spx2	ENSMUSG00000031253	164	22	353	215	151	23	300	80
Ssc5d	ENSMUSG00000035279	158	37	405	221	163	32	347	116
Stab1	ENSMUSG00000042286	1603	325	2076	219	1569	318	2072	151
Stc1	ENSMUSG00000014813	72	10	132	17	71	21	124	24
Stil	ENSMUSG00000028718	13	7	37	11	18	15	36	14
Stmn1	ENSMUSG00000028832	255	12	400	110	218	34	386	85
Sulf1	ENSMUSG00000016918	588	72	1266	375	636	106	916	142
Svep1	ENSMUSG00000028369	454	54	1081	419	488	75	1015	246
Syk	ENSMUSG00000021457	661	54	816	97	624	37	818	114
Synpo2l	ENSMUSG00000039376	2429	160	4589	1397	2488	266	4960	1191
Tacc3	ENSMUSG00000037313	55	17	109	27	41	13	101	32
Tagln2	ENSMUSG00000026547	1222	205	1863	181	1131	206	1710	250
Tax1bp3	ENSMUSG00000040158	636	52	758	26	603	49	731	37
Tcf19	ENSMUSG00000050410	39	7	78	17	36	10	69	16
Tead2	ENSMUSG00000030796	87	19	131	19	76	18	119	12
Tgfb1	ENSMUSG0000002603	550	90	766	73	584	72	754	96
Tgfb1i	ENSMUSG00000035493	530	77	732	148	489	68	651	78
Tgif1	ENSMUSG00000047407	80	8	172	68	80	12	125	17
Thbs1	ENSMUSG00000040152	409	149	2336	862	430	59	1679	388
Thbs3	ENSMUSG00000028047	103	23	225	128	92	40	196	95
Thbs4	ENSMUSG00000021702	98	24	980	1112	104	23	729	572
Thy1	ENSMUSG00000032011	161	30	284	38	162	24	265	26
Timp1	ENSMUSG0000001131	29	17	298	217	27	8	170	133
Timp2	ENSMUSG00000017466	2020	279	2851	462	2083	233	2707	361
Tk1	ENSMUSG00000025574	27	6	65	23	23	5	56	16
Tln1	ENSMUSG00000028465	3433	355	4129	304	3528	301	4361	274
Tlr13	ENSMUSG00000033777	67	17	156	73	54	17	129	34
Tlr4	ENSMUSG00000039005	491	150	724	86	471	25	747	193
Tmem173	ENSMUSG00000024349	169	26	277	47	150	31	216	31
Tmem176b	ENSMUSG00000029810	447	59	695	169	422	18	612	87
Tmem254b	ENSMUSG00000021867	94	24	152	22	90	34	151	21
Tmsb10	ENSMUSG00000079523	1059	131	1943	416	1045	141	1515	201

Tmsb4x	ENSMUSG00000049775	6492	390	9057	1900	6337	792	8278	983
Tnc	ENSMUSG00000028364	43	6	544	443	40	8	407	402
Tnfaip6	ENSMUSG00000053475	16	7	49	21	15	3	40	15
Tnfaip8l1	ENSMUSG00000044469	59	9	106	14	51	10	88	20
Tnfrsf11b	ENSMUSG00000063727	4	4	30	9	8	3	25	12
Tnfrsf12a	ENSMUSG00000023905	569	211	1115	309	580	83	1245	254
Tnfrsf1a	ENSMUSG00000030341	862	76	1114	56	808	94	1077	63
Top2a	ENSMUSG00000020914	156	64	602	224	141	28	511	197
Tpm2	ENSMUSG00000028464	338	60	565	58	358	58	477	79
Tpm3	ENSMUSG00000027940	1515	192	2133	211	1390	166	1854	103
Tpm4	ENSMUSG00000031799	3181	181	4770	635	3020	369	4360	322
Tpx2	ENSMUSG00000027469	56	21	186	55	49	21	165	46
Trem2	ENSMUSG00000023992	35	6	92	48	34	8	74	19
Trim47	ENSMUSG00000020773	322	56	432	50	294	39	391	53
Trim59	ENSMUSG00000034317	45	13	121	42	39	10	82	19
Tspan6	ENSMUSG00000067377	201	18	351	99	188	36	291	45
Ttc9	ENSMUSG00000042734	48	13	109	12	46	8	91	22
Ttk	ENSMUSG00000038379	11	6	50	21	9	2	35	14
Tuba1a	ENSMUSG00000072235	1839	223	2349	176	1762	189	2229	379
Tubb5	ENSMUSG0000001525	1852	114	2383	316	1680	188	2353	298
Tyms	ENSMUSG00000025747	54	5	125	33	37	11	97	35
Tyrobp	ENSMUSG00000030579	196	25	385	134	191	36	314	57
Ube2c	ENSMUSG0000001403	26	8	84	26	25	10	76	27
Uck2	ENSMUSG00000026558	821	87	1664	260	843	95	1668	393
Ugt1a7c	ENSMUSG00000090124	31	6	81	25	36	7	76	31
Uhrf1	ENSMUSG0000001228	52	9	132	55	40	18	111	47
Ulbp1	ENSMUSG00000079685	96	27	174	24	75	13	122	11
Unc93b1	ENSMUSG00000036908	322	73	550	131	355	31	500	38
Vat1	ENSMUSG00000034993	610	35	884	140	594	35	798	66
Vcan	ENSMUSG00000021614	730	115	1503	151	665	105	1354	355
Vim	ENSMUSG00000026728	3763	407	7380	1381	3521	520	6206	983
Xirp2	ENSMUSG00000027022	23026	1933	46990	12463	24085	3291	47862	16560
Xylt1	ENSMUSG00000030657	76	8	167	19	86	14	139	34
Ywhaz	ENSMUSG00000022285	2464	152	2960	156	2391	141	2749	56
Zyx	ENSMUSG00000029860	896	129	1214	76	876	143	1120	93

**Supplementary Table S4.** RNASeq analysis of effects of angiotensin II (AngII) on mRNA expression in hearts from PKN2Het vs WT littermates: mRNAs significantly downregulated by AngII in PKN2Het or WT hearts.

Gene Symbol	Ensembl gene id	WT Vehicle	WT AngII		PKN2Het Vehicle		PKN2Het AngII		
			Mean	SD	Mean	SD	Mean	SD	
March6	ENSMUSG00000039100	4345	470	3364	215	4521	533	3717	463
A530016L24Rik	ENSMUSG00000043122	486	59	252	64	537	84	302	85
Abca12	ENSMUSG00000050296	186	25	118	22	190	14	113	26
Abcc9	ENSMUSG00000030249	9613	652	6487	953	9739	961	7503	994
Acad11	ENSMUSG00000090150	4332	376	3012	486	4068	456	3113	804
Acssl1	ENSMUSG00000027452	6051	350	3795	623	6116	511	4694	536
Adcy9	ENSMUSG00000005580	523	37	386	56	548	56	435	28
Adi1	ENSMUSG00000020629	777	43	587	41	770	25	625	82
Adra1a	ENSMUSG00000045875	454	44	309	38	449	28	324	43
Adrb1	ENSMUSG00000035283	299	27	186	24	312	44	237	7
Aes	ENSMUSG00000054452	8100	309	6557	669	8573	728	7022	440
Ak4	ENSMUSG00000028527	1110	101	673	88	1095	120	841	121
Aldh2	ENSMUSG00000029455	3628	278	2621	303	3753	239	3023	178
Aldh4a1	ENSMUSG00000028737	2051	114	1277	213	2215	312	1569	163
Aldh6a1	ENSMUSG00000021238	4712	450	3354	316	4858	561	3659	653
Aldob	ENSMUSG00000028307	153	33	37	15	130	33	51	29
Angpt1	ENSMUSG00000022309	983	254	585	130	825	181	510	175
Ano10	ENSMUSG00000037949	698	182	344	58	669	131	405	96
Apbb1	ENSMUSG00000037032	1485	207	973	270	1582	132	1096	145
Arel1	ENSMUSG00000042350	1385	91	997	117	1373	120	1084	87
Arfgef1	ENSMUSG00000067851	4031	401	3145	313	4160	428	3482	356
Asb10	ENSMUSG00000038204	1171	63	812	130	1209	144	936	72
Asb14	ENSMUSG00000021898	1693	190	1270	203	1859	69	1299	90
Asb15	ENSMUSG00000029685	1620	111	997	132	1719	167	1139	111
Atp2a2	ENSMUSG00000029467	276075	9196	182185	30616	276406	28699	212684	20219
Bckdha	ENSMUSG00000060376	3198	271	2027	281	3491	476	2369	149
Bckdhb	ENSMUSG00000032263	843	53	580	105	820	64	644	127
Blcap	ENSMUSG00000067787	674	60	518	51	708	57	566	19
Cacna1s	ENSMUSG00000026407	289	41	167	50	318	106	207	31
Calcoco1	ENSMUSG00000023055	2244	90	1682	135	2260	208	1798	84
Camk2a	ENSMUSG00000024617	894	42	584	78	907	103	635	63
Cbx7	ENSMUSG00000053411	375	36	283	55	434	66	306	28
Cdnf	ENSMUSG00000039496	693	83	462	69	638	86	470	25
Clasp1	ENSMUSG00000064302	10042	1348	7016	1532	10721	1184	8158	674
Clasp2	ENSMUSG00000033392	1555	68	1255	49	1588	122	1315	122
Clcn1	ENSMUSG00000029862	122	31	56	16	126	19	52	17
Clpx	ENSMUSG00000015357	2210	180	1776	257	2247	186	1932	167
Cmtm8	ENSMUSG00000041012	193	16	122	26	198	19	133	20
Cmya5	ENSMUSG00000047419	30807	1640	21498	2766	31721	3064	25206	2497
Cngb3	ENSMUSG00000056494	85	21	34	5	96	10	48	18
Cnst	ENSMUSG00000038949	1417	109	1052	101	1496	138	1149	127
Coq8a	ENSMUSG00000026489	8867	811	6241	1021	9606	1491	7168	332
Cpeb3	ENSMUSG00000039652	1712	172	1204	231	1874	247	1337	250
Creg1	ENSMUSG00000040713	2146	83	1671	135	2006	90	1667	106
Crip2	ENSMUSG00000006356	12559	568	9239	1165	12739	1064	10202	689
D10Jhu81e	ENSMUSG00000053329	4564	257	3218	428	4591	348	3636	306
Dcaf11	ENSMUSG00000022214	2685	174	1996	224	2643	170	2142	182
Dcaf8	ENSMUSG00000026554	3228	148	2835	139	3162	236	2954	198
Dcun1d2	ENSMUSG00000038506	1528	101	1151	175	1592	86	1245	86
Dglucy	ENSMUSG00000021185	1025	27	630	95	1021	154	706	146
Dhdh	ENSMUSG00000011382	539	37	412	40	541	58	441	60
Dsg2	ENSMUSG00000044393	2214	147	1452	293	2105	275	1573	277
Ehhadh	ENSMUSG00000022853	319	54	215	36	367	52	263	31
Entpd5	ENSMUSG00000021236	4587	555	2853	380	4318	388	3001	409
Epha4	ENSMUSG00000026235	1430	183	778	139	1532	195	924	149
Esrra	ENSMUSG00000024955	1498	69	1122	160	1612	352	1242	55
Fam174b	ENSMUSG00000078670	5146	309	3201	609	5011	412	3808	373
Fblim1	ENSMUSG0000006219	4020	400	2963	478	4442	528	3364	287

Fgf1	ENSMUSG00000036585	4273	125	2800	289	4103	316	3148	422
Fgf13	ENSMUSG00000031137	912	28	624	84	957	100	687	122
Fgf16	ENSMUSG00000031230	350	35	197	36	325	28	212	47
Fitm2	ENSMUSG00000048486	4343	253	2687	652	4389	466	3182	252
Fktn	ENSMUSG00000028414	919	77	713	82	966	86	734	38
Fyco1	ENSMUSG00000025241	8256	626	6068	819	8149	1328	6602	1438
Gadd45a	ENSMUSG00000036390	237	30	173	8	280	38	199	29
Gal3st3	ENSMUSG00000047658	235	33	123	31	253	42	156	27
Gcat	ENSMUSG00000006378	139	15	88	16	122	23	81	20
Gcdh	ENSMUSG00000003809	1192	92	826	152	1218	47	907	64
Ghr	ENSMUSG00000055737	3256	90	2495	135	3239	69	2574	165
Gid4	ENSMUSG00000018415	1429	66	1151	186	1528	101	1208	39
Gm10435	ENSMUSG00000072902	350	47	240	57	374	40	256	85
Gm10635	ENSMUSG000000111765	62	15	26	11	57	10	29	5
Gm37691	ENSMUSG000000104348	120	14	62	18	123	24	83	16
Gpd11	ENSMUSG00000050627	1532	131	1271	72	1610	184	1401	84
Gpt2	ENSMUSG00000031700	649	55	444	64	689	85	483	73
Gramd1b	ENSMUSG00000040111	802	117	546	52	929	115	696	158
Grcc10	ENSMUSG00000072772	1142	101	905	96	1137	51	918	108
Grm1	ENSMUSG00000019828	796	113	605	58	918	161	761	121
Gstm2	ENSMUSG00000040562	1088	63	815	54	1016	120	792	38
Hadha	ENSMUSG00000025745	29451	2086	19576	3952	28687	2036	22309	1220
Hdac11	ENSMUSG00000034245	385	30	247	18	404	32	306	52
Hdlbp	ENSMUSG00000034088	16562	1228	12760	1097	16946	1402	13742	294
Herpud1	ENSMUSG00000031770	2271	311	1495	173	2164	218	1572	242
Idh3g	ENSMUSG00000002010	6376	459	4785	580	6418	422	4954	479
Ift81	ENSMUSG00000029469	1002	129	666	78	994	49	708	78
Il15	ENSMUSG00000031712	439	60	265	38	422	29	277	62
Inmt	ENSMUSG00000003477	120	30	62	9	125	27	60	31
Iqsec1	ENSMUSG00000034312	2343	237	1649	239	2475	375	1887	147
Isoc1	ENSMUSG00000024601	1090	72	835	76	1154	85	886	108
Ivd	ENSMUSG00000027332	5467	219	3645	686	5738	467	4074	283
Kcnd2	ENSMUSG00000060882	633	53	397	84	534	96	384	46
Kcnj11	ENSMUSG00000096146	2367	103	1635	312	2506	312	1913	137
Kcnj12	ENSMUSG00000042529	362	32	215	47	369	42	263	36
Kcnj3	ENSMUSG00000026824	1558	124	892	227	1560	194	966	194
Kcnj5	ENSMUSG00000032034	1526	103	978	122	1446	143	1137	106
Kcnv2	ENSMUSG00000047298	217	40	101	27	221	15	94	19
Klf15	ENSMUSG00000030087	629	39	379	62	616	39	429	68
Klhdc1	ENSMUSG00000051890	679	63	505	66	737	123	482	72
Klhdc7a	ENSMUSG00000078234	208	40	115	26	215	51	132	33
Klh124	ENSMUSG00000062901	8344	685	6893	406	8712	1112	7374	755
Klh130	ENSMUSG00000026308	803	90	596	82	845	153	665	56
Klh138	ENSMUSG00000022357	594	49	396	86	598	80	398	64
Ldhd	ENSMUSG00000031958	690	79	434	51	734	70	479	49
Lgals4	ENSMUSG00000053964	258	38	159	45	261	30	142	30
Lrrc14b	ENSMUSG00000021579	1627	72	1181	214	1726	119	1267	58
Lrtm1	ENSMUSG00000045776	10990	1420	7948	2173	9808	949	7556	656
Macrod1	ENSMUSG00000036278	1985	82	1475	206	2115	228	1644	157
Maob	ENSMUSG00000040147	1029	117	683	136	1003	67	758	145
Mccc2	ENSMUSG00000021646	1044	126	719	104	1066	137	833	122
Me3	ENSMUSG00000030621	1244	36	938	86	1271	81	1046	52
Mfap3l	ENSMUSG00000031647	512	38	351	27	511	51	378	15
Mgea5	ENSMUSG00000025220	2744	156	2258	103	2825	202	2463	245
Mitf	ENSMUSG00000035158	1007	108	715	103	983	124	817	111
Mlycd	ENSMUSG00000074064	1449	99	1002	186	1535	222	1119	122
Mmab	ENSMUSG00000029575	681	48	453	44	638	56	508	62
Mrgprh	ENSMUSG00000059408	120	15	59	19	121	13	67	15
mt-Rnr2	ENSMUSG00000064339	356240	61989	247940	69255	362883	53161	276407	38517
Mut	ENSMUSG00000023921	2916	284	2169	324	2826	245	2373	210
Mylk3	ENSMUSG00000031698	13367	1180	7949	948	12901	1032	9303	1403
Nadk2	ENSMUSG00000022253	1247	102	792	168	1254	222	893	160
Nceh1	ENSMUSG00000027698	4775	531	3631	517	4935	459	4158	196
Nipsnap2	ENSMUSG00000029432	12499	468	8522	1242	13021	796	9974	916
Osbp2	ENSMUSG00000020435	538	31	388	52	578	65	451	35
Oxr1	ENSMUSG00000022307	1785	149	1475	130	1747	115	1456	95
Oxsm	ENSMUSG00000021786	592	47	470	26	633	71	520	20

Oxsr1	ENSMUSG00000036737	1469	64	1253	72	1563	110	1374	101
P2ry1	ENSMUSG00000027765	592	33	336	93	614	60	420	44
Pank1	ENSMUSG00000033610	1036	54	700	77	1098	87	753	63
Paqr9	ENSMUSG00000064225	1387	188	959	139	1468	178	1110	132
Pcca	ENSMUSG00000041650	1754	109	1194	210	1808	136	1417	61
Pcnt	ENSMUSG00000001151	1516	71	1137	205	1490	140	1194	68
Pde4a	ENSMUSG00000032177	1479	69	1032	200	1596	227	1163	137
Pde4d	ENSMUSG00000021699	566	55	373	47	575	76	416	43
Pdhal	ENSMUSG00000031299	24973	2883	19882	1983	24844	2183	21298	1610
Pdp1	ENSMUSG00000049225	1052	157	827	97	1038	87	873	99
Pdp2	ENSMUSG00000048371	822	182	433	87	839	116	560	111
Pdpr	ENSMUSG00000033624	2409	176	1771	254	2523	330	2118	147
Pex11a	ENSMUSG00000030545	362	28	251	44	360	53	277	16
Pfkfb1	ENSMUSG00000025271	181	54	76	15	125	29	76	31
Pink1	ENSMUSG00000028756	7908	460	5095	582	8315	930	5887	645
Pkia	ENSMUSG00000027499	6489	587	5105	667	6499	450	5564	198
Pkig	ENSMUSG00000035268	1911	58	1637	67	1943	106	1679	127
Pkm	ENSMUSG00000032294	19295	1479	15108	1318	19558	1824	16780	652
Pla2g5	ENSMUSG00000041193	703	60	323	118	617	100	370	76
Pln	ENSMUSG00000038583	103669	9371	75161	8133	106163	7666	81558	8775
Plxnb1	ENSMUSG00000053646	817	113	486	68	762	119	534	62
Pm20d2	ENSMUSG00000054659	458	21	337	55	500	64	387	32
Pnpla8	ENSMUSG00000036257	3505	336	2968	271	3603	216	3140	212
Ppargc1a	ENSMUSG00000029167	1975	310	1550	238	2310	255	1647	126
Ppfibp2	ENSMUSG00000036528	632	102	494	48	689	69	541	29
Ppip5k2	ENSMUSG00000040648	2823	288	1947	183	2670	258	1967	582
Ppm11	ENSMUSG00000027784	1625	159	1031	184	1684	206	1260	149
Ppp1r14c	ENSMUSG00000040653	3104	380	2506	85	3332	336	2807	364
Pptc7	ENSMUSG00000038582	3687	299	2559	451	3939	504	3081	324
Prkab1	ENSMUSG00000029513	625	39	486	57	684	60	543	69
Rap1gap2	ENSMUSG00000038807	2208	274	1592	353	2292	294	1806	108
Rbfox1	ENSMUSG00000008658	634	47	360	59	657	70	426	78
Reep1	ENSMUSG00000052852	440	28	345	23	454	53	354	26
Reep5	ENSMUSG00000005873	6212	260	4792	333	6407	427	5212	316
Rgs2	ENSMUSG00000026360	831	133	501	64	860	81	573	166
Ric8b	ENSMUSG00000035620	1056	84	764	88	1036	119	844	32
Rilpl1	ENSMUSG00000029392	2712	176	2148	322	2829	181	2289	127
Rmnd5a	ENSMUSG00000002222	2488	67	2108	149	2641	123	2117	196
Rpl31	ENSMUSG00000002500	3330	271	1888	478	3250	187	2275	264
Rtn2	ENSMUSG00000030401	979	45	649	92	997	112	733	89
Sdha	ENSMUSG00000021577	26565	1713	17836	2991	26775	2129	20539	1624
Sec31b	ENSMUSG00000051984	190	12	140	15	206	17	142	18
Selenbp1	ENSMUSG00000068874	1432	58	903	170	1401	157	1028	139
Sgcb	ENSMUSG00000029156	2725	146	2351	41	2817	190	2512	150
Slc20a2	ENSMUSG00000037656	3299	120	2345	335	3156	313	2538	136
Slc22a5	ENSMUSG00000018900	515	48	392	19	513	45	415	24
Slc25a34	ENSMUSG00000040740	2458	124	1716	276	2459	202	1859	71
Slc25a42	ENSMUSG00000002346	919	100	557	97	966	156	583	82
Slc27a1	ENSMUSG00000031808	1220	145	877	126	1202	129	879	108
Slc4a3	ENSMUSG00000006576	2856	245	2018	244	3026	328	2319	297
Smim20	ENSMUSG00000061461	843	73	641	62	853	63	664	59
Stom	ENSMUSG00000026880	2813	112	2237	204	2994	287	2470	159
Stum	ENSMUSG00000053963	160	19	64	17	122	38	54	18
Syde2	ENSMUSG00000036863	475	95	306	46	437	39	305	68
Synj2	ENSMUSG00000023805	1330	103	1004	60	1390	140	1030	43
Taf1a	ENSMUSG00000072258	316	29	238	17	323	11	239	23
Tbc1d10c	ENSMUSG00000040247	79	13	45	9	80	16	46	8
Tbc1d16	ENSMUSG00000039976	1680	162	1163	183	1773	217	1329	136
Tbc1d4	ENSMUSG00000033083	2228	153	1576	167	2172	256	1634	160
Tbx5	ENSMUSG00000018263	456	56	299	60	527	87	347	57
Tcea3	ENSMUSG00000001604	1429	35	1076	111	1549	116	1154	106
Tmem150c	ENSMUSG00000050640	201	25	109	24	249	43	146	26
Tmem182	ENSMUSG00000079588	4532	444	3422	366	4747	305	3856	392
Tmem245	ENSMUSG00000055296	3203	419	2375	169	3028	247	2485	165
Tmem63b	ENSMUSG00000036026	1741	102	1317	164	1858	169	1449	124
Tmem65	ENSMUSG00000062373	3732	474	2882	185	3814	575	3099	401
Tnfrsf19	ENSMUSG00000060548	97	27	54	15	91	22	56	12

Tnni3k	ENSMUSG00000040086	2347	262	1468	283	2247	145	1743	187
Trap1	ENSMUSG0000005981	2287	176	1864	73	2431	195	1969	70
Trim7	ENSMUSG00000040350	466	53	297	42	440	107	331	53
Trip10	ENSMUSG00000019487	1361	60	1155	94	1369	30	1142	93
Ttll1	ENSMUSG00000022442	921	104	531	110	965	54	680	86
Txlnb	ENSMUSG00000039891	15534	643	11828	883	16172	1476	12752	915
Uckl1os	ENSMUSG00000010492	61	16	21	7	56	24	31	10
Vldlr	ENSMUSG00000024924	9623	566	7598	786	10008	777	8275	415
Ybx2	ENSMUSG00000018554	158	19	86	33	158	21	98	24
Zfp612	ENSMUSG00000044676	301	27	215	18	304	9	201	39
Zyg11b	ENSMUSG00000034636	2665	223	2061	190	2682	291	2292	252

**Supplementary Table S5.** RNASeq analysis of effects of angiotensin II (AngII) on mRNA expression in hearts from PKN2Het vs WT littermates: mRNAs significantly upregulated by AngII in WT hearts.

Gene Symbol	Ensembl gene id	WT Vehicle		WT AngII		PKN2Het Vehicle		PKN2Het AngII	
		Mean	SD	Mean	SD	Mean	SD	Mean	SD
March1	ENSMUSG00000036469	56	11	114	66	64	15	90	21
1500011B03Rik	ENSMUSG00000072694	30	9	54	13	33	8	48	9
1500015O10Rik	ENSMUSG00000026051	3	2	49	80	5	3	18	14
4930503L19Rik	ENSMUSG00000044906	133	18	213	40	136	22	156	26
9930111J21Rik2	ENSMUSG00000069892	725	103	926	89	721	107	783	91
Abca9	ENSMUSG00000041797	849	55	1144	187	818	92	953	67
Abhd2	ENSMUSG00000039202	898	103	1060	61	933	139	1000	123
AC105304.1	ENSMUSG00000117110	1	2	19	19	2	2	11	8
Acp5	ENSMUSG0000001348	5	2	22	17	6	4	15	9
Actb	ENSMUSG00000029580	7471	1804	10178	1677	7763	1384	9365	1200
Actg1	ENSMUSG00000062825	6824	1047	8916	1194	7413	1015	8405	1266
Actg2	ENSMUSG00000059430	11	6	37	14	12	6	20	12
Actn4	ENSMUSG00000054808	2213	272	2742	211	2012	203	2417	171
Actr2	ENSMUSG00000020152	2099	200	2493	267	2101	71	2352	201
Adam10	ENSMUSG00000054693	1295	82	1540	84	1289	31	1416	75
Adams4	ENSMUSG0000006403	26	22	120	29	38	22	83	38
Adgra2	ENSMUSG00000031486	286	38	404	66	291	29	400	70
Adss	ENSMUSG00000015961	296	25	391	63	284	33	321	15
Aebp1	ENSMUSG00000020473	297	22	678	352	334	100	516	123
Agrn	ENSMUSG00000041936	958	125	1295	154	947	79	1136	70
Ahnak2	ENSMUSG00000072812	300	55	611	330	327	47	473	130
Aida	ENSMUSG00000042901	767	113	1024	80	877	107	902	132
Akr1b8	ENSMUSG00000029762	67	13	106	31	68	10	93	26
Akt3	ENSMUSG00000019699	651	50	856	71	640	112	760	47
Aldh1a3	ENSMUSG00000015134	25	2	51	12	25	7	49	8
Amot	ENSMUSG00000041688	452	43	612	111	514	116	652	97
Antxr1	ENSMUSG00000033420	343	48	747	479	332	36	524	184
Anxa3	ENSMUSG00000029484	637	92	881	124	558	119	714	80
Anxa4	ENSMUSG00000029994	390	35	552	99	380	26	495	39
Anxa8	ENSMUSG00000021950	10	5	45	20	13	5	25	12
Aoah	ENSMUSG00000021322	51	20	105	50	48	14	83	23
Ap2b1	ENSMUSG00000035152	1179	64	1470	164	1223	59	1427	130
Ap3s1	ENSMUSG00000024480	226	22	364	126	251	27	316	37
Apaf1	ENSMUSG00000019979	202	42	332	75	213	32	293	28
Apobec1	ENSMUSG00000040613	119	28	241	144	120	8	163	31
Apoibr	ENSMUSG00000042759	32	3	70	17	32	9	51	18
Apoll1b	ENSMUSG00000091694	7	5	34	9	17	6	37	25
App	ENSMUSG00000022892	3981	381	4939	605	3820	129	4513	126
Aqp8	ENSMUSG00000030762	83	23	156	68	106	26	182	68
Arf3	ENSMUSG00000051853	700	31	853	47	714	16	777	34
Arfip1	ENSMUSG00000074513	425	63	585	108	425	15	463	26
Arhgap23	ENSMUSG00000049807	496	48	632	37	504	37	586	47
Arhgap45	ENSMUSG00000035697	124	18	203	68	131	23	172	35
Arhgdia	ENSMUSG00000025132	2274	183	2741	90	2286	149	2537	205
Arhgef2	ENSMUSG00000028059	885	125	1137	110	951	83	1051	107
Arhgef39	ENSMUSG00000051517	7	3	25	5	7	4	18	6
Armcx2	ENSMUSG00000033436	204	22	300	52	209	17	270	18
Arpc2	ENSMUSG0000006304	2337	43	2757	185	2338	47	2652	121
Arpin	ENSMUSG00000039043	239	19	299	19	258	25	280	26
Arrb2	ENSMUSG00000060216	182	31	313	100	186	36	253	55
Arsb	ENSMUSG00000042082	304	35	427	70	298	13	358	32
Aspn	ENSMUSG00000021388	750	159	3970	5012	798	171	1825	1043
Ass1	ENSMUSG00000076441	79	24	147	71	80	5	118	24
At13	ENSMUSG00000024759	741	53	1024	135	748	50	882	82
Atp6v0a4	ENSMUSG00000038600	9	7	42	23	11	7	25	11
Atp6v1h	ENSMUSG00000033793	486	36	596	56	470	28	561	47
Atp7a	ENSMUSG00000033792	198	11	253	13	197	21	209	17
Atp9a	ENSMUSG00000027546	1025	69	1233	124	1046	42	1120	130
AW551984	ENSMUSG00000038112	5	2	17	8	7	4	17	10

B2m	ENSMUSG00000060802	4421	1037	6550	1100	4422	785	4929	246
B3galt2	ENSMUSG00000033849	372	49	542	57	383	37	471	157
B4galnt1	ENSMUSG00000006731	31	7	66	39	32	6	48	11
B4galt1	ENSMUSG00000028413	1799	176	2095	181	1836	106	2087	131
Baalc	ENSMUSG00000022296	20	5	38	10	18	4	29	7
Bax	ENSMUSG00000003873	210	31	278	16	218	17	271	24
BC037034	ENSMUSG00000036948	67	7	102	13	66	9	74	11
Bcl10	ENSMUSG00000028191	379	38	473	26	405	34	468	34
Bcl2	ENSMUSG00000057329	294	11	378	46	307	30	367	43
Bcl2a1b	ENSMUSG00000089929	18	7	68	61	17	5	44	19
Bcl3	ENSMUSG00000053175	60	35	113	24	70	15	98	24
Bcl6b	ENSMUSG00000000317	820	250	1194	317	923	223	1077	280
Bicc1	ENSMUSG00000014329	681	54	1034	279	743	66	924	94
Bin1	ENSMUSG00000024381	163	26	241	35	165	22	215	15
Bmp2k	ENSMUSG00000034663	222	15	328	62	234	20	306	14
Bora	ENSMUSG00000022070	17	4	37	7	18	8	30	4
C1qtnf3	ENSMUSG00000058914	3	2	341	632	3	2	118	157
C1qtnf5	ENSMUSG00000079592	53	6	100	38	61	17	87	20
C1qtnf7	ENSMUSG00000061535	178	26	294	78	174	31	227	32
C3ar1	ENSMUSG00000040552	234	31	502	241	242	41	380	97
Cacnb3	ENSMUSG00000003352	53	8	108	38	53	6	75	17
Calhm5	ENSMUSG00000049872	49	5	97	18	60	11	89	26
Calm2	ENSMUSG00000036438	2322	263	2921	526	2281	193	2735	103
Camk1d	ENSMUSG00000039145	125	28	197	13	146	26	154	32
Camkk1	ENSMUSG00000020785	29	5	54	12	30	5	42	7
Capn6	ENSMUSG00000067276	8	3	42	52	12	8	24	13
Casp12	ENSMUSG00000025887	208	53	318	96	186	49	260	34
Casp3	ENSMUSG00000031628	113	29	191	45	108	17	171	41
Cfbf	ENSMUSG00000031885	509	26	664	130	518	37	561	32
Ccdc88a	ENSMUSG00000032740	355	54	511	63	310	60	391	78
Ccdc88b	ENSMUSG00000047810	26	4	52	17	31	7	43	4
Ccl12	ENSMUSG00000035352	28	12	76	30	20	5	61	36
Ccr2	ENSMUSG00000049103	85	30	408	389	93	25	233	135
Ccr5	ENSMUSG00000079227	186	40	341	137	159	68	244	42
Cd180	ENSMUSG00000021624	33	12	77	31	53	18	71	11
Cd24a	ENSMUSG00000047139	79	19	145	26	90	14	161	75
Cd2ap	ENSMUSG00000061665	690	32	831	97	667	57	750	87
Cd33	ENSMUSG00000004609	150	35	242	42	149	35	189	29
Cd52	ENSMUSG0000000682	61	22	171	113	54	14	95	23
Cd53	ENSMUSG00000040747	129	18	286	154	144	34	221	59
Cd55	ENSMUSG00000026399	345	57	518	88	369	49	468	57
Cd63	ENSMUSG00000025351	1383	97	1809	371	1430	52	1693	169
Cd80	ENSMUSG00000075122	19	7	60	17	24	9	47	22
Cd83	ENSMUSG00000015396	132	30	202	45	132	31	168	13
Cd86	ENSMUSG00000022901	75	19	139	14	88	32	109	23
Cdc25b	ENSMUSG00000027330	92	22	163	19	92	22	150	40
Cdc42se1	ENSMUSG00000046722	468	71	617	41	442	53	554	68
Cdc6	ENSMUSG00000017499	18	6	40	11	16	6	33	8
Cdc7	ENSMUSG00000029283	20	3	41	10	29	11	30	8
Cdca2	ENSMUSG00000048922	13	3	38	8	27	15	36	10
Cdca4	ENSMUSG00000047832	122	18	180	26	120	24	154	24
Cdk14	ENSMUSG00000028926	200	28	273	53	192	35	226	37
Cdkn3	ENSMUSG00000037628	13	6	27	8	12	2	21	5
Cdr2	ENSMUSG00000030878	234	28	362	52	247	34	334	25
Cdr2l	ENSMUSG00000050910	97	21	164	22	96	12	136	9
Cdt1	ENSMUSG0000006585	24	1	51	16	26	8	47	12
Cemip	ENSMUSG00000052353	1	1	29	37	0	0	17	18
Cenpn	ENSMUSG00000031756	14	5	38	13	16	3	27	10
Cep192	ENSMUSG00000024542	181	30	290	42	205	41	226	32
Cercam	ENSMUSG00000039787	51	4	142	102	51	14	90	27
Cggbp1	ENSMUSG00000054604	811	96	987	62	796	114	900	95
Chaf1a	ENSMUSG0000002835	62	28	147	37	69	14	117	37
Chaf1b	ENSMUSG00000022945	12	2	37	18	18	4	36	9
Chst2	ENSMUSG00000033350	33	6	59	8	44	9	45	10
Chsy3	ENSMUSG00000058152	5	1	14	5	5	2	9	3
Cip2a	ENSMUSG00000033031	56	15	113	30	63	19	81	15
Cks1b	ENSMUSG00000028044	53	13	94	14	55	9	83	13

Clca3a1	ENSMUSG00000056025	11	2	33	21	15	8	17	9
Cldn15	ENSMUSG00000001739	49	9	95	9	66	28	67	17
Clec11a	ENSMUSG00000004473	16	2	53	48	14	4	31	14
Clec12a	ENSMUSG00000053063	76	11	211	106	102	28	134	18
Clec4a1	ENSMUSG00000049037	90	14	212	105	96	15	147	36
Clec4a2	ENSMUSG00000030148	46	12	104	63	40	6	79	23
Clec4a3	ENSMUSG00000043832	54	12	126	46	52	9	86	21
Clspn	ENSMUSG00000042489	17	7	42	12	17	3	38	23
Cnn1	ENSMUSG00000001349	37	23	130	75	42	17	53	24
Cnn2	ENSMUSG00000004665	793	93	1039	52	856	80	1002	98
Cnrip1	ENSMUSG00000044629	67	5	110	32	77	10	96	9
Cntln	ENSMUSG00000038070	189	18	279	45	181	18	235	37
Cntrl	ENSMUSG00000057110	277	35	379	18	284	40	270	21
Col11a1	ENSMUSG00000027966	2	3	52	76	2	2	12	11
Col16a1	ENSMUSG00000040690	187	39	603	471	192	60	420	186
Col1a1	ENSMUSG00000001506	1941	334	10243	9888	2115	63	5954	3420
Col1a2	ENSMUSG00000029661	2657	250	11812	10867	2786	231	7551	4300
Col4a5	ENSMUSG00000031274	763	91	1159	304	773	91	971	147
Col5a3	ENSMUSG00000004098	576	178	985	63	666	103	847	222
Col7a1	ENSMUSG00000025650	4	6	26	21	5	4	11	6
Col8a2	ENSMUSG00000056174	9	5	180	298	14	4	86	85
Col9a2	ENSMUSG00000028626	6	1	31	38	7	4	21	11
Comp	ENSMUSG00000031849	39	8	325	426	69	9	179	129
Copb1	ENSMUSG00000030754	983	86	1212	193	1045	57	1076	62
Coro1a	ENSMUSG00000030707	175	29	270	73	171	24	228	26
Coro1b	ENSMUSG00000024835	688	47	858	53	695	47	802	76
Cplx2	ENSMUSG00000025867	149	21	210	31	160	16	218	24
Cpne8	ENSMUSG00000052560	161	16	246	70	161	15	217	22
Creb3l2	ENSMUSG00000038648	1002	88	1355	234	1018	47	1231	121
Crtap	ENSMUSG00000032431	384	57	511	72	379	32	471	67
Csf2ra	ENSMUSG00000059326	56	11	101	28	65	12	82	17
Csrp1	ENSMUSG00000026421	868	80	1281	109	889	121	1075	145
Cstb	ENSMUSG00000005054	171	14	238	43	175	15	218	32
Cthrc1	ENSMUSG00000054196	3	3	221	380	5	2	92	112
Ctsk	ENSMUSG00000028111	95	23	247	204	90	21	156	59
Ctss	ENSMUSG00000038642	458	93	1279	617	459	103	843	274
Cttn	ENSMUSG00000031078	793	94	1056	113	811	56	962	95
Ctnbp2nl	ENSMUSG00000062127	644	157	873	93	653	151	770	81
Cx3cr1	ENSMUSG00000052336	153	23	369	148	170	25	253	86
Cxcl10	ENSMUSG00000034855	12	4	57	37	12	8	27	6
Cybb	ENSMUSG00000015340	327	42	648	221	360	106	406	69
Cysltr1	ENSMUSG00000052821	54	23	122	68	67	22	119	47
Cyth3	ENSMUSG00000018001	939	142	1235	98	1006	115	1159	89
Cyth4	ENSMUSG00000018008	207	45	374	116	216	29	315	54
D1Ert622e	ENSMUSG00000044768	81	14	134	22	88	9	109	16
Dap	ENSMUSG00000039168	262	38	433	140	293	35	371	55
Dbf4	ENSMUSG00000002297	39	11	81	24	39	8	63	4
Dbnl	ENSMUSG00000020476	472	46	575	30	501	31	573	37
Dck	ENSMUSG00000029366	104	18	188	15	109	4	138	16
Dhx58	ENSMUSG00000017830	37	15	76	24	54	15	63	11
Dkk3	ENSMUSG00000030772	52	16	247	258	56	20	169	78
Dnm1	ENSMUSG00000026825	162	38	244	43	172	24	214	33
Dock11	ENSMUSG00000031093	198	35	312	74	204	30	252	29
Dock7	ENSMUSG00000028556	383	56	520	72	415	36	422	61
Dok3	ENSMUSG00000035711	38	8	70	27	33	8	52	10
Dpep2	ENSMUSG00000053687	21	8	44	15	16	3	33	12
Dpp7	ENSMUSG00000026958	48	11	85	22	56	8	80	17
Dpy19l1	ENSMUSG00000043067	214	23	340	91	229	13	276	30
Dram1	ENSMUSG00000020057	109	11	158	29	104	11	139	11
Dse	ENSMUSG00000039497	182	24	294	74	230	55	247	27
Dsel	ENSMUSG00000038702	152	30	302	163	181	17	233	34
E2f2	ENSMUSG00000018983	15	9	47	2	35	28	45	12
E2f3	ENSMUSG00000016477	259	22	315	27	280	21	306	28
E2f8	ENSMUSG00000046179	31	20	49	20	32	12	50	22
Egr2	ENSMUSG00000037868	32	17	104	54	67	11	86	35
Egr3	ENSMUSG00000033730	55	46	127	33	126	43	192	110
Eif2ak2	ENSMUSG00000024079	457	54	612	78	452	48	564	48

Eif4ebp1	ENSMUSG00000031490	600	42	768	49	633	27	785	117
Elf1	ENSMUSG00000036461	427	66	547	56	479	70	499	46
Eln	ENSMUSG00000029675	512	176	2249	1534	591	55	1327	606
Enpp1	ENSMUSG00000037370	187	9	495	317	181	24	350	178
Epb4112	ENSMUSG00000019978	1216	183	1533	194	1128	76	1296	65
Epst1	ENSMUSG00000022014	40	10	90	32	45	8	66	11
Erc6l	ENSMUSG00000051220	19	8	48	17	17	6	34	13
Esm1	ENSMUSG00000042379	32	4	64	10	34	9	54	17
Etv4	ENSMUSG00000017724	8	5	29	5	8	3	26	18
Etv6	ENSMUSG00000030199	527	36	643	63	544	47	566	37
Evi2a	ENSMUSG00000078771	85	15	172	58	103	15	147	30
Evi2b	ENSMUSG00000093938	37	8	106	37	54	8	77	17
Ezh2	ENSMUSG00000029687	114	28	176	40	98	20	147	19
Fads2	ENSMUSG00000024665	75	13	108	13	83	14	97	12
Fam129a	ENSMUSG00000026483	681	70	925	196	630	59	727	64
Fam167b	ENSMUSG00000050493	7	3	20	8	8	4	17	5
Fam171b	ENSMUSG00000048388	42	7	93	55	48	6	66	20
Fam177a	ENSMUSG00000095595	702	134	843	123	776	69	888	27
Fam83d	ENSMUSG00000027654	6	3	27	7	5	2	17	9
Fam91a1	ENSMUSG00000037119	520	42	707	99	525	28	606	35
Fancd2	ENSMUSG00000034023	13	4	33	8	13	6	28	18
Fap	ENSMUSG000000000392	100	8	185	87	98	34	134	42
Farp1	ENSMUSG00000025555	294	13	417	92	304	53	390	72
Fat1	ENSMUSG00000070047	995	230	1619	361	886	123	1302	330
Fbn2	ENSMUSG00000024598	25	8	112	120	38	10	67	32
Fcer1g	ENSMUSG00000058715	141	25	259	105	135	20	195	28
Fcgr1	ENSMUSG00000015947	58	17	140	69	68	8	103	30
Fermt3	ENSMUSG00000024965	71	21	121	22	77	11	108	24
Fes	ENSMUSG00000053158	170	34	266	19	189	43	230	55
Fgd3	ENSMUSG00000037946	46	14	84	22	51	10	76	20
Fgl2	ENSMUSG00000039899	863	65	1693	575	912	106	1331	391
Fgr	ENSMUSG00000028874	10	5	30	20	9	4	17	11
Fhl1	ENSMUSG00000023092	1773	169	2590	350	1838	138	2464	537
Fibin	ENSMUSG00000074971	181	32	511	420	193	39	346	121
Flt3	ENSMUSG00000042817	2	2	16	13	4	3	8	7
Fmod	ENSMUSG00000041559	30	16	384	621	81	65	169	122
Fmr1	ENSMUSG00000000838	269	36	431	176	300	35	342	37
Fn1	ENSMUSG00000026193	1579	300	7830	6886	1494	199	4711	3367
Foxs1	ENSMUSG00000074676	34	11	64	13	46	5	62	22
Frem1	ENSMUSG00000059049	8	10	51	68	8	4	31	24
Fut11	ENSMUSG00000039357	204	20	286	68	209	19	246	19
Fxyd6	ENSMUSG00000066705	485	36	809	394	515	53	620	96
Fyb	ENSMUSG00000022148	104	44	269	144	111	29	216	57
Fzd1	ENSMUSG00000044674	164	18	259	65	173	23	223	25
G2e3	ENSMUSG00000035293	143	24	208	59	161	20	204	41
Gak	ENSMUSG00000062234	517	39	618	25	529	64	553	30
Garem2	ENSMUSG00000044576	3	3	13	9	3	2	7	4
Gas7	ENSMUSG00000033066	461	108	644	104	455	58	590	51
Gatm	ENSMUSG00000027199	79	9	129	34	80	14	103	20
Gcnt1	ENSMUSG00000038843	85	7	138	43	89	8	117	12
Gcnt4	ENSMUSG00000091387	3	2	26	31	3	1	14	10
Gem	ENSMUSG00000028214	71	22	119	13	95	18	126	28
Gen1	ENSMUSG00000051235	17	8	43	15	30	19	41	16
Gjc1	ENSMUSG00000034520	443	31	538	31	438	34	472	43
Glipr1	ENSMUSG00000056888	19	3	61	50	17	5	34	19
Gm15675	ENSMUSG00000086825	23	4	56	23	34	12	43	15
Gm1966	ENSMUSG00000073902	34	9	90	39	50	9	72	22
Gm2026	ENSMUSG00000078886	29	10	71	41	64	45	50	32
Gm20559	ENSMUSG000000106734	158	25	249	51	169	19	173	37
Gm30873	ENSMUSG000000109341	6	4	25	10	11	7	20	4
Gm36161	ENSMUSG000000114608	18	6	51	47	19	6	34	17
Gm3636	ENSMUSG00000091754	16	5	43	19	24	10	23	5
Gm39214	ENSMUSG000000109754	252	32	351	45	256	25	363	83
Gm42047	ENSMUSG000000110631	86	19	248	70	75	22	169	103
Gm45705	ENSMUSG000000110481	13	3	29	7	14	4	21	3
Gm47761	ENSMUSG000000112478	9	2	26	8	7	2	17	10
Gm49342	ENSMUSG00000021871	79	19	135	20	95	11	98	23

Gm5431	ENSMUSG00000058163	36	7	65	15	44	6	50	7
Gm6377	ENSMUSG00000048621	4	2	18	12	13	16	12	6
Gm8995	ENSMUSG00000063286	770	80	1033	133	749	121	889	142
Gmip	ENSMUSG00000036246	79	23	131	23	79	20	106	20
Gnai2	ENSMUSG00000032562	4185	325	4943	197	4287	161	4768	360
Gnai3	ENSMUSG00000000001	721	11	942	133	676	66	788	53
Gnao1	ENSMUSG00000031748	446	40	615	131	524	114	584	73
Golim4	ENSMUSG00000034109	732	55	1009	144	790	46	896	57
Gpc6	ENSMUSG00000058571	240	29	347	74	228	14	308	59
Gpnmb	ENSMUSG00000029816	23	2	58	33	25	12	38	17
Gpr176	ENSMUSG00000040133	6	3	37	26	7	1	23	18
Gpr34	ENSMUSG00000040229	63	25	126	68	77	29	101	26
Gpr39	ENSMUSG00000026343	4	2	28	20	6	3	21	14
Gpr65	ENSMUSG00000021886	44	9	108	76	42	12	70	21
Gpr68	ENSMUSG00000047415	3	3	18	4	8	2	10	7
Gpx8	ENSMUSG00000021760	491	35	682	134	493	63	644	76
Gria3	ENSMUSG0000001986	27	6	74	55	40	11	71	37
Gsap	ENSMUSG00000039934	66	8	121	24	74	13	95	10
Gxylt2	ENSMUSG00000030074	171	37	519	541	157	23	308	184
Hacd4	ENSMUSG00000028497	224	6	334	92	257	33	288	32
Has2	ENSMUSG00000022367	27	6	50	13	28	8	42	6
Haus8	ENSMUSG00000035439	242	44	381	64	261	50	360	59
Havcr2	ENSMUSG00000020399	17	6	42	21	12	4	23	11
Hbb-bt	ENSMUSG00000073940	3565	1643	6280	1861	4671	1644	8009	3238
Hck	ENSMUSG00000003283	35	10	88	47	39	12	58	8
Hdac1	ENSMUSG00000028800	455	34	557	48	447	37	529	38
Hexa	ENSMUSG00000025232	1121	111	1417	213	1139	67	1382	81
Hexb	ENSMUSG00000021665	487	58	816	323	492	50	666	110
Hjurp	ENSMUSG00000044783	577	122	775	43	589	90	674	87
Hmgb2	ENSMUSG00000054717	115	21	211	30	135	37	202	60
Hmgm3	ENSMUSG00000066456	78	20	130	43	71	15	108	14
Hpgd	ENSMUSG00000031613	182	26	300	44	240	31	258	32
Hpgds	ENSMUSG00000029919	67	16	152	74	91	33	92	21
Hspg2	ENSMUSG00000028763	12506	1017	15279	1628	12610	707	14990	1190
Iffo2	ENSMUSG00000041025	210	56	296	34	208	41	260	55
Ifi203	ENSMUSG00000039997	891	161	1230	255	880	117	940	84
Ifi209	ENSMUSG00000043263	52	15	126	69	50	17	92	45
Ifi211	ENSMUSG00000026536	185	36	351	104	178	18	256	21
Ifi30	ENSMUSG00000031838	101	27	193	76	87	20	127	31
Ifih1	ENSMUSG00000026896	299	32	446	46	329	56	378	53
Ifit1	ENSMUSG00000034459	187	43	329	102	161	24	234	21
Ifit2	ENSMUSG00000045932	547	92	934	140	539	58	669	52
Ifit3	ENSMUSG00000074896	336	93	626	210	311	45	430	29
Ifit3b	ENSMUSG00000062488	122	30	208	57	123	22	150	9
Igf1	ENSMUSG00000020053	384	78	1064	595	422	57	770	126
Igf2bp2	ENSMUSG00000033581	72	26	122	41	102	14	135	38
Igfbp2	ENSMUSG00000039323	1	1	24	20	0	1	4	4
Igfbp5	ENSMUSG00000026185	2981	305	5165	1633	3493	830	4402	921
Ighm	ENSMUSG00000076617	206	22	302	49	234	29	292	34
Igsf10	ENSMUSG00000036334	145	33	315	123	162	38	247	69
Ikzf1	ENSMUSG00000018654	64	21	119	32	75	10	86	10
Il13ra1	ENSMUSG00000017057	1206	209	1526	234	1225	65	1443	213
Il18rap	ENSMUSG00000026068	5	4	17	7	3	2	6	4
Il1b	ENSMUSG00000027398	20	8	71	68	17	7	29	8
Il21r	ENSMUSG00000030745	15	3	46	25	17	2	35	6
Ildr2	ENSMUSG00000040612	25	9	63	21	39	23	51	20
Irf5	ENSMUSG00000029771	73	13	148	22	78	12	119	35
Irf8	ENSMUSG00000041515	118	13	229	76	128	21	193	26
Isg15	ENSMUSG00000035692	59	12	120	28	67	16	93	12
Isg20	ENSMUSG00000039236	86	30	130	16	102	27	144	32
Islr	ENSMUSG00000037206	560	95	865	285	608	50	774	128
Itga4	ENSMUSG00000027009	88	24	170	60	100	20	120	28
Itgav	ENSMUSG00000027087	584	81	920	293	645	110	863	204
Itgax	ENSMUSG00000030789	14	13	49	40	11	3	41	38
Itgb1	ENSMUSG00000025809	10648	748	12926	1642	10469	431	12265	1179
Itgb2	ENSMUSG0000000290	175	40	280	60	156	29	225	46
Itgb3	ENSMUSG00000020689	55	19	135	26	74	35	101	24

Itgb8	ENSMUSG00000025321	44	17	94	45	58	14	57	7
Itgb11	ENSMUSG00000032925	238	42	795	674	281	46	513	150
Itih2	ENSMUSG00000037254	10	2	36	22	10	1	20	5
Itm2a	ENSMUSG00000031239	204	26	483	405	214	32	305	66
Kcne1	ENSMUSG00000039639	91	46	147	42	92	14	127	27
Kctd10	ENSMUSG00000001098	1166	95	1425	67	1193	154	1325	119
Kctd12	ENSMUSG00000098557	889	110	1244	276	915	43	1073	34
Kctd12b	ENSMUSG00000041633	620	130	959	330	830	137	891	240
Kctd15	ENSMUSG00000030499	38	5	65	13	39	8	54	12
Kdelr3	ENSMUSG00000010830	122	17	231	83	128	25	188	48
Kif18a	ENSMUSG00000027115	33	7	55	18	33	3	53	12
Kif20b	ENSMUSG00000024795	44	17	104	56	35	19	80	25
Kirrel	ENSMUSG00000041734	354	32	515	106	351	32	432	45
Klhl29	ENSMUSG00000020627	12	4	36	26	16	6	21	5
Krt18	ENSMUSG00000023043	11	4	41	28	17	8	20	7
Lacc1	ENSMUSG00000044350	110	10	170	40	111	18	129	16
Lair1	ENSMUSG00000055541	93	25	193	59	88	18	152	37
Lbp	ENSMUSG00000016024	114	14	211	51	141	27	174	37
Ldlrad4	ENSMUSG00000024544	207	23	293	57	198	24	230	26
Lhfp	ENSMUSG00000048332	883	63	1348	372	958	40	1113	122
Lilrb4a	ENSMUSG000000112148	184	42	406	123	195	44	266	91
Lix11	ENSMUSG00000049288	862	45	1020	63	903	22	948	26
Lmna	ENSMUSG00000028063	1287	73	1552	83	1330	102	1508	161
Lmnb1	ENSMUSG00000024590	122	21	210	37	129	15	185	47
Lox	ENSMUSG00000024529	89	9	1050	1321	94	21	476	436
Loxl3	ENSMUSG00000000693	104	36	311	233	87	12	196	70
Lpcat2	ENSMUSG00000033192	36	10	94	53	31	6	64	11
Lpp	ENSMUSG00000033306	1398	218	1794	95	1378	115	1689	226
Lpxn	ENSMUSG00000024696	18	5	55	29	22	7	34	9
Lrmp	ENSMUSG00000030263	36	7	68	14	45	10	53	5
Lrrc32	ENSMUSG00000090958	328	91	455	36	361	64	432	52
Lrrc59	ENSMUSG00000020869	766	27	883	28	772	44	888	71
Lsp1	ENSMUSG00000018819	614	136	984	350	600	112	808	176
Lst1	ENSMUSG00000073412	16	5	43	19	20	5	34	7
Ltbp2	ENSMUSG00000002020	94	45	964	1120	126	62	578	514
Ltbp3	ENSMUSG00000024940	530	28	924	412	618	50	772	112
Lum	ENSMUSG00000036446	1447	238	3824	2686	1553	192	2795	564
Lxn	ENSMUSG00000047557	65	9	139	25	70	19	104	26
Lyl1	ENSMUSG00000034041	75	11	111	12	85	3	91	4
Maf	ENSMUSG00000055435	389	56	552	118	424	20	460	80
Maff	ENSMUSG00000042622	133	18	220	64	128	36	187	43
Malt1	ENSMUSG00000032688	196	29	270	27	193	17	212	27
Mapre1	ENSMUSG00000027479	1639	151	1876	92	1651	91	1859	64
Marcks	ENSMUSG00000069662	819	115	1485	784	999	154	1070	121
Mastl	ENSMUSG00000026779	21	19	58	17	22	7	58	28
Matn2	ENSMUSG00000022324	417	57	667	192	429	35	559	39
Mcm5	ENSMUSG00000005410	84	12	162	45	83	19	169	35
Mcm6	ENSMUSG00000026355	230	32	397	77	216	18	363	70
Mcub	ENSMUSG00000027994	41	14	77	15	37	4	50	10
Mdk	ENSMUSG00000027239	26	4	95	130	24	6	43	34
Meg3	ENSMUSG00000021268	123	46	231	107	121	17	140	38
Megf10	ENSMUSG00000024593	19	6	49	31	30	3	40	15
Mex3c	ENSMUSG00000037253	486	50	607	52	503	15	557	37
Mfap2	ENSMUSG00000060572	20	2	69	61	23	4	41	14
Mfap3	ENSMUSG00000020522	454	25	541	33	431	20	503	22
Mgam	ENSMUSG00000068587	9	4	32	24	15	4	30	21
Mgat2	ENSMUSG00000043998	423	27	547	64	443	34	503	31
Mgp	ENSMUSG00000030218	1671	257	3299	1832	1627	149	2424	267
Mirr1	ENSMUSG00000040528	16	6	43	18	16	4	35	10
Mis18a	ENSMUSG00000022978	46	8	79	17	61	14	68	8
Mkrn1	ENSMUSG00000029922	598	102	779	95	681	119	829	128
Mmp14	ENSMUSG00000000957	291	39	862	471	332	50	582	198
Mmp16	ENSMUSG00000028226	14	6	34	13	18	6	22	9
Mns1	ENSMUSG00000032221	9	2	49	8	14	7	28	16
Mob1a	ENSMUSG00000043131	1089	121	1399	155	1053	73	1248	99
Mpeg1	ENSMUSG00000046805	387	93	1323	966	395	77	809	361
Mpz11	ENSMUSG00000026566	252	38	353	54	258	43	287	41

Mrc2	ENSMUSG00000020695	462	41	913	394	473	31	716	159
Ms4a14	ENSMUSG00000099398	18	2	74	52	16	6	34	17
Ms4a4b	ENSMUSG00000056290	4	2	18	15	8	4	9	4
Ms4a4c	ENSMUSG00000024675	8	4	38	33	10	3	16	8
Ms4a6d	ENSMUSG00000024679	61	21	136	54	54	15	109	45
Ms4a7	ENSMUSG00000024672	65	11	296	303	51	5	166	95
Mtfr2	ENSMUSG00000019992	4	2	15	5	3	1	10	2
Mthfd2	ENSMUSG00000005667	41	11	81	14	49	16	81	18
Mtmr11	ENSMUSG00000045934	69	26	114	28	68	30	107	32
Mtpn	ENSMUSG00000029840	1161	76	1505	277	1222	89	1380	115
Mx1	ENSMUSG00000000386	20	10	55	32	17	6	22	11
Mxra8	ENSMUSG00000029070	431	61	782	329	511	145	714	119
Myc	ENSMUSG00000022346	48	8	98	19	58	7	95	39
Myef2	ENSMUSG00000027201	185	24	262	27	174	6	207	19
Myh7	ENSMUSG00000053093	1672	510	20844	27743	2490	1006	11438	8811
Myh9	ENSMUSG00000022443	4467	917	6229	813	4465	679	5733	609
Myl9	ENSMUSG00000067818	507	113	744	105	504	152	536	41
Myo1e	ENSMUSG00000032220	382	52	541	82	377	40	487	59
Myo1g	ENSMUSG00000020437	50	9	89	21	55	12	90	33
Myo5a	ENSMUSG00000034593	359	55	615	165	371	102	518	152
Naalad2	ENSMUSG00000043943	352	43	575	192	346	54	447	64
Nab2	ENSMUSG00000025402	178	29	277	77	177	31	248	30
Nav1	ENSMUSG00000009418	1498	290	1893	171	1457	90	1737	179
Ncapd2	ENSMUSG00000038252	298	45	437	112	363	44	394	55
Nedd9	ENSMUSG00000021365	728	336	1059	86	794	203	936	202
Neil3	ENSMUSG00000039396	10	3	35	11	13	11	23	8
Neurl3	ENSMUSG00000047180	159	33	303	74	176	25	246	35
Nfam1	ENSMUSG00000058099	110	22	202	30	118	21	160	20
Nfkbie	ENSMUSG00000023947	37	6	81	15	38	5	56	8
Nfkbiz	ENSMUSG00000035356	92	25	164	59	103	9	151	32
Nhsl2	ENSMUSG00000079481	276	31	399	49	272	39	339	24
Nkd1	ENSMUSG00000031661	22	8	42	10	25	6	30	7
Nlgn2	ENSMUSG00000051790	167	30	260	63	167	33	228	39
Nmrk2	ENSMUSG00000004939	73	9	158	71	68	15	132	76
Nmt2	ENSMUSG00000026643	286	28	378	59	277	25	339	48
Nnmt	ENSMUSG00000032271	42	5	88	24	47	10	60	8
Nox4	ENSMUSG00000030562	31	5	162	173	29	9	64	30
Npdc1	ENSMUSG00000015094	238	45	344	63	227	27	280	28
Npl	ENSMUSG00000042684	26	8	47	8	28	8	51	12
Npnt	ENSMUSG00000040998	22	7	57	25	31	14	28	9
Nptxr	ENSMUSG00000022421	69	12	105	10	64	14	94	14
Nrep	ENSMUSG00000042834	535	52	997	503	559	60	711	91
Nrros	ENSMUSG00000052384	157	25	231	32	162	27	220	28
Nts	ENSMUSG00000019890	21	8	42	6	25	4	33	13
Nucb2	ENSMUSG00000030659	137	19	239	55	144	20	174	24
Nupr1	ENSMUSG00000030717	60	10	196	120	74	8	130	33
Nusap1	ENSMUSG00000027306	48	17	132	40	45	9	116	36
Nxpe4	ENSMUSG00000044229	315	33	430	45	320	35	379	48
Nxpe5	ENSMUSG00000047592	11	6	35	8	9	4	28	15
Oas1a	ENSMUSG00000052776	82	18	149	24	88	14	121	8
Oas3	ENSMUSG00000032661	6	1	34	18	9	3	18	9
Oasl1	ENSMUSG00000041827	32	9	56	13	38	7	48	5
Oasl2	ENSMUSG00000029561	269	62	498	109	332	69	402	43
Olfr558	ENSMUSG00000070423	167	26	236	25	154	13	204	33
Olfr56	ENSMUSG00000040328	6	3	19	7	8	2	10	5
Omd	ENSMUSG00000048368	16	4	58	62	32	17	29	10
Otulinl	ENSMUSG00000056069	53	9	133	67	61	15	119	66
P2rx7	ENSMUSG00000029468	140	30	223	46	141	24	188	49
P3h1	ENSMUSG00000028641	217	25	313	43	242	18	308	55
P4ha3	ENSMUSG00000051048	2	2	23	32	1	1	11	10
Pak1	ENSMUSG00000030774	34	10	89	41	49	20	57	18
Panx1	ENSMUSG00000031934	35	11	98	49	42	21	76	30
Parp9	ENSMUSG00000022906	467	40	651	71	484	24	548	44
Parpbp	ENSMUSG00000035365	8	4	24	9	7	2	18	11
Pcdh17	ENSMUSG00000035566	299	64	458	76	316	37	426	89
Pcsk5	ENSMUSG00000024713	67	10	129	24	84	4	119	16
Pdgfrl	ENSMUSG00000031595	48	13	182	194	44	4	108	62

Pdk3	ENSMUSG00000035232	44	14	83	17	53	21	69	7
Pdlim2	ENSMUSG00000022090	106	9	175	59	121	17	153	29
Pdlim3	ENSMUSG00000031636	187	22	301	87	190	20	249	48
Pdpn	ENSMUSG00000028583	91	16	188	37	105	17	159	30
Pgm2	ENSMUSG00000029171	116	24	174	30	127	15	159	19
Phf11b	ENSMUSG00000091649	41	10	91	36	39	9	65	19
Phldb2	ENSMUSG00000033149	633	66	824	141	626	28	795	54
Pi15	ENSMUSG00000067780	74	15	180	121	89	17	105	28
Piezo1	ENSMUSG00000014444	764	311	1009	184	762	82	868	67
Piezo2	ENSMUSG00000041482	24	11	103	100	27	10	60	26
Pif1	ENSMUSG00000041064	7	7	20	9	7	4	13	5
Pik3ap1	ENSMUSG00000025017	55	12	132	58	64	10	102	14
Pik3c2a	ENSMUSG00000030660	644	90	821	49	571	41	614	49
Pik3cd	ENSMUSG00000039936	104	25	184	49	123	16	148	46
Pik3cg	ENSMUSG00000020573	96	11	139	24	110	14	125	19
Pik3r5	ENSMUSG00000020901	24	7	70	31	28	9	52	21
Pkd2	ENSMUSG00000034462	934	68	1341	308	928	43	1049	85
Pkhd111	ENSMUSG00000038725	113	45	211	84	195	90	172	61
Pkn3	ENSMUSG00000026785	143	28	220	23	138	15	195	21
Plac8	ENSMUSG00000029322	10	2	54	49	9	5	21	10
Plau	ENSMUSG00000021822	120	25	172	15	122	29	160	33
Plaur	ENSMUSG00000046223	36	7	71	21	37	23	64	15
Pld4	ENSMUSG00000052160	158	21	294	102	174	44	228	58
Plekha4	ENSMUSG00000040428	34	16	87	40	51	13	73	38
Plk1	ENSMUSG00000030867	19	10	48	16	17	7	40	14
Plk4	ENSMUSG00000025758	70	9	110	26	68	16	112	44
Plod3	ENSMUSG00000004846	475	118	658	87	472	51	605	62
Plp2	ENSMUSG00000031146	570	31	793	128	592	14	724	133
Plpp1	ENSMUSG00000021759	1000	50	1160	56	1013	21	1087	43
Pldc2	ENSMUSG00000026748	599	71	840	221	565	51	696	96
Pou2f2	ENSMUSG00000008496	37	5	109	53	61	19	105	35
Ppf1a1	ENSMUSG00000037519	773	148	999	166	867	163	931	191
Ppfibp1	ENSMUSG00000016487	1707	135	2004	276	1903	142	1868	195
Ppib	ENSMUSG00000032383	1085	51	1440	242	1046	78	1281	107
Ppp1r15b	ENSMUSG00000046062	750	74	889	76	775	49	880	44
Ppp1r18	ENSMUSG00000034595	415	70	651	61	435	37	557	57
Pqlc3	ENSMUSG00000045679	95	9	171	87	101	15	126	18
Prelp	ENSMUSG00000041577	1273	232	1575	178	1325	81	1511	142
Prex1	ENSMUSG00000039621	261	20	427	60	278	27	341	38
Prim1	ENSMUSG00000025395	42	9	75	26	45	8	65	14
Prkcd	ENSMUSG00000021948	246	36	398	115	245	27	325	36
Prr51	ENSMUSG00000032841	24	3	49	21	25	8	44	16
Prrt4	ENSMUSG00000079654	41	13	75	15	44	3	68	12
Prss23	ENSMUSG00000039405	314	52	488	126	314	35	361	78
Pstpip1	ENSMUSG00000032322	21	5	54	31	21	3	37	15
Ptafr	ENSMUSG00000056529	107	31	167	16	115	20	154	29
Ptbp1	ENSMUSG00000006498	741	116	1045	159	740	51	886	127
Pthlh	ENSMUSG00000048776	10	3	24	10	10	4	20	5
Ptk2b	ENSMUSG00000059456	161	11	248	52	179	24	246	35
Ptk7	ENSMUSG00000023972	64	11	121	51	79	10	101	16
Ptms	ENSMUSG00000030122	1096	180	1556	255	1175	69	1354	123
Ptn	ENSMUSG00000029838	35	10	527	950	47	13	109	85
Ptpn1	ENSMUSG00000027540	383	52	516	71	406	46	484	90
Ptpn12	ENSMUSG00000028771	720	48	925	82	719	64	779	35
Ptpn18	ENSMUSG00000026126	35	12	64	9	54	15	62	12
Ptpn6	ENSMUSG0000004266	114	27	202	70	107	24	164	25
Ptprc	ENSMUSG00000026395	246	49	533	285	234	45	382	129
Ptpre	ENSMUSG00000041836	163	23	260	20	183	21	214	24
Ptprf	ENSMUSG00000033295	111	21	196	66	107	19	177	20
Rab23	ENSMUSG0000004768	193	52	284	32	226	32	252	58
Rab32	ENSMUSG00000019832	40	12	85	42	46	3	70	12
Rab3i11	ENSMUSG00000024663	211	18	296	51	216	26	283	32
Rab5c	ENSMUSG00000019173	838	81	1059	21	918	29	1032	128
Rab8b	ENSMUSG00000036943	406	32	589	93	439	43	531	48
Rad50	ENSMUSG00000020380	310	33	381	31	339	21	385	26
Rai14	ENSMUSG00000022246	173	18	300	114	173	15	241	57
Rap1b	ENSMUSG00000052681	1590	124	2099	385	1642	155	1892	156

Rasa4	ENSMUSG0000004952	143	26	261	113	138	14	162	33
Rbbp8	ENSMUSG0000041238	177	8	233	32	161	22	196	17
Rbm3	ENSMUSG0000031167	1065	243	1408	328	1097	137	1294	160
Rbp1	ENSMUSG0000046402	203	16	395	267	185	21	311	56
Reps2	ENSMUSG0000040855	67	11	117	35	105	41	101	23
Rflnb	ENSMUSG0000020846	1333	290	1883	230	1446	172	1704	352
Rfx7	ENSMUSG0000037674	332	31	421	33	374	29	376	17
Rgs10	ENSMUSG0000030844	114	9	181	62	108	10	146	24
Rhoa	ENSMUSG0000007815	4789	93	5216	118	4862	194	5112	92
Rhod	ENSMUSG0000041845	59	10	92	15	68	16	66	10
Rhoj	ENSMUSG0000046768	564	95	704	75	573	74	656	48
Rhou	ENSMUSG0000039960	110	28	173	59	135	9	173	41
Rnase6	ENSMUSG0000021880	9	5	29	15	13	7	14	2
Robo1	ENSMUSG0000022883	56	11	110	44	68	14	97	13
Rpl10-ps3	ENSMUSG0000058443	1037	413	1554	348	1563	299	1415	424
Rpl3	ENSMUSG0000060036	3377	296	4471	607	3263	335	4320	344
Rps6ka1	ENSMUSG0000003644	155	10	219	28	140	11	177	26
Rtn4	ENSMUSG0000020458	1597	115	2738	963	1691	68	2291	384
Rtp4	ENSMUSG0000033355	158	33	260	39	177	33	212	32
Runx1	ENSMUSG0000022952	63	29	176	93	54	10	115	46
S1pr2	ENSMUSG0000043895	122	33	225	28	161	13	210	36
Samd14	ENSMUSG0000047181	37	7	72	30	41	5	56	15
Samsn1	ENSMUSG0000022876	14	3	34	12	17	4	26	8
Sat1	ENSMUSG0000025283	655	35	1037	357	699	101	854	124
Sbno2	ENSMUSG0000035673	285	44	452	89	290	31	409	72
Scara3	ENSMUSG0000034463	56	13	114	45	58	2	87	26
Scd2	ENSMUSG0000025203	637	102	838	65	763	157	803	46
Scn1b	ENSMUSG0000019194	235	13	365	140	268	19	330	60
Sc pep1	ENSMUSG0000000278	287	48	480	174	308	44	404	65
Scrn1	ENSMUSG0000019124	212	35	302	33	202	45	226	61
Scube3	ENSMUSG0000038677	5	4	20	12	8	3	16	11
Sdc1	ENSMUSG0000020592	116	15	220	98	124	18	164	39
Sdcbp	ENSMUSG0000028249	2167	214	2679	438	2118	92	2530	189
Sdk1	ENSMUSG0000039683	24	3	57	13	40	21	57	22
Sec16b	ENSMUSG0000026589	57	7	120	43	63	10	73	13
Sele	ENSMUSG0000026582	35	8	70	23	43	4	63	17
Selplg	ENSMUSG0000048163	63	15	127	38	67	10	99	16
Sema6d	ENSMUSG0000027200	1026	136	1377	210	1090	137	1238	97
Serp1	ENSMUSG0000027808	586	74	881	294	591	79	738	92
Serpina3g	ENSMUSG0000041481	9	5	29	16	12	5	21	10
Serpina3i	ENSMUSG0000079014	3	2	17	15	2	2	10	8
Serpina3n	ENSMUSG0000021091	176	100	698	430	134	41	495	374
Serpina1a	ENSMUSG0000044734	77	13	216	200	93	25	137	59
Serpine1	ENSMUSG0000037411	794	250	1688	848	832	284	1309	495
Serpine2	ENSMUSG0000026249	478	38	814	242	497	57	623	60
Serpine1	ENSMUSG0000023224	1822	273	2473	457	1827	186	2279	296
Sertad4	ENSMUSG0000016262	105	17	221	144	112	18	169	32
Sfrp1	ENSMUSG0000031548	345	30	981	861	365	40	683	270
Sfrp2	ENSMUSG0000027996	43	4	313	445	47	8	154	132
Sfxn3	ENSMUSG0000025212	216	19	310	29	224	5	272	31
Sgce	ENSMUSG0000004631	294	28	387	53	287	38	342	18
Sh3bgrl	ENSMUSG0000031246	918	89	1283	246	887	122	1015	78
Shc2	ENSMUSG0000020312	50	9	88	30	52	6	71	5
Shcbp1	ENSMUSG0000022322	19	11	66	49	19	6	42	16
Shisa4	ENSMUSG0000041889	45	8	85	28	49	10	83	18
Shisa5	ENSMUSG0000025647	705	100	1028	56	749	29	862	118
Shtn1	ENSMUSG0000041362	111	11	174	21	133	10	158	33
Siglece	ENSMUSG0000030474	31	11	61	22	29	7	49	8
Sirpa	ENSMUSG0000037902	816	78	1138	211	857	29	986	159
Ska1	ENSMUSG0000036223	3	3	16	11	2	2	11	8
Ska3	ENSMUSG0000021965	7	5	20	4	7	1	19	6
Skil	ENSMUSG0000027660	581	92	881	203	556	78	727	130
Skp2	ENSMUSG0000054115	26	2	53	9	32	9	43	12
Sla	ENSMUSG0000022372	69	14	123	46	60	7	74	15
Slamf7	ENSMUSG0000038179	16	7	59	44	20	9	31	22
Slbp	ENSMUSG0000004642	270	27	364	58	264	33	311	22
Slc15a3	ENSMUSG0000024737	89	19	150	23	90	18	130	28

Slc20a1	ENSMUSG00000027397	373	83	570	141	383	75	430	73
Slc25a24	ENSMUSG00000040322	184	16	278	63	197	22	246	35
Slc25a45	ENSMUSG00000024818	85	11	134	30	87	26	111	13
Slc39a6	ENSMUSG00000024270	135	18	213	64	147	13	187	32
Slc7a8	ENSMUSG00000022180	85	8	120	20	95	6	114	11
Slc9a1	ENSMUSG00000028854	394	28	509	56	454	36	435	54
Slc9a9	ENSMUSG00000031129	122	18	169	14	122	7	161	18
Slco2a1	ENSMUSG00000032548	79	12	158	76	109	32	151	52
Slfn1	ENSMUSG00000078763	6	3	30	22	7	4	14	5
Slfn4	ENSMUSG00000000204	4	3	37	45	3	3	7	6
Slfn8	ENSMUSG00000035208	92	15	162	48	81	9	133	41
Smc4	ENSMUSG00000034349	507	95	871	221	482	64	678	208
Smg1	ENSMUSG00000030655	1722	260	2176	77	1762	176	1909	93
Snhg18	ENSMUSG00000096956	105	9	186	61	111	26	157	23
Snx18	ENSMUSG00000042364	553	47	696	92	562	61	610	52
Snx20	ENSMUSG00000031662	19	11	47	15	23	2	34	9
Snx5	ENSMUSG00000027423	1439	125	1707	156	1541	86	1646	122
Soat1	ENSMUSG00000026600	139	29	253	90	127	33	216	79
Sp3	ENSMUSG00000027109	1028	55	1219	141	1088	81	1139	66
Spi1	ENSMUSG0000002111	75	11	144	49	95	22	131	8
Spidr	ENSMUSG00000041974	67	16	111	18	68	12	82	12
Spin4	ENSMUSG00000071722	30	7	51	5	34	7	38	7
Spn	ENSMUSG00000051457	31	12	75	26	34	10	54	21
Spp1	ENSMUSG00000029304	7	3	219	250	5	2	107	189
Spred1	ENSMUSG00000027351	771	71	991	172	810	79	960	76
Sprr2a2	ENSMUSG00000068893	5	4	45	45	7	3	19	6
Spty2d1	ENSMUSG00000049516	303	36	432	55	340	21	357	39
Sqle	ENSMUSG00000022351	22	13	44	9	32	12	32	12
Srgap1	ENSMUSG00000020121	122	17	179	21	119	24	155	30
Ssh1	ENSMUSG00000042121	389	56	482	27	429	54	403	41
St14	ENSMUSG00000031995	4	1	21	10	6	4	18	19
Star	ENSMUSG00000031574	18	11	140	152	32	27	93	89
Stk26	ENSMUSG00000031112	14	4	39	26	33	20	26	15
Stk32c	ENSMUSG00000015981	20	5	41	5	22	5	29	4
Stt3a	ENSMUSG00000032116	850	44	1211	182	933	75	948	77
Stxbp2	ENSMUSG00000004626	39	12	87	17	33	5	50	10
Sulf2	ENSMUSG00000006800	1067	166	1425	253	1164	107	1386	119
Susd2	ENSMUSG0000006342	39	13	86	24	45	10	49	10
Susd5	ENSMUSG00000086596	20	9	62	31	26	9	31	13
Synpo	ENSMUSG00000043079	2231	119	2747	352	2295	170	2766	301
Syt12	ENSMUSG00000049303	54	21	128	28	50	24	89	45
Tagln	ENSMUSG00000032085	483	160	931	216	458	122	542	128
Taok3	ENSMUSG00000061288	238	28	320	48	253	36	307	26
Tbp11	ENSMUSG00000071359	277	18	347	9	269	16	294	34
Tbx15	ENSMUSG00000027868	14	5	36	21	18	11	36	10
Tbxas1	ENSMUSG00000029925	62	14	104	27	75	23	89	12
Tcaf1	ENSMUSG00000036667	298	59	423	88	292	16	368	39
Tceal9	ENSMUSG00000042712	276	42	454	184	290	28	356	21
Tcirg1	ENSMUSG0000001750	143	21	252	50	181	41	211	53
Tent5a	ENSMUSG00000032265	352	77	521	110	348	40	469	106
Tent5c	ENSMUSG00000044468	180	62	415	151	316	121	530	280
Tep1	ENSMUSG00000006281	281	10	425	52	275	19	343	44
Tgfb1i1	ENSMUSG00000030782	331	73	487	33	326	41	417	38
Tgfb3	ENSMUSG00000021253	358	51	819	586	360	30	577	163
Tgfbr1	ENSMUSG00000007613	473	61	783	295	536	62	608	144
Tgfbr2	ENSMUSG00000032440	1323	221	1904	229	1360	84	1637	48
Tgif2	ENSMUSG00000062175	15	4	33	9	22	11	27	10
Themis2	ENSMUSG00000037731	94	14	167	25	103	12	120	24
Thoc1	ENSMUSG00000024287	393	27	507	81	425	40	457	36
Tifab	ENSMUSG00000049625	51	11	93	26	49	6	72	19
Tlr1	ENSMUSG00000044827	25	12	79	59	23	4	49	22
Tlr2	ENSMUSG00000027995	103	10	196	69	107	15	152	23
Tlr6	ENSMUSG00000051498	15	4	36	10	18	9	18	10
Tlr7	ENSMUSG00000044583	100	10	218	51	119	44	182	57
Tm6sf1	ENSMUSG00000038623	189	36	283	38	193	35	228	22
Tmem119	ENSMUSG00000054675	65	21	180	126	65	6	118	38
Tmem132a	ENSMUSG00000024736	173	25	238	29	190	15	225	33

Tmem165	ENSMUSG00000029234	367	42	504	119	398	39	467	29
Tmem184c	ENSMUSG00000031617	277	31	380	62	313	36	352	23
Tmem198b	ENSMUSG00000047090	101	18	156	32	99	12	129	16
Tmem273	ENSMUSG00000041707	12	5	33	15	17	6	24	6
Tmem45a	ENSMUSG00000022754	60	25	158	66	68	11	112	16
Tmem51	ENSMUSG00000040616	54	4	82	7	68	8	69	12
Tnfrsf1b	ENSMUSG00000028599	240	51	378	73	263	41	340	52
Tnnt3	ENSMUSG00000061723	6	2	29	39	5	3	17	17
Tns3	ENSMUSG00000020422	616	54	885	194	633	54	721	71
Tor3a	ENSMUSG00000060519	274	45	395	49	295	22	340	25
Tram2	ENSMUSG00000041779	231	36	333	42	225	59	272	55
Trf	ENSMUSG00000032554	860	217	1129	103	862	83	1027	78
Trim30a	ENSMUSG00000030921	325	27	481	93	321	43	427	50
Trip13	ENSMUSG00000021569	9	5	30	12	10	2	26	8
Trp53i11	ENSMUSG00000068735	646	173	926	105	688	75	760	211
Tshz3	ENSMUSG00000021217	83	14	129	7	86	15	111	16
Tsku	ENSMUSG00000049580	67	12	104	26	53	7	91	27
Tspan18	ENSMUSG00000027217	290	49	403	41	317	28	366	89
Tspo	ENSMUSG00000041736	297	21	484	201	308	28	397	63
Ttyh3	ENSMUSG00000036565	273	38	397	63	320	15	336	32
Tubb2b	ENSMUSG00000045136	49	15	127	28	62	34	105	43
Txndc5	ENSMUSG00000038991	889	51	1133	196	889	39	1068	85
Ube2l6	ENSMUSG00000027078	317	72	521	98	342	63	524	145
Uchl1	ENSMUSG00000029223	115	13	232	135	124	16	194	68
Ugdh	ENSMUSG00000029201	332	33	438	36	370	92	419	88
Upp1	ENSMUSG00000020407	78	13	127	37	87	15	115	29
Usp18	ENSMUSG00000030107	82	19	133	27	74	13	106	20
Usp6nl	ENSMUSG00000039046	217	31	297	27	260	46	269	17
Vash1	ENSMUSG00000021256	340	36	487	83	322	15	460	115
Vasn	ENSMUSG00000039646	131	17	195	17	135	19	160	13
Vasp	ENSMUSG00000030403	602	62	764	80	624	92	708	80
Vgll3	ENSMUSG00000091243	127	49	249	84	167	31	215	72
Vsir	ENSMUSG00000020101	544	130	797	85	643	20	694	88
Was	ENSMUSG00000031165	34	9	71	17	40	6	48	12
Wipf1	ENSMUSG00000075284	572	54	783	47	562	70	635	43
Wisp1	ENSMUSG00000005124	27	8	174	241	30	12	82	66
Wnt9b	ENSMUSG00000018486	9	5	34	16	8	4	21	10
Wsb1	ENSMUSG00000017677	413	65	588	117	430	59	499	86
Wwtr1	ENSMUSG00000027803	1788	70	2201	189	1899	86	2118	63
Xaf1	ENSMUSG00000040483	194	44	280	32	185	32	215	10
Xcr1	ENSMUSG00000060509	4	4	16	13	3	2	5	4
Yes1	ENSMUSG00000014932	493	48	631	79	517	38	549	53
Yipf5	ENSMUSG00000024487	306	19	418	92	321	20	373	55
Ywhaq	ENSMUSG00000076432	1324	72	1556	97	1256	62	1410	136
Zbp1	ENSMUSG00000027514	37	19	92	33	37	4	63	13
Zdhhc20	ENSMUSG00000021969	297	35	512	168	404	125	438	107
Zfas1	ENSMUSG00000074578	115	9	200	96	116	17	147	30
Zfp185	ENSMUSG00000031351	15	3	69	100	28	22	34	12
Zfp3612	ENSMUSG00000045817	834	75	1082	70	960	66	1042	116
Zfp385b	ENSMUSG00000027016	105	21	153	38	106	21	148	29
Zfp948	ENSMUSG00000067931	153	16	226	55	139	21	197	20
Zmat3	ENSMUSG00000027663	267	23	355	37	287	4	337	50

**Supplementary Table S6.** RNASeq analysis of effects of angiotensin II (AngII) on mRNA expression in hearts from PKN2Het vs WT littermates: mRNAs significantly downregulated by AngII in WT hearts.

Gene Symbol	Ensembl gene id	WT Vehicle		WT AngII		PKN2Het Vehicle		PKN2Het AngII	
		Mean	SD	Mean	SD	Mean	SD	Mean	SD
0610040J01Rik	ENSMUSG00000060512	86	12	50	19	78	10	62	9
1600014C10Rik	ENSMUSG00000054676	741	15	595	54	669	41	652	77
1700123M08Rik	ENSMUSG00000085614	65	5	40	9	59	6	47	7
2010001K21Rik	ENSMUSG00000051606	55	21	18	7	54	24	32	15
2310015K22Rik	ENSMUSG00000101257	17	5	5	2	14	3	6	4
2700097O09Rik	ENSMUSG00000062198	195	23	141	15	172	25	159	20
2900097C17Rik	ENSMUSG00000102869	6799	384	5461	338	6885	478	6050	659
5830417I10Rik	ENSMUSG00000078684	1015	96	743	87	964	152	776	61
A330023F24Rik	ENSMUSG00000096929	201	38	119	33	138	27	115	44
Abcb10	ENSMUSG00000031974	999	42	743	124	1019	76	871	93
Abcb8	ENSMUSG00000028973	1023	86	729	145	1062	134	871	63
Abcd3	ENSMUSG00000028127	2749	274	2096	283	2698	193	2334	334
Abhd10	ENSMUSG00000033157	265	34	203	14	258	14	237	14
AC131339.2	ENSMUSG00000116656	8254	1201	5715	1421	7792	541	6468	972
Acaa2	ENSMUSG00000036880	13252	1380	8259	2391	12324	1059	9258	1215
Acacb	ENSMUSG00000042010	7443	571	5153	1077	7777	973	6190	276
Acad12	ENSMUSG00000042647	1869	179	1262	208	1828	141	1493	156
Acad8	ENSMUSG00000031969	768	60	549	63	690	83	672	41
Acadm	ENSMUSG00000062908	23340	1838	16479	3425	22611	922	17864	1871
Acads	ENSMUSG00000029545	2580	67	1841	326	2630	310	2033	223
Acadsb	ENSMUSG00000030861	2976	193	2400	192	2851	242	2623	299
Acadv1	ENSMUSG00000018574	16703	1281	11802	3040	16035	839	13194	640
Acat1	ENSMUSG00000032047	11595	1306	8601	2045	11394	1310	9863	770
Aco2	ENSMUSG00000022477	41047	2512	30674	4778	41075	2487	35785	2269
Acot2	ENSMUSG00000021226	1314	144	912	240	1349	225	975	53
Acot7	ENSMUSG00000028937	819	45	640	57	804	63	691	52
Acox1	ENSMUSG00000020777	5964	375	4807	434	5983	629	5289	513
Acp6	ENSMUSG00000028093	375	19	285	28	360	30	302	31
Acsl1	ENSMUSG00000018796	21401	1598	15516	3710	21505	1628	18159	1993
Acsl6	ENSMUSG00000020333	322	47	199	38	318	50	264	61
Acsm5	ENSMUSG00000030972	83	17	31	11	61	9	36	8
Acy3	ENSMUSG00000024866	300	15	192	35	310	25	238	34
Adams7	ENSMUSG00000032363	320	21	222	35	323	29	246	59
Adck1	ENSMUSG00000021044	486	19	381	49	484	24	447	35
Adcy1	ENSMUSG00000020431	128	33	66	23	142	11	108	33
Adhfe1	ENSMUSG00000025911	1463	160	926	241	1480	91	1152	46
Adipor2	ENSMUSG00000030168	2471	47	2151	151	2493	164	2345	116
Adra1b	ENSMUSG00000050541	489	73	272	64	473	98	320	63
Afg11	ENSMUSG00000038302	1113	135	844	176	1027	95	958	51
Afg3l1	ENSMUSG00000031967	1302	67	991	162	1222	123	1128	81
Afg3l2	ENSMUSG00000024527	3400	269	2686	386	3367	188	3160	98
Agl	ENSMUSG00000033400	6620	574	5262	429	6615	587	5784	471
Agtpbp1	ENSMUSG00000021557	3401	239	2676	267	3243	152	2747	370
Agtr1a	ENSMUSG00000049115	735	120	525	56	733	94	602	75
AI464131	ENSMUSG00000046312	274	30	170	37	300	45	212	57
Ak1	ENSMUSG00000026817	8786	736	6676	1141	8306	245	7478	570
Ak3	ENSMUSG00000024782	2865	206	2428	194	2737	50	2646	143
Akap1	ENSMUSG00000018428	3302	350	2545	516	3554	412	3012	130
Akr1b3	ENSMUSG00000001642	4099	333	3107	569	4024	229	3471	308
Akr1e1	ENSMUSG00000045410	600	74	471	42	501	55	559	71
Akr7a5	ENSMUSG00000028743	466	29	337	42	459	49	383	48
Akt2	ENSMUSG00000004056	3610	431	2539	315	3460	299	2896	149
Aktip	ENSMUSG00000031667	1230	73	958	87	1211	51	1043	104
Aldh5a1	ENSMUSG00000035936	1096	126	715	113	1087	105	893	121
Aldoa	ENSMUSG00000030695	35858	1289	30804	2263	36705	2352	34386	2290
Alkbh5	ENSMUSG00000042650	2176	139	1835	156	2250	270	1962	35
Alkbh7	ENSMUSG00000002661	389	36	284	50	398	51	341	39
Amd1	ENSMUSG00000075232	2921	695	1957	248	2352	376	2046	448
Anapc13	ENSMUSG00000035048	991	52	835	73	936	44	898	50

Ank	ENSMUSG00000022265	4065	84	3017	442	4145	294	3446	202
Ank2	ENSMUSG00000032826	3236	377	2426	262	3245	406	2934	430
Anks1	ENSMUSG00000024219	1418	123	1011	201	1347	177	1118	141
Anxa11	ENSMUSG00000021866	1492	129	1141	185	1489	130	1259	107
Apba3	ENSMUSG00000004931	676	58	507	64	671	72	610	77
Apobec2	ENSMUSG00000040694	3232	195	2680	271	3255	84	2930	192
Arfgap2	ENSMUSG00000027255	1072	50	921	18	1095	72	979	38
Arhgap26	ENSMUSG00000036452	1156	166	889	88	1003	90	905	186
Arhgef17	ENSMUSG00000032875	1622	105	1309	145	1648	171	1396	65
Arhgef19	ENSMUSG00000028919	631	130	395	97	630	134	502	132
Arl2	ENSMUSG00000024944	429	20	345	25	432	32	371	18
Armc2	ENSMUSG00000071324	597	48	445	104	615	73	517	100
Art3	ENSMUSG00000034842	4846	519	3712	598	4603	497	4111	546
Art5	ENSMUSG00000070424	186	40	126	25	137	17	109	25
As3mt	ENSMUSG0000003559	1028	40	757	113	983	51	838	64
Asb18	ENSMUSG00000067081	499	48	355	63	568	74	485	101
Asb8	ENSMUSG00000048175	1440	34	1106	130	1405	108	1243	39
Atp5a1	ENSMUSG00000025428	73890	5007	52519	8597	73310	4969	61155	3605
Atp5b	ENSMUSG00000025393	81983	4027	60525	7907	80175	3926	68956	5579
Atp5d	ENSMUSG0000003072	5810	313	4470	769	5730	539	5074	535
Atp5e	ENSMUSG00000016252	4682	460	3624	408	4707	229	4130	508
Atp5g3	ENSMUSG00000018770	18004	1331	13448	2291	18271	996	15327	1271
Atp5o	ENSMUSG00000022956	14204	841	11103	1882	13615	536	12332	665
Atrip	ENSMUSG00000025646	240	48	178	13	214	7	169	22
Auh	ENSMUSG00000021460	1320	84	937	128	1302	50	1114	103
B4gat1	ENSMUSG00000047379	686	31	550	51	714	60	593	58
Banf2os	ENSMUSG00000086384	37	10	18	9	34	8	23	6
Bap1	ENSMUSG00000021901	906	50	726	88	873	45	830	87
BB218582	ENSMUSG00000085218	104	20	66	19	93	12	74	18
BC025920	ENSMUSG00000074862	63	12	38	10	58	6	40	6
Bcas2	ENSMUSG00000005687	603	47	499	33	607	16	526	34
Bcat2	ENSMUSG00000030826	1208	96	917	126	1160	104	1012	77
Bcl2l13	ENSMUSG00000009112	1949	142	1520	239	2093	293	1695	182
Bsg	ENSMUSG00000023175	18883	1349	15208	1807	18987	778	17057	1251
Btbd2	ENSMUSG00000003344	522	41	395	30	524	83	414	33
Bzw2	ENSMUSG00000020547	2728	225	2062	260	2680	103	2352	189
C030006K11Rik	ENSMUSG00000116138	646	57	430	81	638	91	512	103
C530005A16Rik	ENSMUSG00000085408	50	10	25	6	47	2	34	5
Cacf1	ENSMUSG00000015488	733	54	563	73	706	29	560	60
Cacnb2	ENSMUSG00000057914	1546	266	1014	149	1369	192	1040	154
Cacng6	ENSMUSG00000078815	34	9	13	6	28	11	13	6
Cadm4	ENSMUSG00000054793	295	26	180	39	288	32	216	22
Calr3	ENSMUSG00000019732	237	30	185	7	218	18	193	10
Cars2	ENSMUSG00000056228	540	40	408	58	563	48	458	53
Ccdc85c	ENSMUSG00000084883	758	52	536	118	780	117	613	80
Ccl11	ENSMUSG00000020676	47	16	18	6	28	8	22	12
Cd59a	ENSMUSG00000032679	1574	127	1303	120	1547	105	1280	69
Cd99l2	ENSMUSG00000035776	1839	81	1579	95	1863	109	1697	59
Cdh2	ENSMUSG00000024304	7013	593	5762	276	7154	806	6155	511
Cdip1	ENSMUSG0000004071	1222	78	994	157	1254	99	1121	69
Cdkl5	ENSMUSG00000031292	275	46	190	15	246	19	225	37
Cdkn1c	ENSMUSG00000037664	381	66	236	40	329	26	256	83
Cds2	ENSMUSG00000058793	4266	154	3435	371	4238	261	3575	214
Cep128	ENSMUSG00000061533	288	24	199	59	257	34	220	53
Cep63	ENSMUSG00000032534	767	47	629	48	738	59	684	37
Ces1d	ENSMUSG00000056973	2184	133	1205	405	1975	180	1372	236
Chchd10	ENSMUSG00000049422	5597	303	4264	732	5732	395	4864	565
Chchd2	ENSMUSG00000070493	5866	649	4709	645	5829	370	5166	564
Chrm2	ENSMUSG00000045613	2913	381	2078	129	2822	350	2290	539
Chrna2	ENSMUSG00000022041	51	20	23	5	42	10	23	6
Cirbp	ENSMUSG00000045193	506	100	381	38	528	31	425	70
Cisd1	ENSMUSG00000037710	2524	194	2038	264	2499	82	2259	149
Clcn3	ENSMUSG00000004319	1219	147	945	108	1163	87	993	110
Clpp	ENSMUSG00000002660	608	48	457	72	598	7	499	95
Clstn1	ENSMUSG00000039953	1769	192	1482	75	1642	58	1584	93
Cluh	ENSMUSG00000020741	5745	385	4121	818	6093	799	5032	263
Cmbl	ENSMUSG00000022235	621	59	470	81	594	54	495	52

Cobll1	ENSMUSG00000034903	1935	295	1391	206	1921	162	1717	245
Cog7	ENSMUSG00000034951	461	24	365	35	450	38	403	33
Colq	ENSMUSG00000057606	238	48	142	30	274	25	195	33
Coq10a	ENSMUSG00000039914	3593	171	2600	450	3601	150	3083	271
Coq2	ENSMUSG00000029319	1358	71	1066	109	1353	65	1154	62
Coq7	ENSMUSG00000030652	1122	100	786	155	1106	99	884	88
Coq9	ENSMUSG00000031782	6190	445	4627	906	6154	410	5544	503
Corin	ENSMUSG00000005220	3746	79	2720	217	3571	374	2889	594
Cox4i1	ENSMUSG00000031818	22284	812	17754	1611	22070	1141	19696	1055
Cox5a	ENSMUSG00000000088	11595	608	8951	1587	11127	414	10060	740
Cox5b	ENSMUSG00000061518	10424	672	8385	1343	10221	301	9039	577
Cox7a1	ENSMUSG00000074218	8954	697	6119	1540	8610	451	7040	827
Cox8b	ENSMUSG00000025488	6504	621	4961	1023	6394	477	5556	903
Cpt2	ENSMUSG00000028607	3334	182	2311	520	3272	298	2688	241
Crat	ENSMUSG00000026853	8544	365	5905	1336	8462	672	6705	567
Cs	ENSMUSG00000005683	24899	2214	17482	3393	24790	1691	20831	1885
Ctnna1	ENSMUSG00000037815	10146	341	7973	731	9700	499	8679	771
Ctsf	ENSMUSG00000083282	632	56	508	41	584	26	503	28
Cul4a	ENSMUSG00000031446	2213	84	1944	75	2181	132	2162	67
Cuta	ENSMUSG00000024194	357	31	286	29	351	28	325	26
Cux2	ENSMUSG00000042589	305	54	194	43	272	63	232	37
Cxadr	ENSMUSG00000022865	914	145	688	47	929	123	924	91
Cyb5d2	ENSMUSG00000057778	378	41	287	32	380	40	322	22
Cyfip2	ENSMUSG00000020340	4903	247	3825	494	5110	622	4425	316
Cyhr1	ENSMUSG00000053929	1686	63	1426	122	1706	105	1462	118
Cyp1a1	ENSMUSG00000032315	14	10	3	1	10	6	3	1
Cyth1	ENSMUSG00000017132	1083	120	785	146	1045	114	943	140
D17H6S53E	ENSMUSG00000043311	205	17	148	28	206	24	200	19
D2hgdh	ENSMUSG00000073609	648	30	491	28	640	53	550	62
D5Ert579e	ENSMUSG00000029190	3086	284	2426	238	2994	183	2459	146
Dap3	ENSMUSG00000068921	1533	99	1172	166	1441	33	1291	61
Ddt	ENSMUSG0000001666	477	14	371	59	468	31	410	47
Decr1	ENSMUSG00000028223	8479	863	5924	1566	7835	344	6512	520
Dele1	ENSMUSG00000024442	2437	95	1683	363	2478	270	2004	115
Dgat2	ENSMUSG00000030747	4953	461	3276	860	4835	519	3984	545
Dhodh	ENSMUSG00000031730	247	18	159	24	232	20	214	23
Dhrs11	ENSMUSG00000034449	676	56	455	62	690	48	551	73
Dhrs4	ENSMUSG00000022210	1099	57	894	97	1070	35	930	39
Diablo	ENSMUSG00000029433	1178	83	980	91	1146	35	1105	48
Dip2c	ENSMUSG00000048264	1657	88	1255	180	1673	186	1363	98
Dirc2	ENSMUSG00000022848	917	63	720	74	897	73	778	36
Dis3l	ENSMUSG00000032396	666	19	538	31	657	38	594	19
Dlst	ENSMUSG0000004789	11654	750	8617	1895	11270	555	10153	788
Dmpk	ENSMUSG00000030409	5934	219	4888	565	5867	505	5423	498
Dnaaf3	ENSMUSG00000055809	112	12	66	8	98	18	67	9
Dnajb2	ENSMUSG00000026203	1197	57	1005	70	1211	30	1066	80
Dnajb9	ENSMUSG00000014905	945	82	775	43	973	79	828	109
Dnajc28	ENSMUSG00000039763	1292	140	949	125	1268	112	1025	90
Doc2g	ENSMUSG00000024871	2878	347	2069	419	3127	217	2451	320
Drosha	ENSMUSG00000022191	1389	86	1151	83	1380	106	1191	65
Dsc2	ENSMUSG00000024331	1098	132	758	132	1038	80	880	140
Dusp18	ENSMUSG00000047205	1193	123	695	186	1165	123	828	151
Dusp23	ENSMUSG00000026544	177	25	131	14	183	13	153	7
Dym	ENSMUSG00000035765	1390	74	1135	99	1419	90	1253	76
Dynll2	ENSMUSG00000020483	8450	781	6147	789	8457	316	7374	749
E2f6	ENSMUSG00000057469	1947	96	1553	144	1933	82	1731	69
Ech1	ENSMUSG00000053898	18987	2037	11742	3859	18009	1245	12749	1792
Echdc3	ENSMUSG00000039063	427	19	300	49	428	30	350	42
Echs1	ENSMUSG00000025465	4828	268	3779	465	4896	284	4167	357
Eci1	ENSMUSG00000024132	3819	262	2675	691	3634	65	3027	306
Ecpas	ENSMUSG00000050812	5520	139	4646	405	5619	641	4989	290
Ecsit	ENSMUSG00000066839	1352	92	1050	152	1386	47	1218	79
Eef1a2	ENSMUSG00000016349	19816	1103	16353	1766	20590	904	18385	1605
Eef1d	ENSMUSG00000055762	2212	97	1867	139	2077	103	2044	101
Efcab2	ENSMUSG00000026495	2803	355	2211	241	2798	209	2383	245
Efnb3	ENSMUSG00000003934	1231	119	643	238	1266	236	811	246
Egflam	ENSMUSG00000042961	374	53	240	63	279	55	262	40

Egln1	ENSMUSG00000031987	9248	229	6578	1044	9122	656	7541	559
Eid2b	ENSMUSG00000070705	191	16	132	14	196	26	154	37
Eml2	ENSMUSG00000040811	379	40	285	35	408	44	337	30
Endog	ENSMUSG00000015337	455	64	312	72	475	50	367	54
Eno3	ENSMUSG00000060600	20868	2272	14909	3162	20388	959	17554	1469
Enpp5	ENSMUSG00000023960	482	40	367	31	452	24	401	59
Entpd4b	ENSMUSG00000022066	1245	62	1009	104	1249	57	1115	37
Ephx2	ENSMUSG00000022040	5045	182	3683	568	4643	192	4079	372
Epm2a	ENSMUSG00000055493	816	72	609	39	825	73	714	58
Erc1	ENSMUSG00000030172	1343	106	1011	106	1205	149	1073	45
Esrrb	ENSMUSG00000021255	570	46	424	77	607	56	500	36
Esrrg	ENSMUSG00000026610	1115	169	852	111	1188	192	986	138
Etfa	ENSMUSG00000032314	11167	800	7804	1484	10775	533	8929	812
Etfb	ENSMUSG00000004610	8827	431	6069	1637	8450	419	6927	725
Etdh	ENSMUSG00000027809	13588	811	9757	2314	12812	772	10703	771
Ext1	ENSMUSG00000028838	505	28	354	91	508	68	427	38
Fam131a	ENSMUSG00000050821	452	30	325	65	445	59	370	46
Fam20b	ENSMUSG00000033557	2462	33	2046	249	2441	169	2285	137
Fam210a	ENSMUSG00000038121	5630	318	3910	672	5594	632	4548	152
Farp2	ENSMUSG00000034066	407	27	323	41	400	28	340	23
Fastkd2	ENSMUSG00000025962	921	102	730	94	816	39	814	51
Fbp2	ENSMUSG00000021456	422	72	243	83	363	23	250	9
Fbxo21	ENSMUSG00000032898	802	70	590	81	829	129	684	55
Fbxo31	ENSMUSG00000052934	1386	125	967	187	1389	148	1079	71
Fbxo32	ENSMUSG00000022358	4438	248	3382	496	4609	317	3689	462
Fdft1	ENSMUSG00000021273	812	58	545	97	811	49	633	82
Fem1a	ENSMUSG00000043683	4314	280	3250	616	4473	492	3867	370
Fh1	ENSMUSG00000026526	7500	576	5659	1050	7018	180	6388	586
Fhod3	ENSMUSG00000034295	6968	897	4787	812	6949	852	5943	560
Fign	ENSMUSG00000075324	264	50	152	48	282	77	222	62
Fkbp4	ENSMUSG00000030357	7033	609	4753	1205	6950	342	5630	654
Flad1	ENSMUSG00000042642	928	42	703	107	840	64	785	91
Fmc1	ENSMUSG00000019689	622	55	458	87	580	55	484	71
Fn3k	ENSMUSG00000025175	262	26	173	19	252	25	208	27
Fndc5	ENSMUSG00000001334	7755	469	5429	1330	7876	453	6619	559
Foxo3	ENSMUSG00000048756	1906	138	1489	235	1807	100	1507	232
Foxo4	ENSMUSG00000042903	1026	58	818	81	1020	106	883	76
Foxo6os	ENSMUSG00000084929	123	20	70	22	91	13	97	30
Fsd2	ENSMUSG00000038663	7461	469	5809	1017	7438	469	6588	359
Fth1	ENSMUSG00000024661	24620	1681	21525	749	25292	1474	22765	1350
Fuz	ENSMUSG00000011658	154	17	113	4	143	29	114	25
Fxr2	ENSMUSG00000018765	2087	79	1668	103	2112	177	1949	154
Gart	ENSMUSG00000022962	791	63	621	72	729	62	724	31
Gcsh	ENSMUSG00000034424	1021	36	874	74	1000	34	954	42
Gfm1	ENSMUSG00000027774	4053	240	3035	442	3973	430	3372	259
Gfm2	ENSMUSG00000021666	1266	144	1001	118	1229	127	1128	100
Gfra1	ENSMUSG00000025089	261	28	179	47	276	25	195	40
Ghitm	ENSMUSG00000041028	10888	1003	9249	687	10712	845	9689	126
Glo1	ENSMUSG00000024026	1952	124	1549	162	1830	76	1663	101
Gm10644	ENSMUSG00000074219	30	3	13	5	21	6	18	7
Gm20619	ENSMUSG00000093482	85	17	53	4	91	12	73	11
Gm29170	ENSMUSG000000100455	84	16	48	12	73	11	60	14
Gm33543	ENSMUSG000000110353	38	12	18	6	30	9	24	10
Gm36827	ENSMUSG000000112327	289	42	195	41	280	51	188	31
Gm37829	ENSMUSG000000104453	1373	82	1009	161	1372	115	1141	137
Gm40604	ENSMUSG000000112800	20	10	8	4	11	3	8	3
Gm43672	ENSMUSG000000106019	412	67	247	76	363	75	322	88
Gm45012	ENSMUSG000000109052	77	14	44	18	83	8	50	6
Gm47547	ENSMUSG000000114196	4410	804	3053	766	4397	589	3371	749
Gm49083	ENSMUSG000000115354	278	31	195	62	260	7	202	31
Gm49130	ENSMUSG000000115234	52	12	23	9	54	13	29	9
Gm49477	ENSMUSG000000116066	359	37	242	50	366	16	279	49
Gm826	ENSMUSG00000074623	78	4	53	10	73	9	60	9
Gna12	ENSMUSG00000000149	3048	223	2381	429	3083	284	2577	277
Gnpat	ENSMUSG00000031985	4943	161	3883	434	4842	240	4332	164
Got1	ENSMUSG00000025190	12937	538	8755	1664	12760	639	10615	1253
Got2	ENSMUSG00000031672	15403	947	11510	1822	15607	1320	13207	1045

Gpd2	ENSMUSG00000026827	401	24	334	32	392	48	398	25
Gpn1	ENSMUSG00000064037	443	41	349	55	348	21	379	15
Gpr155	ENSMUSG00000041762	432	52	326	29	393	31	316	35
Gpr22	ENSMUSG00000044067	1368	315	717	244	1339	221	933	230
Gpr27	ENSMUSG00000072875	177	17	110	8	189	36	153	20
Gpt	ENSMUSG00000022546	376	38	239	62	389	47	298	58
Grb14	ENSMUSG00000026888	3020	238	2239	419	3074	220	2499	294
Gsta4	ENSMUSG00000032348	1102	100	835	91	1063	51	979	106
Gstk1	ENSMUSG00000029864	1045	99	635	177	1034	85	737	172
Gstm1	ENSMUSG00000058135	2900	228	2007	410	2765	233	2247	280
Gstm7	ENSMUSG0000004035	451	36	268	66	397	64	313	83
Gstp1	ENSMUSG00000060803	1530	60	1249	118	1564	76	1343	113
Gstt1	ENSMUSG0000001663	186	22	128	20	182	23	129	13
Gypc	ENSMUSG00000090523	589	35	453	36	560	48	489	47
Gys1	ENSMUSG0000003865	2308	136	1765	214	2462	310	2076	150
Gzmm	ENSMUSG00000054206	67	4	40	12	60	12	51	9
H2-Ke6	ENSMUSG00000073422	624	79	486	54	621	40	499	38
H2afv	ENSMUSG00000041126	582	47	479	48	560	29	511	53
Hadhd	ENSMUSG00000027984	9800	579	6798	1554	9433	502	7758	928
Hadhb	ENSMUSG00000059447	37787	3939	27391	5861	37795	3637	30089	2124
Hbs11	ENSMUSG00000019977	1596	64	1363	99	1582	55	1431	99
Hcn4	ENSMUSG00000032338	215	29	145	22	226	22	167	29
Hdhd2	ENSMUSG00000025421	925	39	718	100	905	51	782	86
Heatr5b	ENSMUSG00000039414	1026	107	806	74	965	134	837	66
Helt	ENSMUSG00000047171	27	9	8	2	21	5	16	10
Herc3	ENSMUSG00000029804	1105	188	784	144	1110	191	995	112
Hibadh	ENSMUSG00000029776	4598	354	3506	554	4704	186	4030	384
Hikeshi	ENSMUSG00000062797	431	18	351	14	437	49	395	29
Hk2	ENSMUSG0000000628	7061	664	5062	953	7161	711	6174	483
Hlf	ENSMUSG00000003949	702	180	377	124	587	150	396	181
Hmgcs2	ENSMUSG00000027875	274	33	184	30	225	17	152	50
Hnmt	ENSMUSG00000026986	222	26	145	18	233	31	181	38
Hopx	ENSMUSG00000059325	3360	233	2164	627	3438	319	2591	663
Hrc	ENSMUSG00000038239	19722	920	12511	2864	19104	720	15198	1393
Hsd17b10	ENSMUSG00000025260	1979	163	1487	242	1984	101	1624	232
Hsd12	ENSMUSG00000028383	5524	757	4049	946	5605	677	4510	583
Hspa5	ENSMUSG00000026864	12991	1134	9421	1954	11342	633	10018	1044
Hspa9	ENSMUSG00000024359	16027	1269	12152	2141	15522	684	14164	919
Hspd1	ENSMUSG00000025980	8960	680	6784	1395	8344	426	7562	640
Htra1	ENSMUSG0000006205	1381	97	1023	118	1387	133	1174	135
Iars2	ENSMUSG00000026618	2409	99	1873	136	2398	100	2171	120
Idh2	ENSMUSG00000030541	25832	1566	18548	3665	26906	2049	21457	2197
Idh3a	ENSMUSG00000032279	10211	1028	7707	867	10029	629	8753	799
Idh3b	ENSMUSG00000027406	11455	1144	8621	1973	11227	459	9312	738
Ids	ENSMUSG00000035847	844	113	686	22	705	81	678	78
Idua	ENSMUSG00000033540	381	15	288	34	343	21	312	19
Il10rb	ENSMUSG00000022969	2740	90	2327	186	2766	76	2592	101
Immt	ENSMUSG00000052337	11137	723	8672	1433	10924	555	9873	547
Imp3	ENSMUSG00000032288	386	37	293	37	353	24	333	39
Insyn1	ENSMUSG00000066607	332	30	244	41	353	22	296	17
Iscal	ENSMUSG00000044792	5523	385	4556	545	5614	212	5191	315
Iscu	ENSMUSG00000025825	1538	101	1296	84	1533	74	1368	132
Isoc2a	ENSMUSG00000086784	619	51	458	90	619	73	511	50
Kars	ENSMUSG00000031948	2130	77	1818	133	2087	64	1922	99
Kcnb1	ENSMUSG00000050556	1529	86	1149	198	1362	171	1226	75
Kcnd3	ENSMUSG00000040896	419	52	304	54	437	49	338	38
Kcng2	ENSMUSG00000059852	1131	114	738	153	1222	266	957	140
Kcnip2	ENSMUSG00000025221	2873	266	2038	321	2700	318	2226	310
Kcnk3	ENSMUSG00000049265	4069	294	2872	660	4507	692	3530	463
Kctd9	ENSMUSG00000034327	1736	135	1293	231	1770	104	1588	97
Khdrbs3	ENSMUSG00000022332	876	67	638	92	898	73	738	119
Kif16b	ENSMUSG00000038844	1579	142	1284	141	1624	143	1458	52
Kif1c	ENSMUSG00000020821	13040	401	10864	1290	13509	1540	11810	481
Kif21a	ENSMUSG00000022629	911	67	703	90	899	40	823	111
Klf9	ENSMUSG00000033863	2073	327	1580	218	1929	244	1672	332
Klhl21	ENSMUSG00000073700	1596	96	1232	219	1629	106	1373	96
Klhl33	ENSMUSG00000090799	489	94	262	86	446	37	313	87

Kpna6	ENSMUSG0000003731	2025	137	1642	186	1978	88	1813	64
Ky	ENSMUSG00000035606	445	33	251	85	458	49	367	57
Kyat1	ENSMUSG00000039648	379	27	294	42	380	16	314	20
L2hgdh	ENSMUSG00000020988	1075	56	746	101	1069	51	876	104
Lclat1	ENSMUSG00000054469	3111	302	2399	376	3091	319	2588	234
Ldhb	ENSMUSG00000030246	22959	1639	15955	3136	22470	933	18647	1684
Letm1	ENSMUSG0000005299	2120	191	1513	340	2063	206	1803	214
Lias	ENSMUSG00000029199	931	93	751	90	903	34	834	53
Limch1	ENSMUSG00000037736	5052	422	3923	326	5049	205	4581	477
Lingo3	ENSMUSG00000051067	229	41	120	47	252	73	159	48
Lmbrd1	ENSMUSG00000073725	1143	53	960	76	1105	87	1035	39
Lmo7	ENSMUSG0000003060	8272	652	6224	773	7881	612	7367	993
Lonp1	ENSMUSG00000041168	2317	80	2025	163	2376	150	2252	87
Lonrf2	ENSMUSG00000048814	202	35	126	24	204	39	153	25
Lpin1	ENSMUSG00000020593	4444	676	2968	594	4769	532	3724	386
Lpl	ENSMUSG00000015568	90429	5374	71420	8174	93258	8317	80525	6094
Lrpprc	ENSMUSG00000024120	4237	451	2986	400	4181	326	3537	377
Lrrc3b	ENSMUSG00000045201	506	44	333	72	477	50	367	53
Lsm14b	ENSMUSG00000039108	972	35	742	85	914	50	896	76
Lynx1	ENSMUSG00000022594	5026	322	3722	716	5034	369	4308	264
Maf1	ENSMUSG00000022553	1093	59	891	57	1121	107	1002	47
Magi3	ENSMUSG00000052539	1616	181	1196	121	1556	176	1327	166
Magt1	ENSMUSG00000031232	1232	137	942	126	1216	90	994	120
Malsu1	ENSMUSG00000029815	281	28	208	15	260	23	236	30
Map10	ENSMUSG00000050930	149	21	98	15	151	17	112	10
Map1lc3a	ENSMUSG00000027602	4603	222	3864	305	4713	378	4049	447
Mapk8ip3	ENSMUSG00000024163	1609	148	1286	127	1571	128	1366	102
Mars2	ENSMUSG00000046994	370	47	284	34	364	34	304	25
Mccc1	ENSMUSG00000027709	2112	94	1589	261	2026	95	1662	118
Mdga1	ENSMUSG00000043557	283	40	180	25	255	46	211	43
Mdh2	ENSMUSG00000019179	16876	703	12970	2129	16369	1034	14499	734
Me1	ENSMUSG00000032418	2846	130	2349	226	2697	138	2438	237
Med121	ENSMUSG00000056476	211	24	139	35	199	27	142	38
Med9	ENSMUSG00000061650	383	8	302	30	383	23	347	23
Mettl7a1	ENSMUSG00000054619	740	30	561	48	684	59	597	63
Mfn1	ENSMUSG00000027668	8217	628	6382	1129	8242	170	7059	753
Mfn2	ENSMUSG00000029020	15414	955	11184	2042	15810	1644	13241	705
Mgme1	ENSMUSG00000027424	350	28	255	46	337	12	267	30
Mgrn1	ENSMUSG00000022517	3397	191	2489	420	3480	322	2787	167
Mhrt	ENSMUSG00000097652	413	27	294	60	414	38	328	38
Migal1	ENSMUSG00000054942	412	61	323	8	409	40	383	35
Mipep	ENSMUSG00000021993	1364	63	983	167	1394	126	1103	71
Mllt6	ENSMUSG00000038437	1839	74	1515	116	1801	105	1533	96
Mlxip	ENSMUSG00000038342	1090	98	876	108	1082	85	963	38
Mmaa	ENSMUSG00000037022	603	23	460	70	572	47	517	37
Mmadhc	ENSMUSG00000026766	1760	184	1400	199	1684	61	1526	84
Mov10l1	ENSMUSG00000015365	912	70	518	82	908	73	735	108
Mpi	ENSMUSG00000032306	1513	105	1202	137	1517	24	1387	104
Mpped2	ENSMUSG00000016386	351	88	229	30	340	24	247	36
Mpst	ENSMUSG00000071711	347	22	269	21	344	35	280	23
Mpv17	ENSMUSG000000107283	1098	32	873	90	1118	80	934	104
Mrpl14	ENSMUSG00000023939	682	54	516	77	739	35	586	87
Mrpl16	ENSMUSG00000024683	961	36	784	75	930	52	848	97
Mrpl28	ENSMUSG00000024181	1210	39	882	132	1171	81	1020	121
Mrpl37	ENSMUSG00000028622	1184	43	904	135	1161	34	1046	74
Mrpl38	ENSMUSG00000020775	704	31	534	72	674	41	611	58
Mrpl39	ENSMUSG00000022889	1365	91	1053	180	1335	40	1087	56
Mrpl4	ENSMUSG00000003299	1028	38	792	138	1029	93	915	137
Mrpl45	ENSMUSG00000018882	1187	97	837	153	1100	58	1043	54
Mrps26	ENSMUSG00000037740	355	39	258	24	351	18	326	26
Mrps35	ENSMUSG00000040112	1312	76	991	219	1236	59	1132	63
Mrps6	ENSMUSG00000039680	361	20	285	16	354	19	300	4
Msrb2	ENSMUSG00000023094	1067	66	775	115	1023	25	865	63
Mtfp1	ENSMUSG00000004748	1636	82	1103	322	1626	114	1320	90
Mtrf11	ENSMUSG00000046671	2563	65	2169	189	2622	122	2390	105
Mtg2	ENSMUSG00000039069	366	31	275	26	387	9	312	16
Mtmmr4	ENSMUSG00000018401	533	95	415	52	508	47	429	38

Mto1	ENSMUSG00000032342	481	27	368	46	450	40	405	41
Mtr	ENSMUSG00000021311	3225	471	2012	528	2736	435	2132	259
Mtus2	ENSMUSG00000029651	2962	248	2267	102	3029	325	2381	425
Myadml2	ENSMUSG00000025141	267	6	178	37	256	34	227	25
Mybbp1a	ENSMUSG00000040463	1302	174	1041	48	1189	167	1099	79
Myh14	ENSMUSG00000030739	1825	190	1436	214	1992	381	1613	123
Myh6	ENSMUSG00000040752	416670	31586	295124	67491	432469	60382	365274	31724
Mylip	ENSMUSG00000038175	408	59	322	55	361	21	336	42
Myzap	ENSMUSG00000041361	8078	741	6069	777	8163	545	7067	721
Nampt	ENSMUSG00000020572	4880	529	3965	206	4631	388	3944	359
Nbas	ENSMUSG00000020576	829	71	596	58	720	104	703	64
Ndrg2	ENSMUSG00000004558	19416	536	16383	1310	19419	1235	17364	725
Ndufa10	ENSMUSG00000026260	9566	706	7436	1132	9920	331	8450	886
Ndufa8	ENSMUSG00000026895	4878	294	3771	635	4757	148	4279	331
Ndufa9	ENSMUSG0000000399	9480	996	7084	1337	9287	369	7867	703
Ndufs1	ENSMUSG00000025968	15975	1815	11734	2163	15650	1579	13236	1027
Ndufs2	ENSMUSG00000013593	16031	729	11634	1773	15858	991	13476	1336
Ndufs3	ENSMUSG00000005510	6047	349	4620	872	5917	121	5197	447
Ndufs7	ENSMUSG00000020153	3525	187	2485	513	3595	317	2923	370
Ndufv1	ENSMUSG00000037916	9773	762	6974	1216	9669	615	8148	626
Nectin2	ENSMUSG00000062300	413	36	310	34	417	41	335	50
Nek9	ENSMUSG00000034290	4497	135	3774	292	4482	346	4215	107
Nfe2l1	ENSMUSG00000038615	10454	393	8704	788	10418	916	9618	241
Nfs1	ENSMUSG00000027618	1552	137	1235	133	1562	117	1353	125
Ngrn	ENSMUSG00000047084	316	43	243	18	297	10	268	29
Nmnat3	ENSMUSG00000032456	318	32	227	37	294	26	237	22
Nomo1	ENSMUSG00000030835	2843	188	2392	196	2879	272	2584	198
Npepps	ENSMUSG00000001441	2325	152	1944	99	2270	128	2110	152
Nprl2	ENSMUSG00000010057	233	23	177	25	218	16	188	17
Nqo2	ENSMUSG00000046949	946	76	768	84	944	37	822	27
Nr1d1	ENSMUSG00000020889	2205	482	1594	392	2278	416	1686	114
Nr3c2	ENSMUSG00000031618	554	97	352	33	533	70	406	87
Nsmce1	ENSMUSG00000030750	572	26	425	55	506	32	480	49
Nsun4	ENSMUSG00000028706	668	48	514	69	656	35	592	35
Nt5c1a	ENSMUSG00000054958	221	21	132	21	214	28	180	22
Nt5dc3	ENSMUSG00000054027	1591	190	1169	296	1701	183	1426	165
Ntn1	ENSMUSG00000020902	1895	146	1435	153	2064	197	1793	251
Nudc	ENSMUSG00000028851	1219	28	997	119	1222	68	1116	61
Nudt3	ENSMUSG00000024213	2420	197	1955	179	2428	117	2144	103
Nudt6	ENSMUSG00000050174	240	31	183	19	270	13	214	24
Oat	ENSMUSG00000030934	4023	214	3428	322	3893	236	3570	97
Ogdh	ENSMUSG00000020456	39640	2492	29734	4328	41635	5116	35518	902
Oma1	ENSMUSG00000035069	520	27	382	67	517	40	433	46
Opa1	ENSMUSG00000038084	5644	514	4210	706	5735	550	5001	562
Oplah	ENSMUSG00000022562	803	117	550	66	755	147	645	45
Oprn	ENSMUSG00000026672	2167	261	1708	294	2308	86	2033	94
Osbp	ENSMUSG00000024687	2871	112	2475	227	3049	216	2682	119
Osbpl2	ENSMUSG00000039050	924	46	750	55	906	59	792	22
Osbpl6	ENSMUSG00000042359	560	64	401	56	579	105	481	24
Osgep	ENSMUSG00000006289	680	53	499	68	589	47	573	41
Otud4	ENSMUSG00000036990	1969	261	1551	87	1916	144	1630	131
Oxall	ENSMUSG00000000959	1341	57	1036	150	1356	195	1142	95
Oxct1	ENSMUSG00000022186	26538	1570	20521	2412	25456	2358	23051	1272
Oxnad1	ENSMUSG00000021906	1147	104	870	148	1159	96	1055	90
Pacsin2	ENSMUSG00000016664	4608	491	3453	568	4770	416	3975	269
Pccb	ENSMUSG00000032527	1749	37	1306	178	1783	212	1458	93
Pcp4l1	ENSMUSG00000038370	3448	91	2643	293	3460	188	3005	313
Pde2a	ENSMUSG000000110195	1585	126	1282	143	1439	108	1257	211
Pdf	ENSMUSG00000078931	565	42	418	72	575	29	492	19
Pdk2	ENSMUSG00000038967	7045	426	4922	991	7351	661	5815	537
Pdss2	ENSMUSG00000038240	428	19	288	48	415	44	365	47
Pdzd2	ENSMUSG00000022197	1958	240	1387	312	1714	300	1447	149
Peg13	ENSMUSG000000106847	1266	135	996	129	1259	67	1062	102
Perm1	ENSMUSG00000078486	6061	537	4239	948	6388	499	5164	309
Pex10	ENSMUSG00000029047	216	17	157	21	236	16	189	19
Pex6	ENSMUSG00000002763	536	39	383	52	543	100	441	44
Pfkl	ENSMUSG00000020277	1893	156	1558	139	1871	165	1710	80

Pfkm	ENSMUSG00000033065	18225	1341	12907	1890	18352	1337	14993	396
Pgm5	ENSMUSG00000041731	2496	117	1972	181	2577	106	2310	218
Phf20	ENSMUSG00000038116	645	141	463	64	547	79	484	111
Phkg1	ENSMUSG00000025537	414	78	217	95	351	52	195	50
Phpt1	ENSMUSG00000036504	592	39	477	58	591	19	515	20
Phyh	ENSMUSG00000026664	9819	550	7600	1012	9908	282	8331	547
Pigg	ENSMUSG00000029263	357	15	277	13	360	32	317	44
Pigv	ENSMUSG00000043257	190	34	113	16	185	35	150	33
Pik3r4	ENSMUSG00000032571	510	63	421	32	453	52	451	38
Pim3	ENSMUSG00000035828	1043	153	638	156	989	141	713	162
Pip4k2c	ENSMUSG00000025417	839	38	718	27	859	49	781	35
Pitpnc1	ENSMUSG00000040430	2019	131	1451	306	1945	148	1677	225
Pitrm1	ENSMUSG00000021193	1183	91	917	87	1076	97	982	47
Plin4	ENSMUSG00000002831	3263	103	2596	321	3280	102	2808	366
Plpbp	ENSMUSG00000031485	1297	158	1038	125	1269	103	1218	88
Pmpca	ENSMUSG00000026926	2809	172	2292	228	2800	157	2538	100
Pnpla2	ENSMUSG00000025509	4617	330	3361	654	4556	476	3773	317
Poldip2	ENSMUSG00000001100	2037	140	1588	200	2103	131	1870	118
Polr2b	ENSMUSG00000029250	1491	97	1240	88	1445	75	1325	88
Polr2e	ENSMUSG00000004667	833	69	697	28	814	44	761	49
Polr2m	ENSMUSG00000032199	4202	139	3527	289	4270	294	3840	106
Ppara	ENSMUSG00000022383	730	69	463	119	639	77	525	69
Ppm1k	ENSMUSG00000037826	2243	337	1519	318	2006	174	1607	419
Ppp1r12b	ENSMUSG00000073557	7349	246	5778	1053	8073	1048	6703	244
Ppp1r26	ENSMUSG00000035829	123	33	63	14	99	6	69	7
Ppp1r3d	ENSMUSG00000049999	323	31	243	23	344	39	274	29
Ppp5c	ENSMUSG00000003099	1134	58	913	91	1135	59	1032	79
Ppt2	ENSMUSG00000015474	570	20	441	69	579	54	505	43
Prdx6	ENSMUSG00000026701	3412	145	2618	272	3250	102	2855	190
Prkaca	ENSMUSG00000005469	4064	153	3118	405	4060	252	3598	192
Prkag1	ENSMUSG00000067713	1480	97	1136	121	1449	53	1228	110
Prkce	ENSMUSG00000045038	1038	123	798	114	1083	139	932	92
Prpf19	ENSMUSG00000024735	3570	220	2865	389	3749	422	3240	103
Prpf8	ENSMUSG00000020850	3805	235	3158	312	3806	301	3465	198
Psap	ENSMUSG00000004207	20301	713	16734	1671	20510	1354	18075	1122
Psmd2	ENSMUSG00000006998	4504	254	3688	415	4294	293	4129	211
Ptcd3	ENSMUSG00000063884	3497	444	2527	522	3299	255	2951	253
Ptov1	ENSMUSG00000038502	994	34	794	32	947	73	875	61
Ptpn3	ENSMUSG00000038764	1516	118	1158	191	1433	94	1204	64
Pttg1	ENSMUSG00000020415	1218	104	917	152	1220	46	1000	82
Pxmp2	ENSMUSG00000029499	803	44	554	114	790	47	628	75
Pygm	ENSMUSG00000032648	19355	1268	13869	2475	19815	1520	16110	975
Qdpr	ENSMUSG00000015806	905	53	716	59	901	38	833	92
Qsox2	ENSMUSG00000036327	354	29	255	33	340	26	293	34
R3hdm4	ENSMUSG00000035781	843	29	689	82	840	52	717	45
Rab12	ENSMUSG00000023460	2932	232	2405	100	2976	158	2577	278
Rab28	ENSMUSG00000029128	1501	127	1261	120	1546	89	1421	64
Rab3a	ENSMUSG00000031840	556	31	385	62	576	29	459	63
Rai2	ENSMUSG00000043518	607	58	481	89	647	60	562	52
Ralgap2	ENSMUSG00000037110	2617	245	1978	383	2581	274	2195	200
Ralgapb	ENSMUSG00000027652	1478	136	1208	120	1466	153	1287	73
Rapsn	ENSMUSG00000002104	164	14	112	16	166	20	118	21
Rasd2	ENSMUSG00000034472	85	16	52	8	87	5	67	16
Rbbp5	ENSMUSG00000026439	503	77	394	43	462	27	433	19
Rbfa	ENSMUSG00000024570	537	27	421	57	552	37	476	23
Rbm20	ENSMUSG00000043639	4345	353	3333	538	4405	474	3671	314
Rbm24	ENSMUSG00000038132	2769	152	2054	213	2701	211	2285	323
Rbpms	ENSMUSG00000031586	2091	178	1725	171	2143	145	1933	119
Rdm1	ENSMUSG00000010362	355	44	260	27	395	55	308	50
Retnla	ENSMUSG00000061100	77	26	28	12	70	10	47	28
Retsat	ENSMUSG00000056666	937	102	713	90	893	134	765	34
Rgs7	ENSMUSG00000026527	36	12	15	6	19	3	25	6
Rhobtb2	ENSMUSG00000022075	496	77	385	66	531	42	452	21
Rhot2	ENSMUSG00000025733	3078	130	2175	480	3032	157	2480	193
Rmnd1	ENSMUSG00000019763	878	53	704	63	926	55	800	97
Rnf114	ENSMUSG00000006418	1224	48	1047	46	1232	102	1117	38
Rpa1	ENSMUSG0000000751	1034	51	817	60	1036	89	910	49

Rpap1	ENSMUSG00000034032	295	38	221	36	319	44	271	27
Rpusd4	ENSMUSG00000032044	283	14	221	31	291	18	238	21
Rragd	ENSMUSG00000028278	3170	310	2413	232	3220	162	2839	371
Rrn3	ENSMUSG00000022682	1172	63	954	93	1149	64	1040	78
Rtn4ip1	ENSMUSG00000019864	1524	104	1118	239	1538	112	1315	140
Rufy1	ENSMUSG00000020375	709	60	558	43	649	12	610	48
Rxrg	ENSMUSG00000015843	1040	79	760	162	1102	94	896	96
Samm50	ENSMUSG00000022437	4316	204	3494	463	4136	107	3926	74
Sbk1	ENSMUSG00000042978	1288	124	1004	171	1329	89	1218	118
Scgb1c1	ENSMUSG00000038801	156	23	101	19	163	23	131	27
Scn4a	ENSMUSG0000001027	691	157	407	125	675	132	480	75
Scn4b	ENSMUSG00000046480	1055	187	607	202	976	267	669	172
Scrn3	ENSMUSG0000008226	772	46	634	36	772	89	686	45
Sdhb	ENSMUSG0000009863	12188	749	9065	1722	11819	503	9978	990
Sdhc	ENSMUSG00000058076	7127	66	5010	729	7101	434	5730	395
Sdr39u1	ENSMUSG00000022223	1168	90	858	177	1171	36	977	118
Sel11	ENSMUSG00000020964	1913	94	1550	157	1805	94	1646	186
Sesn1	ENSMUSG00000038332	2443	189	2090	127	2405	179	2161	117
Sipa112	ENSMUSG0000001995	1430	165	1122	105	1540	153	1327	56
Sirt5	ENSMUSG00000054021	574	24	464	39	573	30	507	40
Slc16a7	ENSMUSG00000020102	227	56	144	27	216	67	189	39
Slc25a11	ENSMUSG00000014606	8077	561	5928	1242	7992	341	6986	662
Slc25a12	ENSMUSG00000027010	4184	351	2893	395	4194	379	3611	151
Slc25a13	ENSMUSG00000015112	2989	324	2199	145	3029	276	2574	268
Slc25a20	ENSMUSG00000032602	3086	349	2262	477	3063	140	2521	210
Slc25a3	ENSMUSG00000061904	25015	1211	18063	2479	25124	1400	20806	1485
Slc25a33	ENSMUSG00000028982	271	36	196	32	254	25	214	18
Slc26a6	ENSMUSG00000023259	159	5	105	24	133	7	122	15
Slc2a4	ENSMUSG00000018566	6195	156	4116	759	6192	600	4937	362
Slc36a2	ENSMUSG00000020264	315	40	215	36	309	9	239	36
Slc38a3	ENSMUSG00000010064	939	97	638	211	1037	121	746	126
Slc41a1	ENSMUSG00000013275	1492	118	1131	142	1374	124	1187	145
Slc4a4	ENSMUSG00000060961	964	160	696	87	861	146	774	132
Slc7a1	ENSMUSG00000041313	1469	249	990	213	1397	281	1151	217
Slc9a8	ENSMUSG00000039463	533	54	422	27	481	53	424	37
Slco3a1	ENSMUSG00000025790	1897	213	1577	239	1938	213	1809	168
Smco1	ENSMUSG00000046345	280	33	173	42	270	15	222	35
Smg5	ENSMUSG0000001415	1134	42	904	93	1081	79	1020	136
Smm11	ENSMUSG00000051989	669	30	545	65	628	41	590	28
Sna3	ENSMUSG0000006587	49	18	24	5	45	14	35	8
Snrpn	ENSMUSG00000102252	939	55	661	136	989	67	760	142
Sod1	ENSMUSG00000022982	3578	226	3002	251	3367	134	3215	151
Sod2	ENSMUSG0000006818	12266	831	8665	1885	11982	506	9979	664
Sord	ENSMUSG00000027227	4541	245	3023	680	4444	324	3516	336
Spr	ENSMUSG00000033735	665	53	505	56	683	71	580	44
Spsb1	ENSMUSG00000039911	519	41	383	46	499	68	431	61
Sptb	ENSMUSG00000021061	3814	253	2892	391	4015	448	3358	226
St3gal3	ENSMUSG00000028538	1047	50	840	121	1048	65	941	63
St6galnac6	ENSMUSG00000026811	1129	64	895	132	1127	72	981	112
Stard10	ENSMUSG00000030688	330	75	189	43	297	12	242	66
Stard7	ENSMUSG00000027367	3728	299	2766	387	3568	81	3253	316
Stk11	ENSMUSG0000003068	1448	37	1205	94	1447	59	1293	70
Ston2	ENSMUSG00000020961	279	82	178	41	317	59	217	35
Stub1	ENSMUSG00000039615	1096	59	905	66	1104	71	1014	92
Suclg1	ENSMUSG00000052738	6364	514	4599	1021	6012	279	5327	363
Suclg2	ENSMUSG00000061838	4105	321	2961	428	4037	119	3294	228
Suox	ENSMUSG00000049858	473	53	354	36	448	32	405	21
Susd6	ENSMUSG00000021133	2324	150	1943	183	2364	108	2034	109
Svip	ENSMUSG00000074093	948	93	733	96	873	98	769	67
Swsap1	ENSMUSG00000051238	126	10	90	15	118	11	105	11
Syt7	ENSMUSG00000024743	873	100	595	126	831	116	700	57
Tango2	ENSMUSG00000013539	2372	272	1812	121	2322	147	1927	149
Tango6	ENSMUSG00000041949	231	19	170	17	230	31	201	14
Tars2	ENSMUSG00000028107	667	59	489	66	606	23	549	66
Tarsl2	ENSMUSG00000030515	1088	105	839	102	1083	60	931	19
Taz	ENSMUSG00000009995	683	45	574	36	641	57	573	45
Tbrg4	ENSMUSG0000000384	909	70	673	136	897	113	763	112

Tcaim	ENSMUSG00000046603	1091	140	752	164	1078	129	865	134
Tcap	ENSMUSG0000007877	15023	5676	9524	3481	11808	3513	10365	2562
Tcp112	ENSMUSG00000020034	2121	130	1478	128	2131	148	1765	222
Tecrl	ENSMUSG00000049537	1305	197	1030	90	1191	128	1094	181
Tent4b	ENSMUSG00000036779	610	55	482	40	562	52	508	45
Tesc	ENSMUSG00000029359	1119	84	854	76	1160	95	937	103
Thrb	ENSMUSG00000021779	495	72	351	62	440	76	311	43
Tmbim6	ENSMUSG00000023010	3804	173	3339	158	3817	189	3501	211
Tmc7	ENSMUSG00000042246	203	26	121	17	221	36	169	29
Tmem135	ENSMUSG00000039428	983	73	725	115	985	79	815	63
Tmem143	ENSMUSG0000002781	1504	67	919	258	1446	221	1083	117
Tmem177	ENSMUSG00000036975	283	12	189	34	271	12	216	21
Tmem250-ps	ENSMUSG00000087679	1255	42	1017	136	1234	98	1140	53
Tmem38a	ENSMUSG00000031791	7478	344	5801	950	7515	482	6828	346
Tmem50b	ENSMUSG00000022964	927	63	728	73	909	32	769	105
Tmem70	ENSMUSG00000025940	1686	231	1310	188	1682	176	1404	135
Tmem82	ENSMUSG00000043085	271	51	168	43	257	20	187	17
Tmem94	ENSMUSG00000020747	1735	172	1255	258	1762	215	1313	178
Tmod1	ENSMUSG00000028328	6866	511	5456	542	6671	424	6180	413
Tmod4	ENSMUSG00000005628	378	37	254	60	361	43	317	59
Tnfaip8	ENSMUSG00000062210	1646	269	1190	267	1502	102	1310	232
Tnip3	ENSMUSG00000044162	52	11	27	13	47	4	42	4
Tnni3	ENSMUSG00000035458	63108	4479	42722	10485	61514	1321	48873	5226
Tnnt2	ENSMUSG00000026414	110161	8926	87055	9068	105408	3834	92241	8335
Tom112	ENSMUSG00000000538	2948	122	2426	287	2928	258	2694	186
Trabd2b	ENSMUSG00000070867	3038	207	2320	372	3187	181	2778	256
Tsc22d1	ENSMUSG00000022010	4439	536	3676	350	4405	178	4019	379
Tspan3	ENSMUSG00000032324	2417	116	2074	132	2505	165	2302	52
Tspyl4	ENSMUSG00000039485	376	62	276	18	382	85	298	73
Ttc19	ENSMUSG00000042298	902	120	684	71	896	69	748	78
Tufm	ENSMUSG00000073838	3132	215	2311	479	3147	191	2714	265
Twnk	ENSMUSG00000025209	604	21	452	67	607	59	505	23
Txnr2	ENSMUSG00000075704	527	35	362	47	464	30	431	49
Ubac2	ENSMUSG00000041765	482	28	351	27	440	56	380	38
Ubl7	ENSMUSG00000055720	695	84	565	67	663	44	641	37
Ubr2	ENSMUSG00000023977	2578	83	1942	289	2546	196	2215	196
Ucp3	ENSMUSG00000032942	1264	355	659	227	1281	331	698	271
Unc45b	ENSMUSG00000018845	3432	81	2694	372	3138	382	2858	156
Uqcc1	ENSMUSG00000005882	3454	270	2476	553	3363	150	2909	228
Uqcrc1	ENSMUSG00000025651	15130	710	10190	2080	15168	907	12233	1293
Uqcrfs1	ENSMUSG00000038462	13197	914	10056	1838	12772	692	11183	890
Urod	ENSMUSG00000028684	800	46	616	62	756	47	678	29
Usf2	ENSMUSG00000058239	1261	122	1046	81	1203	37	1081	60
Vcp	ENSMUSG00000028452	9696	493	8255	496	9439	494	9118	332
Vdac1	ENSMUSG00000020402	17517	801	13326	1578	17010	633	14751	342
Vdac3	ENSMUSG00000008892	6247	446	4930	675	5939	119	5490	330
Vegfb	ENSMUSG00000024962	2831	191	2209	301	2977	265	2434	179
Vps26a	ENSMUSG00000020078	1810	210	1524	43	1767	104	1632	155
Vwa8	ENSMUSG00000058997	6184	159	4148	762	5901	635	4704	407
Wbp2	ENSMUSG00000034341	1379	72	1162	115	1438	101	1294	92
Wdtc1	ENSMUSG00000037622	1386	86	1042	217	1413	154	1245	104
Wfs1	ENSMUSG00000039474	1806	82	1416	252	1797	191	1634	135
Whrn	ENSMUSG00000039137	481	110	307	100	542	79	382	97
Wnk2	ENSMUSG00000037989	1441	166	821	252	1510	204	1013	246
Ybx1	ENSMUSG00000028639	11917	513	10296	764	11978	639	10588	490
Ywhae	ENSMUSG00000020849	5973	224	5142	422	5882	295	5570	239
Zadh2	ENSMUSG00000049090	1687	130	1330	146	1727	133	1433	161
Zfp113	ENSMUSG00000037007	207	26	137	20	206	31	160	32
Zfp536	ENSMUSG00000043456	134	18	70	15	120	18	92	13
Zfp629	ENSMUSG00000045639	654	44	510	45	651	90	565	56
Zfyve21	ENSMUSG00000021286	406	15	295	34	394	31	309	42
Znrf1	ENSMUSG00000033545	850	52	714	48	788	71	705	40

**Supplementary Table S7.** RNASeq analysis of effects of angiotensin II (AngII) on mRNA expression in hearts from PKN2Het vs WT littermates: mRNAs significantly upregulated by AngII in PKN2Het hearts.

Gene Symbol	Ensembl gene id	WT Vehicle		WT AngII		PKN2Het Vehicle		PKN2Het AngII	
		Mean	SD	Mean	SD	Mean	SD	Mean	SD
1500004A13Rik	ENSMUSG00000098912	28	5	38	8	20	7	48	20
4931406P16Rik	ENSMUSG00000066571	1213	197	1375	110	1210	171	1441	195
6430584L05Rik	ENSMUSG00000108228	2	1	7	2	3	1	69	99
AC165271.1	ENSMUSG00000116641	7	2	16	5	5	2	19	12
Adgrd1	ENSMUSG00000044017	191	51	269	56	169	19	249	49
Akap2	ENSMUSG00000038729	3768	234	4279	435	3521	379	4095	258
Aldh1a1	ENSMUSG00000025007	242	27	280	13	215	33	299	35
Ano6	ENSMUSG00000064210	778	83	929	100	694	56	876	34
Anp32b	ENSMUSG00000028333	1235	54	1423	104	1216	59	1418	76
Arhgef12	ENSMUSG00000059495	6349	600	6661	1008	6125	289	7218	254
Arrb1	ENSMUSG00000018909	877	101	1086	152	816	90	1086	112
Atp8b2	ENSMUSG00000060671	531	139	704	103	413	28	673	34
Atxn11	ENSMUSG00000069895	724	111	785	64	708	86	852	141
B3gnt3	ENSMUSG00000031803	234	39	304	15	213	12	289	30
C5ar1	ENSMUSG00000049130	107	17	173	40	78	18	156	56
Capn2	ENSMUSG00000026509	2021	126	2295	152	1873	94	2199	142
Ccl12	ENSMUSG00000035352	28	12	76	30	20	5	61	36
Ccl2	ENSMUSG00000035385	56	15	106	46	42	6	111	80
Cd302	ENSMUSG00000060703	206	18	297	71	176	17	266	37
Cdc42ep4	ENSMUSG00000041598	293	84	306	18	242	49	312	39
Cdc42se1	ENSMUSG00000046722	468	71	617	41	442	53	554	68
Cebpa	ENSMUSG00000034957	116	16	166	28	115	23	164	26
Cenpi	ENSMUSG00000031262	14	6	28	12	6	3	28	9
Ces2e	ENSMUSG00000031886	82	18	89	16	65	19	108	34
Clic5	ENSMUSG00000023959	7647	453	8817	809	7809	595	9603	708
Cmkrlr1	ENSMUSG00000042190	507	144	618	103	422	100	579	89
Col4a3	ENSMUSG00000079465	203	49	299	93	199	27	307	35
Cyb561	ENSMUSG00000019590	237	62	314	54	200	32	299	78
Cyb5r1	ENSMUSG00000026456	363	22	410	23	351	26	444	45
Dbndd2	ENSMUSG00000017734	265	25	310	15	218	53	285	36
Ddah2	ENSMUSG00000007039	240	14	299	36	214	30	292	28
Ddr2	ENSMUSG00000026674	1034	140	1163	154	869	156	1130	83
Dpysl2	ENSMUSG00000022048	377	57	499	48	329	67	433	23
Dsn1	ENSMUSG00000027635	32	10	50	10	25	6	47	8
Eif4a1	ENSMUSG00000059796	3380	300	3664	494	3084	168	3826	261
Elmo1	ENSMUSG00000041112	303	38	395	22	278	56	438	50
Elov11	ENSMUSG00000006390	286	23	361	51	246	37	316	43
Enc1	ENSMUSG00000041773	293	76	382	15	273	69	390	41
Erf	ENSMUSG00000040857	309	56	363	54	285	58	372	48
Fabp5	ENSMUSG00000027533	788	95	996	167	674	83	989	37
Fam102b	ENSMUSG00000040339	516	79	657	85	447	67	598	79
Fgf6	ENSMUSG00000000183	19	11	37	18	16	6	40	17
Fkbp5	ENSMUSG00000024222	356	106	469	65	289	55	412	74
Gba	ENSMUSG00000028048	219	25	275	46	194	36	270	21
Gm10275	ENSMUSG00000069682	2119	213	2280	303	1958	234	2331	159
Gm14005	ENSMUSG00000074813	25	6	32	5	23	3	43	5
Gm15542	ENSMUSG00000083396	41	20	74	30	32	14	92	41
Gm21188	ENSMUSG00000095609	24	11	52	38	12	6	39	17
Gm8430	ENSMUSG00000055093	747	208	891	177	614	182	1041	66
Gngt2	ENSMUSG00000038811	179	19	226	24	170	41	224	28
Hbegf	ENSMUSG00000024486	285	26	375	79	293	20	445	97
Hmox1	ENSMUSG00000005413	189	79	278	49	151	19	270	45
Hnrnpf	ENSMUSG00000042079	2929	181	3120	203	2667	95	3177	258
Hnrnpk	ENSMUSG00000021546	4424	263	4608	377	3979	132	4710	317
Hsp90aa1	ENSMUSG00000021270	4809	792	5821	774	4154	437	5635	799
Id3	ENSMUSG00000007872	547	96	629	46	503	70	613	81
Ier5	ENSMUSG00000056708	536	123	783	105	482	61	803	298
Ilk	ENSMUSG00000030890	1549	39	1714	90	1475	117	1685	57
Itpr2	ENSMUSG00000030287	666	151	771	158	613	94	776	101

Jpt1	ENSMUSG00000020737	841	76	987	49	790	37	1002	107
Jpt2	ENSMUSG00000024165	169	19	197	35	141	33	226	44
Lama2	ENSMUSG00000019899	3507	352	3968	325	3362	180	4015	379
Layn	ENSMUSG00000060594	73	12	116	39	72	19	117	25
Lima1	ENSMUSG00000023022	869	137	1044	86	750	124	1003	145
Ly6a	ENSMUSG00000075602	1892	294	2356	309	1658	287	2262	203
Mad2l1	ENSMUSG00000029910	111	20	150	33	90	23	154	23
Map6	ENSMUSG00000055407	108	31	142	36	87	9	129	34
Mcm10	ENSMUSG00000026669	14	6	30	10	8	7	26	18
Mcm3	ENSMUSG00000041859	156	21	214	41	148	27	240	53
Mcm5	ENSMUSG00000005410	84	12	162	45	83	19	169	35
Mcm6	ENSMUSG00000026355	230	32	397	77	216	18	363	70
Mgat5b	ENSMUSG00000043857	8	5	23	15	9	5	31	24
Mmrn2	ENSMUSG00000041445	1117	202	1171	66	966	115	1226	136
Mob3a	ENSMUSG00000003348	134	17	176	20	115	24	176	43
Mybl1	ENSMUSG00000025912	20	8	40	11	22	4	48	10
Myo1c	ENSMUSG00000017774	2939	140	3445	280	2807	136	3414	203
Ncf2	ENSMUSG00000026480	117	30	183	21	107	29	174	52
Nrp2	ENSMUSG00000025969	1954	236	2425	238	1836	224	2427	166
Nuak1	ENSMUSG00000020032	841	90	1047	199	819	26	1165	278
Nudt18	ENSMUSG00000045211	271	21	330	55	259	36	362	63
Numb	ENSMUSG00000021224	620	116	600	28	522	54	673	44
Nusap1	ENSMUSG00000027306	48	17	132	40	45	9	116	36
Ophn1	ENSMUSG00000031214	212	70	246	57	195	73	284	69
Pald1	ENSMUSG00000020092	474	36	537	61	417	42	544	37
Papln	ENSMUSG00000021223	369	42	478	84	367	37	494	57
Parva	ENSMUSG00000030770	1225	61	1409	154	1113	88	1320	96
Pcolce2	ENSMUSG00000015354	412	82	494	81	352	55	503	72
Pdlim1	ENSMUSG00000055044	1237	36	1524	182	1078	86	1607	176
Pecam1	ENSMUSG00000020717	4184	537	5065	334	3964	407	4742	324
Pid1	ENSMUSG00000045658	275	53	338	14	244	37	314	29
Pilra	ENSMUSG00000046245	31	5	52	15	24	9	52	20
Pole2	ENSMUSG00000020974	16	7	31	8	12	5	33	6
Prg4	ENSMUSG00000006014	323	89	484	130	321	33	596	281
Ptx3	ENSMUSG00000027832	9	5	35	23	8	2	42	47
Rab15	ENSMUSG00000021062	19	12	25	4	11	5	30	8
Rad54l	ENSMUSG00000028702	11	9	22	6	6	2	28	11
Ralb	ENSMUSG00000004451	600	34	674	33	559	34	691	29
Raph1	ENSMUSG00000026014	2057	244	2567	254	1871	214	2337	313
Rasa3	ENSMUSG00000031453	585	66	758	73	582	31	773	108
Rhog	ENSMUSG00000073982	297	22	355	35	256	29	324	32
Ripk3	ENSMUSG00000022221	56	11	90	28	34	8	84	24
Rpl3	ENSMUSG00000060036	3377	296	4471	607	3263	335	4320	344
Rpl39	ENSMUSG00000079641	2170	187	2489	536	1860	274	2471	431
Rps27l	ENSMUSG00000036781	985	107	1026	159	889	103	1140	141
Rras	ENSMUSG00000038387	425	64	533	56	410	35	523	72
Sema7a	ENSMUSG00000038264	731	163	865	32	659	93	882	92
Sh3gl1	ENSMUSG00000032020	234	18	296	44	217	29	272	16
Slc39a1	ENSMUSG00000052310	1324	29	1471	82	1256	48	1467	64
Slc3a2	ENSMUSG00000010095	496	50	522	83	462	51	597	75
Sorbs3	ENSMUSG00000022091	627	75	731	50	570	54	681	36
Spsb4	ENSMUSG00000046997	117	24	148	47	116	20	180	48
Srpx	ENSMUSG00000090084	56	2	104	41	56	6	108	42
Thsd1	ENSMUSG00000031480	201	35	239	30	176	24	246	27
Tinagl1	ENSMUSG00000028776	767	115	841	137	702	142	896	129
Troap	ENSMUSG00000032783	9	3	20	8	5	3	20	13
Tspan9	ENSMUSG00000030352	1563	131	1947	401	1621	98	2180	218
Tubb2a	ENSMUSG00000058672	572	55	703	94	505	25	707	148
Tubb6	ENSMUSG0000001473	337	29	445	93	318	39	459	50
Vsig4	ENSMUSG00000044206	33	11	57	21	28	10	77	29
Wdr1	ENSMUSG0000005103	2521	253	2721	220	2501	131	3026	227
Wfdc17	ENSMUSG00000069792	126	27	205	64	117	24	230	60
Ywhab	ENSMUSG00000018326	2036	61	2287	69	1970	113	2268	129
Ywhah	ENSMUSG00000018965	1422	86	1708	173	1342	151	1658	195

**Supplementary Table S8.** RNASeq analysis of effects of angiotensin II (AngII) on mRNA expression in hearts from PKN2Het vs WT littermates: mRNAs significantly downregulated by AngII in PKN2Het hearts.

Gene Symbol	Ensembl gene id	WT Vehicle		WT AngII		PKN2Het Vehicle		PKN2Het AngII	
		Mean	SD	Mean	SD	Mean	SD	Mean	SD
Abcb7	ENSMUSG0000031333	1213	155	1016	47	1337	171	1067	172
AC161607.1	ENSMUSG00000116903	73	23	44	12	85	11	52	12
Acaca	ENSMUSG0000020532	559	140	447	82	557	121	494	41
Antxr2	ENSMUSG0000029338	3138	199	2527	322	3402	377	2661	386
Arl8b	ENSMUSG0000030105	1872	115	1674	157	2035	143	1684	79
Art4	ENSMUSG0000030217	412	21	326	68	438	37	298	89
Atl2	ENSMUSG0000059811	1046	62	921	131	1052	45	882	97
Atxn2	ENSMUSG0000042605	1186	207	1021	195	1395	65	1084	156
Bicra	ENSMUSG0000070808	259	26	236	41	304	46	218	25
Carnmt1	ENSMUSG0000024726	1249	241	1074	205	1403	244	1098	142
Carns1	ENSMUSG0000075289	373	32	286	27	383	53	289	49
Cited2	ENSMUSG0000039910	544	99	394	73	713	201	447	51
Cog5	ENSMUSG0000035933	1358	209	1191	133	1404	218	1168	103
Dcaf12l1	ENSMUSG0000045284	80	13	49	12	91	12	54	16
Dgke	ENSMUSG0000000276	588	81	456	38	628	87	483	103
Dhtkd1	ENSMUSG0000025815	67	13	46	8	98	24	53	13
Eml5	ENSMUSG0000051166	129	41	106	30	156	42	80	35
Fam84a	ENSMUSG0000020607	17	9	9	4	31	21	9	5
Fam84b	ENSMUSG0000072568	367	45	332	38	416	37	306	21
Fbxo3	ENSMUSG0000027180	1943	149	1714	52	1982	135	1735	155
Fgd4	ENSMUSG0000022788	952	82	788	50	1006	124	808	116
Fnip1	ENSMUSG0000035992	1689	280	1464	146	1814	202	1491	143
Gab1	ENSMUSG0000031714	1294	55	1103	118	1362	98	1139	128
Gm47283	ENSMUSG0000096768	121	68	133	40	164	81	81	49
Hbp1	ENSMUSG0000002996	1726	184	1572	147	1798	134	1552	102
Hccs	ENSMUSG0000031352	997	84	858	98	1041	148	890	60
Hspa12a	ENSMUSG0000025092	841	91	689	87	938	90	730	91
Jmy	ENSMUSG0000021690	1390	158	1200	90	1500	137	1234	114
Kcnh2	ENSMUSG0000038319	847	124	668	110	912	148	635	80
Kcnj2	ENSMUSG0000041695	1344	337	915	199	1453	205	945	234
Laptm4b	ENSMUSG0000022257	953	46	801	57	990	41	803	90
Lysmd4	ENSMUSG0000043831	351	36	275	32	399	40	293	44
Mef2a	ENSMUSG0000030557	4209	341	3602	223	4401	428	3617	183
Mef2d	ENSMUSG000001419	2886	195	2459	352	3285	449	2564	203
Mif4gd	ENSMUSG0000020743	399	41	345	38	434	39	328	28
mt-Nd2	ENSMUSG0000064345	563587	132806	437281	99302	600917	101879	466929	126476
mt-Nd5	ENSMUSG0000064367	810634	162252	639879	106231	854483	106054	682450	132819
Myo5c	ENSMUSG0000033590	102	18	90	31	150	35	66	21
Nnt	ENSMUSG0000025453	5147	1691	3697	588	6332	1498	4488	661
Osbpl1a	ENSMUSG0000044252	1430	127	1177	138	1477	68	1236	73
Pkd2l2	ENSMUSG0000014503	119	20	90	8	123	12	80	8
Plag1	ENSMUSG0000003282	111	11	86	16	110	13	71	14
Plin5	ENSMUSG0000011305	1427	167	1055	258	1589	193	1116	132
Plxnb3	ENSMUSG0000031385	47	14	32	7	53	9	26	4
Pnrc1	ENSMUSG0000040128	1394	186	1223	251	1670	151	1176	94
Prox1	ENSMUSG0000010175	2013	472	1483	298	2390	394	1685	308
Ptpru	ENSMUSG0000028909	76	23	56	21	65	20	34	14
Pygo1	ENSMUSG0000034910	734	66	583	66	821	99	642	73
Retreg1	ENSMUSG0000022270	4914	645	4621	579	5580	346	4633	468
Rorc	ENSMUSG0000028150	820	185	636	99	951	111	730	106
Rsbn11	ENSMUSG0000039968	486	32	495	68	547	61	451	62
Sall4	ENSMUSG0000027547	38	19	25	17	54	31	20	2
Sc5d	ENSMUSG0000032018	453	51	403	59	480	34	405	25
Slc25a22	ENSMUSG0000019082	545	113	458	107	575	57	418	70
Slc25a46	ENSMUSG0000024259	1632	281	1428	165	1805	227	1528	184
Slc40a1	ENSMUSG0000025993	540	85	413	68	525	93	369	33
Slc5a6	ENSMUSG0000006641	210	13	153	42	237	30	148	21
Slc9a2	ENSMUSG0000026062	118	24	98	34	103	34	64	9

Slf1	ENSMUSG00000021597	700	128	591	68	734	132	561	98
Smarcd1	ENSMUSG00000023018	561	16	444	69	610	82	467	65
Sobp	ENSMUSG00000038248	528	23	434	59	594	52	453	47
Sorcs2	ENSMUSG00000029093	323	58	246	26	327	75	216	35
Sp4	ENSMUSG00000025323	262	26	223	14	286	22	209	16
Stk39	ENSMUSG00000027030	2038	169	1731	250	2027	268	1564	136
Tmem161a	ENSMUSG00000002342	695	40	602	58	708	61	579	56
Tmem170b	ENSMUSG00000087370	544	52	444	44	603	78	462	26
Tmem238	ENSMUSG00000030431	17	16	16	5	31	9	10	4
Tob1	ENSMUSG00000037573	692	101	631	35	830	74	668	42
Trmt2b	ENSMUSG0000067369	1295	120	1099	134	1300	53	1109	91
Ttc30a1	ENSMUSG0000075271	133	38	110	17	165	28	117	20
Ttc30b	ENSMUSG0000075273	431	88	337	29	476	71	363	72
Txnip	ENSMUSG0000038393	13919	3376	11722	2478	18708	3486	12475	1810
Ubc	ENSMUSG0000008348	13447	4055	10872	1508	16818	2949	12228	2263
Ube2b	ENSMUSG0000020390	4614	513	4036	428	4668	348	4142	342
Ulk1	ENSMUSG0000029512	1687	77	1424	156	1856	253	1452	92
Vps13a	ENSMUSG0000046230	1184	126	1087	104	1354	142	1101	159
Ythdf3	ENSMUSG0000047213	1491	106	1342	61	1508	114	1305	117
Zbtb18	ENSMUSG0000063659	834	109	672	89	963	89	675	105
Zfp292	ENSMUSG0000039967	872	86	749	89	898	77	715	84

**Supplementary Table S9.** RNASeq data: gene clusters.

Gene Symbol	Ensembl gene id	WT Vehicle		WT AngII		PKN2Het Vehicle		PKN2Het AngII	
		Mean	SD	Mean	SD	Mean	SD	Mean	SD
<b>Complement</b>									
C1qa	ENSMUSG00000036887	895	96	1523	250	883	97	1362	183
C1qb	ENSMUSG00000036905	826	111	1513	429	782	128	1330	245
C1qc	ENSMUSG00000036896	886	106	1454	199	845	131	1290	171
C1qtnf3	ENSMUSG00000058914	3	2	341	632	3	2	118	157
C1qtnf5	ENSMUSG00000079592	53	6	100	38	61	17	87	20
C1qtnf6	ENSMUSG00000022440	122	21	426	250	120	11	348	107
C1qtnf7	ENSMUSG00000061535	178	26	294	78	174	31	227	32
C3ar1	ENSMUSG00000040552	234	31	502	241	242	41	380	97
C4b	ENSMUSG00000073418	231	28	604	141	295	41	861	703
C5ar1	ENSMUSG00000049130	107	17	173	40	78	18	156	56
Cfb	ENSMUSG00000090231	36	7	140	61	33	15	114	78
<b>Extracellular matrix</b>									
Acan	ENSMUSG00000030607	4	3	66	49	3	1	32	34
Aspn	ENSMUSG00000021388	750	159	3970	5012	798	171	1825	1043
Bgn	ENSMUSG00000031375	5175	520	12514	5386	5152	464	9491	2127
Ccdc80	ENSMUSG00000022665	1816	295	3479	1261	1843	168	2847	551
Col11a1	ENSMUSG00000027966	2	3	52	76	2	2	12	11
Col12a1	ENSMUSG00000032332	47	12	495	623	42	10	315	288
Col14a1	ENSMUSG00000022371	466	75	1493	1179	377	75	1075	556
Col15a1	ENSMUSG00000028339	2833	383	5668	1135	3175	509	5335	1392
Col16a1	ENSMUSG00000040690	187	39	603	471	192	60	420	186
Col18a1	ENSMUSG0000001435	248	28	790	244	293	35	541	181
Col1a1	ENSMUSG0000001506	1941	334	10243	9888	2115	63	5954	3420
Col1a2	ENSMUSG00000029661	2657	250	11812	10867	2786	231	7551	4300
Col3a1	ENSMUSG00000026043	5494	744	25906	20347	5871	824	16747	9657
Col4a1	ENSMUSG00000031502	12856	2211	23909	1751	13123	855	20837	3837
Col4a2	ENSMUSG00000031503	9490	1105	15270	591	9814	526	14603	2361
Col4a3	ENSMUSG00000079465	203	49	299	93	199	27	307	35
Col4a4	ENSMUSG00000067158	345	73	497	114	364	54	494	37
Col4a5	ENSMUSG00000031274	763	91	1159	304	773	91	971	147
Col5a1	ENSMUSG00000026837	1205	173	3410	1633	1238	85	2682	1054
Col5a2	ENSMUSG00000026042	878	65	4055	3237	927	105	2738	1563
Col5a3	ENSMUSG0000004098	576	178	985	63	666	103	847	222
Col6a1	ENSMUSG0000001119	2071	252	3943	1376	2047	155	3242	704
Col6a2	ENSMUSG00000020241	2038	291	3824	981	2062	139	3256	743
Col6a3	ENSMUSG00000048126	1170	165	2685	1137	1119	203	1895	452
Col7a1	ENSMUSG00000025650	4	6	26	21	5	4	11	6
Col8a1	ENSMUSG00000068196	704	96	3461	2170	747	153	2473	1081
Col8a2	ENSMUSG00000056174	9	5	180	298	14	4	86	85
Col9a2	ENSMUSG00000028626	6	1	31	38	7	4	21	11
Comp	ENSMUSG00000031849	39	8	325	426	69	9	179	129
Crtap	ENSMUSG00000032431	384	57	511	72	379	32	471	67
Cthrc1	ENSMUSG00000054196	3	3	221	380	5	2	92	112
Ecm1	ENSMUSG00000028108	452	86	696	127	464	82	720	136
Egflam	ENSMUSG00000042961	374	53	240	63	279	55	262	40
Eln	ENSMUSG00000029675	512	176	2249	1534	591	55	1327	606
Fbln2	ENSMUSG00000064080	1827	201	3200	493	1966	214	3008	422
Fbn1	ENSMUSG00000027204	2671	543	7690	2514	3011	303	6532	2277
Fbn2	ENSMUSG00000024598	25	8	112	120	38	10	67	32
Fgl2	ENSMUSG00000039899	863	65	1693	575	912	106	1331	391
Flna	ENSMUSG00000031328	4014	455	5769	673	3783	774	4951	309
Fn1	ENSMUSG00000026193	1579	300	7830	6886	1494	199	4711	3367
Frem1	ENSMUSG00000059049	8	10	51	68	8	4	31	24
Has2	ENSMUSG00000022367	27	6	50	13	28	8	42	6
Hspg2	ENSMUSG00000028763	12506	1017	15279	1628	12610	707	14990	1190
Lama2	ENSMUSG00000019899	3507	352	3968	325	3362	180	4015	379
Lama4	ENSMUSG00000019846	2464	138	3226	192	2291	264	3050	270
Lamb1	ENSMUSG0000002900	2656	308	3500	191	2690	265	3282	467
Lamc1	ENSMUSG00000026478	4969	490	7157	380	5155	283	6688	486

Lox	ENSMUSG00000024529	89	9	1050	1321	94	21	476	436
Lox11	ENSMUSG00000032334	618	97	1447	604	687	57	1181	257
Lox12	ENSMUSG00000034205	724	133	1635	127	683	84	1403	383
Lox13	ENSMUSG0000000693	104	36	311	233	87	12	196	70
Lum	ENSMUSG00000036446	1447	238	3824	2686	1553	192	2795	564
Matn2	ENSMUSG00000022324	417	57	667	192	429	35	559	39
Mfap2	ENSMUSG00000060572	20	2	69	61	23	4	41	14
Mfap3	ENSMUSG00000020522	454	25	541	33	431	20	503	22
Mfap3l	ENSMUSG00000031647	512	38	351	27	511	51	378	15
Mfap4	ENSMUSG00000042436	202	18	1249	1153	245	36	712	324
Mfap5	ENSMUSG00000030116	411	43	1634	1033	404	45	1132	430
Mgp	ENSMUSG00000030218	1671	257	3299	1832	1627	149	2424	267
Mxra7	ENSMUSG00000020814	353	43	549	114	334	33	485	81
Mxra8	ENSMUSG00000029070	431	61	782	329	511	145	714	119
Nid1	ENSMUSG0000005397	3926	530	6347	1387	3634	332	5323	725
Nid2	ENSMUSG00000021806	561	130	914	118	537	62	895	114
Ntn1	ENSMUSG00000020902	1895	146	1435	153	2064	197	1793	251
P3h1	ENSMUSG00000028641	217	25	313	43	242	18	308	55
P3h3	ENSMUSG00000023191	185	14	319	100	179	28	278	54
P4ha3	ENSMUSG00000051048	2	2	23	32	1	1	11	10
Pcolce	ENSMUSG00000029718	778	81	1236	178	675	91	1133	173
Pcolce2	ENSMUSG00000015354	412	82	494	81	352	55	503	72
Plod3	ENSMUSG0000004846	475	118	658	87	472	51	605	62
Postn	ENSMUSG00000027750	1288	354	16369	19036	1325	317	10262	8108
Prg4	ENSMUSG0000006014	323	89	484	130	321	33	596	281
Sparc	ENSMUSG00000018593	7512	635	18831	6579	7355	933	14409	2942
Vcan	ENSMUSG00000021614	730	115	1503	151	665	105	1354	355
<b>Interferon signalling</b>									
Ifi203	ENSMUSG00000039997	891	161	1230	255	880	117	940	84
Ifi204	ENSMUSG00000073489	206	34	433	95	196	40	334	43
Ifi209	ENSMUSG00000043263	52	15	126	69	50	17	92	45
Ifi211	ENSMUSG00000026536	185	36	351	104	178	18	256	21
Ifi2712a	ENSMUSG00000079017	237	35	439	84	218	39	420	49
Ifi30	ENSMUSG00000031838	101	27	193	76	87	20	127	31
Ifih1	ENSMUSG00000026896	299	32	446	46	329	56	378	53
Ifit1	ENSMUSG00000034459	187	43	329	102	161	24	234	21
Ifit2	ENSMUSG00000045932	547	92	934	140	539	58	669	52
Ifit3	ENSMUSG00000074896	336	93	626	210	311	45	430	29
Ifit3b	ENSMUSG00000062488	122	30	208	57	123	22	150	9
Ifitm2	ENSMUSG00000060591	875	131	1176	80	841	117	1097	135
Ifitm3	ENSMUSG00000025492	1226	258	1689	136	1126	147	1515	182
Ifngr1	ENSMUSG00000020009	1109	126	1400	78	1101	128	1324	109
Irf5	ENSMUSG00000029771	73	13	148	22	78	12	119	35
Irf7	ENSMUSG00000025498	220	65	413	114	189	26	332	52
Irf8	ENSMUSG00000041515	118	13	229	76	128	21	193	26
Isg20	ENSMUSG00000039236	86	30	130	16	102	27	144	32
<b>Mitochondria</b>									
Acaa2	ENSMUSG00000036880	13252	1380	8259	2391	12324	1059	9258	1215
Aco2	ENSMUSG00000022477	41047	2512	30674	4778	41075	2487	35785	2269
Afg11	ENSMUSG00000038302	1113	135	844	176	1027	95	958	51
Aldh2	ENSMUSG00000029455	3628	278	2621	303	3753	239	3023	178
Atp5a1	ENSMUSG00000025428	73890	5007	52519	8597	73310	4969	61155	3605
Atp5b	ENSMUSG00000025393	81983	4027	60525	7907	80175	3926	68956	5579
Atp5d	ENSMUSG0000003072	5810	313	4470	769	5730	539	5074	535
Atp5e	ENSMUSG00000016252	4682	460	3624	408	4707	229	4130	508
Atp5g3	ENSMUSG00000018770	18004	1331	13448	2291	18271	996	15327	1271
Atp5o	ENSMUSG00000022956	14204	841	11103	1882	13615	536	12332	665
Bcat2	ENSMUSG00000030826	1208	96	917	126	1160	104	1012	77
Cars2	ENSMUSG00000056228	540	40	408	58	563	48	458	53
Clpp	ENSMUSG0000002660	608	48	457	72	598	7	499	95
Clpx	ENSMUSG00000015357	2210	180	1776	257	2247	186	1932	167
Cluh	ENSMUSG00000020741	5745	385	4121	818	6093	799	5032	263
Coq10a	ENSMUSG00000039914	3593	171	2600	450	3601	150	3083	271
Coq2	ENSMUSG00000029319	1358	71	1066	109	1353	65	1154	62
Coq7	ENSMUSG00000030652	1122	100	786	155	1106	99	884	88

Coq8a	ENSMUSG00000026489	8867	811	6241	1021	9606	1491	7168	332
Coq9	ENSMUSG00000031782	6190	445	4627	906	6154	410	5544	503
Cox4i1	ENSMUSG00000031818	22284	812	17754	1611	22070	1141	19696	1055
Cox5a	ENSMUSG00000000088	11595	608	8951	1587	11127	414	10060	740
Cox5b	ENSMUSG00000061518	10424	672	8385	1343	10221	301	9039	577
Cox7a1	ENSMUSG00000074218	8954	697	6119	1540	8610	451	7040	827
Cox8b	ENSMUSG00000025488	6504	621	4961	1023	6394	477	5556	903
Cs	ENSMUSG0000005683	24899	2214	17482	3393	24790	1691	20831	1885
Decr1	ENSMUSG00000028223	8479	863	5924	1566	7835	344	6512	520
Diablo	ENSMUSG00000029433	1178	83	980	91	1146	35	1105	48
Dlst	ENSMUSG0000004789	11654	750	8617	1895	11270	555	10153	788
Echs1	ENSMUSG00000025465	4828	268	3779	465	4896	284	4167	357
Etfa	ENSMUSG00000032314	11167	800	7804	1484	10775	533	8929	812
Etfb	ENSMUSG0000004610	8827	431	6069	1637	8450	419	6927	725
Etdfh	ENSMUSG00000027809	13588	811	9757	2314	12812	772	10703	771
Fh1	ENSMUSG00000026526	7500	576	5659	1050	7018	180	6388	586
Fmc1	ENSMUSG00000019689	622	55	458	87	580	55	484	71
Gfm1	ENSMUSG00000027774	4053	240	3035	442	3973	430	3372	259
Gfm2	ENSMUSG00000021666	1266	144	1001	118	1229	127	1128	100
Got2	ENSMUSG00000031672	15403	947	11510	1822	15607	1320	13207	1045
Gpd2	ENSMUSG00000026827	401	24	334	32	392	48	398	25
Hccs	ENSMUSG00000031352	997	84	858	98	1041	148	890	60
Iars2	ENSMUSG00000026618	2409	99	1873	136	2398	100	2171	120
Idh2	ENSMUSG00000030541	25832	1566	18548	3665	26906	2049	21457	2197
Idh3a	ENSMUSG00000032279	10211	1028	7707	867	10029	629	8753	799
Idh3b	ENSMUSG00000027406	11455	1144	8621	1973	11227	459	9312	738
Idh3g	ENSMUSG00000002010	6376	459	4785	580	6418	422	4954	479
Immt	ENSMUSG00000052337	11137	723	8672	1433	10924	555	9873	547
Lonp1	ENSMUSG00000041168	2317	80	2025	163	2376	150	2252	87
Malsu1	ENSMUSG00000029815	281	28	208	15	260	23	236	30
Mars2	ENSMUSG00000046994	370	47	284	34	364	34	304	25
Mcub	ENSMUSG00000027994	41	14	77	15	37	4	50	10
Mdh2	ENSMUSG00000019179	16876	703	12970	2129	16369	1034	14499	734
Me3	ENSMUSG00000030621	1244	36	938	86	1271	81	1046	52
Mfn1	ENSMUSG00000027668	8217	628	6382	1129	8242	170	7059	753
Mfn2	ENSMUSG00000029020	15414	955	11184	2042	15810	1644	13241	705
Mgme1	ENSMUSG00000027424	350	28	255	46	337	12	267	30
Migal1	ENSMUSG00000054942	412	61	323	8	409	40	383	35
Mipep	ENSMUSG00000021993	1364	63	983	167	1394	126	1103	71
Mpv17	ENSMUSG00000107283	1098	32	873	90	1118	80	934	104
Mrpl14	ENSMUSG00000023939	682	54	516	77	739	35	586	87
Mrpl16	ENSMUSG00000024683	961	36	784	75	930	52	848	97
Mrpl28	ENSMUSG00000024181	1210	39	882	132	1171	81	1020	121
Mrpl37	ENSMUSG00000028622	1184	43	904	135	1161	34	1046	74
Mrpl38	ENSMUSG00000020775	704	31	534	72	674	41	611	58
Mrpl39	ENSMUSG00000022889	1365	91	1053	180	1335	40	1087	56
Mrpl44	ENSMUSG0000003299	1028	38	792	138	1029	93	915	137
Mrpl45	ENSMUSG00000018882	1187	97	837	153	1100	58	1043	54
Mrps26	ENSMUSG00000037740	355	39	258	24	351	18	326	26
Mrps35	ENSMUSG00000040112	1312	76	991	219	1236	59	1132	63
Mrps6	ENSMUSG00000039680	361	20	285	16	354	19	300	4
mt-Nd2	ENSMUSG00000064345	563587	132806	437281	99302	600917	101879	466929	126476
mt-Nd5	ENSMUSG00000064367	810634	162252	639879	106231	854483	106054	682450	132819
mt-Rnr2	ENSMUSG00000064339	356240	61989	247940	69255	362883	53161	276407	38517
Mtfp1	ENSMUSG0000004748	1636	82	1103	322	1626	114	1320	90
Mtfr11	ENSMUSG00000046671	2563	65	2169	189	2622	122	2390	105
Mtg2	ENSMUSG00000039069	366	31	275	26	387	9	312	16
Mto1	ENSMUSG00000032342	481	27	368	46	450	40	405	41
Nadk2	ENSMUSG00000022253	1247	102	792	168	1254	222	893	160
Ndufa10	ENSMUSG00000026260	9566	706	7436	1132	9920	331	8450	886
Ndufa8	ENSMUSG00000026895	4878	294	3771	635	4757	148	4279	331
Ndufa9	ENSMUSG0000000399	9480	996	7084	1337	9287	369	7867	703
Ndufs1	ENSMUSG00000025968	15975	1815	11734	2163	15650	1579	13236	1027
Ndufs2	ENSMUSG00000013593	16031	729	11634	1773	15858	991	13476	1336
Ndufs3	ENSMUSG00000005510	6047	349	4620	872	5917	121	5197	447
Ndufs7	ENSMUSG00000020153	3525	187	2485	513	3595	317	2923	370
Ndufv1	ENSMUSG00000037916	9773	762	6974	1216	9669	615	8148	626

Ogdh	ENSMUSG00000020456	39640	2492	29734	4328	41635	5116	35518	902
Opa1	ENSMUSG00000038084	5644	514	4210	706	5735	550	5001	562
Oxa11	ENSMUSG00000000959	1341	57	1036	150	1356	195	1142	95
Oxct1	ENSMUSG00000022186	26538	1570	20521	2412	25456	2358	23051	1272
Oxsm	ENSMUSG00000021786	592	47	470	26	633	71	520	20
Pdf	ENSMUSG00000078931	565	42	418	72	575	29	492	19
Pdhal	ENSMUSG00000031299	24973	2883	19882	1983	24844	2183	21298	1610
Pdk2	ENSMUSG00000038967	7045	426	4922	991	7351	661	5815	537
Pdk3	ENSMUSG00000035232	44	14	83	17	53	21	69	7
Pdp1	ENSMUSG00000049225	1052	157	827	97	1038	87	873	99
Pdp2	ENSMUSG00000048371	822	182	433	87	839	116	560	111
Pdpr	ENSMUSG00000033624	2409	176	1771	254	2523	330	2118	147
Pmpca	ENSMUSG00000026926	2809	172	2292	228	2800	157	2538	100
Sdha	ENSMUSG00000021577	26565	1713	17836	2991	26775	2129	20539	1624
Sdhb	ENSMUSG0000009863	12188	749	9065	1722	11819	503	9978	990
Sdhc	ENSMUSG00000058076	7127	66	5010	729	7101	434	5730	395
Sfxn3	ENSMUSG00000025212	216	19	310	29	224	5	272	31
Slc25a11	ENSMUSG00000014606	8077	561	5928	1242	7992	341	6986	662
Slc25a12	ENSMUSG00000027010	4184	351	2893	395	4194	379	3611	151
Slc25a13	ENSMUSG00000015112	2989	324	2199	145	3029	276	2574	268
Slc25a20	ENSMUSG00000032602	3086	349	2262	477	3063	140	2521	210
Slc25a22	ENSMUSG00000019082	545	113	458	107	575	57	418	70
Slc25a24	ENSMUSG00000040322	184	16	278	63	197	22	246	35
Slc25a3	ENSMUSG00000061904	25015	1211	18063	2479	25124	1400	20806	1485
Sod2	ENSMUSG0000006818	12266	831	8665	1885	11982	506	9979	664
Suclg1	ENSMUSG00000052738	6364	514	4599	1021	6012	279	5327	363
Suclg2	ENSMUSG00000061838	4105	321	2961	428	4037	119	3294	228
Tars2	ENSMUSG00000028107	667	59	489	66	606	23	549	66
Tcaim	ENSMUSG00000046603	1091	140	752	164	1078	129	865	134
Tufm	ENSMUSG00000073838	3132	215	2311	479	3147	191	2714	265
Twnk	ENSMUSG00000025209	604	21	452	67	607	59	505	23
Ucp3	ENSMUSG00000032942	1264	355	659	227	1281	331	698	271
Uqcc1	ENSMUSG0000005882	3454	270	2476	553	3363	150	2909	228
Uqcrc1	ENSMUSG00000025651	15130	710	10190	2080	15168	907	12233	1293
Uqcrcf1	ENSMUSG00000038462	13197	914	10056	1838	12772	692	11183	890
Vdac1	ENSMUSG00000020402	17517	801	13326	1578	17010	633	14751	342
Vdac3	ENSMUSG00000008892	6247	446	4930	675	5939	119	5490	330

### Structural

Acta1	ENSMUSG00000031972	6773	1395	24772	10833	8570	3863	28601	14894
Actb	ENSMUSG00000029580	7471	1804	10178	1677	7763	1384	9365	1200
Actg1	ENSMUSG00000062825	6824	1047	8916	1194	7413	1015	8405	1266
Actg2	ENSMUSG00000059430	11	6	37	14	12	6	20	12
Actn1	ENSMUSG00000015143	522	79	925	273	524	61	761	132
Actn4	ENSMUSG00000054808	2213	272	2742	211	2012	203	2417	171
Actr2	ENSMUSG00000020152	2099	200	2493	267	2101	71	2352	201
Actr3	ENSMUSG00000026341	2536	120	3001	264	2399	43	2908	199
Agrn	ENSMUSG00000041936	958	125	1295	154	947	79	1136	70
Aif1	ENSMUSG00000024397	63	12	133	73	51	11	95	13
Ank2	ENSMUSG00000032826	3236	377	2426	262	3245	406	2934	430
Ankrd1	ENSMUSG00000024803	20150	6483	57246	17002	19310	6244	49450	10874
Ankrd23	ENSMUSG00000067653	8223	1670	13521	3447	9104	579	14731	4085
Anks1	ENSMUSG00000024219	1418	123	1011	201	1347	177	1118	141
Anln	ENSMUSG00000036777	56	22	225	55	56	7	174	50
Arpc1b	ENSMUSG00000029622	814	81	1186	179	737	113	1071	150
Arpc2	ENSMUSG0000006304	2337	43	2757	185	2338	47	2652	121
Arpc3	ENSMUSG00000029465	1134	39	1490	168	1115	115	1392	88
Arpc5	ENSMUSG00000008475	864	45	1233	156	871	66	1121	40
Arpin	ENSMUSG00000039043	239	19	299	19	258	25	280	26
Cald1	ENSMUSG00000029761	1649	323	2616	191	1624	256	2205	422
Capg	ENSMUSG00000056737	183	29	364	36	182	36	328	70
Capza1	ENSMUSG00000070372	1251	78	1608	138	1166	148	1428	124
Cfl1	ENSMUSG00000056201	2052	87	2670	304	1872	236	2490	204
Cilp	ENSMUSG00000042254	294	76	3092	3273	401	134	2249	1515
Ckap2	ENSMUSG00000037725	33	16	131	46	25	5	95	45
Ckap2l	ENSMUSG00000048327	30	10	123	39	25	8	110	29
Ckap4	ENSMUSG00000046841	756	159	1094	75	815	103	1104	165

Cnn1	ENSMUSG00000001349	37	23	130	75	42	17	53	24
Cnn2	ENSMUSG00000004665	793	93	1039	52	856	80	1002	98
Cnn3	ENSMUSG00000053931	1009	125	1438	123	955	121	1319	119
Corol1a	ENSMUSG00000030707	175	29	270	73	171	24	228	26
Corol1b	ENSMUSG00000024835	688	47	858	53	695	47	802	76
Cotl1	ENSMUSG00000031827	234	40	369	66	208	50	335	22
Csrp1	ENSMUSG00000026421	868	80	1281	109	889	121	1075	145
Csrp2	ENSMUSG00000020186	180	37	542	354	165	20	315	127
Ctn	ENSMUSG00000031078	793	94	1056	113	811	56	962	95
Dbn1	ENSMUSG00000034675	170	35	385	71	169	25	330	74
Dbn1	ENSMUSG00000020476	472	46	575	30	501	31	573	37
Emilin1	ENSMUSG00000029163	473	106	835	204	519	28	812	91
Eml2	ENSMUSG00000040811	379	40	285	35	408	44	337	30
Eml5	ENSMUSG00000051166	129	41	106	30	156	42	80	35
Enah	ENSMUSG00000022995	2820	352	4077	860	3138	213	4243	467
Fscn1	ENSMUSG00000029581	817	47	1186	92	831	115	1140	241
Ift122	ENSMUSG00000030323	278	32	496	94	309	39	488	78
Ift81	ENSMUSG00000029469	1002	129	666	78	994	49	708	78
Jpt1	ENSMUSG00000020737	841	76	987	49	790	37	1002	107
Jpt2	ENSMUSG00000024165	169	19	197	35	141	33	226	44
Map10	ENSMUSG00000050930	149	21	98	15	151	17	112	10
Map1b	ENSMUSG00000052727	582	102	873	51	444	82	777	113
Map1lc3a	ENSMUSG00000027602	4603	222	3864	305	4713	378	4049	447
Map6	ENSMUSG00000055407	108	31	142	36	87	9	129	34
Mapre1	ENSMUSG00000027479	1639	151	1876	92	1651	91	1859	64
Msn	ENSMUSG00000031207	4381	327	6174	266	4286	400	5734	498
Mybpc2	ENSMUSG00000038670	292	36	901	354	321	110	773	309
Myh10	ENSMUSG00000020900	964	132	1462	186	988	96	1366	213
Myh14	ENSMUSG00000030739	1825	190	1436	214	1992	381	1613	123
Myh6	ENSMUSG00000040752	416670	31586	295124	67491	432469	60382	365274	31724
Myh7	ENSMUSG00000053093	1672	510	20844	27743	2490	1006	11438	8811
Myh9	ENSMUSG00000022443	4467	917	6229	813	4465	679	5733	609
Myl1	ENSMUSG00000061816	777	84	1354	639	674	113	1186	282
Myl6	ENSMUSG00000090841	3039	174	4606	743	2959	365	4098	492
Myl9	ENSMUSG00000067818	507	113	744	105	504	152	536	41
Mylip	ENSMUSG00000038175	408	59	322	55	361	21	336	42
Myo1c	ENSMUSG00000017774	2939	140	3445	280	2807	136	3414	203
Myo1d	ENSMUSG00000035441	367	44	489	47	360	56	474	39
Myo1e	ENSMUSG00000032220	382	52	541	82	377	40	487	59
Myo1f	ENSMUSG00000024300	97	11	170	34	88	10	163	43
Myo1g	ENSMUSG00000020437	50	9	89	21	55	12	90	33
Myo5a	ENSMUSG00000034593	359	55	615	165	371	102	518	152
Myo5c	ENSMUSG00000033590	102	18	90	31	150	35	66	21
Myof	ENSMUSG00000048612	346	89	640	167	312	56	541	78
Nes	ENSMUSG0000004891	1779	216	2677	688	1621	280	2378	347
Pfn1	ENSMUSG00000018293	2349	50	2712	75	2362	104	2642	191
Sgcb	ENSMUSG00000029156	2725	146	2351	41	2817	190	2512	150
Sgce	ENSMUSG0000004631	294	28	387	53	287	38	342	18
Smarcd1	ENSMUSG00000023018	561	16	444	69	610	82	467	65
Sntb2	ENSMUSG00000041308	632	76	913	145	638	68	853	99
Sptb	ENSMUSG00000021061	3814	253	2892	391	4015	448	3358	226
Tagln	ENSMUSG00000032085	483	160	931	216	458	122	542	128
Tagln2	ENSMUSG00000026547	1222	205	1863	181	1131	206	1710	250
Tcap	ENSMUSG00000078777	15023	5676	9524	3481	11808	3513	10365	2562
Tln1	ENSMUSG00000028465	3433	355	4129	304	3528	301	4361	274
Tmod1	ENSMUSG00000028328	6866	511	5456	542	6671	424	6180	413
Tmod4	ENSMUSG0000005628	378	37	254	60	361	43	317	59
Tnni3	ENSMUSG00000035458	63108	4479	42722	10485	61514	1321	48873	5226
Tnnt2	ENSMUSG00000026414	110161	8926	87055	9068	105408	3834	92241	8335
Tnnt3	ENSMUSG00000061723	6	2	29	39	5	3	17	17
Tpm2	ENSMUSG00000028464	338	60	565	58	358	58	477	79
Tpm3	ENSMUSG00000027940	1515	192	2133	211	1390	166	1854	103
Tpm4	ENSMUSG00000031799	3181	181	4770	635	3020	369	4360	322
Ttl1	ENSMUSG00000022442	921	104	531	110	965	54	680	86
Tuba1a	ENSMUSG00000072235	1839	223	2349	176	1762	189	2229	379
Tubb2a	ENSMUSG00000058672	572	55	703	94	505	25	707	148
Tubb2b	ENSMUSG00000045136	49	15	127	28	62	34	105	43

Tubb5	ENSMUSG00000001525	1852	114	2383	316	1680	188	2353	298
Tubb6	ENSMUSG00000001473	337	29	445	93	318	39	459	50
Vim	ENSMUSG00000026728	3763	407	7380	1381	3521	520	6206	983
Was	ENSMUSG00000031165	34	9	71	17	40	6	48	12
Whrn	ENSMUSG00000039137	481	110	307	100	542	79	382	97
Wipf1	ENSMUSG00000075284	572	54	783	47	562	70	635	43
Wisp1	ENSMUSG00000005124	27	8	174	241	30	12	82	66
Xirp2	ENSMUSG00000027022	23026	1933	46990	12463	24085	3291	47862	16560
Zyx	ENSMUSG00000029860	896	129	1214	76	876	143	1120	93

**Supplementary Table S10. Body weights of adult mice.** P values are for body weight after treatment with angiotensin II (AngII) for 7 d relative to baseline body weight (2-way ANOVA with Holm-Sidak's post-test) or for PKN2Het mice relative to wild-type (WT) mice at 42 weeks (t test). There were no significant differences between WT and PKN2Het mice at 12 weeks.

12 weeks		Baseline body weight (g)			Body weight after 7 d AngII (g)			P value
		Mean	SEM	n	Mean	SEM	n	
WT/Vehicle		28.18	0.75	5	28.24	0.72	5	P=0.071
PKN2Het/Vehicle		28.25	0.69	8	27.80	0.80	7	<b>P&lt;0.001</b>
WT/AngII		28.96	0.72	5	28.74	0.56	5	P=0.6235
PKN2/AngII		29.42	0.76	8	28.47	0.72	7	P=0.1847
42 weeks		WT			PKN2Het			
		Mean	SEM	n	Mean	SEM	n	
		35.10	1.40	8	37.24	0.67	11	p=0.151

**Supplementary Table S11. qPCR primers.**

Gene	Sense Primer (5'→3')	Antisense Primer (5'→3')
Gapdh	TCACCACCATGGAGAAGGC	GCTAAGCAGTTGGTGGTGCA
Myh7	CATGCCAACCGTATGGCTG	GTTCCACGATGGCGATGTTTC
Nppa	GATGGATTCAAGAACCTGCTAGA	CTTCCTCAGTCTGCTCACTCA
Nppb	TCCAGCAGAGACCTAAAATTG	CAGTGCAGTACAGCCAAA
Tagln	GACTGCACCTCTCGGCTCAT	CCGAAGCTACTCTCCTTCCA

## Supplementary references

60 Banyasz, T., Lozinskiy, I., Payne, C. E., Edelmann, S., Norton, B., Chen, B., Chen-Izu, Y., Izu, L. T. and Balke, C. W. (2008) Transformation of adult rat cardiac myocytes in primary culture. *Exp Physiol.* **93**, 370-382

61 Cerbai, E., Pino, R., Sartiani, L. and Mugelli, A. (1999) Influence of postnatal-development on I(f) occurrence and properties in neonatal rat ventricular myocytes. *Cardiovasc Res.* **42**, 416-423

## **Chapter 5 - The anti-cancer drug dabrafenib is not cardiotoxic and inhibits cardiac remodelling and fibrosis in a murine model of hypertension**

**Title:** The anti-cancer drug dabrafenib is not cardiotoxic and inhibits cardiac remodelling and fibrosis in a murine model of hypertension.

**Authors:** Daniel N. Meijles, Joshua J. Cull, Susanna T.E. Cooper, Thomas Markou, Michelle A. Hardyman, Stephen J. Fuller, Hajed O. Alharbi, Zoe H.R. Haines, Viridiana Alcantara-Alonso, Peter E. Glennon, Mary N. Sheppard, Peter H. Sugden and Angela Clerk.

**Contributions:** Meijles D.N.: Conceptualization, Resources, Data curation, Formal analysis, Supervision, Funding acquisition, Investigation, Visualisation, Methodology, Writing—original draft, Writing—review and editing. Cull J.J.: Data curation, Validation, Investigation, Methodology. Cooper S.T.E.: Data curation, Formal analysis, Investigation, Methodology. Markou T.: Data curation, Investigation. Hardyman M.A.: Investigation. Fuller S.J.: Data curation, Formal analysis, Investigation. Alharbi H.O.: Investigation. Haines Z.: Investigation. Alcantara-Alonso V.: Investigation. Glennon P.E.: Formal analysis, Methodology. Sheppard M.N.: Resources, Methodology. Sugden P.H.: Writing—review and editing. Clerk A.: Conceptualization, Resources, Data curation, Formal analysis, Supervision, Funding acquisition, Investigation, Visualization, Methodology, Writing—original draft, Project administration, Writing—review and editing.

**DOI:** <https://doi.org/10.1042/CS20210192>

## Research Article

# The anti-cancer drug dabrafenib is not cardiotoxic and inhibits cardiac remodelling and fibrosis in a murine model of hypertension

 Daniel N. Meijles<sup>1,2</sup>, Joshua J. Cull<sup>1</sup>, Susanna T.E. Cooper<sup>2</sup>, Thomais Markou<sup>1</sup>, Michelle A. Hardyman<sup>1</sup>, Stephen J. Fuller<sup>1</sup>, Hajed O. Alharbi<sup>1</sup>, Zoe H.R. Haines<sup>2</sup>, Viridiana Alcantara-Alonso<sup>1</sup>, Peter E. Glennon<sup>3</sup>, Mary N. Sheppard<sup>2,4,5</sup>, Peter H. Sugden<sup>1</sup> and  Angela Clerk<sup>1</sup>

<sup>1</sup>School of Biological Sciences, University of Reading, Reading RG6 2AS, U.K.; <sup>2</sup>Molecular and Clinical Sciences Institute, St George's University of London, London SW17 0RE, U.K.; <sup>3</sup>University Hospitals Coventry and Warwickshire, University Hospital Cardiology Department, Clifford Bridge Road, Coventry CV2 2DX, U.K.; <sup>4</sup>CRY Cardiovascular Pathology Department, St. George's University of London, London, U.K.; <sup>5</sup>St. George's Healthcare NHS Trust, London, U.K.

**Correspondence:** Clerk A. (a.clerk@reading.ac.uk)



Raf kinases signal via extracellular signal-regulated kinases 1/2 (ERK1/2) to drive cell division. Since activating mutations in BRAF (B-Raf proto-oncogene, serine/threonine kinase) are highly oncogenic, BRAF inhibitors including dabrafenib have been developed for cancer. Inhibitors of ERK1/2 signalling used for cancer are cardiotoxic in some patients, raising the question of whether dabrafenib is cardiotoxic. In the heart, ERK1/2 signalling promotes not only cardiomyocyte hypertrophy and is cardioprotective but also promotes fibrosis. Our hypothesis is that ERK1/2 signalling is not required in a non-stressed heart but is required for cardiac remodelling. Thus, dabrafenib may affect the heart in the context of, for example, hypertension. In experiments with cardiomyocytes, cardiac fibroblasts and perfused rat hearts, dabrafenib inhibited ERK1/2 signalling. We assessed the effects of dabrafenib (3 mg/kg/d) on male C57BL/6J mouse hearts *in vivo*. Dabrafenib alone had no overt effects on cardiac function/dimensions (assessed by echocardiography) or cardiac architecture. In mice treated with 0.8 mg/kg/d angiotensin II (AngII) to induce hypertension, dabrafenib inhibited ERK1/2 signalling and suppressed cardiac hypertrophy in both acute (up to 7 d) and chronic (28 d) settings, preserving ejection fraction. At the cellular level, dabrafenib inhibited AngII-induced cardiomyocyte hypertrophy, reduced expression of hypertrophic gene markers and almost completely eliminated the increase in cardiac fibrosis both in interstitial and perivascular regions. Dabrafenib is not overtly cardiotoxic. Moreover, it inhibits maladaptive hypertrophy resulting from AngII-induced hypertension. Thus, Raf is a potential therapeutic target for hypertensive heart disease and drugs such as dabrafenib, developed for cancer, may be used for this purpose.

## Introduction

The extracellular signal-regulated kinase 1/2 (ERK1/2) cascade promotes cell cycle entry and cell division in proliferating cells [1]. In the heart, ERK1/2 signalling promotes cardiomyocyte hypertrophy and, independently of this, is generally cardioprotective [2,3]. Activation of ERK1/2 requires phosphorylation by mitogen-activated protein kinase kinases 1/2 (MKK1/2), which are phosphorylated/activated by the upstream Raf kinases (RAF, BRAF, RAF1) or (in inflammation) Cot/Tpl2 [4,5]. Activation of Raf kinases requires interaction with activated, GTP-bound Ras, which brings the enzyme to the membrane for activation by phosphorylation [4]. Raf kinases operate as homo- or heterodimers. They also require

Received: 19 February 2021

Revised: 18 June 2021

Accepted: 21 June 2021

Accepted Manuscript online:  
30 June 2021

Version of Record published:  
23 July 2021

phosphorylation of specific residues to increase activity (e.g. Ser338/Ser341 in human RAF1) plus dephosphorylation of other residues to permit activation (e.g. Ser43 in human RAF1).

Mutations that activate ERK1/2 signalling cause cancer. Activating mutations in BRAF are particularly prevalent, being associated with ~30% of all cancers and ~60% of melanomas [6,7]. As such, efficacious BRAF inhibitors (e.g. dabrafenib [8]) have been developed for clinical use. Whilst these inhibitors were designed to target oncogenic BRAF, they also inhibit wild-type Raf kinases, and dabrafenib has  $IC_{50}$  values of 5.2 and 6.3 nM for BRAF and RAF1, respectively [8]. The first generation of drugs to be developed are competitive inhibitors acting at the ATP-binding site (i.e. Type 1 or Type 1.5 inhibitors), and these can lock the enzyme in an active conformation. This led to the discovery of the 'Raf paradox' [9], where non-saturating concentrations of drugs can activate ERK1/2 signalling rather than inhibit the pathway. However, not all Raf inhibitors have paradox-inducing abilities, and little is known about their effects in 'normal' cardiac cells, so it is difficult to predict how Raf inhibitors such as dabrafenib affect the heart.

Hypertensive heart disease is a major cause of morbidity and mortality worldwide [10]. Elevated blood pressure induces an initial adaptive response allowing the heart to maintain cardiac output resulting from an increased workload [11]. Terminally differentiated contractile cardiomyocytes become hypertrophied (increase in size), with increases in and adaptation of the myofibrillar apparatus. Over time, however, this adaptative response is unsustainable and contractile function becomes compromised, leading to heart failure. At a cellular level, the switch to failure includes increased cardiomyocyte cell death [12], myocardial inflammation and increased deposition of fibrotic material [13]. While strategies exist to combat elevated blood pressure (e.g. angiotensin-converting enzyme inhibitors [14]), strategies to reduce cardiomyocyte cell death, improve cardiac contractility and reduce fibrosis are urgently needed to treat hypertensive heart failure [15].

ARAF, BRAF and RAF1 are all expressed in human and murine hearts [16]. In cultured rodent cardiomyocytes, RAF1 and ARAF are activated by hypertrophic stimuli such as endothelin-1 [17,18]. Mice with cardiomyocyte-specific expression of a dominant-negative form of RAF1 and subjected to cardiac pressure-overload exhibit increased cardiomyocyte apoptosis resulting in enhanced cardiomyopathy [19,20], consistent with reduced cardioprotection. The role of BRAF in these processes is even less well understood. Here, we investigated the effects of dabrafenib (a Type 1.5 Raf inhibitor) on the heart to determine whether it is likely to be cardiotoxic in hypertension, or if it may protect against hypertensive heart disease. We established that: (1) Raf paradox signalling induced by dabrafenib in cardiac cells is limited; (2) dabrafenib inhibits ERK1/2 activity in isolated cardiac cells, in *ex vivo* perfused adult rat hearts and in a murine model of hypertension induced by angiotensin II (AngII); and (3), inhibition of Raf kinases with dabrafenib reduced cardiomyocyte hypertrophy, cardiac inflammation and cardiac fibrosis induced by AngII in both acute (7 d) and chronic (28 d) treatment conditions. Thus, dabrafenib and, possibly, other Raf kinase inhibitors may be therapeutically useful for treating hypertensive heart disease.

## Materials and methods

### Ethical statement for animal experiments

Procedures were performed in accordance with the European Parliament Directive 2010/63/EU on the protection of animals used for scientific purposes, with local institutional animal care committee procedures (University of Reading) and the U.K. Animals (Scientific Procedures) Act 1986. C57Bl/6J mice, Sprague-Dawley rats and Alzet osmotic minipumps were from Charles River U.K. Details of animal housing, husbandry and welfare are provided in [21].

### *In vivo* mouse studies

Wild-type male (7 wk) C57Bl/6J mice were imported into the BioResource Unit at University of Reading and allowed to acclimatize for 2 weeks before experimentation. Mice were randomly allocated to each treatment group; body weights are provided in Supplementary Table S1. Drug delivery used Alzet osmotic pumps (models 1007D or 1004), filled according to the manufacturer's instructions. Mice received minipumps for delivery of 0.8 mg/kg/d angiotensin II (AngII; Merck) or vehicle (acidified PBS) without/with DMSO/PEG mix [50% (v/v) dimethyl sulphoxide (DMSO), 20% (v/v) polyethylene glycol 400, 5% (v/v) propylene glycol, 0.5% (v/v) Tween 80] or 3 mg/kg/d dabrafenib (Selleck Chemicals) dissolved in DMSO/PEG mix. Separate minipumps were used for AngII and dabrafenib delivery. Minipumps were incubated overnight in sterile PBS (37°C), then implanted subcutaneously under continuous inhalation anaesthesia using isoflurane (induction at 5%, maintenance at 2–2.5%) mixed with 2 l/min O<sub>2</sub>, as previously described [22].

Echocardiography was performed with a Vevo 2100 imaging system using a MS400 18–38 MHz transducer (Visualsonics) as previously described [22]. Left ventricular cardiac dimensions were assessed from short axis M-mode images with the axis placed at the mid-level of the left ventricle at the level of the papillary muscles. Cardiac function

for acute treatments (up to 7 d) was assessed from these images on the basis that the stresses on the hearts are likely to be relatively uniform resulting in minimal deformation of the heart. Thus, the algorithms used are appropriate for comparative data. Data analysis was performed using VevoLAB software (Visualsonics) by independent assessors blinded to intervention. Data were gathered from two M-mode scans at each time point, taking mean values across at least three cardiac cycles for each echocardiogram. The diameter of the aorta was measured with the calliper function from B-mode images at the end of cardiac systole (with the aorta at its widest) and following aortic contraction, taking an average of measurements across three cardiac cycles. Cardiac function and global longitudinal strain were measured in studies with 28 d treatments from B-mode long axis images using Vevo Strain software for speckle tracking. Global circumferential strain was measured using B-mode short axis images.

Mice were killed by CO<sub>2</sub> inhalation followed by cervical dislocation. Hearts were excised quickly, washed in PBS, blotted to remove excess PBS and snap-frozen in liquid N<sub>2</sub> or fixed in 10% buffered formalin for histology.

## Histology and assessment of myocyte size and fibrosis

Histological staining and analysis were performed as previously described [22], assessing general morphology by haematoxylin and eosin (H&E) and fibrosis by Masson's trichrome and picosirius red (PSR). Sections for the study of the effects of dabrafenib on AngII-induced cardiac pathology over 28 d were prepared and stained by HistologiX Limited. Analysis was performed by independent assessors blinded to treatment groups.

## Adult rat heart perfusions

Adult male (300–350 g) Sprague-Dawley rats were used for heart perfusions. Hearts were prepared and perfused in the Langendorff mode as described in [21]. Hearts were perfused for 15 min with Krebs-Henseleit bicarbonate-buffered saline (25 mM NaHCO<sub>3</sub>, 119 mM NaCl, 4.7 mM KCl, 2.5 mM CaCl<sub>2</sub>, 1.2 mM MgSO<sub>4</sub>, 1.2 mM KH<sub>2</sub>PO<sub>4</sub>, pH 7.4, containing 10 mM glucose and equilibrated with 95% O<sub>2</sub>/5% CO<sub>2</sub>) without or with dabrafenib (5 µM) or trametinib (1 µM). Dabrafenib and trametinib were from Selleck Chemicals. Perfusions were continued for 10 min without/with addition of human FGF2 (0.5 µg/ml; Cell Guidance Systems Ltd., U.K.). Hearts were 'freeze-clamped' between aluminium tongs cooled in liquid nitrogen and pulverized under liquid N<sub>2</sub>. Heart powders were stored at -80°C.

## Cell cultures

Neonatal rat cardiomyocytes were prepared and cultured from 2 to 4 d Sprague-Dawley rats as described previously [23]. Human cardiac fibroblasts (PromoCell) were grown in Fibroblast growth medium-3 (FGM3, PromoCell). Fibroblasts were seeded the day before experimentation (at a density to achieve 90% confluence after 24 h) and synchronized overnight in M199 medium containing 0.1% (v/v) foetal calf serum and 100 U/ml penicillin and streptomycin. Cells were exposed to the concentrations of dabrafenib and for the times indicated prior to harvesting for immunoblotting.

## RNA preparation and qPCR

Total RNA was prepared using RNA Bee (AMS Biotechnology Ltd) with 1 ml per 4 × 10<sup>6</sup> cardiomyocytes or 10–15 mg mouse heart powder as previously published [23]. Quantitative PCR (qPCR) was performed as previously described [23], using primers from Invitrogen by Thermo Fisher Scientific. Details of primer sequences are provided in Supplementary Table S2. *Gapdh* was the reference gene for the study, with relative quantification obtained using the  $\Delta Ct$  (threshold cycle) method; relative expression was calculated as  $2^{-\Delta\Delta Ct}$  and normalized to vehicle.

## Sample preparation and immunoblotting

Cells and heart powders were prepared for immunoblotting as published [22], with protein concentrations for equal loading determined by BioRad Bradford assay using bovine serum albumin standards. Proteins were separated by SDS-PAGE on 10% (w/v) polyacrylamide resolving gels with 6% stacking gels and transferred electrophoretically to nitrocellulose using a BioRad semi-dry transfer cell (10 V, 60 min) as described [23]. Proteins were detected using antibodies (1/1000 dilution) to phosphorylated or total ERK1/2 (Cell Signaling Technologies; Cat. Nos. 4377 and 4695, respectively) or *Gapdh* (Cell Signaling Technologies; Cat. No. 2118). Bands were detected by enhanced chemiluminescence using ECL Prime Western Blotting detection reagents with visualization using an ImageQuant LAS4000 system (GE Healthcare). ImageQuant TL 8.1 software (GE Healthcare) was used for densitometric analysis of the bands.

## Image processing

Images were cropped and reorientated for presentation using Photoshop CC then resized in Adobe Illustrator, maintaining the original proportions and using the same resizing factor for all images within a Figure.

## Statistical analysis

Data analysis was performed using Microsoft Excel and GraphPad Prism. Statistical analysis was performed using GraphPad Prism with two-tailed unpaired *t* tests, two-tailed one-way ANOVA or two-tailed two-way ANOVA as indicated. A multiple comparison test was used in combination with ANOVA as indicated in the figure legends. Graphs were plotted with GraphPad Prism 9.0.

## Results

### Dabrafenib inhibits ERK1/2 signalling in cardiac cells and perfused adult rat hearts

Dabrafenib is a Type 1.5 Raf inhibitor that can activate (rather than inhibit) ERK1/2 signalling via the 'Raf paradox' in some cancer cells [9]. We first assessed if dabrafenib activates Raf signalling in primary cardiac cells (neonatal rat cardiomyocytes; human cardiac fibroblasts) *in vitro*. In cardiomyocytes, 10  $\mu$ M dabrafenib inhibited basal ERK1/2 phosphorylation (i.e. activation), with maximal inhibition at  $\sim$ 20 min (Figure 1A). Inhibition was sustained to  $\sim$ 40 min, but by 60 min the inhibitory effect was lost. This may be due to compensatory mechanisms or drug instability in the conditions used. The concentration-dependency of the response was assessed at 20 min. ERK1/2 phosphorylation was inhibited by 10  $\mu$ M dabrafenib in both cell types (Figure 1B,C), with limited effects (activating or inhibitory) at lower doses. We next determined if dabrafenib affects ERK1/2 signalling in intact Langendorff perfused adult male rat hearts, comparing dabrafenib with trametinib, a MKK1/2 inhibitor [24]. Dabrafenib (5  $\mu$ M) and trametinib (1  $\mu$ M) each inhibited basal ERK1/2 phosphorylation (Figure 1D) and agonist-induced activation of ERK1/2 in hearts perfused with FGF2 (Figure 1E). In conclusion, dabrafenib has limited ability to induce Raf paradox signalling in primary cardiac cells, but inhibits at higher concentrations.

### Dabrafenib alone does not significantly affect cardiac function, dimensions or architecture *in vivo*

Since ERK1/2 pathway modulators can cause adverse cardiac events in cancer patients [25], and our data suggest that it inhibits basal ERK1/2 signalling in the heart (Figure 1), we next assessed whether dabrafenib alone has any cardiac effects at baseline in animals *in vivo*. In cancer patients, the recommended dose of dabrafenib is 150 mg, twice daily [26]. With a body weight of 60–100 kg, the dosage would be 3–5 mg/kg/d. We selected a dose at the lower end of this spectrum and male C57Bl/6J mice were implanted with osmotic minipumps for delivery of vehicle or 3 mg/kg/d dabrafenib. The effects on cardiac function/dimensions were assessed by echocardiography. This concentration of dabrafenib had no significant effect on any cardiac parameter studied, whether associated with function (heart rate, cardiac output, ejection fraction, fractional shortening) or dimensions [e.g. left ventricular (LV) wall thickness or internal diameter] (Supplementary Figure S1A and Supplementary Table S3). Dabrafenib also had no effect on cardiac architecture assessed using standard histological staining methods, or any significant effects on mRNA expression of hypertrophic marker genes (*Myh7*, *Nppa* and *Nppb*) assessed by qPCR (Supplementary Figure S1B,C). These findings provide further evidence that dabrafenib is not overtly cardiotoxic and has no immediate adverse cardiac effects in unstressed hearts.

### Dabrafenib inhibits acute hypertensive cardiac remodelling induced by AngII in mice *in vivo*

Although our data with dabrafenib at baseline suggest Raf signalling is not required for maintenance of normal cardiac function, this may be different in the hypertensive heart that undergoes remodelling to maintain function. We therefore treated male C57Bl/6J mice with AngII (0.8 mg/kg/d) to induce hypertension and remodelling as in [22], in the absence or presence of 3 mg/kg/d dabrafenib, initially assessing the effects over 7 d. AngII (24 h) increased cardiac ERK1/2 phosphorylation (i.e. activity) with a significant increase in ERK2 phosphorylation, an effect that was absent with dabrafenib (Figure 2A). We assessed the effects on cardiac dimensions and function at 3 and 7 d by echocardiography (Figure 2B–D; Supplementary Table S3). AngII increased fractional shortening at 3 d, but this was normalized by 7 d (Figure 2C). Dabrafenib inhibited these increases at 3 d, but enhanced the response at 7 d. AngII also significantly increased diastolic and systolic LV wall thickness (WT) as early as 3 d, with decreased LV internal diameter

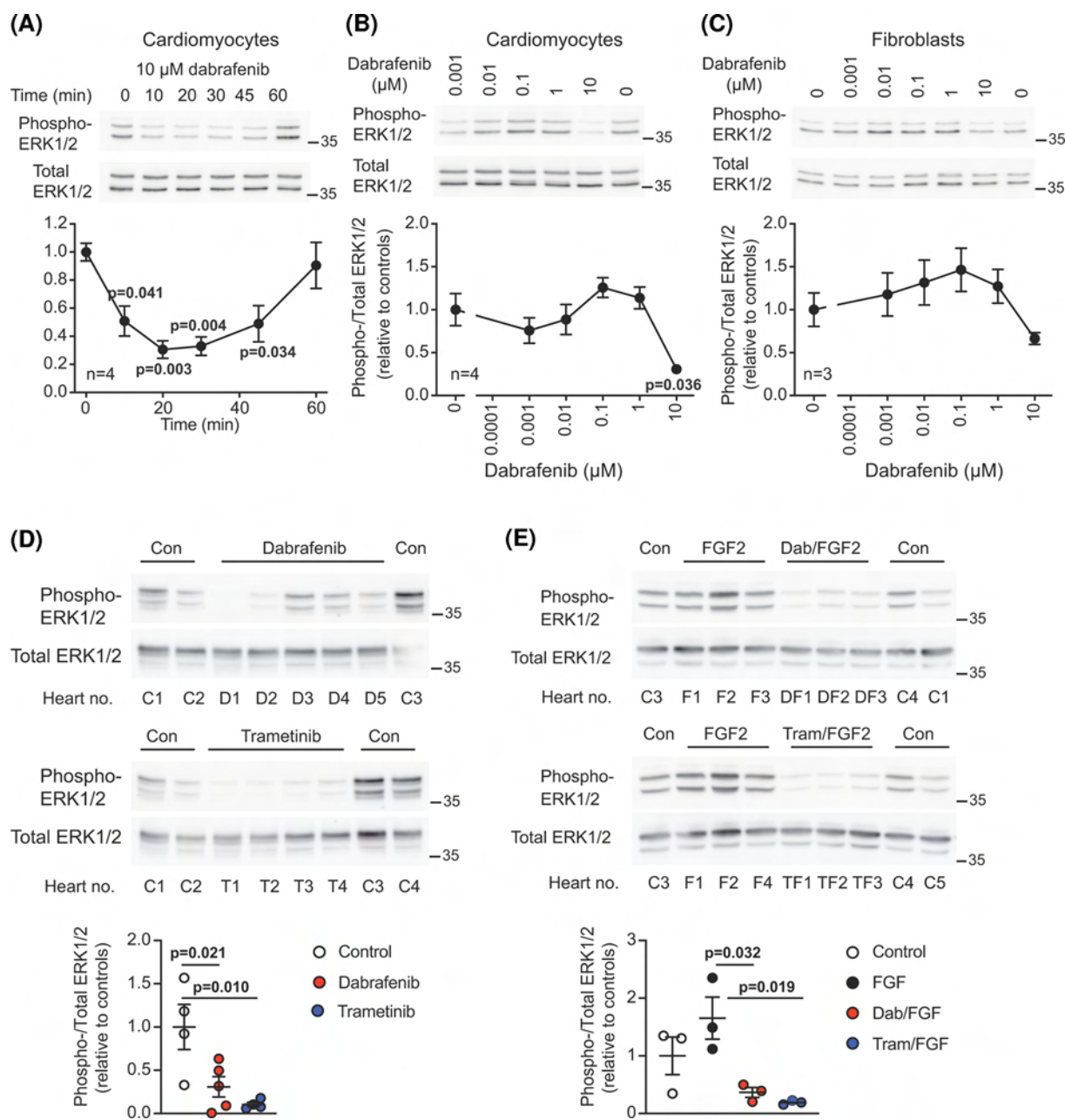


**Figure 1. Dabrafenib inhibits ERK1/2 signalling in the heart**

Neonatal rat cardiomyocytes or human cardiac fibroblasts (as indicated) were exposed to 10 μM dabrafenib for the times indicated (A), or to the indicated concentrations of dabrafenib for 20 min (B and C). Adult male rat hearts were perfused in Langendorff-mode under basal conditions (D) or with 0.5 μg/ml FGF2 (E) without/with 5 μM dabrafenib (Dab) or 1 μM trametinib (Tram) as indicated. Proteins (extracts from  $0.2 \times 10^6$  cells for cardiomyocytes; 20 μg for fibroblasts; 40 μg for hearts) were immunoblotted for phosphorylated (phospho-) or total ERK1/2. Representative blots are shown in the upper panels with positions of relative molecular mass markers on the right of each image. Densitometric analysis is provided in the lower panels. Results are provided as means  $\pm$  SEM for  $n = 3$  or 4 independent cell preparations of hearts as indicated. For (D and E), individual data points are also shown and individual hearts are labelled for direct comparison (C, control; D, dabrafenib; DF, Dab+FGF2; F, FGF2; T, trametinib; TF, Tram+FGF2). Statistical analysis used one-way ANOVA with Holm-Sidak's post-test. In (A and B), significance is given relative to samples with no dabrafenib.

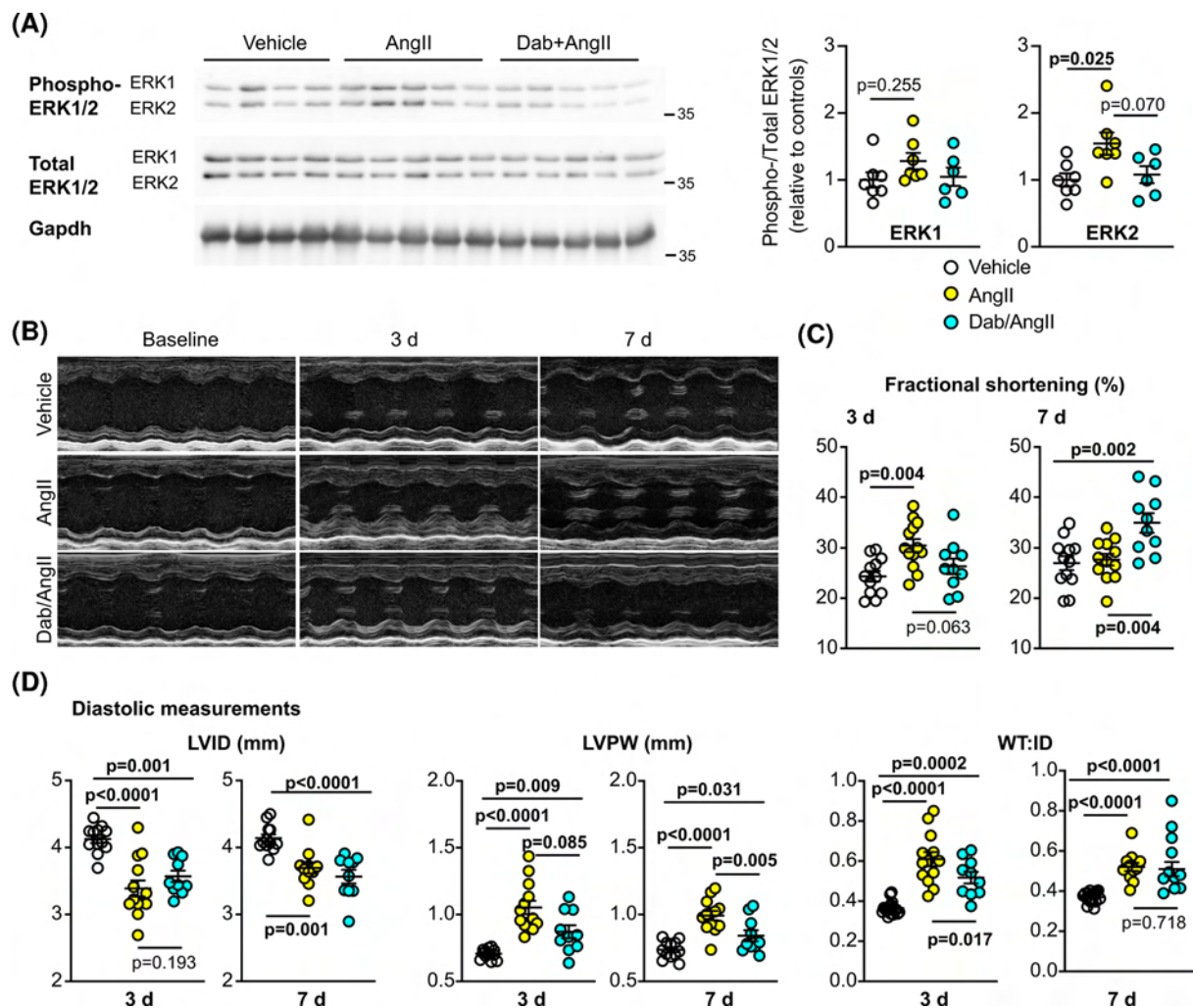


**Figure 2. Dabrafenib inhibits cardiac hypertrophy induced in mice *in vivo* by acute treatment with AngII**

C57BL/6J male mice were treated with vehicle, 0.8 mg/kg/d AngII or 3 mg/kg/d dabrafenib (Dab) with AngII for up to 7 d. (A) Mice were treated for 24 h. Total proteins were extracted from the hearts and 25  $\mu$ g immunoblotted for phosphorylated (phospho-) ERK1/2, total ERK1/2 or Gapdh. Representative immunoblots are on the left with densitometric analysis on the right. (B) Cardiac function and dimensions were assessed using echocardiography. Representative short axis M-mode echocardiograms are shown at baseline and at 3 and 7 d post-treatment. Quantitative assessment of echocardiograms are provided for fractional shortening (C) and diastolic cardiac dimensions (D). All echocardiography data are provided in Supplementary Table S3. LV, left ventricle; ID, internal diameter; PW, posterior wall; WT, wall thickness (anterior wall + posterior wall). Quantification data are individual points with means  $\pm$  SEM. Individual *P* values are shown (one-way ANOVA with Holm-Sidak's post-test).

(ID), resulting in significant increase in the WT:ID ratio (Figure 2D). This is consistent with an early compensatory hypertrophy associated with pressure-overload [27]. Dabrafenib significantly inhibited this response. The increase in wall thickness induced by AngII was sustained through to 7 d, but the change in LVID started to normalize so the WT:ID ratio was reduced relative to 3 d, suggesting that the heart was starting to adapt. Dabrafenib still inhibited the increase in wall thickness induced by AngII at 7 d and the WT:ID ratio remained stable.

To understand the effects of dabrafenib on AngII-induced changes in the heart, we undertook detailed assessment of the changes in gene expression and architecture of the heart after 7 d treatment with AngII. Dabrafenib significantly inhibited the increased cardiac mRNA expression of *Nppa* and *Nppb* induced by AngII at 7 d (Figure 3A), although it did not affect the increase in expression of *Myh7*. At a cellular level, AngII increased cardiomyocyte hypertrophy (with increased cross-sectional area) and cardiac fibrosis (Figure 3B–E). Dabrafenib significantly inhibited

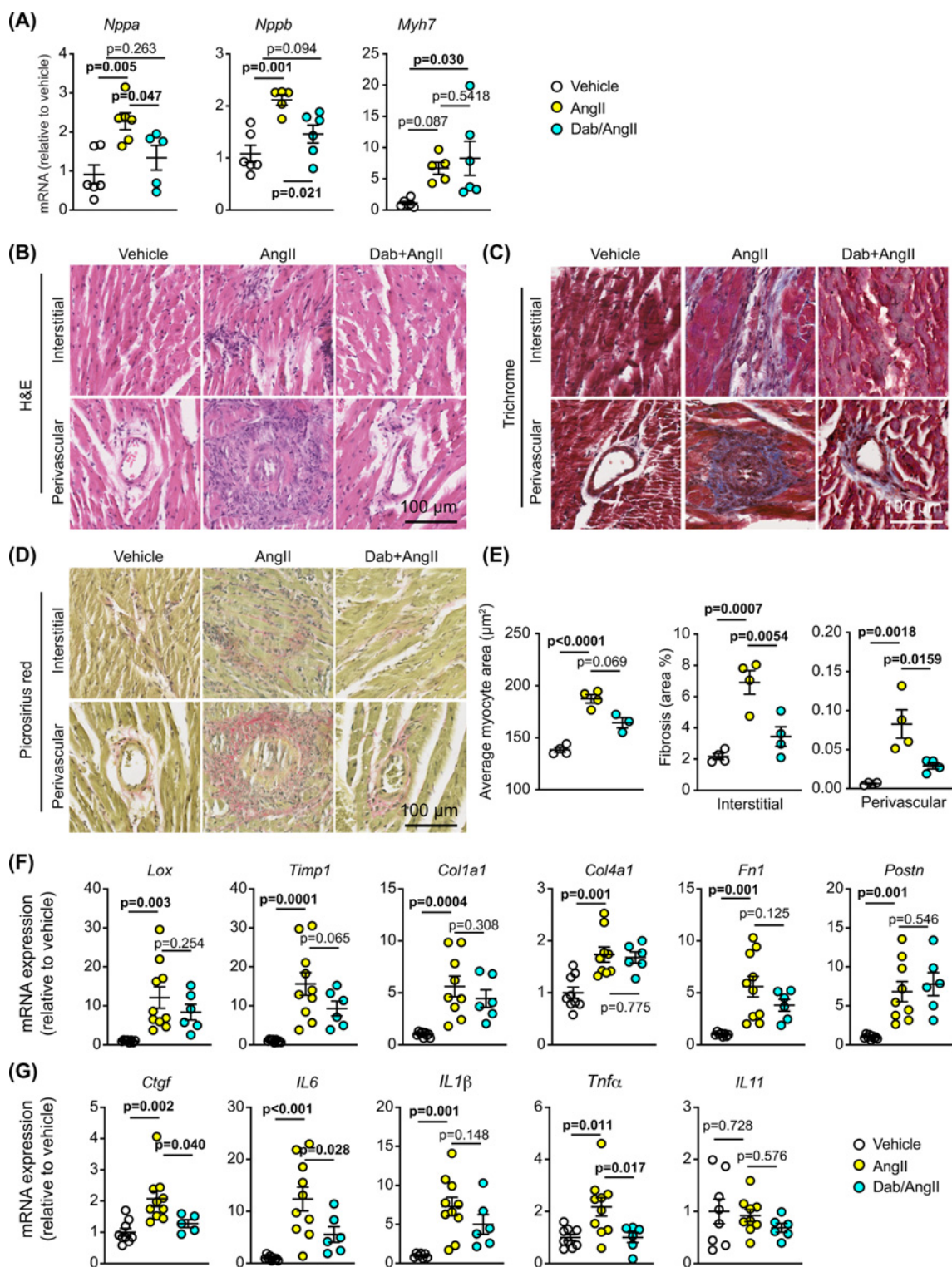


**Figure 3.** Dabrafenib reduces cardiac fibrosis induced in mice *in vivo* by acute treatment with AngII

C57BL/6J male mice were treated with vehicle, 0.8 mg/kg/d AngII or 3 mg/kg/d dabrafenib (Dab) with AngII for 7 d. (A) mRNA expression of *Nppa*, *Nppb* and *Myh7* in mouse hearts was assessed by qPCR. (B) Cardiomyocyte size was assessed using H&E staining (B) with quantification provided in (E) (left panel). Cardiac fibrosis was assessed using trichrome (C) and picrosirius red (D), with quantification provided in (E) (right panels). mRNA expression in mouse hearts of markers of fibrosis (F) or pro-inflammatory cytokines or pro-fibrotic factors (G) was assessed by qPCR. Quantification data are individual points with means  $\pm$  SEM. Individual *P* values are shown (one-way ANOVA with Holm-Sidak's post-test).

AngII-induced cardiomyocyte hypertrophy (Figure 3B,E), and almost eliminated both perivascular and interstitial fibrosis (Figure 3C–E). These effects most likely account for the reduction in cardiac hypertrophy and enhanced function detected by echocardiography (Figure 2C,D; Supplementary Table S3). The increase in expression of mRNAs for fibrosis-associated enzymes (*Lox*, *Timp1*) and extracellular matrix genes (*Col1a1*, *Col4a1*, *Fn1*, *Postn*) induced by AngII were not significantly inhibited by dabrafenib, although there was a trend to a reduced expression (Figure 3F). In contrast, dabrafenib significantly inhibited the increase in mRNAs encoding proinflammatory cytokines and profibrotic factors (*Ctgf*, *IL6*, *IL1 $\beta$* , *Tnf $\alpha$* , *IL11*) induced by AngII at 7 d (Figure 3G). This suggests that one mechanism for the maintenance of cardiac function in dabrafenib-treated hypertensive mice is via reduced myocardial inflammation that potentially impacts on fibrosis and, subsequently, cardiomyocyte hypertrophy. Overall, these studies indicate that dabrafenib moderates cardiac hypertrophy induced acutely by hypertension, with a predominant overall effect on cardiac fibrosis.

## Dabrafenib inhibits hypertensive cardiac remodelling in chronic AngII-infused mice *in vivo*

Given that dabrafenib inhibited cardiac remodelling and fibrosis in hypertensive mice over 7 d, we next assessed if the effects could be sustained over longer periods. Experiments were conducted in male C57Bl/6J mice treated with 3 mg/kg/d dabrafenib or vehicle in the presence/absence of AngII (0.8 mg/kg/d) for 28 d. Dabrafenib alone had no effect on cardiac dimensions/function over this time (Supplementary Table S4). Treatment with AngII for 28 d resulted in increased LV wall thickness whilst maintaining a similar internal diameter (Figure 4A,B; Supplementary Table S5). The increase in wall thickness was inhibited by dabrafenib. To gain insight into the effects on cardiac function, we used echocardiography with 2D speckle-tracking strain analysis of long axis views of the heart. AngII induced clear systolic dysfunction with reduced ejection fraction and fractional shortening, and increased end systolic (not diastolic) volume (Figure 4C). Though not statistically significant, this was associated with an increase in predicted end diastolic left ventricular mass. Functional measurements were supported by strain data (Figure 4D,E; N.B. global longitudinal and circumferential strain measurements are negative values). AngII caused a reduction in global longitudinal and radial strain (measured from the long axis), a result of reduced cardiac contractility. This was associated with reduced global circumferential strain (measured from the short axis view). Dabrafenib had a normalizing effect on all of these parameters. At the cellular level (Figure 5), as with acute hypertension studies (Figure 3), dabrafenib inhibited the increase in cardiomyocyte cross-sectional area induced by AngII, with a significant reduction in *Nppb* mRNA expression, and in perivascular and interstitial fibrosis.

In addition to assessing the cardiac effects of dabrafenib on the response to AngII, we examined the effects on the aorta. AngII (7 d) induced an increase in the medial wall thickness, associated with increased fibrosis (Figure 6A). Dabrafenib reduced the degree of fibrosis, but did not suppress the increase in thickness of medial layer suggesting that the overall response of the aorta to hypertensive pressures was retained. The internal diameter of the ascending aorta was measured in ultrasound images, comparing the difference at the end of cardiac systole (when the aorta is most distended) and following aortic contraction. There was no difference in the diameter of the aorta at the end of cardiac systole between vehicle-treated mice and mice treated with AngII with or without dabrafenib over 7 d (Figure 6B). However, the diameter following aortic contraction was larger in mice treated with AngII, resulting in a smaller ratio between the widest and narrowest measurements. This is consistent with reduced flexibility of the aortic wall. By 28 d, the aortae in mice treated with AngII appeared substantially more rigid than those of either the vehicle-treated mice or mice treated with dabrafenib and AngII, with little change in aortic diameter through the cardiac cycle (Figure 6C,D). Thus, dabrafenib may have additional benefits on the heart by preventing hypertension-induced deterioration of the elasticity of the aorta.

## Discussion

The importance of ERK1/2 signalling in promoting cardiomyocyte hypertrophy and cardioprotection has been known for many years [2,3], but the role of ERK1/2 signalling in promoting cardiac fibrosis has emerged more recently [28–30]. This raises the question of whether it is better to inhibit ERK1/2 and prevent fibrosis or if we should activate ERK1/2 to increase cardioprotection and cardiomyocyte hypertrophy. Furthermore, would inhibiting ERK1/2 to prevent fibrosis be detrimental to cardioprotection and hypertrophy, and vice versa? This dilemma is difficult to resolve at the theoretical level and can only be addressed experimentally. Here, as outlined in the schematic in Figure 7, we show that dabrafenib, a drug which targets the ERK1/2 cascade for cancer and inhibits Raf→ERK1/2 signalling in the heart (Figures 1 and 2), may be useful to reduce cardiac fibrosis in hypertensive heart disease and, although there is concomitant suppression of cardiomyocyte hypertrophy (potentially because of the reduced workload imposed by

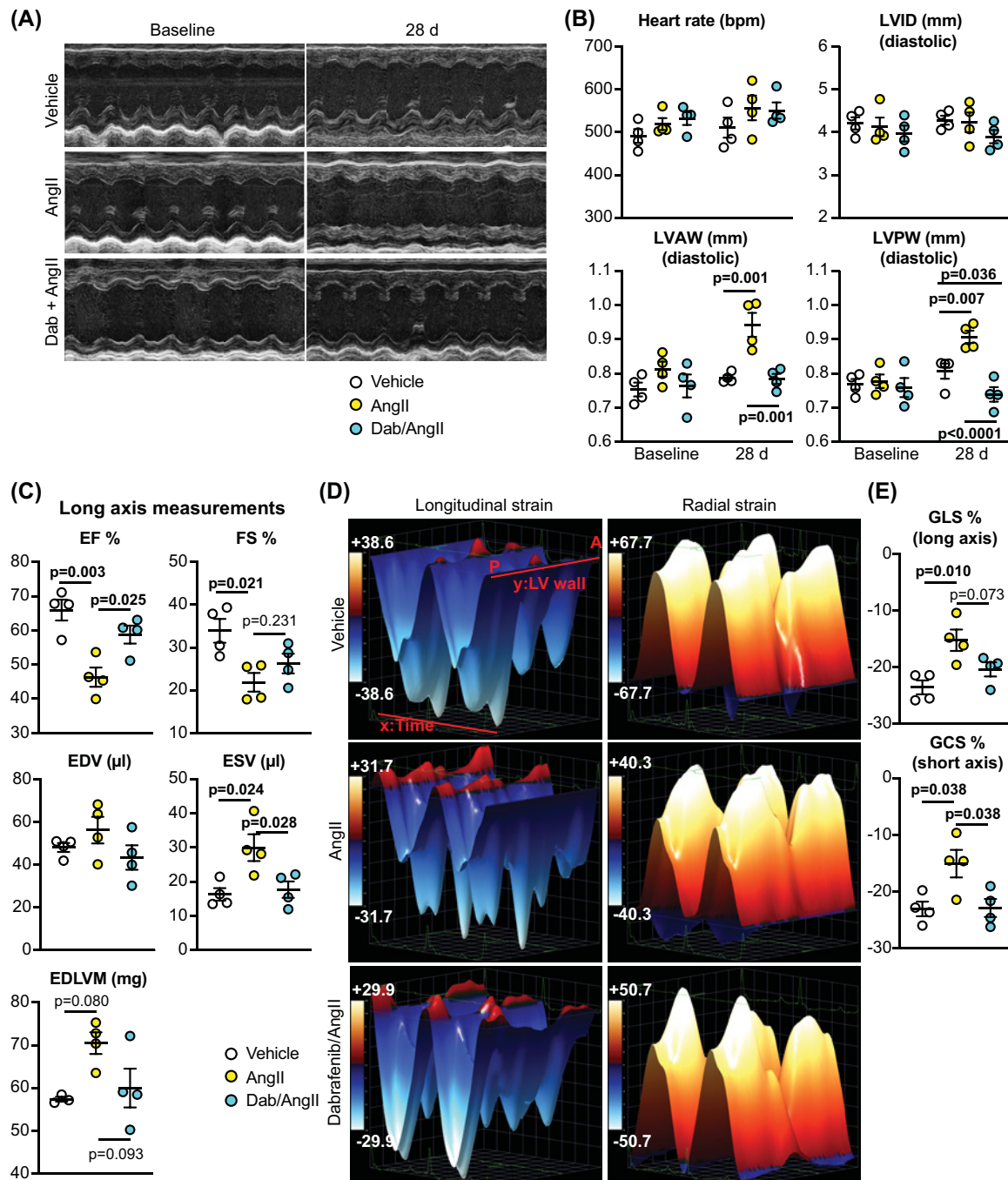


**Figure 4.** Dabrafenib inhibits changes in cardiac dimensions and function induced in mouse hearts by AngII over 28 dP  
 C57BL/6J male mice were treated with vehicle, 0.8 mg/kg/d AngII or 3 mg/kg/d dabrafenib with AngII (28 d). Cardiac function and dimensions were assessed using echocardiography. (A) Representative short axis M-mode echocardiograms from animals at baseline and with 28 d treatment. (B) Quantitative assessment of M-mode echocardiograms showing heart rate and dimensions; AW, anterior wall; LV, left ventricle; ID, internal diameter. All echocardiography data are provided in Supplementary Table S5. (C) Quantification of strain data for B-mode long axis views; EDV, end diastolic volume; EDLVM, end diastolic left ventricular mass; EF, ejection fraction; ESV, end systolic volume; FS, fractional shortening. (D) Representative 3D images showing longitudinal and radial strain assessed from long axis B-mode images. (E) Global longitudinal strain (GLS) and global circumferential strain (GCS) were measured from long and short axis B-mode images, respectively. Quantification data show individual points with means  $\pm$  SEM. Individual *P* values are shown using one-way ANOVA with Holm-Sidak's post-test in (C and E), and two-way ANOVA with Holm-Sidak's post-test in (B).

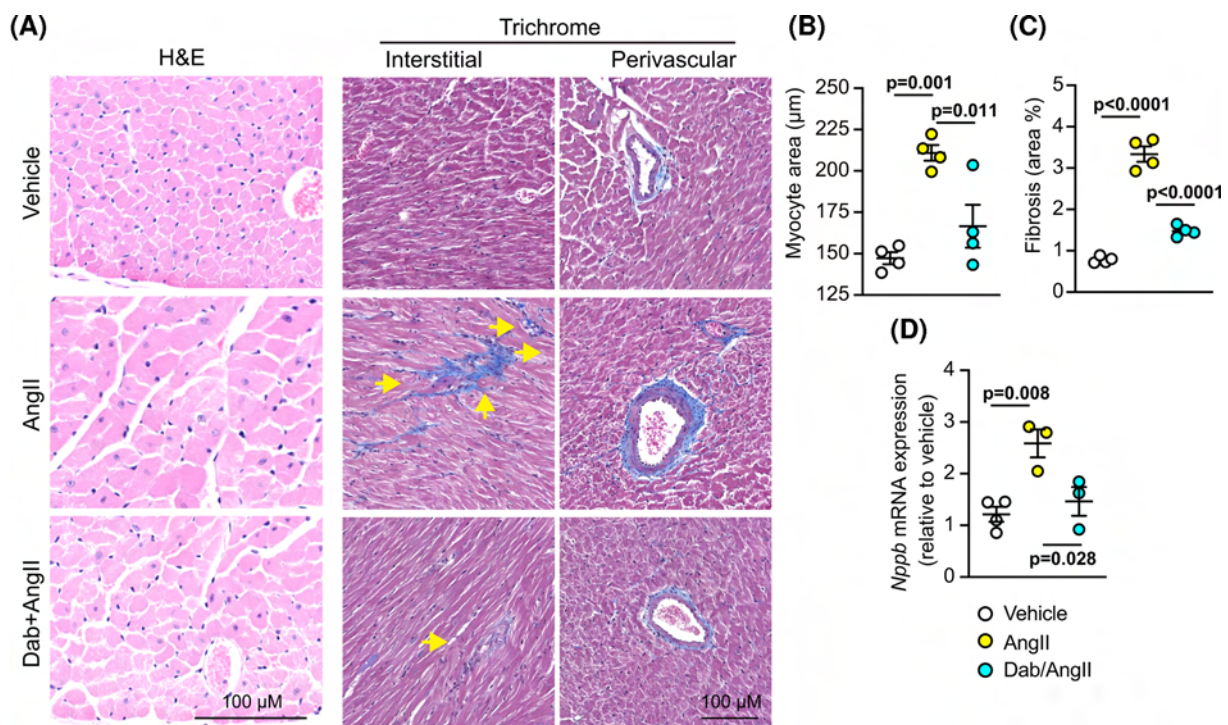


**Figure 5. Dabrafenib inhibits cardiomyocyte hypertrophy and cardiac fibrosis induced in mouse hearts by AngII over 28 d**  
C57BL/6J male mice were treated with vehicle, 0.8 mg/kg/d AngII or 3 mg/kg/d dabrafenib with AngII (28 d). **(A)** Representative images from mouse heart sections stained with H&E (left panels) or Masson's Trichrome (centre and right panels, showing interstitial and perivascular areas, respectively). **(B)** Quantification of cardiomyocyte area from sections stained with H&E. **(C)** Quantification of cardiac fibrosis from sections stained with Trichrome. **(D)** mRNA expression of *Nppb* was measured by qPCR. Quantification data are provided as individual points with means  $\pm$  SEM. Individual *P* values are shown (one-way ANOVA with Holm-Sidak's post-test).

increasing cardiac fibrosis), this does not appear to be detrimental to the heart either in an acute (Figures 2 and 3) or chronic (Figures 4 and 5) setting. The data not only establish Raf kinases as viable therapeutic targets for hypertensive heart disease, but also identify an existing drug in clinical use in humans as a potential therapy.

The importance of BRAF in cancer is well-established, with a number of inhibitors in development or approved for clinical use for an increasing variety of different cancers [6,31]. Dabrafenib is a Raf inhibitor that can activate ERK1/2 via 'Raf paradox' signalling in cancer cells [32]. In contrast, we detected limited paradox-inducing effects of dabrafenib in primary cardiac cells or perfused hearts (Figure 1). Moreover, dabrafenib was as potent as trametinib (a MKK1/2 inhibitor also in clinical use for melanoma [33]) in inhibiting ERK1/2 activity. It is important to consider that Raf inhibitors have generally been studied in cancer cell lines, prone to proliferation and gene mutations which result in relatively fluid signalling pathways. This differs from 'normal' cells that are generally quiescent, possibly highly differentiated and, in the case of cardiomyocytes, terminally differentiated. In these cells, signalling pathways are potentially 'hard-wired' and responses cannot necessarily be extrapolated from those of cancer cells. Dabrafenib did not have significant paradox-inducing effects in the cardiac system, presumably because of a difference in the signalling pathways.

There are increasing problems with cardiotoxicity of anti-cancer drugs [25,34], including those which target the ERK1/2 cascade at the level of MKK1/2 (e.g. trametinib, cobimetinib and selumetinib). Trametinib, alone or in combination with dabrafenib, causes hypertension in up to 26% of patients with decreased ejection fraction in 7–11% of patients [25], and meta-analysis of phase II/III trials of MKK1/2 inhibitors indicate these are on-target effects [33]. In contrast, there are limited reports of cardiotoxicity with dabrafenib monotherapy. Assessment of the FDA's Adverse Event Reporting System for patients receiving either BRAF inhibitors alone or with an MKK1/2 inhibitor (2011–2019; 7712 adverse events), identified just 187 cases of cardiovascular-associated problems resulting from BRAF inhibitor monotherapy [35]. For the monotherapy, 90% of adverse events related to vemurafenib which (unlike dabrafenib) increases QTc interval [36,37].

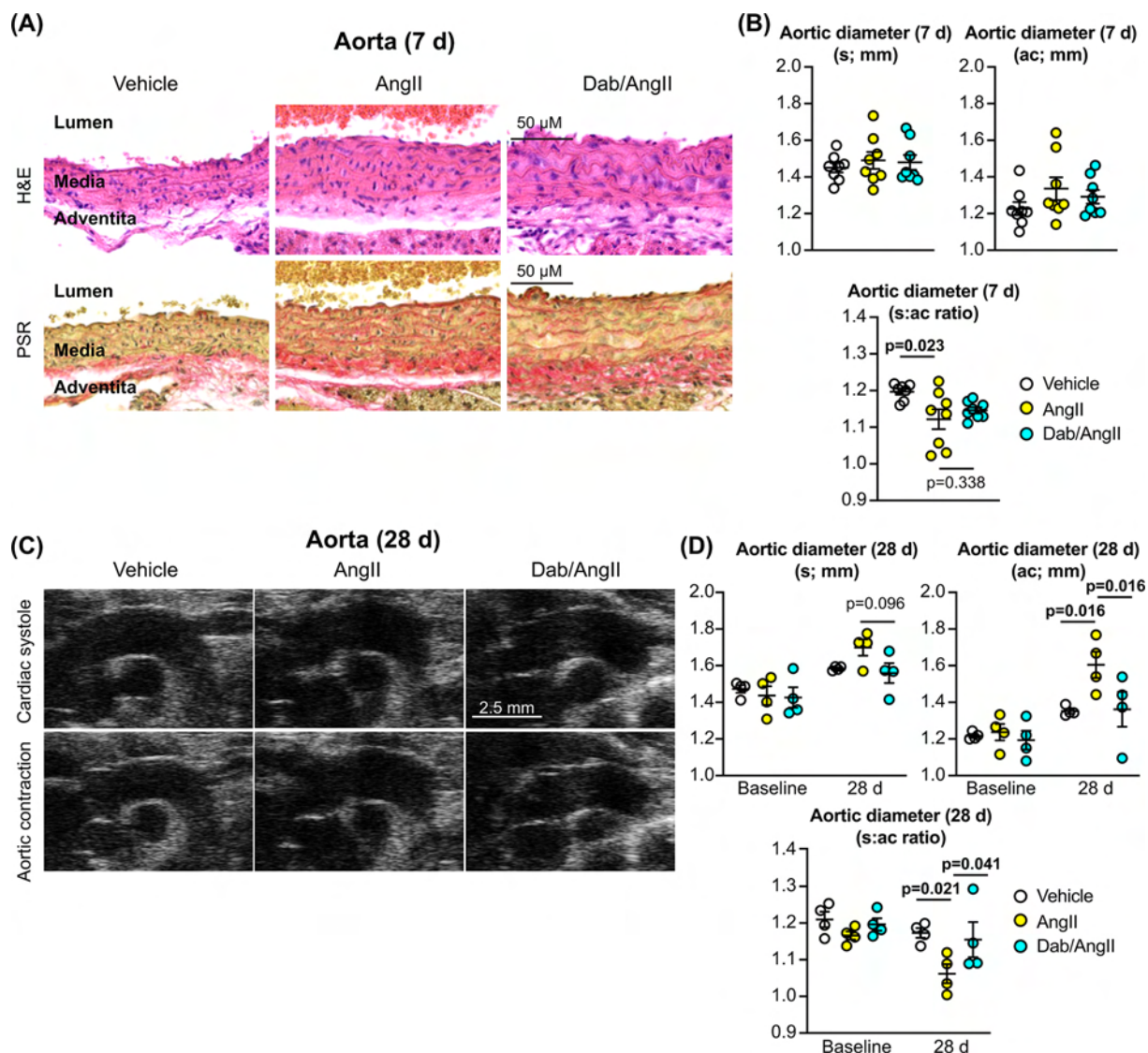


**Figure 6. Effects of dabrafenib on the aorta in mice treated with AngII**

C57BL/6J male mice were treated with vehicle, 0.8 mg/kg/d AngII or 3 mg/kg/d dabrafenib with AngII for 7 or 28 d as indicated. (A) The aorta was fixed and stained with H&E or picrosirius red (PSR). Representative images are shown. (B) Ultrasound B-mode images of the aorta following 7 d treatment were used to measure the internal diameter at the end of cardiac systole (s) with the aorta at its widest diameter, and following aortic contraction (ac). (C) Representative images of the aorta at the end of cardiac systole and following aortic contraction. (D) Ultrasound B-mode images of the aorta following 28 d treatment were used to measure the internal diameter. Quantification data are provided as individual points with means  $\pm$  SEM. Individual  $P$  values are shown using one-way (B) or two-way (D) ANOVA with Holm-Sidak's post-test.

The difference in toxicity between targeting the ERK1/2 cascade at the level of Raf kinases versus MKK1/2 may relate to alternative inputs at the level of MKK1/2. For example, Cot/Tpl2 activates MKK1/2 in some circumstances and is particularly implicated in the inflammatory response [5], and it is clear that  $\alpha_1$ -adrenergic agonists and oxidative stress use an alternative input to MKK1/2 in cardiomyocytes rather than Raf kinases [38,39]. These additional inputs may mean that cardiomyocytes are not compromised by Raf inhibition to the same degree as inhibiting at the level of MKK1/2. Consistent with this, dabrafenib had no significant effect on cardiac function or dimensions *in vivo* in a normotensive setting or any effect on cellular architecture or gene expression (Supplementary Tables S3 and S4; Supplementary Figure S1). In this context, given that a combination Raf plus MKK1/2 inhibitors (e.g. dabrafenib

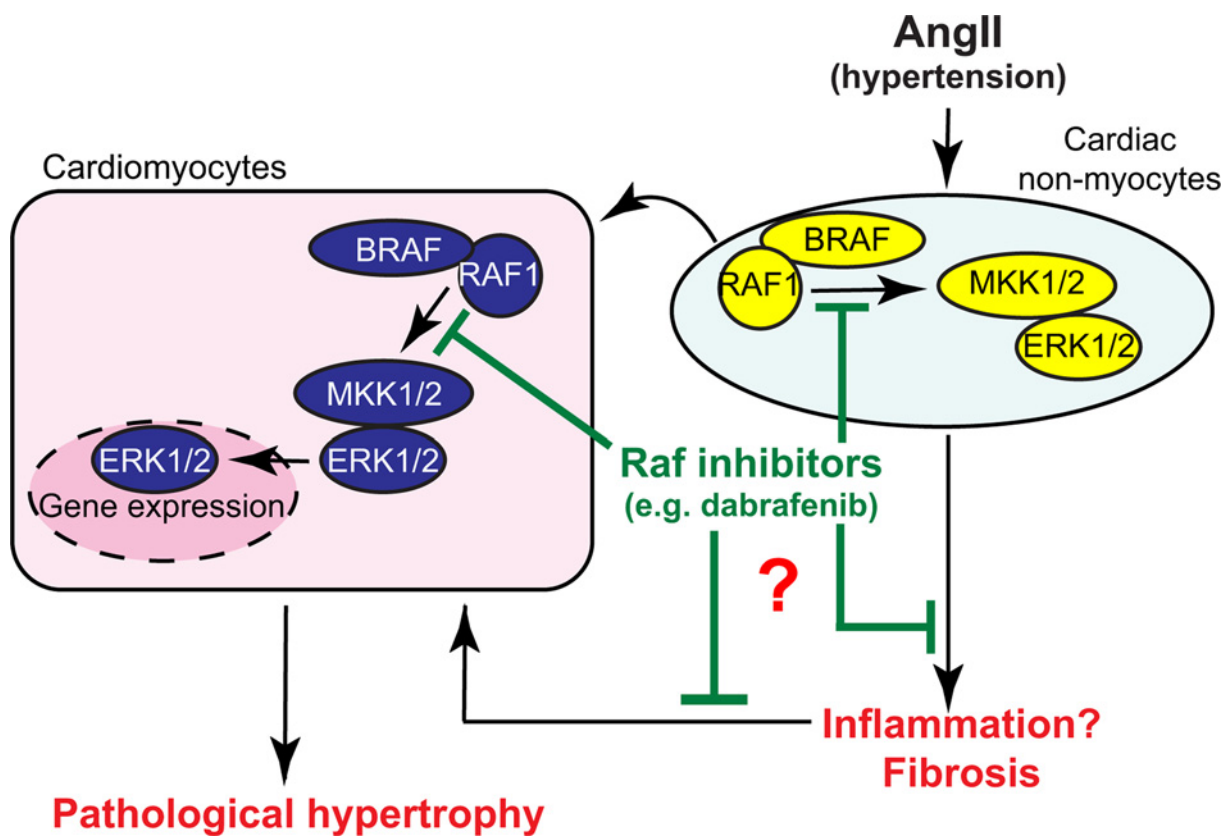


**Figure 7. Schematic representation of the conclusions from this study**

AngII-induced hypertension activates Raf kinases (BRAF and RAF1) in the heart whether directly (particularly in cardiac non-myocytes such as fibroblasts) or indirectly (cardiomyocytes potentially respond to factors released by non-myocytes). Raf kinases signal through the ERK1/2 cascade to promote changes in gene expression and induce phenotypic responses. In cardiomyocytes, this promotes cardiomyocyte hypertrophy to combat increased workload. AngII also increases cardiac inflammation and activates Raf signalling in cardiac non-myocytes promoting cell proliferation and fibrosis. Increased cardiac fibrosis increases the workload on the heart causing further cardiomyocyte hypertrophy. Over time, this leads to pathological remodelling of the hearts that can lead to hypertensive heart disease and failure. Raf inhibitors such as dabrafenib inhibit Raf signalling in both cardiomyocytes and cardiac non-myocytes, reducing cardiac inflammation and fibrosis, reducing cardiomyocyte hypertrophy, and protecting the heart from hypertensive heart disease; ERK, extracellular signal-regulated kinase; MKK, mitogen-activated protein kinase kinase.

with trametinib) is the preferred cancer therapy because of the Raf paradox, patients who experience cardiotoxicity from this regime may still benefit from RAF-targeted monotherapy. Extrapolating further, could dabrafenib be cardioprotective in patients with cancer, undergoing treatments with established cardiotoxicity (e.g. anthracyclines [40])? Moreover, would a cancer environment compromise the cardioprotective effects of dabrafenib on the heart? The answer to the former may depend on the type of toxicity and the underlying mechanism by which dabrafenib exerts its effects; our data suggest the beneficial effects of dabrafenib are likely to be on longer term cardiac remodelling with fibrosis causing cardiac dysfunction rather than acute damage to the myocardium. Addressing the latter question, it seems unlikely that early stage cancer associated with dabrafenib treatment in humans would be likely to affect the cardio-protective effects of dabrafenib given that the heart itself is not prone to cancer (apart from in a very few cases) and metastatic cancers do not (as far as we are aware) invade the heart. However, the systemic effects of later stage cancer and the other treatments that patients receive could influence the responses. Clearly, these issues need to be addressed in preclinical studies and/or the clinic.

Although dabrafenib had no obvious effect in an unstressed heart, it inhibited cardiac adaptation to AngII-induced hypertension suggesting BRAF signalling is important in disease development. We examined the effects of dabrafenib on cardiac adaptation to both acute (up to 7 d) and chronic (28 d) hypertension induced by AngII. Over 3 d, the heart had compensated for the initial insult, with increased LV wall thickness and decreased LV internal diameter, with a

concomitant increase in fractional shortening (Figure 2B–D). This was moderated by dabrafenib. By 7 d, the response to AngII had already changed. Fractional shortening and internal diameters had normalized, but LV wall thickness was still enhanced and this was inhibited by dabrafenib. Dabrafenib also inhibited the increase in cardiomyocyte size and both interstitial and perivascular fibrosis (Figure 3). With chronic AngII treatment, the hearts were beginning to fail, with a significant reduction in ejection fraction and increased LV wall thickness (Figure 4). This was associated with a reduction in global longitudinal and circumferential strain. Notably, dabrafenib inhibited the reduction in ejection fraction and global strain at 28 d. This was accompanied by a reduction in cardiomyocyte size and degree of fibrosis (Figure 5). Thus, our data indicate that dabrafenib may be therapeutically useful for reducing cardiac fibrosis and maintaining cardiac function in hypertensive heart disease. Clearly, further studies are required to establish if this is sustained as the heart decompensates further in response to AngII. Additional studies in other models of heart failure would also help to determine whether the effect of dabrafenib is specific to AngII-associated hypertension or if it is more generally useful in reducing cardiac fibrosis.

An important consideration in terms of potential mechanism is whether or not the effects of dabrafenib on AngII-induced maladaptive remodelling may simply be a consequence of reducing the increase in blood pressure resulting from AngII-treatment. We did not assess blood pressure in this study and this is clearly a limitation of our work. There appears to be no information to suggest that dabrafenib monotherapy reduces blood pressure in patients. Furthermore, trametinib and other MKK1/2 inhibitors promote hypertension in up to 26% of patients, irrespective of whether patients are treated with the MKK1/2 inhibitors alone or in combination with a BRAF inhibitor [25], suggesting that dabrafenib does not mitigate the hypertensive effects of trametinib. In addition, whilst histological assessment of the aortae indicated that dabrafenib reduced fibrosis resulting from AngII-treatment, the medial layer showed a similar degree of thickening with or without dabrafenib (Figure 6A). This suggests that a similar degree of hypertension was induced and the overall response of the aorta to hypertensive pressures was maintained. Nevertheless, although the weight of evidence is generally against the likelihood that dabrafenib reduced the increase in blood pressure induced by AngII-treatment, further studies are clearly required to confirm this experimentally.

Our data suggest that dabrafenib may be useful in treating cardiac fibrosis but, as with all drugs, there are considerations of on-target versus off-target effects. In our studies, dabrafenib most probably inhibits all three Raf kinases, so we cannot be certain which may be driving the ERK1/2 signal in response to AngII (Figure 2A). Assuming the signal is mediated via ERK1/2, the data are consistent with other studies indicating that ERK1/2 signalling in cardiac fibroblasts contributes to cardiac fibrosis. For example, IL11 promotes extracellular matrix production from cardiac fibroblasts via ERK1/2, acting in a post-transcriptional manner [29]. Here, it is necessary to consider the complexities associated with fibrosis. ERK1/2 could influence the rate of synthesis and processing of extracellular matrix proteins, the degree of post-translational modification and cross-linking of collagens, and also the rate of degradation. Our data indicate that at least one of the matrix metalloproteinases (TIMP1) is transcriptionally up-regulated in response to AngII and this is reduced by dabrafenib (Figure 3F). However, for these enzymes, it is more important to assess their overall activities and something which should be considered in the future. It must also be considered that dabrafenib could exert its effects via another pathway (e.g. Raf1 inhibits pro-apoptotic kinases [41,42]) or off-target effects such as inhibition of the pro-apoptotic kinase, RIPK3 [43]. Further studies with different Raf inhibitors are clearly warranted to control for these. Here, it is notable that the cancer field has moved towards development of a different class of inhibitor, Type 2 inhibitors (e.g. PLX8394) that bind exclusively to an inactive conformation of the kinase and are viewed as 'Raf paradox' breakers [44–46]. The cardiac effects of these drugs remain to be investigated.

Whether or not dabrafenib exerts its effects through Raf kinases themselves, it is important to consider the cellular context of the overall response. Our mRNA data suggest that there was increased inflammation in our AngII model of hypertension in mice and this was reduced by dabrafenib (Figure 3G). This remains to be confirmed at the protein level, but increased inflammation is likely to promote cardiac fibrosis [47]. Increasing cardiac fibrosis adds to the workload on the heart, potentially causing further cardiomyocyte hypertrophy. This, in itself, is likely to result in dysfunctional cardiomyocytes and cardiomyocyte death which will then lead to enhanced inflammation. As indicated in Figure 7, dabrafenib may inhibit any of these processes, possibly acting on different target enzymes. Apart from this, our data suggest dabrafenib may preserve the elasticity of the aorta (Figure 6), suggesting it could have a beneficial effect on the vasculature, which would be predicted to benefit the heart. Irrespective of mechanism, our data provide proof-of-principle that drugs such as dabrafenib may be therapeutically useful for reducing cardiac fibrosis. In this respect, there may be competition with other kinase inhibitors, including ASK1 inhibitors that have been in clinical trials for fibrotic diseases such as non-alcoholic steatohepatitis [48]. Our recent studies indicate that the ASK1 inhibitor, selonsertib, does indeed reduce cardiac fibrosis resulting from AngII-induced hypertension [22], but dabrafenib appears at least as effective.

There are, of course, limitations to this study. First, as mentioned above, further studies of the effects of dabrafenib on the increase in blood pressure induced by AngII in our mouse models are necessary. Secondly, we used rat cardiomyocytes and perfused hearts, but conducted the *in vivo* studies in mice. The reasons are technical: the rat systems are well-characterized for *ex vivo* studies, whilst mice are the preferred model for *in vivo* studies. The results were consistent across the species with dabrafenib inhibiting ERK1/2 activities in both, and suppressing cardiac hypertrophy and fibrosis *in vivo*. Thirdly, we only conducted experiments with male mice and these were juveniles. The reasons were purely practical in that it is important to first obtain proof-of-principle data for a relatively focused study. Future studies should consider assessing the effects of dabrafenib on hypertensive heart disease in female animals, in addition to older mice. The latter is particularly important given that the responses are likely to change with age and hypertension is associated with aging. A fourth consideration is the duration of our study. We only assessed the effects of a single dose of dabrafenib on AngII-induced cardiac hypertrophy over 4 weeks, during which time the hearts did not fail whereas most cancer patients are treated for much greater lengths of time with different dosages. However, we did select a dose which is relevant for humans, and cardiac dysfunction has been observed in patients receiving trametinib/dabrafenib combination therapy within 13 days [49], so our data are relevant. Nevertheless, future studies exploring different dosage regimes and more prolonged treatments would be useful. Apart from assessing potential cardiotoxicity over prolonged periods, it will be important to assess whether dabrafenib could, indeed prevent hearts from failing, and to determine if administration of the drug can prevent or even reverse cardiac fibrosis in a heart which is already diseased, a situation more relevant to the human scenario.

The final considerations for our work are the potential implications of using drugs such as dabrafenib for cardiac diseases. Dabrafenib itself does not appear to be cardiotoxic and is generally well-tolerated. There are side effects in cancer patients which are generally managed by dose reduction. The most severe effect is probably an increase in cutaneous squamous cell carcinoma (~12% of patients) [50]. Thus, if dabrafenib were to be used as a therapy for hypertensive heart disease, it may be important to consider dosage monitoring and whether patients have a predisposition for other diseases such as cancer (in the context, perhaps, of 'onco-cardiology'). Nevertheless, reducing cardiac fibrosis with a drug such as dabrafenib may be such a powerful tool in treating cardiac diseases that the benefits could outweigh these costs.

## Clinical perspectives

- **Background:** Inhibitors of the ERK1/2 cascade are used to treat cancer and some have cardiotoxic effects. Oncogenic BRAF (that activates ERK1/2) is a prime target for cancer and dabrafenib was developed as a BRAF inhibitor for melanoma. It is generally used in combination with other drugs, the combinations being cardiotoxic in some patients.
- **Results summary:** Dabrafenib had no overt effects on cardiac function/dimensions (assessed by echocardiography) or cardiac architecture when administered to mice *in vivo*, but inhibited cardiac fibrosis and cardiac hypertrophy in hypertensive mice.
- **Clinical significance:** Since dabrafenib alone did not cause cardiac dysfunction, it may be preferable for use as monotherapy (rather than in combination with other drugs that are cardiotoxic) in some patients with BRAF directed cancers. In addition, dabrafenib (and other similar inhibitors) may be therapeutically beneficial in preventing cardiac hypertrophy and fibrosis in hypertension, thus reducing heart failure development.

## Data Availability

All primary data are available from the corresponding author upon reasonable request. Additional data sharing information is not applicable to this study.

## Competing Interests

Dr Meijles and Prof. Clerk are co-inventors on a patent relating to the use of Raf inhibitors as treatments for fibrosis (WO 2020/161477). The other authors declare that they have no conflict of interest.

## Funding

This work was supported by the British Heart Foundation [grant numbers PG/13/71/30460, PG/17/11/32841, PG/15/24/31367, PG/15/31/31393, FS/18/33/33621, FS/19/24/34262, PG/19/7/34167, PG/19/32/34383]; the Wellcome Trust [grant number 204809/Z/16/Z]; a St. George's University of London PhD studentship (to Z.H.R.H.); and Qassim University, Saudi Arabia (to H.O.A.).

## Open Access

Open access for this article was enabled by the participation of University of Reading in an all-inclusive *Read & Publish* pilot with Portland Press and the Biochemical Society under a transformative agreement with JISC.

## Ethics Approval

Procedures were performed in accordance with the European Parliament Directive 2010/63/EU on the protection of animals used for scientific purposes, with local institutional animal care committee procedures (University of Reading) and with the U.K. Animals (Scientific Procedures) Act 1986.

## CRDiT Author Contribution

**Meijles D.N.:** Conceptualization, Resources, Data curation, Formal analysis, Supervision, Funding acquisition, Investigation, Visualization, Methodology, Writing—original draft, Writing—review and editing. **Cull J.J.:** Data curation, Validation, Investigation, Methodology. **Cooper S.T.E.:** Data curation, Formal analysis, Investigation, Methodology. **Markou T.:** Data curation, Investigation. **Hardyman M.A.:** Investigation. **Fuller S.J.:** Data curation, Formal analysis, Investigation. **Alharbi H.O.:** Investigation. **Haines Z.:** Investigation. **Alcantara-Alonso V.:** Investigation. **Glennon P.E.:** Formal analysis, Methodology. **Sheppard M.N.:** Resources, Methodology. **Sugden P.H.:** Writing—review and editing. **Clerk A.:** Conceptualization, Resources, Data curation, Formal analysis, Supervision, Funding acquisition, Investigation, Visualization, Methodology, Writing—original draft, Project administration, Writing—review and editing.

## Abbreviations

EDV, end diastolic volume; EDLVM, end diastolic left ventricular mass; EF, ejection fraction; ERK, extracellular signal-regulated kinase; ESV, end systolic volume; FS, fractional shortening; LV, left ventricular; MKK, mitogen-activated protein kinase kinase.

## References

- 1 Lavoie, H., Gagnon, J. and Therrien, M. (2020) ERK signalling: a master regulator of cell behaviour, life and fate. *Nat. Rev. Mol. Cell Biol.* **21**, 607–632, <https://doi.org/10.1038/s41580-020-0255-7>
- 2 Kehat, I., Davis, J., Tiburcy, M., Accornero, F., Saba-El-Leil, M.K., Maillet, M. et al. (2011) Extracellular signal-regulated kinases 1 and 2 regulate the balance between eccentric and concentric cardiac growth. *Circ. Res.* **108**, 176–183, <https://doi.org/10.1161/CIRCRESAHA.110.231514>
- 3 Gallo, S., Vitacolonna, A., Bonzano, A., Comoglio, P. and Crepaldi, T. (2019) ERK: a key player in the pathophysiology of cardiac hypertrophy. *Int. J. Mol. Sci.* **20**, 2164, <https://doi.org/10.3390/ijms20092164>
- 4 Matallanas, D., Birtwistle, M., Romano, D., Zebisch, A., Rauch, J., von, Kriegsheim, A. et al. (2011) Raf family kinases: old dogs have learned new tricks. *Genes Cancer* **2**, 232–260, <https://doi.org/10.1177/1947601911407323>
- 5 Xu, D., Matsumoto, M.L., McKenzie, B.S. and Zarrin, A.A. (2018) TPL2 kinase action and control of inflammation. *Pharmacol. Res.* **129**, 188–193, <https://doi.org/10.1016/j.phrs.2017.11.031>
- 6 Roskoski, Jr, R. (2018) Targeting oncogenic Raf protein-serine/threonine kinases in human cancers. *Pharmacol. Res.* **135**, 239–258, <https://doi.org/10.1016/j.phrs.2018.08.013>
- 7 Dhomen, N. and Marais, R. (2007) New insight into *BRAF* mutations in cancer. *Curr. Opin. Genet. Dev.* **17**, 31–39, <https://doi.org/10.1016/j.gde.2006.12.005>
- 8 Rheault, T.R., Stellwagen, J.C., Adjabeng, G.M., Hornberger, K.R., Petrov, K.G., Waterson, A.G. et al. (2013) Discovery of dabrafenib: a selective inhibitor of Raf kinases with antitumor activity against B-Raf-driven tumors. *ACS Med. Chem. Lett.* **4**, 358–362, <https://doi.org/10.1021/ml4000063>
- 9 Durrant, D.E. and Morrison, D.K. (2018) Targeting the Raf kinases in human cancer: the Raf dimer dilemma. *Br. J. Cancer* **118**, 3–8, <https://doi.org/10.1038/bjc.2017.399>
- 10 Savarese, G. and Lund, L.H. (2017) Global public health burden of heart failure. *Card. Fail. Rev.* **3**, 7–11, <https://doi.org/10.15420/cfr.2016:25:2>
- 11 Dorn, II, G.W., Robbins, J. and Sugden, P.H. (2003) Phenotyping hypertrophy: eschew obfuscation. *Circ. Res.* **92**, 1171–1175, <https://doi.org/10.1161/01.RES.0000077012.11088.BC>
- 12 Zhang, J., Liu, D., Zhang, M. and Zhang, Y. (2019) Programmed necrosis in cardiomyocytes: mitochondria, death receptors and beyond. *Br. J. Pharmacol.* **176**, 4319–4339, <https://doi.org/10.1111/bph.14363>
- 13 Suthahar, N., Meijers, W.C., Silljé, H.H.W. and de Boer, R.A. (2017) From inflammation to fibrosis—molecular and cellular mechanisms of myocardial tissue remodelling and perspectives on differential treatment opportunities. *Curr. Heart Fail. Rep.* **14**, 235–250, <https://doi.org/10.1007/s11897-017-0343-y>

14 Messerli, F.H., Bangalore, S., Bavishi, C. and Rimoldi, S.F. (2018) Angiotensin-converting enzyme inhibitors in hypertension: to use or not to use? *J. Am. Coll. Cardiol.* **71**, 1474–1482, <https://doi.org/10.1016/j.jacc.2018.01.058>

15 Tarone, G., Balligand, J.L., Bauersachs, J., Clerk, A., De, Windt, L., Heymans, S. et al. (2014) Targeting myocardial remodelling to develop novel therapies for heart failure: a position paper from the Working Group on Myocardial Function of the European Society of Cardiology. *Eur. J. Heart Fail.* **16**, 494–508, <https://doi.org/10.1002/ejhf.62>

16 Fuller, S.J., Osborne, S.A., Leonard, S.J., Hardyman, M.A., Vaniotis, G., Allen, B.G. et al. (2015) Cardiac protein kinases: the cardiomyocyte kinome and differential kinase expression in human failing hearts. *Cardiovasc. Res.* **108**, 87–98, <https://doi.org/10.1093/cvr/cvv210>

17 Bogoyevitch, M.A., Marshall, C.J. and Sugden, P.H. (1995) Hypertrophic agonists stimulate the activities of the protein kinases c-Raf and A-Raf in cultured ventricular myocytes. *J. Biol. Chem.* **270**, 26303–26310, <https://doi.org/10.1074/jbc.270.44.26303>

18 Clerk, A., Aggeli, I.-K.S., Stathopoulou, K. and Sugden, P.H. (2006) Peptide growth factors signal differentially through protein kinase C to extracellular signal-regulated kinases in neonatal cardiomyocytes. *Cell. Signal.* **18**, 225–235, <https://doi.org/10.1016/j.cellsig.2005.04.005>

19 Harris, I.S., Zhang, S., Treskov, I., Kovacs, A., Weinheimer, C. and Muslin, A.J. (2004) Raf-1 kinase is required for cardiac hypertrophy and cardiomyocyte survival in response to pressure overload. *Circulation* **110**, 718–723, <https://doi.org/10.1161/01.CIR.0000138190.50127.6A>

20 Yamaguchi, O., Watanabe, T., Nishida, K., Kishiwase, K., Higuchi, Y., Takeda, T. et al. (2004) Cardiac-specific disruption of the *c-raf-1* gene induces cardiac dysfunction and apoptosis. *J. Clin. Invest.* **114**, 937–943, <https://doi.org/10.1172/JCI200420317>

21 Meijles, D., Fuller, S.J., Cull, J.J., Alharbi, H.O., Cooper, S.T., Sugden, P.H. et al. (2021) The insulin receptor family and protein kinase B (Akt) are activated in the heart by alkaline pH and  $\alpha_1$ -adrenergic receptors. *Biochem. J.* **478**, 2059–2079, <https://doi.org/10.1042/BCJ20210144>

22 Meijles, D.N., Cull, J.J., Markou, T., Cooper, S.T.E., Haines, Z.H.R., Fuller, S.J. et al. (2020) Redox regulation of cardiac ASK1 (Apoptosis Signal-Regulating Kinase 1) controls p38-MAPK (Mitogen-Activated Protein Kinase) and orchestrates cardiac remodeling to hypertension. *Hypertension* **76**, 1208–1218, <https://doi.org/10.1161/HYPERTENSIONAHA.119.14556>

23 Marshall, A.K., Barrett, O.P., Cullingford, T.E., Shammugasundram, A., Sugden, P.H. and Clerk, A. (2010) ERK1/2 signaling dominates over RhoA signaling in regulating early changes in RNA expression induced by endothelin-1 in neonatal rat cardiomyocytes. *PLoS ONE* **5**, e10027, <https://doi.org/10.1371/journal.pone.0010027>

24 Gilmartin, A.G., Bleam, M.R., Groy, A., Moss, K.G., Minthorn, E.A., Kulkarni, S.G. et al. (2011) GSK1120212 (JTP-74057) is an inhibitor of MEK activity and activation with favorable pharmacokinetic properties for sustained in vivo pathway inhibition. *Clin. Cancer Res.* **17**, 989–1000, <https://doi.org/10.1158/1078-0432.CCR-10-2200>

25 Bronte, E., Bronte, G., Novo, G., Rinaldi, G., Bronte, F., Passiglia, F. et al. (2018) Cardiotoxicity mechanisms of the combination of BRAF-inhibitors and MEK-inhibitors. *Pharmacol. Ther.* **192**, 65–73, <https://doi.org/10.1016/j.pharmthera.2018.06.017>

26 Puszkiel, A., Noé, G., Bellesoeur, A., Kramkine, N., Paludetto, M.-N., Thomas-Schoemann, A. et al. (2019) Clinical pharmacokinetics and pharmacodynamics of dabrafenib. *Clin. Pharmacokinet.* **58**, 451–467, <https://doi.org/10.1007/s40262-018-0703-0>

27 Lindsey, M.L., Kassiri, Z., Virag, J.A.I., de Castro Brás, L.E. and Scherrer-Crosbie, M. (2018) Guidelines for measuring cardiac physiology in mice. *Am. J. Physiol. Heart Circ. Physiol.* **314**, H733–H752, <https://doi.org/10.1152/ajpheart.00339.2017>

28 Thum, T., Gross, C., Fiedler, J., Fischer, T., Kissler, S., Bussen, M. et al. (2008) MicroRNA-21 contributes to myocardial disease by stimulating MAP kinase signalling in fibroblasts. *Nature* **456**, 980–984, <https://doi.org/10.1038/nature07511>

29 Schafer, S., Viswanathan, S., Widjaja, A.A., Lim, W.-W., Moreno-Moral, A., DeLaughter, D.M. et al. (2017) IL-11 is a crucial determinant of cardiovascular fibrosis. *Nature* **552**, 110–115, <https://doi.org/10.1038/nature24676>

30 Sweeney, M., Corden, B. and Cook, S.A. (2020) Targeting cardiac fibrosis in heart failure with preserved ejection fraction: mirage or miracle? *EMBO Mol. Med.* **12**, e10865, <https://doi.org/10.15252/emmm.201910865>

31 Roskoski, Jr, R. (2021) Properties of FDA-approved small molecule protein kinase inhibitors: a 2021 update. *Pharmacol. Res.* **165**, 105463, <https://doi.org/10.1016/j.phrs.2021.105463>

32 King, A.J., Arnone, M.R., Bleam, M.R., Moss, K.G., Yang, J., Fedorowicz, K.E. et al. (2013) Dabrafenib: preclinical characterization, increased efficacy when combined with trametinib, while BRAF/MEK tool combination reduced skin lesions. *PLoS ONE* **8**, e67583, <https://doi.org/10.1371/journal.pone.0067583>

33 Abdel-Rahman, O., ElHalawani, H. and Ahmed, H. (2015) Risk of selected cardiovascular toxicities in patients with cancer treated with MEK inhibitors: a comparative systematic review and meta-analysis. *J. Glob. Oncol.* **1**, 73–82, <https://doi.org/10.1200/JGO.2015.000802>

34 Mincu, R.I., Mahabadi, A.A., Michel, L., Mrotzek, S.M., Schadendorf, D., Rassaf, T. et al. (2019) Cardiovascular adverse events associated with BRAF and MEK inhibitors: a systematic review and meta-analysis. *JAMA Netw. Open* **2**, e198890, <https://doi.org/10.1001/jamanetworkopen.2019.8890>

35 Guha, A., Jain, P., Fradley, M.G., Lenihan, D., Gutierrez, J.M., Jain, C. et al. (2021) Cardiovascular adverse events associated with BRAF versus BRAF/MEK inhibitor: Cross-sectional and longitudinal analysis using two large national registries. *Cancer Med.* **12**, 3862–3872, <https://doi.org/10.1002/cam4.3938>

36 Kloth, J.S.L., Pagani, A., Verboom, M.C., Malovini, A., Napolitano, C., Kruit, W.H.J. et al. (2015) Incidence and relevance of QTc-interval prolongation caused by tyrosine kinase inhibitors. *Br. J. Cancer* **112**, 1011–1016, <https://doi.org/10.1038/bjc.2015.82>

37 Nebot, N., Arkenau, H.T., Infante, J.R., Chandler, J.C., Weickhardt, A., Lickliter, J.D. et al. (2018) Evaluation of the effect of dabrafenib and metabolites on QTc interval in patients with BRAF V600-mutant tumours. *Br. J. Clin. Pharmacol.* **84**, 764–775, <https://doi.org/10.1111/bcp.13488>

38 Clerk, A., Kemp, T.J., Harrison, J.G., Pham, F.H. and Sugden, P.H. (2004) Integration of protein kinase signalling pathways in cardiac myocytes: signalling to and from the extracellular signal-regulated kinases. *Adv. Enzyme. Regul.* **44**, 233–248, <https://doi.org/10.1016/j.advenzreg.2003.11.002>

39 Chiloeches, A., Paterson, H.F., Marais, R., Clerk, A., Marshall, C.J. and Sugden, P.H. (1999) Regulation of Ras-GTP loading and Ras-Raf association in neonatal rat ventricular myocytes by G protein-coupled receptor agonists and phorbol ester. Activation of the ERK cascade by phorbol ester is mediated by Ras. *J. Biol. Chem.* **274**, 19762–19770, <https://doi.org/10.1074/jbc.274.28.19762>

40 Sallustio, B.C. and Boddy, A.V. (2021) Is there scope for better individualisation of anthracycline cancer chemotherapy? *Br. J. Clin. Pharmacol.* **87**, 295–305, <https://doi.org/10.1111/bcp.14628>

41 Chen, J., Fujii, K., Zhang, L., Roberts, T. and Fu, H. (2001) Raf-1 promotes cell survival by antagonizing apoptosis signal-regulating kinase 1 through a MEK-ERK independent mechanism. *Proc. Natl. Acad. Sci. U.S.A.* **98**, 7783–7788, <https://doi.org/10.1073/pnas.141224398>

42 O'Neill, E., Rushworth, L., Baccarini, M. and Kolch, W. (2004) Role of the kinase MIST2 in suppression of apoptosis by the proto-oncogene product Raf-1. *Science* **306**, 2267–2270, <https://doi.org/10.1126/science.1103233>

43 Li, J.-X., Feng, J.-M., Wang, Y., Li, X.-H., Chen, X.-X., Su, Y. et al. (2014) The B-Raf(V600E) inhibitor dabrafenib selectively inhibits RIP3 and alleviates acetaminophen-induced liver injury. *Cell Death Dis.* **5**, e1278, <https://doi.org/10.1038/cddis.2014.241>

44 Tutuka, C.S.A., Andrews, M.C., Mariadason, J.M., Ioannidis, P., Hudson, C., Cebon, J. et al. (2017) PLX8394, a new generation BRAF inhibitor, selectively inhibits BRAF in colonic adenocarcinoma cells and prevents paradoxical MAPK pathway activation. *Mol. Cancer* **16**, 112, <https://doi.org/10.1186/s12943-017-0684-x>

45 Zhang, C., Spevak, W., Zhang, Y., Burton, E.A., Ma, Y., Habets, G. et al. (2015) RAF inhibitors that evade paradoxical MAPK pathway activation. *Nature* **526**, 583–586, <https://doi.org/10.1038/nature14982>

46 Yao, Z., Gao, Y., Su, W., Yaeger, R., Tao, J., Na, N. et al. (2019) RAF inhibitor PLX8394 selectively disrupts BRAF dimers and RAS-independent BRAF-mutant-driven signaling. *Nat. Med.* **25**, 284–291, <https://doi.org/10.1038/s41591-018-0274-5>

47 Smolgovsky, S., Ibeh, U., Tamayo, T.P. and Alcaide, P. (2021) Adding insult to injury - Inflammation at the heart of cardiac fibrosis. *Cell. Signal.* **77**, 109828, <https://doi.org/10.1016/j.cellsig.2020.109828>

48 Ogier, J.M., Nayagam, B.A. and Lockhart, P.J. (2020) ASK1 inhibition: a therapeutic strategy with multi-system benefits. *J. Mol. Med. (Berl.)* **98**, 335–348, <https://doi.org/10.1007/s00109-020-01878-y>

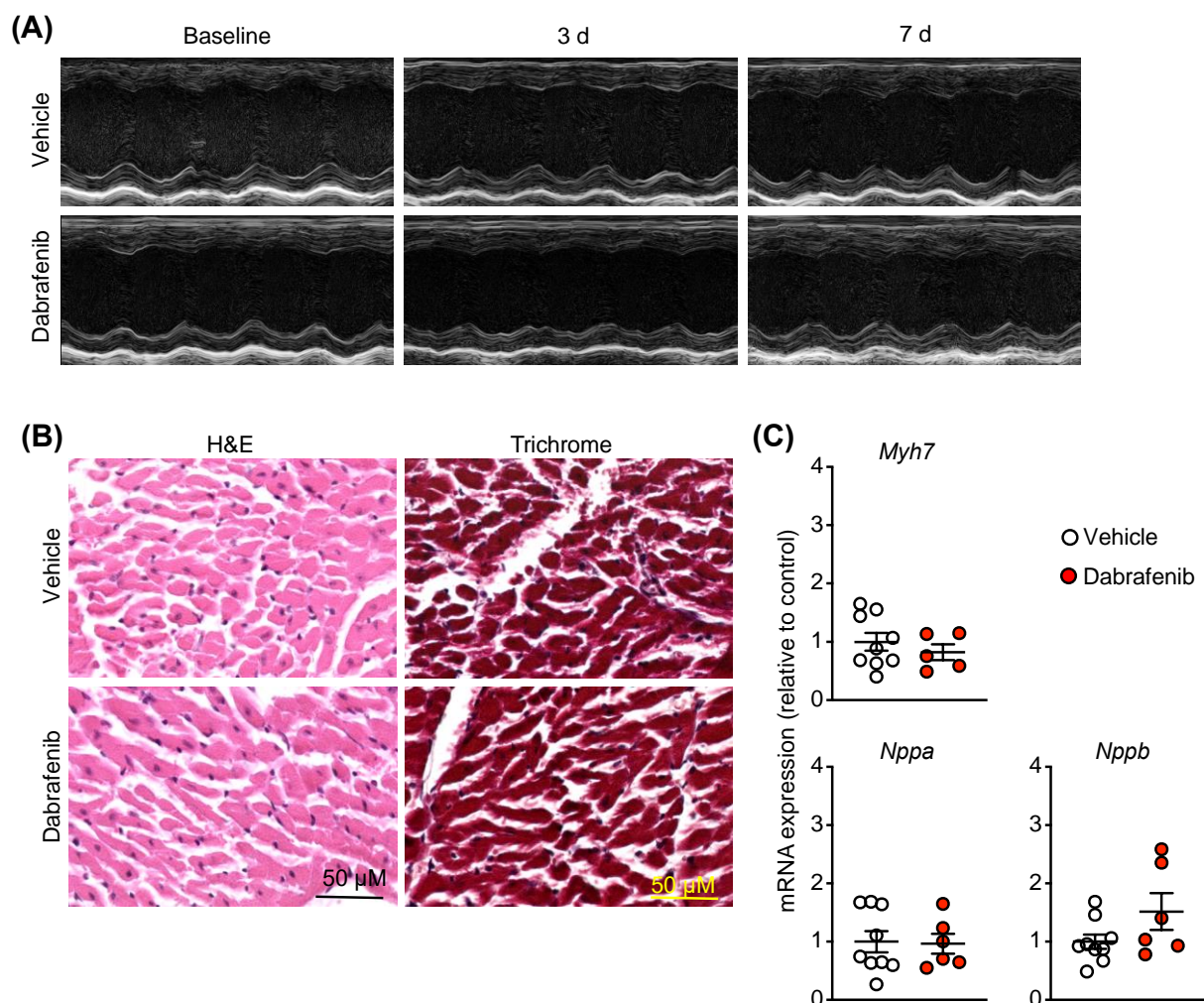
49 Banks, M., Crowell, K., Proctor, A. and Jensen, B.C. (2017) Cardiovascular effects of the MEK inhibitor, trametinib: a case report, literature review, and consideration of mechanism. *Cardiovasc. Toxicol.* **17**, 487–493, <https://doi.org/10.1007/s12012-017-9425-z>

50 Peng, L., Wang, Y., Hong, Y., Ye, X., Shi, P., Zhang, J. et al. (2017) Incidence and relative risk of cutaneous squamous cell carcinoma with single-agent BRAF inhibitor and dual BRAF/MEK inhibitors in cancer patients: a meta-analysis. *Oncotarget* **8**, 83280–83291, <https://doi.org/10.18632/oncotarget.21059>

Meijles et al. The anti-cancer drug dabrafenib is not cardiotoxic and inhibits cardiac remodelling and fibrosis in a murine model of hypertension.

**Supplementary tables and figures**

**Supplementary Figure S1. Acute infusion of mice with dabrafenib had no significant effect on cardiac function/dimensions.** C57BL/6J male mice were treated with vehicle or 3 mg/kg/d dabrafenib for 28 d. **(A)** Echocardiograms were taken at baseline, 3 d or 7 d and analysed, comparing effects of vehicle vs dabrafenib alone. Representative echocardiograms are shown. **(B)** Hearts were fixed and sections stained with haematoxylin and eosin (H&E) or Masson's Trichrome as indicated. Representative sections are shown. **(C)** RNA was extracted from the hearts and mRNA expression measured by qPCR. Results are expressed relative to the means of the vehicle-treated controls. Individual data points are shown with means  $\pm$  SEM.



**Supplementary Table S1. Mouse body weights.** Body weights (BW) are in g. Weights were taken post-minipump insertion (Start) and when mice were culled (End); weights included the minipumps. p values relative to starting weight (2-way ANOVA with Holm-Sidak's post-test).

Study	Condition	BW:Start		BW:End		n
		Mean	SEM	Mean	SEM	
Acute AngII	Vehicle only	26.44	0.60	27.34	0.60	12
	Dabrafenib	26.26	0.40	26.87	0.45	10
	AngII	25.99	0.47	25.82	0.44	13
	Dabrafenib/AngII	25.56	0.26	25.09	0.37	10
Chronic AngII	Vehicle only	28.48	1.08	29.97*	0.84	6
	Dabrafenib	28.33	0.73	29.43*	0.72	6
	AngII	27.43	0.28	28.95*	0.39	4
	Dabrafenib/AngII	26.68	0.69	30.18*	0.57	4

\*p<0.05 relative to starting weight (2-way ANOVA with Holm-Sidak post-test)

**Supplementary Table S2. qPCR primer sequences**

Gene Symbol	Sense Primer (5'→3')	Antisense Primer (5'→3')
<i>Col1a1</i>	TCGTGGCTTCTCTGGTCTC	CCGTTGAGTCCGTCTTGC
<i>Col4a1</i>	CTGGCACAAAAGGGACGAG	ACGTGGCCGAGAATTTCACC
<i>Ctgf</i>	GCACACCGCACAGAACCA	ATGGCAGGCACAGGTCTTG
<i>Ddr2</i>	GCACTTGGTGAATTAATTAGAACATCCTG	GGACAACTAAATGGTCCCTCCC
<i>Fn1</i>	AAGAGGACGTTGCAGAGCTA	AGACACTGGAGACACTGACTAA
<i>IL1b</i>	CAACCAACAAGTGATATTCTCCAT	GGGTGTGCCGTCTTCATTA
<i>IL11</i>	TGACGGAGATCACAGTCTGGA	CGGAGGTAGGACATCAAGTCTAC
<i>IL6</i>	TCCATCCAGTTGCCTTCTTG	GGTCTGTTGGGAGTGGTATC
<i>Lox</i>	GACATTCGCTACACAGGACAT	AACACCAGGTACGGCTTATC
<i>Myh7</i>	GAGATCGAGGACCTGATGG	TCATACTTCTGCTTCCACTCA
<i>Nppa</i>	GATGGATTCAAGAACCTGCTAGA	CTTCCTCAGTCTGCTCACTCA
<i>Nppb</i>	TCCAGCAGAGACCTAAAATTC	CAGTGCAGTACAGCCAAA
<i>Postn</i>	TTCCCTCTCCTGCCCTTATATGC	CCTGATCCGACCCCTGAT
<i>Timp1</i>	TACGCCTACACCCCCAGTCAT	GCCCCGTGATGAGAAACTCTTC
<i>Tnfa</i>	AGCCAGGAGGGAGAACAGA	CAGTGAGTGAAAGGGACAGAAC

**Supplementary Table S3. Echocardiography data: acute effects (baseline, 3 d and 7 d) of dabrafenib *in vivo*.** C57BL/6J male mice were treated with vehicle, 3 mg/kg/d dabrafenib, 0.8 mg/kg/d angiotensin II (AngII) or dabrafenib/AngII for 7 d. Echocardiograms were taken at baseline (BL), 3 d or 7 d. M-mode images from short axis views were taken at the level of the papillary muscles. Data were analysed using VeoLab software. LV, left ventricular; AW, anterior wall; ID, internal diameter; PW, posterior wall; WT, wall thickness (anterior + posterior walls); d, diastole; s, systole.

	Vehicle (n=12)		Dabrafenib (n=10)		AngII (n=13)		Dabrafenib/AngII (n=10)	
Baseline	Mean	SEM	Mean	SEM	Mean	SEM	Mean	SEM
Heart Rate (bpm)	462	8	478	45	458	7	458	8
Ejection Fraction (%)	46.3	1.4	44.6	4.5	44.7	1.0	46.4	2.7
Fractional Shortening (%)	23.0	0.9	22.0	2.3	22.0	0.6	23.1	1.7
LVAW;d (mm)	0.762	0.013	0.779	0.075	0.776	0.015	0.787	0.015
LVAW;s (mm)	1.097	0.018	1.118	0.106	1.108	0.020	1.125	0.027
LVID;d (mm)	4.187	0.043	4.037	0.387	4.117	0.067	3.983	0.079
LVID;s (mm)	3.196	0.050	3.125	0.300	3.197	0.060	3.039	0.085
LVPW;d (mm)	0.713	0.014	0.706	0.068	0.718	0.017	0.704	0.014
LVPW;s (mm)	1.010	0.016	0.993	0.095	0.983	0.020	0.988	0.028
WT:ID; d	0.353	0.004	0.369	0.035	0.364	0.007	0.376	0.011
WT:ID; s	0.663	0.016	0.680	0.066	0.658	0.017	0.704	0.032
3 d	Mean	SEM	Mean	SEM	Mean	SEM	Mean	SEM
Heart Rate (bpm)	491	9	481	46	503	13	511	18
Ejection Fraction (%)	48.5	1.7	46.9	5.1	58.5	1.9	52.1	2.4
Fractional Shortening (%)	24.4	1.1	23.4	2.7	30.5	1.3	26.4	1.6
LVAW;d (mm)	0.787	0.018	0.793	0.077	0.967	0.013	0.956	0.032
LVAW;s (mm)	1.118	0.018	1.141	0.109	1.316	0.018	1.287	0.046
LVID;d (mm)	4.126	0.059	3.987	0.382	3.388	0.121	3.570	0.085
LVID;s (mm)	3.128	0.077	3.028	0.293	2.359	0.119	2.625	0.090
LVPW;d (mm)	0.706	0.011	0.739	0.078	1.053	0.050	0.872	0.049
LVPW;s (mm)	0.993	0.020	1.045	0.107	1.454	0.045	1.161	0.069
WT:ID; d	0.363	0.009	0.386	0.039	0.610	0.035	0.517	0.029
WT:ID; s	0.681	0.025	0.731	0.076	1.222	0.084	0.951	0.066
7 d	Mean	SEM	Mean	SEM	Mean	SEM	Mean	SEM
Heart Rate (bpm)	481	12	486	47	488	12	495	12
Ejection Fraction (%)	52.7	2.2	52.2	5.0	56.2	2.6	64.4	2.5
Fractional Shortening (%)	27.0	1.4	26.6	2.6	29.2	1.9	34.9	1.9
LVAW;d (mm)	0.806	0.019	0.819	0.081	0.936	0.022	0.948	0.043
LVAW;s (mm)	1.183	0.023	1.201	0.116	1.302	0.022	1.358	0.045
LVID;d (mm)	4.138	0.057	3.955	0.383	3.599	0.122	3.565	0.101
LVID;s (mm)	3.031	0.065	2.908	0.284	2.574	0.134	2.325	0.100
LVPW;d (mm)	0.736	0.019	0.769	0.075	0.992	0.034	0.841	0.041
LVPW;s (mm)	1.060	0.025	1.097	0.105	1.370	0.042	1.286	0.052
WT:ID; d	0.374	0.008	0.404	0.040	0.548	0.033	0.510	0.035
WT:ID; s	0.746	0.029	0.799	0.081	1.103	0.110	1.165	0.078

**Supplementary Table S4. Echocardiography data: chronic effects (baseline and 28 d) of dabrafenib *in vivo*.** C57BL/6J male mice were treated with vehicle or 3 mg/kg/d dabrafenib for 28 d. Echocardiograms were taken at baseline (BL) or 28 d. M-mode images from short axis views were taken at the level of the papillary muscles. Data were analysed using VevoLab software. LV, left ventricular; AW, anterior wall; ID, internal diameter; PW, posterior wall; WT, wall thickness (anterior + posterior walls); d, diastole; s, systole.

	Baseline vehicle (n=6)		Baseline dabrafenib (n=6)		28 d vehicle (n=6)		28 d dabrafenib (n=6)	
	Mean	SEM	Mean	SEM	Mean	SEM	Mean	SEM
Heart Rate (bpm)	491	13	519	11	568	22	585	8
Ejection Fraction (%)	54.7	1.9	58.2	2.1	61.6	2.6	63.7	2.4
Fractional Shortening (%)	28.3	1.3	30.5	1.3	32.8	1.8	34.3	1.8
LVAW;d (mm)	0.753	0.016	0.813	0.018	0.796	0.024	0.757	0.018
LVAW;s (mm)	1.001	0.027	1.120	0.022	1.055	0.031	1.053	0.037
LVID;d (mm)	4.208	0.117	4.129	0.178	4.026	0.150	3.994	0.112
LVID;s (mm)	3.028	0.131	2.881	0.180	2.711	0.149	2.629	0.131
LVPW;d (mm)	0.768	0.013	0.777	0.016	0.688	0.019	0.711	0.028
LVPW;s (mm)	1.065	0.020	1.090	0.011	1.079	0.034	1.104	0.031
WT:ID; d	0.363	0.010	0.388	0.018	0.370	0.011	0.369	0.014
WT:ID; s	0.699	0.041	0.781	0.044	0.798	0.045	0.831	0.049

**Supplementary Table S5. Echocardiography data: chronic effects (baseline and 28 d) of dabrafenib *in vivo*.** C57BL/6J male mice were treated with vehicle, 3 mg/kg/d dabrafenib, 0.8 mg/kg/d angiotensin II (AngII) or dabrafenib/AngII for 28 d. Echocardiograms were taken at baseline (BL) or 28 d. M-mode images from short axis views were taken at the level of the papillary muscles. Data were analysed using VevoLab software. LV, left ventricular; AW, anterior wall; ID, internal diameter; PW, posterior wall; WT, wall thickness (anterior + posterior walls); d, diastole; s, systole.

	Vehicle (n=4)		AngII (n=4)		Dabrafenib/AngII (n=4)	
Baseline	Mean	SEM	Mean	SEM	Mean	SEM
Heart Rate (bpm)	491	13	519	11	532	12
Ejection Fraction (%)	54.7	1.9	58.2	2.1	58.9	2.9
Fractional Shortening (%)	28.3	1.3	30.5	1.3	31.0	1.9
LVAW;d (mm)	0.753	0.016	0.813	0.018	0.764	0.027
LVAW;s (mm)	1.001	0.027	1.120	0.022	1.089	0.029
LVID;d (mm)	4.208	0.117	4.129	0.178	3.972	0.153
LVID;s (mm)	3.028	0.131	2.881	0.180	2.752	0.166
LVPW;d (mm)	0.768	0.013	0.777	0.016	0.758	0.023
LVPW;s (mm)	1.065	0.020	1.090	0.011	1.075	0.037
WT:ID; d	0.363	0.010	0.388	0.018	0.385	0.013
WT:ID; s	0.699	0.041	0.781	0.044	0.807	0.059
<hr/>						
28 d	Mean	SEM	Mean	SEM	Mean	SEM
Heart Rate (bpm)	511	19	557	24	551	16
Ejection Fraction (%)	59.6	2.1	47.1	3.8	62.1	2.1
Fractional Shortening (%)	31.6	1.4	23.6	2.3	33.1	1.4
LVAW;d (mm)	0.787	0.006	0.942	0.029	0.784	0.012
LVAW;s (mm)	1.072	0.015	1.192	0.043	1.093	0.009
LVID;d (mm)	4.284	0.086	4.210	0.202	3.899	0.126
LVID;s (mm)	2.929	0.056	3.214	0.173	2.613	0.130
LVPW;d (mm)	0.807	0.018	0.907	0.015	0.739	0.017
LVPW;s (mm)	1.182	0.021	1.143	0.042	1.081	0.026
WT:ID; d	0.373	0.010	0.443	0.019	0.397	0.010
WT:ID; s	0.771	0.013	0.735	0.043	0.846	0.042

**Supplementary Table S6. Echocardiography data: measurements of aortic diameter for effects of dabrafenib *in vivo*.** C57BL/6J male mice were treated with vehicle, 3 mg/kg/d dabrafenib, 0.8 mg/kg/d angiotensin II (AngII) or dabrafenib/AngII for 7 or 28 d. Echocardiograms were taken at baseline (BL), 7 d or 28 d. B-mode images were taken of the ascending aorta and the internal aortic diameter measured at the end of cardiac systole (s) or during diastole (d). Data were analysed using VevoLab software using callipers.

	Vehicle		Dabrafenib		AngII		Dabrafenib/AngII	
	Mean	SEM	Mean	SEM	Mean	SEM	Mean	SEM
<b>7 d (n=8)</b>								
Aortic diameter; s (mm)	1.450	0.026	1.446	0.023	1.490	0.046	1.480	0.040
Aortic diameter; d (mm)	1.227	0.036	1.221	0.019	1.336	0.062	1.292	0.037
Aortic diameter; s:d ratio	1.184	0.015	1.186	0.029	1.122	0.027	1.146	0.008
<b>28 d (n=4)</b>								
Aortic diameter; s (mm)	1.585	0.004	1.523	0.031	1.699	0.036	1.559	0.044
Aortic diameter; d (mm)	1.352	0.011	1.262	0.038	1.605	0.058	1.368	0.073
Aortic diameter; s:d ratio	1.173	0.011	1.209	0.018	1.062	0.021	1.147	0.033

## **Chapter 6 - Discussion and Conclusion**

## 6.1 Key Conclusions from the Research

The systems developed for echocardiography in mice have been used routinely at the University of Reading and were adopted in other institutions (St. George's University of London; Francis Crick Institute, London). They have so far been reported in eight publications (**Appendix I**: (Alharbi *et al.*, 2022; Clerk *et al.*, 2022; Cull *et al.*, 2023; Fuller *et al.*, 2021; Marshall *et al.*, 2022; Meijles, Cull, *et al.*, 2021; Meijles *et al.*, 2020; Meijles, Fuller, *et al.*, 2021)). Of these, the three to which I made the greatest contribution are included in this thesis with the main conclusions as outlined below.

### 6.1.1 The Role of Striatins in the Heart (Chapter 3)

As stated in **Chapter 1**, my primary focus was the roles of striatin and striatin 3 in the heart, the project which I drove to completion (Cull *et al.*, 2023). The data identify the STRIPAK complexes as a novel signalling system involved in the development of pathological cardiac hypertrophy. Expanding our current understanding of this system could provide new therapeutic targets for managing hypertensive heart disease.

The data demonstrate that heterozygous global knockout of STRN, but not STRN3, reduces cardiac hypertrophy induced by AngII in mice, suggesting a role for STRN in the early stages of cardiac dysfunction. With both studies being conducted in parallel, the negative results of the STRN3<sup>+-</sup> mice with the AngII model emphasise the importance of the response displayed with the STRN<sup>+-</sup> mice. The studies with cardiomyocyte-specific deletion of STRN also demonstrate the inhibition of AngII-induced cardiac hypertrophy and fibrosis showing the involvement of these cells specifically. As fibrosis was not significantly impacted in the global STRN<sup>+-</sup> mice, this indicates that global reduction of STRN compromises the cardiac response to AngII by influencing cardiomyocyte hypertrophy without impacting fibrosis. Contrary to this effect, cardiomyocyte STRN knockout reduced AngII-induced fibrosis, as well as AngII-induced cardiac hypertrophy. This suggests there is a compensatory mechanism for maintaining fibrosis when the STRN protein is only partially depleted (global heterozygous model). However, this compensation is lost when the entire STRN gene is deleted in the cardiomyocyte-specific homozygous knockout mice.

The potential cardiac function of STRN3 should not be disregarded. STRN3 is significantly expressed and even upregulated in failing human hearts. In wild-type mice, AngII also increases both STRN and STRN3 expression. Despite this, no significant change in cardiac function or dimensions was detected between the STRN3<sup>+/−</sup> mice and their wild-type littermates, either at baseline or in response to AngII. As our experimental timeline represents the early stages of hypertension-induced cardiac dysfunction (up to 7 days), STRN3 could play a more significant role in the later stages. STRN3 may also influence other cardiac pathologies which have not been explored in this thesis (e.g. myocardial infarction).

The clinical relevance of this study is highlighted by the identification of a novel signalling paradigm, orchestrated by the striatin-based STRIPAK complex. As established in this thesis, the STRIPAK complex seems to be involved in the development of pathophysiological cardiac hypertrophy and, therefore, the progression to heart failure. Therefore, the STRIPAK complex has promise for the development of novel therapeutic targets against it to control cardiac diseases. With over 150 variants of the STRIPAK complex, the challenge for targeting these complexes will be to understand which cells contain which variants, its components and their unique functions. Following this, understanding how these cells independently regulate the STRIPAK variants to enable the complexes to carry out their distinct functions. Clearly, a further understanding of the striatin family and the components of the STRIPAK complex is needed.

### **6.1.2 The Role of PKN2 in the Heart (Chapter 4)**

Previous work on this project was conducted at the Francis Crick Institute and this focused on the role of PKN2 in embryonic development. My contribution to this study was investigating whether PKN2 contributes to the development of hypertension-induced cardiac dysfunction in the adult heart using heterozygous PKN2 global knockout mice (since homozygous deletion of PKN2 is embryonic lethal (Marshall *et al.*, 2022)). The data showed that PKN2 plays a significant role in how the adult heart adapts to pathophysiological (hypertension) but not necessarily physiological (ageing) stressors.

PKN2 clearly plays a crucial role in cardiac development, particularly in the formation of the compact myocardium. Mice with PKN2 knockout in cardiomyocytes have thin

ventricular walls and compromised cardiac function. This developmental disruption presents with 100% of global homozygous PKN2 mice being embryonic lethal and only a third of the cardiomyocyte-specific homozygous PKN2 mice surviving to 4 weeks postnatally. Despite a significant role in development, the cardiac response to PKN2 depletion demonstrated no significant role in the ageing heart. This lack of response was highlighted by no significant differences in cardiac function or dimensions between wild-type and PKN2-deficient mice once they reached middle age (42 weeks). This suggests that PKN2 is not crucial post-development for maintaining heart health under normal conditions. However, when subjected to severe stress associated with hypertension-induced cardiac hypertrophy, a more significant role is presented and PKN2 haploinsufficiency compromised cardiac adaptation to AngII. This is likely a result of the inhibition of cardiomyocyte hypertrophy and fibrosis, presenting as reduced left ventricular hypertrophy and an overall reduction in the increase in left ventricular mass. PKN2 may also have a greater effect on the vasculature than the heart. PKN2 haploinsufficiency was shown to reduce aortic flow, although not pulmonary flow, suggesting a role in regulating blood vessel function. Altogether, these results suggest that PKN2 plays an important role in the adult cardiac response to pathophysiological stressors.

The clinical relevance of this study is that the PKN family could offer therapeutic modalities for both congenital and adult heart diseases. However, further research is needed to develop and trial targeted therapies for the modulation of the PKN family members, the pathways they influence and the consequences of their activation.

### **6.1.3 The Effects of Dabrafenib on the Heart (Chapter 5)**

ERK1/2 signalling has previously been demonstrated to be cardioprotective and plays an important role in the development of cardiomyocyte hypertrophy (Gallo *et al.*, 2019; Kehat *et al.*, 2011). In contrast, the pathway has also been associated with promoting cardiac fibrosis (Lindsey *et al.*, 2018; Schafer *et al.*, 2017; Sweeney *et al.*, 2020), which can be detrimental to cardiac function through excessive scar formation. ERK1/2 also promotes cancer, and this has resulted in the development of several small-molecule inhibitors of the pathway as cancer therapies (Kidger *et al.*, 2020; Lee *et al.*, 2020). However, before applications of these inhibitors can be made clinically for the heart, further research must be conducted to confirm the following uncertainties. Do we inhibit ERK1/2 to prevent fibrosis, potentially compromising its cardioprotective effects? OR do we activate it to

promote heart protection and hypertrophy, potentially risking the development of harmful fibrosis? The only way to resolve these questions is experimentally.

Dabrafenib inhibits RAF family kinases, although it was developed to inhibit specifically the oncogenic form of BRAF, BRAF(V600E). It is commonly used in combination with other cancer treatments to inhibit overactive ERK1/2 signalling resulting from BRAF(V600E) mutations (Eroglu & Ribas, 2016; Long *et al.*, 2016; Robert *et al.*, 2019). Other inhibitors of the ERK1/2 pathway have cardiotoxic effects (Guha *et al.*, 2021; Kloth *et al.*, 2015; Nebot *et al.*, 2018; Peng *et al.*, 2017), with the cardiotoxicity of dabrafenib being unconfirmed. The data from our research suggests that dabrafenib is not cardiotoxic and even has the potential to inhibit maladaptive hypertrophy and fibrosis resulting from hypertension (Meijles, Cull, *et al.*, 2021). The data show that dabrafenib reduces cardiac fibrosis and inhibits maladaptive cardiac hypertrophy resulting from AngII-induced hypertensive heart disease. This was demonstrated by dabrafenib reducing cardiomyocyte hypertrophy, cardiac inflammation and cardiac fibrosis induced by AngII in both acute (7 d) and chronic (28 d) treatment conditions. This finding not only validates RAF kinases as promising therapeutic targets for hypertension-related diseases but also identifies dabrafenib, a medication already in clinical use, as a potential treatment option. This finding is potentially clinically significant. As it is already used in patients, the safety profile is good which could render clinical application of dabrafenib in hypertensive disease more rapid (Eroglu & Ribas, 2016; Long *et al.*, 2016; Robert *et al.*, 2019). Further studies are needed to confirm its efficacy in relation to treatment for hypertension-related cardiovascular diseases. It is also important to determine if dabrafenib can prevent or reverse established fibrosis over an extended timeline.

## 6.2 Theoretical and Practical Implications of *In Vivo* Studies

The development of a standardised and reproducible protocol for *in vivo* echocardiography is essential to ensure the reliability and comparability of data across preclinical mouse studies of the heart. Investigating and uncovering the roles of genes in signalling pathways, within tissues or even the organism as a whole, unlocks the potential for new therapeutic targets for diseases. However, there are many considerations for such research as discussed in this section.

### 6.2.1 Choice of Preclinical Model and Use of Genetically-Altered Mice

The studies all use mice with a single genetic background, the C57Bl/6J background. There can be significant differences between the substrains of C57Bl/6 mice. For example, C57BL/6N mice are not suitable for cardiac research because they respond differently, generally more severely, to pressure overload compared to C57BL/6J mice (Garcia-Menendez *et al.*, 2013). Therefore, the C57Bl/6J mice are used widely for cardiovascular studies.

This is why both lines used in the striatin study ("Knockout first" STRN<sup>tm1a(KOMP)WT<sub>Si</sub></sup> and STRN3<sup>tm1a(KOMP)WT<sub>Si</sub></sup> mice), that were originally on a C57Bl/6N background, were transferred onto a C57Bl/6J background through at least eight generations of backcrossing. The goal was to replace the C57Bl/6N genetics with C57Bl/6J genetics while retaining the traits of the Strn/Strn3 mice. The reason for backcrossing for at least eight generations is to "purify" the genetic background. Each generation of backcrossing introduces a 50% chance of inheriting the unwanted C57Bl/6N genetics. By performing multiple rounds of backcrossing, the proportion of C57Bl/6N genetics decreases exponentially with each generation. After eight generations, the resulting population will have over 99% of its genetic makeup derived from the C57Bl/6J background, reducing the impact of any remaining C57Bl/6N genome.

However, despite significant backcrossing the background genetics of these mice were not identical to the C57Bl/6J genome. This is demonstrated by comparing the global heterozygous Strn/Strn3 strains (Cull *et al.*, 2023) to the C57Bl/6J mice obtained for the Dabrafenib study (Meijles, Cull, *et al.*, 2021). The backcrossed Strn/Strn3 mice demonstrated notably higher mortality rates. A likely explanation is that despite the extensive efforts, further rounds of backcrossing were necessary to fully eliminate undesirable genetic influences from the original C57Bl/6N background.

All of the studies in this thesis used the same model of hypertension, 0.8 mg/kg/d AngII. As explained in **Chapter 2**, AngII is a peptide hormone involved in regulating blood pressure and associated with heart failure (Nehme *et al.*, 2019; Patel *et al.*, 2017; Pugliese *et al.*, 2020; Sayer & Bhat, 2014) and is commonly used in research to induce high blood pressure. For our studies, a moderate concentration of Ang II (0.8 mg/kg/d) (Patel *et al.*, 2018) was utilised to induce hypertension, rather than a subpressor dose

(e.g., 0.288 mg/kg/d) (Izumiya *et al.*, 2003) or a dose more associated with sudden cardiac death (e.g., >2.0 mg/kg/d). The 0.8 mg/kg/d AngII concentration was chosen because it effectively triggers hypertension at our experimental timepoints, allowing us to study early-stage mechanisms and associated pathophysiology without causing severe side effects.

Having decided on the basic features of the model (background strain and disease model) the next consideration was the gene/system in question and how to investigate the role of individual genes. This decision depended on the research objectives as well as the characteristics and establishment of the gene or pathway under investigation. Two of the studies in this thesis used genetically-altered mice focusing on gene deletion to assess the effects over an extended period (global knockout for STRN, STRN3 or PKN2) or in a specific context (cardiomyocyte STRN or PKN2 in the adult heart) (Cull *et al.*, 2023; Marshall *et al.*, 2022) as discussed more in the next section. Genetically-altered mice can provide an assessment of the gene's role throughout the developmental processes but also into adulthood, determining the long-term consequences of the manipulated gene.

## 6.2.2 Selection of Genetically Altered Model for Gene Deletion

### (i) Global Gene Deletion vs Cell-Specific Gene Knockout

As discussed in **section 2.5**, there are several options for gene deletion in mice. Global gene deletion involves the elimination of a gene throughout the entire organism such that the targeted gene is deleted or inactivated in all tissues of the body (Davey & MacLean, 2006). Mouse models with global gene deletion serve as a valuable tool for proof-of-concept studies, but there can be problems with this approach. A major problem with the original system which relies on constitutive gene deletion is the possibility that homozygous gene deletion of essential genes required for development may result in embryonic lethality (Justice *et al.*, 2011). This was the case for STRN and STRN3 (**Chapter 3**) (Cull *et al.*, 2023) and PKN2 (**Chapter 4**) (Marshall *et al.*, 2022). To avoid this, global heterozygous STRN, STRN3 and PKN2 mice were utilised for the studies. In all cases, the heterozygotes appeared normal compared with wild-type littermates but, for STRN and PKN2, a cardiac phenotype was revealed when hearts were stressed by treatment with AngII. However, since the knockout is applied systemically, any observed changes in specific organs, such as the heart, cannot be definitively linked to the function of that gene in that particular tissue. This is due to the possibility that the observed effect

may be a secondary consequence of or influenced by the primary effect in another tissue (e.g. the lungs), which could indirectly influence the tissue under investigation (e.g. the heart) (Davey & MacLean, 2006). Thus, we cannot be certain from the studies in **Chapters 3 and 4** that the effects of STRN or PKN2 haploinsufficiency were due to knockdown in cardiomyocytes or the heart as a whole and did not result from, for example, hormonal effects or deficiencies in innervation.

Cell-specific gene deletion models can resolve this issue, allowing for the elimination of a gene in a specific cell type, with the other cell types retaining the original gene (Davey & MacLean, 2006; Huang *et al.*, 2021; Yan *et al.*, 2015). This allows for more accurate assessment of the gene's function within a particular tissue or organ, without the confounding effects of systemic gene deletion. Such specificity allows for a more nuanced understanding of a gene's function and can help to identify potential therapeutic targets for disease treatment. As cell-specific knockouts provide more precise information, they are not as useful in evaluating the overall effect of a gene. For example, the cell-specific model may determine that the gene has no role in the organ or disease being investigated despite a significant role in other cell types within the organism relating to the disease. For this reason, they are not ideal models for concept validation.

Cell-specificity is achieved by targeting the machinery for gene deletion to a cell type using a cell-specific promoter. For cardiomyocytes, there are several that are used, the most common being the promoter for Myh6 (alpha-myosin heavy chain) (Huang *et al.*, 2021; Yan *et al.*, 2015). The advantage of this is that Myh6 is largely only expressed in the adult ventricle from birth so gene deletion does not occur during embryonic development avoiding the potential for embryonic lethality. The Myh6 promoter was used for cardiomyocyte-specific STRN knockout (**Chapter 3**) (Cull *et al.*, 2023). Other cardiomyocyte specific promoters may be expressed during embryonic development as with the study of PKN2 (**Chapter 4**) (Marshall *et al.*, 2022). Here, SM22 $\alpha$  and XMLC2 promoters were used for cardiomyocyte-specific PKN2 knockout mice. As previously mentioned, this model was a constitutive model of gene deletion and the mice demonstrated severe cardiac developmental defects from birth. Only ~1/3 of the offspring of the SM22 $\alpha$ -Cre $^{+/-}$  Pkn2 $^{fl/fl}$  mice survived to 4 weeks postnatally. Further studies using the Myh6 promoter for cardiomyocyte-specific gene deletion of PKN2 may be more revealing.

## **(ii) Method of Gene Deletion: The CRE Enzyme and Constitutive vs Inducible Specific Knockouts**

The Cre recombinase enzyme is generally used for genetic manipulation in mice. However, it can have detrimental effects to the heart at high levels of expression (Bersell *et al.*, 2013; McLellan *et al.*, 2017) and if enzyme activity is not controlled constitutive expression of the enzyme results in constitutive gene knockout. Constitutive knockouts involve the permanent and complete elimination of a gene's function, removing the activity of the targeted gene throughout the time that the enzyme is expressed. This approach is particularly useful when researchers aim to understand the fundamental, baseline functions of a gene. Conversely, inducible knockouts offer researchers the ability to modulate gene expression in a controlled manner (Saunders, 2011). Inducible systems employ regulatory elements that respond to experimental interventions, allowing researchers to control when the target gene is deleted. For Cre, an established method for regulating enzyme activity is to use a form of the enzyme which is flanked by binding sites for oestrogen from the oestrogen receptor which have been modified for binding of tamoxifen (Sohal *et al.*, 2001). Thus, the enzyme is only activated in the presence of tamoxifen (i.e. it is used for tamoxifen-inducible gene deletion). If this form of Cre is placed under control of the Myh6 promoter, it is also only expressed in cardiomyocytes.

Despite both being conditional models, the models used for the STRN (inducible gene deletion) and PKN2 (constitutive gene deletion) projects demonstrate these differences and their consequences. For STRN, a tamoxifen-inducible Cre system was used with tamoxifen administered after baseline echocardiography at 7 weeks resulting in conditional deletion not only after birth, but only in the adult (Cull *et al.*, 2023). This method bypassed the developmental issues and embryonic lethality present in the global homozygous model. In contrast, the PKN2 model utilised a non-inducible form of CRE resulting in constitutive knockout. Therefore, the PKN2 gene is absent throughout the entire development and lifespan of the animal. Although the PKN mice survived through to birth, they died around birth because the hearts could not undergo the necessary post-birth remodelling (Marshall *et al.*, 2022).

### **6.2.3 Use of Small Molecule Inhibitors**

An alternative way to investigate the role of an enzyme in a response such as cardiac hypertrophy is to use a selective small molecular inhibitor. Numerous inhibitors have been produced to inhibit protein kinases, generally as potential therapies for cancer (Bhullar *et al.*, 2018). Apart from general problems with toxicity, one major problem is that the drugs can have off-target effects due to a lack of specificity of the drugs. However, recently produced inhibitors that are now in use for cancer such as those that inhibit the ERK1/2 cascade generally have great specificity (Ullah *et al.*, 2022). Another problem can be toxicity resulting from on-target effects in other tissues and several anti-cancer drugs can be cardiotoxic in some patients (Bhullar *et al.*, 2018). The publication in **Chapter 5** took a different approach from genetically-modified mice. This study investigated the effects of a pharmacological inhibitor (dabrafenib) that was designed to target BRAF but which inhibits the RAF family kinases in general (Meijles, Cull, *et al.*, 2021; Rheault *et al.*, 2013; Ullah *et al.*, 2022). This may be viewed as a more immediate and adaptable approach by enabling the study of the acute responses to the drug or assessing the therapeutic potential of targeting the drug-specific pathways. There are challenges in availability of small molecule inhibitors including specificity for the target of interest, toxicity, and appropriate dosage. However, as dabrafenib is already used clinically to treat cancer in patients, it is clearly specific, safe for use in mice and information to establish an appropriate dosage.

In the cancer field, drug administration commonly involves oral dosing (Budha *et al.*, 2012; Cardoso *et al.*, 2018; Fujita *et al.*, 2017; Kim *et al.*, 2017). Oral dosing requires multiple administrations to maintain the therapeutic drug level. Consequentially, the drug concentration in the blood fluctuates from high (upon dosing) to low (before dosing), leading to inconsistent efficacy or side effects of the drug simply due to variation in drug availability (Almoshari, 2022; Keraliya *et al.*, 2012). Our research team uses osmotic minipumps (as in (Alharbi *et al.*, 2022; Clerk *et al.*, 2022; Cull *et al.*, 2023; Fuller *et al.*, 2021; Marshall *et al.*, 2022; Meijles, Cull, *et al.*, 2021; Meijles *et al.*, 2020; Meijles, Fuller, *et al.*, 2021)). These provide a consistent and steady delivery of medication over a set period (days to weeks dependant on the minipump), eliminating the need for frequent dosing. This consistency ensures therapeutic thresholds are maintained, potentially improving treatment efficacy and minimising side effects associated with peaks and troughs of drug administration/withdrawal (Almoshari, 2022; Keraliya *et al.*, 2012; Patel *et al.*, 2021). Minipumps also bypass the digestive system, ensuring optimal drug absorption and enabling drugs with poor oral bioavailability to be utilised. Thus, dosing using minipumps reduces variability in drug exposure, as the drugs are released at a constant, predetermined flow rate, leading to more accurate research data. Moreover, although

surgery is required for implantation, there is an overall reduction in animal stress and handling associated with gavage, contributing to improved animal welfare.

Osmotic minipumps do have several limitations that need to be considered (Almoshari, 2022; Patel *et al.*, 2021). Firstly, minipump implantation requires a surgical procedure, adding to the complexity, potential risks, and stressors of the overall experiment. Additional monitoring is therefore required to detect any side effects or malfunction of the minipump implantation, adding to the overall management burden. Moreover, certain pharmaceutical formulations are incompatible with the osmotic minipumps, restricting their applicability. For example, many drugs are insoluble in water but dissolve in DMSO. However, minipumps can only tolerate 50% DMSO so we needed to develop a process for solubilisation of protein inhibitors in DMSO prior to mixing with other reagents and detergents (40% polyethylene glycol, 10% propylene glycol, 1% Tween 80). In comparison to oral dosing, the cost associated with osmotic minipumps is substantially higher for the minipumps themselves and the surgery (Almoshari, 2022). These limitations highlight the need for careful evaluation of the suitability and feasibility of minipump application prior to experimentation.

### **6.3.2 Limitations of *In Vivo* Studies with Preclinical Models of Disease**

Due to the inherent complexity and variability of living systems, *in vivo* studies face significant challenges in controlling all potentially influencing factors both internal and external to the animal (Voelkl *et al.*, 2020). This difficulty makes it challenging to draw definitive conclusions about the effect of the gene/drug/pathway being studied. While comparisons to human genetics and disease aetiologies can be made, the innate differences between species can limit the direct applicability of rodent findings to humans (McGonigle & Ruggeri, 2014).

The potential for species-specific responses to treatments can complicate the translation of results to humans. This is especially pronounced in complex diseases with multifaceted genetic and environmental components (Voelkl *et al.*, 2020). Despite these limitations, *in vivo* models allow researchers to study specific diseases and their mechanisms in real-time in a living organism, allowing for the chance to test the safety and efficacy of novel treatments prior to human trials (Franco, 2013; Robinson *et al.*, 2019). Nevertheless, to

make the models most relevant to disease it is increasingly important to take into consideration additional factors such as age and sex.

**(i) Age.** Classification of mice as a “young” or “old” depends on the context of the research and the strain being used. For example, in C57BL/6 mice, “young” adults are categorised as 3-6 months old, while “old” adults can be 18-24+ months (Yanai & Endo, 2021). As the lifespan of genetically-altered mice may be strain-specific (since mutations may alter their lifespan), the definition of young or old mice is not straightforward. The age of the mouse presents age-related challenges that should be considered prior to the research. Younger mice are typically lean and gain weight steadily until reaching maturity. Older mice may lose muscle mass and gain fat, leading to increased body weight despite decreased lean tissue (Messa *et al.*, 2020; Petr *et al.*, 2021)

An increased fat-to-body weight ratio can lead to increased absorption of the drug from the bloodstream into the adipose tissue, resulting in inaccurate dosing of the mouse (Cho *et al.*, 2013). As the mice age, they experience a decline in organ, metabolism, and stem cell function (Liu *et al.*, 2022; Petr *et al.*, 2021) compared to younger mice, introducing more confounding factors which may affect the variables being investigated. Maintaining older animals comes with increased expense compared to younger mice. Similarly, the older mice have a reduced experimental turnover as it takes much longer to obtain the required age before the experiments even start.

For the studies in this thesis, hypertension was induced by pharmacological intervention (using angiotensin II) in young mice (8-10 weeks) to avoid problems with aging mice whilst enabling the accurate and rapid assessment of the effect of genetic alteration or drug administration on the heart. However, the studies with PKN2 heterozygous gene deletion (**Chapter 4**) enabled a comparison of young and old (~1 year) mice. These data illustrated the change in cardiac function.

**(ii) Sex.** As referenced in **Chapter 1**, the studies in this thesis used male mice only. The oestrous cycle in female mice can introduce variability in data due to hormonal fluctuations. These hormonal cycles affect various organ systems and responses to treatment, and can add complexity to data interpretation and experimental design (Milner

*et al.*, 2008). In the study of STRN and STRN3, the intention was to convert the original global constitutive line(s) into a model for cardiomyocyte-specific, tamoxifen-induced conditional line. As an oestrogen receptor antagonist, tamoxifen has greater potential for unanticipated effects in female mice than in males.

At the time the studies were initiated, the Myh6-CRE model with tamoxifen-inducibility had not been characterised in female mice. Therefore, the study focused only on males. However, in an ancillary study of cardiomyocyte BRAF knockout to which I contributed, the effects of phenylephrine on male and female hearts were compared. Unlike male hearts, tamoxifen administration in female mice led to a slight but significant decrease in cardiomyocyte size (Alharbi *et al.*, 2022). While tamoxifen generally clears within 2-3 days (Sohal *et al.*, 2001), its pharmacokinetics may differ in females or this specific mouse line, potentially causing residual effects at the experiment's conclusion (11 days post-injection). Given tamoxifen's antagonism to oestrogen and oestrogen's known role in promoting PKB/Akt signalling within female hearts (Camper-Kirby *et al.*, 2001; Sugden & Clerk, 2001), it's possible that the observed decrease in cardiomyocyte size is consequential of tamoxifen's interference with the hormone. Clearly, more research on females is needed.

### **6.3 Concluding Remarks**

Cardiovascular diseases remain a significant global challenge, affecting billions of adults every year, with hypertension and heart failure being two of the most common diseases. With the future of treatments heading towards personalised medicine, developing protein-specific treatments could improve the survival of patients affected by mutations in these genes. The selection of appropriate mouse models is paramount to an accurate assessment of the hypothesis associated with these genes. Echocardiography provides a cheap and minimally invasive method of assessing the effect of these genes and the novel treatments targeting them.

## **References**

- (IMPC), I. M. P. C. (2023). *Allele details for Strntm1a(KOMP)Wtsi*. Retrieved 18 December from [http://www.mousephenotype.org/data/alleles/MGI:1333757/tm1a\(KOMP\)Wtsi](http://www.mousephenotype.org/data/alleles/MGI:1333757/tm1a(KOMP)Wtsi)
- Abais-Battad, J. M., Alsheikh, A. J., Pan, X., Fehrenbach, D. J., Dasinger, J. H., Lund, H., Roberts, M. L., Kriegel, A. J., Cowley, A. W., Jr., Kidambi, S., Kotchen, T. A., Liu, P., Liang, M., & Mattson, D. L. (2019). Dietary Effects on Dahl Salt-Sensitive Hypertension, Renal Damage, and the T Lymphocyte Transcriptome. *Hypertension*, 74(4), 854-863. <https://doi.org/10.1161/HYPERTENSIONAHA.119.12927>
- Ahuja, P., Sdek, P., & MacLellan, W. R. (2007). Cardiac Myocyte Cell Cycle Control in Development, Disease, and Regeneration. *Physiological Reviews*, 87(2), 521-544. <https://doi.org/10.1152/physrev.00032.2006>
- Aimo, A., Kollia, E., Ntritsos, G., Barison, A., Masci, P.-G., Figliozi, S., Klettas, D., Stamatelopoulos, K., Delialis, D., Emdin, M., & Georgopoulos, G. (2021). Echocardiography versus computed tomography and cardiac magnetic resonance for the detection of left heart thrombosis: a systematic review and meta-analysis. *Clinical Research in Cardiology*, 110(11), 1697-1703. <https://doi.org/10.1007/s00392-020-01741-7>
- Alberts, B., Johnson, A., Lewis, J., Raff, M., Roberts, K., & Walter, P. (2002). *Molecular Biology of the Cell, 4th edition*. Garland Science.
- Alharbi, H. O., Hardyman, M. A., Cull, J. J., Markou, T., Cooper, S. T. E., Glennon, P. E., Fuller, S. J., Sugden, P. H., & Clerk, A. (2022). Cardiomyocyte BRAF is a key signalling intermediate in cardiac hypertrophy in mice. *Clin Sci (Lond)*, 136(22), 1661-1681. <https://doi.org/10.1042/CS20220607>
- Ali, E. S., Akter, S., Ramproshad, S., Mondal, B., Riaz, T. A., Islam, M. T., Khan, I. N., Docea, A. O., Calina, D., Sharifi-Rad, J., & Cho, W. C. (2022). Targeting Ras-ERK cascade by bioactive natural products for potential treatment of cancer: an updated overview. *Cancer Cell International*, 22(1), 246. <https://doi.org/10.1186/s12935-022-02666-z>
- Almoshari, Y. (2022). Osmotic Pump Drug Delivery Systems-A Comprehensive Review. *Pharmaceuticals (Basel)*, 15(11). <https://doi.org/10.3390/ph15111430>
- Altman, D. (2020). Myosin Work and Motility, Mechanism of. In G. Roberts & A. Watts (Eds.), *Encyclopedia of Biophysics* (pp. 1-12). Springer Berlin Heidelberg. [https://doi.org/10.1007/978-3-642-35943-9\\_754-1](https://doi.org/10.1007/978-3-642-35943-9_754-1)

- Ames, M. K., Atkins, C. E., & Pitt, B. (2019). The renin-angiotensin-aldosterone system and its suppression. *J Vet Intern Med*, 33(2), 363-382.  
<https://doi.org/10.1111/jvim.15454>
- Ancion, A., Tridetti, J., Nguyen Trung, M.-L., Oury, C., & Lancellotti, P. (2019). A Review of the Role of Bradykinin and Nitric Oxide in the Cardioprotective Action of Angiotensin-Converting Enzyme Inhibitors: Focus on Perindopril. *Cardiology and Therapy*, 8(2), 179-191. <https://doi.org/10.1007/s40119-019-00150-w>
- Anthamatten, A. (2023). Diabetes and Heart Failure. In K. M. S. Hayes & N. R. Dellise (Eds.), *Managing Heart Failure in Primary Care: A Case Study Approach* (pp. 177-204). Springer International Publishing. [https://doi.org/10.1007/978-3-031-20193-6\\_12](https://doi.org/10.1007/978-3-031-20193-6_12)
- Antzelevitch, C., & Patocskai, B. (2016). Brugada Syndrome: Clinical, Genetic, Molecular, Cellular, and Ionic Aspects. *Curr Probl Cardiol*, 41(1), 7-57.  
<https://doi.org/10.1016/j.cpcardiol.2015.06.002>
- Appel, L. J., Moore, T. J., Obarzanek, E., Vollmer, W. M., Svetkey, L. P., Sacks, F. M., Bray, G. A., Vogt, T. M., Cutler, J. A., Windhauser, M. M., Lin, P. H., & Karanja, N. (1997). A clinical trial of the effects of dietary patterns on blood pressure. DASH Collaborative Research Group. *N Engl J Med*, 336(16), 1117-1124.  
<https://doi.org/10.1056/nejm199704173361601>
- Avruch, J., Khokhlatchev, A., Kyriakis, J. M., Luo, Z., Tzivion, G., Vavvas, D., & Zhang, X. F. (2001). Ras activation of the Raf kinase: tyrosine kinase recruitment of the MAP kinase cascade. *Recent Prog Horm Res*, 56, 127-155.  
<https://doi.org/10.1210/rp.56.1.127>
- Bahar, M. E., Kim, H. J., & Kim, D. R. (2023). Targeting the RAS/RAF/MAPK pathway for cancer therapy: from mechanism to clinical studies. *Signal Transduct Target Ther*, 8(1), 455. <https://doi.org/10.1038/s41392-023-01705-z>
- Banerjee, P. (2017). Heart failure: a story of damage, fatigue and injury? *Open Heart*, 4(2), e000684. <https://doi.org/10.1136/openhrt-2017-000684>
- Barros, V. N. (2019). The heart cycle: review. *MOJ Womens Health*, 8(1), 66-69.  
<https://doi.org/10.15406/mojwh.2019.08.00214>
- Bartelds, B., Douwes, J. M., & Berger, R. M. F. (2021). The Right Ventricle in Congenital Heart Diseases. In S. P. Gaine, R. Naeije, & A. J. Peacock (Eds.), *The Right Heart* (pp. 183-203). Springer International Publishing.  
[https://doi.org/10.1007/978-3-030-78255-9\\_13](https://doi.org/10.1007/978-3-030-78255-9_13)
- Baskaran, R., & Velmurugan, B. K. (2018). Protein phosphatase 2A as therapeutic targets in various disease models. *Life Sciences*, 210, 40-46.  
<https://doi.org/https://doi.org/10.1016/j.lfs.2018.08.063>

- Bersell, K., Choudhury, S., Mollova, M., Polizzotti, B. D., Ganapathy, B., Walsh, S., Wadugu, B., Arab, S., & Kühn, B. (2013). Moderate and high amounts of tamoxifen in aMHC-MerCreMer mice induce a DNA damage response, leading to heart failure and death. *Disease models & mechanisms*, 6(6), 1459-1469. <https://doi.org/10.1242/dmm.010447>
- Bhullar, K. S., Lagarón, N. O., McGowan, E. M., Parmar, I., Jha, A., Hubbard, B. P., & Rupasinghe, H. P. V. (2018). Kinase-targeted cancer therapies: progress, challenges and future directions. *Molecular Cancer*, 17(1), 48. <https://doi.org/10.1186/s12943-018-0804-2>
- Boone, M., & Deen, P. M. (2008). Physiology and pathophysiology of the vasopressin-regulated renal water reabsorption. *Pflugers Arch*, 456(6), 1005-1024. <https://doi.org/10.1007/s00424-008-0498-1>
- Boron, W. F., & Boulpaep, E. L. (2012). *Medical Physiology, 2e Updated Edition E-Book: with STUDENT CONSULT Online Access*. Elsevier Health Sciences. [https://books.google.co.uk/books?id=54mxMgO5H\\_YC](https://books.google.co.uk/books?id=54mxMgO5H_YC)
- Bottle, A., Kim, D., Aylin, P., Cowie, M. R., Majeed, A., & Hayhoe, B. (2018). Routes to diagnosis of heart failure: observational study using linked data in England. *Heart*, 104(7), 600-605. <https://doi.org/10.1136/heartjnl-2017-312183>
- Boyden, P. A., Hirose, M., & Dun, W. (2010). Cardiac Purkinje cells. *Heart Rhythm*, 7(1), 127-135. <https://doi.org/10.1016/j.hrthm.2009.09.017>
- Budha, N. R., Frymoyer, A., Smelick, G. S., Jin, J. Y., Yago, M. R., Dresser, M. J., Holden, S. N., Benet, L. Z., & Ware, J. A. (2012). Drug absorption interactions between oral targeted anticancer agents and PPIs: is pH-dependent solubility the Achilles heel of targeted therapy? *Clin Pharmacol Ther*, 92(2), 203-213. <https://doi.org/10.1038/clpt.2012.73>
- Camper-Kirby, D., Welch, S., Walker, A., Shiraishi, I., Setchell, K. D., Schaefer, E., Kajstura, J., Anversa, P., & Sussman, M. A. (2001). Myocardial Akt activation and gender: increased nuclear activity in females versus males. *Circ Res*, 88(10), 1020-1027. <https://doi.org/10.1161/hh1001.090858>
- Cardoso, E., Csajka, C., Schneider, M. P., & Widmer, N. (2018). Effect of Adherence on Pharmacokinetic/Pharmacodynamic Relationships of Oral Targeted Anticancer Drugs. *Clin Pharmacokinet*, 57(1), 1-6. <https://doi.org/10.1007/s40262-017-0571-z>
- Carmeliet, P. (2005). Angiogenesis in life, disease and medicine. *Nature*, 438(7070), 932-936. <https://doi.org/10.1038/nature04478>
- Chambers, C. H., & Matthews, G. (2019). Cardiac Cycle. In D. Chambers, C. Huang, & G. Matthews (Eds.), *Basic Physiology for Anaesthetists* (2 ed., pp. 117-120). Cambridge University Press. <https://doi.org/DOI: 10.1017/9781108565011.031>

- Charrin, S., & Alcover, A. (2006). Role of ERM (ezrin-radixin-moesin) proteins in T lymphocyte polarization, immune synapse formation and in T cell receptor-mediated signaling. *Front Biosci*, 11, 1987-1997. <https://doi.org/10.2741/1940>
- Chen, M. J., Dixon, J. E., & Manning, G. (2017). Genomics and evolution of protein phosphatases. *Sci Signal*, 10(474). <https://doi.org/10.1126/scisignal.aag1796>
- Cho, S.-J., Yoon, I.-S., & Kim, D.-D. (2013). Obesity-related physiological changes and their pharmacokinetic consequences. *Journal of Pharmaceutical Investigation*, 43(3), 161-169. <https://doi.org/10.1007/s40005-013-0073-4>
- Clerk, A., Meijles, D. N., Hardyman, M. A., Fuller, S. J., Chothani, S. P., Cull, J. J., Cooper, S. T. E., Alharbi, H. O., Vanezis, K., Felkin, L. E., Markou, T., Leonard, S. J., Shaw, S. W., Rackham, O. J. L., Cook, S. A., Glennon, P. E., Sheppard, M. N., Sembrat, J. C., Rojas, M., . . . Sugden, P. H. (2022). Cardiomyocyte BRAF and type 1 RAF inhibitors promote cardiomyocyte and cardiac hypertrophy in mice *in vivo*. *Biochem J*, 479(3), 401-424. <https://doi.org/10.1042/bcj20210615>
- Conrad, N., Judge, A., Tran, J., Mohseni, H., Hedgecott, D., Crespillo, A. P., Allison, M., Hemingway, H., Cleland, J. G., McMurray, J. J. V., & Rahimi, K. (2018). Temporal trends and patterns in heart failure incidence: a population-based study of 4 million individuals. *Lancet*, 391(10120), 572-580. [https://doi.org/10.1016/S0140-6736\(17\)32520-5](https://doi.org/10.1016/S0140-6736(17)32520-5)
- Cull, J., Cooper, S., Alharbi, H., Chothani, S., Rackham, O., Meijles, D., Dash, P., Kerkelä, R., Ruparelia, N., Sugden, P., & Clerk, A. (2023). *Striatin plays a major role in angiotensin II-induced cardiomyocyte and cardiac hypertrophy in mice* *in vivo*. Cold Spring Harbor Laboratory. <https://dx.doi.org/10.1101/2023.10.21.563397>
- da Silva, A. C. R., & Reinach, F. C. (1991). Calcium binding induces conformational changes in muscle regulatory proteins. *Trends in Biochemical Sciences*, 16, 53-57. [https://doi.org/https://doi.org/10.1016/0968-0004\(91\)90024-P](https://doi.org/https://doi.org/10.1016/0968-0004(91)90024-P)
- Damman, K., Valente, M. A. E., Voors, A. A., O'Connor, C. M., van Veldhuisen, D. J., & Hillege, H. L. (2013). Renal impairment, worsening renal function, and outcome in patients with heart failure: an updated meta-analysis. *European Heart Journal*, 35(7), 455-469. <https://doi.org/10.1093/eurheartj/eht386>
- Danno, S., Kubouchi, K., Mehruba, M., Abe, M., Natsume, R., Sakimura, K., Eguchi, S., Oka, M., Hirashima, M., Yasuda, H., & Mukai, H. (2017). PKN2 is essential for mouse embryonic development and proliferation of mouse fibroblasts. *Genes Cells*, 22(2), 220-236. <https://doi.org/10.1111/gtc.12470>
- Davey, R. A., & MacLean, H. E. (2006). Current and future approaches using genetically modified mice in endocrine research. *American Journal of Physiology-*

*Endocrinology and Metabolism*, 291(3), E429-E438.

<https://doi.org/10.1152/ajpendo.00124.2006>

- David, F. W. (2018). The Role of Tropomyosin in Cardiac Function and Disease. In K. Ozgur (Ed.), *Cardiac Diseases and Interventions in 21st Century* (pp. Ch. 2). IntechOpen. <https://doi.org/10.5772/intechopen.81420>
- Delpire, E. (2009). The mammalian family of sterile 20p-like protein kinases. *Pflugers Arch*, 458(5), 953-967. <https://doi.org/10.1007/s00424-009-0674-y>
- Dickinson, H. O., Campbell, F., Beyer, F. R., Nicolson, D. J., Cook, J. V., Ford, G. A., & Mason, J. M. (2008). Relaxation therapies for the management of primary hypertension in adults: a Cochrane review. *Journal of Human Hypertension*, 22(12), 809-820. <https://doi.org/10.1038/jhh.2008.65>
- Ding, J., Yu, M., Jiang, J., Luo, Y., Zhang, Q., Wang, S., Yang, F., Wang, A., Wang, L., Zhuang, M., Wu, S., Zhang, Q., Xia, Y., & Lu, D. (2020). Angiotensin II Decreases Endothelial Nitric Oxide Synthase Phosphorylation via AT1R Nox/ROS/PP2A Pathway [Original Research]. *Frontiers in Physiology*, 11. <https://doi.org/10.3389/fphys.2020.566410>
- Doggrell, S. A., & Brown, L. (1998). Rat models of hypertension, cardiac hypertrophy and failure. *Cardiovascular Research*, 39(1), 89-105. [https://doi.org/10.1016/s0008-6363\(98\)00076-5](https://doi.org/10.1016/s0008-6363(98)00076-5)
- Dorn, G. W., 2nd, Robbins, J., & Sugden, P. H. (2003). Phenotyping hypertrophy: eschew obfuscation. *Circ Res*, 92(11), 1171-1175. <https://doi.org/10.1161/01.Res.0000077012.11088.Bc>
- Dutta, S., & Mukherjee, K. (2019). Multifractal approach to study of salt induced hypertension and baroreflex dysfunction in salt sensitive Dahl rats. *Physica A: Statistical Mechanics and its Applications*, 515, 526-536. <https://doi.org/https://doi.org/10.1016/j.physa.2018.09.105>
- El Marjou, F., Jouhanneau, C., & Krndija, D. (2021). Targeted TransgenicTransgenic Mice Using CRISPRClustered regularly interspaced short palindromic repeats (CRISPR)/Cas9 Technology. In K. Ancelin & M. Borensztein (Eds.), *Epigenetic Reprogramming During Mouse Embryogenesis: Methods and Protocols* (pp. 125-141). Springer US. [https://doi.org/10.1007/978-1-0716-0958-3\\_9](https://doi.org/10.1007/978-1-0716-0958-3_9)
- Eroglu, Z., & Ribas, A. (2016). Combination therapy with BRAF and MEK inhibitors for melanoma: latest evidence and place in therapy. *Ther Adv Med Oncol*, 8(1), 48-56. <https://doi.org/10.1177/1758834015616934>
- Failer, T., Amponsah-Offeh, M., Neuwirth, A., Kourtzelis, I., Subramanian, P., Mirtschink, P., Peitzsch, M., Matschke, K., Tugtekin, S. M., Kajikawa, T., Li, X., Steglich, A., Gembardt, F., Wegner, A. C., Hugo, C., Hajishengallis, G., Chavakis, T.,

Deussen, A., Todorov, V., & Kopaliani, I. (2022). Developmental endothelial locus-1 protects from hypertension-induced cardiovascular remodeling via immunomodulation. *The Journal of Clinical Investigation*, 132(6). <https://doi.org/10.1172/JCI126155>

- Flecknell, P. (2002). Replacement, reduction and refinement. *Altex*, 19(2), 73-78.
- Fletcher, D. A., & Mullins, R. D. (2010). Cell mechanics and the cytoskeleton. *Nature*, 463(7280), 485-492. <https://doi.org/10.1038/nature08908>
- Forough, R., Scarcello, C., & Perkins, M. (2011). Cardiac biomarkers: a focus on cardiac regeneration. *J Tehran Heart Cent*, 6(4), 179-186. <https://www.ncbi.nlm.nih.gov/pubmed/23074366>
- Franco, N. H. (2013). Animal Experiments in Biomedical Research: A Historical Perspective. *Animals*, 3(1), 238-273. <https://www.mdpi.com/2076-2615/3/1/238>
- Fuentes, N., & Silveyra, P. (2019). Estrogen receptor signaling mechanisms. *Adv Protein Chem Struct Biol*, 116, 135-170. <https://doi.org/10.1016/bs.apcsb.2019.01.001>
- Fujita, K. I., Ishida, H., Kubota, Y., & Sasaki, Y. (2017). Toxicities of Receptor Tyrosine Kinase Inhibitors in Cancer Pharmacotherapy: Management with Clinical Pharmacology. *Curr Drug Metab*, 18(3), 186-198. <https://doi.org/10.2174/1389200218666170105165832>
- Fuller, S. J., Edmunds, N. S., McGuffin, L. J., Hardyman, M. A., Cull, J. J., Alharbi, H. O., Meijles, D. N., Sugden, P. H., & Clerk, A. (2021). MAP4K4 expression in cardiomyocytes: multiple isoforms, multiple phosphorylations and interactions with striatins. *Biochem J*, 478(11), 2121-2143. <https://doi.org/10.1042/bcj20210003>
- Fuller, S. J., McGuffin, L. J., Marshall, A. K., Giraldo, A., Pikkarainen, S., Clerk, A., & Sugden, P. H. (2012). A novel non-canonical mechanism of regulation of MST3 (mammalian Sterile20-related kinase 3). *Biochem J*, 442(3), 595-610. <https://doi.org/10.1042/bj20112000>
- Gallo, S., Vitacolonna, A., Bonzano, A., Comoglio, P., & Crepaldi, T. (2019). ERK: A Key Player in the Pathophysiology of Cardiac Hypertrophy. *Int J Mol Sci*, 20(9). <https://doi.org/10.3390/ijms20092164>
- Garbi M, D'hooge J, & Shkolnik E. (2016). General principles of echocardiography. In P. Lancellotti, J. L. Zamorano, G. Habib, & L. Badano (Eds.), *The EACVI Textbook of Echocardiography* (pp. 0). Oxford University Press. <https://doi.org/10.1093/med/9780198726012.003.0001>
- Garbi, M., D'Hooge, J., & Shkolnik, E. (2016). The general principles of echocardiography - chapter of The EACVI Textbook of Echocardiography. In.
- Garcia-Menendez, L., Karamanlidis, G., Kolwicz, S., & Tian, R. (2013). Substrain specific response to cardiac pressure overload in C57BL/6 mice. *Am J Physiol Heart Circ Physiol*, 305(3), H397-402. <https://doi.org/10.1152/ajpheart.00088.2013>

- Garza, A. E., Rariy, C. M., Sun, B., Williams, J., Lasky-Su, J., Baudrand, R., Yao, T., Moize, B., Hafiz, W. M., Romero, J. R., Adler, G. K., Ferri, C., Hopkins, P. N., Pojoga, L. H., & Williams, G. H. (2015). Variants in striatin gene are associated with salt-sensitive blood pressure in mice and humans. *Hypertension*, 65(1), 211-217. <https://doi.org/10.1161/HYPERTENSIONAHA.114.04233>
- Garza, A. E., Trefts, E., Katayama Rangel, I. A., Brooks, D., Baudrand, R., Moize, B., Romero, J. R., Ranjit, S., Treesaranuwattana, T., Yao, T. M., Adler, G. K., Pojoga, L. H., & Williams, G. H. (2020). Striatin heterozygous mice are more sensitive to aldosterone-induced injury. *J Endocrinol*, 245(3), 439-450. <https://doi.org/10.1530/joe-19-0562>
- Georgiopoulou, V. V., Kalogeropoulos, A. P., & Butler, J. (2012). Heart failure in hypertension: prevention and treatment. *Drugs*, 72(10), 1373-1398. <https://doi.org/10.2165/11631100-00000000-00000>
- Gholami, S. K., Heydarpour, M., Williams, J. S., Pojoga, L. H., Adler, G. K., Williams, G. H., & Romero, J. R. (2024). Striatin Gene Variants Are Associated With Salt Sensitivity of Blood Pressure by Mechanisms That Differ in Women and Men. *Hypertension*, 81(2), 330-339. <https://doi.org/doi:10.1161/HYPERTENSIONAHA.123.21955>
- Goetsch, M. R., Wagle, A. A., Valilis, E. M., Razavi, A. C., McEvoy, J. W., Blumenthal, R. S., & Whelton, S. P. (2021). Dietary and Lifestyle Modification for the Prevention and Treatment of Hypertension. *Current Cardiovascular Risk Reports*, 15(10), 21. <https://doi.org/10.1007/s12170-021-00683-7>
- Gordon, A. M., Homsher, E., & Regnier, M. (2000). Regulation of Contraction in Striated Muscle. *Physiological Reviews*, 80(2), 853-924. <https://doi.org/10.1152/physrev.2000.80.2.853>
- Gordon, J., Hwang, J., Carrier, K. J., Jones, C. A., Kern, Q. L., Moreno, C. S., Karas, R. H., & Pallas, D. C. (2011). Protein phosphatase 2a (PP2A) binds within the oligomerization domain of striatin and regulates the phosphorylation and activation of the mammalian Ste20-Like kinase Mst3. *BMC Biochem*, 12, 54. <https://doi.org/10.1186/1471-2091-12-54>
- Goudreault, M., D'Ambrosio, L. M., Kean, M. J., Mullin, M. J., Larsen, B. G., Sanchez, A., Chaudhry, S., Chen, G. I., Sicheri, F., Nesvizhskii, A. I., Aebersold, R., Raught, B., & Gingras, A. C. (2009). A PP2A phosphatase high density interaction network identifies a novel striatin-interacting phosphatase and kinase complex linked to the cerebral cavernous malformation 3 (CCM3) protein. *Mol Cell Proteomics*, 8(1), 157-171. <https://doi.org/10.1074/mcp.M800266-MCP200>

- Gourdie, R. G., Dimmeler, S., & Kohl, P. (2016). Novel therapeutic strategies targeting fibroblasts and fibrosis in heart disease. *Nat Rev Drug Discov*, 15(9), 620-638. <https://doi.org/10.1038/nrd.2016.89>
- Grant, M. D., Mann, R. D., Kristenson, S. D., Buck, R. M., Mendoza, J. D., Reese, J. M., Grant, D. W., & Roberge, E. A. (2021). Transthoracic Echocardiography: Beginner's Guide with Emphasis on Blind Spots as Identified with CT and MRI. *Radiographics*, 41(4), 1022-1042. <https://doi.org/10.1148/rq.2021200142>
- Grossman, W., & Paulus, W. J. (2013). Myocardial stress and hypertrophy: a complex interface between biophysics and cardiac remodeling. *The Journal of Clinical Investigation*, 123(9), 3701-3703. <https://doi.org/10.1172/JCI69830>
- Gubra. (2021). *ANGII-PE mouse*. Retrieved 20 March from [https://www.gubra.dk/wp-content/uploads/2021/09/Gubra\\_AngII-PE\\_mouse.pdf](https://www.gubra.dk/wp-content/uploads/2021/09/Gubra_AngII-PE_mouse.pdf)
- Guha, A., Jain, P., Fradley, M. G., Lenihan, D., Gutierrez, J. M., Jain, C., de Lima, M., Barnholtz-Sloan, J. S., Oliveira, G. H., Dowlati, A., & Al-Kindi, S. (2021). Cardiovascular adverse events associated with BRAF versus BRAF/MEK inhibitor: Cross-sectional and longitudinal analysis using two large national registries. *Cancer Medicine*, 10(12), 3862-3872. <https://doi.org/https://doi.org/10.1002/cam4.3938>
- Gupta, T., Connors, M., Tan, J. W., Manosroi, W., Ahmed, N., Ting, P. Y., Garza, A. E., Romero, J. R., Hopkins, P. N., Williams, J. S., & Williams, G. H. (2017). Striatin Gene Polymorphic Variants Are Associated With Salt Sensitive Blood Pressure in Normotensives and Hypertensives. *Am J Hypertens*, 31(1), 124-131. <https://doi.org/10.1093/ajh/hpx146>
- Gusev, N. B. (2013). Troponin. In R. H. Kretsinger, V. N. Uversky, & E. A. Permyakov (Eds.), *Encyclopedia of Metalloproteins* (pp. 2258-2263). Springer New York. [https://doi.org/10.1007/978-1-4614-1533-6\\_56](https://doi.org/10.1007/978-1-4614-1533-6_56)
- Guzzo, R. M., Salih, M., Moore, E. D., & Tuana, B. S. (2005). Molecular properties of cardiac tail-anchored membrane protein SLMAP are consistent with structural role in arrangement of excitation-contraction coupling apparatus. *Am J Physiol Heart Circ Physiol*, 288(4), H1810-1819. <https://doi.org/10.1152/ajpheart.01015.2004>
- Haggerty, C. M., Mattingly, A. C., Gong, M. C., Su, W., Daugherty, A., & Fornwalt, B. K. (2015). Telemetric Blood Pressure Assessment in Angiotensin II-Infused ApoE-/Mice: 28 Day Natural History and Comparison to Tail-Cuff Measurements. *PLOS ONE*, 10(6), e0130723. <https://doi.org/10.1371/journal.pone.0130723>
- Henderson, C. A., & Gregorio, C. C. (2015). Dynamics of Actin in the Heart: Defining Thin Filament Length. In E. Ehler (Ed.), *Cardiac Cytoarchitecture: How to Maintain a Working Heart* (pp. 71-88). Springer International Publishing. [https://doi.org/10.1007/978-3-319-15263-9\\_4](https://doi.org/10.1007/978-3-319-15263-9_4)

- Hinderer, S., & Schenke-Layland, K. (2019). Cardiac fibrosis - A short review of causes and therapeutic strategies. *Adv Drug Deliv Rev*, 146, 77-82.  
<https://doi.org/10.1016/j.addr.2019.05.011>
- Huang, X., Yan, L., Kou, S., Meng, J., Lu, Z., Lin, C.-P., Liu, C., & Zhang, H. (2021). Generation and characterization of a Myh6-driven Cre knockin mouse line. *Transgenic Research*, 30(6), 821-835. <https://doi.org/10.1007/s11248-021-00285-4>
- Hubrecht, R. C., & Carter, E. (2019). The 3Rs and Humane Experimental Technique: Implementing Change. *Animals (Basel)*, 9(10). <https://doi.org/10.3390/ani9100754>
- Humphrey, J. D. (2021). Mechanisms of Vascular Remodeling in Hypertension. *Am J Hypertens*, 34(5), 432-441. <https://doi.org/10.1093/ajh/hpaa195>
- Hwang, J., & Pallas, D. C. (2014). STRIPAK complexes: structure, biological function, and involvement in human diseases. *Int J Biochem Cell Biol*, 47, 118-148.  
<https://doi.org/10.1016/j.biocel.2013.11.021>
- Iacobazzi, D., Suleiman, M. S., Ghorbel, M., George, S. J., Caputo, M., & Tulloh, R. M. (2016). Cellular and molecular basis of RV hypertrophy in congenital heart disease. *Heart*, 102(1), 12. <https://doi.org/10.1136/heartjnl-2015-308348>
- Ishikawa, T., Sato, A., Marcou, C. A., Tester, D. J., Ackerman, M. J., Crotti, L., Schwartz, P. J., On, Y. K., Park, J. E., Nakamura, K., Hiraoka, M., Nakazawa, K., Sakurada, H., Arimura, T., Makita, N., & Kimura, A. (2012). A novel disease gene for Brugada syndrome: sarcolemmal membrane-associated protein gene mutations impair intracellular trafficking of hNav1.5. *Circ Arrhythm Electrophysiol*, 5(6), 1098-1107.  
<https://doi.org/10.1161/circep.111.969972>
- Izumiya, Y., Kim, S., Izumi, Y., Yoshida, K., Yoshiyama, M., Matsuzawa, A., Ichijo, H., & Iwao, H. (2003). Apoptosis Signal-Regulating Kinase 1 Plays a Pivotal Role in Angiotensin II-Induced Cardiac Hypertrophy and Remodeling. *Circulation Research*, 93(9), 874-883. <https://doi.org/doi:10.1161/01.RES.0000100665.67510.F5>
- Jain, B. P., Pandey, S., Saleem, N., Tanti, G. K., Mishra, S., & Goswami, S. K. (2017). SG2NA is a regulator of endoplasmic reticulum (ER) homeostasis as its depletion leads to ER stress. *Cell Stress Chaperones*, 22(6), 853-866.  
<https://doi.org/10.1007/s12192-017-0816-7>
- Jama, H. A., Muralitharan, R. R., Xu, C., O'Donnell, J. A., Bertagnolli, M., Broughton, B. R. S., Head, G. A., & Marques, F. Z. (2022). Rodent models of hypertension. *British Journal of Pharmacology*, 179(5), 918-937.  
<https://doi.org/https://doi.org/10.1111/bph.15650>
- Jiang, W., Xiong, Y., Li, X., & Yang, Y. (2021). Cardiac Fibrosis: Cellular Effectors, Molecular Pathways, and Exosomal Roles [Review]. *Frontiers in Cardiovascular Medicine*, 8. <https://doi.org/10.3389/fcvm.2021.715258>

- Justice, M. J., Siracusa, L. D., & Stewart, A. F. (2011). Technical approaches for mouse models of human disease. *Disease Models & Mechanisms*, 4(3), 305-310. <https://doi.org/10.1242/dmm.000901>
- Kannan, A., & Janardhanan, R. (2014). Hypertension as a Risk Factor for Heart Failure. *Current Hypertension Reports*, 16(7), 447. <https://doi.org/10.1007/s11906-014-0447-7>
- Kartha, C. C. (2021). Cardiomyocytes in Heart Failure. In C. C. Kartha (Ed.), *Cardiomyocytes in Health and Disease* (pp. 245-255). Springer International Publishing. [https://doi.org/10.1007/978-3-030-85536-9\\_15](https://doi.org/10.1007/978-3-030-85536-9_15)
- Kean, M. J., Ceccarelli, D. F., Goudreault, M., Sanches, M., Tate, S., Larsen, B., Gibson, L. C., Derry, W. B., Scott, I. C., Pelletier, L., Baillie, G. S., Sicheri, F., & Gingras, A. C. (2011). Structure-function analysis of core STRIPAK Proteins: a signaling complex implicated in Golgi polarization. *J Biol Chem*, 286(28), 25065-25075. <https://doi.org/10.1074/jbc.M110.214486>
- Kehat, I., Davis, J., Tiburcy, M., Accornero, F., Saba-El-Leil, M. K., Maillet, M., York, A. J., Lorenz, J. N., Zimmermann, W. H., Meloche, S., & Molkentin, J. D. (2011). Extracellular signal-regulated kinases 1 and 2 regulate the balance between eccentric and concentric cardiac growth. *Circ Res*, 108(2), 176-183. <https://doi.org/10.1161/circresaha.110.231514>
- Kemp, C. D., & Conte, J. V. (2012). The pathophysiology of heart failure. *Cardiovasc Pathol*, 21(5), 365-371. <https://doi.org/10.1016/j.carpath.2011.11.007>
- Kendall, R. T., & Feghali-Bostwick, C. A. (2014). Fibroblasts in fibrosis: novel roles and mediators [Review]. *Frontiers in Pharmacology*, 5. <https://doi.org/10.3389/fphar.2014.00123>
- Keraliya, R. A., Patel, C., Patel, P., Keraliya, V., Soni, T. G., Patel, R. C., & Patel, M. M. (2012). Osmotic drug delivery system as a part of modified release dosage form. *ISRN Pharm*, 2012, 528079. <https://doi.org/10.5402/2012/528079>
- Khalil, H., & Zeltser, R. (2023). Antihypertensive Medications. In *StatPearls*. <https://www.ncbi.nlm.nih.gov/pubmed/32119466>
- Kidger, A. M., Munck, J. M., Saini, H. K., Balmanno, K., Minihane, E., Courtin, A., Graham, B., O'Reilly, M., Odle, R., & Cook, S. J. (2020). Dual-Mechanism ERK1/2 Inhibitors Exploit a Distinct Binding Mode to Block Phosphorylation and Nuclear Accumulation of ERK1/2. *Molecular Cancer Therapeutics*, 19(2), 525-539. <https://doi.org/10.1158/1535-7163.Mct-19-0505>
- Kim, H. Y., Martin, J. H., McLachlan, A. J., & Boddy, A. V. (2017). Precision dosing of targeted anticancer drugs—challenges in the real world. *Translational Cancer Research*, S1500-S1511. <https://tcr.amegroups.org/article/view/16980>

- Kim, J. W., Berrios, C., Kim, M., Schade, A. E., Adelman, G., Yeerna, H., Damato, E., Iniguez, A. B., Florens, L., Washburn, M. P., Stegmaier, K., Gray, N. S., Tamayo, P., Gjoerup, O., Marto, J. A., DeCaprio, J., & Hahn, W. C. (2020). STRIPAK directs PP2A activity toward MAP4K4 to promote oncogenic transformation of human cells. *eLife*, 9, e53003. <https://doi.org/10.7554/eLife.53003>
- Kinno, M., Nagpal, P., Horgan, S., & Waller, A. H. (2017). Comparison of Echocardiography, Cardiac Magnetic Resonance, and Computed Tomographic Imaging for the Evaluation of Left Ventricular Myocardial Function: Part 2 (Diastolic and Regional Assessment). *Current Cardiology Reports*, 19(1), 6. <https://doi.org/10.1007/s11886-017-0816-3>
- Kloth, J. S. L., Pagani, A., Verboom, M. C., Malovini, A., Napolitano, C., Kruit, W. H. J., Sleijfer, S., Steeghs, N., Zambelli, A., & Mathijssen, R. H. J. (2015). Incidence and relevance of QTc-interval prolongation caused by tyrosine kinase inhibitors. *British Journal of Cancer*, 112(6), 1011-1016. <https://doi.org/10.1038/bjc.2015.82>
- Knight, P. J. (2023). Getting to the heart of thick-filament structure. *Nature*, 623(7988), 703-704. <https://doi.org/10.1038/d41586-023-03307-9>
- Kong, T., Liu, M., Ji, B., Bai, B., Cheng, B., & Wang, C. (2019). Role of the Extracellular Signal-Regulated Kinase 1/2 Signaling Pathway in Ischemia-Reperfusion Injury [Review]. *Frontiers in Physiology*, 10. <https://doi.org/10.3389/fphys.2019.01038>
- Kotob, S. E. (2021). "Review Article: An Overview of Cellular Signal Transduction Pathway". *Biomedical Journal of Scientific & Technical Research*, 38(2). <https://doi.org/10.26717/bjstr.2021.38.006133>
- Kuck, U., Radchenko, D., & Teichert, I. (2019). STRIPAK, a highly conserved signaling complex, controls multiple eukaryotic cellular and developmental processes and is linked with human diseases. *Biol Chem*, 400(8), 1005-1022. <https://doi.org/10.1515/hsz-2019-0173>
- Kurtz, T. W., & Morris, R. C., Jr. (1985). Hypertension in the recently weaned Dahl salt-sensitive rat despite a diet deficient in sodium chloride. *Science*, 230(4727), 808-810. <https://doi.org/10.1126/science.4059913>
- Landa, I., & Knauf, J. A. (2019). Mouse Models as a Tool for Understanding Progression in Braf(V600E)-Driven Thyroid Cancers. *Endocrinol Metab (Seoul)*, 34(1), 11-22. <https://doi.org/10.3803/EnM.2019.34.1.11>
- Lavoie, H., Gagnon, J., & Therrien, M. (2020). ERK signalling: a master regulator of cell behaviour, life and fate. *Nat Rev Mol Cell Biol*, 21(10), 607-632. <https://doi.org/10.1038/s41580-020-0255-7>
- Lawson, C. A., Zaccardi, F., Squire, I., Okhai, H., Davies, M., Huang, W., Mamas, M., Lam, C. S. P., Khunti, K., & Kadam, U. T. (2020). Risk Factors for Heart Failure: 20-

Year Population-Based Trends by Sex, Socioeconomic Status, and Ethnicity. *Circ Heart Fail*, 13(2), e006472. <https://doi.org/10.1161/CIRCHEARTFAILURE.119.006472>

- Lee, S., Rauch, J., & Kolch, W. (2020). Targeting MAPK Signaling in Cancer: Mechanisms of Drug Resistance and Sensitivity. *International Journal of Molecular Sciences*, 21(3), 1102. <https://www.mdpi.com/1422-0067/21/3/1102>
- Li, H., Liu, Q., Wang, S., Huang, L., Huang, S., Yue, Y., Feng, K., & Wu, Z. (2022). A New Minimally Invasive Method of Transverse Aortic Constriction in Mice. *Journal of Cardiovascular Translational Research*, 15(3), 635-643. <https://doi.org/10.1007/s12265-021-10170-4>
- Lin, C.-J., Lin, C.-Y., Chen, C.-H., Zhou, B., & Chang, C.-P. (2012). Partitioning the heart: mechanisms of cardiac septation and valve development. *Development (Cambridge, England)*, 139(18), 3277-3299. <https://doi.org/10.1242/dev.063495>
- Lindsey, M. L., Kassiri, Z., Virag, J. A. I., Brás, L. E. d. C., & Scherrer-Crosbie, M. (2018). Guidelines for measuring cardiac physiology in mice. *American Journal of Physiology-Heart and Circulatory Physiology*, 314(4), H733-H752. <https://doi.org/10.1152/ajpheart.00339.2017>
- Liu, B., Li, A., Gao, M., Qin, Y., & Gong, G. (2020). Modified Protocol for A Mouse Heart Failure Model Using Minimally Invasive Transverse Aortic Constriction. *STAR Protoc*, 1(3), 100186. <https://doi.org/10.1016/j.xpro.2020.100186>
- Liu, B., Qu, J., Zhang, W., Izpisua Belmonte, J. C., & Liu, G.-H. (2022). A stem cell aging framework, from mechanisms to interventions. *Cell Reports*, 41(3). <https://doi.org/10.1016/j.celrep.2022.111451>
- Long, G. V., Grob, J. J., Nathan, P., Ribas, A., Robert, C., Schadendorf, D., Lane, S. R., Mak, C., Legenne, P., Flaherty, K. T., & Davies, M. A. (2016). Factors predictive of response, disease progression, and overall survival after dabrafenib and trametinib combination treatment: a pooled analysis of individual patient data from randomised trials. *Lancet Oncol*, 17(12), 1743-1754. [https://doi.org/10.1016/s1470-2045\(16\)30578-2](https://doi.org/10.1016/s1470-2045(16)30578-2)
- Lu, H., Howatt, D. A., Balakrishnan, A., Moorleghen, J. J., Rateri, D. L., Cassis, L. A., & Daugherty, A. (2015). Subcutaneous Angiotensin II Infusion using Osmotic Pumps Induces Aortic Aneurysms in Mice. *J Vis Exp*(103). <https://doi.org/10.3791/53191>
- Ma, S., Meng, Z., Chen, R., & Guan, K. L. (2019). The Hippo Pathway: Biology and Pathophysiology. *Annu Rev Biochem*, 88, 577-604. <https://doi.org/10.1146/annurev-biochem-013118-111829>
- Ma, X., Zeng, W., Wang, L., Cheng, R., Zhao, Z., Huang, C., Sun, Z., Tao, P., Wang, T., Zhang, J., Liu, L., Duan, X., & Niu, D. (2022). Validation of reliable safe harbor

locus for efficient porcine transgenesis. *Functional & Integrative Genomics*, 22(4), 553-563. <https://doi.org/10.1007/s10142-022-00859-3>

- Ma, Y., Zhang, L., & Huang, X. (2014). Genome modification by CRISPR/Cas9. *Febs j*, 281(23), 5186-5193. <https://doi.org/10.1111/febs.13110>
- Maas, A., Rosano, G., Cifkova, R., Chieffo, A., van Dijken, D., Hamoda, H., Kunadian, V., Laan, E., Lambrinoudaki, I., Maclaran, K., Panay, N., Stevenson, J. C., van Trotsenburg, M., & Collins, P. (2021). Cardiovascular health after menopause transition, pregnancy disorders, and other gynaecologic conditions: a consensus document from European cardiologists, gynaecologists, and endocrinologists. *Eur Heart J*, 42(10), 967-984. <https://doi.org/10.1093/eurheartj/ehaa1044>
- MacArthur Clark, J. (2018). The 3Rs in research: a contemporary approach to replacement, reduction and refinement. *Br J Nutr*, 120(s1), S1-s7. <https://doi.org/10.1017/s0007114517002227>
- Maeda, D., Dotare, T., Matsue, Y., Teramoto, K., Sunayama, T., Tromp, J., & Minamino, T. (2023). Blood pressure in heart failure management and prevention. *Hypertension Research*, 46(4), 817-833. <https://doi.org/10.1038/s41440-022-01158-x>
- Maik-Rachline, G., Cohen, I., & Seger, R. (2018). RAF, MEK and ERK Inhibitors as Anti-Cancer Drugs: Intrinsic and Acquired Resistance as a Major Therapeutic Challenge. In Y. Yarden & M. Elkabets (Eds.), *Resistance to Anti-Cancer Therapeutics Targeting Receptor Tyrosine Kinases and Downstream Pathways* (pp. 89-116). Springer International Publishing. [https://doi.org/10.1007/978-3-319-67932-7\\_5](https://doi.org/10.1007/978-3-319-67932-7_5)
- Man, J., Barnett, P., & Christoffels, V. M. (2018). Structure and function of the Nppa-Nppb cluster locus during heart development and disease. *Cell Mol Life Sci*, 75(8), 1435-1444. <https://doi.org/10.1007/s00018-017-2737-0>
- Mangini, S., Pires, P. V., Braga, F. G., & Bacal, F. (2013). Decompensated heart failure. *Einstein (Sao Paulo)*, 11(3), 383-391. <https://doi.org/10.1590/s1679-45082013000300022>
- Marampon, F., Ciccarelli, C., & Zani, B. M. (2019). Biological Rationale for Targeting MEK/ERK Pathways in Anti-Cancer Therapy and to Potentiate Tumour Responses to Radiation. *International Journal of Molecular Sciences*, 20(10), 2530. <https://www.mdpi.com/1422-0067/20/10/2530>
- Marshall, J. J. T., Cull, J. J., Alharbi, H. O., Zaw Thin, M., Cooper, S. T. E., Barrington, C., Vanyai, H., Snoeks, T., Siow, B., Suárez-Bonnet, A., Herbert, E., Stuckey, D. J., Cameron, A. J. M., Prin, F., Cook, A. C., Priestnall, S. L., Chotani, S., Rackham, O. J. L., Mejiles, D. N., . . . Parker, P. J. (2022). PKN2 deficiency leads both to prenatal 'congenital' cardiomyopathy and defective angiotensin II stress responses. *Biochem J*, 479(13), 1467-1486. <https://doi.org/10.1042/bcj20220281>

- Masenga, S. K., & Kirabo, A. (2023). Hypertensive heart disease: risk factors, complications and mechanisms. *Front Cardiovasc Med*, 10, 1205475. <https://doi.org/10.3389/fcvm.2023.1205475>
- McGonigle, P., & Ruggeri, B. (2014). Animal models of human disease: Challenges in enabling translation. *Biochemical Pharmacology*, 87(1), 162-171. <https://doi.org/https://doi.org/10.1016/j.bcp.2013.08.006>
- McLellan, M. A., Rosenthal, N. A., & Pinto, A. R. (2017). Cre-loxP-Mediated Recombination: General Principles and Experimental Considerations. *Curr Protoc Mouse Biol*, 7(1), 1-12. <https://doi.org/10.1002/cpmo.22>
- Mehta, P. K., & Griendling, K. K. (2007). Angiotensin II cell signaling: physiological and pathological effects in the cardiovascular system. *Am J Physiol Cell Physiol*, 292(1), C82-97. <https://doi.org/10.1152/ajpcell.00287.2006>
- Meijles, D. N., Cull, J. J., Cooper, S. T. E., Markou, T., Hardyman, M. A., Fuller, S. J., Alharbi, H. O., Haines, Z. H. R., Alcantara-Alonso, V., Glennon, P. E., Sheppard, M. N., Sugden, P. H., & Clerk, A. (2021). The anti-cancer drug dabrafenib is not cardiotoxic and inhibits cardiac remodelling and fibrosis in a murine model of hypertension. *Clin Sci (Lond)*, 135(14), 1631-1647. <https://doi.org/10.1042/cs20210192>
- Meijles, D. N., Cull, J. J., Markou, T., Cooper, S. T. E., Haines, Z. H. R., Fuller, S. J., O'Gara, P., Sheppard, M. N., Harding, S. E., Sugden, P. H., & Clerk, A. (2020). Redox Regulation of Cardiac ASK1 (Apoptosis Signal-Regulating Kinase 1) Controls p38-MAPK (Mitogen-Activated Protein Kinase) and Orchestrates Cardiac Remodeling to Hypertension. *Hypertension*, 76(4), 1208-1218. <https://doi.org/10.1161/hypertensionaha.119.14556>
- Meijles, D. N., Fuller, S. J., Cull, J. J., Alharbi, H. O., Cooper, S. T. E., Sugden, P. H., & Clerk, A. (2021). The insulin receptor family and protein kinase B (Akt) are activated in the heart by alkaline pH and  $\alpha$ 1-adrenergic receptors. *Biochem J*, 478(11), 2059-2079. <https://doi.org/10.1042/bcj20210144>
- Messa, G. A. M., Piasecki, M., Hurst, J., Hill, C., Tallis, J., & Degens, H. (2020). The impact of a high-fat diet in mice is dependent on duration and age, and differs between muscles. *Journal of Experimental Biology*, 223(6). <https://doi.org/10.1242/jeb.217117>
- Meurs, K. M., Stern, J. A., Sisson, D. D., Kittleson, M. D., Cunningham, S. M., Ames, M. K., Atkins, C. E., DeFrancesco, T., Hodge, T. E., Keene, B. W., Reina Doreste, Y., Leuthy, M., Motsinger-Reif, A. A., & Tou, S. P. (2013). Association of dilated cardiomyopathy with the striatin mutation genotype in boxer dogs. *J Vet Intern Med*, 27(6), 1437-1440. <https://doi.org/10.1111/jvim.12163>

- Mills, K. T., Stefanescu, A., & He, J. (2020). The global epidemiology of hypertension. *Nat Rev Nephrol*, 16(4), 223-237. <https://doi.org/10.1038/s41581-019-0244-2>
- Milner, T. A., Drake, C. T., Lessard, A., Waters, E. M., Torres-Reveron, A., Graustein, B., Mitterling, K., Frys, K., & Iadecola, C. (2008). Angiotensin II-induced hypertension differentially affects estrogen and progestin receptors in central autonomic regulatory areas of female rats. *Exp Neurol*, 212(2), 393-406. <https://doi.org/10.1016/j.expneurol.2008.04.021>
- Miranda-Silva, D., Lima, T., Rodrigues, P., Leite-Moreira, A., & Falcão-Pires, I. (2021). Mechanisms underlying the pathophysiology of heart failure with preserved ejection fraction: the tip of the iceberg. *Heart Failure Reviews*, 26(3), 453-478. <https://doi.org/10.1007/s10741-020-10042-0>
- Moore-Morris, T., Guimaraes-Camboa, N., Yutzey, K. E., Puceat, M., & Evans, S. M. (2015). Cardiac fibroblasts: from development to heart failure. *J Mol Med (Berl)*, 93(8), 823-830. <https://doi.org/10.1007/s00109-015-1314-y>
- Moreno, C. S., Park, S., Nelson, K., Ashby, D., Hubalek, F., Lane, W. S., & Pallas, D. C. (2000). WD40 repeat proteins striatin and S/G(2) nuclear autoantigen are members of a novel family of calmodulin-binding proteins that associate with protein phosphatase 2A. *J Biol Chem*, 275(8), 5257-5263. <https://doi.org/10.1074/jbc.275.8.5257>
- Moreth, K., Fischer, R., Fuchs, H., Gailus-Durner, V., Wurst, W., Katus, H. A., Bekeredjian, R., & Hrabě de Angelis, M. (2014). High-throughput phenotypic assessment of cardiac physiology in four commonly used inbred mouse strains. *Journal of Comparative Physiology B*, 184(6), 763-775. <https://doi.org/10.1007/s00360-014-0830-3>
- Mori, S., Tretter, J. T., Spicer, D. E., Bolender, D. L., & Anderson, R. H. (2019). What is the real cardiac anatomy? *Clin Anat*, 32(3), 288-309. <https://doi.org/10.1002/ca.23340>
- Muasya, J., & Mulwa, P. (2023). Pilot Study, a Neglected Part of Qualitative and Quantitative Research Process: Evidence from Selected PhD Thesis and Dissertations. *Higher Education Research*, 8(4), 115-123. <https://doi.org/10.11648/i.her.20230804.11>
- Müller, A. L., & Dhalla, N. S. (2013). Differences in Concentric Cardiac Hypertrophy and Eccentric Hypertrophy. In B. Ostadal & N. S. Dhalla (Eds.), *Cardiac Adaptations: Molecular Mechanisms* (pp. 147-166). Springer New York. [https://doi.org/10.1007/978-1-4614-5203-4\\_8](https://doi.org/10.1007/978-1-4614-5203-4_8)

- Muñoz-Chápuli, R., Quesada, A. R., & Ángel Medina, M. (2004). Angiogenesis and signal transduction in endothelial cells. *Cellular and Molecular Life Sciences CMLS*, 61(17), 2224-2243. <https://doi.org/10.1007/s00018-004-4070-7>
- Muñoz-Santos, D., Montoliu, L., & Fernández, A. (2020). Generation of Genetically Modified Mice Using CRISPR/Cas9. In C. Costa (Ed.), *Xenotransplantation: Methods and Protocols* (pp. 129-138). Springer US. [https://doi.org/10.1007/978-1-0716-0255-3\\_9](https://doi.org/10.1007/978-1-0716-0255-3_9)
- Murphy, S. P., Ibrahim, N. E., & Januzzi, J. L., Jr. (2020). Heart Failure With Reduced Ejection Fraction: A Review. *JAMA*, 324(5), 488-504. <https://doi.org/10.1001/jama.2020.10262>
- Myat, A., Redwood, S. R., Qureshi, A. C., Spertus, J. A., & Williams, B. (2012). Resistant hypertension. *BMJ : British Medical Journal*, 345, e7473. <https://doi.org/10.1136/bmj.e7473>
- Nadar, S. K., & Lip, G. Y. H. (2021). The heart in hypertension. *Journal of Human Hypertension*, 35(5), 383-386. <https://doi.org/10.1038/s41371-020-00427-x>
- Nader, M. (2019). The SLMAP/Striatin complex: An emerging regulator of normal and abnormal cardiac excitation-contraction coupling. *Eur J Pharmacol*, 858, 172491. <https://doi.org/10.1016/j.ejphar.2019.172491>
- Nader, M., Alotaibi, S., Alsolme, E., Khalil, B., Abu-Zaid, A., Alsomali, R., Bakheet, D., & Dzimir, N. (2017). Cardiac striatin interacts with caveolin-3 and calmodulin in a calcium sensitive manner and regulates cardiomyocyte spontaneous contraction rate. *Can J Physiol Pharmacol*, 95(10), 1306-1312. <https://doi.org/10.1139/cjpp-2017-0155>
- Nader, M., Westendorp, B., Hawari, O., Salih, M., Stewart, A. F., Leenen, F. H., & Tuana, B. S. (2012). Tail-anchored membrane protein SLMAP is a novel regulator of cardiac function at the sarcoplasmic reticulum. *Am J Physiol Heart Circ Physiol*, 302(5), H1138-1145. <https://doi.org/10.1152/ajpheart.00872.2011>
- Nakamura, M., & Sadoshima, J. (2018). Mechanisms of physiological and pathological cardiac hypertrophy. *Nat Rev Cardiol*, 15(7), 387-407. <https://doi.org/10.1038/s41569-018-0007-y>
- Narkiewicz, K. (2006). Diagnosis and management of hypertension in obesity. *Obesity Reviews*, 7(2), 155-162. <https://doi.org/https://doi.org/10.1111/j.1467-789X.2006.00226.x>
- Nebot, N., Arkenau, H.-T., Infante, J. R., Chandler, J. C., Weickhardt, A., Lickliter, J. D., Sarantopoulos, J., Gordon, M. S., Mak, G., St-Pierre, A., Tang, L., Mookerjee, B., Carson, S. W., Hayes, S., & Grossmann, K. F. (2018). Evaluation of the effect of dabrafenib and metabolites on QTc interval in patients with BRAF V600–mutant

tumours. *British Journal of Clinical Pharmacology*, 84(4), 764-775.

<https://doi.org/https://doi.org/10.1111/bcp.13488>

- Nehme, A., Zouein, F. A., Zayeri, Z. D., & Zibara, K. (2019). An Update on the Tissue Renin Angiotensin System and Its Role in Physiology and Pathology. *J Cardiovasc Dev Dis*, 6(2). <https://doi.org/10.3390/jcdd6020014>
- Nicholls, M. (2019). Neutralizing MAP4K4: Mark Nicholls speaks to Prof. Michael Schneider at Imperial College London, about a potential new treatment that could help minimize cardiomyocyte injury after a myocardial infarction. *European Heart Journal*, 40(22), 1752-1753. <https://doi.org/10.1093/eurheartj/ehz365>
- Noubiap, J. J., Nansseu, J. R., Nyaga, U. F., Sime, P. S., Francis, I., & Bigna, J. J. (2019). Global prevalence of resistant hypertension: a meta-analysis of data from 3.2 million patients. *Heart*, 105(2), 98-105. <https://doi.org/10.1136/heartjnl-2018-313599>
- Oka, T., Akazawa, H., Naito, A. T., & Komuro, I. (2014). Angiogenesis and cardiac hypertrophy: maintenance of cardiac function and causative roles in heart failure. *Circ Res*, 114(3), 565-571. <https://doi.org/10.1161/circresaha.114.300507>
- Ovalle, W. K., & Nahirney, P. C. (2013). *Netter's Essential Histology: with Student Consult Access*. Elsevier Health Sciences. <https://books.google.co.uk/books?id=toBDtreNf9cC>
- Pan, S., & Zhang, W. (2021). Molecules in Signal Pathways. In S. Pan & J. Tang (Eds.), *Clinical Molecular Diagnostics* (pp. 139-154). Springer Singapore. [https://doi.org/10.1007/978-981-16-1037-0\\_11](https://doi.org/10.1007/978-981-16-1037-0_11)
- Pandey, K. N. (2021). Molecular Signaling Mechanisms and Function of Natriuretic Peptide Receptor-A in the Pathophysiology of Cardiovascular Homeostasis. *Front Physiol*, 12, 693099. <https://doi.org/10.3389/fphys.2021.693099>
- Parati, G., Goncalves, A., Soergel, D., Bruno, R. M., Caiani, E. G., Gerdts, E., Mahfoud, F., Mantovani, L., McManus, R. J., Santalucia, P., & Kahan, T. (2022). New perspectives for hypertension management: progress in methodological and technological developments. *European Journal of Preventive Cardiology*, 30(1), 48-60. <https://doi.org/10.1093/eurjpc/zwac203>
- Parker, M. M., & Wigger, M. (2023). Cardiorenal Syndrome, Chronic Kidney Disease, Anemia, and Heart Failure. In K. M. S. Hayes & N. R. Dellise (Eds.), *Managing Heart Failure in Primary Care: A Case Study Approach* (pp. 157-175). Springer International Publishing. [https://doi.org/10.1007/978-3-031-20193-6\\_11](https://doi.org/10.1007/978-3-031-20193-6_11)
- Patel, J., Douglas, G., Kerr, A. G., Hale, A. B., & Channon, K. M. (2018). Effect of irradiation and bone marrow transplantation on angiotensin II-induced aortic inflammation in ApoE knockout mice. *Atherosclerosis*, 276, 74-82. <https://doi.org/https://doi.org/10.1016/j.atherosclerosis.2018.07.019>

- Patel, J., Parikh, S., & Patel, S. (2021). Comprehensive review on osmotic drug delivery system. *World Journal of Pharmaceutical Research*, 10, 523-550. <https://doi.org/10.20959/wjpr20215-20303>
- Patel, S., Rauf, A., Khan, H., & Abu-Izneid, T. (2017). Renin-angiotensin-aldosterone (RAAS): The ubiquitous system for homeostasis and pathologies. *Biomedicine & Pharmacotherapy*, 94, 317-325. <https://doi.org/https://doi.org/10.1016/j.biopha.2017.07.091>
- Peng, L., Wang, Y., Hong, Y., Ye, X., Shi, P., Zhang, J., & Zhao, Q. (2017). Incidence and relative risk of cutaneous squamous cell carcinoma with single-agent BRAF inhibitor and dual BRAF/MEK inhibitors in cancer patients: a meta-analysis. *Oncotarget*, 8(47). <https://www.oncotarget.com/article/21059/text/>
- Petr, M. A., Alfaras, I., Krawcyzk, M., Bair, W.-N., Mitchell, S. J., Morrell, C. H., Studenski, S. A., Price, N. L., Fishbein, K. W., Spencer, R. G., Scheibye-Knudsen, M., Lakatta, E. G., Ferrucci, L., Aon, M. A., Bernier, M., & de Cabo, R. (2021). A cross-sectional study of functional and metabolic changes during aging through the lifespan in male mice. *eLife*, 10, e62952. <https://doi.org/10.7554/eLife.62952>
- Phuah, Y., Tan, Y. X., Zaghloul, S., Sim, S., Wong, J., Usmani, S., Snell, L., Thavabalan, K., García-Pérez, C. L., Kumar, N. S., Glatzel, H., Ahmad, R. R., Candilio, L., Bray, J. J. H., Ahmed, M., & Providencia, R. (2023). A systematic review and meta-analysis of transthoracic echocardiogram vs. cardiac magnetic resonance imaging for the detection of left ventricular thrombus. *European Heart Journal - Imaging Methods and Practice*, 1(2). <https://doi.org/10.1093/ehjimp/qyad041>
- Pinto, A. R., Ilinykh, A., Ivey, M. J., Kuwabara, J. T., D'Antoni, M. L., Debuque, R., Chandran, A., Wang, L., Arora, K., Rosenthal, N. A., & Tallquist, M. D. (2016). Revisiting Cardiac Cellular Composition. *Circulation Research*, 118(3), 400-409. <https://doi.org/doi:10.1161/CIRCRESAHA.115.307778>
- Plikus, M. V., Wang, X., Sinha, S., Forte, E., Thompson, S. M., Herzog, E. L., Driskell, R. R., Rosenthal, N., Biernaskie, J., & Horsley, V. (2021). Fibroblasts: Origins, definitions, and functions in health and disease. *Cell*, 184(15), 3852-3872. <https://doi.org/10.1016/j.cell.2021.06.024>
- Plotnik, J. P., Budka, J. A., Ferris, M. W., & Hollenhorst, P. C. (2014). ETS1 is a genome-wide effector of RAS/ERK signaling in epithelial cells. *Nucleic Acids Research*, 42(19), 11928-11940. <https://doi.org/10.1093/nar/gku929>
- Pollock, J. D., & Makaryus, A. N. (2024). Physiology, Cardiac Cycle. In *StatPearls*. StatPearls Publishing Copyright © 2024, StatPearls Publishing LLC.

- Powers, J. D., Malingen, S. A., Regnier, M., & Daniel, T. L. (2021). The Sliding Filament Theory Since Andrew Huxley: Multiscale and Multidisciplinary Muscle Research. *Annual Review of Biophysics*, 50(1), 373-400. <https://doi.org/10.1146/annurev-biophys-110320-062613>
- Prescott, M. J. (2017). The Three Rs. In *The International Encyclopedia of Primatology* (pp. 1-5). <https://doi.org/https://doi.org/10.1002/9781119179313.wbprim0220>
- Pugliese, N. R., Masi, S., & Taddei, S. (2020). The renin-angiotensin-aldosterone system: a crossroad from arterial hypertension to heart failure. *Heart Failure Reviews*, 25(1), 31-42. <https://doi.org/10.1007/s10741-019-09855-5>
- Quétier, I., Jacqueline, Spencer-Dene, B., Lachmann, S., Casamassima, A., Franco, C., Escuin, S., Joseph, Baskaran, P., Rajeeve, V., Howell, M., Andrew, Stamp, G., Rosewell, I., Cutillas, P., Gerhardt, H., Peter, & Angus. (2016). Knockout of the PKN Family of Rho Effector Kinases Reveals a Non-redundant Role for PKN2 in Developmental Mesoderm Expansion. *Cell Reports*, 14(3), 440-448. <https://doi.org/10.1016/j.celrep.2015.12.049>
- Redfield, M. M., & Borlaug, B. A. (2023). Heart Failure With Preserved Ejection Fraction: A Review. *JAMA*, 329(10), 827-838. <https://doi.org/10.1001/jama.2023.2020>
- Retta, S. F., & Glading, A. J. (2016). Oxidative stress and inflammation in cerebral cavernous malformation disease pathogenesis: Two sides of the same coin. *Int J Biochem Cell Biol*, 81(Pt B), 254-270. <https://doi.org/10.1016/j.biocel.2016.09.011>
- Rheault, T. R., Stellwagen, J. C., Adjabeng, G. M., Hornberger, K. R., Petrov, K. G., Waterson, A. G., Dickerson, S. H., Mook, R. A., Jr., Laquerre, S. G., King, A. J., Rossanese, O. W., Arnone, M. R., Smitheman, K. N., Kane-Carson, L. S., Han, C., Moorthy, G. S., Moss, K. G., & Uehling, D. E. (2013). Discovery of Dabrafenib: A Selective Inhibitor of Raf Kinases with Antitumor Activity against B-Raf-Driven Tumors. *ACS Medicinal Chemistry Letters*, 4(3), 358-362. <https://doi.org/10.1021/ml4000063>
- Richards, E., Lopez, M. J., & Maani, C. V. (2023). *Phenylephrine*. StatPearls Publishing, Treasure Island (FL). <http://europepmc.org/abstract/MED/30521222>
- Richmond, J. (2002). Refinement, reduction, and replacement of animal use for regulatory testing: future improvements and implementation within the regulatory framework. *Ilar j*, 43 Suppl, S63-68. [https://doi.org/10.1093/ilar.43.suppl\\_1.s63](https://doi.org/10.1093/ilar.43.suppl_1.s63)
- Robert, C., Grob, J. J., Stroyakovskiy, D., Karaszewska, B., Hauschild, A., Levchenko, E., Chiarion Sileni, V., Schachter, J., Garbe, C., Bondarenko, I., Gogas, H., Mandalá, M., Haanen, J. B. A. G., Lebbé, C., Mackiewicz, A., Rutkowski, P., Nathan, P. D., Ribas, A., Davies, M. A., . . . Long, G. V. (2019). Five-Year Outcomes with Dabrafenib

plus Trametinib in Metastatic Melanoma. *New England Journal of Medicine*, 381(7), 626-636. <https://doi.org/10.1056/NEJMoa1904059>

- Robinson, N. B., Krieger, K., Khan, F. M., Huffman, W., Chang, M., Naik, A., Yongle, R., Hameed, I., Krieger, K., Girardi, L. N., & Gaudino, M. (2019). The current state of animal models in research: A review. *International Journal of Surgery*, 72, 9-13. <https://doi.org/https://doi.org/10.1016/j.ijsu.2019.10.015>
- Rog-Zielinska, E. A., Norris, R. A., Kohl, P., & Markwald, R. (2016). The Living Scar-- Cardiac Fibroblasts and the Injured Heart. *Trends Mol Med*, 22(2), 99-114. <https://doi.org/10.1016/j.molmed.2015.12.006>
- Rosenkranz, S. (2004). TGF-beta1 and angiotensin networking in cardiac remodeling. *Cardiovasc Res*, 63(3), 423-432. <https://doi.org/10.1016/j.cardiores.2004.04.030>
- Ruwhof, C., & van der Laarse, A. (2000). Mechanical stress-induced cardiac hypertrophy: mechanisms and signal transduction pathways. *Cardiovascular Research*, 47(1), 23-37. [https://doi.org/10.1016/s0008-6363\(00\)00076-6](https://doi.org/10.1016/s0008-6363(00)00076-6)
- Sanghamitra, M., Talukder, I., Singarapu, N., Sindhu, K. V., Kateriya, S., & Goswami, S. K. (2008). WD-40 repeat protein SG2NA has multiple splice variants with tissue restricted and growth responsive properties. *Gene*, 420(1), 48-56. <https://doi.org/10.1016/j.gene.2008.04.016>
- Saunders, T. L. (2011). Inducible Transgenic Mouse Models. In M. H. Hofker & J. van Deursen (Eds.), *Transgenic Mouse Methods and Protocols* (pp. 103-115). Humana Press. [https://doi.org/10.1007/978-1-60761-974-1\\_7](https://doi.org/10.1007/978-1-60761-974-1_7)
- Savarese, G., Becher, P. M., Lund, L. H., Seferovic, P., Rosano, G. M. C., & Coats, A. J. S. (2023). Global burden of heart failure: a comprehensive and updated review of epidemiology. *Cardiovasc Res*, 118(17), 3272-3287. <https://doi.org/10.1093/cvr/cvac013>
- Saxton, A., Tariq, M. A., & Bordoni, B. (2023). Anatomy, Thorax, Cardiac Muscle. In *StatPearls*. StatPearls Publishing Copyright © 2023, StatPearls Publishing LLC. <https://www.ncbi.nlm.nih.gov/books/NBK535355/#:~:text=Cardiomyocytes%20contain%20many%20mitochondria%20to,the%20demands%20of%20muscle%20contraction.>
- Sayer, G., & Bhat, G. (2014). The Renin-Angiotensin-Aldosterone System and Heart Failure. *Cardiology Clinics*, 32(1), 21-32. <https://doi.org/https://doi.org/10.1016/j.ccl.2013.09.002>
- Schafer, S., Viswanathan, S., Widjaja, A. A., Lim, W.-W., Moreno-Moral, A., DeLaughter, D. M., Ng, B., Patone, G., Chow, K., Khin, E., Tan, J., Chothani, S. P., Ye, L., Rackham, O. J. L., Ko, N. S. J., Sahib, N. E., Pua, C. J., Zhen, N. T. G., Xie,

C., . . . Cook, S. A. (2017). IL-11 is a crucial determinant of cardiovascular fibrosis. *Nature*, 552(7683), 110-115. <https://doi.org/10.1038/nature24676>

- Sears, R., Nuckolls, F., Haura, E., Taya, Y., Tamai, K., & Nevins, J. R. (2000). Multiple Ras-dependent phosphorylation pathways regulate Myc protein stability. *Genes Dev*, 14(19), 2501-2514. <https://doi.org/10.1101/gad.836800>
- Segura, A. M., Frazier, O. H., & Buja, L. M. (2014). Fibrosis and heart failure. *Heart Fail Rev*, 19(2), 173-185. <https://doi.org/10.1007/s10741-012-9365-4>
- Seo, G., Han, H., Vargas, R. E., Yang, B., Li, X., & Wang, W. (2020). MAP4K Interactome Reveals STRN4 as a Key STRIPAK Complex Component in Hippo Pathway Regulation. *Cell Rep*, 32(1), 107860. <https://doi.org/10.1016/j.celrep.2020.107860>
- Sergienko, N. M., Donner, D. G., Delbridge, L. M. D., McMullen, J. R., & Weeks, K. L. (2022). Protein phosphatase 2A in the healthy and failing heart: New insights and therapeutic opportunities. *Cell Signal*, 91, 110213. <https://doi.org/10.1016/j.cellsig.2021.110213>
- Seymour, A.-M. L., Giles, L., Ball, V., Miller, J. J., Clarke, K., Carr, C. A., & Tyler, D. J. (2015). In vivo assessment of cardiac metabolism and function in the abdominal aortic banding model of compensated cardiac hypertrophy. *Cardiovascular Research*, 106(2), 249-260. <https://doi.org/10.1093/cvr/cvv101>
- Shchemelinin, I., Sefc, L., & Necas, E. (2006). Protein kinases, their function and implication in cancer and other diseases. *Folia Biol (Praha)*, 52(3), 81-100.
- Shi, Z., Jiao, S., & Zhou, Z. (2016). STRIPAK complexes in cell signaling and cancer. *Oncogene*, 35(35), 4549-4557. <https://doi.org/10.1038/onc.2016.9>
- Shibuya, M. (2011). Vascular Endothelial Growth Factor (VEGF) and Its Receptor (VEGFR) Signaling in Angiogenesis: A Crucial Target for Anti- and Pro-Angiogenic Therapies. *Genes Cancer*, 2(12), 1097-1105. <https://doi.org/10.1177/1947601911423031>
- Shimizu, I., & Minamino, T. (2016). Physiological and pathological cardiac hypertrophy. *J Mol Cell Cardiol*, 97, 245-262. <https://doi.org/10.1016/j.yjmcc.2016.06.001>
- Simmonds, S. J., Cuijpers, I., Heymans, S., & Jones, E. A. V. (2020). Cellular and Molecular Differences between HFpEF and HFrEF: A Step Ahead in an Improved Pathological Understanding. *Cells*, 9(1). <https://doi.org/10.3390/cells9010242>
- Skarnes, W. C., Rosen, B., West, A. P., Koutsourakis, M., Bushell, W., Iyer, V., Mujica, A. O., Thomas, M., Harrow, J., Cox, T., Jackson, D., Severin, J., Biggs, P., Fu, J., Nefedov, M., de Jong, P. J., Stewart, A. F., & Bradley, A. (2011). A conditional

knockout resource for the genome-wide study of mouse gene function. *Nature*, 474(7351), 337-342. <https://doi.org/10.1038/nature10163>

- Skwarek-Maruszewska, A., Hotulainen, P., Mattila, P. K., & Lappalainen, P. (2009). Contractility-dependent actin dynamics in cardiomyocyte sarcomeres. *Journal of Cell Science*, 122(12), 2119-2126. <https://doi.org/10.1242/jcs.046805>
- Sohal, D. S., Nghiem, M., Crackower, M. A., Witt, S. A., Kimball, T. R., Tymitz, K. M., Penninger, J. M., & Molkentin, J. D. (2001). Temporally Regulated and Tissue-Specific Gene Manipulations in the Adult and Embryonic Heart Using a Tamoxifen-Inducible Cre Protein. *Circulation Research*, 89(1), 20-25. <https://doi.org/doi:10.1161/hh1301.092687>
- Sophocleous, G., Owen, D., & Mott, H. R. (2021). The structure and function of protein kinase C-related kinases (PRKs). *Biochem Soc Trans*, 49(1), 217-235. <https://doi.org/10.1042/BST20200466>
- Sotoodehnia, N., Isaacs, A., de Bakker, P. I. W., Dörr, M., Newton-Cheh, C., Nolte, I. M., van der Harst, P., Müller, M., Eijgelsheim, M., Alonso, A., Hicks, A. A., Padmanabhan, S., Hayward, C., Smith, A. V., Polasek, O., Giovannone, S., Fu, J., Magnani, J. W., Marciante, K. D., . . . Arking, D. E. (2010). Common variants in 22 loci are associated with QRS duration and cardiac ventricular conduction. *Nature Genetics*, 42(12), 1068-1076. <https://doi.org/10.1038/ng.716>
- Spudich, J. A. (2001). The myosin swinging cross-bridge model. *Nature Reviews Molecular Cell Biology*, 2(5), 387-392. <https://doi.org/10.1038/35073086>
- Steckelings, U. M., Kloet, A., & Sumners, C. (2017). Centrally Mediated Cardiovascular Actions of the Angiotensin II Type 2 Receptor. *Trends Endocrinol Metab*, 28(9), 684-693. <https://doi.org/10.1016/j.tem.2017.06.002>
- Stone, I. B., Green, J., Koefoed, A. W., Hornik, E. S., Williams, J. S., Adler, G. K., & Williams, G. H. (2021). Striatin genotype-based, mineralocorticoid receptor antagonist-driven clinical trial: study rationale and design. *Pharmacogenet Genomics*, 31(4), 83-88. <https://doi.org/10.1097/fpc.0000000000000425>
- Stranges, S., Wu, T., Dorn, J. M., Freudenheim, J. L., Muti, P., Farinaro, E., Russell, M., Nohajski, T. H., & Trevisan, M. (2004). Relationship of Alcohol Drinking Pattern to Risk of Hypertension. *Hypertension*, 44(6), 813-819. <https://doi.org/doi:10.1161/01.HYP.0000146537.03103.f2>
- Sugden, P. H., & Clerk, A. (2001). Akt like a woman: gender differences in susceptibility to cardiovascular disease. *Circ Res*, 88(10), 975-977. <https://doi.org/10.1161/hh1001.091864>
- Susic, D., & Frohlich, E. D. (2000). Hypertension and the heart. *Current Hypertension Reports*, 2(6), 565-569. <https://doi.org/10.1007/s11906-996-0042-7>

- Susic, D., & Frohlich, E. D. (2011). Hypertensive Cardiovascular and Renal Disease and Target Organ Damage: Lessons from Animal Models. *Cardiorenal Med*, 1(3), 139-146. <https://doi.org/10.1159/000329334>
- Sweeney, M., Corden, B., & Cook, S. A. (2020). Targeting cardiac fibrosis in heart failure with preserved ejection fraction: mirage or miracle? *EMBO Molecular Medicine*, 12(10), e10865. <https://doi.org/https://doi.org/10.15252/emmm.201910865>
- Tanos, T., Marinissen, M. J., Leskow, F. C., Hochbaum, D., Martinetto, H., Gutkind, J. S., & Coso, O. A. (2005). Phosphorylation of c-Fos by Members of the p38 MAPK Family: ROLE IN THE AP-1 RESPONSE TO UV LIGHT \*. *Journal of Biological Chemistry*, 280(19), 18842-18852. <https://doi.org/10.1074/jbc.M500620200>
- Tanti, G. K., Pandey, P., Shreya, S., & Jain, B. P. (2023). Striatin family proteins: The neglected scaffolds. *Biochim Biophys Acta Mol Cell Res*, 1870(3), 119430. <https://doi.org/10.1016/j.bbamcr.2023.119430>
- Tardiff, J. C. (2006). Cardiac hypertrophy: stressing out the heart. *The Journal of Clinical Investigation*, 116(6), 1467-1470. <https://doi.org/10.1172/JCI28884>
- Thomas, M., & Tikellis, C. (2009). Losing Control: Positive and Negative Feedback in the Renin Angiotensin System. *Current Hypertension Reviews*, 5, 222-226. <https://doi.org/10.2174/157340209788921194>
- Tombor, L. S., & Dimmeler, S. (2022). Why is endothelial resilience key to maintain cardiac health? *Basic Research in Cardiology*, 117(1), 35. <https://doi.org/10.1007/s00395-022-00941-8>
- Tremoleda, J. L., Kerton, A., & Gsell, W. (2012). Anaesthesia and physiological monitoring during in vivo imaging of laboratory rodents: considerations on experimental outcomes and animal welfare. *EJNMMI Research*, 2(1), 44. <https://doi.org/10.1186/2191-219X-2-44>
- Ullah, R., Yin, Q., Snell, A. H., & Wan, L. (2022). RAF-MEK-ERK pathway in cancer evolution and treatment. *Seminars in Cancer Biology*, 85, 123-154. <https://doi.org/https://doi.org/10.1016/j.semcan.2021.05.010>
- Vidal-Petiot, E., Greenlaw, N., Ford, I., Ferrari, R., Fox, K. M., Tardif, J. C., Tendera, M., Parkhomenko, A., Bhatt, D. L., & Steg, P. G. (2018). Relationships Between Components of Blood Pressure and Cardiovascular Events in Patients with Stable Coronary Artery Disease and Hypertension. *Hypertension*, 71(1), 168-176. <https://doi.org/10.1161/hypertensionaha.117.10204>
- VisualSonics, F. (2008a). *How to Perform the Most Commonly Used Measurements in the Cardiac Measurements Package and the Generated Calculations of Cardiac Function using the Veo® 2100*. Retrieved 13/03/2024 from

[https://www.visualsonics.com/sites/default/files/AN\\_2100\\_Cv\\_Cardiac\\_Measurements\\_ver1.0.pdf](https://www.visualsonics.com/sites/default/files/AN_2100_Cv_Cardiac_Measurements_ver1.0.pdf)

- VisualSonics, F. (2008b). *MKT02620 Imaging Guides: Small Animal Echocardiography using the Vevo Imaging Systems Rev 1.0.* . Retrieved 13/03/2024 from <https://bcf.technion.ac.il/wp-content/uploads/2015/10/MKT02620-IGEchocardiography-Rev-1.0.pdf>
- Voelkl, B., Altman, N. S., Forsman, A., Forstmeier, W., Gurevitch, J., Jaric, I., Karp, N. A., Kas, M. J., Schielzeth, H., Van de Castele, T., & Würbel, H. (2020). Reproducibility of animal research in light of biological variation. *Nature Reviews Neuroscience*, 21(7), 384-393. <https://doi.org/10.1038/s41583-020-0313-3>
- Vonk Noordegraaf, A., & Galiè, N. (2011). The role of the right ventricle in pulmonary arterial hypertension. *Eur Respir Rev*, 20(122), 243-253. <https://doi.org/10.1183/09059180.00006511>
- Wagh, V., Doss, M. X., Sabour, D., Niemann, R., Meganathan, K., Jagtap, S., Gaspar, J. A., Ardestani, M. A., Papadopoulos, S., Gajewski, M., Winkler, J., Hescheler, J., & Sachinidis, A. (2014). Fam40b is required for lineage commitment of murine embryonic stem cells. *Cell Death Dis*, 5, e1320. <https://doi.org/10.1038/cddis.2014.273>
- Wakimoto, T., Matsunaga, S., Takai, A., & Fusetani, N. (2002). Insight into Binding of Calyculin A to Protein Phosphatase 1: Isolation of Hemicalyculin A and Chemical Transformation of Calyculin A. *Chemistry & Biology*, 9(3), 309-319. [https://doi.org/10.1016/S1074-5521\(02\)00118-7](https://doi.org/10.1016/S1074-5521(02)00118-7)
- Wang, S., Binder, P., Fang, Q., Wang, Z., Xiao, W., Liu, W., & Wang, X. (2018). Endoplasmic reticulum stress in the heart: insights into mechanisms and drug targets. *Br J Pharmacol*, 175(8), 1293-1304. <https://doi.org/10.1111/bph.13888>
- Watson, S. (2023). *Family History and Your Heart Failure Risk*. WebMD. Retrieved 16 November from webmd.com
- Wells, D. J., Playle, L. C., Enser, W. E. J., Flecknell, P. A., Gardiner, M. A., Holland, J., Howard, B. R., Hubrecht, R., Humphreys, K. R., Jackson, I. J., Lane, N., Maconochie, M., Mason, G., Morton, D. B., Raymond, R., Robinson, V., Smith, J. A., & Watt, N. (2006). Assessing the welfare of genetically altered mice. *Laboratory Animals*, 40(2), 111-114. <https://doi.org/10.1258/002367706776318971>
- Whelton, P. K., Carey, R. M., Aronow, W. S., Casey, D. E., Jr., Collins, K. J., Dennison Himmelfarb, C., DePalma, S. M., Gidding, S., Jamerson, K. A., Jones, D. W., MacLaughlin, E. J., Muntner, P., Ovbiagele, B., Smith, S. C., Jr., Spencer, C. C., Stafford, R. S., Taler, S. J., Thomas, R. J., Williams, K. A., Sr., . . . Wright, J. T., Jr. (2018). 2017 ACC/AHA/AAPA/ABC/ACPM/AGS/APhA/ASH/ASPC/NMA/PCNA

Guideline for the Prevention, Detection, Evaluation, and Management of High Blood Pressure in Adults: A Report of the American College of Cardiology/American Heart Association Task Force on Clinical Practice Guidelines. *Hypertension*, 71(6), e13-e115. <https://doi.org/10.1161/hyp.0000000000000065>

- Whitaker, R. H. (2018). Anatomy of the heart. *Medicine*, 46(8), 423-426. <https://doi.org/https://doi.org/10.1016/j.mpmed.2018.05.010>
- Wiesel, P., Mazzolai, L., Nussberger, J., & Pedrazzini, T. (1997). Two-kidney, one clip and one-kidney, one clip hypertension in mice. *Hypertension*, 29(4), 1025-1030. <https://doi.org/10.1161/01.hyp.29.4.1025>
- Williams, J. L., Paudyal, A., Awad, S., Nicholson, J., Grzesik, D., Botta, J., Meimarinou, E., Maharaj, A. V., Stewart, M., Tinker, A., Cox, R. D., & Metherell, L. A. (2020). Mylk3 null C57BL/6N mice develop cardiomyopathy, whereas Nnt null C57BL/6J mice do not. *Life Science Alliance*, 3(4), e201900593. <https://doi.org/10.26508/lsa.201900593>
- Wong, P. C. (2014). Science of Ultrasound and Echocardiography. In P. C. Wong & W. C. Miller-Hance (Eds.), *Transesophageal Echocardiography for Congenital Heart Disease* (pp. 1-48). Springer London. [https://doi.org/10.1007/978-1-84800-064-3\\_1](https://doi.org/10.1007/978-1-84800-064-3_1)
- World Health Organization. (2023). *Hypertension*. World Health Organization Retrieved 15 November from <https://www.who.int/news-room/fact-sheets/detail/hypertension>
- Yan, J., Zhang, L., Sultana, N., Park, D. S., Shekhar, A., Bu, L., Hu, J., Razzaque, S., & Cai, C.-L. (2015). A Murine Myh6MerCreMer Knock-In Allele Specifically Mediates Temporal Genetic Deletion in Cardiomyocytes after Tamoxifen Induction. *PLOS ONE*, 10(7), e0133472. <https://doi.org/10.1371/journal.pone.0133472>
- Yanai, S., & Endo, S. (2021). Functional Aging in Male C57BL/6J Mice Across the Life-Span: A Systematic Behavioral Analysis of Motor, Emotional, and Memory Function to Define an Aging Phenotype [Original Research]. *Frontiers in Aging Neuroscience*, 13. <https://doi.org/10.3389/fnagi.2021.697621>
- Yang, H., Wang, H., & Jaenisch, R. (2014). Generating genetically modified mice using CRISPR/Cas-mediated genome engineering. *Nature Protocols*, 9(8), 1956-1968. <https://doi.org/10.1038/nprot.2014.134>
- Zarich, N., Oliva, J. L., Martínez, N., Jorge, R., Ballester, A., Gutiérrez-Eisman, S., García-Vargas, S., & Rojas, J. M. (2006). Grb2 Is a Negative Modulator of the Intrinsic Ras-GEF Activity of hSos1. *Molecular Biology of the Cell*, 17(8), 3591-3597. <https://doi.org/10.1091/mbc.e05-12-1104>
- Zhang, Y., Mignone, J., & MacLellan, W. R. (2015). Cardiac Regeneration and Stem Cells. *Physiol Rev*, 95(4), 1189-1204. <https://doi.org/10.1152/physrev.00021.2014>

- Zhihao, L., Jingyu, N., Lan, L., Michael, S., Rui, G., Xiyun, B., Xiaozhi, L., & Guanwei, F. (2020). SERCA2a: a key protein in the Ca<sup>2+</sup> cycle of the heart failure. *Heart Failure Reviews*, 25(3), 523-535. <https://doi.org/10.1007/s10741-019-09873-3>
- Zhou, P., & Pu, W. T. (2016). Recounting Cardiac Cellular Composition. *Circ Res*, 118(3), 368-370. <https://doi.org/10.1161/CIRCRESAHA.116.308139>
- Zhou, Z., Liu, Z., Gao, X., & Long, Q. (2021). Mitochondrial respiration in C57BL/6 substrains varies in response to myocardial infarction. *Journal of Bioenergetics and Biomembranes*, 53(2), 119-127. <https://doi.org/10.1007/s10863-021-09884-6>

## **Appendix**

### **Appendix I: Publications**

- Alharbi, H. O., Hardyman, M. A., Cull, J. J., Markou, T., Cooper, S. T. E., Glennon, P. E., Fuller, S. J., Sugden, P. H., & Clerk, A. (2022). Cardiomyocyte BRAF is a key signalling intermediate in cardiac hypertrophy in mice. *Clin Sci (Lond)*, 136(22), 1661-1681. <https://doi.org/10.1042/CS20220607>
- Clerk, A., Meijles, D. N., Hardyman, M. A., Fuller, S. J., Chothani, S. P., Cull, J. J., Cooper, S. T. E., Alharbi, H. O., Vanezis, K., Felkin, L. E., Markou, T., Leonard, S. J., Shaw, S. W., Rackham, O. J. L., Cook, S. A., Glennon, P. E., Sheppard, M. N., Sembrat, J. C., Rojas, M., . . . Sugden, P. H. (2022). Cardiomyocyte BRAF and type 1 RAF inhibitors promote cardiomyocyte and cardiac hypertrophy in mice *in vivo*. *Biochem J*, 479(3), 401-424. <https://doi.org/10.1042/bcj20210615>
- Cull, J., Cooper, S., Alharbi, H., Chothani, S., Rackham, O., Meijles, D., Dash, P., Kerkelä, R., Ruparelia, N., Sugden, P., & Clerk, A. (2023). *Striatin plays a major role in angiotensin II-induced cardiomyocyte and cardiac hypertrophy in mice* *in vivo*. Cold Spring Harbor Laboratory. <https://dx.doi.org/10.1101/2023.10.21.563397>
- Fuller, S. J., Edmunds, N. S., McGuffin, L. J., Hardyman, M. A., Cull, J. J., Alharbi, H. O., Meijles, D. N., Sugden, P. H., & Clerk, A. (2021). MAP4K4 expression in cardiomyocytes: multiple isoforms, multiple phosphorylations and interactions with striatins. *Biochem J*, 478(11), 2121-2143. <https://doi.org/10.1042/bcj20210003>
- Marshall, J. J. T., Cull, J. J., Alharbi, H. O., Zaw Thin, M., Cooper, S. T. E., Barrington, C., Vanyai, H., Snoeks, T., Siow, B., Suárez-Bonnet, A., Herbert, E., Stuckey, D. J., Cameron, A. J. M., Prin, F., Cook, A. C., Priestnall, S. L., Chotani, S., Rackham, O. J. L., Meijles, D. N., . . . Parker, P. J. (2022). PKN2 deficiency leads both to prenatal 'congenital' cardiomyopathy and defective angiotensin II stress responses. *Biochem J*, 479(13), 1467-1486. <https://doi.org/10.1042/bcj20220281>
- Meijles, D. N., Cull, J. J., Cooper, S. T. E., Markou, T., Hardyman, M. A., Fuller, S. J., Alharbi, H. O., Haines, Z. H. R., Alcantara-Alonso, V., Glennon, P. E., Sheppard, M. N., Sugden, P. H., & Clerk, A. (2021). The anti-cancer drug dabrafenib is not cardiotoxic and inhibits cardiac remodelling and fibrosis in a murine model of hypertension. *Clin Sci (Lond)*, 135(14), 1631-1647. <https://doi.org/10.1042/cs20210192>
- Meijles, D. N., Cull, J. J., Markou, T., Cooper, S. T. E., Haines, Z. H. R., Fuller, S. J., O'Gara, P., Sheppard, M. N., Harding, S. E., Sugden, P. H., & Clerk, A. (2020). Redox Regulation of Cardiac ASK1 (Apoptosis Signal-Regulating Kinase 1) Controls p38-MAPK (Mitogen-Activated Protein Kinase) and Orchestrates Cardiac Remodeling to

Hypertension. *Hypertension*, 76(4), 1208-1218.

<https://doi.org/10.1161/hypertensionaha.119.14556>

- Meijles, D. N., Fuller, S. J., Cull, J. J., Alharbi, H. O., Cooper, S. T. E., Sugden, P. H., & Clerk, A. (2021). The insulin receptor family and protein kinase B (Akt) are activated in the heart by alkaline pH and  $\alpha$ 1-adrenergic receptors. *Biochem J*, 478(11), 2059-2079. <https://doi.org/10.1042/bcj20210144>